DATE ENTERED SEP 23 1971

ORNL
MASTER COPY

ORNL-4706
UC-4 – Chemistry

CHEMISTRY DIVISION ANNUAL PROGRESS REPORT

FOR PERIOD ENDING MAY 20, 1971

OAK RIDGE NATIONAL LABORATORY
operated by
UNION CARBIDE CORPORATION
for the
U.S. ATOMIC ENERGY COMMISSION

Printed in the United States of America. Available from
National Technical Information Service
U.S. Department of Commerce
5285 Port Royal Road, Springfield, Virginia 22151
Price: Printed Copy $3.00; Microfiche $0.95

This report was prepared as an account of work sponsored by the United States Government. Neither the United States nor the United States Atomic Energy Commission, nor any of their employees, nor any of their contractors, subcontractors, or their employees, makes any warranty, express or implied, or assumes any legal liability or responsibility for the accuracy, completeness or usefulness of any information, apparatus, product or process disclosed, or represents that its use would not infringe privately owned rights.

ORNL-4706

Contract No. W-7405-eng-26

CHEMISTRY DIVISION ANNUAL PROGRESS REPORT

for Period Ending May 20, 1971

E. H. Taylor, Director
Sheldon Datz, Associate Director
Ralph Livingston, Associate Director
B. H. Ketelle, Assistant Director

G. E. Moore, Editor of Annual Report

SEPTEMBER 1971

OAK RIDGE NATIONAL LABORATORY
Oak Ridge, Tennessee
operated by
UNION CARBIDE CORPORATION
for the
U. S. ATOMIC ENERGY COMMISSION

Reports previously issued in this series are as follows:

ORNL-2386	Period Ending June 20, 1957
ORNL-2584	Period Ending June 20, 1958
ORNL-2782	Period Ending June 20, 1959
ORNL-2983	Period Ending June 20, 1960
ORNL-3176	Period Ending June 20, 1961
ORNL-3320	Period Ending June 20, 1962
ORNL-3488	Period Ending June 20, 1963
ORNL-3679	Period Ending June 20, 1964
ORNL-3832	Period Ending May 20, 1965
ORNL-3994	Period Ending May 20, 1966
ORNL-4164	Period Ending May 20, 1967
ORNL-4306	Period Ending May 20, 1968
ORNL-4437	Period Ending May 20, 1969
ORNL-4581	Period Ending May 20, 1970

Contents

INTRODUCTION ix

1. NUCLEAR CHEMISTRY

The Return to $A = 49$ 1
Levels in ^{101}Ru Populated by the Decay of ^{101}Tc 3
Energy Levels of ^{104}Pd Populated by the Beta Decay of 43-sec ^{104g}Rh and 4.41-min ^{104m}Rh 5
Decay of ^{72}As to the Levels of ^{72}Ge 9
Level Structure of ^{108}Pd Populated in the Decay of 2.42-min ^{108}Ag 12
Coulomb Excitation and In-Beam Reaction Gamma Spectroscopy 12
In-Beam Gamma-Ray Spectroscopy of the Tin Isotopes 13
The Decay of ^{136}Pr and the Level Structure of ^{136}Ce 14
New Alpha Emitters with $N = 86$ and $N = 87$: ^{156}Tm and Isomers of ^{154}Ho and ^{153}Ho 15
The Decay of ^{158}Eu to Levels in ^{158}Gd 19
Band-Mixing Anomalies in ^{178}Hf 21
The Decay of ^{194}Au to the Levels of ^{194}Pt 23
Abundances of the Primordial Radionuclides K, Th, and U in Apollo 12 Lunar Samples by Nondestructive Gamma-Ray Spectrometry: Implications for Origin of Lunar Soils 25
Cosmogenic Radionuclide Concentrations and Exposure Ages of Lunar Samples from Apollo 12 29

2. CHEMISTRY AND PHYSICS OF TRANSURANIUM ELEMENTS

Inclusion of Charged-Particle Emission and Fission in Nuclear Reaction Calculations 32
Analysis of the Interactions of Protons with ^{232}Th and ^{231}Pa 34
Coulomb Excitation Studies of Even-Even Transuranium Nuclei Using Alpha Particles 36
Properties of Ground-State Rotational Bands of Heavy Even-Even Nuclei 38
Multiple Coulomb Excitation of Heavy Elements with ORIC Heavy-Ion Beams 40
Charged Particles from High-Energy Oxygen-Ion-Induced Reactions 42
Studies of (H.I.,αxn) Reactions 44
Determination of the Half-Lives of ^{246}Cm and ^{248}Cm by Absolute Specific Activity Techniques 46
The Thermal Cross Sections and Resonance Integrals for Neutron Capture of ^{249}Cf, ^{250}Cf, and ^{251}Cf 47
Evaluation of ^{251}Cf "Burnout" Experiment 51
The Thermal Cross Section and Resonance Integral for Neutron Fission of ^{252}Cf 53
The Neutron Capture Thermal Cross Sections and Resonance Integrals of ^{244}Pu and ^{245}Pu 55
K X-Ray Energies and Relative Transition Probabilities of Curium, Berkelium, Californium, and Einsteinium 56

Electron Binding Energies and L-Shell Fluorescent Yields in Curium 58
The Unequivocal Identification of Transfermium Elements Using X-Ray Techniques 60
The Alpha Decay of ^{255}No and States in ^{251}Fm 62
On the $M2$ Transition Probability between the $5/2^+[622\uparrow] \rightleftharpoons 9/2^-[734\uparrow]$ Nilsson States 64
The New Nuclide ^{259}No 65
Search for Element 106 67
Radioactivity Associated with Pleochroic Halos 69
Search for Superheavy Elements in Nature 69
Search for Superheavy Elements with Neutron Multiplicity Counters 71
Electron-Transfer and $f \rightarrow d$ Absorption Bands of Some Lanthanide and Actinide Complexes and the Standard III-IV Oxidation Potentials for Each Member of the Lanthanide and Actinide Series 71
Solution Absorption Spectra of Bk(III) and Bk(IV) and the Formal Potential of the Bk(IV)-Bk(III) Couple in Several Media 72
Thiocyanate Complexes of Trivalent Actinides 72
Thermodynamic Systematics among the Members of the Lanthanide and Actinide Series 73
Theoretical Treatment of the Energy Differences between $f^q d^1 s^2$ and $f^{q+1} s^2$ Electron Configurations for Lanthanide and Actinide Atomic Vapors 73
Electron Spectrometry of Actinides and Actinide Compounds 74
Intramolecular Energy Transfer and Sensitized Luminescence in an Einsteinium β-Diketone Chelate and the Lower-Lying Electronic Energy Levels of Es(III) 76
Noncovalent Character in the Chemical Bonds of the Lanthanide(III) and the Actinide(III) Tricyclopentadienides 76
Samarium Triindenide: Crystal and Molecular Structure 77
Crystal and Molecular Structure of Triindenyluranium Chloride 78
Method for the Direct Determination of Ligands 80
Ligands in Solvated Lanthanide Halides 81
Crystallographic Studies on $Cs_2NaNdCl_6$ and $Cs_2NaDyCl_6$ 81
Preparation and Properties of Cs_3NdCl_6 and $Cs_2NaNdCl_6$ 82
Studies with Heptavalent Neptunium 83
The Crystal Structure of Americium Sulfate Octahydrate 83
The Dioxide of Long-Lived ^{248}Cm 84
Some Properties of Berkelium Metal 85
Ionic Radii from Transplutonium Trichlorides 86
Neutron Multiplicity Counter 87
Fast-Closing Protective Valve at ORIC 89

3. ISOTOPE CHEMISTRY

Fractionation of Carbon Isotopes: The CYANEX System 91
Photochemistry of Chlorine 91
Oxygen-17 Facility 91

Molecular Spectroscopy 92
Isotopic Mass Spectrometry 97
Comparative Isotopic Carbon Analyses of CO and CO_2 98
Exchange of Oxygen between CO_2(g) and V_2O_5(s) 98

4. RADIATION CHEMISTRY

Ozone Formation in the Pulse Radiolysis and Flash Photolysis of Oxygen 100
Absorption Spectrum and Reaction Kinetics of the HO_2 Radical in the Gas Phase 102
Radiation Chemistry of Gaseous Methane 103
Photooxidation and Fluorescence of Cerium(III) in Aqueous Sulfuric Acid Solutions 104
Reduction of Cerium(IV) by Hydrogen Peroxide: Dependence of Reaction Rate on Hammett's Acidity Function 105
Reduction of Cerium(IV) by Nitrous Acid in Aqueous Nitric Acid Solutions 106
Energy Transfer and the Radiolysis of Aliphatic Carboxylic Acids 107

RADIATION AND HOT-ATOM CHEMISTRY OF INORGANIC CRYSTALLINE SOLIDS

A Raman Spectral Study of the ^{60}Co Gamma Radiolysis of ^{18}O-Enriched Polycrystalline KNO_2 111

5. ORGANIC CHEMISTRY

Preparation of Vinyl Esters 113
The Deamination of 1-Cyclopentylethylamine 113
Solvolysis of 3-Phenyl-2-bromopropanal 114
The Mechanism of the Diels-Alder Reaction. Attempts to Prepare Unusual Hydrocarbons 114
Heats of Formation of 3-Aryl-2,3-dimethyl-2-butyl Cations in Super Acids 115
The Mechanism of Hydride Shift in Norbornyl Cations 116
A Deuterium Tracer Study of 6,1,2-Hydride Shift in Substituted Norbornyl Cations 116
Preparation and Purification of *p*-Sexiphenyl 117

6. PHYSICAL CHEMISTRY

AQUEOUS SYSTEMS

Free Energies of Electrolyte Mixtures 119
A Simple Equation for the Prediction of the Activity Coefficient Value of Each Component in Aqueous Electrolyte Mixtures 121
Parameters for Calculating the Activity Coefficient of Each Component in HCl-RbCl, HCl-CsCl, HCl-$SrCl_2$, and HCl-$BaCl_2$ Mixtures to Ionic Strength 3 125
Osmotic and Activity Coefficients for Mixtures of Cesium Chloride and Barium Chloride in Water at 25° 127
Estimation of Solute Activity Coefficients in Dilute Aqueous Mixtures at 25°: Comparisons with Predictions from the Guggenheim Theory of Solutions 127

Heats of Dilution of Aqueous Solutions of Sodium Salts of Carboxylic Acids 128
Thermodynamics of Aqueous Solutions of Tetrabutylammonium Carboxylates. Model Systems for the Hydrophobic Interaction in Proteins 129
The Effect of Dimethyl Sulfoxide (DMSO) on Hydrophobic Interactions: Heats of Dilution of Tetrabutylammonium Bromide in the Mixed Solvent System Water-DMSO 131
Tracer Diffusion Coefficients of HTO and $^{36}Cl^-$ in Cation Exchangers 133
Theory of the Porous-Frit Method of Measuring Self-Diffusion Constants 134
Mass Transport Studies 135
Adsorption of Cd(II) and Hg(II) on Anion Exchangers from Chloride Solutions 138
Activity Coefficients of NaCl in Water-Organic Mixtures 139
Density of Water-Organic Mixtures at 25°C 140
Hyperfiltration with Dynamically Formed Membranes 140
Organic Polyelectrolytes for Hyperfiltration Tests 145
Some Remarks on the Integration of the Extended Nernst-Planck Equations in the Hyperfiltration of Multicomponent Solutions 146
Geometric Effects in Piezodialysis through Charge-Mosaic Membranes 148
Cross-Flow Filtration of Sewage Effluents 148

MOLTEN SALTS AND RELATED NONAQUEOUS SYSTEMS

A Reference Electrode System for Use in Fluoride Melts 150
Free Energy of Formation of Lanthanide Halides 152
Enthalpy of Uranium Tetrafluoride from 298 to 1400°K: Enthalpy and Entropy of Fusion 153
Enthalpy of Lithium Fluoroborate from 298 to 700°K: Enthalpy and Entropy of Fusion 154
High-Temperature Crystal Chemistry of Tetrafluoroborates and Structurally Related Compounds 155
Excess Free Energy in Some Binary Molten-Salt Mixtures with a Common Cation 155
"ThOF": Trivalent Thorium? 158
Polarizability Change for Halide Ions (X^-) on Forming Complex Ions (BF_4^-) or Molecules ZX_n 159
Magnetic Susceptibility of Titanium(II) Tetrachloroaluminate 161
Raman Spectra of the High-Temperature Phase of Polycrystalline $NaBF_4$ 162
Raman Spectra of BeF_4^{2-} in Molten LiF and NaF to 686°C 163
Raman Spectral Studies of Molten Lithium Nitrate–Lithium Perchlorate Mixtures 165

CALORIMETRY

Low-Temperature Heat Capacity of ^{7}Li Hydride and ^{7}Li Deuteride 168
Enthalpies of Orthorhombic and Cubic Lead Difluoride. The Order-Disorder Transition in the Cubic Phase 171

ELECTROCHEMISTRY

Hydrous Oxides of Technetium in Its Lower Valencies 173
Electrochemistry of Technetium and of Iron Containing Technetium 174
Electrochemical Behavior of Titanium 175

Potentiostatic Method for the Determination of Specific Conductance 177
Hydrogen Production with a Suspension Electrode in a Flow Cell 178
Electrochemical Pretreatment of Sea Water for pH Control and Bicarbonate Removal 181
Electrochemical Method for Analysis of Dissolved Oxygen in the Parts-per-Billion Range 182

7. CHEMICAL PHYSICS

NEUTRON AND X-RAY DIFFRACTION

The Crystal and Molecular Structure of the "Anomalous Acetate" of Katonic Acid. A Severely Twisted Carbon-Carbon Double Bond 183
The Crystal Structure of 3-Hydroxyxanthine Dihydrate, a Tumor-Inducing Chemical Agent 185
Precise X-Ray Crystal-Structure Analysis of Decachlororuthenocene 187
Precise X-Ray Crystal-Structure Analysis of 1,1′-Diethoxyoctachloroferrocene 190
Crystal and Molecular Structure of α,α'-Trehalose Dihydrate 192
Characterization of the Thermal Motion in Trisacetylacetonatochromium(III) 195
Crystal and Molecular Structure of Trimercury Chloroaluminate, $Hg_3(AlCl_4)_2$ 198
X-Ray and Neutron Diffraction Study of Xenon Hexafluoride 200
A Computer Program to Aid in the Understanding of Interatomic Forces in Molecules and Crystals 201
A Method for Predicting the Conformation of the Isolated Molecule of an Organic Compound from Its Crystal Structure 202
The Calculation of Potential-Energy Parameters from the Vibrational Frequencies of Ethane 203
A Convenient Way of Applying Constraints in a Crystallographic Least-Squares Refinement 204
Least-Squares Refinement of Measurements for Crystal Absorption Corrections 204
A New Formulism for Reporting the Precision of Crystal Structure Parameters 205
ORTEP-II: A Crystal-Structure Graphics Program with Elimination of Overlap 207
Computer-Controlled Neutron Diffractometer for the Study of Liquids 208
Liquid Gallium: Comparison of X-Ray and Neutron Diffraction Data 209
The Mean Spherical Model: Solution of an Integral Equation for the Structure of Liquid Metals 210
Liquid Water: Molecular Correlation Functions from X-Ray Diffraction 211
X-Ray Diffraction Study of the System BeF_2-LiF 212
Diffraction Studies on Aqueous Electrolyte Solutions 213

INFRARED AND RAMAN SPECTROSCOPY

Effects of Density and State on the Profiles and Integrated Intensities of Near-Infrared Absorption Bands of H_2O 214
Spectrophotometry of Liquids and Solutions over Wide Ranges of Temperature and Pressure 216
Measurement of Infrared Emission Spectra of Molten Salts by Fourier Transform Spectroscopy 217
Polarized Raman Spectra of β-Quartz 218
Dynamics of β-Quartz Structures of Vitreous SiO_2 and BeF_2 221
Raman and Infrared Spectral Studies of Anhydrous Li_2CO_3 and Na_2CO_3 223

Determination of Longitudinal Optical Mode Frequencies by Polarized Specular Reflectance (PSR) Infrared Spectroscopy 226

Polarized Vibrational Spectra of Potassium Chlorate 229

The Crystal Structure of $Sr(NO_3)_2$, $Ca(NO_3)_2$, $Ba(NO_3)_2$, and $Pb(NO_3)_2$: An Infrared and Raman Study 230

Raman and Infrared Spectra of Anhydrous $Zn(NO_3)_2$, $Cd(NO_3)_2$, and $Ca(NO_3)_2$: A Study of the Phase Changes in $Ca(NO_3)_2$ 232

MICROWAVE AND RADIO-FREQUENCY SPECTROSCOPY

Paramagnetic Resonance Studies of Liquids during Photolysis 235

Paramagnetic Resonance Studies of Gamma-Irradiated Inorganic Single Crystals at Low Temperature 237

ELECTRON SPECTROSCOPY

Electron Spectroscopy 237

Study of Chemical Bonding in Transition Metal Compounds by Use of Photoelectron Spectroscopy 238

Manifestation of Atomic Dynamics through the Auger Effect 240

Excitation Accompanying Photoionization in Atoms and Molecules and Its Relationship to Electron Correlation 241

Determination of the *K-LL* Auger Spectra of O_2, N_2, CO, NO, H_2O, and CO_2 241

Resonance *K* Excitation and Auger Decay of the Nitrogen Molecule 241

Calculations Using Atomic Wave Functions 243

ATOMIC AND MOLECULAR COLLISIONS

Ionizing Collisions of Fast Alkali Atoms with Cl_2, Br_2, and O_2 244

Differentiation in *L* Subshell Vacancy Production in Iodine Ions by Atomic Collisions at 15 to 60 MeV 246

Charge-Changing Collisions of Channeled Oxygen Ions in Gold 249

MASS SPECTROMETRY AND RELATED TECHNIQUES

The Radiolysis of Methane in the Electric-Field Source 250

Characterization of Volatile and Nonvolatile Solids Obtained from the Gas Phase Radiolysis of Pentaborane-9 251

PUBLICATIONS 253

PAPERS PRESENTED AT SCIENTIFIC AND TECHNICAL MEETINGS 260

LECTURES 265

SUPPLEMENTARY ACTIVITIES 267

Introduction

No innovations in the Annual Report this year. Everything should be where you expect it.

The new directions mentioned a year ago occupied the attention of more and more members of the staff, but only at the level of proposal writing, not in the conduct of research that would appear herein. Perhaps next year. The most extensive proposals and the ones we are counting on most heavily represent continuation and extension of the present Water Research Program, but groups as diverse as the Transuranium Research Laboratory, Organic Chemistry, and Molecular Beams found areas in which their capabilities might be usefully applied to certain environmental problems.

Despite the distractions of proposal writing, our usual product, research results, appeared at a somewhat increased rate. In addition to the usual selection, these included: some interesting observations in fields long under study (the gas-phase spectrum and some rate constants of HO_2; precise neutron and x-ray diffraction data for liquid gallium, showing complete equivalence); some new applications of old techniques (electron spectrometry of the actinides; unequivocal identification of transfermium elements by the Moseley technique); and an invention (the measurement of electrolytic conductance by a potentiostatic method).

By next year, some of the new directions we propose to take will be opened or closed. No matter how that goes, however, we are already committed to dropping a few of our present areas of research. These changes in our research program will be somewhat gradual in order to minimize the waste of past effort, but in the case of our one production activity, the oxygen-17 plant, it is already shut down.

1. Nuclear Chemistry

THE RETURN TO $A = 49$[1]

E. Eichler S. Raman[2]

Like a never empty bowl, the modest little nucleus ^{49}Ca reveals new insights at every reexamination. Last year[3] we discussed the results of our attempt to determine the spin of the important 4507-keV level. In addition, we tentatively listed a number of new weak transitions. Now we have confirmed the existence of the low-intensity lines by a variation of the "mobile" source experiment. A ^{49}Ca source was prepared, counted for about 4 min, moved closer to the detector to restore the initial counting rate, and counted again for 4 min. This procedure was repeated for a total counting time of 45 min. The areas of the gamma-ray peaks were computed relative to the area of the double-escape peak of the well-established 3084.4-keV gamma ray. Those gamma rays with constant relative areas over four half-lives of counting were designated as legitimate.

The 143.2- and 1408.9-keV gamma energies were determined in two separate runs by counting ^{49}Ca sources with ^{57}Co and ^{60}Co sources respectively. The 143.2-keV gamma energy measurement was done with a 0.25-cm^3 Ge(Li) x-ray detector [the other measurements were made with a 6.5% Ge(Li) detector]. These two gamma peaks, together with the three peaks associated with the 3084.4-keV gamma ray, served as internal calibration standards.

The decay scheme in Fig. 1.1, based on the present and previous study[4] of ^{49}Ca decay, includes all of the observed gamma rays. The levels at 2228.6 and 2371.8 keV are well established from ^{50}Ti(d,^{3}He) studies.[5] Since the β^- disintegration energy[6] $Q^- = 5263 \pm 5$ keV and since there are no known levels below 2.22 MeV from reaction studies,[6] the 3084.4-, 4071.9-, and 4738.2-keV gamma rays must be ground-state transitions. The three levels thus established have also been excited in stripping reactions.[7–9] Vingiani, Chilosi, and Bruynesteyn[10] have observed high-energy gamma rays from resonance proton capture leading to a level at 3513 ± 5 keV. Therefore, we have assigned the 1288.4- and 1144.5-keV gamma rays as deexciting a level at 3516.6 keV. Finally, the 4493.3-keV level is established by our 1409-3084 keV correlation studies.

The lifetime $T_{1/2} = 1.40 \pm 0.09$ nsec measured by Chilosi and Vingiani[11] for the 2371.8-keV level and the gamma-branching ratio measured in this work imply that the 143.2-keV gamma transition (assumed to be $M1$) is hindered by a factor of 2500 ± 400 and the 2371.7-keV gamma transition ($M2$) by a factor of 470 ± 70 over the Moszkowski estimates.

With simple proton configurations of the type $[(f_{7/2})^2_0(d^{-1}_{3/2})]_{3/2^+}$ and $[(f_{7/2})^1(d_{3/2})^4_0]_{7/2^-}$ for the ^{49}Sc 2371.8-keV level and the ground state, respectively, the $M2$ transition is expected to proceed at nearly the single-particle rate. The observed $M2$ hindrance can be understood within the framework of calculations by Kurath and Lawson[12] and by Lawson and Macfarlane.[13] In these calculations, the authors have shown that $M2$ inhibition will result in cases where the wave function of the hole state has appreciable core-excited components. Specifically, the authors have compared observed $M2$ transition rates in ^{43,45,47}Sc isotopes with those calculated using wave functions projected from the appropriate Nilsson wave functions. The extension of these calculations by Lawson[14] to the ^{49}Sc case leads to a 19% admixture of $[(f_{7/2})^2_2(d_{3/2})^{-1}]_{3/2^+}$ core-excited components in the eigenfunctions for the $^3/_2{}^+$ hole state and a resulting $M2$ hindrance (in Moszkowski units) of 170. A shell-model calculation, also by Lawson,[14] leads to similar $M2$ inhibition, but in this case the probability of core excitation is only about 12%. Experimentally, the presence of core excitation is suggested by the $d_{3/2}$ pickup strength of 3.39 [≈15% lower than the maximum of 4.0] for the 2372-keV level obtained by Newman and Hiebert[5] from the ^{50}Ti(d,^{3}He) reaction.

Since an $s_{1/2}$ strength of 2.14 was also obtained by Newman and Hiebert[5] for the 2228.6-keV level, this level is probably due to single-hole excitations of the type $[(f_{7/2})^2_0(s_{1/2})^{-1}]_{1/2^+}$. The strong $M1$ inhibition of the 143.2-keV gamma transition immediately follows from l-forbiddenness. The observation[11] that the 2228.9-keV $E3$ transition proceeds at close to single-particle speed is also consistent with a pure $[(f_{7/2})^2_0(s_{1/2})^{-1}]_{1/2^+}$ configuration for the 2228.6-keV level.

As a natural extension of the study of ^{49}Ca decay, we have investigated the decay of ^{49}Sc to levels in ^{49}Ti.

ORNL-DWG. 70-14620

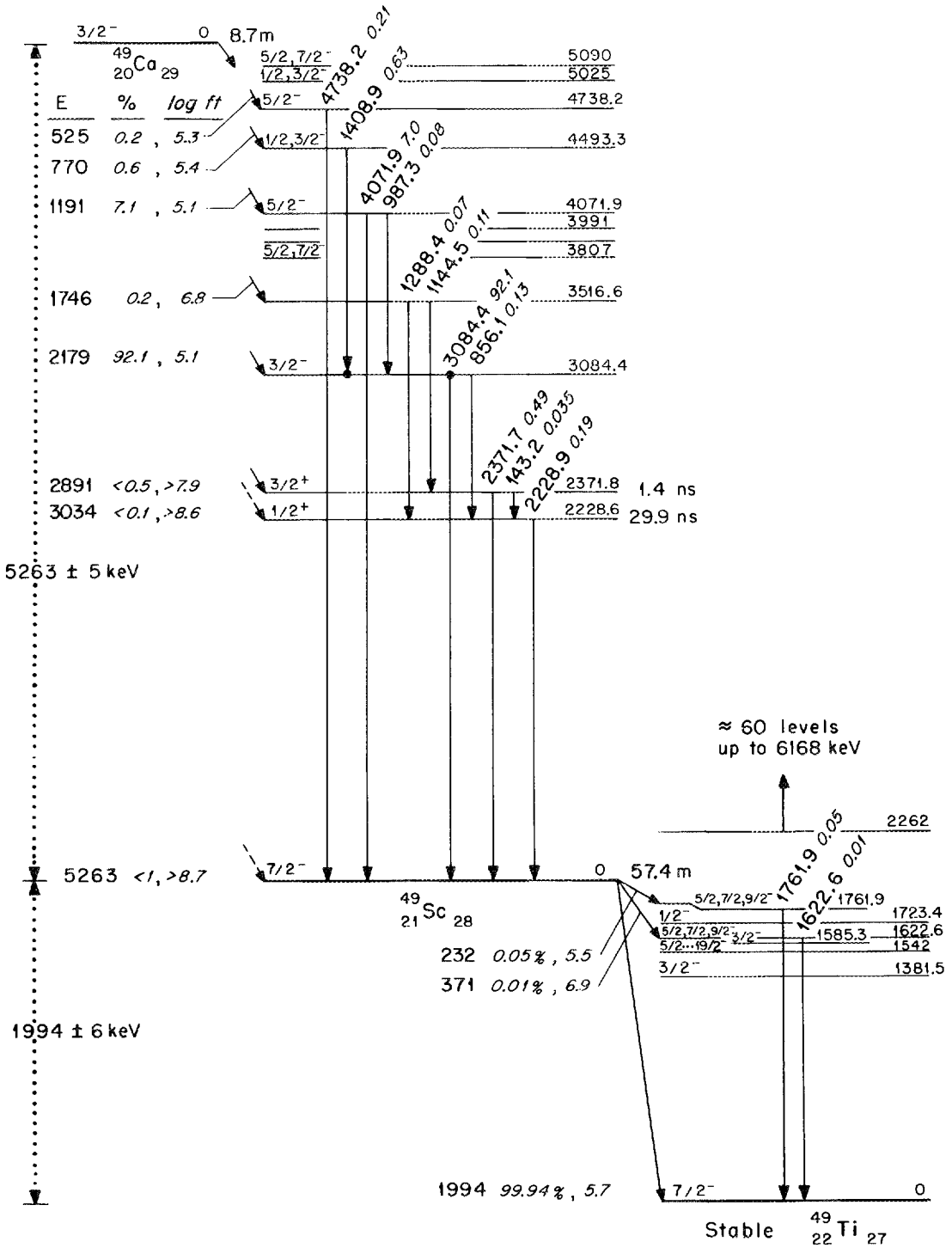

Fig. 1.1. Proposed decay scheme for 8.7-min ^{49}Ca and ^{49}Sc.

The only previous report of gamma-ray emission in ^{49}Sc decay is that by Rezanka et al.,[15] who observed [with an NaI(Tl) detector] a single gamma ray of energy 1.78 ± 0.04 MeV and intensity 0.03 per 100 decays of ^{49}Sc. We studied the ^{49}Sc decay by first preparing an intense ^{49}Ca source. After an elapsed interval of 100 min, by which time virtually all of ^{49}Ca had decayed to ^{49}Sc, the gamma spectrum counted for 1 hr showed two peaks superimposed on the bremsstrahlung background. These two peaks were observed to decay with the half-life of ^{49}Sc ($T_{1/2}$ = 57.4 min). With energy calibrations provided by the gamma radiations from ^{38}Cl and ThC″ sources, the gamma energies were determined to be 1622.6 ± 0.6 and 1761.9 ± 0.3 keV with absolute intensities of 0.01 ± 0.003% and 0.05 ± 0.01%. These transitions are included in the level scheme of Fig. 1.1.

1. See also, *Phys. Div. Annu. Progr. Rep. Dec. 31, 1970*, ORNL-4659, p. 65.
2. Nuclear Data Project.
3. E. Eichler, *Chem. Div. Annu. Progr. Rep. May 20, 1970*, ORNL-4581, p. 1.
4. G. Chilosi, G. D. O'Kelley, and E. Eichler, *Nucl. Phys. A* **136**, 649 (1969).
5. E. Newman and J. C. Hiebert, *Nucl. Phys. A* **110**, 366 (1968).
6. S. Raman, *Nuclear Data Sheets* **B4**, 397 (1970); W. B. Ewbank and S. Raman, "Adjusted Mass Differences," ibid. **B4**, 439 (1970).
7. D. D. Armstrong and A. G. Blair, *Phys. Rev.* **140**, B1226 (1965).
8. J. R. Erskine, A. Marinov, and J. P. Schiffer, *Phys. Rev.* **142**, 633 (1966).
9. T. B. Grandy et al., *Nucl. Phys. A* **113**, 353 (1968).
10. G. B. Vingiani, G. Chilosi, and W. Bruynesteyn, *Phys. Lett. B* **26**, 285 (1968).
11. G. Chilosi and G. B. Vingiani, *Phys. Lett. B* **27**, 81 (1968).
12. D. Kurath and R. D. Lawson, *Phys. Rev.* **161**, 915 (1967).
13. R. D. Lawson and M. H. Macfarlane, *Phys. Rev. Lett.* **14**, 152 (1965).
14. R. D. Lawson, private communication, November 1970.
15. I. Rezanka et al., *J. Inorg. Nucl. Chem.* **18**, 13 (1961).

LEVELS IN ^{101}Ru POPULATED BY THE DECAY OF ^{101}Tc[1]

N. K. Aras[2] G. Chilosi[4]
P. Fettweis[3] G. D. O'Kelley

An experimental investigation of the energy levels of ^{101}Ru has been in progress for several years. The decays of 3.0-year ^{101g}Rh (I^π = $1/2^-$) and 4.4-day ^{101m}Rh (I^π = $9/2^+$) have yielded important information concerning the level structure of ^{101}Ru, and these results have been published.[5] Our preliminary study[6] of the decay of 14.6-min ^{101}Tc (I^π = $9/2^+$) to levels of ^{101}Ru has been extended by recent high-resolution gamma-ray spectrometry, and a revised decay scheme has been determined.

Gamma-ray energies and intensities were measured with a high-efficiency, high-resolution Ge(Li) detector. Gamma-gamma coincidence relationships between some of the intense gamma transitions were determined by use of two 7.5- by 7.5-cm NaI(Tl) scintillation detectors set 120° apart and connected to a two-parameter pulse-height analyzer for data acquisition. Beta energies were determined with a well-type anthracene scintillation spectrometer. Beta-gamma coincidence relationships were studied with anthracene and NaI(Tl) detectors.

Sources of ^{101}Tc were chemically separated from a large sample of 14-min ^{101}Mo, which in turn was prepared by neutron capture on ^{100}Mo. Several of the gamma energies assigned to the decay of ^{101}Tc were disturbingly similar in energy to gamma energies of ^{101}Mo. Careful comparisons between ^{101}Tc and ^{101}Mo spectra showed that the ^{101}Tc peaks in question do happen to lie very close in energy to ^{101}Mo gamma-ray peaks (see Table 1.1).

Table 1.1 gives the energies and intensities of all gamma rays observed in a ^{101}Tc source, as well as a comparison with the energy values of the same lines observed in Coulomb excitation.[7] Intensities are corrected for internal conversion, which is especially important for the 127-keV gamma ray. Also listed are the neighboring ^{101}Mo lines and their intensities relative to the 307-keV line of ^{101}Tc in the gamma-ray spectrum of a ^{101}Mo source measured 45 min after irradiation.

The most energetic beta-ray group in the decay of ^{101}Tc has an energy of 1.31 ± 0.03 MeV and is in coincidence with the 307-keV gamma ray. An inner beta group of energy 1.07 ± 0.03 MeV is in coincidence with the 545-keV gamma ray.

The decay scheme shown in Fig. 1.2 accounts for all of the gamma rays for which coincidence data were obtained. Some levels were assigned from energy sums alone, if more than one gamma-ray cascade yielded the same level energy. No coincidence data are available for the 674.0- and 826.2-keV gamma rays, and their energies do not correspond to any of the differences between established levels. These unassigned gamma rays may correspond to ground-state transitions. The level scheme of Fig. 1.2 is self-consistent and agrees with data from Coulomb excitation[7] of ^{101}Ru and decay of the ^{101}Rh isomers.[5]

Table 1.1. Gamma rays of ^{101}Tc observed in the present work and their transition intensities compared with corresponding lines observed by Coulomb excitation

Also given are energies and intensities of gamma rays of ^{101}Mo which lie particularly close to some established ^{101}Tc lines

^{101}Tc source separated from ^{101}Mo		E_γ (keV), Coulomb excitation[a]	^{101}Mo source measured 45 min after the end of the irradiation	
E_γ (keV)	I_γ (%)		E_γ[b] (keV)	I_γ relative to the 307-keV transition
72.5 ± 1	0.01 ± 0.005			
84.8 ± 1.4	0.04 ± 0.005			
127.1 ± 0.2	1.5 ± 0.2	127.2 ± 0.2		
179.4 ± 0.3	0.3 ± 0.03			
184.0 ± 0.3	1.4 ± 0.02	184.1 ± 0.1		
233.7 ± 0.3	0.1 ± 0.02	233.7 ± 0.1		
238.3 ± 0.3	0.3 ± 0.03	238.1 ± 0.1		
295.2 ± 0.5	0.04 ± 0.01	294.8 ± 0.2		
306.7 ± 0.2	90.0 ± 9.0	306.8 ± 0.2		
321.7 ± 0.5	0.04 ± 0.006			
383.1 ± 0.5	0.02 ± 0.003			
393.0 ± 0.3	0.06 ± 0.007			
413.0 ± 0.5	0.02 ± 0.004	413.1 ± 0.2		
422.5 ± 0.5	0.03 ± 0.005	422.0 ± 0.1	421.4	0.22
488.1 ± 0.5	0.03 ± 0.005	489.1 ± 0.2		
515.9 ± 0.2	0.08 ± 0.009		513.2	1.8
531.1 ± 0.2	0.8 ± 0.08		532.7	0.9
544.6 ± 0.2	4.8 ± 0.5	544.9		
602.8 ± 0.5	0.01 ± 0.005			
616.9 ± 0.3	0.03 ± 0.005	616.3 ± 0.3		
621.7 ± 0.2	0.07 ± 0.008	623.2 ± 0.6		
626.7 ± 0.2	0.4 ± 0.04		625.5	0.4
631.7 ± 0.5	0.04 ± 0.003			
674.0 ± 0.5	0.02 ± 0.003			
694.3 ± 0.2	0.06 ± 0.007		695.2	3.5
715.6 ± 0.2	0.06 ± 0.006		712.7	2.1
720.0 ± 0.2	0.2 ± 0.02	720.1 ± 0.2		
811.1 ± 0.2	0.06 ± 0.007			
826.2 ± 0.5	0.002 ± 0.001			
842.7 ± 0.2	0.2 ± 0.02			
911.9 ± 0.3	0.01 ± 0.002			
928.5 ± 0.2	0.09 ± 0.03	928.9 ± 1.5		
938.1 ± 0.2	0.08 ± 0.008		933.8	2.1

[a]Kistner and Schwarzschild, ref. 7. Only those gamma rays which were also observed in the present work are listed.

[b]Only those lines which lie close to ^{101}Tc lines are listed.

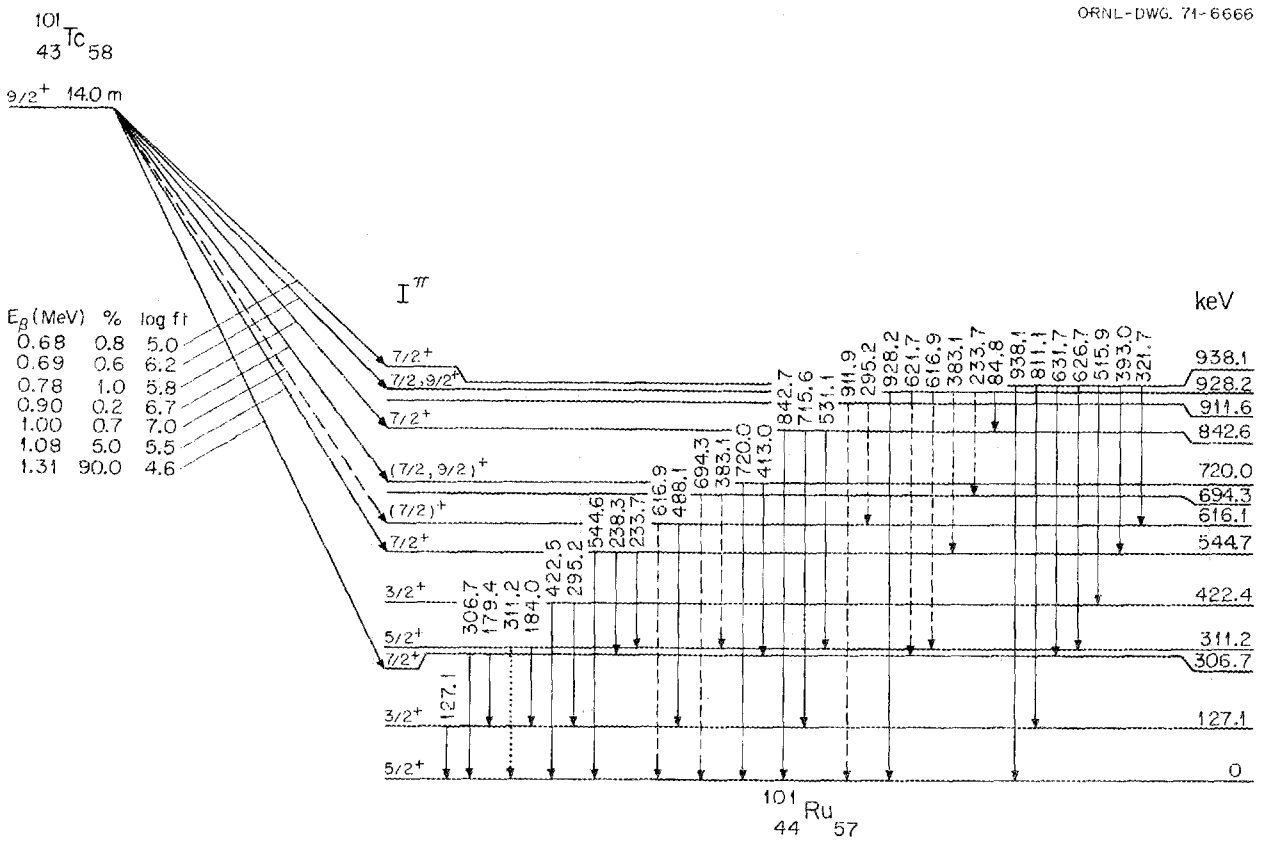

Fig. 1.2. Proposed decay scheme of ^{101}Tc. Dashed lines denote weak transitions, whose assignment may be uncertain. The 311.2-keV line was not observed directly in the present work.

Our decay scheme of ^{101}Tc is in excellent agreement with results recently published by Siwamogsatham and Easterday[8] in all major respects. A level at 1001 keV (694 + 307) was proposed by Siwamogsatham and Easterday, in agreement with a level seen in nuclear reaction spectroscopy. We find no evidence for a 306.7-694.3 keV cascade in our gamma-gamma coincidence studies, although the low intensity of the 694.3-keV transition does not allow us to rule out the excitation of a level at 1001.1 keV in the decay of ^{101}Tc. Siwamogsatham and Easterday also propose a level at 674 keV, supported only by a single gamma-ray transition. As noted above, we recognize this possibility but choose not to include this transition in Fig. 1.2 because of the lack of supporting evidence.

1. Summary of a paper accepted for publication in *Nuclear Physics*.
2. Middle East Technical University, Ankara, Turkey.
3. Centre d'Etude de l'Energie Nucléaire, Mol, Belgium.
4. Istituto di Fisica Superiore, Università di Napoli, Napoli, Italy.

5. N. K. Aras, G. D. O'Kelley, and G. Chilosi, *Phys. Rev.* **146**, 869 (1966).
6. N. K. Aras, G. D. O'Kelley, and G. Chilosi, *Chem. Div. Annu. Prog. Rep. May 20, 1965*, ORNL-3832, p. 13.
7. O. C. Kistner and A. Z. Schwarzschild, *Phys. Rev.* **154**, 1182 (1967).
8. B. Siwamogsatham and H. T. Easterday, *Nucl. Phys. A* **162**, 42 (1971).

ENERGY LEVELS OF ^{104}Pd POPULATED BY THE BETA DECAY OF 43-sec ^{104g}Rh AND 4.41-min ^{104m}Rh

N. C. Singhal[1] E. Eichler
N. R. Johnson J. H. Hamilton[2]

In a continuation of our study of properties of the two-phonon quadrupole state in spherical nuclei, we have utilized the beta decay of the 43-sec 1^+ ^{104g}Rh and the 4.41-min 5^+ ^{104m}Rh. We have studied the decay of these isomers with high-resolution Ge(Li) detectors in the singles and coincidence mode and also have performed NaI-Ge(Li) directional correlation measurements on the four different cascades.

The ^{104}Rh sources were produced by irradiating Rh metal foil in the Oak Ridge Research Reactor. In order to study the two activities independently, we utilized the principle of differential activation. When the 43-sec ^{104g}Rh was to be emphasized, the irradiation time was about 1 to 2 sec, whereas for the 4.41-min ^{104m}Rh decay study it varied from 20 to 50 sec. For the 4.41-min ^{104m}Rh decay study the counting was started 7 to 10 min after the end of irradiation in order to allow the independently produced 43-sec ^{104g}Rh activity to decay.

The gamma-ray singles spectrum for the equilibrium source of 43-sec ^{104g}Rh and 4.41-min ^{104m}Rh measured with a 6.5% Ge(Li) detector is shown in Fig. 1.3. This spectrum is the result of summing the individual spectra obtained from a succession of 14 sources counted over a period of 4 hr; each source was counted for ≈15 min. During each counting period the source-to-detector distance was decreased every 15 sec (from 30 cm to 10 cm) to maintain a constant count rate of $\approx 1.5 \times 10^4$ per second. By moving the sources we increased their effective half-life and also avoided any shift in the peak position which might arise from the varying count rate. The low-energy (≤300 keV) singles spectrum for 4.41-min ^{104m}Rh decay was measured with a Ge(Li) x-ray detector having a surface area of 75 mm^2.

Energies and intensities of the gamma rays assigned to the decay of ^{104m}Rh and ^{104g}Rh are summarized in Table 1.2. Energies of the prominent transitions were obtained by counting the ^{104m}Rh sources simultaneously with IAEA calibration sources (^{22}Na, ^{137}Cs, ^{60}Co, ^{88}Y), and in turn these strong lines were later used as calibration lines for other relatively weaker gamma rays.

Our results agree quite well with those of Ionescu and Kern,[4] except that they failed to observe the 629.6-, 839.9-, 1264.8-, and 1689.1-keV gamma rays.

Coincidence measurements were performed with two Ge(Li) detectors with active volumes of 35 and 40 cm^3. The coincidence events were analyzed in a two-parameter mode with two 4096-channel analog-to-digital converters and then recorded as elements of the type X_iY_i on a magnetic tape. In order to achieve maximum coincidence efficiency, the two detectors were arranged in 180° geometry. A lead absorber (0.6 mm thick) was placed in front of each detector face to stop 2.44-MeV beta rays and the low-energy gamma

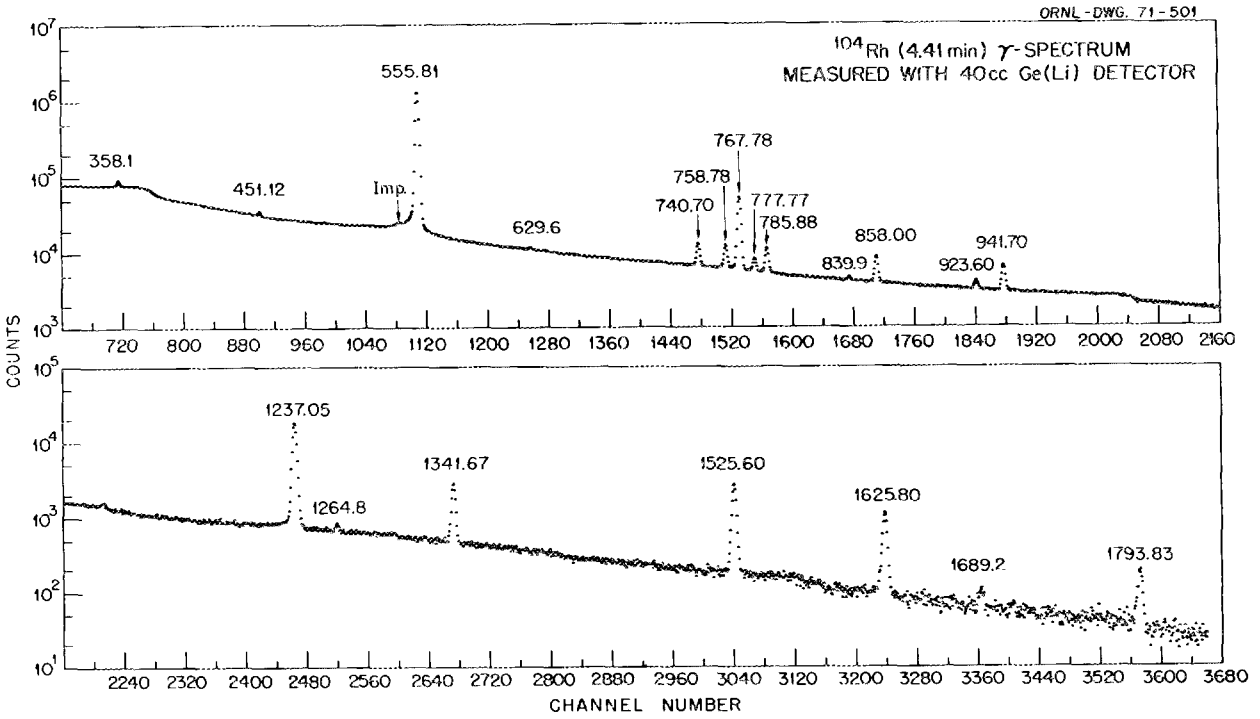

Fig. 1.3. Singles gamma-ray spectrum from the decay of 43-sec and 4.41-min ^{104}Rh (equilibrium source). This spectrum was obtained by allowing ^{104}Rh sources to decay for 8 to 10 min before the counting was started.

Table 1.2a. Energies and intensities of gamma rays from the beta decay of the 43-sec and 4.41-min isomers of ^{104}Rh

Transition energy (keV)	Relative intensity
358.12 ± 0.15	0.81 ± 0.06
451.18 ± 0.12	0.29 ± 0.03
555.81 ± 0.04	100
629.6 ± 0.4	0.05 ± 0.02
740.69 ± 0.05[a]	0.66 ± 0.04
758.78 ± 0.06[a]	0.72 ± 0.04
767.78 ± 0.05[a]	5.02 ± 0.26
777.77 ± 0.07	0.29 ± 0.03
785.88 ± 0.05	0.66 ± 0.04
839.90 ± 0.10[a]	0.05 ± 0.015
858.00 ± 0.06[a]	0.55 ± 0.04
923.62 ± 0.10[a]	0.14 ± 0.02
941.72 ± 0.06[a]	0.52 ± 0.03
1237.05 ± 0.05	3.61 ± 0.19
1264.84 ± 0.15	0.03 ± 0.01
1341.67 ± 0.07	0.50 ± 0.03
1526.60 ± 0.06[a]	0.61 ± 0.04
1625.76 ± 0.07[a]	0.30 ± 0.02
1689.1 ± 0.3	0.021 ± 0.006
1793.83 ± 0.09	0.05 ± 0.006

[a]These transitions are from states populated directly from the beta decay of ^{104m}Rh.

Table 1.2b. Energies and intensities of the gamma rays following the decay of 4.41-min ^{104m}Rh to 43-sec ^{104g}Rh

Energy[a] (keV)	Intensity
51.43	100
77.55	5.1 ± 0.3
97.11	6.2 ± 0.3

[a]These energies are taken from ref. 5.

rays. The coincidence data were integrated for a total of 28 irradiations over a period of 7 hr, each source being counted for about 15 min.

These coincidence data (total of 3 million events) were sorted on the ORNL IBM 360/90 computer by using the program MPASORT.[3] We extracted the spectrum in coincidence with each of the 18 gamma rays assigned to the decay of ^{104m}Rh. Three of these coincidence spectra, which illustrate some of the important features of the level scheme, are shown in Fig. 1.4. We were able to establish a definite coincidence relationship between 16 of the 18 gamma rays observed in the ^{104}Rh singles spectrum. The coinci-

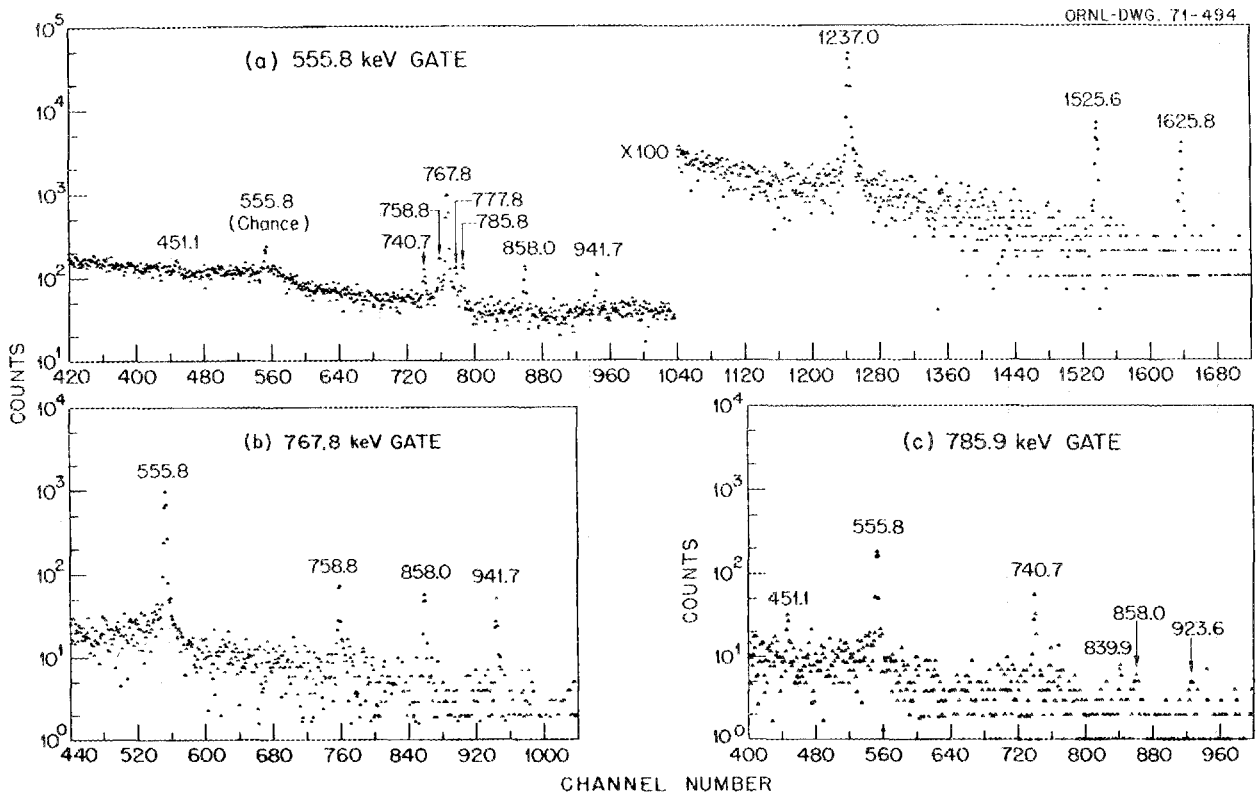

Fig. 1.4. Selected gamma-gamma coincidence spectra obtained with a two-parameter Ge(Li)-Ge(Li) coincidence system.

dence relationship between the 555.8-keV gamma ray and two weak gamma rays at 1264.8 and 1689.1 keV was established from the data obtained with an NaI-Ge(Li) coincidence arrangement.

Directional correlation measurements were made on four cascades involving the 555.8-keV ground-state transition and the four gamma rays that feed it by using a 3- by 3-in. NaI scintillator and a 40-cm^3 Ge(Li) detector combination. The correlation coefficients A_2 and A_4 were corrected for the finite solid angle effects of the detectors. The perturbation factors G_2 and G_4 were assumed to be unity since the lifetime of the intermediate 555.8-keV state is very short. In Fig. 1.5 we show a comparison between the experimental and theoretical values of A_2 and A_4 for the four cascades (555.8-767.8, 555.8-777.8, 555.8-785.9, and 555.8-1237.0 keV).

We have constructed a decay scheme of the ^{104}Rh isomers, as shown in Fig. 1.6, from our data and have made spin assignments based on the directional correlations, log *ft* values, and gamma-ray branching ratios.

Qualitatively, ^{104}Pd, like other Pd isotopes, appears to be a good vibrational nucleus. In the vibrational picture we can associate the 555.81-keV level with the one-phonon vibration and the 1323.59-keV (4^+), 1333.58-keV (0^+), and 1341.68-keV (2^+) levels with the two-phonon triplet. This is one of the closest lying triplets reported so far. From our directional correlation measurements we obtain an $M1$ admixture of $\leqslant 3\%$ for the $2^{+\prime} \rightarrow 2^+$ cascade transition. The ratio of the reduced transition probabilities of cascade to crossover from the $2^{+\prime}$ state is found as

$$B(E2, 2^{+\prime} \rightarrow 2^+)/B(E2, 2^{+\prime} \rightarrow 0^+) = 19.2 \pm 1.6.$$

These values are similar to the values reported for other Pd isotopes and are in good agreement with the predictions of the vibrational model.

The higher-lying states at 1792.83 keV (0^+), 1820.4 keV (2^+), and 2082.38 keV (4^+) could be three of the expected five members (0^+, 2^+, 3^+, 4^+, 6^+) of the three-phonon quintet. If the 1820.4-keV (2^+) level should be a three-phonon state, one would expect an enhanced $E2$ transition to the 1341.68-keV 4^+ level. This weak 478-keV transition (expected intensity ~0.1) is probably masked by high Compton background. The 2082.38-keV (4^+) and 1792.83-keV (0^+) levels do have

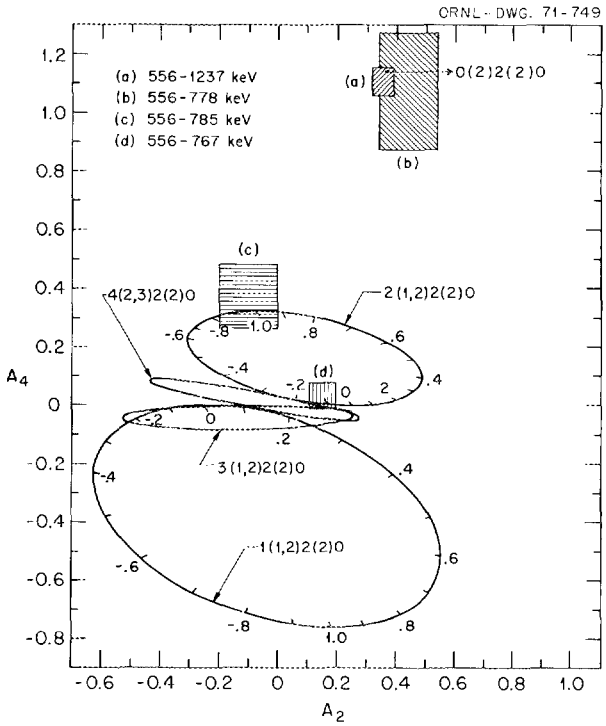

Fig. 1.5. Comparison of measured A_2 and A_4 (shaded rectangles) with theoretical values for $J(1,2)2(2)0$, $J = 1-4$, cascades. The numbers on the curves are $\delta = 1/(1 + |\delta|)$, where δ is the mixing ratio parameter.

large relative reduced transition probabilities to the 1341.68-keV ($2^{+\prime}$) and 1323.59-keV (4^+) levels as compared with the $B(E2)$ to the 555.81-keV (2^+) level. These characteristics support the three-phonon character for the 2082.38- and 1792.83-keV levels. However, the log *ft* value of 5.4 for the 1792.83-keV (0^+) level may suggest that this level is a two-quasi-particle excitation.

---

1. Graduate research assistant from Vanderbilt University, Nashville, Tenn.
2. Physics Department, Vanderbilt University, Nashville, Tenn.
3. A. F. Kluk, private communication.
4. V. A. Ionescu and J. Kern, *Helv. Phys. Acta* **42**, 575 (1969).
5. C. M. Lederer, J. M. Hollander, and I. Perlman, *Table of Isotopes*, 6th ed., Wiley, New York, 1967.

ORNL-DWG. 70-138658

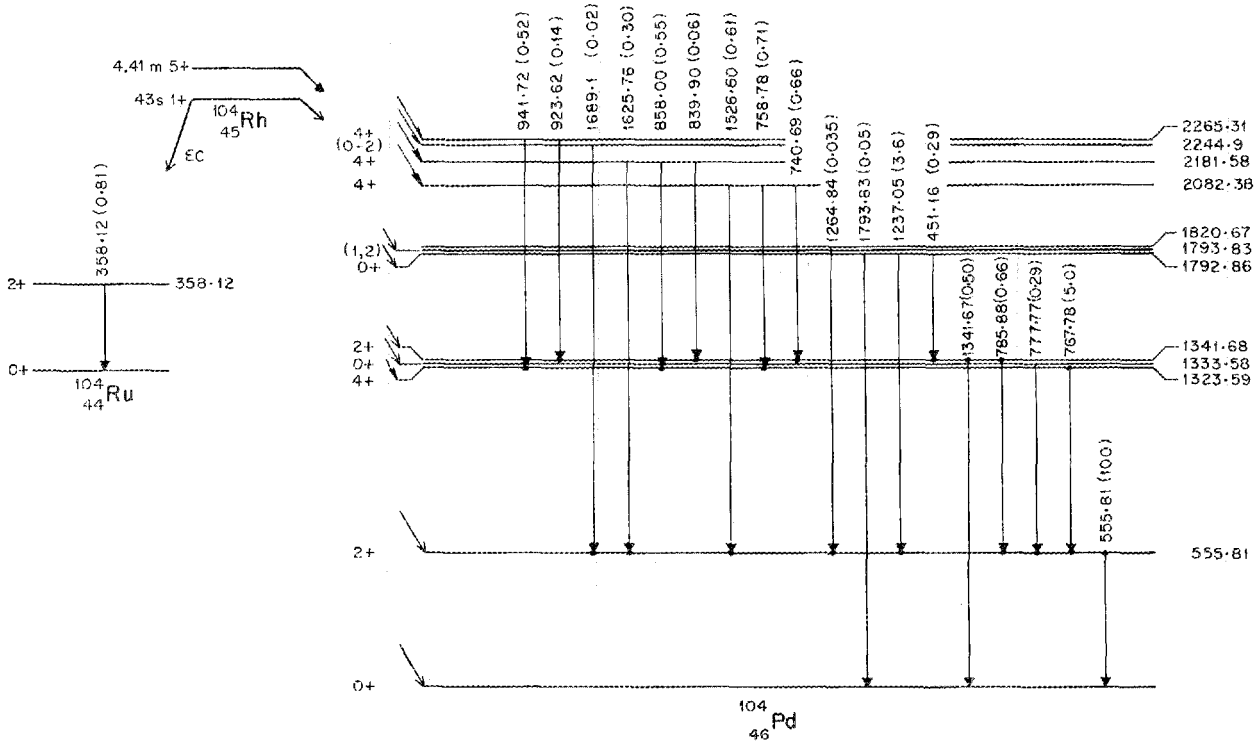

Fig. 1.6. Proposed decay scheme of ^{104}Rh. The closed circle at the head of an arrow indicates that a definite coincidence relationship was observed between that transition and the one or more gamma rays cascading into the level.

DECAY OF ^{72}As TO THE LEVELS OF ^{72}Ge

A. C. Rester[1] A. V. Ramayya[1]
J. H. Hamilton[1] N. R. Johnson

The nucleus ^{72}Ge is most interesting in that some of its low-lying excited states appear to be reasonably well interpreted in terms of a vibrational model, while others are not described at all by this interpretation. In an effort to understand the behavior in this nucleus more clearly, we have made a detailed investigation of its level properties up to 4 MeV as populated by the decay of 26-hr ^{72}As. These measurements have involved a variety of techniques including: (1) gamma-ray singles measurements with a large-volume, high-resolution Ge(Li) detector; (2) two-parameter gamma-gamma coincidence studies with Ge(Li) detectors; and (3) internal conversion spectrum measurements with an Si(Li) detector.

Since there is only a single gamma ray at 46 keV in the 8.4-day decay of ^{72}Se to ^{72}As, a source of ^{72}Se was made in order to take advantage of its much longer half-life compared with ^{72}As. The ^{72}Se source, produced on the Oak Ridge Isochronous Cyclotron via the reaction ^{70}Ge(α,2n)^{72}Se, was purified by standard chemical techniques.

In this work, 60 gamma-ray transitions were observed, and the energies and intensities of these are listed in Table 1.3. During the course of these experiments, Camp[2] also reported on the decay of ^{72}As. For the most part the data in the table are in agreement with Camp,[2] the primary difference being that the error limits on our energy values are considerably less than those assigned by him. The data in this table and from our gamma-gamma coincidence and electron measurements are best summarized by the ^{72}Ge level scheme proposed in Fig. 1.7.

From Coulomb excitation measurements[3,4] as well as from inelastic proton and deuteron scattering,[5,6] both the 834- and 1464-keV levels appear to have a rather strong collective character. This is consistent with the identification of these levels as one- and two-quadrupole phonon states respectively. The decay character-

Table 1.3. Energies and relative intensities of gamma rays in ^{72}Ge from the decay of ^{72}As

Energy (keV)	Relative intensity	Energy (keV)	Relative intensity
113.1 ± 0.2	0.036 ± 0.004	2105.9 ± 0.3	0.93 ± 0.09
142.5 ± 0.2	0.010 ± 0.004	2109.8 ± 0.3	0.28 ± 0.03
428.5 ± 0.2	0.083 ± 0.008	2116.7 ± 0.4	0.041 ± 0.006
600.93 ± 0.05	0.40 ± 0.02	2201.74 ± 0.09	0.65 ± 0.02
629.93 ± 0.05	10.2 ± 0.3	2214.1 ± 0.02	0.043 ± 0.006
786.43 ± 0.05	0.54 ± 0.02	2248.5 ± 0.1	0.42 ± 0.02
834.00 ± 0.03	100	2339.8 ± 0.2	0.043 ± 0.005
879.2 ± 0.2	0.032 ± 0.005	2402.9 ± 0.1	0.14 ± 0.01
894.27 ± 0.05	0.99 ± 0.03	2491.0 ± 0.2	0.041 ± 0.006
905.3 ± 0.2	0.049 ± 0.005	2507.9 ± 0.1	0.42 ± 0.02
911.8 ± 0.2	0.070 ± 0.009	2515.4 ± 0.2	0.029 ± 0.005
938.8 ± 0.2	0.10 ± 0.01	2521.8 ± 0.2	0.059 ± 0.005
942 ± 1	0.020 ± 0.004	2585.0 ± 0.3	0.12 ± 0.01
999.84 ± 0.08	0.037 ± 0.005	2621.5 ± 0.1	0.49 ± 0.02
1031 ± 1	0.035 ± 0.007	2844.2 ± 0.4	0.087 ± 0.006
1050.76 ± 0.05	1.23 ± 0.04	2860 ± 1	0.04 ± 0.01
1193.9 ± 0.1	0.12 ± 0.01	2864 ± 1	0.02 ± 0.01
1215.14 ± 0.05	0.29 ± 0.02	2898.6 ± 0.4	0.035 ± 0.005
1230.8 ± 0.1	0.099 ± 0.007	2940.1 ± 0.1	0.42 ± 0.02
1276.8 ± 0.2	0.046 ± 0.005	2982.1 ± 0.2	0.24 ± 0.03
1390.44 ± 0.05	0.30 ± 0.01	3094.3 ± 0.2	0.18 ± 0.01
1464.0 ± 0.07	1.43 ± 0.05	3112.4 ± 0.3	0.10 ± 0.01
1475.91 ± 0.07	0.63 ± 0.02	3150.0 ± 0.3	0.10 ± 0.01
1523 ± 1	0.014 ± 0.003	3161 ± 1	0.010 ± 0.003
1568.2 ± 0.1	0.18 ± 0.01	3337.7 ± 0.4	0.028 ± 0.004
1581.3 ± 0.3	0.051 ± 0.006	3398 ± 1	0.008 ± 0.004
1680.7 ± 0.1	0.15 ± 0.01	3550.4 ± 0.8	0.031 ± 0.005
1710.90 ± 0.07	0.34 ± 0.02	3803.6 ± 0.3	0.11 ± 0.02
1921 ± 1	0.06 ± 0.02	3872.0 ± 0.5	0.006 ± 0.002
1991.14 ± 0.08	0.48 ± 0.02	3995.0 ± 0.3	0.08 ± 0.02

istics of the 1728-keV level suggest that it may be another member (4^+) of the two-phonon triplet, while the properties of the 2064-keV (3^+) and 2464-keV (3^+, 4^+) levels are suggestive of three-phonon states.

The one feature of the ^{72}Ge low-lying states that is in complete conflict with the vibrational picture is the appearance of a $0^{+\prime}$ level as the first excited state. It is very likely that this $0^{+\prime}$ state can be explained within the shell-model framework as has[7] a similar $0^{+\prime}$ state in ^{90}Zr. The latter nucleus has $N = 50$ (closed neutron shell) and $Z = 40$ (closed proton subshell). Ford[7] has described the $0^{+\prime}$ state in ^{90}Zr in terms of the excitation from the ground-state configuration of a pair of protons to $g_{9/2}$ orbits. The large pairing energy associated with the excitation of a $g_{9/2}$ proton pair is sufficient to drop the $0^{+\prime}$ level below the 5^- level of the $(p_{1/2}g_{9/2})$ configuration. Since ^{90}Zr has a closed neutron shell, neutron-pair excitation was ignored. In ^{72}Ge, $N = 40$ (closed neutron subshell) and $Z = 32$, so that the $0^{+\prime}$ state in this nucleus may be described in terms of the excitation of a pair of neutrons to $g_{9/2}$ orbits or a pair of protons to $f_{5/2}$ orbits. However, such a simple explanation seems unlikely since $N = 40$ is not a major closed shell and $Z = 32$ is four protons above a closed shell. If excitation of pairs of particles is the origin of this $0^{+\prime}$ state, it would seem more probable that in the case of neutron excitations in ^{72}Ge, proton excitations are not ignorable and vice versa. This point was made by Hübenthal, Monnand, and Moussa[8] with regard to the recently discovered first excited $0^{+\prime}$ state in ^{98}Mo.

Although the appearance of this low-lying excited 0^+ state in ^{72}Ge can be reasonably well accounted for in terms of the promotion of a pair of particles, this simple picture does not explain the presence of a sizable monopole matrix element for the $0^{+\prime} \rightarrow 0^+$ transition. Eichler, Stelson, and Dickens[9] recently made an accurate determination of $\rho = 0.10$, where ρ is the reduced nuclear monopole matrix element. As has been pointed out by Church and Weneser,[10] monopole transitions

ORNL-DWG. 69-14189B

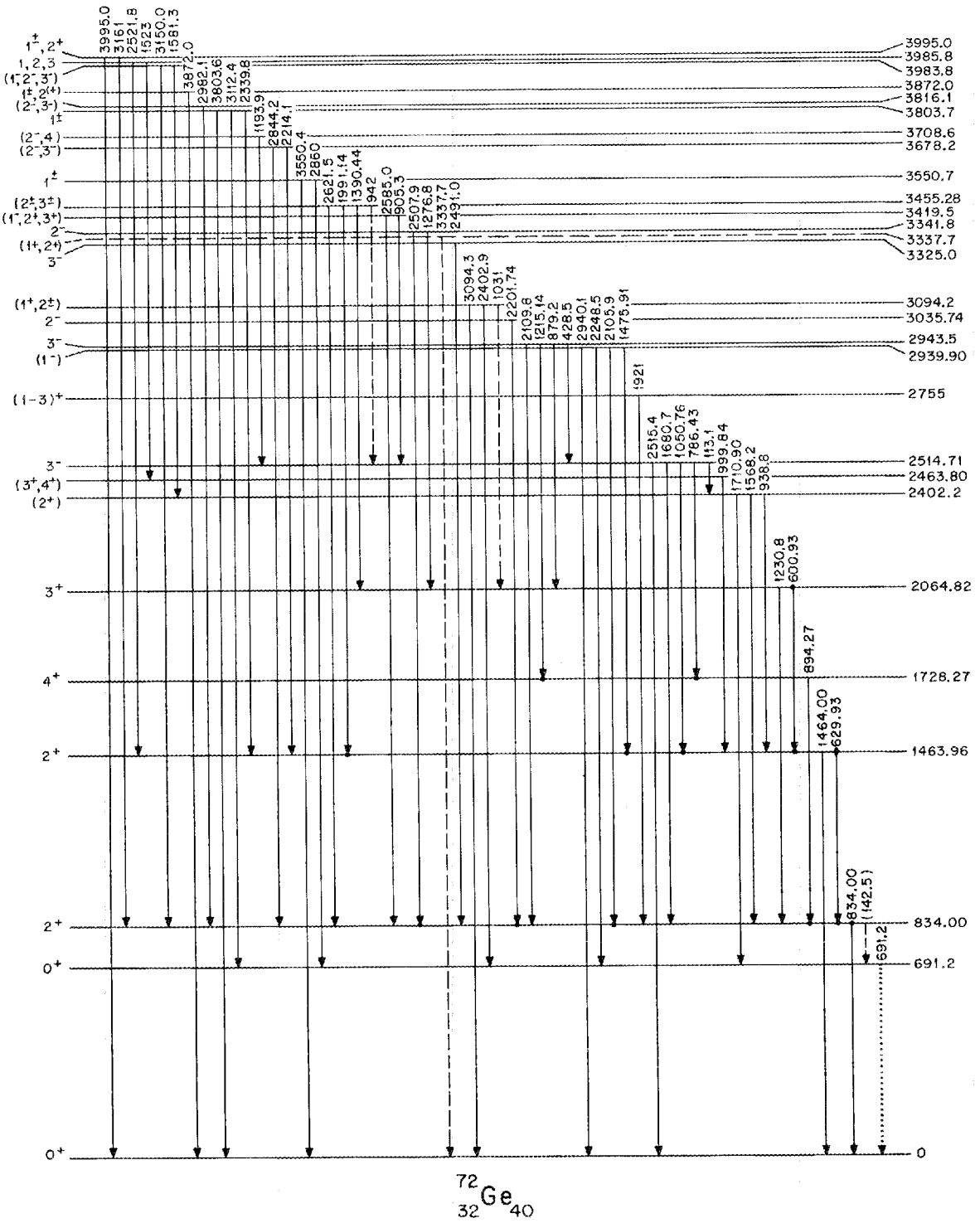

Fig. 1.7. Levels in ^{72}Ge populated by the decay of ^{72}As. The dashed levels are tentative assignments. The 691.2-keV transition, which proceeds totally by internal conversion, is dashed.

between pure states of this type are forbidden because the monopole operator is diagonal in the angular variables. However, $E0$ emission can be accounted for on the basis of configuration mixing if the mixing involves different radial dependences. Calculations by Schiff[11] for ^{12}C have shown that values of ρ up to about 0.1 can be explained in terms of a configuration mixing picture, which fact lends some support for this interpretation in the ^{72}Ge case.

1. Vanderbilt University, Nashville, Tenn.
2. D. C. Camp, *Nucl. Phys. A* **121**, 561 (1968).
3. A. H. Wapstra, G. J. Nijgh, and R. van Lieshout, *Nuclear Spectroscopy Tables*, p. 58, North-Holland, Amsterdam, 1959.
4. B. L. Robinson and R. W. Fink, *Rev. Mod. Phys.* **32**, 117 (1960).
5. P. H. Stelson and L. Grodzins, *Nucl. Data, Sect. A* **1**, 21 (1965).
6. Yu. P. Gangrskii and I. Kh. Lemberg, *Sov. Phys. JETP* **15**, 711 (1962).
7. K. W. Ford, *Phys. Rev.* **98**, 1516 (1955).
8. K. Hübenthal, E. Monnand, and A. Moussa, *Nucl. Phys. A* **128**, 577 (1969).
9. E. Eichler, P. H. Stelson, and J. K. Dickens, *Nucl. Phys. A* **120**, 622 (1968).
10. E. L. Church and J. Weneser, *Phys. Rev.* **103**, 1035 (1956).
11. L. I. Schiff, *Phys. Rev.* **98**, 1281 (1955).

LEVEL STRUCTURE OF ^{108}Pd POPULATED IN THE DECAY OF 2.42-min ^{108}Ag

N. C. Singhal[1] E. Eichler
N. R. Johnson J. H. Hamilton[2]

We are presently investigating the properties of the low-lying excited states of ^{108}Pd as populated in the ^{108}Ag decay by use of a high-resolution, large-volume Ge(Li) detector. A total of 11 gamma rays have been assigned to the ^{108}Ag decay. The energies and intensities of these gamma rays as obtained from a preliminary analysis of the data are listed in Table 1.4. These values are in excellent agreement with those of Okano et al.;[3] however, our values are determined to much better accuracy. From the results of the NaI-Ge(Li) coincidence measurements, we are able to establish energy levels in ^{108}Pd at 930.9, 1052.8, 1314.2, 1441.1, and 1539.9 keV, again in agreement with ref. 3.

Gamma-gamma directional correlation measurements have been performed on three different cascades (618.9-433.9 keV, 880.3-433.9 keV, and 1007.2-433.9 keV) with an NaI-Ge(Li) detector combination. The results of the directional correlation measurements are listed in Table 1.5. The spins of the levels at 1052.8, 1314.2, and 1441.1 keV can be uniquely determined as J = 0, 0, and 2, respectively, from the directional correlation coefficients. Contrary to the measurements of Okano et al.,[3] we find that the 1007.2-keV transition is predominantly $E2$ ($\geqslant$98%), which is consistent with the interpretation of this level as a three-phonon vibrational state.

Table 1.4. Energies and relative intensities of gamma rays emitted in the decay of 2.42-min ^{108}Ag

Gamma-ray energy (keV)	Relative intensity
433.95 ± 0.04	100
497.6 ± 0.2	0.33 ± 0.11
(509.7 ± 0.5)[a]	
511.01	Annihilation
618.85 ± 0.05	56.2 ± 2.6
632.98 ± 0.05	355 ± 18
880.26 ± 0.10	0.62 ± 0.10
931.2 ± 0.3	0.13 ± 0.02
1007.22 ± 0.06	2.83 ± 0.15
1106.00 ± 0.07	0.31 ± 0.06
1441.14 ± 0.09	0.62 ± 0.05
1539.9 ± 0.2	0.22 ± 0.02

[a]There is some evidence for a gamma ray of this energy.

Table 1.5. Directional correlation coefficients and assigned spin sequences

Cascade (keV)	Directional correlation coefficients		Spin sequence and mixing ratio
	A_2	A_4	
618.9-433.9	0.34 ± 0.02	1.28 ± 0.04	0-2-0
880.3-433.9	0.19 ± 0.19	1.00 ± 0.35	0-2-0
1007.2-433.9	−0.04 ± 0.07	0.32 ± 0.14	2-2-0, $\delta \geqslant (\lvert 7.0 \rvert)$

1. Graduate research assistant from Vanderbilt University, Nashville, Tenn.
2. Physics Department, Vanderbilt University, Nashville, Tenn.
3. K. Okano et al., *Nucl. Phys. A* **164**, 545 (1971).

COULOMB EXCITATION AND IN-BEAM REACTION GAMMA SPECTROSCOPY

E. Eichler R. L. Hahn
N. R. Johnson C. E. Bemis, Jr.

The heavy-ion in-beam spectroscopy program at ORIC has gained in both momentum and breadth. Out

of the Coulomb excitation studies have come extremely interesting results bearing on the validity of nuclear collective motion. A more detailed account of this work is given elsewhere.[1] In collaboration with the Physics and Electronuclear Divisions we have also begun a program of nuclear reaction gamma-ray spectroscopy.[2] These two kinds of research exploit the enormous potential of heavy-ion beams in diverse but mutually complementary ways. The prospect of even heavier projectiles at ORIC heralds exciting new avenues of research.

1. E Eichler, N. R. Johnson, C. E. Bemis, Jr., R. O. Sayer, D. C. Hensley, and M. R. Schmorak, "Multiple Coulomb Excitation of Heavy Elements with ORIC Heavy-Ion Beams," chap. 2, this report.

2. J. B. Ball, E. Eichler, J. L. C. Ford, Jr., R. L. Hahn, N. R. Johnson, R. L. Robinson, P. H. Stelson, and K. S. Toth, "In-Beam Gamma-Ray Spectroscopy of the Tin Isotopes," the following contribution, this report.

IN-BEAM GAMMA-RAY SPECTROSCOPY OF THE TIN ISOTOPES[1]

J. B. Ball[2] N. R. Johnson
E. Eichler R. L. Robinson[3]
J. L. C. Ford, Jr.[3] P. H. Stelson[3]
R. L. Hahn K. S. Toth[2]

The observation of gamma rays following (H.I.,xn) reactions has proved to be a powerful tool for investigating nuclei off the stability line.[4,5] The high-energy heavy-ion beams now available from ORIC allow this technique to be applied to nuclei and mass regions which were formerly inaccessible. As an initial project we have used the (^{16}O,xn) reactions on all the stable molybdenum isotopes to excite levels in tin nuclei. Oxygen beams of energies 71.5, 80, and 90 MeV were used. Figure 1.8 depicts a 200-keV portion of the entire series of spectra, indicating the great complexity of gamma radiation observed.

In general, as we progress to isotopes with smaller neutron excess, the cross sections for the (H.I.,xn) reactions decrease, probably due to increased competition with charged-particle emission. This factor may make it impossible to study nuclei at the limit of particle stability (i.e., at the "proton drip line") as has been stressed by Diamond.[5] We plan to investigate charged-particle emission in future experiments. It may be possible to obtain readily identifiable and less complex spectra by observing gamma rays in coincidence with alpha particles emitted in such a reaction as ^{92}Mo(^{20}Ne,$\alpha 2n$)^{106}Sn.

1. See also, *Phys. Div. Annu. Progr. Rep. Dec. 31, 1970*, ORNL-4659, p. 37, and *Electronucl. Div. Annu. Progr. Rep. Dec. 31, 1970*, ORNL-4649, p. 63.

2. Electronuclear Division.

3. Physics Division.

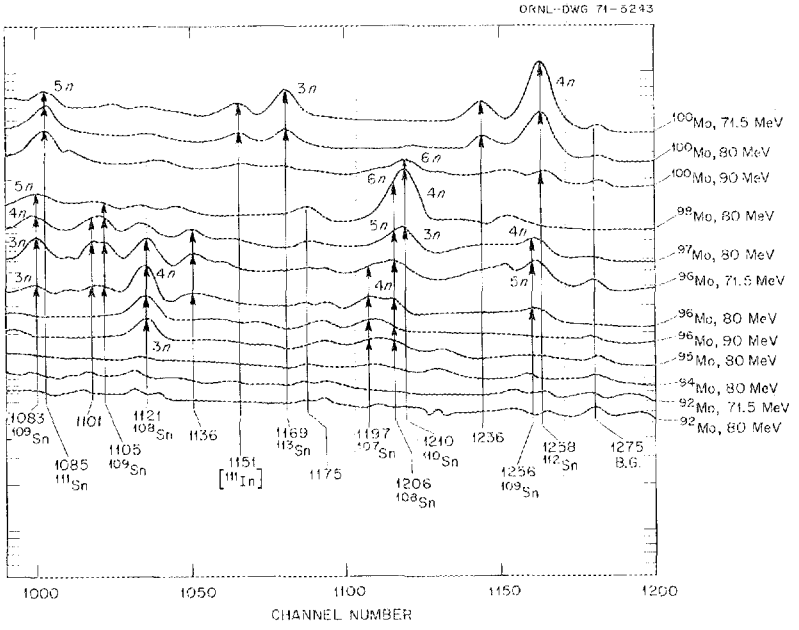

Fig. 1.8. Gamma spectra from 1100 to 1300 keV resulting from 71.5-, 80-, and 90-MeV ^{16}O ion bombardment of all the stable isotopes of molybdenum. On the right are given the targets and oxygen energies. Below the spectra the peaks marked by arrows are identified with energies (in keV) and nuclei in which they occur.

4. F. S. Stephens, *Proceedings of the International Conference on Properties of Nuclear States*, Montreal, Canada, p. 127, Les Presses de L'Université de Montreal, 1969.

5. R. M. Diamond, *Conference on the Properties of Nuclei Far from the Region of Beta Stability*, Leysin, Switzerland, 1970; UCRL-19961 (1970); and to be published.

THE DECAY OF ^{136}Pr AND THE LEVEL STRUCTURE OF ^{136}Ce[1]

B. H. Ketelle A. R. Brosi J. R. Van Hise[2]

The instrumentation for rapid accumulation of gamma-gamma coincidence data described last year[3] has been used to study the decay schemes of several of the new rare-earth isotopes discovered in earlier work on this program. On the basis of observed coincidences, detailed energy level structures populated in the decay of ^{136}Nd, ^{137}Nd, ^{135}Pr, and ^{136}Pr have been elucidated. Only in the case of the decay of ^{136}Pr do we have sufficient information from other kinds of experiments to make reasonably firm spin and parity assignments to the energy levels populated. The energy level diagram deduced for ^{136}Ce is shown in Fig. 1.9.

The low-lying levels of ^{136}Ce populated by ^{136}Pr decay can be separated into two different sequences on the basis of beta decay transition probabilities to the various levels and gamma transition probabilities between them. A 0^+, 2^+, 4^+ sequence suggests the

ORNL-DWG. 71-2586

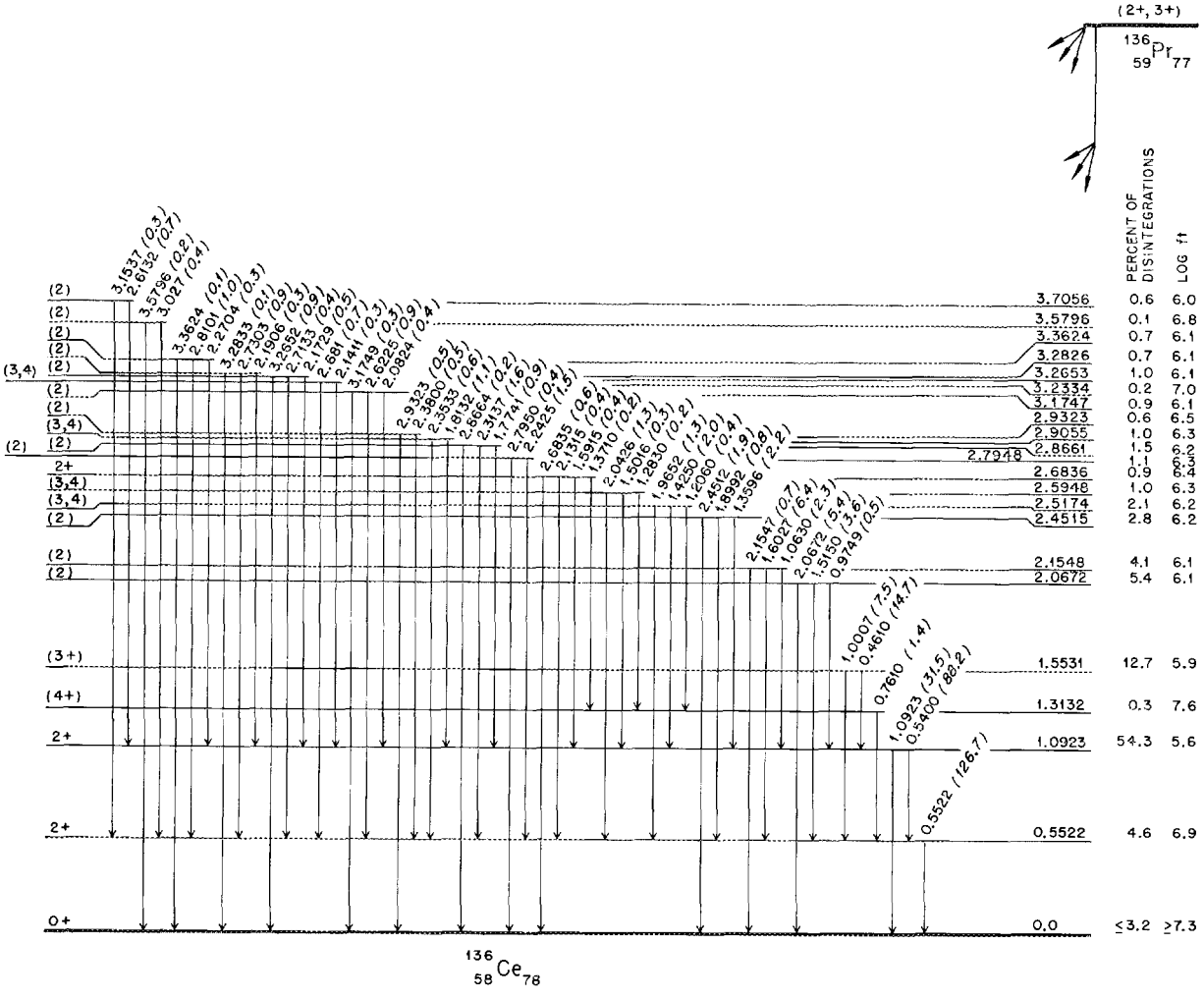

Fig. 1.9. ^{136}Pr decay scheme.

ORNL-DWG. 71-2573

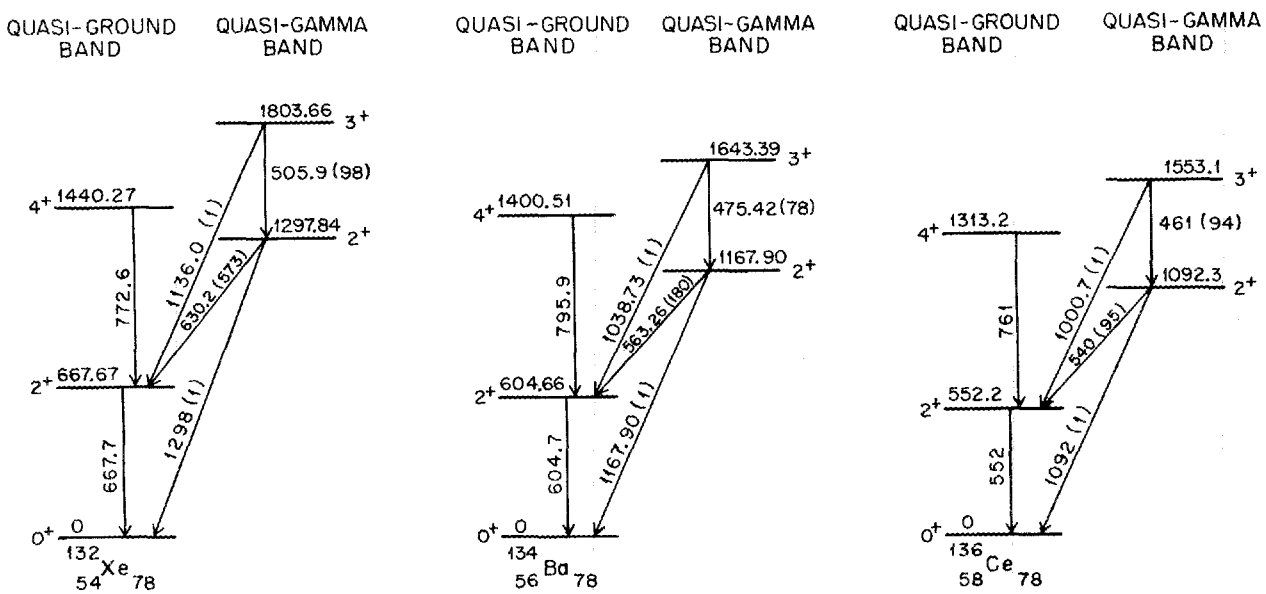

Fig. 1.10. Energy-level structures of nuclei with 78 neutrons. Reduced transition probabilities are given in parentheses for transitions from the 2^+ and 3^+ levels of the quasi-gamma band.

ground-state rotational band in deformed nuclei, while a 2^+, 3^+ sequence appears similar to what is called the gamma band in deformed nuclei.

The "in-beam" work of Ward[4] et al. showed that the low-mass-number cerium nuclei have quasi-rotational levels with energies which increase with increasing neutron number. Even though ^{136}Ce and ^{138}Ce are close to the 82-neutron shell closure, the energies of their 2^+ and 4^+ levels fall on smooth energy vs neutron number curves with the lower-neutron-number cerium isotopes.

The other 78-neutron even-even isotopes which have been studied, ^{132}Xe and ^{134}Ba, also have levels[5-7] which can be separated into sequences analogous to those observed in ^{136}Ce. A comparison of the quasi-ground and quasi-gamma bands of ^{132}Xe, ^{134}Ba, and ^{136}Ce is shown in Fig. 1.10. The energies of the corresponding levels in these three nuclides decrease with increasing proton number. This suggests increasing nuclear deformation as the number of protons beyond the 50-proton shell increases. This change in nuclear deformation is also suggested by the changes with atomic number of the reduced transition probabilities. The suggestion of nuclear deformation at a neutron number of 78 is consistent with the prediction of nuclear deformation near this region by Marshalek, Person, and Sheline.[8]

1. Substantially the same work was reported in *Electronucl. Div. Annu. Progr. Rep. Dec. 31, 1970,* ORNL-4649, p. 28.
2. Present address: Tri-State College, Angola, Ind.
3. B. H. Ketelle and A. R. Brosi, *Chem. Div. Annu. Progr. Rep. May 20, 1970,* ORNL-4581, p. 6.
4. D. Ward, R. M. Diamond, and F. S. Stevens, *Nucl. Phys. A* **117**, 309 (1968).
5. Zh. Zhelev et al., *Bull. Acad. Sci. USSR, Phys. Ser.* 32(10), 1497 (1968).
6. Most recently studied by D. C. Camp, R. A. Meyer, and J. R. Van Hise, "Decay of ^{134}Ce to Levels of ^{134}Ba," to be submitted for publication.
7. J. H. Hamilton, H. K. Carter, and J. J. Pinajian, *Phys. Rev. C* **1**, 666 (1970).
8. E. Marshalek, L. W. Person, and R. K. Sheline, *Rev. Mod. Phys.* **35**, 108 (1963).

NEW ALPHA EMITTERS WITH $N = 86$ AND $N = 87$: ^{156}Tm AND ISOMERS OF ^{154}Ho AND ^{153}Ho[1]

K. S. Toth[2] R. L. Hahn M. A. Ijaz[3]

The work reported here is part of a program that deals with the production and characterization of new

rare-earth alpha emitters with neutron numbers equal to 86 and 87. Earlier reports[4,5] discussed the properties of ^{153,154}Ho, ^{155}Er, and ^{156,157}Yb nuclides produced by bombarding enriched targets of ^{156}Dy and ^{162}Er with protons, alpha particles, and ^{3}He ions. The present work is concerned with new radioactive species which were produced by bombarding various rare-earth targets with the 103-MeV quadruply charged ^{14}N ions available at the ORIC.

Two basic techniques were used in this work to determine mass assignments. The first involved the measurement of yield curves for the production of new activities, which were then compared with yield curves for the production of known isotopes and with yield curves calculated from the statistical model of nuclear reactions (as developed in a computer code by Sikkeland; e.g., see ref. 6). The second technique involved the establishment of a parent-daughter relationship between a known and a new alpha radioactivity.

The experiments were performed with a gas-jet system.[7] Targets consisted of thin layers of enriched rare-earth oxides, ~0.3 mg/cm^2, electrodeposited onto nickel supporting foils. During irradiation, targets were positioned so that the ^{14}N beam first passed through the backing foil and then the oxide deposit; the maximum available ^{14}N energy was 88.4 MeV. Radioactive recoil nuclei ejected from these thin targets were stopped in helium gas in a "high-pressure" chamber (~0.2 to 2 atm) and then carried by the gas through a very small orifice into a "low-pressure" chamber (~0.2 to 0.5 torr), where they were deposited on a catcher foil. A rapidly driven wheel conveyed the collected radioactivity to a position in front of an alpha-particle detector in ~0.2 sec.

Alpha-particle spectra were measured with an Si(Au) detector. A precision pulser, together with a ^{244}Cm source, was used to set the energy scale of these spectrometers, but internal calibration standards, with energy values taken from the measurements of Golovkov et al.,[8] were used to determine precisely the energies of the various alpha groups observed.

Isomers of ^{153}Ho and ^{154}Ho

Previously, we had discussed the properties of ^{153}Ho and ^{154}Ho which were produced by bombarding ^{156}Dy with protons.[9] Holmium-153 had an alpha-decay energy of 3.97 ± 0.02 MeV and a half-life of 9.3 ± 0.5 min, while ^{154}Ho decayed with a half-life of 11.8 ± 1.0 min and emitted alpha particles of 3.91 ± 0.02 MeV. Since then Golovkov et al.[8] measured the alpha-decay energies more accurately with the use of a magnetic spectrograph. Their energy values (and half-lives) are as follows: ^{153}Ho, 4.010 ± 0.005 MeV (7–9 min) and ^{154}Ho, 3.933 ± 0.005 MeV (10–12 min).

The neighboring nuclides, ^{151}Ho and ^{152}Ho, are each known[10] to have both high- and low-spin isomers that decay by alpha emission. Because we had produced the above-mentioned ^{153}Ho and ^{154}Ho alpha emitters in proton irradiations, we felt, by analogy with the known pairs of isomers in ^{151}Ho and ^{152}Ho, that these species represented decay from the low-spin isomers. We thus undertook a search for the postulated high-spin isomers by bombarding neodymium targets with ^{14}N ions.

First, a series of irradiations of ^{144}Nd with ^{14}N ions was made at different bombarding energies. With the available ^{14}N energy, the 9.3-min ^{153}Ho (4.010 MeV) and 11.8-min ^{154}Ho (3.933 MeV) radioactive species were produced, respectively, in (^{14}N,5n) and (^{14}N,4n) reactions on ^{144}Nd. In addition to other known alpha groups, two new alpha peaks were observed at 3.91 and 3.72 MeV, with half-lives of 2.0 ± 0.1 and 3.0 ± 0.3 min respectively.

To help interpret these data, a similar investigation was made with a ^{142}Nd target. Here the (^{14}N,5n) and (^{14}N,4n) reactions lead to the well-established nuclides ^{151}Ho and ^{152}Ho. Alpha groups corresponding to both isomers in the two nuclei together with the 3.91- and 4.010-MeV alpha peaks were observed. The 3.933-MeV (^{154}Ho) and 3.72-MeV alpha groups, however, were not observed. This result was not unexpected because statistical model calculations[6] indicated that the yield of the ^{142}Nd(^{14}N,2n)^{154}Ho reaction was severely reduced by the Coulomb barrier; that is, its maximum value at ~59 MeV was about 100 times less than that for the corresponding (^{14}N,3n) reaction.

Figure 1.11 shows yields as a function of incident energy observed in the ^{14}N bombardments of ^{142}Nd and ^{144}Nd. Consider first Fig. 1.11*a*, where the yield data, measured with ^{142}Nd as the target nucleus, are shown for the low- and high-spin isomers of ^{151}Ho and ^{152}Ho. Clearly, the yields for the low-spin isomers peak at lower bombarding energies than do those for the corresponding high-spin isomers. This point was noted by Macfarlane and Griffioen[10] in their investigations of rare-earth alpha emitters with heavy ions. They attributed the shift in the excitation function to the competition of gamma-ray emission with nucleon evaporation in the decay of high angular momentum states of the compound nucleus.

Figure 1.11*b* shows the yields obtained with the ^{144}Nd target for ^{153}Ho (4.010 MeV), ^{154}Ho (3.933 MeV), and the 3.72- and 3.91-MeV alpha groups. The

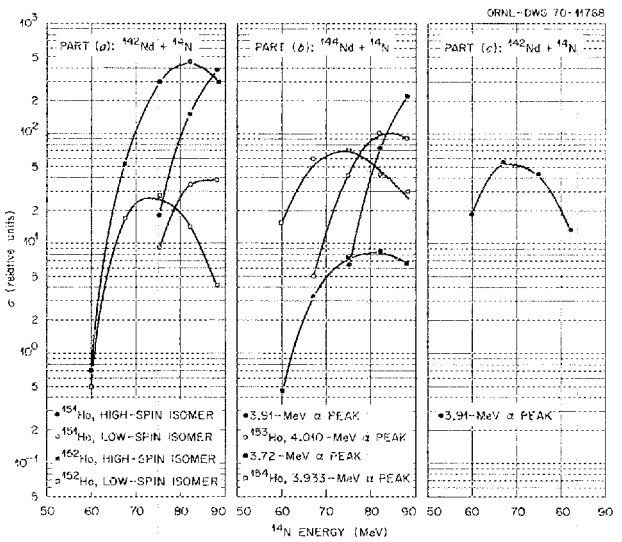

Fig. 1.11. Yields as a function of incident energy measured for various holmium alpha groups. (*a*) Yields for the production of the high- and low-spin isomers of ^{151}Ho and ^{152}Ho in ^{14}N bombardments of ^{142}Nd. (*b*) Yields for the 3.91-, 4.010-, 3.72-, and 3.933-MeV alpha groups observed in ^{14}N bombardments of ^{144}Nd. (*c*) Yield for the production of the 3.91-MeV alpha peak in ^{14}N bombardments of ^{142}Nd. Curves drawn only for ease of presentation.

similarity in behavior of the yield curves for ^{153}Ho and ^{154}Ho with those shown in *a* for the low-spin isomers of ^{151}Ho and ^{152}Ho is quite apparent. It is also seen that the yield data for the 3.72-MeV alpha group in *b* peak at essentially the same bombarding energy as the data points for the high-spin isomer of ^{152}Ho (Fig. 1.11*a*). This evidence, together with the fact that the 3.72-MeV group was not seen in the ^{142}Nd bombardments [as is expected for the product of a (^{14}N,2*n*) reaction], strongly suggests that it represents alpha decay from a high-spin state in ^{154}Ho. The yield curve for the 3.91-MeV alpha group in Fig. 1.11*b* has not reached a maximum in the bombarding energy range investigated, but its shape is consistent with that observed for the ^{151}Ho high-spin isomer in Fig. 1.11*a*.

Yield data for the 3.91-MeV alpha group obtained in the ^{142}Nd bombardments are shown in Fig. 1.11*c*. It is seen that the peak of the yield curve is at ~70 MeV. This observation is also consistent with the alpha group being due to the decay of the high-spin isomer of ^{153}Ho [the ^{142}Nd(^{14}N,3*n*) product] in view of the fact that the high-spin (^{14}N,4*n*) products reach their maximum yields at ~82 MeV.

In Fig. 1.12 the experimental yield data are compared with excitation functions calculated from the statistical model[6] for (^{14}N,4*n*) and (^{14}N,5*n*) reactions induced on targets of ^{142}Nd and ^{144}Nd. The calculations, indicated by dashed curves, are normalized to the data points, which now represent the sum of the yields for both isomers in each holmium isotope. (The 3.91- and 3.72-MeV alpha groups are assumed to be due to the decay of high-spin isomers in ^{153}Ho and ^{154}Ho respectively.) The calculated excitation functions reproduce the energy dependence of the experimental yield data reasonably well.

The yield data shown in Figs. 1.11 and 1.12 cannot by themselves rule out the possibility that the two new alpha emitters are either dysprosium or terbium isotopes produced in (^{14}N,*pxn*) and (^{14}N,*αxn*) reactions. These possibilities were eliminated in a series of cross bombardments, involving the bombardment of ^{140}Ce

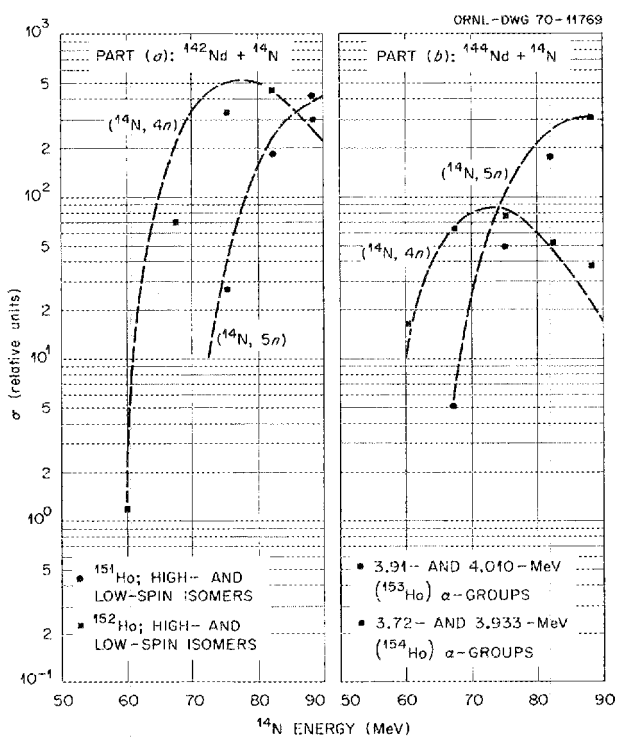

Fig. 1.12. Experimental yield data compared with excitation functions (dashed curves) calculated from the statistical model for (^{14}N,4*n*) and (^{14}N,5*n*) reactions induced on targets of ^{142}Nd (*a*) and ^{144}Nd (*b*). The calculated curves are normalized to the data points which represent the sum of the yields for both isomers in each holmium isotope.

and ^{141}Pr with ^{14}N ions and ^{144}Nd with ^{12}C ions. Holmium nuclei cannot be produced with these three target and projectile combinations, and indeed, the 3.72- and 3.91-MeV alpha groups were not observed.

From shell-model considerations, the $h_{11/2}$ and $d_{5/2}$ proton orbitals are likely to account for the isomers in ^{153}Ho ($Z = 67$, $N = 86$). One may therefore speculate that the new 3.91-MeV alpha group represents decay from the $h_{11/2}$ state of ^{153}Ho to the high-spin isomer in ^{149}Tb (see ref. 11) and that the 4.010-MeV alpha emitter decays from the ^{153}Ho $d_{5/2}$ state to a low-spin state in ^{149}Tb. It is, however, not possible to state which of the two isomers represents the ground state in ^{153}Ho.

Based on alpha-decay energy systematics and on the known level structure of ^{146}Eu, we previously proposed[5] that the spin of the ^{150}Tb ground state is low. Then, since the spin of 11.8-min ^{154}Ho has been measured[12] to be 1, its alpha decay very likely proceeds to the ground state of ^{150}Tb. The 3-min ^{154}Ho isomer presumably decays to a high-spin state in ^{150}Tb. As in the case of ^{153}Ho it is not possible to say which of the two alpha-emitting states in ^{154}Ho is the ground state.

Thulium-156

The 84- and 85-neutron thulium nuclides, ^{153}Tm and ^{154}Tm, were first found by Macfarlane,[13] who reported that these isotopes decayed essentially only by alpha emission. Because the 86- and 87-neutron nuclides, for a given element, characteristically have alpha/total branching ratios that are reduced by a factor of 100 to 1000 relative to 84- and 85-neutron nuclei, it is not surprising that ^{155}Tm and ^{156}Tm have as yet remained unreported. We undertook a search for these isotopes via the reactions ^{144}Sm(^{14}N,3n)^{155}Tm and ^{147}Sm(^{14}N,5n)^{156}Tm. The ^{14}N energy, 88.4 MeV, is too low to induce the ^{147}Sm(^{14}N,6n)^{155}Tm reaction with any reasonable probability, and the ^{144}Sm(^{14}N,2n) reaction to produce ^{156}Tm was not expected to be observed.

Bombardments for varying lengths of time at different energies were made with both samarium targets. It was found that in addition to (^{14}N,xn) reactions, (^{14}N,pxn) and (^{14}N,αxn) reactions also have large cross sections. The independent production of the ^{151}Ho and ^{152}Ho isomers in these (^{14}N,αxn) reactions has served to complicate the identification of ^{155}Tm, which appears to have a half-life and an alpha-decay energy quite similar to those of the high-spin isomer in its alpha-decay daughter, ^{151}Ho. The search for and identification of ^{155}Tm is therefore still in progress.

The assignment of a new radioactivity, with half-life of 77 ± 10 sec, turned out to be more straightforward even though its alpha-decay energy, 4.23 ± 0.01 MeV, is essentially the same as that of 7-min ^{150}Dy. The yield curve for this new alpha group was measured, and its shape was found to be consistent with that expected for a ^{147}Sm(^{14}N,5n) low-spin product. Its mass assignment, however, is based on firmer evidence; a parent-daughter relationship was established between it and the low-spin isomer in ^{152}Ho. Figure 1.13 shows the decay data obtained for the 4.38-MeV alpha group known to be associated with the ^{152}Ho low-spin isomer. Least-squares analysis indicated a genetic relationship between two radioactive components, one with a half-life of 2.38 min and the other with a 77-sec half-life. Because the 2.38-min half-life is that of the low-spin isomer of ^{152}Ho, the parent-daughter relationship establishes the existence of a new thulium nuclide, ^{156}Tm. The fact that it apparently populates a low-spin isomer would indicate that the new alpha group represents decay from a state with a low spin.

The results obtained in this work are listed in Table 1.6.

Table 1.6. New alpha emitters

Nuclide	Half-life	Alpha-decay energy (MeV)
^{156}Tm (low-spin isomer)	77 ± 10 sec	4.23 ± 0.01
^{154}Ho (high-spin isomer)	3.0 ± 0.3 min	3.72 ± 0.01
^{153}Ho (high-spin isomer)	2.0 ± 0.1 min	3.91 ± 0.01

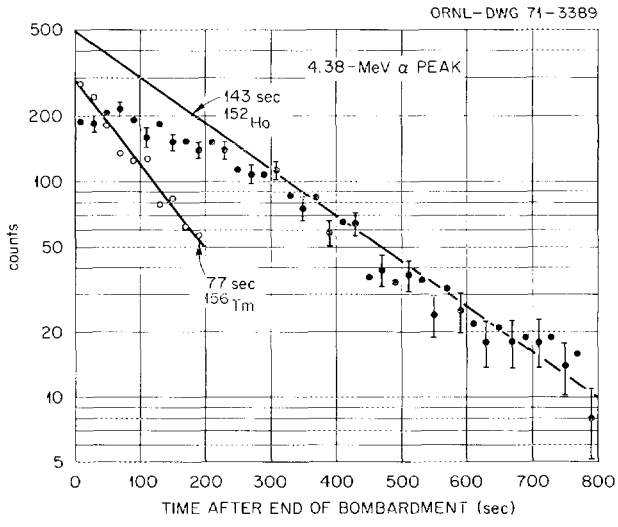

Fig. 1.13. Decay data obtained for the 4.38-MeV alpha group observed in ^{14}N bombardments of ^{147}Sm. The growth of ^{152}Ho establishes the assignment of the 77-sec activity to alpha-decaying ^{156}Tm.

1. A similar report has appeared in *Electronucl. Div. Annu. Progr. Rep. Dec. 31, 1970,* ORNL-4649, p. 65.
2. Electronuclear Division.
3. Physics Department, Virginia Polytechnic Institute, Blacksburg.
4. K. S. Toth et al., *Chem. Div. Annu. Progr. Rep. May 20, 1969,* ORNL-4437, p. 7.
5. K. S. Toth et al., *Chem. Div. Annu. Progr. Rep. May 20, 1970,* ORNL-4581, pp. 7–14.
6. T. Sikkeland, A. Ghiorso, and M. J. Nurmia, *Phys. Rev.* **172,** 1232 (1968).
7. R. L. Hahn et al., *Chem. Div. Annu. Progr. Rep. May 20, 1969,* ORNL-4437, p. 37.
8. N. A. Golovkov, S. K. Khvan, and V. G. Chumin, p. 27 in *Proceedings of the International Symposium on Nuclear Structure,* Dubna, 1968, IAEA, Vienna, 1969.
9. R. L. Hahn, K. S. Toth, and T. H. Handley, *Phys. Rev.* **163,** 1291 (1967).
10. R. D. Macfarlane and R. D. Griffioen, *Phys. Rev.* **130,** 1491 (1963).
11. R. D. Macfarlane, *Phys. Rev.* **126,** 274 (1962).
12. C. Ekström et al., *Nucl. Phys. A* **135,** 289 (1969).
13. R. D. Macfarlane, *Phys. Rev.* **136,** B941 (1964).

THE DECAY OF ^{158}Eu TO LEVELS IN ^{158}Gd

A. F. Kluk[1] N. R. Johnson J. H. Hamilton[2]

Studies of the beta decay of ^{158}Eu have been completed this past year with both singles and multiparameter coincidence experiments being performed by use of large-volume, high-resolution Ge(Li) detectors. Many sources of 46-min ^{158}Eu were prepared from the (d,α) reaction on ^{160}Gd. Targets of Gd_2O_3 (95.95% enriched in ^{160}Gd) were bombarded with 13.5-MeV deuterons at ORIC, and extensive chemical purification of Eu was then performed.

While primary emphasis has been devoted to the analysis of the properties of the collective levels of ^{158}Gd, a detailed analysis of all the levels has been done, and a decay scheme has been proposed (Fig. 1.14). Accurate energies and intensities have been determined for 129 transitions, of which 79 have been placed in a ^{158}Gd level scheme consisting of 27 levels.

We have observed the 2^+ and 3^+ members of the γ-vibrational band and are particularly interested in the electric quadrupole transition probabilities from these levels to the 0^+, 2^+, and 4^+ members of the ground-state rotational band. A search was made for the 0^+ and 2^+ members of the β band, which previously had been reported in (d,d') reaction work[3] and in (n,γ) studies,[4,5] but no evidence for them was found.

Our interest in these levels stems from our earlier studies,[6] in which we were unable to account theoretically for the $B(E2)$ ratios from the β band in ^{152}Sm and ^{154}Gd, which are just at the onset of permanent nuclear deformation. The theory, which was thought to describe the $B(E2)$ ratios from the γ band, consists of a perturbational treatment of the simple adiabatic model of an axially symmetric deformed nucleus. This treatment is necessary to account for the mixing of the wave functions of the vibrational and rotational bands. There result corrections to the gamma-ray branching ratios from this band mixing whose spin-independent part is given as a function of a term called a mixing parameter Z. According to the theory, this parameter should have a consistent value for all branching ratios from a given band. If mixing between the β- and γ-vibrational bands is considered, a second spin-independent mixing parameter $Z_{\beta\gamma}$ is obtained.

The values which we obtain for Z_γ, the mixing parameter for the γ-vibrational band, for ^{158}Gd are listed in column 5 of Table 1.7 and are compared with the values obtained from the ^{158}Tb decay studies of Paperiello et al.[7] in column 6. Using our value of Z_γ from the 3^+ level, where no mixing of the β- and γ-vibrational bands is expected to occur, we can determine the effects of including β-γ mixing. The resulting values of $Z_{\beta\gamma}$ are listed in column 7. It will be noted that our values of Z_γ are close to zero and less than the values for ^{152}Sm, ^{154}Gd, and ^{156}Gd, which are about 0.08 (ref. 6), 0.10 (ref. 6), and 0.03 (ref. 8) respectively. While all the values for Z_γ do not overlap, the inclusion of β-γ mixing does not improve the consistency of the Z_γ values appreciably. Thus, although considerably less mixing occurs between the γ-vibration and the ground-state band for ^{158}Gd, which is considered to be more strongly deformed than the above three nuclei, a consistent value for Z_γ is not obtained. This probably implies that we must search for other admixtures in the wave function of the ^{158}Gd γ vibration.

---

1. Oak Ridge Graduate Fellow from Vanderbilt University, Nashville, Tenn., under appointment with Oak Ridge Associated Universities.
2. Physics Department, Vanderbilt University, Nashville, Tenn.

3. R. Block, B. Elbek, and P. O. Tjom, *Nucl. Phys. A* **91,** 576 (1967).
4. R. C. Greenwood and C. W. Reich, Idaho Nuclear Corporation, Progress Report No. IN-1317, p. 78 (1970).
5. L. V. Groshev, et al., *Izv. Akad. Nauk SSSR, Ser. Fiz.* **26,** 1119 (1962); *Bull. Acad. Sci. USSR, Phys. Ser.* **26,** 1127 (1962).
6. L. L. Riedinger, N. R. Johnson, and J. H. Hamilton, *Phys. Rev. Lett.* **19,** 1243 (1967), and *Phys. Rev.* **179,** 1214 (1969).
7. C. J. Paperiello, E. G. Funk, and J. W. Mihelich, *Nucl. Phys. A* **140,** 261 (1970).
8. D. J. McMillan, J. H. Hamilton, and J. J. Pinajian, submitted to *Phys. Rev.*

ORNL-DWG. 71-211A

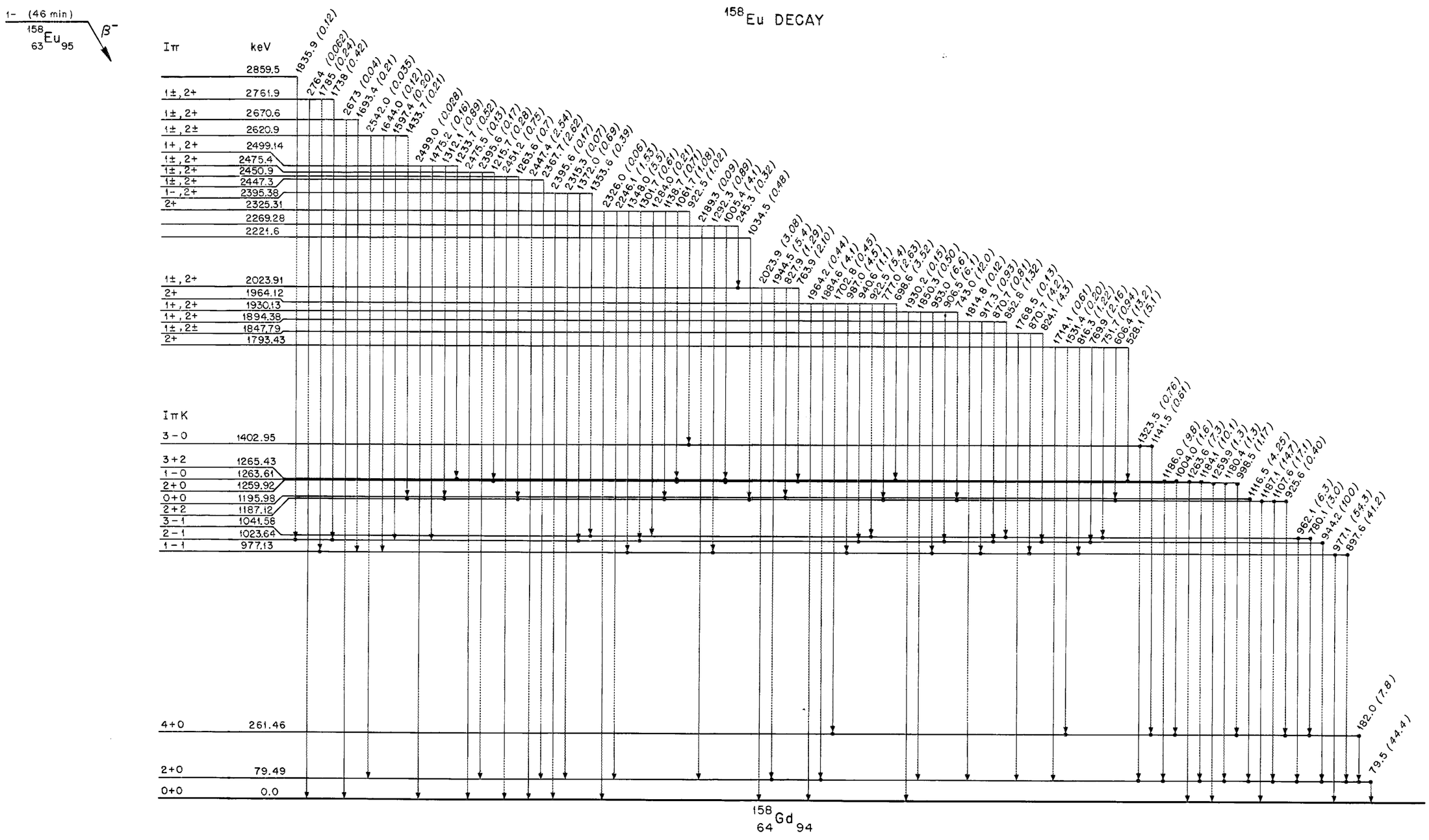

Fig. 1.14. Level scheme of ^{158}Gd from the decay of ^{158}Eu. Energies (in keV) and relative intensities are given for each transition.

Table 1.7. Ratios of reduced transition probabilities for transitions from the γ-vibrational band of ^{158}Gd to the ground-state rotational band

$\frac{I_i^\pi \to I_f^\pi}{I_i^\pi \to I'_f{}^\pi}$	$\frac{E(I_i \to I_f)}{E(I_i \to I'_f)}$	$\frac{B(E2, K_i I_i \to K_f I_f)}{B(E2, K_i I_i \to K_f I'_f)}$ Experimental value	Adiabatic theory	Z_γ Present work	Paperiello et al.[a]	$Z_{\beta\gamma}$
				$\times 10^{-3}$	$\times 10^{-3}$	$\times 10^{-3}$
$\frac{2^+ \to 0^+}{2^+ \to 2^+}$	$\frac{1187.12}{1107.63}$	0.608 (33)	0.70	24 (9)	41 (15)	−23 (9)
$\frac{2^+ \to 4^+}{2^+ \to 2^+}$	$\frac{925.6}{1107.63}$	0.057 (12)	0.05	9 (17)	9 (16)	8 (9)
$\frac{2^+ \to 0^+}{2^+ \to 4^+}$	$\frac{1187.12}{925.6}$	10.6 (25)	13.9	14 (13)	17 (12)	22 (16)
$\frac{3^+ \to 2^+}{3^+ \to 4^+}$	$\frac{1004.2}{1185.97}$	0.368 (38)	0.40	−7 (7)		

[a]Calculated from data of Paperiello et al.[7]

BAND-MIXING ANOMALIES IN ^{178}Hf

J. H. Hamilton[1] P. E. Little[1]
A. V. Ramayya[1] N. R. Johnson

In a previous report[2] we gave an account of some of the preliminary measurements on the amount of magnetic dipole ($M1$) radiation in the transition from the 2^+ member of the β-vibrational band to the 2^+ member of the ground-state band of ^{178}Hf. A knowledge of the $M1$ radiation is very important to an understanding of the anomalous behavior reported for the ratios of reduced electric quadrupole transition probabilities from such states (e.g., see refs. 3 and 4).

These angular correlation measurements have now been repeated to yield highly accurate values of the amount of $M1$ radiation present both in the 1183.4-keV transition from the 2^+ member of the β band of this nucleus and in the corresponding transition from the 2^+ 1496-keV level of another $K = 0$ band.

Our angular correlation results[5] yield the value $(85.6\,^{+1.1}_{-2.1})\%$ for the $M1$ admixture in the 1183.4-keV transition ($2_\beta^+ \to 2_g^+$). This value is in agreement with that previously obtained only with NaI detectors by Nielsen et al.[6] However, the present error limits are a factor of 4 smaller than theirs. In the case of the other $2^+ \to 2^+$ transition (1403 keV) we find an $M1$ admixture of $(61\,^{+0.7}_{-1.2})\%$.

The relative intensities of the transitions from the 1276-keV 2^+ state as obtained with our large-volume, high-efficiency Ge(Li) detector are given in Table 1.8 along with the previous results.[6,7] From our gamma-ray intensity data, an $M1$ admixture of $(73.0 \pm 1.3)\%$ in the $2^+ \to 2^+$ 1183-keV transition would yield a consistent value for the spin-independent band-mixing parameter Z_β for the various branching ratios from the 1276-keV 2^+ state. When one subtracts the 85.6% $M1$ admixture in this $2^+ \to 2^+$ transition found from our γ-$\gamma(\theta)$ work, it is impossible to find a consistent Z_β value. It takes six standard deviations in the γ-$\gamma(\theta)$ work or ten standard deviations in our branching-ratio data for the $M1$ admixtures obtained in these two ways to agree. As a consequence we are forced to conclude that while the $M1$ admixture is large from this state in ^{178}Hf, the branching-ratio data are in no better agreement with theory than in ^{154}Gd. Thus, this work does not confirm the expectation of Mottelson[8] as earlier reported,[6] and it removes the one case that appeared to fit the suggested new theoretical description with large $M1$ admixtures.

A similar analysis has been performed for the next 2^+ level at 1496 keV, and the results are shown also in Table 1.8, where our gamma-ray intensities are compared with the early results of Nielsen et al.[9] Since the branching ratios agree with a $K = 0$ assignment after subtracting a 61% $M1$ admixture in the $2^+ \to 2^+$ transition, one is tempted to identify this as a β-vibrational state. However, to assign one of the known 0^+ states as the ground-state member of such a

Table 1.8. Relative intensities and branching ratios from the 1276.6- and 1496.1-keV 2^+ ($K = 0$) levels in ^{178}Hf populated in the decay of ^{178}Ta

Energy (keV)	Transition	Gamma intensity			Experimental relative $B(E2)$ values,[a] present work			Theoretical relative $B(E2)$ values for Z_β values[b] of:			
		Ref. 7	Ref. 6	This work	$M1 = 0$	$M1 = 73\%$	$M1 = 85.6^{+1.1\%}_{-2.1\%}$	0	0.020	0.026	0.040
970.0	$2^+ \to 4^+$	3.66 ± 0.21	3.57 ± 1.09	3.54 ± 0.18	86.9 ± 4.4	322 ± 16	603^{+35}_{-32}	180	295	323	437
1183.4	$2^+ \to 2^+$	11.00	11.00	11.00	100	100	100	100	100	100	100
1276.6	$2^+ \to 0^+$	2.52 ± 0.20	2.07 ± 0.64	2.22 ± 0.10	13.8 ± 0.6	51.1 ± 2.2	$95.8^{+4.7}_{-4.3}$	70	54	51.2	40
		Ref. 9		This work	$M1 = 0$	$M1 = 62.5\%$	$M1 = 61^{+0.7\%}_{-1.2\%}$	0	−0.020	−0.040	−0.060
1189.5	$2^+ \to 4^+$	4.65		5.66 ± 0.28	12.9 ± 0.6	34.4 ± 1.6	33.1 ± 1.6	180	93.3	34.8	4.6
1402.9	$2^+ \to 2^+$	100		100.0	100	100	100	100	100	100	100
1496.1	$2^+ \to 0^+$	65.9		56.3 ± 1.9	40.8 ± 1.4	109 ± 3.7	$104.6^{+3.8}_{-3.6}$	70	87.4	108	129

[a]These values are for various $M1$ components in the 1183.4- and 1402.9-keV $2^+ \to 2^+$ transitions as indicated.

[b]The notation here is the same as refs. 3 and 4. The lower half of the table is for the 1496.1-keV level, and the Z_β values are negative.

β-vibrational band would yield a moment of inertia quite different from that of the ground-state band. Nielsen et al.[9] already have pointed out that the electron capture feeding to the 1496-keV level is a factor of 2 higher than predicted by Alaga's rules for a rotational band built on either the 1434- or 1444-keV 0^+ states. A more serious problem is the $E0$ strength of the 1403-keV $2^+ \rightarrow 2^+$ transition. Our electron data and that of earlier work[6,9] indicate that the $E0$ strength of the 1403-keV transition is about ten times weaker than that of the 1183-keV transition.

The implications of these results are that the levels in ^{178}Hf previously reported[6,9] as β vibrational in character are not. It certainly is true that the ^{178}Hf $K = 0$ bands are quite different in structure than in ^{154}Gd. One is clearly left with the problem of the anomalous branching ratios from the β bands, as there is at present no case where there is an adequate theoretical description to explain the branching patterns from these states of the "β-vibrational" type.

1. Vanderbilt University, Nashville, Tenn.
2. J. H. Hamilton et al., *Chem. Div. Annu. Progr. Rep. May 20, 1970,* ORNL-4581, p. 17.
3. L. L. Riedinger, N. R. Johnson, and J. H. Hamilton, *Phys. Rev. Lett.* **19**, 1243 (1967).
4. L. L. Riedinger, N. R. Johnson, and J. H. Hamilton, *Phys. Rev.* **179**, 1214 (1969).
5. J. H. Hamilton et al., *Phys. Rev. Lett.* **25**, 946 (1970).
6. H. L. Nielsen, K. B. Nielsen, and N. Rud, *Phys. Rev. Lett. B* **27**, 150 (1968).
7. T. A. Siddiqi, R. C. Carlson, and G. T. Emery, *Bull. Amer. Phys. Soc.* **14**, 1174 (1969).
8. B. R. Mottelson, *J. Phys. Soc. Jap., Suppl.* **24**, 87 (1968).
9. H. L. Nielsen et al., *Nucl. Phys. A* **93**, 385 (1967).

THE DECAY OF ^{194}Au TO THE LEVELS OF ^{194}Pt[1]

G. D. Benson[2] R. G. Albridge[2]
A. V. Ramayya[2] G. D. O'Kelley

The gamma rays emitted following the decay of the 39.5-hr ground state of ^{194}Au (spin and parity 1^-) to levels in ^{194}Pt have been studied extensively in an effort to remove some of the uncertainties from the decay scheme derived from previous work. The energies and intensities of 93 gamma rays were determined with a high-efficiency, high-resolution Ge(Li) spectrometer. In addition, nine weak lines were seen in the singles spectra which could not be positively assigned to the ^{194}Au decay on the basis of half-life or coincidence relationships.

Energies were measured by recording the spectrum of a source composed of a mixture of ^{194}Au and several radionuclide standards. From such spectra the energies of several prominent gamma lines were obtained, and these energies in turn were used as internal standards for the determination of the weaker lines. The energy calibration was accomplished with a computer program which fitted the standard lines to a second-degree polynomial by the method of least squares. These careful energy measurements disclosed significant disagreements with earlier values for the high-energy gamma rays by Bergman and Bäckström,[3] who used a magnetic internal-conversion spectrometer. Our energies of strong transitions at high energies measured by Ge(Li) spectrometry were as much as 0.3 to 0.5 keV lower. Our results were verified by comparison of energies of escape peaks with energies of full-energy peaks of high-energy gamma rays.

The K-conversion coefficients of transitions in ^{194}Pt were calculated from the relative gamma-ray intensities in the present work and the internal-conversion electron intensities that were determined by Bergman and Bäckström.[3] The relative gamma-ray and electron intensities were normalized by use of the theoretical internal conversion coefficient[4] for the intense $E2$ transition of 328.47 keV from the 2^+ first excited state to the 0^+ ground state of ^{194}Pt.

Gamma-gamma coincidence measurements were performed with two Ge(Li) detectors in a 90° geometry coupled to a two-parameter analyzer. Gamma coincidence spectra obtained by gating on 34 transitions were analyzed. The coincidence relationships, extensive data on multipolarities of the gamma transitions derived from internal conversion coefficients, and precise transition energies and intensities were used to construct the consistent level scheme for ^{194}Pt shown in Fig. 1.15.

Reduced transition rates, $B(E2)$, for transitions from states in ^{194}Pt and energy spacings suggest that the low-lying states of ^{194}Pt are vibrational in character. We have interpreted the 622-keV (2^+) and 811-keV (4^+) levels as members of a two-phonon triplet and the 923-keV (3^+), 1229-keV ($2, 3, 4^+$), 1267-keV (0^+), and 1374-keV (6^+) levels as possible members of a three-phonon quintet. In addition, we observed the ground-state transition from the 1432-keV (3^-) level, which we interpret as an octupole vibrational state.

We have also compared our experimental results with recent calculations by Kumar and Baranger,[5] who applied the pairing-plus-quadrupole model of residual interactions to calculations of properties of states of even isotopes of W, Os, and Pt. The model does not yield accurate energies of the first few excited states, nor does it account for the large number of low-lying states observed experimentally. Further, experimental ratios of $B(E2)$ values generally do not agree well with

ORNL-DWG. 69-5248

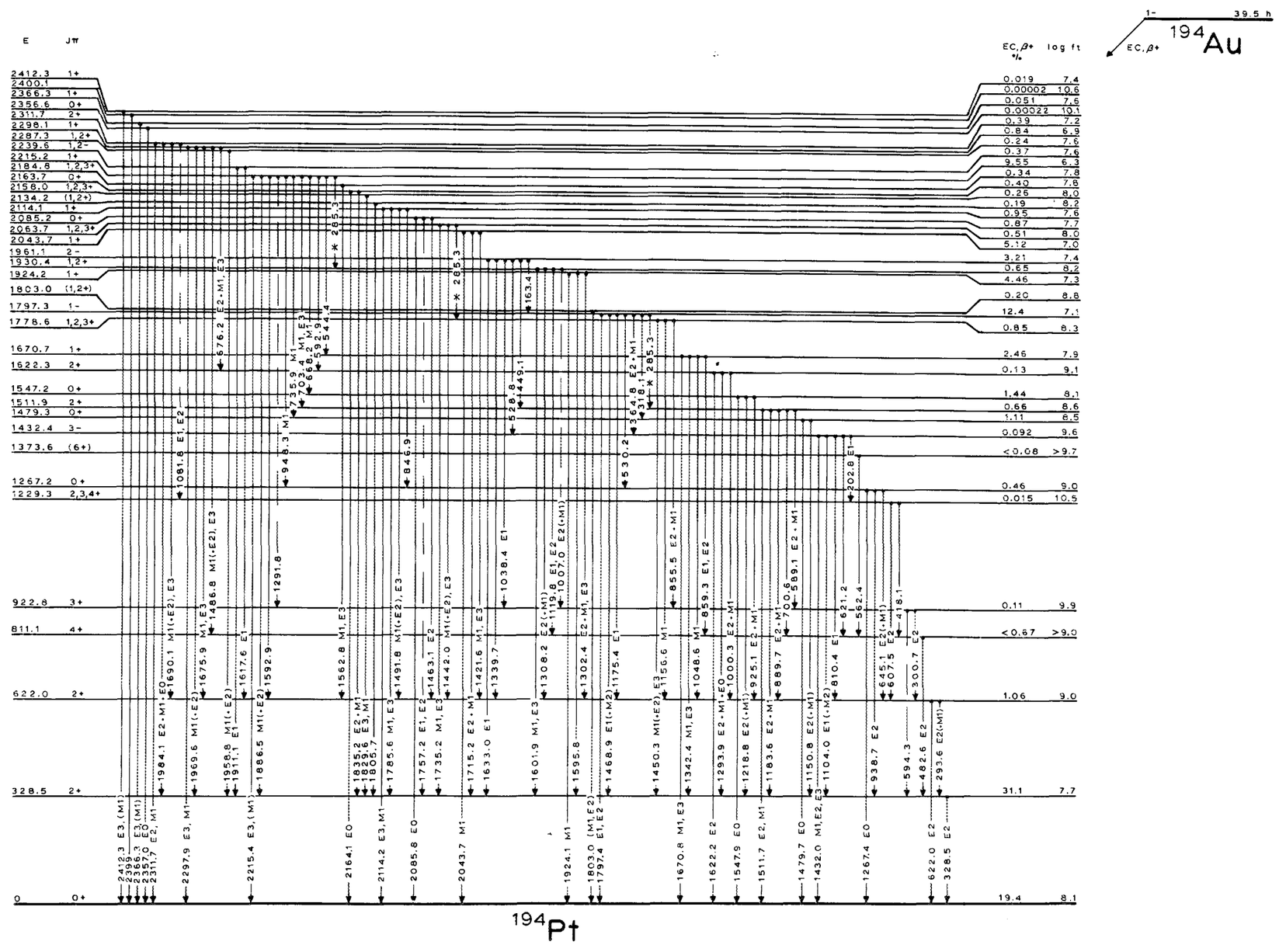

Fig. 1.15. Proposed decay scheme of ^{194}Au. Energy values are in keV. Gamma transitions whose placement may be doubtful are shown by dashed lines.

the values calculated by Kumar and Baranger. Thus, the pairing-plus-quadrupole model does not appear to provide an adequate description of the levels of ^{194}Pt.

---

1. Summary of a paper published in *Nucl. Phys. A* **150**, 311 (1970).
2. Vanderbilt University, Nashville, Tenn.
3. O. Bergman and G. Bäckström, *Nucl. Phys.* **55**, 529 (1964).
4. L. A. Sliv and I. M. Band, p. 1639 in *Alpha-, Beta- and Gamma-Ray Spectroscopy*, K. Siegbahn, ed., North-Holland, Amsterdam, 1965.
5. K. Kumar and M. Baranger, *Nucl. Phys. A* **122**, 273 (1968).

ABUNDANCES OF THE PRIMORDIAL RADIONUCLIDES K, Th, AND U IN APOLLO 12 LUNAR SAMPLES BY NONDESTRUCTIVE GAMMA-RAY SPECTROMETRY: IMPLICATIONS FOR ORIGIN OF LUNAR SOILS[1]

G. D. O'Kelley V. A. McKay[4]
P. R. Bell[2] K. J. Northcutt[3]
J. S. Eldridge[3] R. T. Roseberry[4]
E. Schonfeld[5]

A suite of lunar samples from the Ocean of Storms were examined by nondestructive gamma-ray spectrometry at the Lunar Receiving Laboratory (LRL), Houston, Texas, during the Apollo 12 mission. Preliminary data from this study were reported earlier.[6] More recently, the data analyses have been refined, and additional samples have been analyzed.

The gamma scintillation coincidence spectrometer used at the LRL for analysis of most of the samples, calibration procedures, and associated data reduction techniques were described previously. A second system at ORNL with detectors identical to those used at the LRL was used to analyze two of the samples (12002,20 and 12013,11). Analyses for K, Th, and U are presented in Table 1.9. Error statements in the table are quite conservative estimates and include overall errors from counting statistics, geometrical uncertainties, and calibration errors.

Analysis of Rocks and Fines

The large amount of material studied (about 40% of the total mass of Apollo 12 samples) permits some detailed comparisons to be made between the concentrations shown in Table 1.9 and comparable measurements carried out on Apollo 11 samples by various investigators. The crystalline rocks of Apollo 11 appeared to fall into two chemical groups with different alkali metal concentrations. Our Apollo 11 work showed that one chemical group had average K, Th, and U concentrations of about 500, 1.0, and 0.25 ppm respectively; the other group had average K, Th, and U concentrations of about 2400, 3.3, and 0.8 ppm respectively.

All of the crystalline rocks of Apollo 12 we have examined resemble the low-potassium group of Apollo 11 and have average concentrations of K, Th, and U of about 520, 0.97, and 0.25 ppm respectively. These Apollo 12 samples show remarkably small deviations from the average values.

The fines and breccia from the Ocean of Storms are quite different from the crystalline rocks in several respects. The concentrations of the radioactive elements K, Th, and U are much higher and more variable in the fines and breccia than in the crystalline rocks. The average K/U ratio for fines and breccia is only about 1300 (see Table 1.9), compared with an average value of about 2100 for the crystalline rocks. It is important to note that the mass ratio Th/U is approximately 3.8 for all materials listed in Table 1.9 except for sample 12013, in good agreement with average Th/U ratios for Tranquillity Base materials and for terrestrial materials. The concentrations of K, U, and Th in the fines and breccia from the Apollo 11 site were intermediate between the respective concentrations for the two chemical classes of crystalline rocks. It appeared on this basis that the fines and breccia might have been derived from the crystalline rocks at the Sea of Tranquillity; however, more detailed chemical studies later showed that Apollo 11 soil contained other components differing slightly from the crystalline rocks in composition. Clearly, the crystalline rocks whose concentrations are given in Table 1.9 could not alone have formed the Apollo 12 fines and breccia.

The depletion of volatile elements observed in lunar materials is thought to be characteristic of the whole moon. Studies of the primordial radioactive elements are particularly useful in this connection, because the ratios of K (a volatile element) to U (a refractory element) for common terrestrial rock types are remarkably constant over a wide range of K concentration. Thus, the K/U ratio appears to be a result of early chemical fractionation and is not affected by later igneous processes.

In Fig. 1.16 we show a plot of K/U mass ratios as a function of potassium concentration, normalized to 18 wt % silicon. Data on lunar samples are from our gamma spectrometry studies and from other chemical analyses reported in the literature. It is clear that eucrites, carbonaceous chondrites, and ordinary chondrites fall into groups which are distinct from one

Table 1.9. Concentrations of primordial radionuclides in lunar samples[a]

Sample	Weight (g)	K (ppm)	Th (ppm)	U (ppm)	K/U mass ratio	Th/U mass ratio
			Crystalline rocks			
12002, 0	1529	450 ± 20	0.89 ± 0.06	0.23 ± 0.02	1960 ± 192	3.87 ± 0.42
12002, 20	260	425 ± 21	0.73 ± 0.04	0.21 ± 0.02	2020 ± 216	3.50 ± 0.39
12002, 30	46	440 ± 20	0.86 ± 0.06	0.22 ± 0.02	2000 ± 212	3.91 ± 0.45
12004, 1	502	469 ± 33	0.92 ± 0.09	0.24 ± 0.03	1960 ± 282	3.83 ± 0.61
12021, 0	1877	500 ± 50	0.98 ± 0.10	0.26 ± 0.03	1920 ± 292	3.77 ± 0.53
12039, 0	255	673 ± 40	1.20 ± 0.06	0.31 ± 0.03	2170 ± 246	3.87 ± 0.42
12051, 0	1660	530 ± 50	1.00 ± 0.10	0.26 ± 0.03	2040 ± 304	3.85 ± 0.59
12052, 1	201	540 ± 20	1.03 ± 0.06	0.27 ± 0.02	2000 ± 166	3.82 ± 0.36
12053, 0	879	535 ± 40	1.06 ± 0.11	0.28 ± 0.03	1910 ± 244	3.79 ± 0.57
12054, 0	687	530 ± 35	0.79 ± 0.08	0.22 ± 0.03	2410 ± 365	3.59 ± 0.61
12062, 0	739	510 ± 35	0.83 ± 0.09	0.22 ± 0.03	2320 ± 354	3.78 ± 0.66
12064, 0	1214	520 ± 35	0.87 ± 0.09	0.23 ± 0.02	2260 ± 248	3.78 ± 0.51
12065, 0	2109	510 ± 50	1.06 ± 0.11	0.27 ± 0.03	1890 ± 280	3.92 ± 0.54
Average, crystalline rocks					2066	3.79 ± 0.14
			Fines			
12032, 16	89.6	3100 ± 100	8.8 ± 0.2	2.35 ± 0.07	1320 ± 58	3.75 ± 0.14
12070, 0	354	2030 ± 120	6.25 ± 0.50	1.65 ± 0.16	1230 ± 140	3.79 ± 0.48
			Breccia			
12034, 0	155	4560 ± 130	13.1 ± 0.3	3.4 ± 0.2	1341 ± 88	3.85 ± 0.24
12073, 0	405	2960 ± 90	8.45 ± 0.10	2.19 ± 0.08	1352 ± 68	3.86 ± 0.15
Average, fines and breccia					1311	3.81 ± 0.14
			Rock 12013			
12013, 0	80.0	20,400 ± 600	34.2 ± 0.8	10.3 ± 0.5	1980 ± 112	3.32 ± 0.18
12013, 11	66.2	21,100 ± 600	32.2 ± 1.4	9.8 ± 1.0	2160 ± 228	3.29 ± 0.36

[a]Standardization for assay of K, Th, and U assumed terrestrial isotopic abundances and equilibrium of Th and U decay series.

another and from either lunar or terrestrial materials. It may be noted that on these systematics the tektites fall within the terrestrial group. The meteorites fall on a common "trend line" for which the product of the K and U concentrations is approximately constant. In contrast, both the earth and the moon possess constant K/U ratios characteristic of each planet.

The values of K/U for lunar material appear to be separable into five distinct groups, as shown in Fig. 1.16: (1) Apollo 12 rocks + low-K Apollo 11 rocks; (2) Apollo 11 fines and breccia; (3) high-K Apollo 11 rocks; (4) Apollo 12 fines and breccia; and (5) rock 12013. An analysis of the relationships between these "islands" in the K/U systematics suggests that samples at the two landing sites are products of two separate magmatic processes.

Rock 12013 and the Origin of Apollo 12 Fines and Breccia

Sample 12013 proved to be one of the most interesting samples studied. Our gamma-ray spectrometry measurements during the preliminary examination showed clearly that the specimen was dramatically different from all lunar samples previously examined.[6] The concentrations of K and U were about 40 times the average concentrations of the crystalline rocks of Apollo 12 and about 10 times the concentrations of the high-K rocks of Apollo 11. At the bottom of Table 1.9 we show a refined analysis of our data on the whole rock (12013,0) and an additional measurement on the 66-g piece (12013,11) which remained after samples were cut for destructive analy-

sis. Despite the inhomogeneity of this breccia on a microscopic scale, the primordial radionuclide concentrations from our two measurements on large rock fragments agree very well with each other. The Th/U ratio is distinctly different, namely, 3.3, compared with 3.8 for other Apollo 12 material.

It is interesting to speculate on the possible role of rock 12013 or one of its components in forming the Apollo 12 fines and breccia. Our K/U systematics in Fig. 1.16 suggest that the required material to mix with the crystalline rocks must have a low K/U ratio of about 1000 and a K concentration of about 5000 to

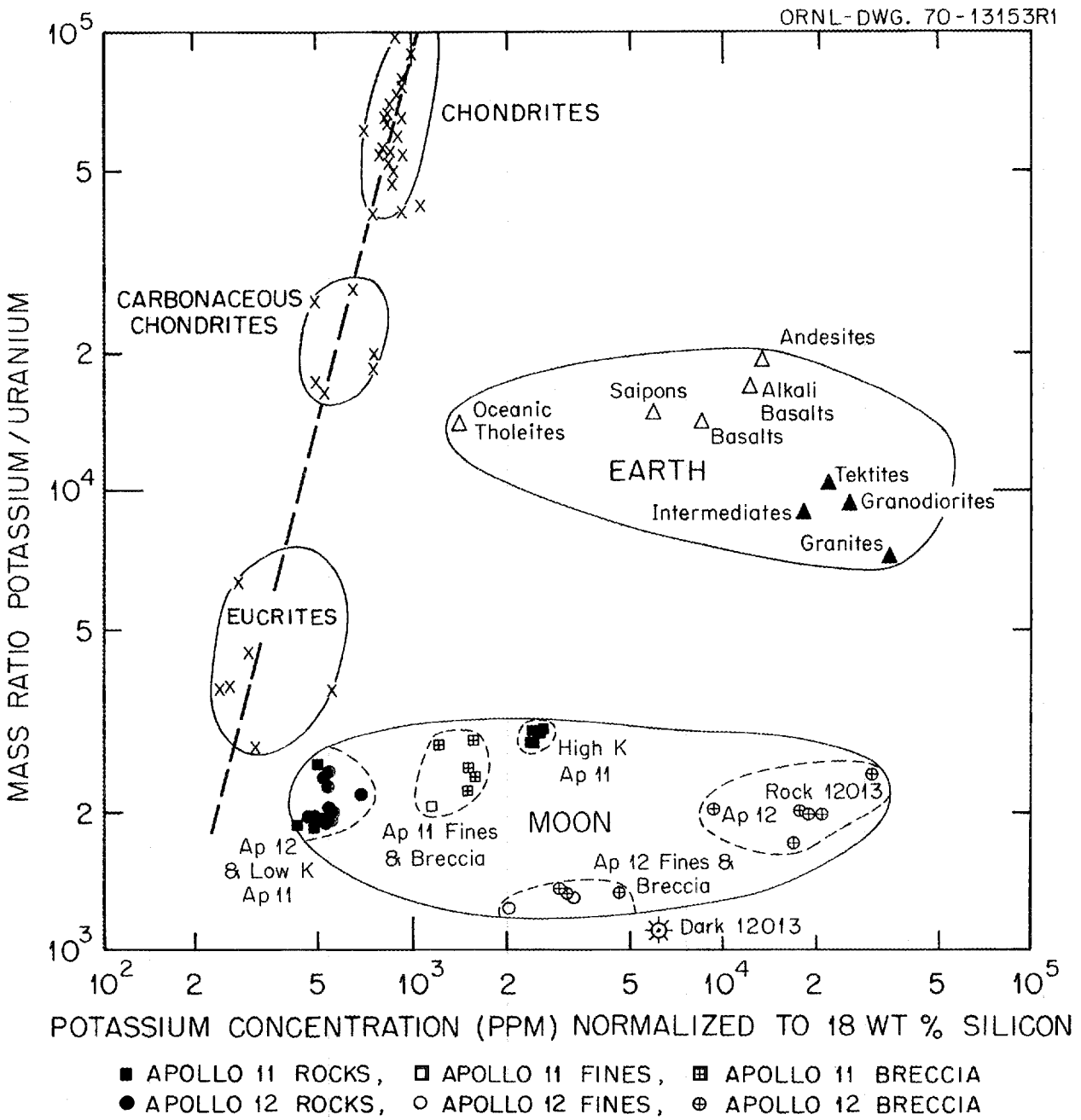

Fig. 1.16. Plot of mass ratios K/U as a function of K concentration normalized to 18 wt % Si. The distinct grouping of meteorites and terrestrial and lunar materials is apparent.

7000 ppm. Further, since our Th/U ratios of Table 1.9 show that the fines, breccia, and crystalline rocks all have a common Th/U ratio of 3.8, not all of the constituents of 12013 can be common to the lunar soil.

Studies on 12013 have disclosed a general chemical similarity between the light and the gray material, which, taken together, are distinct from the dark material. Chemical analyses from the literature on these two components of 12013 show that the average K concentration is 6500 ppm for the dark material and 25,500 ppm for the light and the gray, in fair agreement with our measured concentration of about 20,000 ppm averaged over the whole rock. The light material is too high in potassium to be the missing component. Further, Wakita and Schmitt[7] report a range of 2.3 to 3.2 for the Th/U ratio, which also militates against the light material. However, Tatsumoto[8] found dark material from 12013 which had a U concentration of 5.7 ppm and a "normal" Th/U mass ratio of 3.7. Thus, it appears that a component of 12013 with a K concentration of 6500 ppm, a K/U ratio of ~1100, and a Th/U ratio of 3.8 does exist and may be the component required to form the lunar fines and breccia from the crystalline rocks. This point has been added to the K/U systematics of Fig. 1.16. These results strongly support the suggestions of Hubbard, Gast, and Wiesmann[9] and Schnetzler, Philpotts, and Bottino[10] that the dark component of 12013 may be a major component of the lunar soil.

A simple two-component mixing model was fitted to the K and U concentrations of three soil samples and two breccia samples from Apollo 12. Mixing was assumed to occur between basaltic material of 520 ppm K and 0.25 ppm U and a foreign component of 6500 ppm K. The data are best fitted by a U concentration of 5.2 ppm in the foreign component. Samples (and percent foreign component) are: soils 12032 (43%), 12033 (54%), 12070 (27%); and breccia 12034 (66%), 12073 (40%).

Gas Retention Ages

The elemental analyses for K, Th, and U reported in Table 1.9 may be combined with rare-gas concentrations to estimate crystallization ages of rocks. In Table 1.10 we show gas retention ages for eight samples. Although the K-^{40}Ar and U,Th-^{4}He ages are reasonably concordant for 12002, 12004, and 12064, the U,Th-^{4}He ages are consistently younger than the K-^{40}Ar ages. The low U,Th-^{4}He ages for 12062, 12065, and 12013 suggest that these rocks have experienced significant heating accompanied by preferential loss of He.

Table 1.10. Estimation of gas retention ages of lunar samples

Sample	K-^{40}Ar (10^9 years)	U,Th-^{4}He (10^9 years)
12002	2.55[a]	2.32[a]
12004	2.92[a]	2.69[a]
12021	3.22[b]	
12052	2.34[b]	
12062	2.61[c]	1.22[d]
12064	3.10[a]	2.69[a]
12065	2.79[a]	1.95[a]
12013	3.37[c]	1.47[c]

[a]Rare-gas concentrations from ref. 12; K, Th, U concentrations from Table 1.9.

[b]Rare-gas concentrations from ref. 13; K, Th, U concentrations from Table 1.9.

[c]Rare-gas concentrations from refs. 6 and 14; K, Th, U concentrations from Table 1.9.

[d]Rare-gas concentrations from ref. 6; Th and U concentrations from Table 1.9.

Gas retention ages of large samples are generally found to give somewhat shorter ages than those obtained by other methods. However, the K-^{40}Ar ages of Table 1.10 for 12004, 12021, and 12064 show evidence of little or no loss of radiogenic argon. Our results compare well with ages of these Apollo 12 rocks reported at the 1971 Lunar Science Conference by other groups using different isotopic clocks. None of the Apollo 12 rocks we have studied have exhibited an age as high as the 3.97×10^9 years we determined[11] for Apollo 11 rock 10003.

---

1. Sponsored by the National Aeronautics and Space Administration through interagency agreements with the U.S. Atomic Energy Commission. Summary of a paper in press in the *Proceedings of the Second Lunar Science Conference,* to be published in *Geochimica et Cosmochimica Acta.*
2. Director's Division.
3. Analytical Chemistry Division.
4. Instrumentation and Controls Division.
5. NASA Manned Spacecraft Center, Houston, Tex.
6. Lunar Sample Preliminary Examination Team (including P. R. Bell, J. S. Eldridge, V. A. McKay, G. D. O'Kelley, and R. T. Roseberry), *Science* **167**, 1325–39 (1970); *Chem. Div. Annu. Progr. Rep. May 20, 1970,* ORNL-4581, pp. 25–27.
7. H. Wakita and R. A. Schmitt, *Earth Planet. Sci. Lett.* **9**, 169–76 (1970).
8. M. Tatsumoto, *Earth Planet. Sci. Lett.* **9**, 193–200 (1970).
9. N. J. Hubbard, P. W. Gast, and H. Wiesmann, *Earth Planet. Sci. Lett.* **9**, 181–84 (1970).
10. C. C. Schnetzler, J. A. Philpotts, and M. L. Bottino, *Earth Planet. Sci. Lett.* **9**, 185–92 (1970).

11. G. D. O'Kelley et al., *Proceedings of the Apollo 11 Lunar Science Conference, Geochim. Cosmochim. Acta,* Suppl. 1, vol. 2, pp. 1407–1423, Pergamon, 1970.
12. H. Hintenberger, H. Weber, and N. Takaoka, *Apollo 12 Lunar Science Conference,* unpublished proceedings, 1971.
13. K. Marti and G. W. Lugmair, *Apollo 12 Lunar Science Conference,* unpublished proceedings, 1971.
14. O. A. Schaeffer et al., *Science* **170**, 161–62 (1970).

COSMOGENIC RADIONUCLIDE CONCENTRATIONS AND EXPOSURE AGES OF LUNAR SAMPLES FROM APOLLO 12[1]

G. D. O'Kelley V. A. McKay[4]
P. R. Bell[2] K. J. Northcutt[3]
J. S. Eldridge[3] R. T. Roseberry[4]
E. Schonfeld[5]

Cosmogenic radionuclide abundances in lunar samples from the Ocean of Storms were determined nondestructively by gamma-ray spectrometry. Several radionuclides of interest have short half-lives, and for this reason, most of the data reported below were recorded at the Lunar Receiving Laboratory (LRL), Houston, Texas, during the preliminary examination of the Apollo 12 samples. Preliminary values of ^{22}Na and ^{26}Al concentrations for some of the samples were published;[6] since that early account the analyses of the data have been refined to obtain quantitative radionuclide concentrations of other cosmogenic species, and additional samples have been analyzed.

Several gamma-ray spectrometers were used in the course of this study. An NaI(Tl) scintillation coincidence spectrometer with an associated on-line data acquisition system described previously,[7] together with a Ge(Li) spectrometer, permitted rapid analyses of samples at the LRL during the sample quarantine period, so that nuclides of short half-life could be determined. Some studies at later times were carried out at ORNL on an NaI(Tl) spectrometer similar to the scintillation spectrometer at the LRL.

The first Apollo 12 sample for radioactivity determination (12002,0) was received from the LRL Sample Laboratory on November 28, 1969, about 8.4 days after liftoff from the moon. Methods of data acquisition and data analysis were essentially the same as those we used to analyze Apollo 11 samples.[7] Yields of short-lived nuclides were corrected to the time of liftoff from the lunar surface, 1426 GMT, November 20, 1969.

Cosmogenic Radionuclide Concentrations

Results are given in Table 1.11. The general concentration patterns resemble those we observed for spallogenic radionuclides in the Apollo 11 samples;[7] however, a number of subtle differences were noted due to effects of chemical composition and shielding. The data of Table 1.11 were recorded on large samples, usually a rock or a large fragment of a rock. Sample weights are listed in Table 1.9 of the previous paper. As observed in all gamma-ray spectrometry studies of lunar samples, the high concentrations of Th and U make difficult the determination of weak gamma-ray components. Because of the short times available for some of the measurements, it was not possible to determine all eight nuclides listed in Table 1.11 for all of the samples. Rock 12002 was the most carefully studied of all our samples, and a rather complete radionuclide pattern was obtained.

Sample 12002,30 was a 46-g piece cut from the top of oriented rock 12002,0, and the data in Table 1.11 were obtained before 12002,30 was submitted to destructive analysis by Finkel et al.[8] to determine depth variations of cosmogenic nuclides. As expected, high concentrations of ^{26}Al and ^{22}Na were seen, in excess of the production by galactic protons, which is estimated to be about 41 dis min^{-1} kg^{-1}. The concentration of ^{54}Mn has also been enhanced over the nominal galactic production value by solar proton bombardment, while ^{56}Co, which is almost totally produced by solar flares, manifests a large concentration in the surface piece (12002,30) over that of the whole rock (12002,0). In contrast, breccia 12034 was buried about 15 cm and so was shielded from solar protons; hence the concentration of ^{54}Mn is low and ^{56}Co is undetectable.

For the other rocks of Table 1.11 excess ^{26}Al is observed over that produced by galactic protons, with a moderate excess of ^{22}Na. These results, together with the ^{56}Co concentrations of Table 1.11, show that the rocks in question were at least partially exposed on the lunar surface.

Rocks 12054, 12062, and 12064 show evidence of recent low exposure. Within experimental errors it is not possible to decide whether the low values of ^{26}Al are due to partial shielding from solar protons or whether the ^{26}Al did not attain saturation. Galactic proton exposure ages suggest that samples 12062 and 12064 have been near, but not on, the lunar surface for the last 150 to 200 m.y. (million years), so these rocks probably received a low exposure to solar protons. Another possible explanation would be a high surface erosion rate, but it does not seem consistent to propose that certain rocks erode rapidly while others do not.

The two soil samples we examined appear to have been taken from quite different depths. The high concentrations of ^{22}Na and ^{26}Al, and especially the

Table 1.11. Concentrations (dis min^{-1} kg^{-1}) of spallogenic radionuclides in Apollo 12 samples[a]

Values for short-lived nuclides have been corrected to 1426 GMT, Nov. 20, 1969

Sample[b]	Type[c]	^{22}Na	^{26}Al	^{46}Sc	^{48}V	^{52}Mn	^{54}Mn	^{56}Co	^{60}Co
12002, 0	B	42 ± 3	75 ± 6	3.5 ± 1.0	13 ± 3	31 ± 12	38 ± 3	33 ± 4	0.55 ± 0.30
12002, 20	B	47 ± 3	67 ± 5						0.73 ± 0.65
12002, 30	B	86 ± 3	126 ± 6				50 ± 5	148 ± 20	
12004, 1	A	53 ± 5	90 ± 6	3.7 ± 1.5			35 ± 4	34 ± 8	<2.6
12039, 0	B	43 ± 5	95 ± 7	<6.0			37 ± 6	40 ± 10	
12052, 1	A	40 ± 6	75 ± 6				27 ± 7	26 ± 10	
12053, 0	A	40 ± 6	81 ± 12	7.0 ± 2.0	20 ± 5		35 ± 5	32 ± 6	<1.0
12054, 0	B	39 ± 7	50 ± 10	5.0 ± 2.0			36 ± 5	40 ± 10	<1.0
12062, 0	AB	30 ± 5	57 ± 9	5.0 ± 2.0	9 ± 3		31 ± 6	7 ± 4	
12064, 0	B	40 ± 5	51 ± 5	5.0 ± 2.0	22 ± 6	33 ± 18	35 ± 3	32 ± 6	<1.0
12013, 0	C	50 ± 10	115 ± 16	<15			<66	50 ± 30	<8.0
12013, 11	C	26 ± 10	90 ± 10						
12034, 0	C	29 ± 5	45 ± 5	<10	<60		16 ± 8	<16	<4.0
12073, 0	C	63 ± 7	110 ± 10	<10			28 ± 7	47 ± 12	
12032, 16	D	48 ± 6	100 ± 7	<10			27 ± 7	<30	<2.0
12070, 0	D	70 ± 8	146 ± 16				41 ± 10	55 ± 14	<1.5

[a]Upper limits are 2σ, evaluated from least-squares analysis.

[b]A zero following the five-digit sample number designates a whole rock or fines sample.

[c]Petrologic type: A, fine-grained crystalline rock; B, coarse-grained crystalline rock; AB, crystalline rock of intermediate grain size; C, breccia; D, fines.

high ^{56}Co, are consistent with near-surface sampling for 12070. The sample of 12032 apparently came from a deeper zone, about 5 cm below the surface.

The concentrations of ^{46}Sc in samples from Apollo 12 are about 2.4 times lower than those we found in Apollo 11 samples.[7] This reduction reflects the lower concentration of Ti target nuclei in the samples from the Ocean of Storms.

Despite delays in obtaining samples during the preliminary examination, 5.7-day ^{52}Mn was determined in two rocks and 16-day ^{48}V was determined in four rocks. The ^{52}Mn yields are approximately as expected from the chemical composition and correlate well with the ^{54}Mn yields. Most of the ^{48}V was produced by solar protons via the reaction $^{48}Ti(p,n)^{48}V$ during the solar flare of November 3, 1970. The ^{48}V and ^{56}Co concentrations of rock 12062 show that this rock was partially shielded from solar protons.

Thermal-Neutron Flux

Cobalt-60 has a half-life of only 5.3 years and is produced with a high cross section (37 b) by thermal-neutron capture in ^{59}Co. The concentration of ^{60}Co in lunar material can be employed to calculate the neutron flux characteristic of recent steady-state production on the lunar surface. Such information is a useful complement to fluxes deduced from mass spectrometric measurements of isotopic anomalies in Gd. The Gd isotope ratios yield an integrated thermal-neutron flux which requires a meaningful exposure age before an average flux can be obtained. Lunar rocks endure such a complex history that the average flux obtained mass spectrometrically may not represent the most recent flux to the accuracy desired.

In Table 1.11 we show that in the case of rock 12002,0 a value of 0.55 ± 0.30 dis min^{-1} kg^{-1} was obtained for the ^{60}Co concentration, from which we derive a value for the thermal-neutron flux of 0.35 ± 0.18 neutron cm^{-2} sec^{-1}. Our result for the flux in this sample of mass density 20 g/cm^2 is in good agreement with the depth dependence of thermal-neutron fluxes measured mass spectrometrically by Marti and Lugmair[9] in lunar material of about 18 to 150 g/cm^2. Our result for 12002 is also in agreement with the theoretical value of 0.23 ± 0.06 neutron cm^{-2} sec^{-1} calculated by Armstrong and Alsmiller,[10] who averaged the solar maximum and minimum fluxes and included nominal Apollo 11 rare-earth concentrations in the lunar surface composition.

Exposure Ages

Estimates of cosmic-ray exposure ages were made on seven rocks by the ^{22}Na-^{22}Ne method[7] and agree well with ^{3}He ages from the literature. Exposure ages ranged from 48 m.y. (12013) to 251 m.y. (12064).

Rocks of relatively shorter exposure age (12002, 12004, 12013, 12053) all were collected in the Ocean of Storms north of a line connecting the north rim of Bench Crater and the center of Surveyor Crater. Rocks 12062, 12064, and 12065 have significantly longer exposure ages and were collected south of this line, which appears to be a boundary associated with Middle Crescent Crater. As shown by Warner and Anderson,[11] most of the crystalline rocks north of this diffuse boundary are porphyritic basalts, while those to the south are granular and ophitic basalts. The model proposed by Warner and Anderson to account for this distribution tentatively associated with Middle Crescent Crater suggests that the area north of the boundary would be strewn with ejecta of somewhat more recent exposure than the region to the south, which might be rich in older regolith material. Although this conclusion is speculative and is based on relatively few exposure ages, our data lend qualitative support to the model of Warner and Anderson.

1. Sponsored by the National Aeronautics and Space Administration through interagency agreements with the U.S. Atomic Energy Commission. Summary of a paper accepted for publication in *Proceedings of the Second Lunar Science Conference,* to be published in *Geochimica et Cosmochimica Acta.*

2. Director's Division.
3. Analytical Chemistry Division.
4. Instrumentation and Controls Division.
5. NASA Manned Spacecraft Center, Houston, Tex.
6. Lunar Sample Preliminary Examination Team (including P. R. Bell, J. S. Eldridge, V. A. McKay, G. D. O'Kelley, and R. T. Roseberry), *Science* **167**, 1325–39 (1970).

7. G. D. O'Kelley et al., *Proceedings of the Apollo 11 Lunar Science Conference, Geochim. Cosmochim. Acta, Suppl. 1,* vol. 2, pp. 1407–23, Pergamon, 1971.
8. R. C. Finkel et al., "Depth Variation of Cosmogenic Nuclides in a Lunar Surface Rock," *Apollo 12 Lunar Science Conference,* unpublished proceedings, 1971.
9. K. Marti and G. W. Lugmair, "^{81}Kr-Kr and K-^{40}Ar Ages, Cosmic-Ray Spallation Products and Neutron Effects in Apollo 11 and Apollo 12 Lunar Samples," *Apollo 12 Lunar Science Conference,* unpublished proceedings, 1971.
10. T. W. Armstrong and R. G. Alsmiller, Jr., "Calculation of Cosmogenic Radionuclides in the Moon and Comparison with Apollo Measurements," *Apollo 12 Lunar Science Conference,* unpublished proceedings, 1971.
11. J. L. Warner and D. H. Anderson, "Lunar Crystalline Rocks: Petrology, Geology, and Origin," *Apollo 12 Lunar Science Conference,* unpublished proceedings, 1971.

2. Chemistry and Physics of Transuranium Elements

INCLUSION OF CHARGED-PARTICLE EMISSION AND FISSION IN NUCLEAR REACTION CALCULATIONS[1]

R. L. Hahn O. W. Hermann[2]

In proton-induced reactions on actinide targets, the yields of radioactive products from reactions involving the emission of charged particles are often comparable with or larger than the yields from reactions involving only neutron emission. This observation[3–5] has prompted us to consider in detail[1,6] how to include effects due to charged-particle emission, neutron emission, and fission in existing nuclear reaction calculations.[7,8] We shall discuss here the results of these considerations, and then, in the following report,[9] compare calculated excitation functions with experimental values.[3,5]

The calculations are performed within the framework of a model that treats a nuclear reaction as an intranuclear cascade followed by compound-nucleus decay.[7,8] Because it is not clear how to treat a collective nuclear phenomenon like fission as a series of nucleon-nucleon interactions in the intranuclear cascade, we assume, as has been done by others,[4,5,10] that fission occurs only during compound-nucleus decay. However, we do not, as has been traditional, confine ourselves solely to the competition between fission and neutron emission, but perform a more general calculation that includes the possibility of charged-particle evaporation as well.

We express the cross section for evaporation from compound nucleus c of x particles, in competition with fission, as[1]

$$\sigma(c, x, f) = \sigma_c \left[\prod_{i=1}^{x} P_i\right] \left\{ \prod_{i=1}^{x} [\Gamma_n/(\Gamma_n + \Gamma_f)]_i \right\}, \quad (1)$$

where σ_c is the compound-nucleus formation cross section, $\Pi P_i = P_x$ is the probability that the x particles are evaporated, and the term in the second set of brackets is the probability that particle emission, and not fission, occurs. Note that P_x is not restricted to neutrons but can include charged-particle emission also. The form of Eq. (1) is especially useful because the competition between particle emission and fission enters as a separate factor. Existing codes[7,8] essentially calculate the cross section for evaporation of x particles, *without fission*, as

$$\sigma(c, x) = \sigma_c \left[\prod_{i=1}^{x} P_i\right]. \quad (2)$$

So it is a rather straightforward task to modify these codes to include fission effects, as in Eq. (1). We use the empirically derived formula of Sikkeland et al.[10] to evaluate (Γ_n/Γ_f) for use in Eq. (1),[1]

$$\log_{10} (\Gamma_n/\Gamma_f) = -0.276Z + \begin{matrix} 5.46 + 0.14N \text{ for } N \leqslant 153 \\ 19.23 + 0.05N \text{ for } N \geqslant 153 \end{matrix}. \quad (3)$$

For odd-Z nuclei, 0.12 must be added to the equation.

To illustrate the results of our calculations, we refer to Fig. 2.1, which presents computed excitation functions of selected reactions for the system ^{231}Pa + p. Here the curves in the left half of the figure are for the case in which no intranuclear cascade takes place; instead the incident proton is assumed to interact with ^{231}Pa to form compound nucleus ^{232}U. The case labeled "without fission" is based on the use of Eq. (2), while the results called "with fission" are calculated with Eqs. (1) and (3). The curves in the right half of Fig. 2.1 are for the case in which the intranuclear cascade first occurs, followed by decay of the resulting compound nuclei. Note that the calculations for the cascade, "with fission," consider fission competition only during the compound-nucleus part of the reaction; as mentioned above, fission is assumed not to occur during the initial cascade process.

Let us first examine the curves labeled "compound nucleus." Without fission competition, the (p,xn) cross sections peak at $\sim 10^3$ mb, while the (p,pxn) curves have maximum values of ~60 to 80 mb. When fission competition is included, all of the cross sections decrease by at least a factor of $\sim 10^3$. The $(p,5n)$ peak is now lower than the $(p,4n)$ curve because fission competition increases with the number of evaporated particles. Note

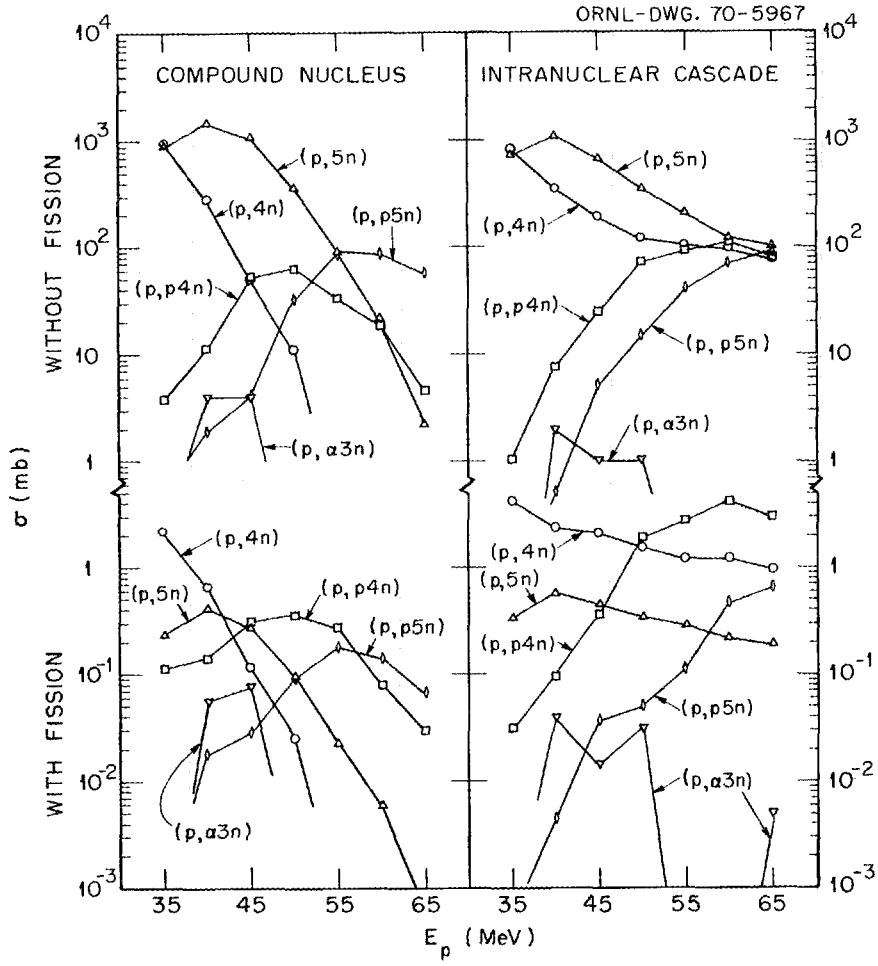

Fig. 2.1. Calculated excitation functions for selected nuclear reactions of ^{231}Pa + p. Results are shown, with and without fission competition, as obtained for compound-nucleus decay only (left side) and for the intranuclear cascade followed by compound-nucleus decay (right side).

that while the (p,pxn) cross sections have also decreased due to the effect of fission, they have not been as drastically reduced as have the (p,xn) values. In fact, the $(p,p4n)$ curve has approximately the same maximum value as the $(p,5n)$ curve, an effect associated with the decreased fissionability of the intermediate nuclei resulting from proton emission [see Eq. (3)]. The $(p,\alpha 3n)$ curve, although calculated with poor statistics, also increases relative to the (p,xn) curves when fission is included in the calculations.

The shapes of the excitation functions for the emission of charged particles change when the fission process is considered. This result occurs because several reaction paths, with ensuing different fission-competition factors, are possible in such reactions; for example, the $(p,p4n)$, $(p,d3n)$, and $(p,t2n)$ reactions all may contribute to the calculated $(p,p4n)$ curve. For (p,xn) reactions, the reaction path is uniquely determined, and so only the magnitudes, but not the shapes of the excitation functions, change when fission is allowed.

When compound-nucleus decay, without fission, is preceded by the intranuclear cascade, we notice, as shown in the upper right part of Fig. 2.1, that the (p,xn) curves have characteristic high-energy tails and that the (p,pxn) curves do not vary as rapidly with proton energy as they do when only compound-nucleus decay occurs. These results clearly are due to the fact that a distribution of excited compound nuclei are produced in the cascade instead of only ^{232}U. Note, however, that peak values of the various cross-section curves are not very different for the cases labeled "compound nucleus" and "intranuclear cascade" (without fission).

But when the fission process is also included in the cascade-plus-compound-nucleus calculation, the (p,pxn) curves are seen to increase significantly relative to the (p,xn) curves. For example, $\sigma(p,p4n) = 4$ mb and $\sigma(p,5n) = 0.6$ mb at their respective maxima. The major causes of this effect are: (1) the increase with increasing bombarding energy of the number of particles emitted during the cascade phase of the reaction, resulting in fewer particles that have to be evaporated, in competition with fission, to form a given product; (2) the large contribution of cascade protons, instead of evaporation protons, to the calculated (p,pxn) cross sections; and (3) the neglect of fission during the cascade process.

In summary, the main points of Fig. 2.1 are: (1) the cross sections for (p,pxn) reactions in the absence of fission are ≈10% of the (p,xn) values for either the pure compound-nucleus or intranuclear cascade calculations; and (2) inclusion of fission greatly enhances the (p,pxn) values relative to the (p,xn) cross sections, the increase being larger for the intranuclear cascade.

We also mention that we have enlarged the nuclear reaction calculations[7,8] so as to be able to calculate the kinetic-energy and angular distributions and ranges of product recoil nuclei. The details of these calculations are discussed in ref. 1.

Copies of these codes are available to outside users through the Radiation Shielding Information Center at ORNL.

---

1. A more detailed discussion of this subject is given by R. L. Hahn and O. W. Hermann, *Inclusion of Fission and Charged-Particle Emission in Calculations of Nuclear Reactions; Computed Energies, Angles, and Ranges of Recoil Nuclei,* ORNL-TM-3179 (Apr. 7, 1971).

2. Mathematics Division.

3. R. L. Hahn, K. S. Toth, and M. F. Roche, *Chem. Div. Annu. Progr. Rep. May 20, 1970,* ORNL-4581, p. 28.

4. E. K. Hyde, I. Perlman, and G. T. Seaborg, *The Nuclear Properties of the Heavy Elements,* vol. III, Prentice-Hall, Englewood Cliffs, N.J., 1964.

5. See, for example, M. Lefort, G. N. Simonoff, and X. Tarrago, *Nucl. Phys.* 25, 216 (1961); C. Brun and G. N. Simonoff, *J. Phys. (Paris)* 23, 12 (1962); H. Gauvin, *J. Phys. (Paris)* 24, 836 (1963); and B. Gatty, M. Lefort, and X. Tarrago, *J. Phys. (Paris)* 29, 45 (1968).

6. R. L. Hahn, *Chem. Div. Annu. Progr. Rep. May 20, 1970,* ORNL-4581, p. 30.

7. H. W. Bertini, *Phys. Rev.* **131**, 1801 (1963); also *Monte Carlo Calculations on Intranuclear Cascades,* ORNL-3383 (1963).

8. H. W. Bertini, M. P. Guthrie, and O. W. Hermann, *Instructions for the Operation of Codes Associated with MECC3, a Preliminary Version of an Intranuclear Cascade Calculation for Nuclear Reactions,* ORNL-4564 (May 1971).

9. R. L. Hahn, K. S. Toth, and M. F. Roche, "Analysis of the Interactions of Protons with ^{232}Th and ^{231}Pa," the following contribution, this report.

10. T. Sikkeland, A. Ghiorso, and M. J. Nurmia, *Phys. Rev.* **172**, 1232 (1968).

ANALYSIS OF THE INTERACTIONS OF PROTONS WITH ^{232}Th AND ^{231}Pa

R. L. Hahn K. S. Toth[1] M. F. Roche[2]

Data for the reactions of $p + {}^{231}$Pa, as presented last year,[3] led us to the consideration of nuclear reaction calculations as just described.[4] In this report we shall evaluate these calculations by comparing calculated excitation functions with data for proton-induced reactions.

Because our data for ^{231}Pa + p are not in the form of absolute cross sections, and so require additional discussion, we begin by showing the data from Lefort's group[5] at Orsay for reactions of ^{232}Th with protons. In Fig. 2.2 the points represent absolute cross sections determined by radiochemical processing of irradiated ^{232}Th targets. Because the experimental values are <100 mb, and because, as illustrated in Fig. 2.1 (previous contribution), calculated cross sections for

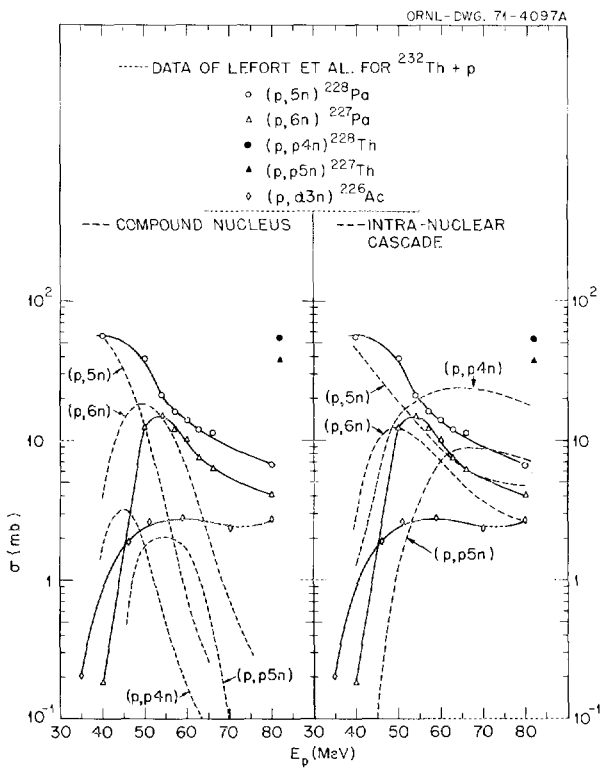

Fig. 2.2. Comparison of cross-section data of Lefort et al. (ref. 5) for ^{232}Th + p with predictions of the compound-nucleus and intranuclear cascade models. Fission competition effects were included in all calculations.

(p,xn) reactions have large values (several hundred millibarns) when fission is not considered, all of the calculated curves in Fig. 2.2 *do* include the effects of fission competition. The dashed curves on the left side of Fig. 2.2 represent the various decay modes of compound nucleus ^{233}Pa formed by the interaction of ^{232}Th + p. Although the peak values of the ($p,5n$) and ($p,6n$) excitation functions are reproduced by the calculations, the rapid decrease of the calculated curves with increasing energy does not reproduce the experimentally observed high-energy tails. And the calculated (p,pxn) curves are several orders of magnitude smaller than the two experimental points measured at 82 MeV.

The right side of Fig. 2.2 presents calculated excitation functions obtained by assuming that the reactions proceed via an intranuclear cascade (see ref. 4 for details of the calculation). Although not ideal, the fit to the data is much improved relative to the curves obtained from the compound-nucleus model alone. The high-energy tails of the (p,xn) data are indeed predicted by the calculations. And the ($p,p4n$) and ($p,p5n$) calculated curves have nonnegligible values at 82 MeV, although they are smaller than the experimental cross sections by factors of ~4 and ~6 respectively.

Note that neither assumption about the reaction mechanism, compound nucleus nor intranuclear cascade, succeeds in predicting cross sections for the ($p,\alpha 3n$) reaction that even approximate the measured values of ~2 mb; the predicted values are so small that they do not appear on the graph. This result is not unexpected for the compound-nucleus model, where Coulomb-barrier effects reduce the probability of charged-particle emission. But, as we have observed, the emission of charged particles, or at least of protons, is appreciable during the intranuclear cascade. However, only neutrons and protons can be emitted during the cascade; to explain the data, one apparently must postulate that nuclear aggregates, namely alpha particles, are also emitted during the cascade.[6]

Our data for the reactions ^{231}Pa + p, shown in Fig. 2.3, were obtained by collecting recoil nuclei ejected from the ^{231}Pa target. An angle of 34° with respect to the beam direction was subtended by the catcher foils. The experimental yields have been corrected for differences in beam intensity, bombardment time, decay after bombardment, and alpha/total branching ratios, but not for target-thickness effects. The ordinates of Fig. 2.3 are thus proportional to the product of the reaction cross section and the range of the recoil nucleus within the target.

In Fig. 2.4 we compare our calculated results with the data for ^{231}Pa + p. The effects of fission are included. Because Fig. 2.2 indicated that the intranuclear cascade improved the agreement between theory and experiment *vis-à-vis* the compound-nucleus model, the calcu-

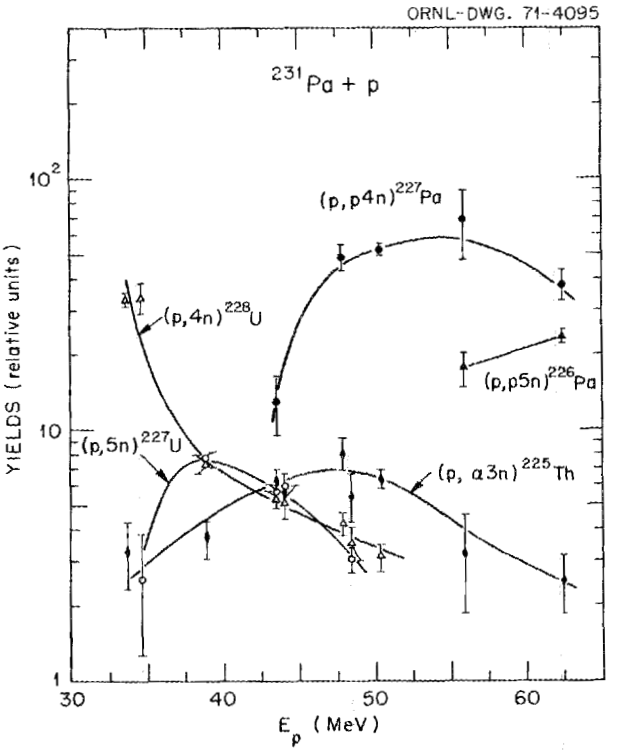

Fig. 2.3. Data obtained for the reactions ^{231}Pa + p by collecting recoil nuclei that escape from the ^{231}Pa target.

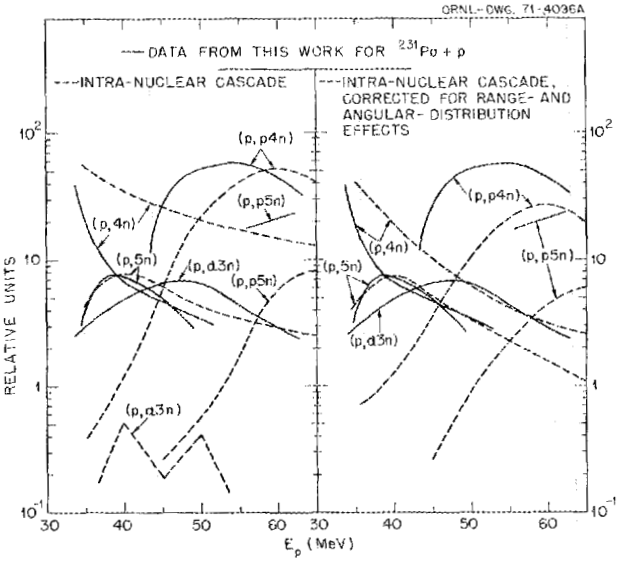

Fig. 2.4. Comparison of the intranuclear cascade calculations, including fission, with the data for ^{231}Pa + p. The curves in the right half of the figure also include effects attributable to the ranges and angular distributions of the recoil nuclei.

lated curves in Fig. 2.4 are based on the cascade model. The left side of the figure presents calculated curves that are directly proportional to reaction cross section; the calculations are normalized to the data at the peak of the $(p,5n)$ reaction. We see that the (p,pxn) reactions are correctly predicted to be predominant above 45 MeV. But the predicted high-energy tails of the (p,xn) reactions, which agree with the data so nicely in the $^{232}Th + p$ case, appear to be excessive here.

To account for this discrepancy, we calculated the angular distributions and ranges of the recoil nuclei, as discussed in ref. 4. We were thus able to take into account in our calculations how the experiments were carried out, correcting the predicted cross-section values to represent the yields of nuclei that recoiled from the target within an angle of 34° with respect to the beam. Calculated values in units of the product of cross section and recoil range are shown on the right side of Fig. 2.4; again the values have been normalized to the peak of the $(p,5n)$ data. The high-energy tailing previously obtained in the calculations has clearly diminished. And the $(p,p4n)$ and $(p,p5n)$ calculated curves, although smaller than the experimental values by factors of ~2 and ~4, respectively, are correctly predicted to have significant yields above 45 MeV. Conversely, the poor agreement between calculated and experimental $(p,\alpha 3n)$ curves is made even worse by including corrections due to recoil effects.

In summary, we note that the large yields of (p,pxn) reactions observed in the interactions of protons (<85 MeV) with ^{232}Th and ^{231}Pa can be understood in terms of a nuclear model that considers (1) that the reaction proceeds via an intranuclear cascade and (2) that fission competes with neutron and charged-particle emission during the compound-nucleus phase of the deexcitation process. Inclusion of range and angular-distribution effects allows us to consider experiments in which collimated recoil nuclei are detected.

1. Electronuclear Division.
2. Electronuclear Division; present address, Argonne National Laboratory, Argonne, Ill.
3. R. L. Hahn, K. S. Toth, and M. F. Roche, *Chem. Div. Annu. Progr. Rep. May 20, 1970*, ORNL-4581, p. 28.
4. R. L. Hahn and O. W. Hermann, "Inclusion of Charged-Particle Emission and Fission in Nuclear Reaction Calculations," the preceding contribution, this report.
5. M. Lefort, G. N. Simonoff, and X. Tarrago, *Nucl. Phys.* **25**, 216 (1961); C. Brun and G. N. Simonoff, *J. Phys. (Paris)* **23**, 12 (1962).
6. H. Gauvin, M. Lefort, and X. Tarrago, *Nucl. Phys.* **39**, 447 (1962).

COULOMB EXCITATION STUDIES OF EVEN-EVEN TRANSURANIUM NUCLEI USING ALPHA PARTICLES

C. E. Bemis, Jr. R. Robinson[1]
J. L. C. Ford, Jr.[1] F. K. McGowan[1]
P. H. Stelson[1] W. T. Milner[1]

We are using inelastically scattered alpha particles in a systematic Coulomb-excitation program to study the properties of states and the nuclear deformation of even-even transuranium nuclei. These studies are performed using 17- to 18-MeV ^4He ions accelerated in the Oak Ridge EN tandem accelerator. Inelastically scattered alpha particles from suitable targets are detected on the focal plane of an Enge split-pole spectrograph using a 20-cm-long position-sensitive proportional counter of the type designed by Borkowski and Kopp.[2,3] The position resolution of this detector is ~0.7 mm, corresponding to an energy resolution of 9 keV FWHM for 15-MeV alphas.

Isotopically pure targets are directly prepared using the 150-cm isotope separator in the Transuranium Research Laboratory. The appropriate singly charged ion beam in the separator is retarded to an energy of 4 keV and refocused to yield a target spot 0.06 cm wide by 1 cm long. This target approximates the correct source dimensions of the Enge analyzing magnet under the conditions of our experiments. Targets are usually collected on thin Ni foil and contain a total of ~1 μg of material (20 μg/cm^2).

To date we have excited the first 2^+ and 4^+ states of a number of even-even transuranium nuclei using this method. A typical spectrum is shown in Fig. 2.5 for incident 18-MeV alpha particles scattered from ^{238}U at a laboratory angle of 150°.

The measurement of a transition probability involves the determination of the ratio of an inelastic scattering peak to the elastic peak, which may be performed with great precision using our high-resolution data; extremely accurate transition probabilities may be determined as a result. Transition probabilities were determined with the aid of the Winther–de Boer computer program assuming the excitation probabilities of the 2^+ and 4^+ states obey the rotational prediction. Our $B(E2)$ value for the excitation of the 2^+ state in ^{238}U, (11.65 ± 0.06) e^2 b^2, is one of the most accurate $B(E2)$ values known.

Our preliminary results for the 2^+ excitation in ^{234}U, ^{236}U, ^{238}Pu, ^{240}Pu, ^{242}Pu, ^{244}Pu, and ^{246}Cm, determined using 17.00-MeV alphas scattered at 150°, are given in Table 2.1.

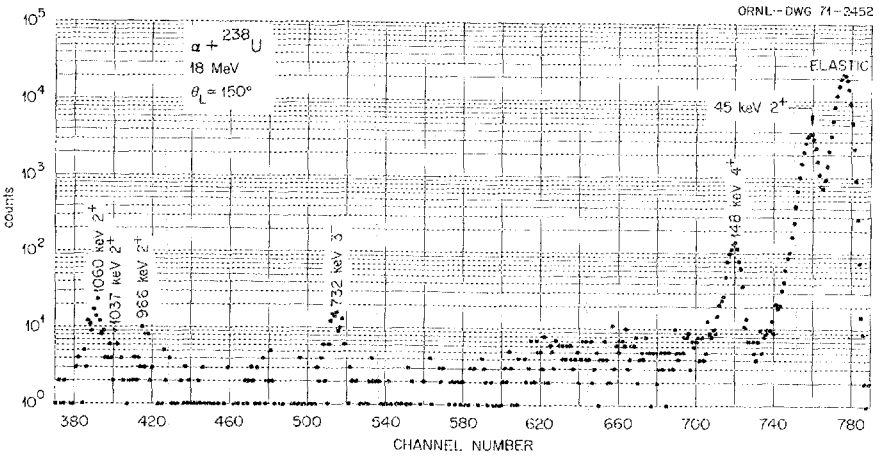

Fig. 2.5. Inelastically scattered alpha-particle spectrum at a laboratory angle of 150° for 18-MeV alphas incident on ^{238}U.

Table 2.1. Transition probabilities for the excitation of the 2_g^+ states of even-even transuranium nuclides

Nucleus	$B(E2)$ (e^2b^2)
^{234}U	10.45 ± 0.26
^{236}U	11.75 ± 0.23
^{238}U	11.65 ± 0.06
^{238}Pu	12.55 ± 0.25
^{240}Pu	12.55 ± 0.22
^{242}Pu	13.37 ± 0.24
^{244}Pu	13.81 ± 0.30
^{246}Cm	15.20 ± 0.45

The $B(E2)$ values can be related to the intrinsic quadrupole moment Q_0 of the ground state of these nuclei using the relation

$$Q_0{}^2 = \frac{16\pi}{5e^2} B(E2; 0^+ \to 2^+) .$$

The intrinsic quadrupole moments in turn may be interpreted directly in terms of the nuclear deformation. We have combined the results of our work with the published data of other workers in Fig. 2.6, which shows the intrinsic quadrupole moments as a function of A. The increase in nuclear deformation from $A = 220$ to 250 as determined by the magnitude of Q_0 is striking. Our experiments are being extended to include the higher transuranics ^{244}Cm, ^{248}Cm, ^{250}Cf, and ^{252}Cf, as well as to provide more accurate data below uranium by inclusion of ^{226}Ra, ^{228}Ra, ^{228}Th, ^{230}Th, ^{232}Th, and ^{232}U.

1. Physics Division.

2. C. J. Borkowski and M. K. Kopp, *Rev. Sci. Instrum.* **39**, 1515 (1968).

3. C. J. Borkowski and M. K. Kopp, *IEEE Trans. Nucl. Sci.* **NS17**(3), 340 (1970).

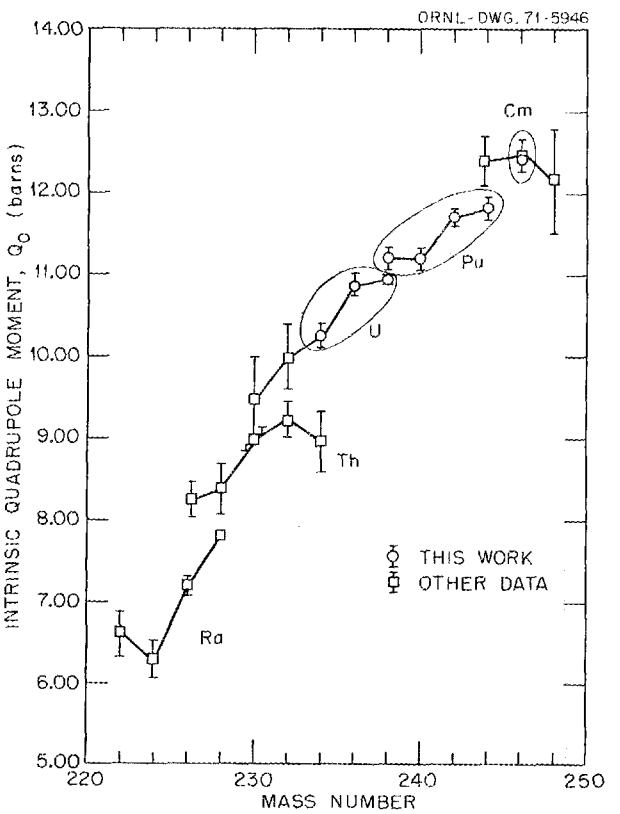

Fig. 2.6. Intrinsic quadrupole moments for the ground states of even-even nuclei as determined from experimental $B(E2; 0^+ \to 2^+)$ values. Our data are represented by the circles and those of others by boxes.

PROPERTIES OF GROUND-STATE ROTATIONAL BANDS OF HEAVY EVEN-EVEN NUCLEI

C. E. Bemis, Jr. M. J. Zender[1] M. R. Schmorak[2]

The use of small ultrahigh-resolution Ge(Li) detectors has enabled us to measure the weak gamma rays following the alpha decay of even-even nuclei in the transuranium element region. For the cases investigated, it has been possible to observe directly the $E2$ deexcitation gamma rays in the daughter ground-state rotational bands up to spin 8^+ in ^{234}U and ^{236}U. Alpha-decay branching to these states ($l = 8$) is typically of the order of 1 part in 10^7 alpha decays. We have used high-isotopically-enriched sources (≥99.99% by mass) of the parent activity to avoid interferences from other radioactivities in the measurements. For all cases studied the $2^+ \rightarrow 0^+$ gamma-ray energy could be determined to an accuracy of ~10 eV and the $4^+ \rightarrow 2^+$ and higher-order transitions to similar accuracies. The determination of alpha-branching ratios to states in the ground-state bands was accomplished by measuring the absolute gamma-ray intensities from sources whose absolute disintegration rate was measured by alpha counting in a calibrated low-geometry alpha chamber or by normalization of relative gamma-ray intensities to previously determined alpha branching to the 2^+ states. Our results

Table 2.2. Alpha branches to ground-state rotational bands

Final nucleus	J^π	I_α(%), this work	I_α(%), NDS[a]	Alpha hindrance factor[b]	α_T[c]
^{232}Th	2^+	(26)	26	1.19	337
	4^+	0.15 ± 0.02	0.26	27.3	6.9
^{234}U	2^+	(28.4)	28.4	1.4	746
	4^+	0.091 ± 0.005	0.11	117	13.7
	6^+	0.0024 ± 0.0002	0.005	540	2.17
	8^+	$(1.2 \pm 0.2) \times 10^{-5}$	8.6×10^{-6}	5700	0.738
^{236}U	2^+	(24)	24	1.65	612
	4^+	0.096 ± 0.005	0.091	90	11.2
	6^+	0.0012 ± 0.0003	0.002	610	1.78
	8^+	$(2.9 \pm 0.4) \times 10^{-5}$		8000	0.60
^{238}U	2^+	(21.1)	21.1	1.9	635
	4^+	0.090 ± 0.009		83	11.6
	6^+	0.0012 ± 0.0004		440	1.85
^{240}Pu	2^+	(23.6)	23.6	1.91	932
	4^+	0.027 ± 0.003	0.02	440	17.1
	6^+	0.0036 ± 0.0004	0.0034	500	2.51
	8^+		$\approx 4 \times 10^{-5}$		

[a]From a recent compilation of M. Schmorak and Y. A. Ellis, *Nuclear Data Sheets*, B4-6-1970.

[b]The hindrance factors were calculated from our experimental alpha branches using the technique described in the introduction to *Nuclear Data Sheets*, B5-3-1971.

[c]The total internal conversion coefficients used for deriving the alpha branching from the gamma intensities are calculated from the tables of L. A. Sliv and I. M. Band, in *Alpha-, Beta-, and Gamma-Ray Spectroscopy*, K. Siegbahn, ed., vol. 2, p. 1639, North-Holland, Amsterdam, 1965.

Table 2.3. Gamma-ray energies (in eV) for transitions within the ground-state bands of heavy even-even nuclei

Transition	^{232}Th	^{234}U	^{236}U	^{238}U	^{240}Pu
$2^+ \rightarrow 0^+$	49,369 ± 9	43,491 ± 9	45,242 ± 6	44,915 ± 13	42,824 ± 8
$4^+ \rightarrow 2^+$	112,750 ± 15	99,850 ± 10	104,233 ± 5	103,499 ± 35	98,860 ± 13
$6^+ \rightarrow 4^+$		152,719 ± 19	160,310 ± 8	158,800 ± 80	152,630 ± 20
$8^+ \rightarrow 6^+$		201,000 ± 60	212,400 ± 100		

Table 2.4. Comparison of experimental level energies with predictions of the rotational model (BM) and the variable moment of inertia (VMI) model

J^π	Experimental E (keV)	Experimental $\pm\Delta E$ (eV)	Least squares adjusted E (calc), VMI (keV)	Least squares adjusted E (calc), BM (keV)
			^{232}Th	
2^+	49.369	9	49.385	49.239
4^+	162.119	18	162.096	162.286
6^+	333.7	550	333.16	333.72
8^+	556.9	700	556.81	559.6
10^+	827.8	1000	827.56	827.4
12^+	1138.5	1000	1140.61	1126.2
14^+			1491.87	
			$\sigma^2 = 2.6$	$\sigma^2 = 98$
			$g_0 = 0.0603$	$A = 8.246$
			$C = 0.933$	$B = -6.58$
			^{236}U	
2^+	45.242	6	45.250	45.215
4^+	149.475	8	149.473	149.479
6^+	309.785	13	309.775	309.816
8^+	522.185	100	522.42	521.55
10^+			783.42	
12^+			1088.94	
14^+			1435.46	
			$\sigma^2 = 3.9$	$\sigma^2 = 33$
			$g_0 = 0.0660$	$A = 7.562$
			$C = 1.265$	$B = -4.42$
			^{240}Pu	
2^+	42.824	8	42.822	42.811
4^+	141.684	15	141.688	141.707
6^+	294.314	25	294.312	294.302
8^+	500	3000	497.65	497
10^+			748.34	
12^+			1043.03	
14^+			1378.55	
			$\sigma^2 = 0.38$	$\sigma^2 = 2.3$
			$g_0 = 0.0698$	$A = 7.156$
			$C = 1.325$	$B = -3.55$

J^π	Experimental E (keV)	Experimental $\pm\Delta E$ (eV)	Least squares adjusted E (calc), VMI (keV)	Least squares adjusted E (calc), BM (keV)
			^{234}U	
2^+	43.491	9	43.513	43.423
4^+	143.341	14	143.344	143.318
6^+	296.060	24	295.989	296.269
8^+	497.077	40	497.147	496.904
10^+			742.46	
12^+			1027.92	
14^+			1350.00	
			$\sigma^2 = 9.0$	$\sigma^2 = 77.1$
			$g_0 = 0.0686$	$A = 7.268$
			$C = 0.851$	$B = -5.08$
			^{238}U	
2^+	44.915	12	44.930	44.835
4^+	148.414	37	148.353	148.361
6^+	307.214	87	307.272	307.96
8^+	518.3	550	517.85	519.52
10^+	776.6	800	776.05	777.44
12^+	1077.8	1000	1077.97	1074.62
14^+	1416.8	2500	1420.11	1402.4
			$\sigma^2 = 1.5$	$\sigma^2 = 19.5$
			$g_0 = 0.0665$	$A = 7.496$
			$C = 1.179$	$B = -3.89$

Notes: $E_{BM} = AJ(J+1) + BJ^2(J+1)^2$, A in keV, B in eV.

$$E_{VMI} = \tfrac{1}{2}C(g-g_0)^2 + \frac{J(J+1)}{2g}, \frac{\partial E}{\partial g} = 0, g \text{ in keV}^{-1}, C \text{ in } 10^6 \text{ (keV)}^3.$$

$$\sigma^2 = \frac{\chi^2}{\text{D.F.}} = \Sigma \frac{[E_i(\text{calc}) - E_i(\text{exp})]^2}{(\Delta E_i)^2} \Big/ (\text{number of levels} - 2).$$

for the alpha branching to the ground-state bands in ^{232}Th, ^{234}U, ^{236}U, ^{238}U, and ^{240}Pu are summarized in Table 2.2. Gamma-ray abundances were corrected for internal conversion to yield total transition intensities and hence the alpha-decay branching.

Using our accurately measured gamma-ray transition energies as listed in Table 2.3, we have compared the energies of the states in the ground-state bands with predictions of the second-order rotational model prescription of Bohr-Mottelson[3] (BM) and with the variable moment of inertia prescription (VMI) of Mariscotti, Scharff-Goldhaber, and Buck.[4] We have used least-squares fitting techniques to obtain the best fits to the experimental data. Since both prescriptions contain two adjustable parameters, the goodness of fit should provide which of the models is better. We have combined our results with the Coulomb excitation results of Stephens, Diamond, and Perlman[5] for ^{232}Th and ^{238}U to provide data on higher spin members of the ground-state bands for these cases. The comparison of the experimental level energies with the predictions of the BM and VMI models is given in Table 2.4. The values for σ^2, which is a criterion for the goodness of fit, dramatically favor the VMI prediction. Our results are being prepared for publication.

1. Oak Ridge Associated Universities Research Participant from Fresno State College, Fresno, Calif., summer 1969.
2. Nuclear Data Project.

3. A. Bohr and B. Mottelson, *At. Energ.* **14**, 41 (1961).
4. M. A. J. Mariscotti, G. Scharff-Goldhaber, and B. Buck, *Phys. Rev.* **178**, 1864 (1969).
5. F. S. Stephens, Jr., R. M. Diamond, and I. Perlman, *Phys. Rev. Lett.* **3**, 435 (1959).

MULTIPLE COULOMB EXCITATION OF HEAVY ELEMENTS WITH ORIC HEAVY-ION BEAMS[1]

E. Eichler — R. O. Sayer[2]
N. R. Johnson — D. C. Hensley[3]
C. E. Bemis, Jr. — M. R. Schmorak[4]

The Coulomb excitation program initiated last year at the Oak Ridge Isochronous Cyclotron to investigate collective properties of nuclei in the little-explored actinide region has borne fruit this year. Beams of 80-MeV ^{16}O ions, 100-MeV ^{20}Ne ions, and 145-MeV ^{40}Ar ions from the new ORIC heavy-ion source[5] were used to populate levels up to the 12^+ state in the ground-state rotational bands of ^{238}U and ^{242}Pu. Previously, only the first excited state of ^{242}Pu was known.

Large-volume Ge(Li) detectors were used to observe the deexcitation gamma rays in singles and in coincidence with heavy ions backscattered into an annular Si surface barrier counter. A high-resolution Ge(Li) x-ray detector was also used to study the lower-energy transitions.

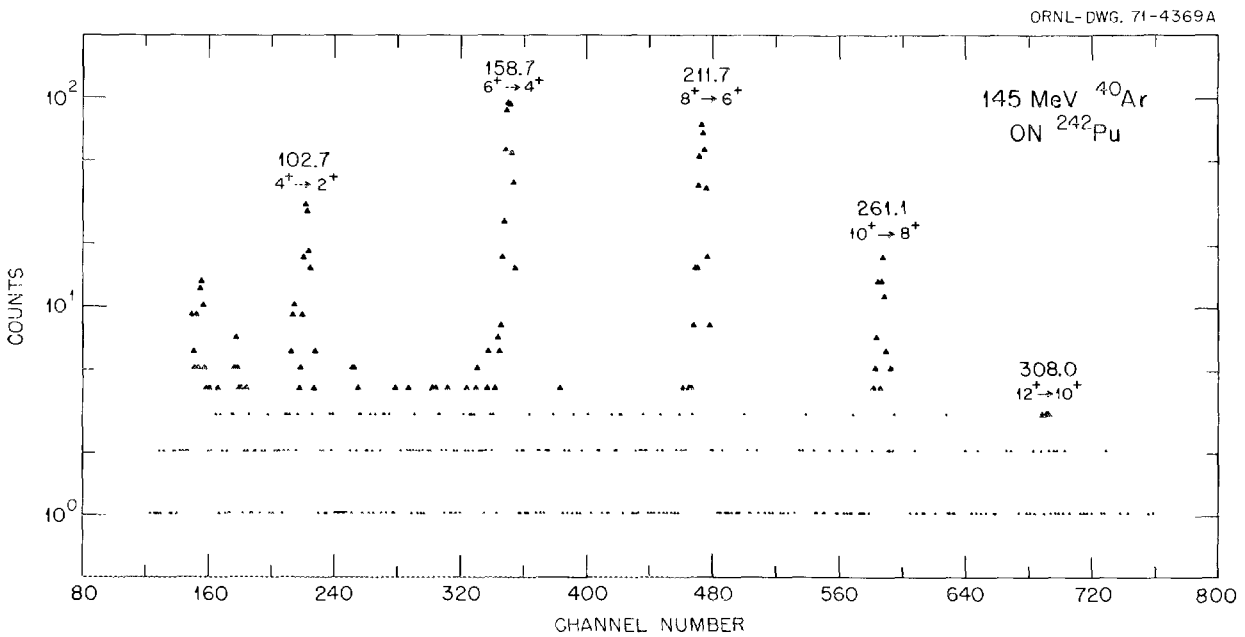

Fig. 2.7. Gamma spectrum from states in ^{242}Pu Coulomb excited by 145-MeV ^{40}Ar.

Targetry presents special problems with the heavy elements. There are ten nuclides in this region with $t_{1/2}$ > 5000 years and thus suitable for Coulomb excitation. However, only the thorium and uranium isotopes are now available in sufficient quantities for preparation of metallic self-supporting targets. One achievement of the year was our successful use of a 400-μg/cm^2 $^{242}PuO_2$ target deposited on a 0.1-mg/cm^2 Ni backing. This kind of target can be studied only by the heavy-ion-backscatter–coincidence method.

Our primary goal is to measure ground-state rotational band energies and transition rates for all available heavy element targets. Very accurate energies were obtained for the $4 \rightarrow 2$ and $6 \rightarrow 4$ transitions in ^{238}U and ^{232}Th with the high-resolution x-ray detector in the singles mode. Energies for levels up to the 12^+ state in ^{238}U and ^{242}Pu were measured with the large Ge(Li) detectors in ^{16}O-gamma experiments. In Fig. 2.7 is shown a spectrum of gamma rays in coincidence with 145-MeV ^{40}Ar ions backscattered from a ^{242}Pu target.

Table 2.5 presents the ground-band energies for ^{232}Th, ^{238}U, and ^{242}Pu determined from our best data and those of refs. 6 and 8. The experimental energies are compared with energies predicted by a two-parameter version of the Bohr-Mottelson[9] formula and with those predicted by the variable moment of inertia (VMI) model of Mariscotti, Scharff-Goldhaber, and Buck,[10] also a two-parameter fit. All energy levels were used in the least-squares fit. The VMI predictions agree extremely well with experiment: usually better than 100 eV. Only with ^{242}Pu does the BM approach give comparable – though still inferior – accuracy.

The singles spectra from ^{20}Ne Coulomb excitation of ^{238}U revealed 13 states in the octupole, β, and γ vibrational bands.[7,11]

Table 2.5. Ground-state rotational levels in ^{232}Th, ^{238}U, and ^{242}Pu

J^π	E (keV), experimental	VMI		BM	
		E_{calc} (keV)	Diff.	E_{calc} (keV)	Diff.
		^{232}Th			
2^+	49.37 ± 0.01[a]	49.39	0.02	49.24	0.13
4^+	162.12 ± 0.02[a]	162.09	−0.03	162.29	0.17
6^+	333.12 ± 0.06	333.12	0.00	333.72	0.60
8^+	556.9 ± 0.6[b]	556.70	−0.2	559.6	2.70
10^+	827.2 ± 0.7[b]	827.33	0.1	827.4	0.20
12^+	1137.9 ± 1.2[b]	1140.19	2.3	1126.2	11.7
		^{238}U			
2^+	44.92 ± 0.01[a]	44.93	0.01	44.85	−0.07
4^+	148.29 ± 0.05	148.31	0.02	148.30	0.01
6^+	307.13 ± 0.07	307.10	−0.03	307.48	0.35
8^+	517.54 ± 0.12	517.42	−0.12	517.90	0.36
10^+	775.33 ± 0.16	775.17	−0.16	773.43	−1.9
12^+	1074.8 ± 0.6	1076.45	1.6	1066.3	−8.5
14^+	1414.0 ± 2.0[b]	1417.71	3.7	1387.0	−27.0
		^{242}Pu			
2^+	44.50 ± 0.06	44.49	−0.01	44.39	−0.11
4^+	147.25 ± 0.12	147.24	−0.01	147.12	−0.13
6^+	305.95 ± 0.16	305.99	0.04	306.12	0.17
8^+	517.67 ± 0.19	517.66	−0.01	518.19	0.52
10^+	778.8 ± 0.6	778.87	0.07	778.92	0.12
12^+	1086.8 ± 2.0	1086.19	−0.6	1082.8	−4.0

[a]Reference 6.

[b]Reference 8.

1. A preliminary account of this work appeared in *Electronucl. Div. Annu. Progr. Rep. Dec. 31, 1970*, ORNL-4649, p. 69.
2. Physics Department, Furman University, Greenville, S.C.
3. Electronuclear Division.
4. Nuclear Data Project.
5. E. D. Hudson, M. L. Mallory, and S. W. Mosko, *High Performance Heavy-Ion Source for Cyclotrons*, ORNL-TM-3391 (May 1971).
6. C. E. Bemis, Jr., M. R. Schmorak, and M. J. Zender, *Phys. Rev.*, to be published; also C. E. Bemis, Jr., M. J. Zender, and M. R. Schmorak, "Properties of Ground-State Rotational Bands of Heavy Even-Even Nuclei," the preceding contribution, this report.
7. F. K. McGowan, W. T. Milner, R. L. Robinson, and P. H. Stelson, *Bull. Amer. Phys. Soc.* **16**, 493 (1971).
8. F. S. Stephens, R. M. Diamond, and I. Perlman, p. 208 in *Coulomb Excitation*, ed. by K. Alder and A. Winther, Academic, New York, 1966.
9. A. Bohr and B. R. Mottelson, *At. Energ.* **14**, 41 (1961).
10. M. A. J. Mariscotti, G. Scharff-Goldhaber, and B. Buck, *Phys. Rev.* **178**, 1864 (1969).
11. Th. W. Elze and J. R. Huizenga, *Bull. Amer. Phys. Soc.* **16**, 537 (1971).

CHARGED PARTICLES FROM HIGH-ENERGY OXYGEN-ION-INDUCED REACTIONS[1]

J. B. Ball[2] R. L. Hahn
C. E. Bemis, Jr. R. L. Robinson[3]
J. L. C. Ford, Jr.[3] K. S. Toth[2]

Although heavy ions promise a number of unique advantages for nuclear physics, heavy-ion reactions are still relatively unexplored, particularly at higher energies. The reaction mechanisms involved, the dependence of the emitted masses on the energy and masses of the colliding nuclei, and the character of the states excited are largely open questions. The present report concerns measurements with the high-energy oxygen beam of the Oak Ridge Isochronous Cyclotron in a study of the above problems.

In the initial experiments, a 140-MeV ^{16}O beam was used to bombard targets of ^{46}Ti, ^{116}Cd, and ^{238}U. Reaction products were detected at laboratory angles of 20, 25, 35, and 45°. The emitted masses were identified by a $dE/dx \times E$ counter telescope consisting of 26- and 300-μ-deep semiconductor detectors. Measurements were made with and without a biased amplifier following the E detector amplifier. The data were accumulated in a 50 × 400 channel $\Delta E \times E$ matrix in the memory of the 20,000-channel Victoreen analyzer. A photograph of the cathode ray tube display appears in Fig. 2.8, showing the data from the $^{16}O + {}^{238}U$ reaction at an angle of 25°. The groups correspond to the isotopes of He, Li, Be or B, C, N, O, F, and Ne as one moves along the y or ΔE axis. However, the resolution of the system was not adequate to separate different isotopes of a given atomic number. Evidently, the nuclear system formed at these energies can fragment into many different nuclear species. The heaviest emitted mass observed in such spectra decreased as the target mass decreased. Thus, while Na was observed in the $^{16}O + {}^{238}U$ data, Ne was the heaviest mass identified in the ^{116}Cd irradiation.

The energy spectra accumulated at a laboratory angle (θ_L) of 20° for the C, N, O, and F isotopes emitted from the ^{116}Cd target are shown in Fig. 2.9. The energy resolution was about 750 keV and is apparently largely due to the target thickness of 200 $\mu g/cm^2$ and the entrance aperture of the detector. Despite the poor statistics, peaks were observed in the oxygen and nitrogen spectra at all θ_L except 45°. The highest-energy peak in the nitrogen spectrum occurs at an energy corresponding to the ground-state group from the $^{116}Cd(^{16}O,{}^{15}N)$ reaction. The strongest peak observed in the oxygen spectrum after that due to elastic scattering may be attributed to the $(^{16}O,{}^{17}O)$ reaction. However, these peaks may also be due to excitation of high-lying states in other reaction channels, and further work must be done to determine their origin.

Fig. 2.8. Multiparameter-analyzer CRT display of $\Delta E \times E$ data from the $^{16}O + {}^{238}U$ reaction at an angle of 25°. The loci correspond to the isotopes of He, Li, Be or B, C, N, O, F, and Ne as one moves along the y or ΔE axis.

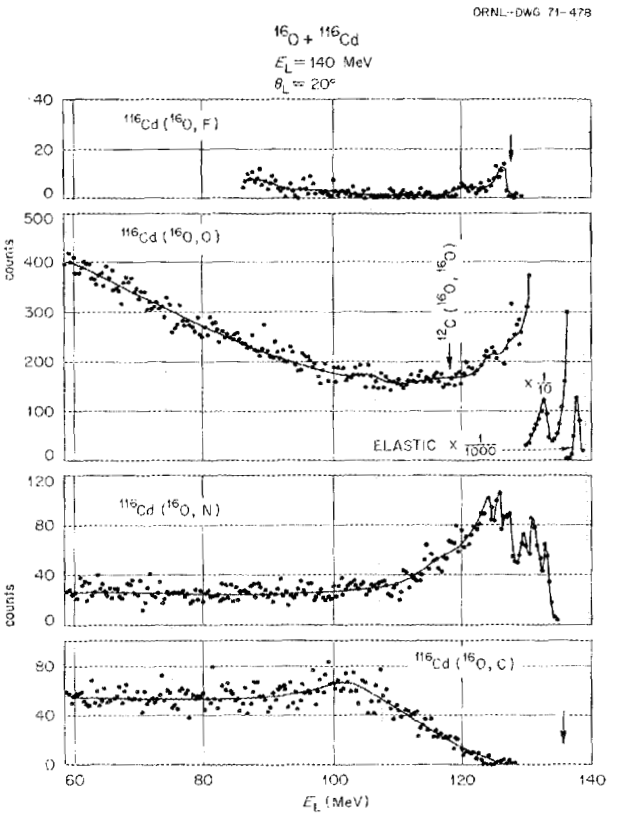

Fig. 2.9. Energy spectra of C, N, O, and F products from the $^{16}O + ^{116}Cd$ reaction at 140 MeV.

No discernible structure appeared in the carbon and fluorine data which was reproducible from angle to angle except for the peak at the high-energy end of the fluorine spectrum. The arrows in Fig. 2.9 indicate the energies at which the ground-state groups from the (^{16}O,^{12}C) and (^{16}O,^{17}F) reactions are expected. The peak in the fluorine spectrum occurs about 1.4 MeV below the ground-state group. Similar peaks have been observed in other (^{16}O,F) reactions at comparable energies and were attributed to a grazing-reaction mechanism rather than compound-nucleus formation.[4]

The (^{16}O,^{12}C) reaction is a particularly interesting one, as it can proceed by an alpha-particle transfer. The absence of any structure in this reaction near the ground state accompanied by a large yield corresponding to highly excited states has been reported in other (^{16}O,^{12}C) work.[5]

The relative cross sections for the Li, Be or B, C, N, O, and F isotopes emitted from the ^{116}Cd target and detected at an angle of 25° are shown in Fig. 2.10. Note that the oxygen value does not include the contribution of the elastic peak. The angular distributions for O, N, and C from the ^{116}Cd target appear in Fig. 2.11. The absolute cross-section scale for C and N was established by normalizing the ^{16}O elastic-peak data to the calculated Rutherford scattering cross section. Of interest is the fact that the data do not display any structure but rather decrease exponentially with increasing angle: an order of magnitude decrease in 10 to 15°. This feature of heavy-ion reactions has been noted in other types of reactions and limits the nuclear structure information which can be obtained from such angular distributions.[6,7] The elastic scattering is expected to decrease exponentially beyond about 20° as Fresnel diffraction effects begin to dominate the cross section.[8]

This survey of heavy-ion transfer reactions is being expanded to include additional heavy targets, such as ^{206}Pb, ^{207}Pb, and ^{209}Bi. More complete angular distributions than presented here will be obtained, as will excitation functions. Other projectile ions available at ORIC, such as ^{12}C, ^{14}N, and ^{20}Ne, will also be employed. Finally, use of the broad-range mass spectro-

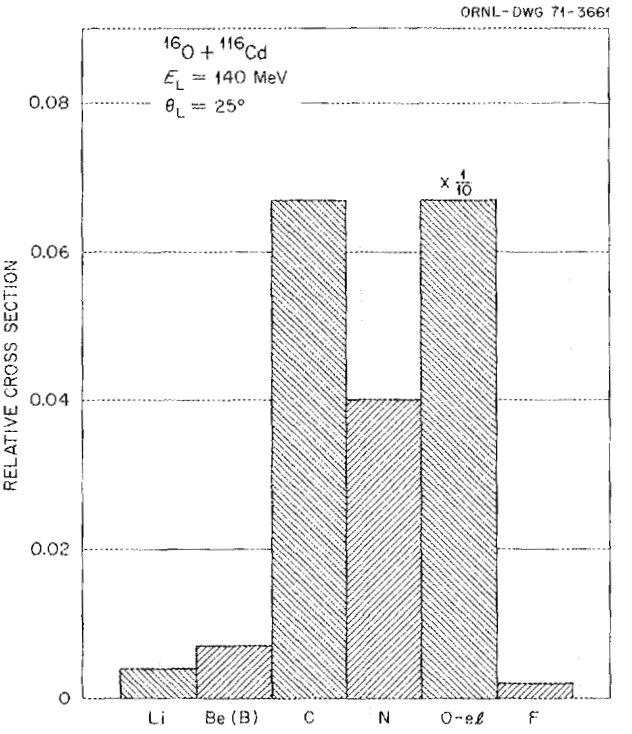

Fig. 2.10. Relative cross sections at an angle of 25° for the emission of Li, Be or B, C, N, O (excluding elastic scattering), and F from the ^{116}Cd target.

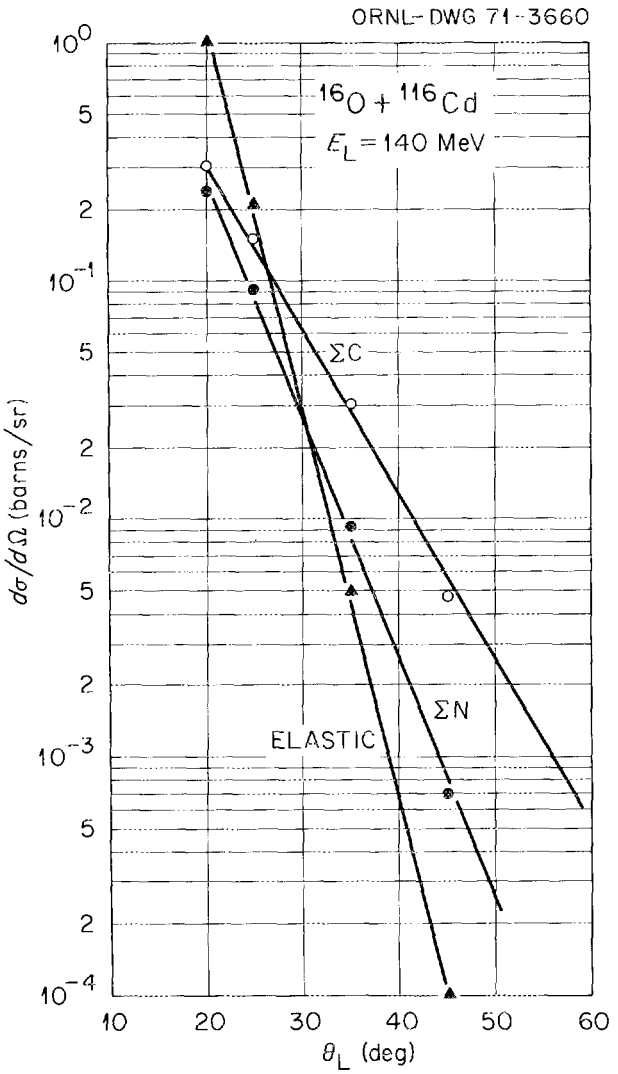

Fig. 2.11. Angular distribution of C, N, and elastically scattered O from the ^{116}Cd target. The ordinate scale refers to the C and N data; for the elastic peak, the values are given relative to the cross sections for Rutherford scattering.

graph with position-sensitive detectors should markedly improve mass and energy resolution and should simplify the interpretation of these interesting reactions.

1. Prior reports on this work have appeared in *Electronucl. Div. Annu. Progr. Rep. Dec. 31, 1970,* ORNL-4649, p. 61, and *Phys. Div. Annu. Progr. Rep. Dec. 31, 1970,* ORNL-4659, p. 49.
2. Electronuclear Division.
3. Physics Division.
4. C. F. Grindnev, V. V. Volkov, and J. Wilczynski, *Nucl. Phys. A* **142**, 385 (1970).
5. J. C. Faivre et al., *Phys. Rev. Lett.* **24**, 1188 (1970).
6. M. W. Sachs, C. Chasman, and D. A. Bromley, *Phys. Rev.* **139**, B92 (1965).
7. J. Birnbaum, J. C. Overley, and D. A. Bromley, *Phys. Rev.* **157**, 787 (1967).
8. W. E. Frahn, *Nucl. Phys.* **75**, 577 (1966).

STUDIES OF (H.I., αxn) REACTIONS[1]

R. L. Hahn K. S. Toth[2]
P. F. Dittner O. L. Keller
P. J. Hammons

The cross sections of (H.I.,xn) reactions of actinide elements characteristically are small, from microbarns to nanobarns, because of the strong competition between fission and nucleon emission. However, it has been observed at Berkeley[3] and at Dubna[4] that, in some instances, heavy-ion reactions involving charged-particle emission, specifically (H.I.,αxn), have yields that are much larger than those of the corresponding (H.I.,xn) reactions. (We must note here that the terminology "αxn" does not necessarily mean that alpha particles are always emitted in the reaction. Because only the radioactive products have been observed, it is also possible that particles such as ^{3}He or ^{6}He, or perhaps two protons, are emitted.) Because of the possible significance of such reactions for the production of very heavy new isotopes and for the elucidation of the mechanisms of heavy-ion reactions with heavy elements, we have begun a program to study (H.I.,αxn) reactions.

To date, we have measured excitation functions by the gas-jet technique[5] for the following reactions that all lead to ^{245}Cf and ^{244}Cf: ^{238}U(^{12}C, $5n$ and $6n$), ^{239}Pu(^{12}C, $\alpha 2n$ and $\alpha 3n$), ^{235}U(^{16}O, $\alpha 2n$ and $\alpha 3n$), ^{237}Np(^{14}N, $\alpha 2n$ and $\alpha 3n$), and, to some extent, ^{233}U(^{18}O, $\alpha 2n$ and $\alpha 3n$). The data for the (H.I.,αxn) reactions indicate that $\sigma(^{12}C) > \sigma(^{16}O) > \sigma(^{14}N)$. This trend is interpreted as evidence for the dependence of the cross section upon the nature of the fragment that is transferred into the nucleus.

In addition to the relative measurements made with the gas-jet system, absolute cross-section values for the ^{238}U(^{12}C,xn) and ^{239}Pu(^{12}C,αxn) reactions were determined in experiments in which thick targets were irradiated and the resultant Cf activities chemically purified for alpha-particle counting. The excitation functions for the ^{238}U + ^{12}C reactions were found to be similar to data presented by Sikkeland et al.[6] and to be consistent with expectations based on the compound-nucleus model.[6,7]

The results of a preliminary analysis of the ^{239}Pu + ^{12}C data are presented in Fig. 2.12. We note that the

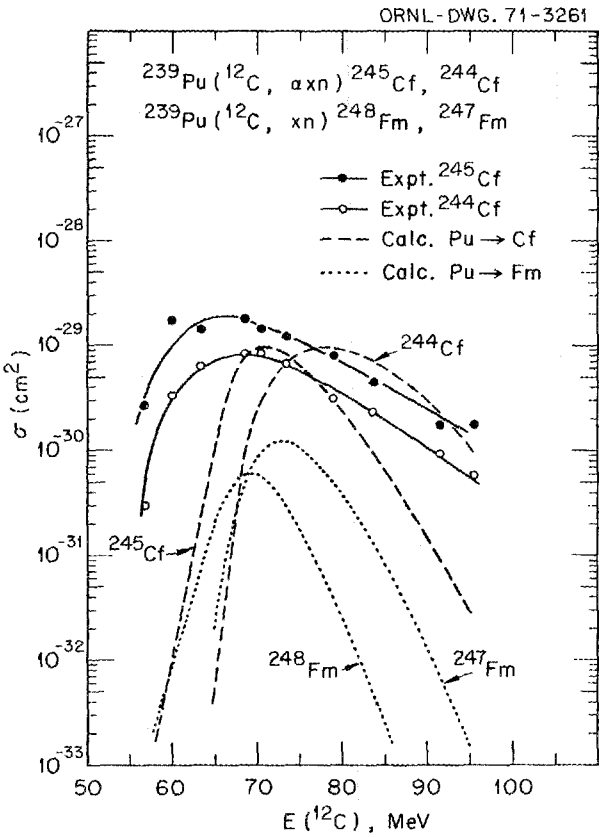

Fig. 2.12. Experimental and calculated excitation functions for ^{239}Pu(^{12}C,αxn) reactions leading to ^{245}Cf and ^{244}Cf, and calculated excitation functions for the ^{239}Pu(^{12}C,xn)^{248}Fm, ^{247}Fm reactions.

^{239}Pu(^{12}C,αxn) peak cross sections are ~10 μb. Experiments carried out with the gas-jet system to measure the cross sections of Fm nuclides from the ^{239}Pu(^{12}C,xn) reaction did not yield any activities ascribable to Fm isotopes. From the upper limits on Fm production derived from these experiments, we conclude that the yields of the (^{12}C,αxn) reactions on ^{239}Pu are ~50 to 300 times larger than the corresponding (^{12}C,xn) reactions.

Calculated curves for the (^{12}C,xn) and (^{12}C,αxn) reactions on ^{239}Pu are also shown in Fig. 2.12. The dotted curves for ^{248}Fm and ^{247}Fm are based on the compound-nucleus model, including the effects of competition between neutron evaporation and fission.[7] While not as low as our estimated upper limit values, the calculated peak cross sections for the Fm nuclides are ~1 μb, an order of magnitude smaller than the experimental Cf yields. This observation is important because the probability of charged-particle emission from heavy compound nuclei is small due to the large Coulomb barriers involved; the model predicts σ(H.I.,xn) $\gg$ σ(H.I.,αxn). Thus, the relatively large measured (^{12}C,αxn) cross sections must be ascribed to non-compound-nucleus processes.

In an initial attempt to treat (H.I.,αxn) reactions on heavy nuclei, Sikkeland[8] has constructed a model containing the following salient points:

1. compound-nucleus formation from target + projectile occurs only for those angular-momentum components of the projectile that are below a cutoff value l_c;
2. grazing collisions occur above l_c;
3. in a grazing encounter, part of the incoming heavy ion can be transferred to the target nucleus, leaving an alpha particle behind as one of the products of the reaction (e.g., if ^{12}C is the projectile, ^{8}Be transfers to the target);
4. the nucleus so formed by the transfer is treated as a compound nucleus, with neutron emission and fission as its main modes of decay.

The results of a calculation with this model for the ^{239}Pu(^{12}C,αxn) reaction are shown as the dashed curves in Fig. 2.12. We see that the calculation approximately reproduces the magnitudes of the observed (^{12}C,αxn) cross sections and indeed predicts much larger cross sections than for the corresponding (^{12}C,xn) reactions.

To learn more about the mechanisms of these reactions, we have recently begun to investigate their characteristics in greater detail. Initial experiments involved measuring the recoil-range distributions of ^{245}Cf produced in ^{238}U(^{12}C,5n) and ^{239}Pu(^{12}C,α2n) reactions at 67 MeV. Stacks of thin carbon foils, each 20 or 40 μg/cm^2, were placed directly behind the targets to collect the Cf recoils. The data from these early measurements, which sampled the angular interval from 0 to 10° with respect to the ^{12}C beam, are shown in Fig. 2.13. The relative alpha activity due to ^{245}Cf observed in each catcher foil is plotted vs total catcher thickness. Since recoil range is a function of recoil energy, these data reflect the kinetic energy distributions of the recoiling nuclei and so yield information about the reaction mechanisms involved.

For example, the range distribution for the ^{238}U(^{12}C,5n) reaction is observed to be approximately symmetrical, with an average value of ~150 μg/cm^2. Now, if the interaction of ^{238}U with a 67-MeV ^{12}C ion forms a compound nucleus, its range in carbon is expected to be 145 μg/cm^2. But, because of small contributions to the motion of the recoiling nucleus

from the neutrons, which are emitted symmetrically about 90° in the center-of-mass system, with a Maxwellian energy distribution, the final recoiling nucleus will be characterized by a symmetric distribution of ranges centered about an average value $\gtrsim$145 μg/cm^2. This description clearly fits our data; we conclude that the ^{238}U(^{12}C,5n) reaction proceeds via compound-nucleus formation and decay.

The range distribution for the ^{239}Pu(^{12}C,α2n) reaction, also given in Fig. 2.13, is striking because it differs from that for the ^{238}U + ^{12}C case. The average range for ^{239}Pu + ^{12}C is $\gtrsim$160 μg/cm^2, and there is a pronounced skewness in the distribution at large ranges, whereas no activity was observed above 240 μg/cm^2 in the uranium experiment.

These qualitative differences between the range distributions shown in Fig. 2.13 indicate that some other mechanism besides (or in addition to) compound-nucleus formation is operative in the (^{12}C,αxn) reaction. More data for this reaction are clearly needed.

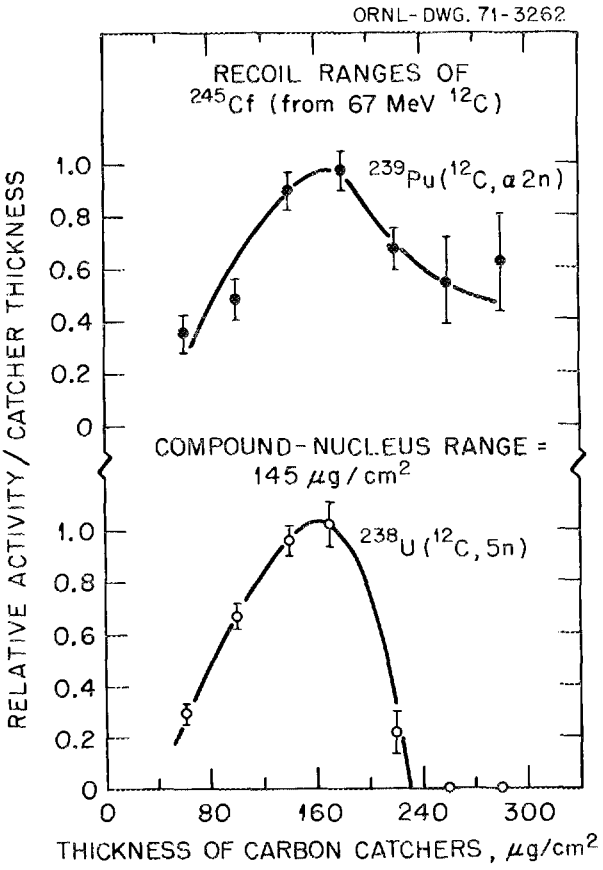

Fig. 2.13. Recoil range distributions measured at an angle of 0° for ^{245}Cf produced in the ^{238}U(^{12}C,5n) and ^{239}Pu(^{12}C,α2n) reactions.

Accordingly, in future experiments we shall determine the angular distribution of the ^{245}Cf recoils as well as measure the range distributions at angles other than 0° and at energies >67 MeV.

1. A preliminary account of this work appeared in *Electronucl. Div. Annu. Progr. Rep. Dec. 31, 1970*, ORNL-4649, p. 69.
2. Electronuclear Division.
3. P. Eskola et al., *Phys. Rev. C* 2, 1058 (1970).
4. I. Zvara, private communication.
5. R. L. Hahn et al., *Chem. Div. Annu. Progr. Rep. May 20, 1969*, ORNL-4437, p. 37.
6. T. Sikkeland, J. Maly, and D. F. Lebeck, *Phys. Rev.* **169**, 1000 (1968).
7. T. Sikkeland, A. Ghiorso, and M. J. Nurmia, *Phys. Rev.* **172**, 1232 (1968).
8. T. Sikkeland, private communication.

DETERMINATION OF THE HALF-LIVES OF ^{246}Cm AND ^{248}Cm BY ABSOLUTE SPECIFIC ACTIVITY TECHNIQUES

C. E. Bemis, Jr. J. R. Stokely[2]
J. E. McCracken[1] R. D. Baybarz[3]
R. E. Eby[2]

We have measured the partial alpha half-lives for ^{246}Cm and ^{248}Cm and the partial spontaneous-fission half-life for ^{248}Cm using an absolute specific-activity technique. The absolute quantities of curium were determined microchemically (~0.5 μmole) using a complexometric titration with ethylenediaminetetraacetic acid (EDTA) and determining the excess EDTA added to the curium samples coulometrically. The chemical determinations were combined with isotopic abundances determined mass spectrometrically, absolute alpha-activity measurements, and alpha-spectral measurements to determine the partial alpha half-lives for ^{246}Cm and ^{248}Cm and the partial spontaneous-fission half-life for ^{248}Cm. Our results are reported in Table 2.6.

This work is reported in more detail elsewhere.[5]

1. Graduate student assignee to Analytical Chemistry Division.
2. Analytical Chemistry Division.
3. Chemical Technology Division.
4. D. N. Metta, H. Diamond, and F. R. Kelly, *J. Inorg. Nucl. Chem.* **31**, 1245 (1969).
5. J. E. McCracken, J. R. Stokely, R. D. Baybarz, C. E. Bemis, Jr., and R. Eby, accepted for publication in *J. Inorg. Nucl. Chem.*

Table 2.6. Results of absolute half-life measurements for ^{246}Cm and ^{248}Cm

Isotope	Measured quantity	Value
^{246}Cm	Partial alpha $t_{1/2}$	4655 ± 40 years
	Partial SF $t_{1/2}$	(1.80 ± 0.01) × 10^7 years[a]
	Total $t_{1/2}$	4654 ± 40 years
^{248}Cm	Partial alpha $t_{1/2}$	(3.703 ± 0.032) × 10^5 years
	Partial SF $t_{1/2}$	(4.115 ± 0.034) × 10^6 years
	Alpha/SF ratio	11.11 ± 0.04
	Total $t_{1/2}$	(3.397 ± 0.032) × 10^5 years
^{248}Cm/^{246}Cm	Partial alpha $t_{1/2}$ ratio	79.55 ± 0.29

[a]Values reported by Metta, Diamond, and Kelly (ref. 4).

THE THERMAL CROSS SECTIONS AND RESONANCE INTEGRALS FOR NEUTRON CAPTURE OF ^{249}Cf, ^{250}Cf, AND ^{251}Cf

J. Halperin C. E. Bemis, Jr.
R. E. Druschel R. E. Eby[1]

The nuclides ^{249}Cf, ^{250}Cf, and ^{251}Cf are important intermediates in high-flux reactors producing ^{252}Cf. The neutron cross sections for these nuclides bear on the evaluation of a thermal-neutron reactor spectrum vs an intermediate-energy reactor spectrum for the production of ^{252}Cf, as well as on nuclear systematics for these heavy nuclides. By irradiating pure samples of ^{249}Cf and ^{250}Cf with neutrons under controlled and carefully monitored conditions and by precision mass spectrometric determinations of isotopic ratios, we have measured both the thermal-neutron capture cross sections and the capture resonance integrals of ^{249,250,251}Cf. Although not a primary goal of the experiment, the data are sufficiently precise to allow estimating the absorption cross section of ^{251}Cf as well. The nuclide sequence is shown in Eq. (1).

$$\begin{array}{ccccccc} & \nearrow (n,f) & & & & \nearrow (n,f) & \\ {}^{249}\mathrm{Cf} & \xrightarrow{(n,\gamma)} & {}^{250}\mathrm{Cf} & \xrightarrow{(n,\gamma)} & {}^{251}\mathrm{Cf} & \xrightarrow{(n,\gamma)} & {}^{252}\mathrm{Cf} \\ & \alpha \downarrow 13.1\mathrm{y} & & \alpha \downarrow 892\mathrm{y} & & \alpha, \mathrm{SF} \downarrow 2.65\mathrm{y} & \end{array} \qquad (1)$$

Experimental

Samples of isotopically enriched californium of ~100 ng were deposited in fused silica capsules. In each irradiation a set of three such capsules was arranged linearly within an aluminum container, and each end capsule was encased in a cadmium neutron filter. The cadmium filters were 1- by 1-cm cylinders of 0.040 in. wall thickness. A neutron flux monitor was placed at each end of each silica capsule. The monitors used in these irradiations consisted of dilute alloys (0.151%) of cobalt in aluminum. The samples were irradiated continuously at constant power in a hydraulic tube facility of the ORR at a thermal flux of ~2 × 10^{14} neutrons cm^{-2} sec^{-1} and an epithermal flux per unit ln E of ~ 2 × 10^{13} neutrons cm^{-2} sec^{-1}. The irradiation data are summarized in Table 2.7. The neutron fluxes were evaluated from measurements of the 1.33-MeV gamma rays of the 5.26-year ^{60}Co using an NaI detector and calculated on the basis of σ_{2200} = 37.0 b and I = 75 b.

Mass spectrometric analyses of both the irradiated and the original californium samples were carried out. The californium was electrodeposited on platinum wires and placed into rhenium canoe-type filaments in the spectrometer source. Resistive heating of the rhenium filament produced thermal ionization of the californium, which was analyzed in the two-stage mass spectrometer. Typically 10-ng samples of californium in the source provided sufficient ions for analysis. The mass spectrometric data are summarized in Tables 2.8 and 2.9.

Discussion

The neutron reaction rates in thermal reactor spectra may be satisfactorily expressed in terms of a model in which the thermal-neutron flux, ϕ_{th}, is described by a Maxwellian distribution characterized by $E_T = kT$ and an epithermal component which has a dE/E distribution. This latter distribution extends from a lower limit of about $5E_T$ and ranges over ~7 orders of magnitude in energy until it merges into the unmoderated fission neutron spectrum. Cadmium serves as a suitable thermal-neutron filter with an energy cutoff near 0.5 eV,

Table 2.7. Summary of neutron irradiation data[a]

Experiment	Irradiation time (sec)	Average thermal flux (neutrons cm^{-2} sec^{-1})	Average epithermal flux per ln E (neutrons cm^{-2} sec^{-1})
	$\times 10^5$	$\times 10^{14}$	$\times 10^{14}$
37C-1	3.454	1.94_5	1.98_2
-2	3.454	1.94_5	$(1.96_2)^b$
-3	3.454	1.94_5	1.92_2
37D-1	4.320	1.88_6	1.98_4
-2	4.320	1.88_6	$(1.94_8)^b$
-3	4.320	1.88_6	1.91_1
45A-1	2.597	1.76_0	1.82_5
-2	2.597	1.76_0	$(1.85_4)^b$
-3	2.597	1.76_0	1.88_2

[a]Based upon ^{60}Co (σ_{2200} = 37.0 b, I = 75 b).

[b]Interpolated.

Table 2.8. Mass analyses of ^{249}Cf samples

Experiment	Sample	$\frac{^{250}Cf}{^{249}Cf}$ (at. %)	$\frac{^{251}Cf}{^{249}Cf}$ (at. %)	$\frac{^{252}Cf}{^{249}Cf}$ (at. %)
37C[a]	Cd filter, 1	$0.507_9 \pm 0.005$	0.0208 ± 0.001	$<3 \times 10^{-4}$
	Cd filter, 3	$0.480_2 \pm 0.005$	0.0189 ± 0.001	$<3 \times 10^{-4}$
	Unfiltered, 2	$3.59_6 \pm 0.02$	$0.347_0 \pm 0.004$	0.0208 ± 0.001
37D[b]	Cd filter, 1	0.630 ± 0.006	0.0330 ± 0.001	$<10^{-3}$
	Cd filter, 3	0.614 ± 0.006	0.0317 ± 0.001	$<10^{-3}$
	Unfiltered, 2	$4.38_8 \pm 0.02$	$0.526_2 \pm 0.005$	0.0463 ± 0.001
	Unirradiated	$<5 \times 10^{-4}$	$<5 \times 10^{-4}$	$<5 \times 10^{-4}$

[a]Mass analysis carried out 50 days following irradiation.

[b]Mass analysis carried out 28 days following irradiation.

Table 2.9. Mass analyses of ^{250}Cf samples

Experiment	Sample	$\frac{^{251}Cf}{^{250}Cf}$ (at. %)	$\frac{^{252}Cf}{^{250}Cf}$ (at. %)
45A[a]	Cd filter, 1	$8.08_0 \pm 0.04$	$0.274_9 \pm 0.002$
	Cd filter, 3	$8.12_2 \pm 0.04$	$0.278_8 \pm 0.002$
	Unfiltered, 2	15.83 ± 0.06	1.605 ± 0.008
	Unirradiated	$2.40_8 \pm 0.01$	$0.223_4 \pm 0.002$

[a]Mass analysis carried out 26 days following irradiation.

enabling discrimination between these two principal components of the neutron spectrum. The reaction rates may conveniently be evaluated in terms of the integrated rates over the thermal distribution,

$$R_{th} = \int_{th} \phi(E)\, \sigma(E)\, dE\,,$$

which when suitably normalized can be expressed as the product of a thermal-neutron flux ϕ_{th} and thermal-neutron cross section σ_{th}, so that $R_{th} = \phi_{th}\sigma_{th}$. Similarly, the epithermal reaction rate,

$$R_{epi} = \int_{epi} \phi(E)\, \sigma(E)\, dE\,,$$

can be expressed in terms of the appropriately defined mean flux ϕ_{epi} (the epithermal-neutron flux per unit ln E) and the resonance integral

$$I = \int_{epi} \sigma(E)\, dE/E\,,$$

so that $R_{epi} = \phi_{epi} I$. The conventions used here have been described in detail elsewhere.[2]

The distribution of nuclide concentration following the reactor irradiation is calculated in terms of a series of consecutive first-order reactions and a combining of the two spectral components in the neutron distribution. The integrated form of the equations used to evaluate the cross sections takes the form

$$N_n/N_0 = \left(\prod_{i=1}^{n} a_i\right) \sum_{j=1}^{n} \frac{(e^{-(b_j - b_0)t} - 1)}{\prod_{\substack{i=0 \\ i \neq j}}^{n} (b_i - b_j)}\,, \qquad (2)$$

where a = formation constant = $\phi\sigma^c$ and b = removal constant = $\phi\sigma^a$ for each component nuclide in the starting mixture. In Eq. (2), ϕ is taken as either the epithermal or thermal flux and σ as either the resonance integral or the effective cross section,

$$\sigma_{eff} = \sigma_{th} + (\phi_{epi}/\phi_{th})\, I\,,$$

respectively. The superscripts c and a refer to capture and absorption (i.e., fission plus capture). The terms $N_0 ... N_n$ refer to the series of nuclides produced by successive neutron addition.

^{251}Cf Absorption

In a system of consecutive first-order nuclide transmutations involving no unmeasured branching, the rate constants can be evaluated completely from a set of measurements yielding the concentration of each component in the nuclide sequence (to within the limits of accuracy of the measurements). However, in the present sequence, a branching which was not measured directly does occur due to fission at both ^{249}Cf and ^{251}Cf [see Eq. (1)]. The thermal fission cross section and resonance integral of ^{249}Cf have been measured,[3,4] but there is considerable uncertainty in the fission cross section of ^{251}Cf. However, it has been possible to estimate this branching in the current experiment. Irradiations 37C and 37D are similar in all respects except that the reactants in 37D were more nearly completely converted (i.e., the proportion of each nuclide transmuted was greater in 37D than in 37C). Using an iterative calculational procedure, this difference in the degree of "burnout" allows an evaluation of the absorption cross section of ^{251}Cf.

By calculating the ratio of σ_{250}'s for the two runs 37C and D, which are expressed in terms of the mass ratio (251/250) and neutron fluence [see Eq. (2)], the value of the parameter $(\sigma^a{}_{251} - \sigma^a{}_{250})_{eff}$ for which this ratio becomes unity can be determined. Since runs 37C and D were mass analyzed on the same date and were quite similar in all respects, the precision in the ratios of the mass analyses and neutron fluences exceeds their absolute accuracy and permits evaluating $\sigma^a{}_{251}$ with greater accuracy than would otherwise be possible. This allows the derivation of a consistent set of cross sections for the reactions in Eq. (1). For the conditions of runs 37C and D (see Table 2.7), the parameter $(\sigma^a{}_{251} - \sigma^a{}_{250})_{eff}$ = 3700 ± 1200 b is derived, resulting in an effective absorption cross section for ^{251}Cf of $\sigma^a{}_{251}$(eff) ≃ 6900 b with an estimated uncertainty of ~20%. However, this error only introduces an ~1% uncertainty in the calculation of $\sigma^c{}_{249}$ and ~2% in $\sigma^c{}_{251}$, but an ~7% uncertainty in $\sigma^c{}_{250}$. The propagation of error from this source is relatively small for the resonance integral measurements because of the tenfold lower epithermal flux intensity.

^{249}Cf Capture

The branching for ^{249}Cf fission was taken into account using $\sigma^f{}_{249}$ = 1670 b[3,4] and $I^f{}_{249}$ = 2110 b.[3] The sensitivity of the cross section, $\sigma^c{}_{249}$, is such that a 15% change in $\sigma^f{}_{249}$ introduces less than a 1% change in $\sigma^c{}_{249}$. The variation of $\sigma^c{}_{249}$ in terms of the parameter $(\sigma^a{}_{251} - \sigma^a{}_{250})_{eff}$ which is used in the evaluation of $\sigma^a{}_{250}$ is shown in Table 2.10. It is apparent that a variation of 2000 b introduces less than a 1% change in $\sigma^c{}_{249}$. The average value of the thermal capture cross section, $\sigma^c{}_{249}$(th), is listed in the last column based upon the measured value of $I^c{}_{249}$ = 765 b discussed below. Since the evaluation of $\sigma^c{}_{250}$

Table 2.10. Dependence of $\sigma^c{}_{249}$ upon $(\sigma^a{}_{251} - \sigma^a{}_{250})_{eff}$

$(\sigma^a{}_{251} - \sigma^a{}_{250})_{eff}$ (b)	$\sigma^c{}_{249}$(eff) (b)		Average $\sigma^c{}_{249}$(eff) (b)	Average $\sigma^c{}_{249}$(th)* (b)
	37C	37D		
1000	567	537	552	474
3000	570	541	555	477
5000	573	545	559	481
7000	577	551	564	486

*Based upon $I^c{}_{249}$ = 765 b.

Table 2.11. Summary of ^{249}Cf cross sections

Experiment	ϕ_{th}/ϕ_{epi}	I^c_{249} (b)	σ^c_{249}(eff)* (b)	σ^c_{249}(th) (b)
37C	9.68_3	769 755	571	492
37D	9.96_5	768 768	543	464
		av 765 ± 35		av 478 ± 25

*Based upon $(\sigma^a_{251} - \sigma^a_{250})_{eff}$ = 3700 b.

yielded a best fit for the parameter $(\sigma^a_{251} - \sigma^a_{250})_{eff}$ = 3700 b, we estimate σ^c_{249}(th) = 478 ± 25 b. This may be compared with values of 270 and 300 b used by the Savannah River and the TRU groups to correlate their data.[5,6]

The results of the four measurements of the resonance capture integral of ^{249}Cf are summarized in Table 2.11, and the average is taken as I^c_{249} = 765 ± 35 b. Because of the lower epithermal flux, uncertainties introduced due to error in other cross sections are negligible. The present value may be compared with the value of I^c_{249} = 1030 b from Hennelly.[5] The values of the effective and thermal cross sections are also listed in columns 4 and 5, respectively, of Table 2.11. The parameter $\alpha = \sigma_c/\sigma_f$ is of interest for a fissionable nuclide and is calculated as α_{th} = 0.29 and α_{epi} = 0.36 for ^{249}Cf derived from these results.

^{250}Cf Capture

The measurement of the ^{250}Cf cross section was made in irradiations starting with both ^{250}Cf and ^{249}Cf. In the former case (45A) the ^{251}Cf produced was a first-order product; in the latter case (37C and D) the ^{251}Cf was the product of a second-order reaction. The higher isotopic ratios for first-order reactions lead to somewhat greater accuracies in that measurement (see Tables 2.8 and 2.9), and these are reflected in the weighted averages. The variation of I^c_{250} is illustrated in Table 2.12 and is relatively insensitive to the assumed value of I^a_{251}. On the basis[7] of I^a_{251} = 7000 b, the value of I^c_{250} = 11,600 ± 500 b is derived. This compares with I^c_{250} = 4975 b used by the Savannah River group.[5]

Similarly, the variation of σ^c_{250}(eff) with the parameter $(\sigma^a_{251} - \sigma^a_{250})_{eff}$ is shown in Table 2.13. An ~180-b change in σ^c_{250}(eff) results from a 2000-b variation in that parameter. The ^{250}Cf thermal cross sections are summarized in Table 2.14. Column 3 lists

Table 2.12. Dependence of I^c_{250} upon I^a_{251}

I^a_{251} (b)	$I^c_{250} \times 10^{-4}$ (b)*			
	37C	37D	45A	Weighted average
3,000	1.18_1	1.21_3	1.13_1	1.14_1
7,000	1.19_2	1.22_7	1.15_2	1.16_1
13,000	1.20_8	1.24_8	1.17_9	1.18_6
17,000	1.21_9	1.26_3	1.20_0	1.20_6

*Each entry is the mean of two determinations.

Table 2.13. Dependence of σ^c_{250}(eff) upon $(\sigma^a_{251} - \sigma^a_{250})_{eff}$

$(\sigma^a_{251} - \sigma^a_{250})_{eff}$ (b)	σ^c_{250}(eff) (b)			
	37C	37D	45A	Weighted average
1000	3024	2945	3017	3006
3000	3161	3116	3202	3181
5000	3299	3292	3392	3360
7000	3444	3473	3585	3543

Table 2.14. Summary of ^{250}Cf thermal cross sections

Experiment	$\frac{\phi_{th}}{\phi_{epi}}$	σ_{250}(eff)* (b)	σ_{250}(th) (b)
37C	9.68_3	3209	2010
37D	9.96_5	3178	2013
45A	9.48_2	3269	2045
		Weighted av	2034 ± 200

*Based upon $(\sigma^a_{251} - \sigma^a_{250})$ = 3700 b, I^a_{251} = 7000 b, $I^c_{250} = 1.16_1 \times 10^4$ b.

the measured effective cross sections for the three irradiations. The derived thermal cross sections are shown in the last column; the weighted average of $\sigma^c_{250}(\text{th}) = 2030 \pm 200$ b. The larger uncertainty in this measurement is due to the sensitivity of this cross section to the more poorly known value of σ^a_{251}. This value may be compared with 1485 and 2000 b, given by the Savannah River group and the TRU group respectively.

^{251}Cf Capture

The determination of the ^{251}Cf capture cross section is dependent upon the measurement of the mass ratio N_{252}/N_{251}. In the irradiation of the ^{249}Cf (37C and D), too little conversion to ^{252}Cf was realized by this third-order reaction in the filtered irradiation to enable evaluating the resonance integral. However, the unfiltered irradiation provided sufficient ^{252}Cf to measure $\sigma^c_{251}(\text{eff})$. The ^{250}Cf irradiation (45A) produced adequate quantities of ^{252}Cf to evaluate both σ^c_{251} and I^c_{251}. The low value of the absorption cross section of ^{252}Cf implies a negligible effect on the ^{251}Cf measurement. However, we used $\sigma^a_{252} = 65$ b and $I^a_{252} = 150$ b in this calculation.[3,8]

The dependence of I^c_{251} on the value of I^a_{251} is relatively slight. A factor of 2 change in the current estimate of the latter[7] makes only a 1% change in the value of I^c_{251}. Using the value of $I_a = 7000$ b, we report that $I^c_{251} = 1600 \pm 30$ b. Hennelly[5] gives $I^c_{251} = 730$ b for this parameter. The variation of $\sigma^c_{251}(\text{eff})$ as a function of $(\sigma^a_{251} - \sigma^a_{250})_{\text{eff}}$ is shown in Table 2.15. For the value of the parameter $(\sigma^a_{251} - \sigma^a_{250})_{\text{eff}} = 3700$ b, we report $\sigma^c_{251}(\text{eff}) = 3022 \pm 150$ b. By subtracting the epithermal contribution, the thermal capture cross section may be evaluated as $\sigma^c_{251}(\text{th}) = 2850 \pm 150$ b. This latter value may again be compared with a value of about 1980 b used by both the Savannah River and the TRU groups[5,6] to correlate nuclide yields in their respective reactors.

Table 2.15. Dependence of σ^c_{251} upon $(\sigma^a_{251} - \sigma^a_{250})_{\text{eff}}$

$(\sigma^a_{251} - \sigma^a_{250})_{\text{eff}}$ (b)	$\sigma^c_{251}(\text{eff})$ (b)			
	37C	37D	45A	Weighted average
1000	2942	3003	3103	3089
3000	2901	2957	3053	3040
5000	2865	2907	3003	2990
7000	2821	2846	2956	2942

1. Analytical Chemistry Division.
2. R. W. Stoughton and J. Halperin, *Nucl. Sci. Eng.* 6, 100 (1959).
3. R. W. Benjamin, K. W. MacMurdo, and J. D. Spencer, "Neutron Induced Fission Cross Sections for $^{244-248}$Cm and ^{249}Cf," presented at the Third Conference on Neutron Cross Sections and Technology, Knoxville, Tenn., Mar. 15–17, 1971.
4. J. Halperin, J. H. Oliver, and R. W. Stoughton, *Chem. Div. Annu. Progr. Rep. May 20, 1970,* ORNL-4581, p. 37.
5. E. J. Hennelly, "The Heavy Actinide Cross Section Story," presented at the Third Conference on Neutron Cross Sections and Technology, Knoxville, Tenn., Mar. 15–17, 1971.
6. W. D. Burch, J. E. Bigelow, and L. J. King, *Semiannual Report of Production, Status, and Plans for Period Ending June 30, 1970. Transuranium Processing Plant,* ORNL-4588, p. 31.
7. C. E. Bemis, Jr. et al., "Evaluation of ^{251}Cf 'Burnout' Experiment," following contribution, this report.
8. J. Halperin, J. H. Oliver, and R. W. Stoughton, "The Thermal Cross Section and Resonance Integral for Neutron Fission of ^{252}Cf," another contribution in this chapter, this report.

EVALUATION OF ^{251}Cf "BURNOUT" EXPERIMENT

C. E. Bemis, Jr. R. E. Druschel
R. D. Baybarz[1] J. Halperin

As a by-product of an experiment previously reported[2] on the measurement of the neutron absorption cross section of ^{257}Fm, it was possible to make certain observations bearing on the absorption and capture cross sections of ^{251}Cf. Because of the special interest at this time in ^{251}Cf as an intermediate in the production of ^{252}Cf, these data have been evaluated.

Cadmium-filtered and unfiltered samples of actinides containing picogram quantities of ^{251}Cf were irradiated in the hydraulic-tube facility of the ORR with cobalt monitors in a configuration which facilitated determination of the integrated neutron flux in the sample. These were irradiated to a thermal-neutron fluence of 6.27×10^{19} neutrons/cm^2 in a position where the ratio of thermal flux to epithermal flux per unit ln E was equal to 9.56. The evaluation of the absorption cross section of ^{251}Cf was to be made by comparing the ^{251}Cf content of each of the irradiated samples with that of a portion of the original sample.

The actinide sample contained $\sim 10^9$ atoms of the 892-year alpha-emitting ^{251}Cf, which represented only a few percent of the alpha activity of the sample. Since this quantity was too small to determine by mass spectrometry, the alpha spectrum was measured using a surface-barrier-detector–pulse-height-analysis system. It was possible to make measurements on the 5.667-MeV (34.7%) and 5.844-MeV (27.8%) peaks of ^{251}Cf even though 18.1-year ^{244}Cm [5.806 MeV (76.4%) and

5.76 MeV (23.6%)] had been added to the sample in much larger amounts to provide a standard of comparison for the "burnout" experiment.

The analysis was carried out by first quantitatively separating the actinides as a group on an anion exchange column from various fission product contaminants in the irradiated samples. The alpha-spectrum analysis of these samples established the ratio of ^{252}Cf to ^{244}Cm. The ^{252}Cf peaks [6.118 MeV (84.5%) and 6.075 MeV (15.5%), 2.65 years half-life, 3.1% spontaneous-fission branch] are amply separated in energy from the ^{244}Cm and are of comparable intensity, permitting a precise determination of ^{252}Cf/^{244}Cm. However, the ^{251}Cf/^{244}Cm ratio cannot be directly evaluated because of the overlapping of the ^{244}Cm and the ^{251}Cf peaks. The sample was redissolved and passed through a cation exchange column using an α-hydroxyisobutyric acid eluent, thus separating the curium and californium fractions by a nominal factor in excess of 10^3. The ^{251}Cf/^{252}Cf ratio was then determined from the alpha spectrum of this latter sample. The product of these two measured ratios yielded the desired value of ^{251}Cf/^{244}Cm.

The ratio of ^{251}Cf/^{244}Cm in the original unirradiated sample was determined similarly. Since no ^{252}Cf was initially present in this sample, an amount of ^{252}Cf activity comparable with the ^{244}Cm present was added and the ratio accurately measured through its alpha spectrum. Again an α-hydroxyisobutyric acid column separation served to remove the curium from the californium fraction, permitting the determination of the ^{251}Cf/^{252}Cf ratio and thus the value of ^{251}Cf/^{244}Cm.

The determination of the absorption cross section of the ^{251}Cf depends upon comparing the ratio ^{251}Cf/^{244}Cm in the irradiated samples with that in the unirradiated sample. Since only ~0.1% of the ^{244}Cm is transmuted in the unfiltered irradiation (less in the filtered irradiation), the correction can be accurately applied, and the absorption cross section of ^{251}Cf can be accurately expressed as

$$\sigma^a{}_{251}(\text{eff}) = (1/\phi t)\ln(N^o{}_{251}/N_{251})\,. \qquad (1)$$

The superscripts a, c (used later), and o refer to absorption, to capture, and to the original unirradiated sample respectively. The subscript is the mass number of the nuclide in question and is unambiguous in this context. The terms ϕt and σ refer either to the thermal-neutron fluence and effective thermal cross section or the epithermal fluence per unit ln E and the resonance integral, $I^a = \int \sigma^a(E)\,dE/E$, respectively.

It should be noted that the low alpha-decay rates of the ^{251}Cf necessitated counting times of several days. The ^{251}Cf alpha spectra in samples 1 and 3 appeared quite pure by comparison with known ^{251}Cf alpha spectra. (The measured ratios are listed in Table 2.16). However, the spectrum of sample 2 was poorly defined and was inconsistent with the known abundances in the fine structure. Thus the latter sample could not be used to evaluate the thermal absorption cross section. From samples 1 and 3, the resonance absorption integral of ^{251}Cf can be deduced as $I^a{}_{251} \approx 7000$ b. The uncertainty in the cross section, about 50%, reflects the low burnout achieved in the filtered irradiation.

From the ratio of ^{252}Cf to ^{251}Cf the capture cross section can be evaluated similarly. An expression for the capture neutron cross section is

$$\sigma^c{}_{251}(\text{eff}) = \frac{(N_{252}/N_{251})(\sigma^a{}_{251} - \sigma^a{}_{252})}{\exp[\phi t(\sigma^a{}_{251} - \sigma^a{}_{252})] - 1}\,, \qquad (2)$$

where the thermal-neutron parameters are required for $\sigma^c{}_{251}$(eff) and the epithermal parameters for $I^c{}_{251}$. The evaluation of $\sigma^c{}_{251}$ is dependent upon the absorption cross sections of ^{252}Cf and ^{251}Cf. The former is small and has been characterized;[3,4] it introduces no significant error in the calculation. Values of $\sigma^a{}_{252}$(eff) = 65 b and $I^a{}_{252}$ = 150 b were taken for these parameters. The resonance capture integral could be directly determined in this experiment and was found to be $I^c{}_{251} \approx 1620 \pm 100$ b. The sensitivity of the measurement is such that changing the assumed value of $I^a{}_{251}$ by a factor of 2 makes less than a 2% change in $I^c{}_{251}$. This value is in good agreement with that reported elsewhere.[5] The data further permit the evaluation of $\sigma^c{}_{251}$, dependent upon $\sigma^a{}_{251}$, and thus place a significant restraint on this parameter. The values of $\sigma^c{}_{251}$ are given in Table 2.17 as a function of $\sigma^a{}_{251}$. These results are consistent with reported[5] values of $\sigma^c{}_{251}$(eff) ≅ 3000 b and $\sigma^a{}_{251}$(eff) ≅ 6700 b.

Table 2.16. Alpha spectrum data for ^{251}Cf samples

Sample No.	^{251}Cf counts	Atom ratio	
		^{252}Cf/^{251}Cf	^{251}Cf/^{244}Cm
1, unirradiated	2407	$0.0170_0{}^a$	8.97_5
2, unfiltered radiation	1434	0.166_2	8.43_9
3, filtered radiation	4041	0.0108_8	8.56_0

[a] ^{252}Cf added.

1. Chemical Technology Division.
2. C. E. Bemis, Jr., et al., *Chem. Div. Annu. Progr. Rep. May 20, 1970,* ORNL-4581, p. 43.
3. J. Halperin et al., *Nucl. Sci. Eng.* 37, 228 (1969).
4. J. Halperin, J. H. Oliver, and R. W. Stoughton, "The Thermal Cross Section and Resonance Integral for Neutron Fission of ^{252}Cf," the following contribution, this report.
5. J. Halperin et al., "The Thermal Cross Sections and Resonance Integrals for Neutron Capture of ^{249}Cf, ^{250}Cf, and ^{251}Cf," the preceding contribution, this report.

Table 2.17. Cross-section dependence of σ^c_{251} upon σ^a_{251}

σ^a_{251}(eff) (b)	σ^c_{251}(eff) (b)	σ^f_{251}(eff) (b)	α_{251}*
2000	2657		
3500	2782	718	3.9
5000	2910	2090	1.4
6500	3041	3459	0.88
8000	3177	4823	0.66
9500	3315	6185	0.54
11000	3458	7542	0.46

*$\alpha = \sigma^c/\sigma^f$.

THE THERMAL CROSS SECTION AND RESONANCE INTEGRAL FOR NEUTRON FISSION OF ^{252}Cf

J. Halperin J. H. Oliver
R. W. Stoughton

The neutron-induced fissionability of ^{252}Cf is of special interest, of course, to the program involving its production and also as an example of an even-even nuclide undergoing subthreshold fission (compare ^{232}U, ^{238}Pu, ^{244}Cm). Although ^{252}Cf was first identified in 1954 and sizable samples have since become available, this measurement has proved to be quite difficult. The origin of the experimental problem lies in its high spontaneous-fission rate. Although ^{252}Cf decays predominantly by alpha emission with a 2.73-year half-life, there is a spontaneous-fission branching with an 85.5-year half-life. This high spontaneous-fission rate implies that in-pile measurements need to be made in neutron fluxes in excess of 10^{13} neutrons cm^{-2} sec^{-1}. This is beyond the usual range for fission chambers positioned in reactor fluxes, and signal to noise is too unfavorable for the accelerator pulsed-beam neutrons using the time-of-flight technique.

We have used the method of solid-state track recording to evaluate both the fission thermal cross section and the resonance integral of ^{252}Cf. The technique is applicable because it lends itself to the use of picogram-size samples and a detector that can be used in a high-flux region of a reactor. The method has been described,[1] and we have used a similar technique involving polycarbonate plastic film as a fission detector for unfiltered reactor spectra and muscovite in cadmium-filtered irradiations. For the latter case, we have replaced the earlier polyethylene sample holder with holders made of either polytetrafluoroethylene or polychlorotrifluoroethylene to minimize moderation of our epithermal-neutron spectrum. The tracks in the mica are developed by etching in concentrated HF for an hour at room temperature. We find the efficiency of the mica detector equal to that of Lexan within the limits of our error, (92 ± 2)%. Both Mn and Au neutron monitors were used to evaluate the thermal and epithermal components of the reactor spectrum. The measurements have been normalized to σ_{2200}(Au) = 98.8 b, I(Au) = 1580 b, σ_{2200}(Mn) = 13.3 b, and I(Mn) = 14.5 b. Our ^{252}Cf sample was isotopically quite pure, containing ~0.1% ^{251}Cf and 0.01% ^{249}Cf. This fissionable nuclide contamination resulted in a 4-b correction to the thermal cross-section measurement and a 5-b correction to the resonance integral. Since the experiment is sensitive to the presence of any fissionable isotope (e.g., ^{235}U, ^{239,241}Pu, ^{245,247}Cm) in picogram quantities, below the limit detectable by alpha counting, stringent requirements are placed on the chemical purity of the sample. The californium sample was purified by a series of α-hydroxyisobutyric acid cation exchange column separations. The product from the third column was judged pure by continuing the separation through two additional columns: the number of fission tracks observed by neutron-induced fission in the product from the fifth column was indistinguishable from that of the third, although the original sample was heavily contaminated with fissionable nuclides.

These irradiations were carried out in the pneumatic tube facility of the ORR, where the thermal-neutron flux was measured as ~5 × 10^{13} neutrons cm^{-2} sec^{-1} and where the ratio of the thermal to epithermal flux per unit ln E was ~35. For convenience in the microscopic examination of the tracks, the irradiations were timed to yield 1000 to 2000 tracks per experiment. The major difficulty was associated with the need for utmost speed in the handling of the ^{252}Cf-source—mica and —Lexan detector system. The goal was to permit the source and detector to be in contact for a minimum time prior to and following the irradiation. This permitted the registration of the minimum number of ^{252}Cf *spontaneous* fission tracks compared with those produced by *induced* fission while in the reactor.

In the unfiltered experiments the fraction of tracks due to neutron-induced fission ranged from 30 to 50% of the total number of tracks recorded. In the filtered irradiation, the value ranged from 6 to 15% and was the principal limitation in the accuracy of the measurement.

The data are summarized in Tables 2.18 and 2.19, in which the second column lists the fluence, and the third column lists the ^{252}Cf content of the sample at the time of the measurement. The number of observed fission tracks counted under the microscope is listed in column 4. The computed number of tracks due to the known spontaneous-fission rate of the sample is given in column 5. The last column lists the calculated cross section for each run. The weighted average of 12 determinations of the effective fission cross section of ^{252}Cf was measured as σ^f_{252}(eff) = 35 ± 4 b. The weighted average of seven determinations of the fission

Table 2.18. Fission cross section of ^{252}Cf

Experiment	Thermal fluence (neutrons/cm^2)	Number of ^{252}Cf atoms	Total number of fission tracks observed	Number of spontaneous-fission tracks (computed)	σ^f_{252}(eff) (b)
	$\times 10^{14}$	$\times 10^{10}$			
A-3	5.94	2.98	1381	902	25.4
4	4.98	2.95	1095	642	29.5
6	5.54	2.91	1831	1126	39.2
9	6.50	2.88	1756	1046	33.6
10	6.85	2.86	1673	912	34.3
12	7.63	2.84	1868	1068	32.5
B-2	4.76	3.12	1410	881	34.7
5	5.12	3.08	2106	1439	37.7
6	7.71	3.07	2557	1672	33.0
7	6.38	3.05	2083	1183	41.7
8	6.44	3.04	1913	1012	41.5
9	9.71	3.02	2169	1002	35.3
					Weighted av 34.9 ± 4

Table 2.19. Fission resonance integral of ^{252}Cf

Experiment	Epithermal fluence per unit ln E (neutrons/cm^2)	Number of ^{252}Cf atoms	Total number of fission tracks observed	Number of spontaneous-fission tracks (computed)	I^f_{252} (b)
	$\times 10^{14}$	$\times 10^{10}$			
A-20	0.561	2.58	1213	1022	138
22	0.379	2.53	1000	910	97
23	0.401	2.51	1009	924	87
24	0.343	2.48	826	773	63
B-20	0.558	2.65	1109	1028	54
22	0.331	2.58	1010	910	121
23	0.346	2.54	1130	1008	143
					Weighted av 110 ± 30

resonance integral is similarly reported as $I^f_{252} = 110 \pm 30$ b. The thermal cross section $[\sigma_{th} = \sigma_{eff} - (\phi_{epi}/\phi_{th})I]$ is thus determined as $\sigma^f_{252} = 32 \pm 4$ b. Combined with the previously reported[2] capture cross sections, $\sigma^c_{252}(th) = 21$ b and $I^c_{252} = 43$ b, the capture-to-fission ratio parameters are $\alpha_{th} = 0.66$ and $\alpha_{epi} = 0.4$.

By correlating yields in the production of ^{252}Cf at the TRU facility, Bigelow[3] observed that the reported capture cross sections did not account for the ^{252}Cf burnout and that his data were consistent with a fission cross section of 30 to 50 b. Furthermore, fission product analyses of reirradiated ^{252}Cf suggested values of σ^f_{252} ranging from ~20 b to upward of 100 b. Hennelly,[4] from similar considerations at Savannah River, suggested $\sigma^f_{252} = 6$ b and $I^f_{252} = 12$ b. Recently, Moore et al. reported[5] the results of measurements using a nuclear explosion in which numerous fission resonances were seen in ^{252}Cf for neutron energies from 20 eV to 5 MeV. He observed that the fission width of four resonances for which shape fitting was possible exceeded the estimated gamma width. He reports a fission resonance integral above 20 eV as 56 ± 5 b. These data confirm the substantially higher fission cross sections for ^{252}Cf than the capture values, leading to values of the parameter α of less than unity.

1. J. Halperin, J. H. Oliver, and R. W. Stoughton, *Chem. Div. Annu. Progr. Rep. May 20, 1970*, ORNL-4581, p. 37.
2. J. Halperin et al., *Nucl. Sci. Eng.* **37**, 228 (1969).
3. J. E. Bigelow, personal communication (September 1970).
4. E. J. Hennelly, "The Heavy Actinide Cross Section Story," presented at the Third Conference on Neutron Cross Sections and Technology, Knoxville, Tenn., Mar. 15–17, 1971.
5. M. S. Moore, J. H. McNally, and R. D. Baybarz, "The Neutron-Induced Fission Cross Section of ^{252}Cf," presented at the Third Conference on Neutron Cross Sections and Technology, Knoxville, Tenn., Mar. 15–17, 1971.

THE NEUTRON CAPTURE THERMAL CROSS SECTIONS AND RESONANCE INTEGRALS OF ^{244}Pu AND ^{245}Pu

R. E. Druschel J. Halperin
R. E. Eby[1]

In the very high-flux reactors devoted to the production of californium isotopes, somewhat less than 0.5% of the ^{242}Pu consumed leads to ^{244}Pu. See Eq. (1):

$$
\begin{array}{ccccccccc}
 & & & & & & {}^{245}Cm & & {}^{246}Cm \\
 & & & & & & \beta^- \uparrow 2.0\ \text{hr} & & \beta^- \uparrow 25\ \text{min} \\
 & & & & & & {}^{245}Am & & {}^{246}Am \\
 & & \beta^- \uparrow 5.0\ \text{hr} & & & & \beta^- \uparrow 10.5\ \text{hr} & & \beta^- \uparrow 10.85\ \text{days} \\
{}^{242}Pu & \xrightarrow{(n,\gamma)} & {}^{243}Pu & \xrightarrow{(n,\gamma)} & {}^{244}Pu & \xrightarrow{(n,\gamma)} & {}^{245}Pu & \xrightarrow{(n,\gamma)} & {}^{246}Pu \\
\alpha \downarrow 3.87 \times 10^5\ \text{years} & & & & \alpha \downarrow 8.28 \times 10^7\ \text{years} & & & &
\end{array}
\qquad (1)
$$

However, ^{244}Pu is of especial interest in geochronology, and recent evidence[2] appears to have confirmed its presence as an extinct radioactivity in meteoritic material. Furthermore, its relatively long half-life leads to the interesting possibility of handling macro quantities of plutonium with minimal complications due to alpha radioactivity (e.g., radiolytic effects of aqueous solutions of ^{239}Pu) as well as minimal radiation hazard.

We have measured the thermal-neutron capture cross section and resonance integral of the 8.28×10^7-year ^{244}Pu and the 10.5-hr ^{245}Pu. The measurements have been made by irradiating samples of ^{244}Pu of greater than 99% isotopic purity in cadmium-filtered and unfiltered configurations. The irradiations have been carried out in both the ORR and the BSR using dilute cobalt alloys to evaluate neutron fluence. The data have as yet been only incompletely evaluated and are therefore reported here as preliminary values.

^{244}Pu

The thermal cross section of ^{244}Pu was measured in two separate sorts of experiments. One irradiation was carried out in the D_2O tank of the BSR, which provides a highly thermalized neutron spectrum (comparable with the thermal column of a graphite reactor). The ratio of $\phi_{epi}/\phi_{th} < 3000$. Following the irradiation the

plutonium was chemically purified by a rare-earth fluoride precipitation. This was followed by adsorption onto an anion exchange column in a strong HCl medium. The ^{244}Pu was assayed by alpha counting and the ^{245}Pu-^{245}Am equilibrium mixture determined by 4π beta counting on thin film mounts. A nonlinear least-squares fit of the decay served to evaluate the characteristic 10.5-hr period and the amount of the 245-mass chain produced from the irradiated ^{244}Pu.

A second set of irradiations including both cadmium-filtered and unfiltered neutrons was carried out in which the ratio of the 245-mass chain produced to the initial ^{244}Pu was determined mass spectrometrically using an isotopic dilution technique. The ^{244}Pu was measured by adding a known amount of very pure ^{242}Pu to the sample. After equilibration, the mass ratio ^{244}Pu/^{242}Pu was determined with a two-stage mass spectrometer using a thermal ionization source and electron multiplier detectors. The ^{245}Cm formed in the irradiations was similarly evaluated mass spectrometrically by adding to the sample an accurately known quantity of isotopically pure ^{246}Cm. A satisfactory agreement between the two measurements of the thermal cross section of ^{244}Pu was obtained. The results of the experiment are summarized in Table 2.20. A value of $\sigma^c{}_{2200}(^{244}\mathrm{Pu}) = 1.70 \pm 0.1$ b is reported for the 2200-m/sec cross section of ^{244}Pu. The resonance integral $I(^{244}\mathrm{Pu}) = 45 \pm 4$ b has been similarly measured in our isotopic dilution experiment.

^{245}Pu

A prolonged irradiation of ^{244}Pu at constant reactor power using both cadmium-filtered and unfiltered neutrons was carried out to produce the 10.85-day ^{246}Pu. (Thermal fluence = 1.90×10^{20} neutrons/cm^2 and $\phi_{th}/\phi_{epi} = 10.1$.) Following chemical purification of the plutonium, the ^{246}Pu was assayed by measuring the intensity of both the 800-keV (24.3%) and the 1079-keV (31.6%) gammas in the decay of the 25-min ^{246}Am. The latter nuclide is in equilibrium with the ^{246}Pu parent, and the decay was followed for several half-lives. Using the gamma intensities given by Orth[3] and an estimated value for $\alpha(^{245}\mathrm{Pu}) \cong 1$, a thermal capture cross section $\sigma^c{}_{th}(^{245}\mathrm{Pu}) = 150 \pm 30$ b and a capture resonance integral $I^c(^{245}\mathrm{Pu}) = 220 \pm 40$ b can be reported.

The thermal cross section of ^{244}Pu measured here is in substantial agreement with earlier estimates, whereas the capture cross section of ^{245}Pu is somewhat lower than the 260 b listed by Holden.[4] There appear to be no other measurements extant for the resonance integrals reported here.

Table 2.20. Capture cross section of ^{244}Pu

Irradiation	Thermal fluence (neutrons/cm^2)	Epithermal fluence (neutrons/cm^2)	$\sigma^c{}_{2200}$ (b)	I^c (b)
	$\times 10^{18}$	$\times 10^{18}$		
I	0.0187_3	$<6 \times 10^{-7}$	1.69	
L-2	32.2	3.67[a]	1.70	
L-1		3.58		45
L-1		3.76		46

[a]Interpolated value.

1. Analytical Chemistry Division.
2. E. C. Alexander, Jr., et al., *Science* 172, 837 (1971).
3. C. J. Orth, *Phys. Rev.* 148, 1226 (1966).
4. N. E. Holden and F. W. Walker, *Chart of the Nuclides*, General Electric Co., Schenectady, N.Y., 1969.

K X-RAY ENERGIES AND RELATIVE TRANSITION PROBABILITIES OF CURIUM, BERKELIUM, CALIFORNIUM, AND EINSTEINIUM

P. F. Dittner C. E. Bemis, Jr.

Accurate data on x-ray energies and relative transition probabilities (RTP) are needed for unambiguously identifying a given element. Standard x-ray fluorescence techniques have been used to determine the energies and RTP's for most elements through americium.[1,2] Scarcity of material and high specific activity precludes the use of the aforementioned techniques beyond americium. However, one can exploit the radioactive decay of suitable radioactive nuclides to observe *K* x-ray emission from the daughter elements. Thus a fraction of the alpha decay of ^{249}Cf and ^{254}Es leads to excited nuclear states in ^{245}Cm and ^{250}Bk respectively. Some of the nuclei in excited states above the *K*-shell binding energy of the daughter are then internally converted in the *K* shell. The subsequent filling of the *K* vacancies results in Cm and Bk *K* x-ray emission. Similarly, the beta decay of ^{250}Bk leads to excited nuclear states in ^{250}Cf resulting finally in Cf *K* x-ray emission. A decay process which produces *K*-shell vacancies directly is electron capture. We produced ^{251}Fm at the ORIC by bombarding a ^{249}Cf target with 30-MeV alphas via the ^{249}Cf$(\alpha,2n)^{251}$Fm reaction.

The x rays from the various sources impinged upon a high-resolution (500 eV FWHM at 122 keV) Ge(Li)

Table 2.21. K x-ray energies (eV)

Element	$K_{\alpha 2}$ ($K - L_{II}$)		$K_{\alpha 1}$ ($K - L_{III}$)		$K_{\beta 3}$ ($K - M_{II}$)		$K_{\beta 1}$ ($K - M_{III}$)	
	Experiment	Theory	Experiment	Theory	Experiment	Theory	Experiment	Theory
Curium	104,589(5)	104,607(105)	109,273(5)	109,287(109)	122,289(6)	122,315(122)	123,407(6)	123,433(123)
Berkelium	107,165(6)	107,214(107)	112,112(6)	112,146(112)	125,478(10)	125,437(125)	126,582(10)	126,618(127)
Californium	109,818(5)	109,864(110)	115,031(5)	115,060(115)	128,599(7)	128,615(129)	129,816(7)	129,864(130)
Einsteinium	112,501(10)	112,581(113)	118,018(10)	118,057(118)	131,848(20)	131,874(132)	133,188(20)	133,193(133)

Table 2.22. K-shell binding energies (eV) obtained from $K_{\alpha 1}$, $K_{\alpha 2}$, $K_{\beta 3}$, and $K_{\beta 1}$ energies and L_{II}, L_{III}, M_{II}, and M_{III} binding energies

Z	Element	$K_{\alpha 1} + L_{III}$	$K_{\alpha 2} + L_{II}$	$K_{\beta 3} + M_{II}$	$K_{\beta 1} + M_{III}$	K binding energy	
						Experiment	Theory
96	Curium	128,243	128,246	128,235	128,246	128,243(6)	128,261(128)
97	Berkelium	131,564	131,550	131,625	131,559	131,566(17)	131,586(132)
98	Californium	134,912	134,916	134,915	134,905	134,913(7)	134,967(135)

photon detector. The pulses were further amplified and stored in a 4096-channel MCA. Spectra of the appropriate x-ray source and a ^{182}Ta source were recorded simultaneously, and the energies of the Cm, Bk, and Cf K x rays were determined relative to the well-known energies (±2 eV) of the ^{182}Ta gamma rays.[3] The decay of 1.5-day ^{251}Es following that of the 7-hr ^{251}Fm facilitated the simultaneous recording of the Cf and Es K x-ray spectra, and the Es K x-ray energies were determined relative to those of Cf.

K-series RTP's were determined by correcting the measured photopeak areas for background and for the energy-dependent detection efficiency. Calibrated sources of ^{57}Co, ^{241}Am, ^{113}Sn, ^{203}Hg, ^{137}Cs, ^{243}Am, and ^{240}Pu were used to establish points on an absolute detection efficiency vs energy curve.

In order to isolate the Bk x rays (resulting in the decay of ^{254}Es) from those of Cf, an alpha-photon coincidence spectrum was accumulated. By allowing the parent activity, ^{251}Fm, to decay for 48 hr and then accumulating the photons from the source, a "clean" Cf x-ray spectrum was obtained. This spectrum was then used to correct the region of overlap (Es $K'_{\beta 1}$ with Cf $K'_{\beta 2}$) in the Es x-ray spectrum obtained during the first 48 hr from the ^{251}Fm source.

The measured K x-ray energies, together with the calculated values of Carlson et al.,[4] are shown in Table 2.21. Using available values[5-7] for the binding energies of the L_{II}, L_{III}, M_{II}, and M_{III} shells and our K x-ray energies, we have calculated the K-shell binding energies for Cm, Bk, and Cf as shown in Table 2.22. The relative transition probabilities are shown in Table 2.23. Transitions from higher shells (N, O, etc.), although observed, could not be resolved into transitions from specific subshells (i.e., N_{IV} or O_{III}), and therefore their average energies and relative transition probabilities are not listed. Our measured transition probabilities agree quite well with recent calculations of Lu et al.[8]

Table 2.23. Relative transition probabilities of K x rays

$K_{\alpha 1} = 1000$

Element	$K_{\alpha 2}$ ($K - L_{II}$)	$K_{\beta 3}$ ($K - M_{II}$)	$K_{\beta 1}$ ($K - M_{III}$)
Curium	632(6)	112(2)	230(7)
Berkelium	643(8)	126(4)	222(10)
Californium	657(8)	133(4)	259(10)
Einsteinium	666(11)	134(6)	242(12)

1. J. A. Bearden, *Rev. Mod. Phys.* 39, 78 (1967).
2. G. C. Nelson, B. G. Saunders, and S. I. Salem, *Z. Phys.* **235**, 308 (1970).
3. R. C. Greenwood, R. G. Helmer, and R. J. Gehrke, *Nucl. Instrum. Methods* 77, 141 (1970).
4. T. A. Carlson et al., *Nucl. Phys. A* **135**, 57 (1969).
5. J. M. Hollander et al., *Ark. Fys.* **28**, 375 (1965).

6. I. Ahmad et al., *Phys. Rev. C* 3, 380 (1971).
7. Y. Y. Chu, M. Perlman, C. E. Bemis, Jr., and P. F. Dittner (to be published).
8. C. C. Lu, F. B. Malik, and T. A. Carlson (to be published).

ELECTRON BINDING ENERGIES AND *L*-SHELL FLUORESCENT YIELDS IN CURIUM

P. F. Dittner Y. Y. Chu[1]
C. E. Bemis, Jr. M. L. Perlman[1]

We have recently determined electron binding energies in curium by combining precision internal-conversion kinetic-energy measurements with gamma-ray energy measurements. To augment these binding energy determinations and to extend the measurements to those electron shells not readily studied by the internal-conversion method, we have measured both the *K*-series and *L*-series x-ray emission lines of curium using suitable radioactivities.

Internal conversion lines resulting from the $2^+ \rightarrow 0^+$ $E2$ transition in ^{246}Cm from the alpha decay of isotopically pure sources of ^{250}Cf were studied using the Brookhaven 50-cm $\pi\sqrt{2}$ electron spectrometer. Electron kinetic energies for the $L_I \rightarrow M_{III}, N_{II}, N_{III}$, and $O_{II,III}$ lines from this transition were determined from the measured electron momenta and are accurate to approximately ±10 eV. The $2^+ \rightarrow 0^+$ gamma-ray transition and the *L* x-ray emission lines in the decay of ^{250}Cf were measured using a small planar Ge(Li) detector. The measured gamma-ray energy resolution was ~250 eV FWHM in the curium *L* x-ray energy region. The energies of the most intense *L* x-ray lines of curium were determined relative to those of uranium produced in the decay of ^{240}Pu, and the $2^+ \rightarrow 0^+$ gamma-ray energy was determined relative to the $K_{\alpha 1}$ and $K_{\alpha 2}$ lines of europium. The energies of these lines used as standards are known[2] to an accuracy of ~1 part in 10^5 as determined using the latest values of the fundamental constants.[3] Under the conditions of our experiment, peak centroids were determined to ~0.1 channel, which corresponds to an accuracy of ~2 eV.

The *L* x-ray spectrum from the decay of ^{250}Cf is shown in Fig. 2.14. We have extrapolated the radiative transition probabilities of Scofield[4] from $Z = 92$ to $Z = 96$ and normalized them to the experimental intensities for the $L_{\alpha 1}$, $L_{\beta 1}$, and $L_{\gamma 4}$ lines. The extrapolated intensities account for the experimental spectrum remarkably well, indicating that the *L* Auger yields in this region show little discontinuity. The *L* x-ray energies and intensities as derived above are listed in Table 2.24 together with the energy of the $2^+ \rightarrow 0^+$ gamma ray in ^{246}Cm, all from the decay of ^{250}Cf.

The *K* x-ray energy spectrum of curium following the alpha decay of ^{249}Cf was measured using the techniques outlined above.

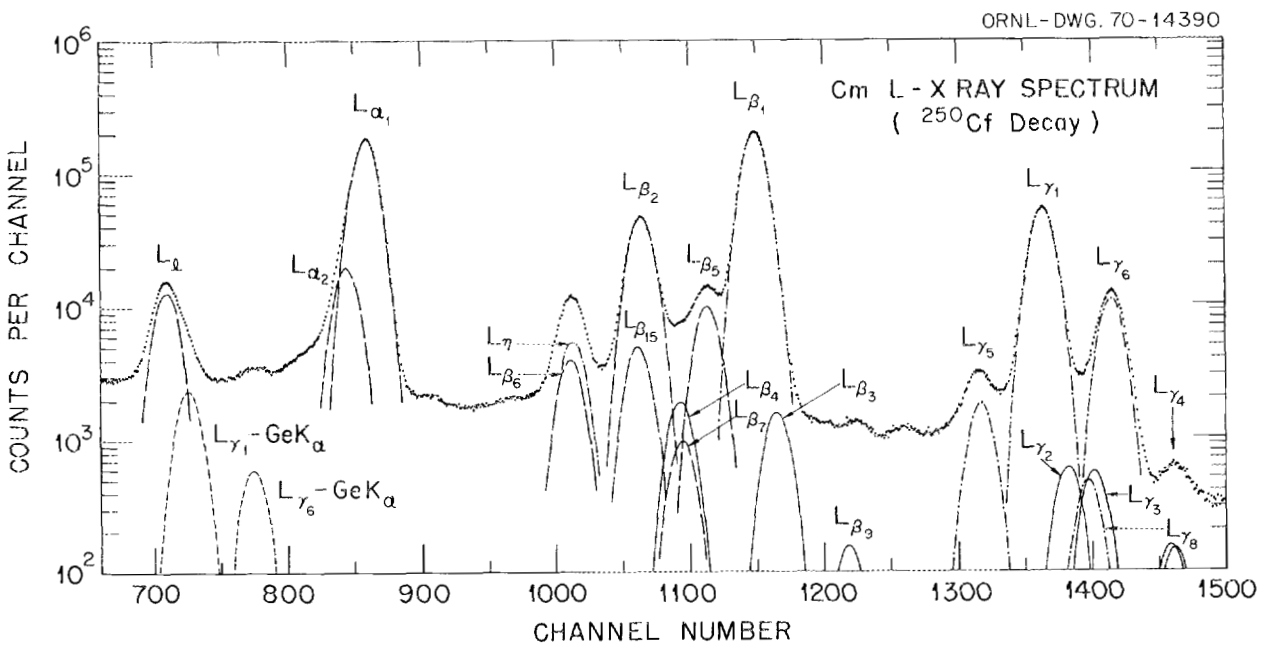

Fig. 2.14. *L* **x-ray energy spectrum for curium in the alpha decay of ^{250}Cf.** The x-ray lines result from vacancies in the L_I (——), L_{II} (-·-·-), and L_{III} (-----) shells.

By combining the L x-ray energies for the $L_{\alpha 1}$, $L_{\beta 2}$, $L_{\beta 1}$, $L_{\gamma 5}$, $L_{\gamma 1}$, and $L_{\gamma 6}$ lines, the K x-ray energies of the $K_{\alpha 2}$, $K_{\alpha 1}$, $K_{\beta 3}$, and $K_{\beta 1}$ lines, together with the internal-conversion electron energies and gamma-ray energy, we were able to derive electron binding energies for the $K \to N_V$, $O_{II} \to O_{IV}$, and P_{III} electrons. These values are listed in Table 2.25 together with the method used to determine the binding energies. We have also compared our experimental binding energies with the theoretical values of Carlson et al.[5]

Table 2.24. Energies and relative intensities of the most intense L x-ray lines in Cm from the decay of ^{250}Cf, and the energy of the $2^+ \to 0^+$ gamma ray in ^{246}Cm

Line designation	Energy[a] (keV)	Relative intensity[b] ($L_{\beta 1}$ = 1.000)
L_l ($L_{III} - M_I$)	12.650 ± 0.002	0.080
$L_{\alpha 2}$ ($L_{III} - M_{IV}$)	(14.745 ± 0.014)	0.126
$L_{\alpha 1}$ ($L_{III} - M_V$)	14.959 ± 0.002	1.082
$L_{\beta 6}$ ($L_{III} - N_I$)	(17.299 ± 0.016)	0.022
$L_{\beta 15}$ ($L_{III} - N_{IV}$)	(18.049 ± 0.016)	0.026
$L_{\beta 2}$ ($L_{III} - N_V$)	18.113 ± 0.002	0.238
$L_{\beta 7}$ ($L_{III} - O_I$)		0.005
$L_{\beta 5}$ ($L_{III} - O_{IV,V}$)		0.054
L_η ($L_{II} - M_I$)	(17.331 ± 0.016)	0.030
$L_{\beta 1}$ ($L_{II} - M_{IV}$)	19.426 ± 0.002	1.000
$L_{\gamma 5}$ ($L_{II} - N_I$)	21.980 ± 0.008	0.008
$L_{\gamma 1}$ ($L_{II} - N_{IV}$)	22.730 ± 0.002	0.241
$L_{\gamma 8}$ ($L_{II} - O_I$)		0.002
$L_{\gamma 6}$ ($L_{II} - O_{IV}$)	23.519 ± 0.002	0.049
$L_{\beta 4}$ ($L_I - M_{II}$)	(18.568 ± 0.025)	0.998×10^{-2}
$L_{\beta 3}$ ($L_I - M_{III}$)	(19.680 ± 0.025)	0.768×10^{-2}
$L_{\beta 10}$ ($L_I - M_{IV}$)	(20.287 ± 0.022)	0.054×10^{-2}
$L_{\beta 9}$ ($L_I - M_V$)	(20.500 ± 0.024)	0.073×10^{-2}
$L_{\gamma 2}$ ($L_I - N_{II}$)	(23.018 ± 0.025)	0.275×10^{-2}
$L_{\gamma 3}$ ($L_I - N_{III}$)	(23.318 ± 0.025)	0.244×10^{-2}
$L_{\gamma 4}$ { ($L_I - O_{II}$)	(24.219 ± 0.026)	0.133×10^{-2}
$L_{\gamma 4}$ { ($L_I - O_{III}$)	(24.286 ± 0.024)	
$2^+ \to 0^+$(^{246}Cm)	42.852 ± 0.005	$(5.83 \pm 0.12) \times 10^{-3}$
ΣL_I x rays (experimental intensity)		0.0255 ± 0.0050
ΣL_{II} x rays (experimental intensity)		1.33 ± 0.03
ΣL_{III} x rays (experimental intensity)		1.63 ± 0.03

[a]Calculated energy values using our experimental binding energies are given in parentheses; other values are experimental measurements.

[b]Relative intensities are based on extrapolations of the radiative transition probabilities of Scofield [*Phys. Rev.* **179**, 9 (1969)] and normalized to the experimental intensities for $L_{\alpha 1}$ (L_{III}), $L_{\beta 1}$ (L_{II}), and to $L_{\gamma 4}$ (L_I).

Values for the fluorescence yields in the L subshells may be obtained from the photon intensity data and the L subshell internal-conversion coefficients. Recalling that the subshell fluorescence yield, ω_i, is the probability per vacancy in the ith subshell that a photon is emitted in an electromagnetic transition to that subshell, one obtains the equations

$$\omega_I = I(\Sigma L_I)/I_\gamma \alpha_I \,, \tag{1}$$

$$\omega_{II} = I(\Sigma L_{II})/I_\gamma(\alpha_{II} + \alpha_I f_{I,II}) \,, \tag{2}$$

$$\omega_{III} = I(\Sigma L_{III})/I_\gamma[\alpha_{III} + \alpha_{II} f_{II,III} + \alpha_I(f_{I,III} + f_{I,II} f_{II,III})] \,. \tag{3}$$

In these equations $I(\Sigma L_i)$ is the intensity sum for all the L x-ray lines corresponding to transitions to the L_i subshell, I_γ is the intensity of the 42.852-keV unconverted gamma ray, α_i is the L_i subshell internal-conversion coefficient of the 42.852-keV transition, and f_{ij} is the Coster-Kronig probability for transfer of the vacancy from the ith to the jth subshell. Internal-conversion coefficients for this nuclear transition have been measured,[6] and the results are in accord with theoretical values.[7] With the theoretical value 15.7 for α_I and photon intensities from Table 2.24, Eq. (1) yields directly the result

$$\omega_I = 0.28 \pm 0.06 \,.$$

The relatively large uncertainty is associated with the fact that most of $I(\Sigma L_I)$ has been deduced from its weak $L_{\gamma 4}$ components.

For the evaluation of ω_{II} from Eq. (2), knowledge of $f_{I,II}$ is not critical; α_{II} is large in comparison with α_I and even if $f_{I,II}$ were as much as $1 - 0.28 = 0.72$, the contribution of the $\alpha_I f_{I,II}$ term would be less than 3%. With $\alpha_{II} = 421$ and $f_{I,II}$ taken to be 0.1, a reasonable choice,[8] Eq. (2) yields

$$\omega_{II} = 0.54 \pm 0.02 \,.$$

Evaluation of ω_{III} from Eq. (3) is fairly straightforward. Here the value of α_{III}, 349, is comparable with that of α_{II}, and $f_{II,III}$ is therefore important. Recently, McGeorge and Fink have measured this quantity for Cm and have reported $f_{II,III} = 0.188 \pm 0.019$.[9] For the sake of completeness the α_I term may be included; and if $f_{I,III}$ is taken to be 0.55,[8] one finds

$$\omega_{III} = 0.63 \pm 0.02 \,.$$

Table 2.25. Electron binding energies in curium

Electron shell	Binding energy (keV)		Scheme for binding energy determination[c]
	Experiment[a]	Theory[b]	
$K\ (1s_{1/2})$	128.243 ± 0.006	128.261	$K_{\alpha 2}$ + BE(L_{II}), $K_{\alpha 1}$ + BE(L_{III}), $K_{\beta 3}$ + BE(M_{II}), $K_{\beta 1}$ + BE(M_{III})
$L_I\ (2s_{1/2})$	24.518 ± 0.021	24.523	E_γ − IC(L_I)
$L_{II}\ (2p_{1/2})$	23.654 ± 0.011	23.654	E_γ − IC(L_{II})
$L_{III}\ (2p_{3/2})$	18.973 ± 0.011	18.974	E_γ − IC(L_{III})
$M_I\ (3s_{1/2})$	6.323 ± 0.011	6.313	BE(L_{III}) − L_l
$M_{II}\ (3p_{1/2})$	5.946 ± 0.013	5.946	E_γ − IC(M_{II})
$M_{III}\ (3p_{3/2})$	4.839 ± 0.013	4.828	E_γ − IC(M_{III})
$M_{IV}\ (3d_{3/2})$	4.228 ± 0.011	4.236	BE(L_{II}) − $L_{\beta 1}$
$M_V\ (3d_{5/2})$	4.014 ± 0.011	4.014	BE(L_{III}) − $L_{\alpha 1}$
$N_I\ (4s_{1/2})$	1.674 ± 0.012	1.664	BE(L_{II}) − $L_{\gamma 5}$
$N_{II}\ (4p_{1/2})$	1.500 ± 0.014	1.493	E_γ − IC(N_{II})
$N_{III}\ (4p_{3/2})$	1.200 ± 0.014	1.194	E_γ − IC(N_{III})
$N_{IV}\ (4d_{3/2})$	0.924 ± 0.011		BE(L_{II}) − $L_{\gamma 1}$
$N_V\ (4d_{5/2})$	0.860 ± 0.011		BE(L_{III}) − $L_{\beta 2}$
$O_{II}\ (5p_{1/2})$	0.299 ± 0.016		E_γ − IC(O_{II})
$O_{III}\ (5p_{3/2})$	0.232 ± 0.012		E_γ − IC(O_{III})
$O_{IV}\ (5d_{3/2})$	0.135 ± 0.011		BE(L_{II}) − $L_{\gamma 6}$
$P_{III}\ (6p_{3/2})$	0.033 ± 0.027		E_γ − IC(P_{III})

[a]Errors are approximately standard deviations based on uncertainties in the measurements. The result for the K shell is a weighted average.

[b]Reference 5. Uncertainty in the theoretical values is stated to be ±0.1% for the K binding energies, ±0.2% for the L shell, and ±0.5% for the M and N shells.

[c]$K_{\alpha 1}$, $L_{\beta 2}$, etc., in this column are photon energies, BE(L_{III}) is an electron binding energy, E_γ is the gamma-ray energy (42.852 keV), and IC(M_{II}) is the kinetic energy of the electron from the M_{II} subshell internally converted in the deexcitation of the 42.852-keV state of ^{246}Cm.

1. Chemistry Department, Brookhaven National Laboratory, Upton, N.Y.
2. J. A. Bearden, *Rev. Mod. Phys.* **39**, 78 (1967).
3. B. N. Taylor, W. H. Parker, and D. N. Langenberg, *Rev. Mod. Phys.* **41**, 375 (1969).
4. J. H. Scofield, *Phys. Rev.* **179**, 9 (1969).
5. T. A. Carlson et al., *Nucl. Phys. A* **135**, 57 (1969).
6. Y. Y. Chu and M. L. Perlman, *Phys. Rev. C* **3**, 2021 (1971).
7. Theoretical values for the L subshell internal-conversion coefficients were interpolated from the tables of R. S. Hager and E. C. Seltzer, *Nucl. Data, Sect. A* **4**, 1 (1968).
8. R. W. Fink et al., *Rev. Mod. Phys.* **38**, 513 (1966).
9. J. C. McGeorge and R. W. Fink, *Bull. Amer. Phys. Soc.* **16**, 578 (1971).

THE UNEQUIVOCAL IDENTIFICATION OF TRANSFERMIUM ELEMENTS USING X-RAY TECHNIQUES[1]

C. E. Bemis, Jr. R. L. Hahn
P. F. Dittner D. C. Hensley[2]
C. D. Goodman[2] R. J. Silva

Identification of the atomic number of an element by its characteristic K-series x rays was first applied by Moseley[3] in establishing parts of the periodic table, and this method has been more recently applied to confirming the identification of artificially produced ele-

ments, such as technetium ($Z = 43$) and promethium ($Z = 61$).[4]

With a simple modification, however, this x-ray identification method can be extended to the identification and study of many of the transfermium elements, even though these elements must be examined a few atoms at a time. We have used this extended method in a study of ^{251}Fm and in a confirmation of the identification of ^{255}No.

Our technique relies on the coincident observation of characteristic K-series x rays from the daughter element and of alpha particles from the alpha decay of the parent element. This will be possible if the alpha decay of the parent proceeds to excited nuclear states in the daughter nucleus which subsequently deexcite by the internal-conversion process. The characteristic K-series x rays of the daughter element then result from atomic rearrangements following K-shell internal conversion. Since the observed alpha particle has $Z = 2$, the identification of the K-series x rays from the daughter element (with atomic number $Z - 2$) provides an equally precise identification of the parent element with atomic number Z.

We produced the 200-sec ^{255}No isotope in the ^{249}Cf(^{12}C,$\alpha 2n$) reaction using a beam of $^{12}C^{4+}$ ions accelerated in the Oak Ridge Isochronous Cyclotron. The recoiling reaction products were thermalized in a helium-filled gas-jet collection assembly, pumped through a small orifice, and deposited on a 23-mg/cm^2 Ni disk. After a 6-min bombardment cycle, the disk was pneumatically transferred a distance of about 30 m to a coincidence counting assembly. During the accumulation of a total integrated current of ^{12}C ions of about 10 particle-μA-hr, approximately 180 bombardment-counting cycles were completed, and about 7000 alpha particles from the decay of ^{255}No were detected.

The three linear pulses constituting a valid coincidence event, namely, alpha-particle energy, photon energy, and time correlation, were digitized sequentially using one fast on-line 8192-channel analyzer and then transferred to a computer for storage.[5] All alpha events were recorded whether accompanied by a coincidence photon or not.

Our singles alpha spectrum for the decay of ^{255}No is shown in Fig. 2.15. This spectrum, with considerably better energy resolution, is essentially identical to the spectrum recently reported by Eskola et al.[6] for the same reaction. Figure 2.16 shows a portion of the photon energy spectrum for the photons observed in coincidence with all of the ^{255}No alpha groups. The observed lines have been identified as corresponding to Fm K-series x rays for the following reasons: the energies of these lines are in excellent agreement with values calculated[7] for Fm K-series x rays, and the relative line intensities are in good agreement with those expected for Fm K-series x rays.[7] Since these x rays are

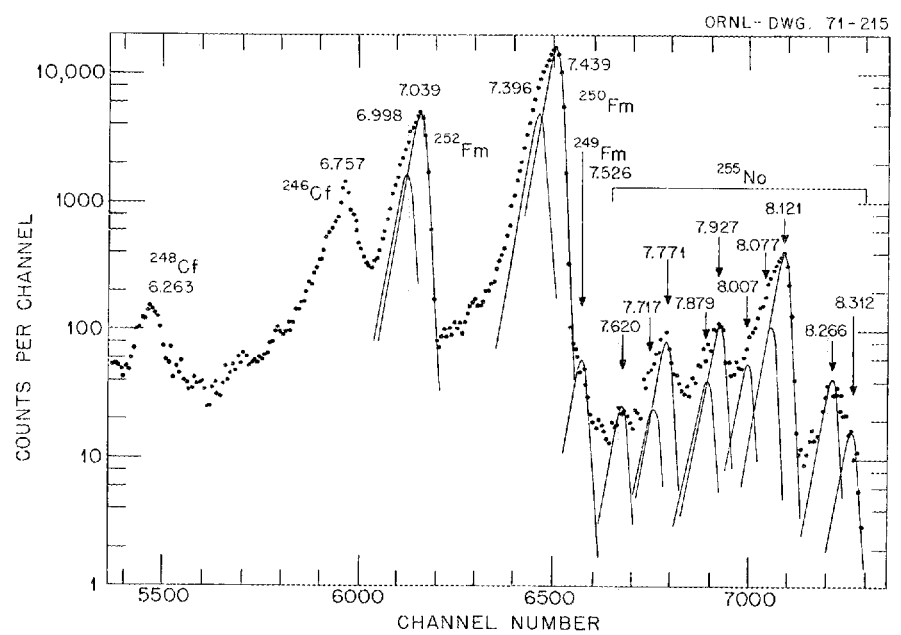

Fig. 2.15. Alpha spectrum observed for the reaction products of 72.3-MeV $^{12}C^{4+}$ ions on ^{249}Cf.

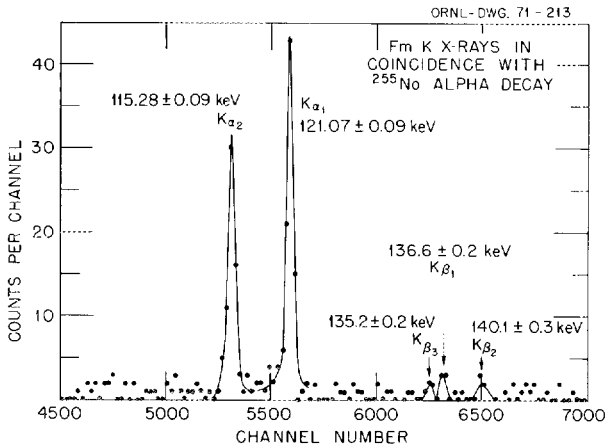

Fig. 2.16. A portion of the photon spectrum in coincidence with alpha particles from the decay of ^{255}No. The observation of Fm K-series x rays constitutes an unequivocal identification of Z = 102, nobelium.

uniquely associated with fermium (Z = 100) and since the x rays were in coincidence with alpha particles (Z = 2), the identification of nobelium (Z = 102) is unequivocal.

Based on our experience with the identification of nobelium, we feel that a conclusive atomic number identification could be obtained with the observation of far fewer coincident events than were obtained in this experiment. We are currently applying this technique to the identification and study of alpha-active isotopes of other transfermium elements which include 4.5-sec ^{257}104, 31-sec ^{256}Lr, and 1.6-sec ^{260}105. Our unequivocal identification of nobelium has been the subject of a recent publication which should be referred to for further details.[8]

THE ALPHA DECAY OF ^{255}No AND STATES IN ^{251}Fm

C. E. Bemis, Jr. D. C. Hensley[1]
P. F. Dittner C. D. Goodman[1]
R. J. Silva

The experiments[2] designed to provide an unequivocal identification of the atomic number of nobelium (Z = 102) by coincident observation of K-series x rays of Fm in coincidence with the alpha decay of ^{255}No have also provided detailed information on the level scheme for ^{251}Fm. Ten alpha groups in the ^{255}No decay have been identified, and their energies, intensities, and alpha-decay hindrance factors are listed in Table 2.26.

Analysis of our prompt and delayed alpha–K-x-ray and alpha–gamma-ray coincidence data indicates that approximately 43% of the observed K-series x rays result from the internal conversion of a transition from the state in ^{251}Fm at 191 keV. All of the K-series x rays in coincidence with the alpha groups with energies of 8.121, 8.077, and 8.007 MeV are delayed, and we derive a lifetime for the state at 191 keV of 15.2 ± 2.3 μsec. The alpha–x-ray delayed-coincidence curve for these transitions is shown in Fig. 2.17. A 187.2-keV gamma ray in prompt coincidence with the 7.927- and 7.879-MeV alpha transitions has been established as $E2$ or admixed $E2$-$M1$ multipolarity using conversion coefficients derived from our data. The gamma rays and x

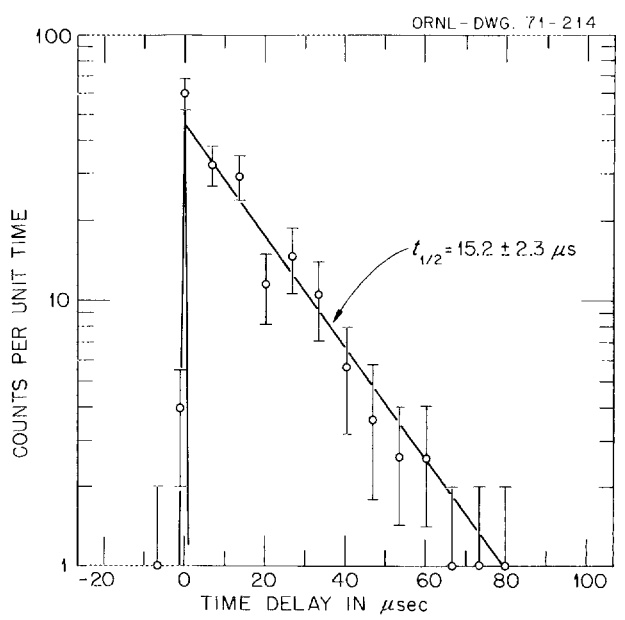

Fig. 2.17. Delayed alpha–x-ray coincidence curve for the 191-keV state in ^{251}Fm.

1. See also *Electronucl. Div. Annu. Progr. Rep. Dec. 31, 1970,* ORNL-4649, p. 69.
2. Electronuclear Division.
3. H. G. Moseley, *Phil. Mag.* **26**, 1024 (1913); **27**, 703 (1914).
4. L. E. Burkhart, W. F. Peed, and B. G. Saunders, *Phys. Rev.* **73**, 347 (1948); L. E. Burkhart, W. F. Peed, and E. J. Spitzer, *Phys. Rev.* **75**, 86 (1949).
5. C. D. Goodman, C. A. Ludemann, D. C. Hensley, R. Kurz, and E. W. Anderson, *Proceedings of IEEE 1970 Nuclear Science Symposium,* Nov. 4–6, 1970, New York (to be published).
6. P. Eskola et al., *Phys. Rev. C* **2**, 1058 (1970).
7. C. E. Bemis, Jr., P. F. Dittner, D. C. Hensley, C. D. Goodman, and R. J. Silva, "The Alpha Decay of ^{255}No and States in ^{251}Fm," the following contribution, this report.
8. P. F. Dittner et al., *Phys. Rev. Lett.* **26**, 1037 (1971).

ORNL-DWG. 71-745A

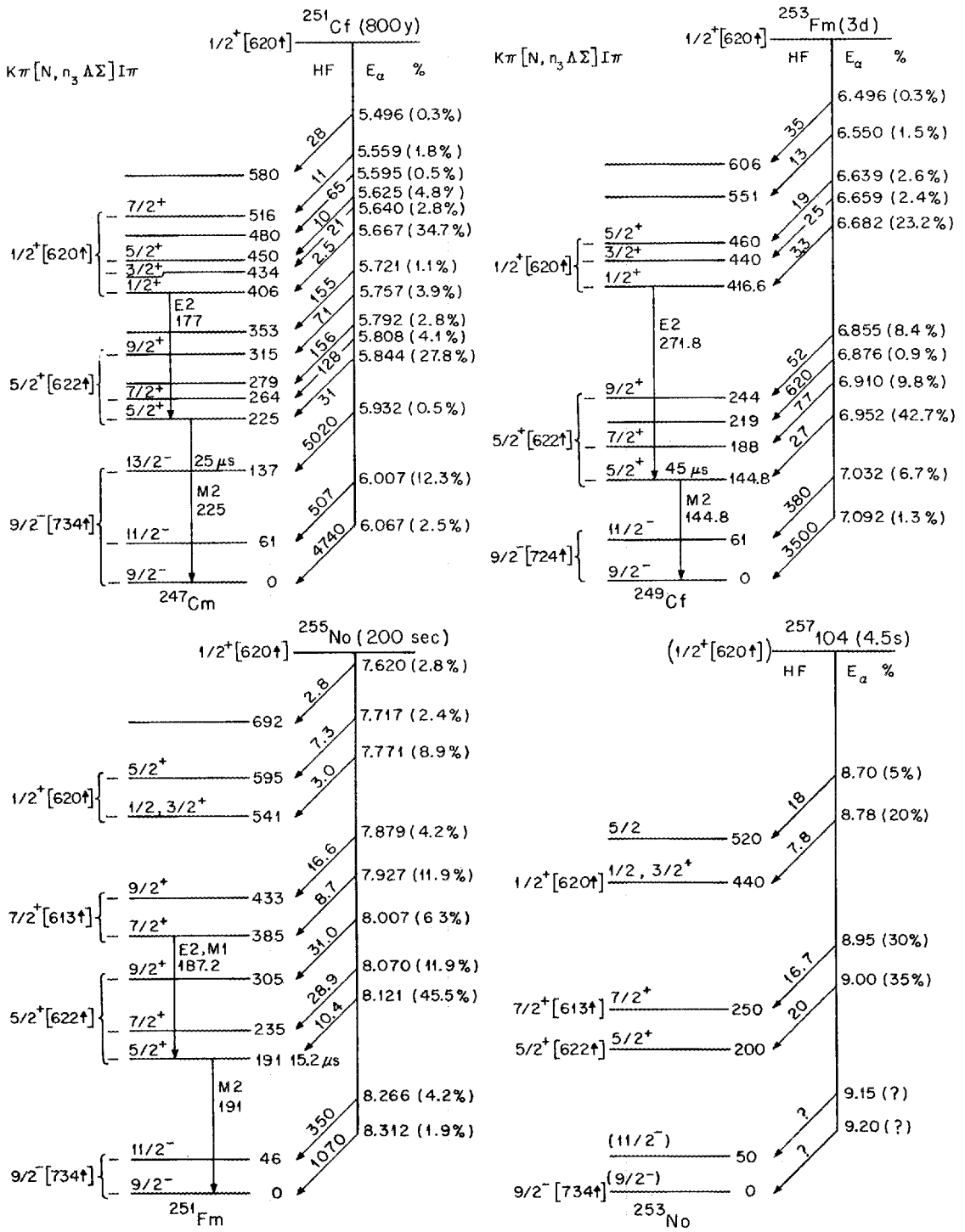

Fig. 2.18. Decay schemes for the $N = 151$ nuclides ^{247}Cm and ^{249}Cf and the ^{251}Fm results from this work. The data for ^{253}No from the alpha decay of ^{257}104 are interpreted from the data of Ghiorso et al., ref. 3.

rays observed in the decay of ^{255}No are listed in Table 2.27.

We have combined all of our data, including alpha energies, intensities, and hindrance factors together with gamma-ray energies, intensities, and conversion coefficients, and have derived the level scheme for ^{251}Fm shown in the lower left corner of Fig. 2.18. The level schemes for the other well-established N = 151 nuclides, ^{247}Cm and ^{249}Cf, are also shown in Fig. 2.18 for comparison. The data for ^{253}No from the alpha decay of ^{257}104 have been judiciously derived from the data of Ghiorso et al.[3] The similarity, as expected for all odd-A N = 151 nuclides, is striking nonetheless. It is interesting to note that our results for the decay of ^{255}No represent the first case for detailed nuclear spectroscopic investigations above Z = 100 apart from singles alpha spectroscopy. Our results are being prepared for publication.

Table 2.26. Summary of alpha-spectra data for ^{255}No

Alpha energy (MeV)	Intensity (%)	Excited-state energy (keV)	Hindrance factor
8.312 ± 0.009	1.9 ± 0.1	0	1070
8.266 ± 0.008	4.2 ± 0.4	46	350
8.121 ± 0.006	45.5 ± 1.3	191	10.4
8.077 ± 0.009	11.9 ± 1.6	235	28.9
8.007 ± 0.011	6.3 ± 1.1	305	31.0
7.927 ± 0.007	11.9 ± 0.7	385	8.7
7.879 ± 0.011	4.2 ± 0.4	433	16.6
7.771 ± 0.007	8.9 ± 0.7	541	3.0
7.717 ± 0.011	2.4 ± 0.4	595	7.3
(7.620 ± 0.010)	(2.8 ± 0.4)	(692)	(2.8)

Table 2.27. A. Gamma rays and x rays observed in the decay of ^{255}No

Transition energy (keV)	Photon intensity[a] (%)	Notes
115.28 ± 0.09 (Fm $K_{\alpha 2}$)	19.4 ± 2.3	$K_{\alpha 2}/K_{\alpha 1}$ = 0.65 ± 0.10
121.07 ± 0.09 (Fm $K_{\alpha 1}$)	29.9 ± 3.0	
135.2 ± 0.2 (Fm $K_{\beta 3}$)	2.2 ± 1.0	
136.6 ± 0.2 (Fm $K_{\beta 1}$)	2.6 ± 1.0	
140.1 ± 0.3 (Fm $K_{\beta 2'}$)	1.9 ± 0.9	
Σ Fm K x rays	56.0 ± 4.1	
1.87.2 ± 0.2 ($M1$ or $E2$)	5.5 ± 2.5	$\alpha_K = 1.4^{+2.1}_{-0.6}$ $\alpha_T = 1.9^{+4.9}_{-1.2}$ Theory $\alpha_T(M1)$ = 8.02 $\alpha_T(E2)$ = 1.66

[a]Absolute per ^{255}No alpha decay.

B. Fm K x rays per ^{255}No alpha group

Alpha group	K x ray intensity per alpha (%)	
	Prompt	Delayed
To $\frac{5}{2}^+$[622↑] band		37 ± 11
To $\frac{7}{2}^+$[613↑] band	47 ± 11	61 ± 14
To $\frac{1}{2}^+$[620↑] band	87 ± 12	38 ± 15

1. Electronuclear Division.
2. C. E. Bemis, Jr., P. F. Dittner, C. D. Goodman, R. L. Hahn, D. C. Hensley, and R. J. Silva, "The Unequivocal Identification of Transfermium Elements Using X-Ray Techniques," the preceding contribution, this report.
3. A. Ghiorso et al., *Phys. Rev. Lett.* **22**, 1317 (1969).

ON THE $M2$ TRANSITION PROBABILITY BETWEEN THE $\frac{5}{2}^+$[622↑] ⇌ $\frac{9}{2}^-$[734↑] NILSSON STATES

C. E. Bemis, Jr. D. C. Hensley[1]
P. F. Dittner K. Kumar[2]
C. D. Goodman[1] R. J. Silva

Magnetic quadrupole transitions, $M2$, have been observed between the same pair of intrinsic single-particle Nilsson states in the heavy-mass deformed region for N = 151 nuclides. These cases are for the $\frac{5}{2}^+$[622↑] → $\frac{9}{2}^-$[734↑] transitions in ^{247}Cm (ref. 3), ^{249}Cf (ref. 4), and ^{251}Fm (ref. 5). Very little information is available for $M2$ transitions in the deformed regions, and little information exists for transition probabilities for two or more cases of transitions of any multipolarity between the same pair of intrinsic Nilsson states. The three cases of $M2$ transitions listed above are the exception and have caught our interest.

We have derived the transition probabilities, $B(M2)$, for these cases using lifetime information and total conversion coefficients interpolated from the tables of Hager and Seltzer.[6] These $B(M2)$ values are listed in Table 2.28, together with the retardation factors, F_w, relative to the Weisskopf single-particle estimate, which provide a reference point for the relative speed of the transitions.

Using the wave functions by Chi[7] for particle states in a Nilsson well in the $j \cdot m$ coupling scheme rather than the more mathematically cumbersome Nilsson wave

Table 2.28. Magnetic quadrupole transition probabilities for the $5/2^+[622\uparrow] \rightarrow 9/2^-[734\uparrow]$ neutron transition

Case	E_γ (keV)	$T_{1/2}$ (total) (μsec)	α (total)	$B(M2)^a$ (e^2cm^4)	$F_w{}^b$
				$\times 10^{-55}$	
^{247}Cm	225	23 ± 3	12.4	2.90 ± 0.35	244 ± 29
^{249}Cf	144.8	45 ± 5	67.9	2.83 ± 0.32	250 ± 28
^{251}Fm	190	15.2 ± 2.3	30.2	4.76 ± 0.72	150 ± 30

[a] $1/\tau_\gamma(\text{sec}) = 1.24 \times 10^{61} \cdot E_\gamma{}^5\ (\text{MeV}) \cdot B(M2)\ (e^2\text{cm}^4)$.
[b] Retardation relative to Weisskopf estimate using $r_0 = 1.2$ F.

functions ($l \cdot s$ coupling scheme), we have derived the theoretical $B(M2)$ values. We have taken $g^{\text{eff}} = 0.6g^{\text{free}}$ and have used a pairing energy $\Delta = 12/\sqrt{A}$ (MeV). For a deformation $\delta = 0.3$, the transitions are retarded by about a factor of 1.6 → 2.8, which is very satisfying agreement.

The transition probabilities for all three $M2$ transitions considered here are nearly equal within the errors of experiment and are in essential agreement with theoretical values. These facts perhaps indicate that the two Nilsson states involved for the three cases studied, the $5/2^+[622\uparrow]$ and $9/2^-[734\uparrow]$ orbitals, are nearly pure single-particle states. We have estimated the half-life of the proposed $5/2^+[622\uparrow]$ state[5] at 200 keV in ^{253}No, which is populated in the alpha decay of ^{257}104, to be ~12 μsec. This half-life may be determined in a manner similar to those of the other $N = 151$ cases and should provide further insight to the $5/2^+[622\uparrow] \rightarrow 9/2^-[734\uparrow]$ $M2$ transitions.

1. Electronuclear Division.
2. Neutron Physics Division.
3. A. Chetham-Strode, Jr., et al., *Nucl. Phys. A* **107**, 645 (1968).
4. I. Ahmad et al., *Phys. Rev.* **164**, 1537 (1967).
5. C. E. Bemis, Jr., P. F. Dittner, D. C. Hensley, C. D. Goodman, and R. J. Silva, "The Alpha Decay of ^{255}No and States in ^{251}Fm," the preceding contribution, this report.
6. R. S. Hager and E. C. Seltzer, *Nucl. Data, Sect. A* **4**, 1 (1968).
7. B. Chi, *Nucl. Phys.* **83**, 97 (1966).

THE NEW NUCLIDE ^{259}No[1]

R. J. Silva P. F. Dittner
M. L. Mallory P. J. Hammons
O. L. Keller

Nobelium-255, with a half-life of 185 sec, was the longest-lived isotope of element 102 known; however, semiempirical correlations of alpha, beta, and spontaneous-fission decay half-lives for the heaviest elements suggest an order-of-magnitude longer half-life for ^{259}No. A longer-lived isotope would be extremely valuable for carrying out further chemical studies on nobelium; therefore, a search for a new, long-lived alpha-emitting isotope of element 102 with mass 259 has been carried out through bombardment of ^{248}Cm with ^{18}O ions from the Oak Ridge Isochronous Cyclotron via the (^{18}O,$\alpha 3n$) reaction.

A 350-μg/cm^2 target of ^{248}Cm was prepared by electrodeposition of the curium nitrate from an isopropyl alcohol solution onto a ½-mil-thick Be backing foil and converted to the oxide by heating to ~600°C. The $^{18}O^{5+}$-ion beam was collimated to the target area (0.25 cm^2) and degraded from 123 MeV to desired energies between 88 and 106 MeV with Be foils. The product atoms recoiling from the target were stopped in He and collected by "gas jet" onto a platinum catcher foil on the end of a rabbit. The foil could be pneumatically transferred to the laboratory area in a few seconds for alpha-particle energy analysis.

The bombardment, gas-jet collection, and rabbit systems, as well as the basic electronic system, used in these experiments have been described elsewhere.[2] The energy resolution of the alpha detection system was about 25 keV FWHM at 22% geometry.

Figure 2.19 shows an alpha-particle energy spectrum accumulated from eight 2-hr bombardments of the target with 97-MeV oxygen ions. This bombarding energy produced the highest yield of product (~20 counts per particle-microampere-hour). We believe the rather broad peak at 7.52 MeV is due to ^{259}No decay. The peaks at 7.60 and 7.68 MeV are also thought to be associated with ^{259}No. The half-life was determined to be 1.5 ± 0.5 hr, as also shown in Fig. 2.19. This activity was not produced when the target was bombarded with ^{12}C and ^{16}O ions; however, in the latter case, ^{257}No from the (^{16}O,$\alpha 3n$) reaction was observed.

The long half-life allowed us to carry out chemical separation of the nobelium from other elements produced in the target using cation-exchange column techniques. Figure 2.20 shows preliminary results on the elution position of the 7.52-MeV alpha activity relative to Y, Ba, Sr, and Fm using 3 M ammonium α-hydroxyisobutyrate (pH 5.0) as eluent. The Fm was produced in the bombardment from the (^{18}O,$2\alpha xn$) reaction, while ^{133}Ba, ^{90}Sr, and ^{90}Y were added in tracer quantities. The arrow indicates the expected elution position for nobelium relative to the tracers from a 2-mm-diam by 2-cm-long Dowex 50-X12 resin bed heated to 75°C.[3]

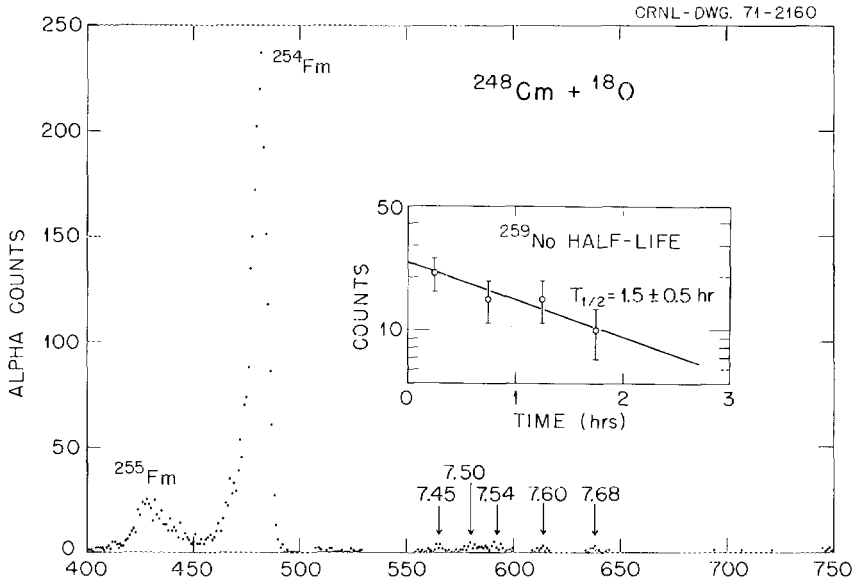

Fig. 2.19. Alpha-particle energy spectra accumulated from bombardments of ^{248}Cm with 97-MeV ^{18}O ions. Also shown is the half-life derived from the time distribution of the 7.50- to 7.68-MeV alpha-particle groups.

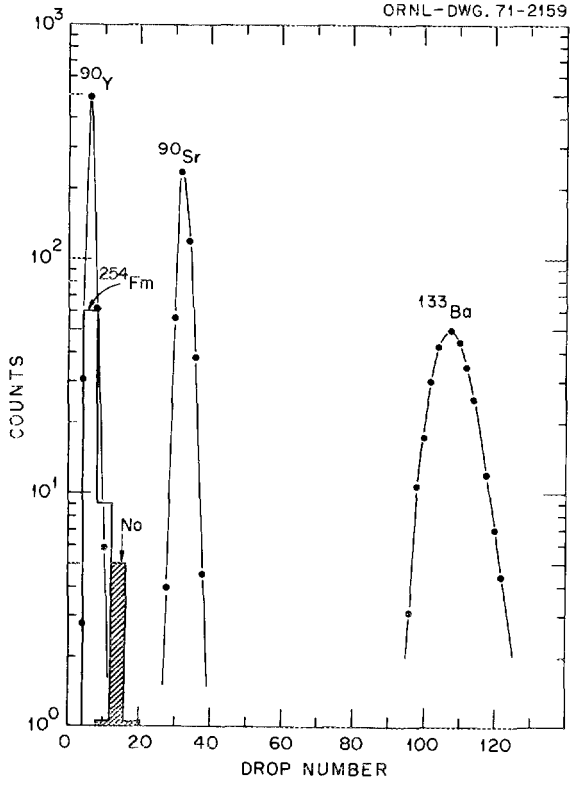

Fig. 2.20. Cation exchange column elution of the 7.52-MeV alpha activity and tracer quantities of elements of groups II (Sr, Ba) and III (Y, Fm) of the chemical periodic table. The arrow indicates the expected elution position for element 102.

The energy and half-life of the 7.52-MeV alpha activity agree reasonably well with those expected[4] for ^{259}No assuming decay to excited nuclear states. The ground state of ^{259}No is expected to be $9/2^+$ from the odd 157th neutron in the [615↓] Nilsson level, as is the case with ^{257}Fm. The ground state of the daughter, ^{255}Fm, is $7/2^+$[613↑]. One expects alpha decay between different Nilsson states to be hindered, while favored decay should take place to an excited $9/2^+$[615↓] level in ^{255}Fm. From ^{257}Fm decay, this state is known to be at about 250 keV above ground state in ^{253}Cf. The alpha group at 7.68 MeV could possibly be the hindered ground-state-to-ground-state band decay in ^{259}No.

From the trends in spontaneous-fission half-lives given by even-even nuclides, one might have expected a much shorter half-life for ^{259}No than observed due to spontaneous-fission decay; however, odd-A nuclides also experience a retardation in spontaneous-fission decay lifetimes. In particular, unusually large hindrance factors ($\sim 10^{10}-10^{12}$) over even-even trends seem to be associated with $N = 157$ nuclides (^{257}Fm,^{261}104) compared with the hindrance factors of 10^5-10^7 for most other odd-A or odd-odd-type nuclides.

The alpha-particle energy of 7.52 MeV corresponds to a decay energy (Q_α) of 7.64 MeV. The partial alpha half-life for unhindered decay calculated from this Q_α is 1.47 hr,[5] in good agreement with the observed value. Apparently electron capture and spontaneous fission

are not significant competing modes of decay; however, only a very cursory search has been made.

Work is in progress to study chemically separated samples in more detail and to establish the genetic linkage between the proposed ^{259}No and its decay daughter, ^{255}Fm.

1. A similar contribution has appeared in *Electronucl. Div. Annu. Progr. Rep. Dec. 31, 1970*, ORNL-4649, p. 72.
2. R. J. Silva et al., *Phys. Rev. C* **2**, 1948 (1970).
3. J. Maly et al., *Science* **160**, 1114 (1968).
4. V. E. Viola, Jr., and G. T. Seaborg, *J. Inorg. Nucl. Chem.* **28**, 741 (1966).
5. J. O. Rasmussen and C. J. Gallagher, *J. Inorg. Nucl. Chem.* **3**, 333 (1957). Calculated values were normalized to fit half-lives of known even-even alpha emitters in this region.

SEARCH FOR ELEMENT 106

R. D. Baybarz[1] R. L. Hahn
C. E. Bemis, Jr. D. C. Hensley[2]
P. F. Dittner O. L. Keller
E. Eichler M. L. Mallory
C. D. Goodman[2] R. J. Silva

The development of high-energy and high-intensity beams of oxygen ions at the ORIC and the availability of relatively large quantities of ^{249}Cf produced at the HFIR and Transuranium Processing Plant have made it possible to search for the new element 106 via the ^{249}Cf(^{18}O,4n)^{263}106 reaction. In order to search for new elements, it is essential to have reasonably accurate

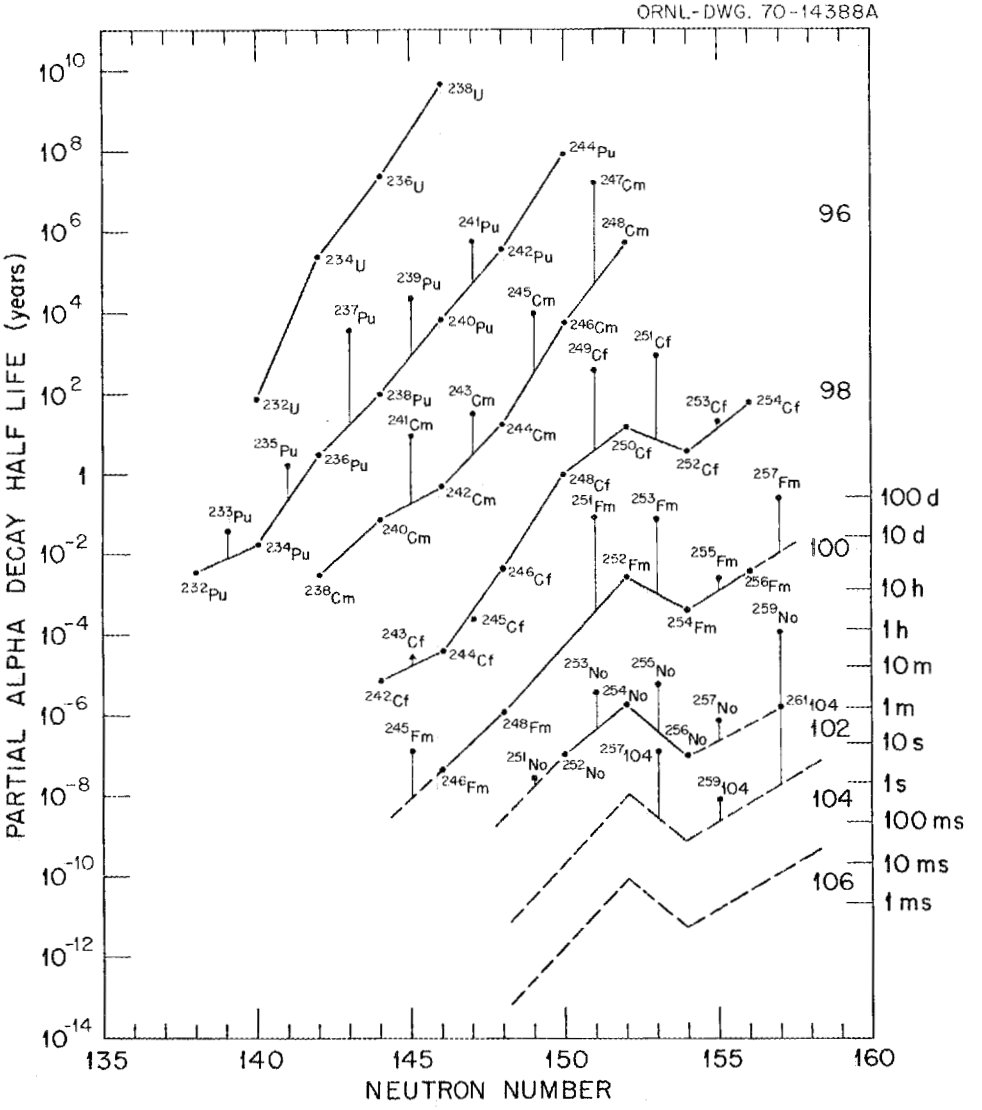

Fig. 2.21. Alpha-decay half-lives as a function of neutron number for even-Z transuranium nuclides. The solid lines connect even-even nuclide points, while the dotted lines are predicted trends.

predictions of their half-lives and production cross sections; it is virtually impossible to design experiments without them, and they are frequently the key to success.

Figures 2.21 and 2.22 show plots of experimentally determined alpha and spontaneous-fission half-lives for a number of transuranium elements. The data are most conveniently presented as a series of two-dimensional plots, each of constant atomic number, of the half-lives as a function of neutron number. The most smoothly varying correlations are obtained for plots of nuclei with even numbers of protons and neutrons. In all cases, varying degrees of retardation in alpha and spontaneous-fission decay are exhibited by nuclei with odd numbers of protons and/or neutrons due to the effect of the unpaired particles.

As can be seen in Figs. 2.21 and 2.22, for a given Z, alpha-decay half-lives increase (i.e., alpha-decay energies decrease) while spontaneous-fission half-lives decrease with increasing neutron number above the $N = 152$ subshell. The selection of $^{263}106$ as the best candidate (longest lived) for our search results from a compromise between these two effects. We estimate the energy of the most prominent alpha-particle group in the decay of $^{263}106$ to be 9.25 ± 0.25 MeV, giving a partial alpha half-life between 100 msec and 2 sec. Assuming the same spontaneous-fission retardation factor (10^{10} – 10^{12}) for $^{263}106$ as is observed for the other $N = 157$ nuclides, that is, ^{257}Fm, ^{259}No, and $^{261}104$, we estimate a partial half-life for spontaneous fission of a few seconds. The electron-capture half-life is expected to be several hours.[3]

The most successful predictions of heavy-ion cross sections for the production of the heaviest elements are due to the scheme of Sikkeland.[4] Figure 2.23 shows computer-calculated excitation functions for the reaction ^{249}Cf(^{18}O,xn) to produce isotopes of element 106. (These estimates are usually good to a factor of 3.) The peak production cross section for $^{263}106$ is predicted to be 2×10^{-34} cm^2 at a bombarding energy of 97 MeV. Irradiating a 450-μg/cm^2 target of ^{249}Cf with 0.5 particle-μA of ^{18}O, one can hope to produce approximately 40 atoms/day; however, somewhat fewer than half are measurable due to counting geometry and mechanical losses of our present system.

Using our recoil gas-jet system,[5] modified to observe very short half-life activities ($T_{1/2} < 100$ msec), we have made a preliminary search for an alpha-emitting isotope of element 106 with the properties discussed above. Unfortunately, short-lived neutron-deficient iso-

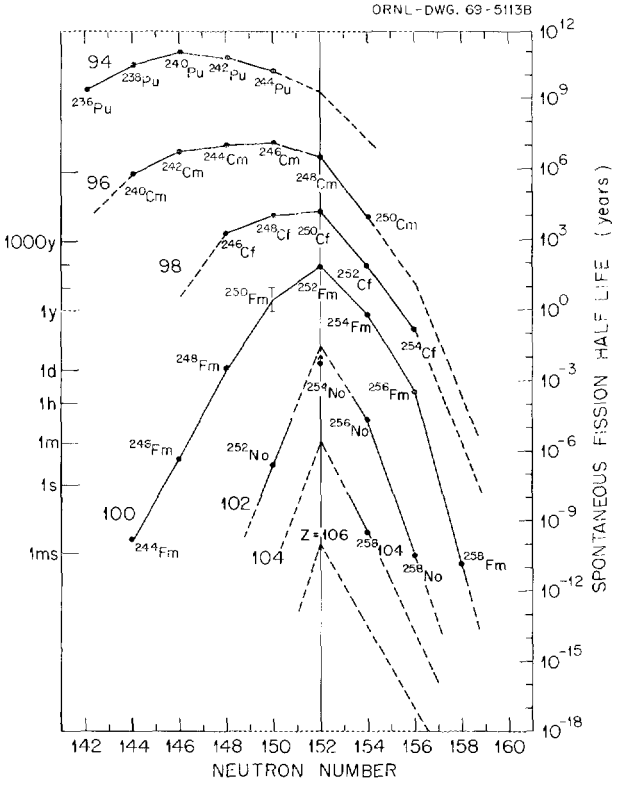

Fig. 2.22. Spontaneous-fission decay half-lives as a function of neutron number for even-Z transuranium elements. The solid lines connect even-even nuclide points, while the dotted lines are predicted trends.

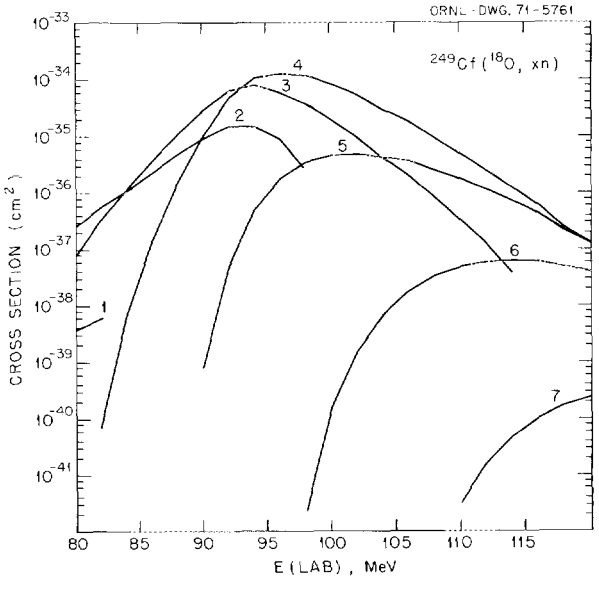

Fig. 2.23. Computer-calculated excitation functions for the ^{249}Cf(^{18}O,xn)$^{267-x}106$ reactions. Numbers on curves are the number of neutrons.

topes of elements in the Pb to Th region, produced from small amounts of impurities in the target, gave rise to background peaks in the 9.0-to-9.5-MeV energy range and obscured the few events expected for the decay of $^{263}106$.

Experiments are now being directed toward development of a capillary system[6] for the rapid transport of the product atoms several feet from the bombardment assembly into a shielded area where more sophisticated coincidence experiments (alpha–x-ray or parent-daughter) or fast gas-phase chemical separations may be carried out to select from the background and identify the activity due to element 106.

1. Chemical Technology Division.
2. Electronuclear Division.
3. V. E. Viola, Jr., and G. T. Seaborg, *J. Inorg. Nucl. Chem.* **28**, 697 (1966).
4. T. Sikkeland, A. Ghiorso, and M. Nurmia, *Phys. Rev.* **172**, 1232 (1968).
5. R. L. Hahn, *Chem. Div. Annu. Progr. Rep. May 20, 1968*, ORNL-4306, p. 37.
6. R. D. MacFarlane et al., *Nucl. Instrum. Methods* **73**, 285 (1969).

RADIOACTIVITY ASSOCIATED WITH PLEOCHROIC HALOS

R. V. Gentry[1] J. W. Boyle

The identification of various types of radioactivity associated with pleochroic halos has until recently been primarily a problem of relating halo ring radii with energies of known alpha emitters. Autoradiographic studies, alpha-recoil, and fission-track techniques have also been utilized as secondary analytical techniques. Even so, several halo sizes which cannot be directly related to known alpha emitters still exist. Giant halos with radii more than twice as large as normal radii have been found and subsequently reported.[2] If the giant halos did indeed arise from alpha activity, the energies involved range to about 15 MeV or more. Dwarf halos with radii much less than normal radii have also been found. Like the giant halos the dwarf halos are extremely rare, and their known occurrence is limited to very specific sites. In the case of the dwarf halos, if they arise from alpha radioactivity, the radii imply the existence not only of alpha emission less than 1 MeV, but of several different alpha energies in the 1-to-3-MeV range, which apparently cannot be attributed to any known alpha emitters. An intriguing question is whether the scattered reports of very low-energy alpha activity over the last 40 years can be related to the origin of the dwarf halos. These possibilities have been described in more detail.[3] Improved autoradiographic techniques as well as alpha-particle spectroscopy are planned to ascertain whether very low-energy alpha activity is present in certain samples containing the dwarf halos. Also, the newly developed ion microprobe mass spectrometer shows promise of being capable of analyzing the isotopic as well as the elemental composition of even the very small halo inclusions. Isotopic analyses of polonium halo inclusions using the ion microprobe have revealed Pb isotopic ratios differing from any previously reported values. Apparently large isotopic variations are locked within very small halo inclusions.[3]

1. Visiting scientist from the Institute of Planetary Science, Columbia Union College, Takoma Park, Md.
2. R. V. Gentry, *Science* **169**, 670 (1970).
3. R. V. Gentry, *Science* (in press).

SEARCH FOR SUPERHEAVY ELEMENTS IN NATURE

J. S. Drury D. A. Lee

The search for superheavy elements in nature continued along several lines of endeavor.

Field trips were made to southwest Colorado and Ontario to obtain large (100-lb) samples of ores and mill concentrates for use in the new ORNL neutron multiplicity counter.[1] Thirty-one hundred pounds of lead, zinc, copper, silver, and gold ores and mill concentrates were obtained from the Emperius and Homestake Mines at Creede, Colorado, the Dixilyn Operations and the American Standard Metals Company at Silverton, Colorado, and the Idarado Mine at Telluride, Colorado. In the Sudbury basin, samples of pentlandite, chalcopyrite, pyrrhotite, and norite were obtained from the following mines: Totten, Creighton, Copper Cliff North, Clarabelle, Frood-Stobie, Falconbridge, Maclennan, Strathcona, and Levack. One-hundred-pound samples of ore concentrates were also obtained from the following mills: Frood-Stobie, Creighton, Levack, Copper Cliff, Coniston, Falconbridge, and Strathcona. Dust samples of similar amount were obtained from smelters located at Copper Cliff, Coniston, Falconbridge, and Strathcona. In addition, approximately 150 lb of rock were collected at the abandoned Vermillion Mine, where samples of high precious metal content (sperrylite) had recently been found. In all, about 110 samples, weighing approxi-

mately 5.5 tons, were obtained for the Neutron Multiplicity Counting Program.[2]

In another phase of the search, samples of the following ores or minerals were examined, by means of the "fire-assay" technique and spontaneous-fission counting,[3] for the presence of superheavy elements more noble than silver:

Sample	Source
Amphibole	Chvaletice, Bohemia, and San Benito County, Calif.
Barite	Potasi, Mo.
Basalt	Laacher See, Germany, Falkensten, Norway, Linz, Germany, and Pisgah Crater, Calif.
Chalocite	Superior, Ariz.
Chromite	Transvaal, South Africa, and Southern Rhodesia
Columbite	Keystone, S.D.
Enstatite	Norway and Nye County, Mont.
Gabbro	San Diego County, Calif., and Wichita Mountains, Okla.
Ilmenite	Hoback Range, Wyo., and St. Urbain, Canada
Magnetite	Marmora, Canada
Peridotite	Lowell, Vt.
Psilomelane	Dona Ana County, N.M.
Pyrolusite	Lake Valley, N.M.
Pyrrhotite	Sudbury, Canada
Rutile	Nelson County, Va.

Among the ores and minerals collected were some which were mechanically amenable to the analytical procedures described above but which seemed likely, on the basis of present theory, to contain superheavy elements *less* noble than gold (e.g., 114–120). These samples should not benefit from the fire-assay concentration step if the chemical properties of the superheavy elements are as presently predicted. Nevertheless, we chose to process these samples on the grounds that the present state of the art of predicting the chemical properties of the superheavy elements is at best uncertain. This set of samples included:

Sample	Source
Celestite	Torreon, Mexico
Gadolinite	Norway
Galena	Galena, Kan.
Molybdenite	Climax, Colo.
Monazite	Elk Mountain, N.M.
Stibnite	San Benito County, Calif.
Strontianite	Hamm, Westphalia

No evidence for spontaneous fission was detected in any of the foregoing samples.

Although ekaosmium (108) should occur in ultrabasic rocks with the platinum metal group, there is some question that such samples could be concentrated and detected via the fire-assay technique because of the expected volatility of the tetroxide. For this reason we developed a wet chemical method to concentrate element 108 in our samples. The various ores were pulverized and placed in a still[4] with 350 μg of osmium and a mixture of mineral acids. The volatile osmium tetroxide (and presumably the tetroxide of ekaosmium, if present) distilled and was collected in traps containing various liquids, of which water appeared to be most satisfactory. These solutions were electrolyzed to deposit osmium on nickel disks for fission counting. Samples processed in this manner included: basalt, chromite, columbite, enstatite, gadolinite, magnetite, monazite, peridotite, pyrolusite, rutile, and stibnite from sources previously identified. In addition, chalcopyrite from the Falconbridge Mine, Sudbury, Canada, was processed, as well as biotite samples from a Norwegian quarry and sinter-treated dust from a Western lead processing plant. No fission activity was observed in any of these samples.

Element 119 (ekafrancium) is expected to have properties resembling the alkali metals. Several Norwegian micas containing numerous pleochroic halos were thought to be potentially interesting sources for this element. These samples were processed as follows. The mineral was treated with HF to remove silica and yield soluble alkali metal fluorides. The latter were leached from the residues with water and precipitated with sodium tetraphenylboron. This precipitate was dissolved in acetone and treated with hydrochloric acid to decompose the complex. The water-immiscible phenylboron was extracted with *p*-xylene, and the alkali metal salts in the aqueous phase were evaporated on a disk for spontaneous-fission counting. None of the mica samples containing pleochroic halos gave evidence of spontaneous fission.

Element 120 (ekaradium) was sought in minerals known to contain alkaline earths. The alkali metals in the samples were removed as described above, and the residues were leached with HCl. Iron was extracted with Adogen-364 (a long-chain tertiary amine) in *p*-xylene. Aluminum, rare earths, and similar elements were precipitated with ammonium hydroxide. The alkaline earths were precipitated with ammonium oxalate. After ignition and conversion of the alkaline earths to nitrates, calcium was extracted with methanol, barium was precipitated as the chromate, and the remainder was collected as a strontium fraction. Each fraction was plated on disks for spontaneous fission counting. The ores treated in this manner were strontianite, celestite, monazite, rutile, gadolinite, barite, and peridotite, as described above. No spontaneous fission was observed in these samples.

1. R. L. Macklin, F. M. Glass, J. Halperin, R. T. Roseberry, R. W. Stoughton, and M. Tobias, "Neutron Multiplicity Counter," another contribution in this chapter, this report.
2. J. Halperin, E. Cheifetz, J. S. Drury, R. V. Gentry, E. R. Giusti, R. C. Jared, R. M. Milton, R. L. Macklin, R. W. Stoughton, and S. G. Thompson, "Search for Superheavy Elements with Neutron Multiplicity Counters," the following contribution, this report.
3. J. S. Drury, *Chem. Div. Annu. Progr. Rep. May 20, 1970*, p. 46.
4. G. H. Faye, *Anal. Chem.* 37, 696 (1965).

SEARCH FOR SUPERHEAVY ELEMENTS WITH NEUTRON MULTIPLICITY COUNTERS

J. Halperin — R. C. Jared[1]
E. Cheifetz[1] — R. M. Milton[3]
J. S. Drury — R. L. Macklin[4]
R. V. Gentry[2] — R. W. Stoughton
E. R. Giusti[1] — S. G. Thompson[1]

The following samples were counted for several days each in the ORNL ^{3}He multiplicity counter:[5] 1 kg of silica gel previously used for sorbing and desorbing gases in the Linde plant for producing noble gases; 1 liter of gas, which contained an appreciable amount of xenon, from the Linde plant; 50 g of mica which contained dwarf halos; 130 g of monazite ore which was found adjacent to mica containing giant halos; 15 kg of ore from Colorado containing lead sulfide, barium sulfate, and some gold; and 15 kg of flue dust from a copper smelter from the Sudbury region in Canada. In addition, about 20 kg of each of the following samples were sent to UC-LRL and counted on their neutron multiplicity scintillation counter:[6] lead sulfide concentrate that has a relatively high ^{204}Pb content, from Ivigtut, Greenland; bastnasite ($CeFCO_3$) ore from California; and both a copper and a nickel concentrate from a mill in the Sudbury region in Canada. None of the above samples showed multiple neutron counts in excess of background, which, in the case of the latter four samples, indicates a spontaneous-fission half-life of the major metallic components in excess of about 5×10^{22} years. (Alternatively, if the half-life of the superheavy element is 10^9 years, an upper limit of 10^{-14} g of superheavy element per gram of sample is indicated.)

Recently Marinov and coworkers[7] chemically separated various fractions from a tungsten target irradiated with 10^{18} protons of 24 GeV at CERN. In the mercury fraction they found 93 fission fragment counts in 37 days which they thought might result from spontaneous fission of an isotope of ekamercury. Because of these findings, colleagues at BNL sent us two tungsten targets which had been irradiated with about 10^{17} protons of 28 GeV. With the lower irradiation, we did not expect to see any multiple neutron events whether or not Marinov and coworkers[7] correctly interpreted their results. Indeed, we did not see any neutron events above background.

We shall continue our search for superheavy elements both in nature and in accelerator targets.

---

1. Lawrence Radiation Laboratory, University of California, Berkeley.
2. Visiting scientist from the Institute of Planetary Science, Columbia Union College, Takoma Park, Md.
3. Union Carbide Corp., Linde Laboratories, Tarrytown, N.Y.
4. Physics Division.
5. R. L. Macklin, F. M. Glass, J. Halperin, R. T. Roseberry, R. W. Stoughton, and M. Tobias, "Neutron Multiplicity Counter," another contribution in this chapter, this report.
6. The UC-LRL neutron multiplicity counter is located 800 ft underground; it has a lower multiple-neutron background than the ORNL counter because of this greater shielding against cosmic-ray muons which, in striking large samples containing materials of relatively high atomic number, give rise to countable multiple-neutron events.
7. A. Marinov et al., *Nature (London)* 229, 464 (1971).

ELECTRON-TRANSFER AND $f \rightarrow d$ ABSORPTION BANDS OF SOME LANTHANIDE AND ACTINIDE COMPLEXES AND THE STANDARD III-IV OXIDATION POTENTIALS FOR EACH MEMBER OF THE LANTHANIDE AND ACTINIDE SERIES[1]

L. J. Nugent — J. L. Burnett[3]
R. D. Baybarz[2] — J. L. Ryan[4]

Best values for the standard III-IV oxidation potentials for each member of the lanthanide series and for each member of the actinide series are obtained from a variety of sources, namely, from the direct electrode measurements reported in the literature, from linear plots of electron-transfer absorption band energy for various Ln(IV) and An(IV) complexes vs the respective III-IV potential, from linear plots of $f \rightarrow d$ absorption band energy for various Ln(III) and An(III) complexes vs the respective III-IV potential, and from theoretical correlations using refined electron-spin-pairing-energy theory. Two major results of this work are: (1) the M III-IV potentials for M = Cm, Cf, Pr, and Tb are all within -3.2 ± 0.3 V, and (2) the indication that the unknown oxidation states Cf(IV), Es(IV), Pm(IV), Sm(IV), Fm(IV), and possibly Md(IV), listed in the order of decreasing stability, may be stabilized in various media. Altogether, the results are in excellent accord with the actinide hypothesis.

1. To appear in August issue of *J. Inorg. Nucl. Chem.* (1971).
2. Chemical Technology Division.
3. Present address: Division of Research, U.S. Atomic Energy Commission, Washington, D.C.
4. Pacific Northwest Laboratories, Richland, Wash.

SOLUTION ABSORPTION SPECTRA OF Bk(III) AND Bk(IV) AND THE FORMAL POTENTIAL OF THE Bk(IV)-Bk(III) COUPLE IN SEVERAL MEDIA[1]

R. D. Baybarz[2] J. R. Stokely[3]
J. R. Peterson[4]

The absorption spectrum of Bk(III) in 1 *M* $DClO_4$ – 99.9% D_2O was studied over the spectral region 200 to 1700 nm. Thirteen new absorption bands below 320 nm, including the previously unreported $f \rightarrow d$ transition bands at 242 and 212 nm, were observed. The absorption spectra of electrolytically produced Bk(IV) in 1 *M* $HClO_4$, 1 *M* H_2SO_4, 2 *M* K_2CO_3, 7.5 *M* H_3PO_4, and in 0.5 *M* di(2-ethylhexyl)phosphoric acid in dodecane were also investigated. The Bk(IV) spectrum was found to be characterized by a very strong electron transfer band at ~280 nm and only weak bands, corresponding to "forbidden" $f \rightarrow f$ transitions, in the visible wavelength region. Molar absorptivities were determined for the various bands in both the Bk(III) and Bk(IV) spectra. These Bk(IV) spectral determinations were made in conjunction with direct potentiometric measurements of the formal reduction potential of the Bk(IV)-Bk(III) couple in the various aqueous media mentioned above, as well as in 1 *M* HNO_3. The values derived from the appropriate Nernst equation plots range from +1.30 V vs S.C.E. in 1.0 *M* $HClO_4$ to +0.02 V in 2 *M* K_2CO_3.

1. Abstract of paper submitted to *J. Inorg. Nucl. Chem.*
2. Chemical Technology Division.
3. Analytical Chemistry Division.
4. Consultant; Department of Chemistry, University of Tennessee, Knoxville.

THIOCYANATE COMPLEXES OF TRIVALENT ACTINIDES[1]

H. D. Harmon[2] C. F. Coleman[3]
W. J. McDowell[3] J. R. Peterson[4]

Study of the aqueous thiocyanate complexes of the trivalent transplutonium actinides[5] continued by means of distribution equilibria with the cation-exchange extractant di(2-ethylhexyl)phosphoric acid (HDEHP). The resulting values of the overall formation constants for the mono-, di-, and trithiocyanate complexes in sodium thiocyanate–sodium perchlorate solution at constant ionic strength ($I = 1$) are listed in Table 2.29. These formation constants, β_1, β_2, and β_3, are defined by:

$$M^{3+} + nSCN^- \rightleftharpoons M(SCN)_n^{(3-n)+} ,$$

$$\beta_n = [M(SCN)_n^{(3-n)+}] / [M^{3+}] [SCN^-]^n .$$

Previous workers have not reported formation constants for all three complexes and have not agreed on the species identified. One report gave β_1 and β_2 for Pu, Am, Cm, and Cf,[6] while two others gave β_1 and β_3 for Am[7,8] and Cm.[8] The error limits given in Table 2.29 are the standard deviation of fitting of each constant to the distribution data. The large error limits for the dithiocyanate complexes leave questionable the true existence of that complex species; at present our β_2 values can only be considered approximate upper limits.

Plots of β vs Z were examined for the "tetrad effect."[9,10,11] The tetrad grouping from curium to einsteinium is apparent in β_3 (Fig. 2.24) but not in β_1 or β_2 (Fig. 2.25). This suggests that bonding significantly affecting the $5f$ electrons occurs in the tri- but not the mono- or dithiocyanate complexes. This in turn is consistent with the trithiocyanate complex being inner sphere and the mono- and dithiocyanate complexes being outer sphere.[6]

Returning to the apparent values for β_2 (Fig. 2.25), if this species does indeed exist, the extent of its formation decreases with increasing atomic number from americium to einsteinium. This might suggest that the degree of covalent bonding increases with Z, causing a relative decrease in the tendency to form outer-sphere complexes. In support of this suggestion, it may be noted that rate constants for the hydration of trivalent lanthanide ions change rapidly in the analogous region Eu-Gd-Tb and that this has been interpreted as a sharp decrease in coordination number.[12]

Table 2.29. Formation constants for thiocyanate complexes of trivalent actinides

Aqueous $NaSCN$-$NaClO_4$ solution, ionic strength = 1, pH = 2; error limit is the standard deviation of fitting

	β_1	β_2	β_3
Americium	2.3 ± 0.1	1.1 ± 0.4	0.69 ± 0.28
Curium	2.8 ± 0.2	0.9 ± 0.6	0.84 ± 0.47
Berkelium	3.1 ± 0.2	0.3 ± 0.7	2.3 ± 0.6
Californium	3.7 ± 0.2	0.3 ± 0.6	2.6 ± 0.5
Einsteinium	3.6 ± 0.2	0.04 ± 0.71	2.9 ± 0.5

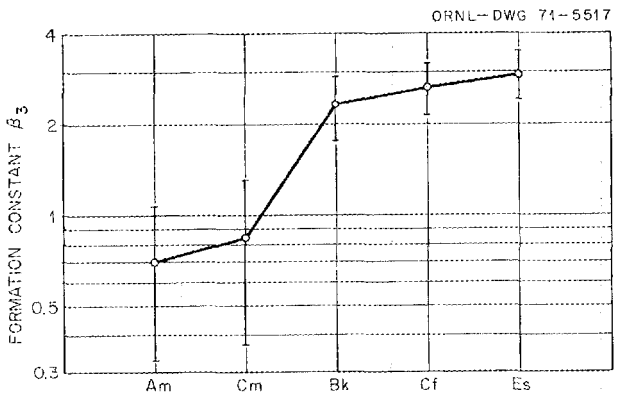

Fig. 2.24. Formation constant β_3 for actinide trithiocyanate complexes, showing "tetrad effect." Ionic strength is constant at 1 *M* (NaSCN + $NaClO_4$), pH 2. The error bars represent the standard deviation of fitting of each formation constant to the solvent extraction distribution data.

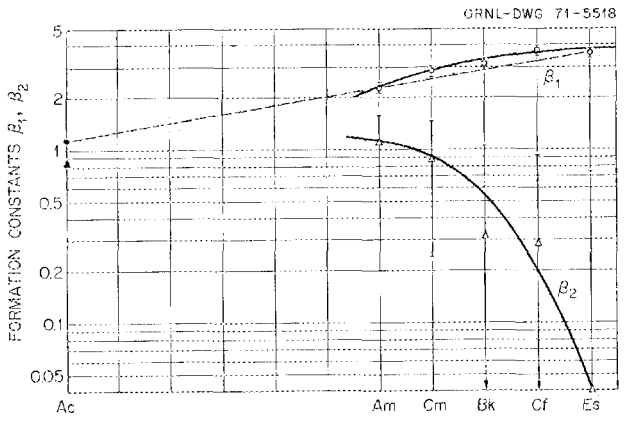

Fig. 2.25. Formation constants β_1 and β_2 for actinide mono- and dithiocyanate complexes. Actinium points from ref. 13.

The values for β_1 increase slightly with Z. It is of interest to note that a straight line through these log β_1 points (Fig. 2.25) also passes through the log β_1 point for $Ac(SCN)^{2+}$.[13] This is consistent with the concept that the monothiocyanates are outer-sphere complexes with stability dependent on electrostatic forces. This suggests extrapolation of the same line for prediction of β_1 values for the monothiocyanate complexes of the actinides beyond einsteinium.

1. Also appears in *Chem. Technol. Div. Annu. Progr. Rep. Mar. 31, 1971,* ORNL-4682, p. 123; submitted to *J. Inorg. Nucl. Chem.*
2. National Defense Education Act Title IV Fellow from the University of Tennessee, Knoxville.
3. Chemical Technology Division.
4. Consultant; Department of Chemistry, University of Tennessee, Knoxville.
5. *Chem. Technol. Div. Annu. Progr. Rep. May 31, 1970,* ORNL-4572, p. 187.
6. G. R. Choppin and J. Ketels, *J. Inorg. Nucl. Chem.* **27**, 1335 (1965).
7. T. Sekine, *Acta Chem. Scand.* **19**, 1519 (1965).
8. I. A. Lebedev and G. N. Yakovlev, *Radiokhimiya* **4**, 3046 (1962).
9. D. F. Peppard et al., *J. Inorg. Nucl. Chem.* **32**, 339 (1970).
10. D. F. Peppard, G. W. Mason, and S. Lewey, *J. Inorg. Nucl. Chem.* **31**, 2271 (1969).
11. I. Fidelis and S. Siekierski, *J. Inorg. Nucl. Chem.* **28**, 185 (1966).
12. D. G. Karraker, *J. Chem. Educ.* **47**, 424 (1970).
13. C. L. Rao, C. J. Shahani, and K. A. Mathew, *Inorg. Nucl. Chem. Lett.* **4**, 655 (1968).

THERMODYNAMIC SYSTEMATICS AMONG THE MEMBERS OF THE LANTHANIDE AND ACTINIDE SERIES[1]

L. J. Nugent J. L. Burnett[2]
L. R. Morss[3]

The thermodynamic data for the lanthanide and actinide metals (M) can be combined with the relative energies of the two lowest electronic configurations of the neutral gaseous atoms and the aqueous M III-IV oxidation potentials to show that systematic relationships exist which account for the irregular variations in the heats of formation $\Delta H_f^\circ[M(III)_{aq}]$ and $\Delta H_f^\circ[M(IV)_{aq}]$ as a function of atomic number. The observed systematics provides a check on some of the previously reported thermodynamic properties for the members of these series, and it provides a basis for the calculation of $\Delta H_f^\circ[M(III)_{aq}]$ and $\Delta H_f^\circ[M(IV)_{aq}]$ in each case where this information is not otherwise known.

1. To be submitted to *J. Chem. Thermodyn.*
2. Present address: Division of Research, U.S. Atomic Energy Commission, Washington, D.C.
3. Department of Chemistry, Purdue University, Lafayette, Ind.

THEORETICAL TREATMENT OF THE ENERGY DIFFERENCES BETWEEN $f^q d^1 s^2$ AND $f^{q+1} s^2$ ELECTRON CONFIGURATIONS FOR LANTHANIDE AND ACTINIDE ATOMIC VAPORS[1]

L. J. Nugent K. L. Vander Sluis[2]

The difference between the lowest energy level of the $f^q d^1 s^2$ electron configuration and the lowest energy level of the $f^{q+1} s^2$ electron configuration for the metal vapors of nine members of the lanthanide series and

four members of the actinide series are shown to be neatly and simply correlated by an adaptation of refined electron-spin-pairing-energy theory. The theory is also used to extrapolate the corresponding energy differences for those lanthanide and actinide metal vapors where this information was previously undetermined. The results are helpful as a guide in making spectral assignments and are generally useful in correlating the thermodynamic properties of the chemical compounds of the lanthanide and actinide series. The theoretical basis of the treatment should also be applicable for correlating the relative energies of other electron configurations in these metal atoms and ions.

1. To appear in August issue of *J. Opt. Soc. Amer.* (1971).
2. Physics Division.

ELECTRON SPECTROMETRY OF ACTINIDES AND ACTINIDE COMPOUNDS

M. O. Krause F. Wuilleumier[1]

A double-focusing electrostatic energy analyzer has been installed at the Transuranium Research Laboratory and adapted to the special requirements imposed by the hazards of handling transuranium elements. In particular, the source chamber and the sample-loading chamber have been redesigned and rebuilt.

With the present instrument the electronic structure of the actinides and their compounds can be studied using as probes either x rays of 1 to 2 keV energy, x rays of 100 to 200 eV, resonance radiation between 10 and 40 eV from gas discharges, or electrons over a wide range of energies. In addition, transitions between lightly bound electronic levels can be measured by converting the electron energy analyzer into a unique ultrasoft x-ray spectrometer.[2] The capability of the instrument is illustrated by way of the Au $4f$ (Mg $K\alpha$) and Pt $4f$ (Mg $K\alpha$) photoelectron lines which are plotted in Fig. 2.26. An effective resolution of about 1 eV (FWHM) can be achieved using the Mg $K\alpha$ doublet, width 0.65 eV, and an instrumental resolution of $\Delta E/E = 0.05\%$.

As part of the program of determining binding energies of electrons in elements beyond Pu, we have obtained preliminary results on binding energies of the N, O, P, and Q electrons of Am. Figure 2.27 shows as an example the $4f$ doublet represented as the Am $4f$ (Al $K\alpha$) photolines, which are 14.3(1) eV apart. Theoretical values of the spin splitting, 14.1 eV,[3] 14.4 eV,[4] or 15.3 eV,[5] compare favorably with the experimental determination, while values from theory and semiempirical extrapolations[6] of the binding energies lie somewhat above our experimental values of $E(N_6) = 463.6(5)$ eV and $E(N_7) = 449.3(5)$ eV. Deviations of 10 to 20 eV have been found for other level energies of Am which have been measured so far. When experimental and theoretical results are compared, we should remember that theory produces level energies of free atoms referred to the vacuum level, while experiments such as ours yield level energies of bound atoms referred to the Fermi level. As a consequence, theoretical values should lie above experimental values by 2 to 6 eV. Additional differences can arise from chemical shifts of core electron levels depending upon the chemical compound investigated. In this experiment, americium is believed to be present as $Am(OH)_3$ with a possible small admixture of the sesquioxide. Although measurement of level energies of Am in various compounds and in its metallic state are of intrinsic value, a rigorous test of theory will have to come from an experiment involving free Am atoms. Such an experiment of the photoionization of Am vapor is being prepared.

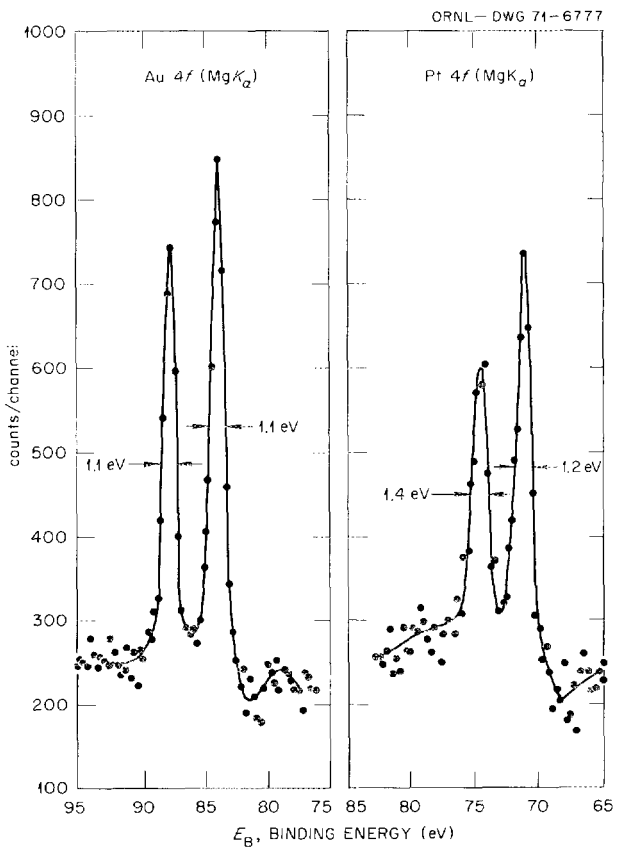

Fig. 2.26. The $4f$ doublets of Au and Pt excited by Mg $K\alpha$ x rays. $\Delta E/E = 0.05\%$.

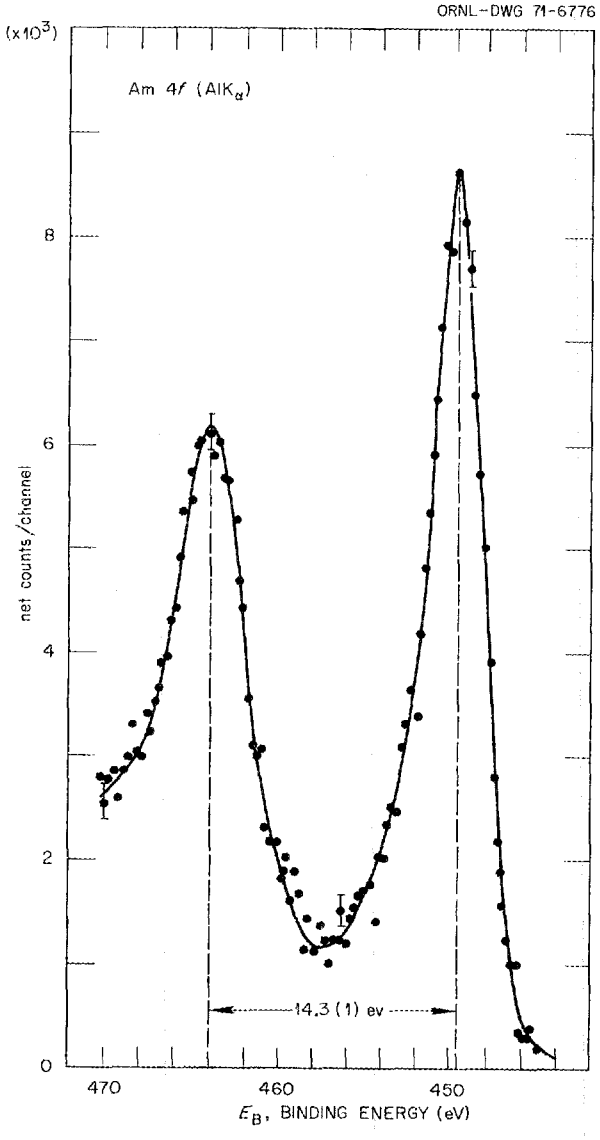

Fig. 2.27. The 4*f* doublet of Am excited by Al *Kα* x rays. A sample of 25 μg of ^{241}Am was electrodeposited on Pt as $Am(OH)_3$. $\Delta E/E = 0.16\%$.

In investigating the actinides a major interest centers around the identification of the 5*f* electrons which may appear as "atomic states," as "pure bands," or as "hybridized bands," depending upon the chemical state. In the gaseous state the angular momentum quantum is best inferred from angular distribution measurements of photoelectrons; in the solid state it must be deduced, however, from the variation in energy of photoionization cross sections. Cross sections, σ, for electrons with different l numbers often vary in a characteristic manner, and, in fact, vary quite distinctly for 5*f* electrons in the range from threshold to about 200 eV. For example, according to a free-atom model calculation,[7] σ_{5f} for $Z = 99$ rises rapidly from a small value of 2 Mb at 30 eV to 20 Mb at 90 eV and then drops off to less than 1 Mb near 200 eV. It is this possibility to identify orbitals, especially the 5*f* orbitals, by the energy dependence of σ that led us to search for good photon sources in the range from 100 to 200 eV. Narrow and intense lines, the $M\zeta$ x rays, shown in Fig. 2.28, were found in the elements Y, Zr, Nb, and Mo. In a first utilization[8] of these lines we were able to study with accuracy the photoexcitation of a K electron of He to the L level concomitant with the photoionization of the other K electron, which is a process having the small cross section of about 1 kb between 100 and 200 eV. X-ray transitions offer additional information on electronic structure and dynamics, and soft x-ray emission spectra are particularly useful in complementing photoelectron spectra of the band structure of solids. As implicitly contained in Fig. 2.28 or in any other photoelectron spectrum, such spectra represent images of the x-ray spectra of the excitation source, and the electron spectrometer has assumed the role of an x-ray spectrometer. Simply speaking, instead of fixing x-ray energy, $h\nu$, and deducing electron binding energy, E_B, from the measured kinetic energy E_{kin} of the photoelectron according to $E_{kin} = h\nu - E_B$, we now fix E_B by choosing a certain level of an appropriate

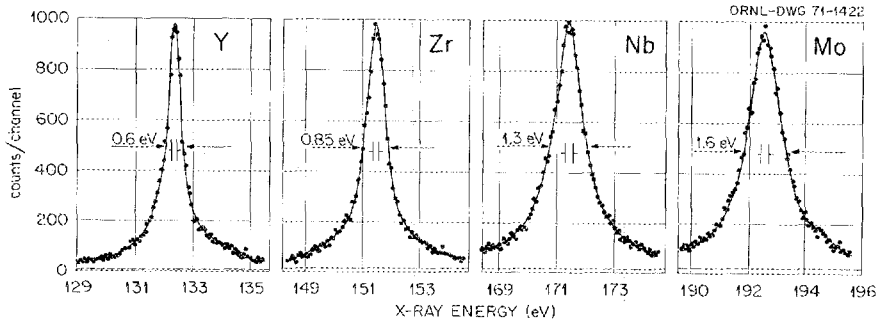

Fig. 2.28. Ne 2*p* (X *Mζ*) photolines, X = Y, Zr, Nb, and Mo. These profiles bear close resemblance to the corresponding *Mζ* x-ray profiles. $\Delta E/E = 0.15\%$; instrumental window indicated inside peaks.

converter atom and deduce $h\nu$ from E_{kin}. The relationship between photoelectron spectrum $I_e\, dE$ and x-ray spectrum $I_x\, dE$ is given by

$$I_e\, dE = GNT\eta E_e \frac{d\sigma_{nl}}{d\Omega}\bigg|_\phi I_x\, dE\,, \qquad (1)$$

where

G = geometry factor of source-converter-analyzer setup,

N = number of converter atoms,

T = transmission of window between source and converter,

η = detector efficiency,

E_e = energy of photoelectron,

$\frac{d\sigma_{nl}}{d\Omega}\Big|_\phi$ = differential photoionization cross section of nl subshell of selected converter atom at angle ϕ between photon and photoelectron direction.

Since it is possible to determine the above quantities with accuracy, we have available a unique x-ray spectrometer of well-known characteristics. This instrument has advantages especially in the soft and ultrasoft x-ray region where an atomic subshell nl of narrow width and large σ_{nl} can be selected as converter, so that a resolution of about 0.1 eV can be obtained. Furthermore, if an angle of ϕ = 54.75° is chosen, the differential cross section $d\sigma_{nl}/d\Omega$ can be replaced by the total cross section σ_{nl} times a constant. It should be noted that $I_x\, dE$ is the spectrum of the x rays as they escape the surface of the target into a cone determined by the geometry of the setup.

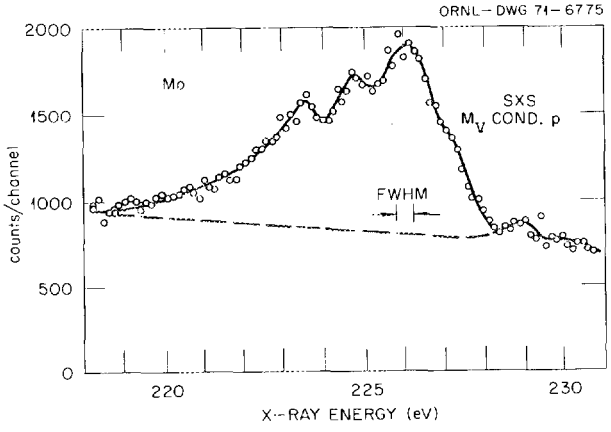

Fig. 2.29. X-ray emission band M_V-cond(p) band of Mo, as observed by means of the photoelectron spectrum Ne 2p [M_V-cond(p) band]. Minor corrections to the spectrum omitted. $\Delta E/E$ = 0.15%. The small contribution of the M_{IV} emission band can be seen above 228 eV.

Figure 2.29 illustrates the use of the analyzer as x-ray spectrometer, showing the x-ray band of transitions from the M_5 level of Mo to the conduction (p) band. Under the assumption of constant transition probabilities, the plot corresponds to the density of the electronic states with p symmetry, and it is gratifying to note for the first time the occurrence of three peaks in the spectrum as theory predicts.

1. Guest scientist from Laboratoire de Chimie Physique de la Faculté des Sciences de Paris, Paris, France.

2. M. O. Krause, *Chem. Phys. Lett.* (in press); M. O. Krause and F. Wuilleumier, *Phys. Lett.* (in press).

3. T. A. Carlson et al., *Eigenvalues, Radial Expectation Values, and Potentials for Free Atoms from Z = 2 to 126 as Calculated from Relativistic Hartree-Fock-Slater Atomic Wave Functions*, ORNL-4614 (December 1970).

4. T. A. Carlson and B. P. Pullen, *Eigenvalues for Elements from Z = 2 to 103 in a Good Approximation to Relativistic Hartree-Fock Solutions*, ORNL-4393 (April 1969).

5. J. Mann, private communication, 1970.

6. W. Lotz, *J. Opt. Soc. Amer.* **60**, 206 (1970).

7. F. Combet-Farnoux, private communication, 1971.

8. F. Wuilleumier and M. O. Krause, to be published.

INTRAMOLECULAR ENERGY TRANSFER AND SENSITIZED LUMINESCENCE IN AN EINSTEINIUM β-DIKETONE CHELATE AND THE LOWER-LYING ELECTRONIC ENERGY LEVELS OF Es(III)[1]

L. J. Nugent G. K. Werner[3]
R. D. Baybarz[2] H. A. Friedman[2]

Ultraviolet-light-excited energy transfer and sensitized luminescence have been induced in an $^{253}Es^{3+}$ β-diketone chelate. The measurements and calculations show that the first excited (J = 7) energy level in the $5f^{10}$ electronic configuration of Es^{3+} is at 9600 cm^{-1} in aqueous 1 M $HClO_4$ solution, and this fixes the Landé parameter ζ_{5f}(aq) for Es^{3+} near +3600 cm^{-1}.

1. Abstract of published paper, *Chem. Phys. Lett.* **7**, 179 (1970).

2. Chemical Technology Division.

3. Physics Division.

NONCOVALENT CHARACTER IN THE CHEMICAL BONDS OF THE LANTHANIDE(III) AND THE ACTINIDE(III) TRICYCLOPENTADIENIDES[1]

L. J. Nugent G. K. Werner[3]
P. G. Laubereau[2] K. L. Vander Sluis[3]

The absorption and uv-excited emission spectra of several microcrystals of $^{248}Cm(C_5H_5)_3$ have been

measured throughout the visible region of the spectrum. One line group in each spectrum can be clearly assigned to the transition: $J = 7/2$ (first excited state) $\leftrightarrow J = 7/2$ (ground state). This group shows a large ($\sim$1680 cm^{-1}) ligand-field splitting and a baricenter of intensity at 15,920 cm^{-1}. By comparing the latter with the corresponding value for $Cm(III)_{aq}$, the nephelauxetic parameter $d\beta$ for Cm(III) in $Cm(C_5H_5)_3$ is estimated to be 0.050 ± 0.004; this corresponds to a covalency in these organometallic bonds of about (2.5 ± 0.2)% relative to the corresponding bonds of $Cm(III)_{aq}$. Similar considerations based on the published[4] absorption spectrum of $Am(C_5H_5)_3$ lead to an organometallic bond covalency in the latter of about (2.8 ± 0.2)% relative to the corresponding bonds of $Am(III)_{aq}$.

The above covalencies for $Am(C_5H_5)_3$ and $Cm(C_5H_5)_3$, representative of the actinide series, are compared with those for $Pr(C_5H_5)_3$, $Nd(C_5H_5)_3$, and $Er(C_5H_5)_3$, representative of the lanthanide series; and it is concluded that although the actinides are more covalent than the lanthanides, as expected, all of these compounds are highly ionic in their organometallic chemical bonding. They should, therefore, be designated as lanthanide or actinide tricyclopentadienides, rather than as "tricyclopentadienyls" as has been the practice among various authors in recent publications.

1. Abstract of published paper, *J. Organometal. Chem.* **27**, 365 (1971).
2. Visiting scientist from the Federal Republic of Germany, Bonn.
3. Physics Division.
4. R. Pappalardo, W. T. Carnall, and P. R. Fields, *J. Chem. Phys.* **51**, 842 (1969).

SAMARIUM TRIINDENIDE: CRYSTAL AND MOLECULAR STRUCTURE

J. L. Atwood[1] J. H. Burns
P. G. Laubereau[2]

A preliminary report on the synthesis and structure determination of crystals of $Sm(C_9H_7)_3$ was given last year.[3] Least-squares refinement of the structural parameters has been completed, and a description of the results is presented here.

Figure 2.30 shows one molecule of $Sm(C_9H_7)_3$ (hydrogen atoms not included), in which it is seen that the five-membered rings form an approximately trigonal array around the Sm atom; the six-membered rings do not obey the trigonal symmetry, probably to achieve packing efficiency. The somewhat analogous tricyclopentadienides of lanthanides and actinides are ionic,[4] and this compound is expected to be also; the symmetrical distribution of C-Sm distances is consistent with electrostatic attraction, although it does not prove it. The Sm-C bonds reported[5] to exist in $Sm(C_5H_5)_3$ bear no resemblance to the symmetrical structure shown here.

Figure 2.31 shows how the $Sm(C_9H_7)_3$ molecules fill the orthorhombic unit cell, and Table 2.30 lists intramolecular distances.

1. Chemistry Department, University of Alabama, University.
2. Visiting scientist from the Federal Republic of Germany, Bonn.
3. J. L. Atwood, J. H. Burns, and P. G. Laubereau, *Chem. Div. Annu. Progr. Rep. May 20, 1970*, ORNL-4581, p. 57.
4. L. J. Nugent et al., *J. Organometal. Chem.* **27**, 365 (1971); also the preceding contribution, this report.
5. C. H. Wong, T. Lee, and Y. Lee, *Acta Crystallogr., Sect. B* **25**, 2580 (1969).

ORNL-DWG. 71-5466

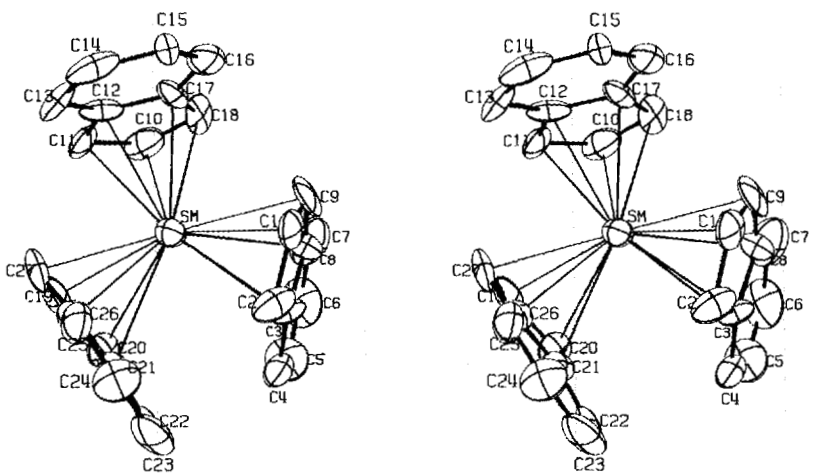

Fig. 2.30. Stereoscopic view of one molecule of $Sm(C_9H_7)_3$. Hydrogen atoms are not included.

ORNL-DWG. 71-5464

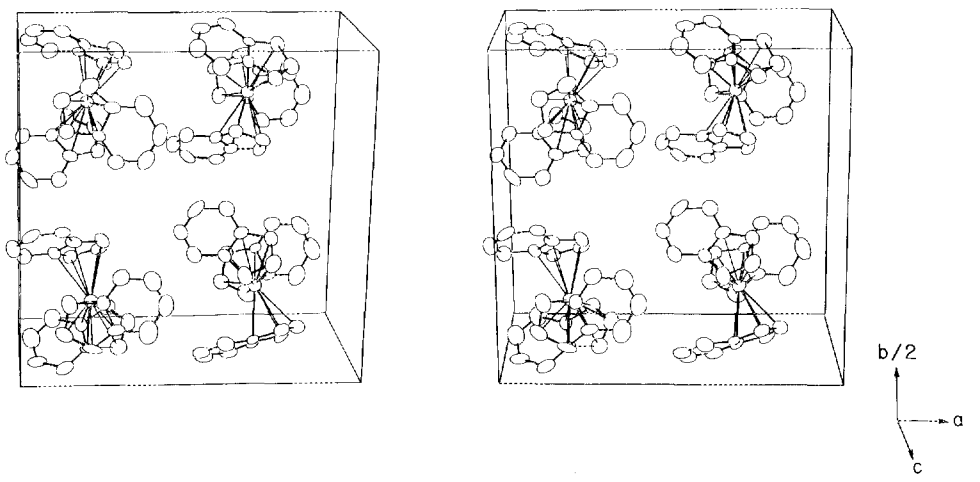

Fig. 2.31. Stereoscopic view of one-half of a unit cell of the crystal structure of $Sm(C_9H_7)_3$.

Table 2.30. Intramolecular distances (Å) in $Sm(C_9H_7)_3$

C-C	*d*	C-C	*d*	Sm-C	*d*
1-2	1.47	15-16	1.39	1	2.71
2-3	1.48	16-17	1.40	2	2.68
3-4	1.45	17-18	1.50	3	2.77
4-5	1.38	18-10	1.40	8	2.77
5-6	1.34	12-17	1.41	9	2.73
6-7	1.51	19-20	1.42	10	2.72
7-8	1.44	20-21	1.40	11	2.78
8-9	1.42	21-22	1.42	12	2.71
9-1	1.42	22-23	1.44	17	2.70
3-8	1.46	23-24	1.41	18	2.76
10-11	1.45	24-25	1.35	19	2.70
11-12	1.47	25-26	1.42	20	2.80
12-13	1.47	26-27	1.44	21	2.86
13-14	1.41	27-19	1.43	26	2.75
14-15	1.37	21-26	1.45	27	2.69

CRYSTAL AND MOLECULAR STRUCTURE OF TRIINDENYLURANIUM CHLORIDE

J. H. Burns P. G. Laubereau[1]

Our studies of organometallic compounds of lanthanides and actinides were extended by use of the indenyl ligand, $C_9H_7^-$, to form carbon-to-metal bonds. This ligand, which is less symmetrical than the cyclopentadienyl ring previously used,[2] was chosen with the hope that it would produce ordered structures. This was the case, and crystals of $U(C_9H_7)_3Cl$ (ref. 3) and $Sm(C_9H_7)_3$ (ref. 4) were made, and their structure was determined by the heavy-atom method with diffractometer-collected data.

Figure 2.32 shows one molecule of $U(C_9H_7)_3Cl$ in which the U is tetrahedrally surrounded by three five-membered rings and a chlorine atom. The uranium atom is bonded to the carbon atoms of the five-membered rings of the three indenyl ring systems at distances given in Table 2.31. Bond lengths and angles within the indenyl rings are given in Fig. 2.33. The U-Cl distance is 2.593(3) Å, comparable with that in $(C_5H_5)_3UCl$, which is 2.559 Å. Packing of the molecules in the orthorhombic unit cell, $a = 8.58$ Å, $b = 14.24$ Å, $c = 16.73$ Å, is shown in Fig. 2.34.

Some inferences can be drawn regarding the nature of the metal-to-ring bonding. Because of the U-C distances and the orientation of the indenyl moieties, σ bonding to a single C atom is ruled out. The essentially equivalent U-C distances could mean ionic bonding, or they could mean covalent bonding through an orbital involving all five C atoms. The U-C distances of 2.67–2.89 Å correspond closely to the value of 2.65 Å in the sandwich-bonded uranocene and to the range 2.68–2.82 Å in the less accurately known structure of

Table 2.31. Distances (Å) from uranium to ring carbons in $U(C_9H_7)_3Cl$

Bond	*d*	Bond	*d*	Bond	*d*
U–C(1)	2.71	U–C(18)	2.71	U–C(19)	2.67
–C(9)	2.73	–C(10)	2.72	–C(27)	2.69
–C(2)	2.77	–C(11)	2.77	–C(20)	2.73
–C(8)	2.86	–C(17)	2.79	–C(26)	2.88
–C(3)	2.87	–C(12)	2.87	–C(21)	2.89

ORNL-DWG. 70-13868

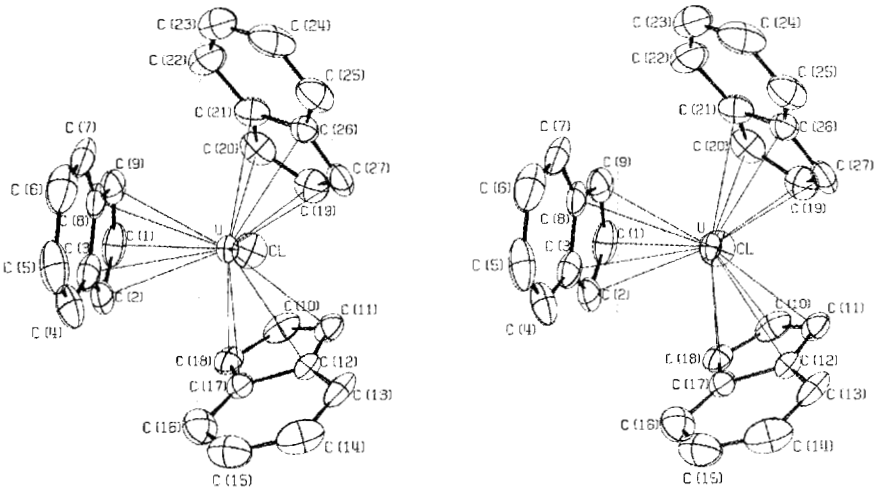

Fig. 2.32. Stereoscopic drawing of one molecule of $U(C_9H_7)_3Cl$.

ORNL-DWG. 70-13866A

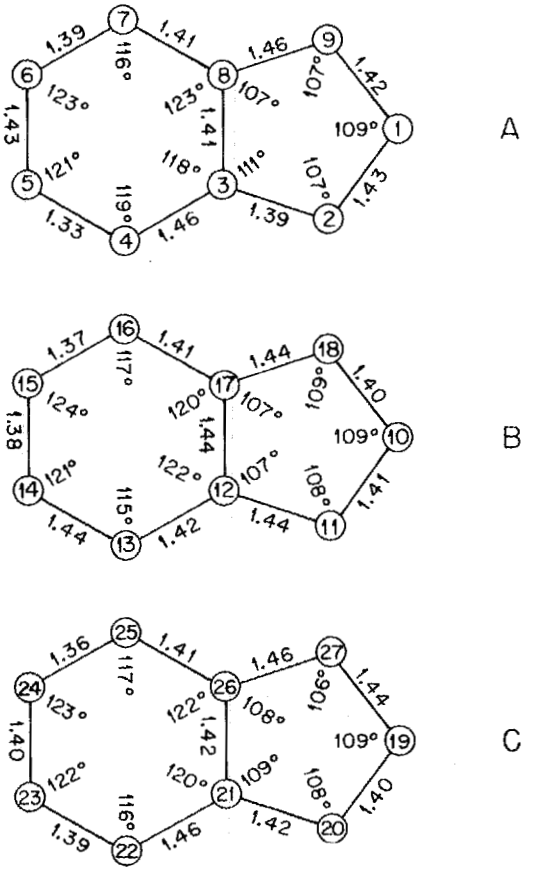

Fig. 2.33. Bond lengths and angles in the indenyl rings of $U(C_9H_7)_3Cl$.

ORNL-DWG. 70-13867

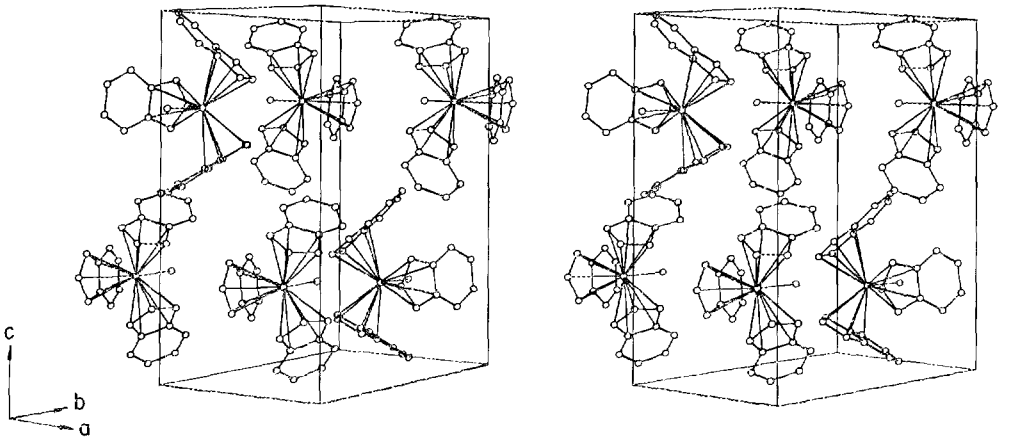

Fig. 2.34. Stereoscopic drawing of the contents of 1½ unit cells of $U(C_9H_7)_3Cl$ to show packing.

$(C_5H_5)_3UCl$.[5] This latter compound exhibits chemical evidence of its covalency and is structurally similar to $(C_9H_7)_3UCl$, which suggests that the latter compound may have covalent character in its U-C bonds.

1. Guest scientist from the Federal Republic of Germany, Bonn.
2. P. G. Laubereau, J. H. Burns, and L. Ganguly, *Chem. Div. Annu. Progr. Rep. May 20, 1970*, ORNL-4581, p. 52.
3. P. G. Laubereau, L. Ganguly, J. H. Burns, B. M. Benjamin, J. L. Atwood, and J. Selbin, *Inorg. Chem.* **10** (1971), in press.
4. J. L. Atwood, J. H. Burns, and P. G. Laubereau, *Chem. Div. Annu. Progr. Rep. May 20, 1970*, ORNL-4581, p. 57.
5. C. H. Wong, Y. M. Yen, and T. Y. Lee, *Acta Crystallogr.* **18**, 340 (1965).

METHOD FOR THE DIRECT DETERMINATION OF LIGANDS

C. E. Higgins W. H. Baldwin

Earlier methods for the analysis of solvate composition of salts depended on an indirect method.[1] The method reported here provides, on very small samples, both qualitative identification (including water) and quantitative estimation of ligands present.

Our long-term interest is in the products of the reaction of small quantities of actinides with organic molecules. In view of the small amounts of actinides available, we have chosen to use a method that gives a residual product after evaporation of by-products and excess reagents from the reaction mixture. It will be necessary to know the composition of the solid products of such reactions. First it was believed advantageous to make and analyze lanthanide chloride adducts of the type expected with the actinides.

Gas chromatography offers a sensitive method for the analysis of the ligands if the ligand can be quantitatively released from the salt and collected. For this purpose it is necessary to dissolve the solvate in a solvent which will replace the ligand. In our method we used tributyl phosphate (TBP), containing a known weight of isopropyl alcohol (10 wt %) as internal standard, to displace water, methanol, and ethanol ligands. Two milliliters of this TBP solution was added to 0.2–0.5 millimole of solvate; heating to 80° was sometimes necessary to complete the dissolution. The isopropyl alcohol and ligand were distilled from the solution and collected in a receiver cooled in dry ice. The pressure was lowered during the distillation to 1 torr while the TBP solution was warmed to 50–60° for 30 min. Water was quantitatively removed in one treatment, but complete removal of ethanol required two.

Analysis of the receiver contents was performed on a 1-m long, 2-mm-ID stainless steel column containing 80–100 mesh Porapak Q with helium flowing at 40 or 50 ml/min; column temperatures were maintained at 100 or 125°C. The ratio of ligand to isopropyl alcohol was found by comparison of peak height ratios or area ratios to those obtained using known weight ratios. As little as 1 μg/μl could be detected with the thermal conductivity detector, and increased sensitivity should be possible using more sensitive detectors. It may be possible to inject an organic solution containing the solvate directly into the GC; a short preliminary column for trapping the salt and for releasing the ligand could be connected to the chromatographic column.

Using the TBP displacement method we have analyzed hydrated cerous chloride and uranyl nitrate for water content. The results were quantitative, though usually about 5% higher than those obtained by Karl Fischer titration.

Similar tests with other ligands are being made using other gas chromatographic columns. For example, a special column of 10% poly(ethylene imine) on chrom T at 125°C with a helium flow of 50 ml/min has been used for the analysis of amines and water.

1. S. N. Misra, T. N. Misra, and R. C. Mehrotra, *J. Inorg. Nucl. Chem.* 27, 105 (1965).

LIGANDS IN SOLVATED LANTHANIDE HALIDES

C. E. Higgins W. H. Baldwin

Lanthanide halide alcoholates result both from the solution of the anhydrous salt in alcohols[1] and from the reaction of hydrated salts with dimethoxypropane (DMP) or triethyl orthoformate. Using the TBP displacement method[2] we found that the residue from the evaporation in vacuo at room temperature of DMP and known amounts of hydrated cerous or yttrium chloride contained two methanol molecules per $LnCl_3$ molecule. Similarly, reaction with triethyl orthoformate (and subsequent removal by evaporation of reaction byproducts and excess reagents) resulted in an ethanol: $LnCl_3$ ratio of 2.0. Misra et al.[1] have reported trisalcoholates resulting from the reaction of anhydrous lanthanide halides with alcohols and by azeotropic distillation of water from $LnCl_3$ hydrates mixed with solutions of alcohols and benzene. The discrepancy in the number of alcoholate residues, two in our case and three in theirs,[1] is probably the result of our more extensive drying in vacuo of the product.

In contrast, heating the hydrated lanthanide chlorides in refluxing DMP led to competing reactions and incomplete dehydration. When yttrium oxide was dissolved in a slight excess of aqueous HCl and was treated with refluxing DMP for 2.5 hr, a purple solution resulted. The purple solid recovered on evaporation in vacuo had the composition $YCl_3 \cdot 1.9MeOH \cdot 0.3H_2O$. Similarly, $CeCl_3 \cdot 6H_2O$ in refluxing DMP yielded $CeCl_3 \cdot 1.6MeOH \cdot 0.6H_2O$. Heating the hydrates in triethyl orthoformate at ~80°C formed anhydrous halide diethanolates; however, there was a slight halide deficiency (Cl:Y = 2.7).

1. S. N. Misra, T. N. Misra, and R. C. Mehrotra, *J. Inorg. Nucl. Chem.* 27, 105 (1965).
2. C. E. Higgins and W. H. Baldwin, "Method for the Direct Determination of Ligands," the preceding contribution, this report.

CRYSTALLOGRAPHIC STUDIES ON $Cs_2NaNdCl_6$ AND $Cs_2NaDyCl_6$

J. H. Burns

A series of isomorphous compounds of the empirical formula Cs_2NaMCl_6, where M is a trivalent lanthanide or actinide, was prepared by Morss et al.,[1] and the cubic unit-cell parameters were determined by x-ray diffraction. Of interest to us were the compounds containing Pu, Am, and Bk, because in the proposed cryolite structure, the trivalent ions are octahedrally coordinated by chloride ions, a promising case for comparison of ionic sizes.

As examples widely spaced in ionic size, single-crystal specimens of $Cs_2NaNdCl_6$ and $Cs_2NaDyCl_6$ were provided by L. R. Morss, Purdue University, and we have determined their crystal structures by x-ray diffraction. The atomic parameters are given in Table 2.32, and the structure is shown in Fig. 2.35, which depicts the atoms by their thermal ellipsoids. The Cl atom was described in two ways: (1) constrained to the x axis and given anisotropic thermal motion (Fig. 2.35) or (2) put in the general xyz position, requiring disorder, and given isotropic thermal motion. Table 2.32 contains both sets of refined parameters. Interatomic distances (Å) listed below were calculated from the disordered model.

Distance	Length in --	
	Nd compound	Dy compound
Na-Cl	2.763	2.760
Cs-Cl	3.590	3.602
M-Cl	2.713	2.634

Table 2.32. Crystal structure parameters for $Cs_2NaNdCl_6$ and $Cs_2NaDyCl_6$

Atom	x	y	z	$\bar{u}^2$(Å^2)
		$Cs_2NaNdCl_6$		
Cs	0.25	0.25	0.25	0.042
Na	0.0	0.0	0.0	0.024
Nd	0.5	0.5	0.5	0.015
Cl				
(aniso.)	0.2524	0	0	0.015,0.067
(disord.)	0.2523	0.0097	0.0243	(0.015)
		$Cs_2NaDyCl_6$		
Cs	0.25	0.25	0.25	0.035
Na	0.0	0.0	0.0	0.023
Dy	0.5	0.5	0.5	0.014
Cl				
(aniso.)	0.2560	0.0	0.0	0.015,0.052
(disord.)	0.2559	0.0224	0.0038	(0.015)

ORNL-DWG. 71-5465

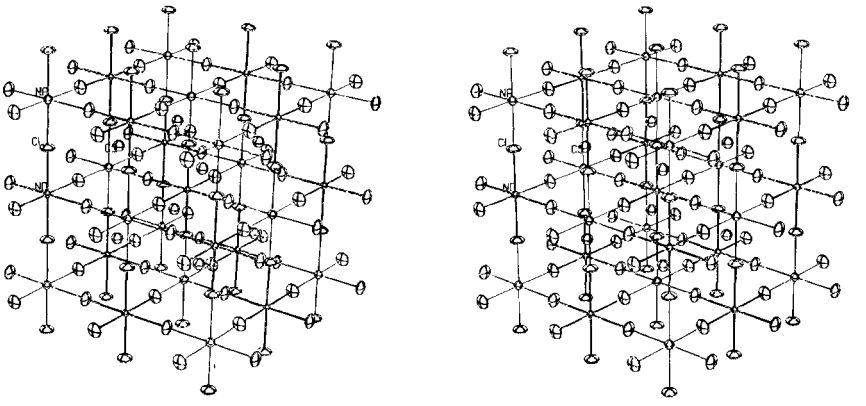

Fig. 2.35. Stereoscopic view of a unit cube of $Cs_2NaNdCl_6$ with the chloride atom in anisotropic motion.

From this list it is seen that the alkali metal to chloride distances were in close agreement between the two compounds, while the lanthanide to chloride distances showed the characteristic contraction. From the reported[1] unit-cell dimensions for the Pu, Am, and Bk compounds and the structures determined here, it is clear that the elements Pu, Am, and Bk show the actinide contraction in their corresponding compounds, but the exact amount depends on their (unknown) chloride parameters.

1. L. R. Morss et al., *Inorg. Chem.* 9, 1771 (1970).

PREPARATION AND PROPERTIES OF Cs_3NdCl_6 AND $Cs_2NaNdCl_6$

J. N. Stevenson[1] L. J. Nugent
J. R. Peterson[2]

During the course of preliminary experiments to develop techniques and equipment for the preparation of Cs_3CmCl_6 and $Cs_2NaCmCl_6$ (using ^{248}Cm), samples of Cs_3NdCl_6 and $Cs_2NaNdCl_6$ were prepared, and some of their properties were determined.

Stoichiometric amounts of anhydrous $NdCl_3$ and CsCl were mixed in a reaction vessel, evacuated, and heated to about 115°C. Anhydrous HCl gas was then introduced and the temperature increased until the sample melted. The Cs_3NdCl_6 product appeared to be light blue under fluorescent room lighting. The preparation of $Cs_2NaNdCl_6$ was carried out similarly, with the addition of the stoichiometric amount of NaCl, evacuation and heating to 520°C before introduction of HCl, and heating of the reaction mixture to 1000°C. The color of the product was like that of Cs_3NdCl_6.

Samples of both products were examined by standard powder methods. Tricesium neodymium(III) chloride exhibited an apparent tetragonal structure with a_0 = 5.68 Å and c_0 = 10.69 Å; however, several weak lines could not be indexed on the basis of this structure. The dicesium sodium neodymium(III) chloride exhibited a face-centered cubic cryolite structure with a_0 = 10.892 Å, which is in good agreement with the 10.889-Å value reported by Morss.[3]

The melting point of the $Cs_2NaNdCl_6$ compound was determined under 0.5 atm HCl pressure to be about 700°C, whereas that for the Cs_3NdCl_6 compound was found to be about 820°C. In addition, an apparent phase change was observed for Cs_3NdCl_6 at a temperature of about 375°C. A high-temperature x-ray camera will be used to study in greater detail this apparent phase transformation. Similar behavior for Cs_3NdCl_6 has been observed previously.[4]

The reflectance spectrum of each compound was measured using a Cary 14 recording spectrophotometer. The two spectra are, in general, very similar, but clearly not identical. The absorption lines for $Cs_2NaNdCl_6$ were generally stronger than those for Cs_3NdCl_6. Maximum absorption for both compounds occurs in the 17,500–16,100 cm^{-1} range. This peak for $Cs_2NaNdCl_6$ centers about 17,200 cm^{-1}. The corresponding peak for Cs_3NdCl_6 centers about 17,000 cm^{-1}, with a minor component at about 17,200 cm^{-1}. Other absorption peaks occur for both compounds with centers about 19,000, 13,000, 12,300, and 11,400 cm^{-1}.

1. Oak Ridge Graduate Fellow from the University of Tennessee, Knoxville, under appointment with the Oak Ridge Associated Universities.
2. Consultant; Department of Chemistry, University of Tennessee, Knoxville.
3. L. R. Morss et al., *Inorg. Chem.*, 9, 1771 (1970).
4. Sun In'-Chzhu and I. S. Morozov, *Zh. Neorg. Khim.* 3, 1914 (1958).

STUDIES WITH HEPTAVALENT NEPTUNIUM

W. H. Baldwin J. R. Stokely[1]
J. H. Burns G. K. Werner[2]

The existence of Np(VII) was established by Spitsyn et al.[3] in 1969. They prepared Np in this valence state in alkaline solution and also in the solid compound $Co(NH_3)_6NpO_5 \cdot 3H_2O$. These workers, and also Jorgensen,[4] speculated on the nature of the NpO_5^{3-} ion. We have an effort under way to prepare the above compound, and perhaps others, in a form suitable for x-ray diffraction study in order to characterize ions containing Np(VII).

The published method[5] of preparation, ozonization of Np(V) in NaOH solution, was employed to prepare Np(VII). Very dark green solutions were obtained at a concentration of about 4 mg of Np(VII) per milliliter. Addition of $Co(NH_3)_6Cl_3$ solution precipitated brilliant green crystals of about 20 μ in largest dimension, too small for single-crystal diffraction. A coulometric analysis for Np gave (44.3 ± 0.4)% (theoretical = 44.5%). From this analysis and the method of preparation we believe these crystals to be $Co(NH_3)_6NpO_5 \cdot 3H_2O$, but efforts to increase their size by various procedures failed. X-ray powder diffraction yielded a pattern containing the following (first eight) interplanar spacings (in Å): 6.66, s; 5.90, m; 5.65, w; 5.44, m; 5.27, vs; 4.23, ms; 3.86, s; 3.69, s.

When solutions of Np(VII) and $Co(NH_3)_6Cl_3$ were allowed to diffuse slowly together through a layer of 1 *M* NaOH, crystals having a needle-like form and an intense red color (so as to appear black) were obtained. These grew to 150 μ in length, but the number produced in each preparation was rather limited; hence, conventional chemical analysis has not been possible thus far. We have established the presence of neptunium from neutron-activation and gamma-ray analyses, and that the crystals contain Np(VII) from absorption spectra. A structural analysis by single-crystal methods is in progress and is expected to yield the empirical formula of the compound. Crystals are monoclinic, $C2/c$, with a = 10.865 Å, b = 10.597 Å, c = 14.867 Å, and β = 115°13′. These data do not correspond to the powder pattern above; therefore the two substances are of different crystal structures although they may be polymorphic forms of the same compound.

1. Analytical Chemistry Division.
2. Physics Division.
3. V. I. Spitsyn et al., *J. Inorg. Nucl. Chem.* 31, 2733 (1969).
4. C. K. Jorgensen, *Chem. Phys. Lett.* 2, 549 (1968).
5. A. J. Zielen and D. Cohen, *J. Phys. Chem.* 74, 394 (1970).

THE CRYSTAL STRUCTURE OF AMERICIUM SULFATE OCTAHYDRATE

J. H. Burns R. D. Baybarz[1]

Determination of the type of coordination exhibited by a lanthanide or actinide ion when it is crystallized from aqueous solution is of interest because it indicates the complexing ability of the anion relative to water, it suggests the type of coordination in solution, and, in the solid, the crystal field symmetry is obtained for use in explaining magnetic behavior of the M^{3+} ions. The only previous work relevant to the present problem is a partial structure determination[2] on $Nd_2(SO_4)_3 \cdot 8H_2O$, in which the Nd was concluded to have face-centered trigonal prismatic 9-coordination. We have found that $Am_2(SO_4)_3 \cdot 8H_2O$ is isostructural with the Nd compound and has, in fact, the Am in dodecahedral 8-coordination.

The crystal symmetry is monoclinic, $C2/c$, with a = 13.62 Å, b = 6.84 Å, c = 11.840 Å, β = 102.67°, and Z = 4. In Fig. 2.36 is shown the part of the structure occupying one-half the unit cell. The Am ions are all crystallographically equivalent and are each coordinated by the oxygen atoms from four sulfate ions and four water molecules. In the drawing the sulfate ions are recognized as regular tetrahedra, while the water molecules are shown only as oxygen atoms attached to the Am ions. Hydrogen atoms were not located, but there are numerous O ... O distances suggestive of hydrogen bonding. The structure is also cross-linked by each sulfate being shared by two or more Am ions. The Am–O distances range from 2.38 to 2.55 Å, and the S–O distances from 1.45 to 1.50 Å.

1. Chemical Technology Division.
2. D. R. Fitzwater and R. E. Rundle, *Structure of Neodymium Sulfate Octahydrate,* Ames Laboratory Report No. ISC-241 (1952).

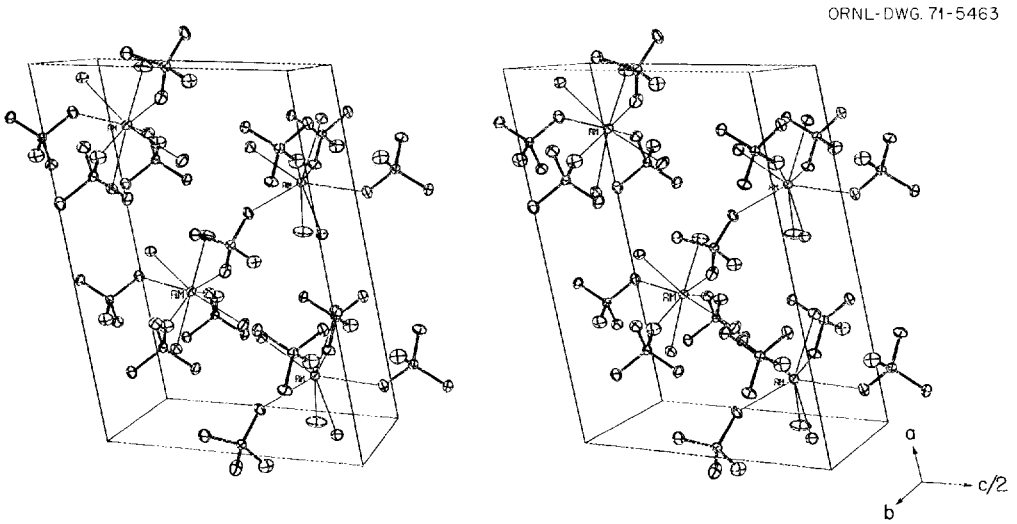

Fig. 2.36. Steroscopic view of one-half the unit cell contents of $Am_2(SO_4)_3 \cdot 8H_2O$.

THE DIOXIDE OF LONG-LIVED ^{248}Cm

J. R. Peterson[1] J. Fuger[2]

In an effort to study the properties of curium in the absence of intense self-irradiation, a systematic study has been undertaken utilizing the recently available long-lived curium isotope of mass number 248 ($t_{1/2}$ = 3.5 × 10^5 years). The ^{248}Cm made available for this study was "milked" from a ^{252}Cf "cow"[3] and then underwent the standard purification procedure for small quantities of actinides.[4] The purified curium was loaded into single beads of preleached Dowex 50W-X4 ion exchange resin and pretreated Dowex chelating resin A-1. These beads were subsequently calcined in air or oxygen to form curium sesquioxide. The curium dioxide samples were prepared by treatment of the sesquioxide with oxygen gas at temperatures below 400°C. The dioxide stoichiometry was assumed, since direct determination was deemed impossible on the 1- to 2-μg scale employed.

The various samples were subjected to analysis by standard x-ray powder diffraction methods. All samples prepared were found to exhibit the face-centered cubic (fcc) fluorite-type structure. The room-temperature average lattice parameter was 5.359 ± 0.002 Å, where the error limit represents the 95% confidence level calculated using the standard statistical method for the average of five independent determinations. This value is significantly smaller than the previously accepted value of 5.372 ± 0.003 Å (ref. 5) but is in excellent agreement with the value of 5.359 ± 0.001 Å obtained by Noé on a freshly prepared sample of $^{244}CmO_2$.[6] In addition, Noé has shown that the lattice constant for $^{244}CmO_2$ increases with time, reaching the saturation value in about 1.6 days.[6] The increase of lattice constant with time is attributed to self-irradiation effects. Such radiation-induced expansion was not expected in the $^{248}CmO_2$ samples and, indeed, was not observed over the eight months of this study.

Plots of the cubic lattice parameters of the actinide dioxides and the corresponding calculated tetravalent ionic radii [0.880 Å for Cm(IV)] vs atomic number are given in Fig. 2.37. Included on the lattice parameter plot are the old literature value for $^{244}CmO_2$[5] and a value for CfO_2 derived from a sample prepared by Baybarz et al.[7] Although our lattice parameter for CmO_2 greatly reduces the apparent cusp there, it does not eliminate it entirely. Of equal importance, however, is the fact that no cusp is evident at berkelium, corresponding to the half-filled $5f^7$ electron configuration. Thus, it appears that the magnitude of the half-filled shell effect is small compared with the precision with which these lattice constants have been determined.

---

1. Consultant; Department of Chemistry, University of Tennessee, Knoxville. Work carried out in part at the ORNL Transuranium Research Laboratory and in part at the University of Liège while in residence as a North Atlantic Treaty Organization Postdoctoral Fellow in Science.

2. Nuclear Chemistry Laboratory, University of Liège, 2 rue A. Stevart, 4000 Liège, Belgium.

3. D. E. Ferguson et al., *Chem. Technol. Div. Annu. Progr. Rep. May 31, 1970,* ORNL-4572, p. 119.

4. R. D. Baybarz, J. B. Knauer, and P. B. Orr, *Final Isolation and Purification of the Transplutonium Elements from the Last Six TRU Campaigns*, ORNL-4672, to be published.
5. L. B. Asprey et al., *J. Amer. Chem. Soc.* 77, 1707 (1955).
6. M. Noé and J. Fuger, *Inorg. Nucl. Chem. Lett.* 7, 421 (1971).
7. R. D. Baybarz, R. G. Haire, and J. A. Fahey, submitted to *J. Inorg. Nucl. Chem.*

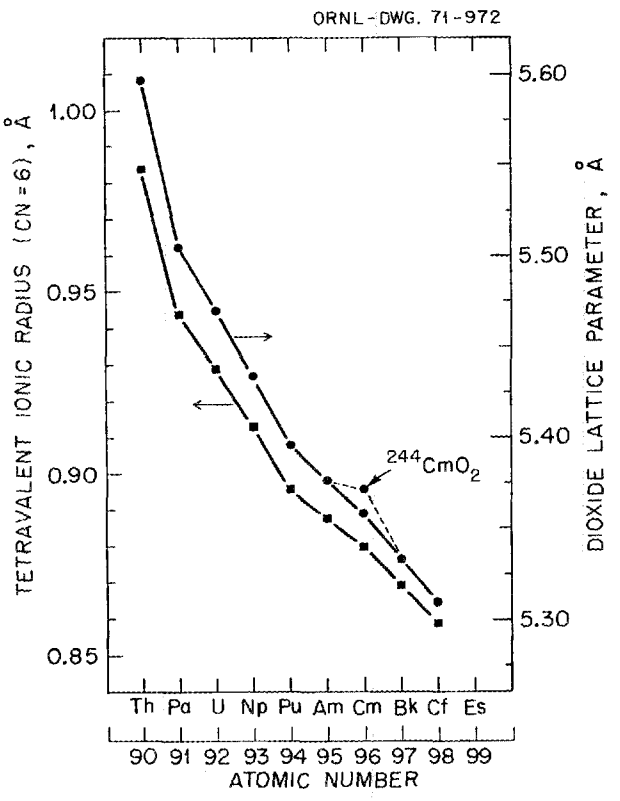

Fig. 2.37. Actinide dioxide lattice parameters and corresponding calculated tetravalent ionic radii.

SOME PROPERTIES OF BERKELIUM METAL[1]

J. A. Fahey[2] R. D. Baybarz[4]
J. R. Peterson[3] D. K. Fujita[5]

The initial preparation of berkelium metal was reported previously.[6] Additional work since that time has provided the following information concerning the physical and chemical properties of berkelium metal.

Berkelium metal exhibits two allotropic modifications, the face-centered cubic (fcc) and the double hexagonal closest-packed (dhcp). The average room-temperature fcc lattice parameter is $a_0 = 4.997 \pm 0.004$ Å, where the error limit represents the 95% confidence level calculated using the standard statistical method for the average of ten independent determinations. The average room-temperature dhcp lattice parameters are $a_0 = 3.416 \pm 0.003$ Å and $c_0 = 11.069 \pm 0.007$ Å, where the error limits represent again the 95% confidence level for the average of six independent determinations. The results derived from the observed lattice constants of the two forms of Bk metal are presented in Table 2.33.

Our data indicate that the fcc phase is the high-temperature phase with respect to the dhcp phase, representing behavior analogous to that observed in La, Ce, Am, and possibly Cm. The definitive answer to the phase relationship question should come from careful high-temperature x-ray studies of metal samples large enough to produce satisfactory diffraction patterns in reasonable exposure times.

The difference in metallic radii of the two allotropes of Bk is attributed to a differing metallic valence in the two forms. Magnetic susceptibility measurements were carried out in an effort to detect significant differences in the magnetic behavior of the two metallic phases that would support the suspected differences in their electronic nature.[7] The results, though preliminary in nature, indicate that berkelium is a predominantly trivalent metal.

During the course of this work attempts were made to prepare Am, Cm, and Cf metals utilizing the same technique as for Bk metal, that is, by Li reduction of the metal trifluoride at a suitable temperature. From these experiments we have estimated, primarily on the basis of product yields, the relative order of volatility of the four metals to be: Cm $\ll$ Bk $<$ Am $\ll$ Cf.

Utilizing the method of Ordway[8] the melting point of Bk metal was determined to be 986 ± 25°C. This value is the average of two independent determinations on samples weighing about 5 μg. The error limit given represents the 90% confidence level. This value is consistent with the preparative conditions employed;[6]

Table 2.33. Crystallographic data for berkelium metal

Crystal structure	fcc	dhcp
Space group	$Fm3m$ (O_h^5)	$P6_3/mmc$ (D_{6h}^4)
Metal atom position	4 Bk in a	2 Bk in a; 2 Bk in c
Lattice constants, Å	4.997 ± 0.004	3.416 ± 0.003 11.069 ± 0.007
Atomic volume, Å^3 ($Z = 4$)[a]	31.19	27.96
X-ray density, g/cc	13.25	14.78
Axial ratio, c_0/a_0	1.000	3.240
Metallic radius, Å (CN = 12)	1.76_7	1.70_4

[a]Z denotes number of atoms per unit cell.

however, it is considerably lower than the 1675°C estimate of Matthias et al.[9]

A sample of berkelium hydride has been prepared by treatment of the metal at 225°C with hydrogen gas and found to exhibit an fcc structure with $a_0 = 5.23 \pm 0.01$ Å. By analogy to lanthanide and other actinide hydride systems, it is thought that the composition of the sample is BkH_{2+x}, where $x < 1$. The trihydride would be expected to exhibit a hexagonal structure.

In the series of Bk metal preparations, two products appeared metallic, but were somewhat brittle, and were found to exhibit an fcc structure with $a_0 = 4.964$ Å, significantly smaller than the parameter associated with the fcc form of metallic Bk. The preparative conditions for these two samples might have been favorable for monoxide formation. However, attempts to prove or disprove that this fcc phase corresponds to berkelium monoxide have been unsuccessful. High-temperature x-ray studies of Bk metal should demonstrate whether or not this fcc phase is another metal phase.

It is apparent that the metallic properties of Bk do not correspond to those of Tb, its lanthanide analog. In fact, taken as a whole, the observed properties of Bk metal and the apparent high volatility of Cf metal are consistent with a trend toward enhanced stability of the divalent state in the transcurium metals.

1. Summary of a paper submitted to *J. Inorg. Nucl. Chem.*
2. Oak Ridge Graduate Fellow from the University of Tennessee, Knoxville, under appointment with the Oak Ridge Associated Universities. Present address: Chemistry Department, Bronx Community College, Bronx, N.Y.
3. Consultant; Department of Chemistry, University of Tennessee, Knoxville.
4. Chemical Technology Division.
5. Graduate student, University of California (Berkeley), Lawrence Radiation Laboratory. Present address: Department of Zoology, University of California, Davis.
6. J. R. Peterson, J. A. Fahey, and R. D. Baybarz, *Chem. Div. Annu. Progr. Rep. May 20, 1969,* ORNL-4437, p. 35.
7. D. K. Fujita, Ph.D. dissertation, University of California, Lawrence Radiation Laboratory Report UCRL-19507 (November 1969).
8. F. Ordway, *J. Res. Nat. Bur. Stand.* 48(2), 152 (1952).
9. B. T. Matthias et al., *Phys. Rev. Lett.* 18, 781 (1967).

IONIC RADII FROM TRANSPLUTONIUM TRICHLORIDES

J. H. Burns J. R. Peterson[1]
R. D. Baybarz[2]

Our work[3] on the refinement of crystal structures of the anhydrous transplutonium trichlorides using melt-grown single crystals has continued. We obtained a crystal of $^{249}CfCl_3$ having the hexagonal UCl_3 structure type and refined the unit-cell dimensions and chloride positional parameters using diffractometer data. The least-squares adjusted parameters are as follows: $a = 7.379(1)$ Å and $c = 4.0900(5)$ Å,

	x	y	z	β_{11}	β_{22}	β_{33}	β_{12}
Cf	1/3	2/3	1/4	0.0054(2)	0.0054	0.0113(5)	0.0027
Cl	0.3902(6)	0.3019(6)	1/4	0.0060(7)	0.0052(6)	0.0186(19)	0.0030(6)

The bond distances of primary interest are Cf-Cl(equatorial) = 2.924(4) Å and Cf-Cl(apical) = 2.815(3) Å.

Ionic radii have been derived from our crystal-structure determinations of the metal-to-chloride distances in these transplutonium trichlorides. It is assumed that when an actinide and a lanthanide ion, in isomorphous structures, have the same distance to chlorine, then that actinide has the same radius as the lanthanide. The radii of trivalent lanthanide ions are well known.[4] By making comparisons of this type the following radius values (Å) were obtained (estimated values in parentheses):

Am^{3+}	0.984
Cm^{3+}	0.973
Bk^{3+}	(0.952)
Cf^{3+}	0.935
Es^{3+}	(0.922)

The previously reported[3] dimorphism of $CfCl_3$ was studied by use of a high-temperature x-ray diffraction camera. The transformation: $CfCl_3$(hexagonal) $\rightleftharpoons$ $CfCl_3$(orthorhombic) is apparently a very sluggish one; we were able to observe the transformation but could not reproduce it in a controlled manner, even though the sample was carried through several cycles of heating, annealing, and cooling. The transition temperature is still unknown, as is the identity of the high-temperature equilibrium form.

1. Consultant; Department of Chemistry, University of Tennessee, Knoxville.
2. Chemical Technology Division.
3. J. H. Burns and J. R. Peterson, *Chem. Div. Annu. Progr. Rep. May 20, 1970,* ORNL-4581, p. 57.
4. D. H. Templeton and C. H. Dauben, *J. Amer. Chem. Soc.* 76, 5237 (1954).

NEUTRON MULTIPLICITY COUNTER[1]

R. L. Macklin[2] R. T. Roseberry[3]
F. M. Glass[3] R. W. Stoughton
J. Halperin M. Tobias[4]

In recent years a number of estimates and calculations have been made which imply that nuclei of atomic number near 114 (and near certain higher closed shells of neutrons and protons as well) may be relatively stable.[5] The range of estimates of this stability encompasses the possibility that half-lives of nuclides in this "island of stability"[5] are long enough that detectable quantities may be found in nature -- provided that they are formed at all during nucleosynthesis in stellar interiors. Further, the possible production of such superheavy nuclei directly in accelerators has been receiving increasing attention from experimenters. Although heavy-ion beams with the requisite energies to penetrate the heavy-element Coulomb barriers have not yet been produced (the Super Hilac is due to start up at the end of 1971), recent reports have excited interest in the possibility of indirectly producing such superheavy nuclides. By using multi-GeV beams of protons or electrons (which do exist now in a number of accelerators) on heavy-element targets, it may be possible to form spallation products of sufficient energy to interact with the heavy-element substrate to form superheavy elements. A search for such nuclides is in progress in many laboratories throughout the world; evidence for the existence of such superheavy nuclides may even have been obtained by Marinov[6] at the Rutherford Laboratory, Flerov[7] at Dubna, or Bhandari[8] at the Tata Institute.

The superheavy nuclei or their decay products can be expected to fission spontaneously. The fission process in turn involves the emission of a variable number of neutrons, and the detection of these neutrons provides a sensitive means of detecting these nuclides. Since fast neutrons are highly penetrating, the technique lends itself to examining large samples (hundreds of grams per square centimeter) without prior chemical preparation. We have assembled a neutron multiplicity counter with the capacity of detecting neutrons emitted in spontaneous fission. The sensitivity of the instrument is ~1 spontaneous fission event per day. It provides a capability of examining large natural samples (~50-kg samples of ores, concentrates, etc.) for neutron emission. Such samples, in general, would not require chemical preparation, which involves the added risk of losses in the effort to concentrate superheavy elements of yet unknown chemical behavior.

The only known spontaneous-fission emitter in nature is ^{238}U with $T_{1/2}$ (S.F.) $\simeq 10^{16}$ years (0.6 fission day^{-1} mg^{-1}). In this connection $\bar{\nu}$, the average number of neutrons per fission, for ^{238}U is 2.0, and even the highest-mass spontaneously fissioning nuclide[9] yet measured, ^{257}Fm, yields $\bar{\nu} < 4$. Although $\bar{\nu}$ for a superheavy element is, of course, not known, it has been variously estimated that $\bar{\nu}(^{298}114) \simeq 10$ for binary fission.[10] Thus the predicted high value of $\bar{\nu}$ for superheavy elements leads to the possibility of a distinctive characterization of a superheavy nuclide by neutron multiplicity counting, which enables distinguishing it from all presently known nuclides. A further characteristic of the current counter design is its insensitivity to gamma radiation. It is perhaps 10^4-fold less sensitive than the gadolinium-loaded scintillation tank detector. Gamma-ray sources at the roentgen-per-hour level can be tolerated in the instrument.

Figures 2.38 and 2.39 show an overall isometric view and schematic cross section, respectively, of the neutron multiplicity counter. The sample chamber of the counter is a 9-in.-diam, 20-in.-long cylinder. This provides over 20 liters of sample volume; depending upon the density of the material, samples of 50 kg and larger can be accommodated. The detection system consists of an array of 20 ^3He-filled proportional counters, symmetrically spaced along the sample volume and embedded in a paraffin matrix to moderate the fast neutrons emitted in fission. This moderating region is 6 in. in radial extent, and the ^3He counters which penetrate it are contained within each of twenty 1.25-in.-diam aluminum tubes parallel to the cylindrical axis of the sample chamber. Ten of these tubes are on the circumference of the sample volume, and the other ten tubes are equally spaced on a circular row 1.25 in. radially displaced from the first row; this spacing was found to be optimal by Monte Carlo calculation. A sheet of 40-mil cadmium about the outside of this moderating region plus two additional inches of paraffin serves to shield the counter from possible outside sources of neutrons. The overall length is 36 in., of which the inner 20 in. parallels the counter sensitive volume. Two paraffin-filled end plugs 8 in. long close the sample volume and function as end neutron reflector-moderator and external neutron shield. The cylindrical assembly is encased in a ⅛-in. steel shell and is supported by a rectangular frame on casters. The entire assembly weighs about 800 lb.

The detector tubes are filled with ^3He to 6 atm pressure and are operated as proportional counters with a 1400-V positive anode bias with the aluminum shell at ground potential. The gas mixture contains 11% Kr to

minimize energy losses to the wall and 1% CO_2 to minimize ion recombination. The resolution of each detector was measured to be better than 5% FWHM. The output of the detectors, in pairs, is fed to ten preamplifiers which are mounted on the face of the steel shell to minimize cable lengths. The preamplifier output is carried to an amplifier–single-channel-analyzer unit in an adjacent instrument rack. A SCA window was selected to encompass as much signal as possible to enhance the system efficiency. This corresponds normally to accepting pulses lying between 0.1 and 1.0 MeV. (Q for $^3He(n,p)^3H$ is 765 keV.) The output of the discriminator is fed into a buffer memory, where as many as ten events may be stored and outputted to a fast printer according to preset logical requirements. A 2-Mc timer controls the rate of "word" transfer within the memory. Following the detection of an event in any channel, a gate is opened for a preset but variable interval of time from 0 to 1000 μsec (~500 μsec is currently used), and multiplicities are noted. The output of the system is such that each detected event is printed out to identify the channel of origin, the time of detection of the event measured in microseconds, whether the event took place under the anticoincidence "umbrella," and a coded symbol which allows rapid recognition of the multiplicity number in which the event is found (i.e., the number of neutron captures recorded within the preset intervals). Thus, it is possible to examine the distribution in time of all the events recorded within one multiplicity period so that

ORNL-DWG 71-5523A

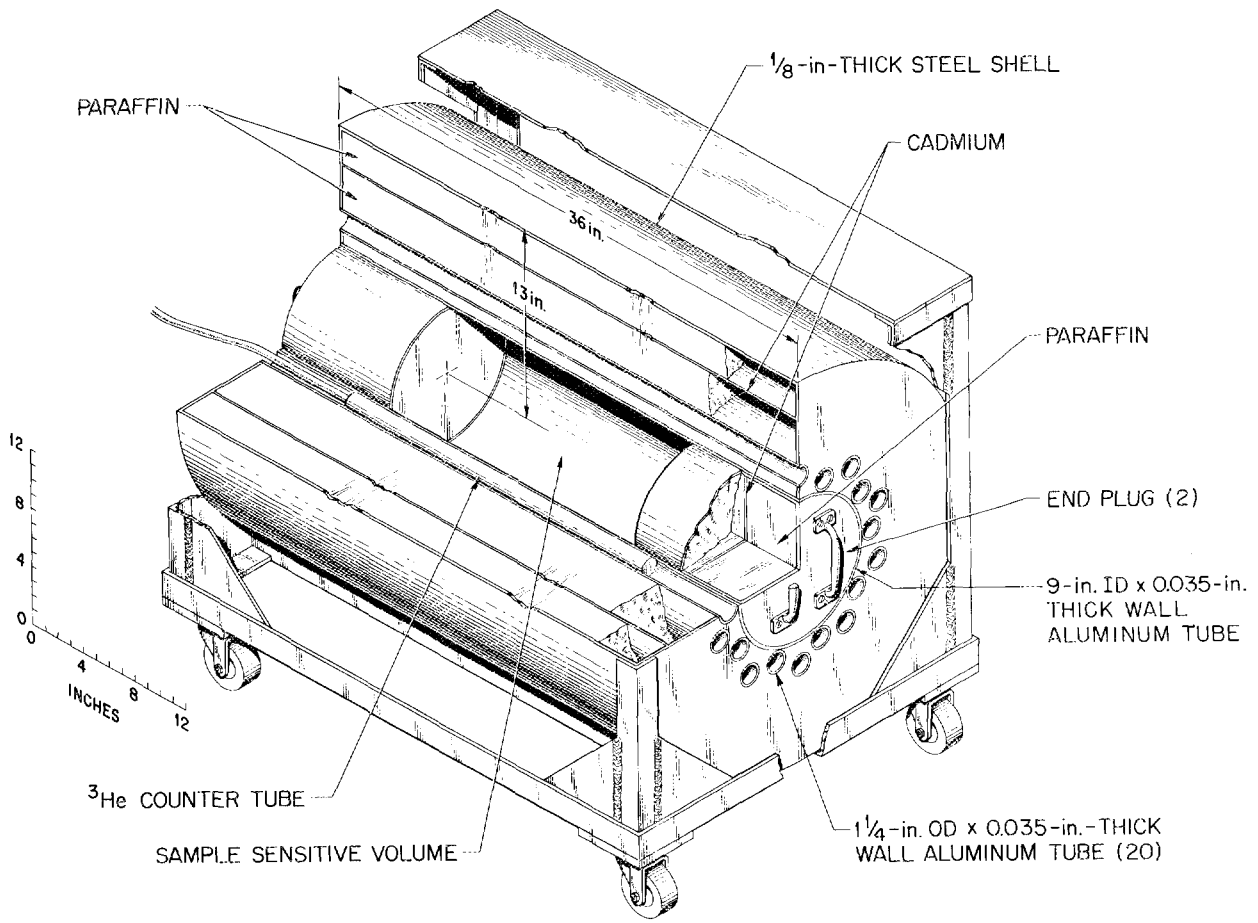

Fig. 2.38. Isometric view of neutron multiplicity counter.

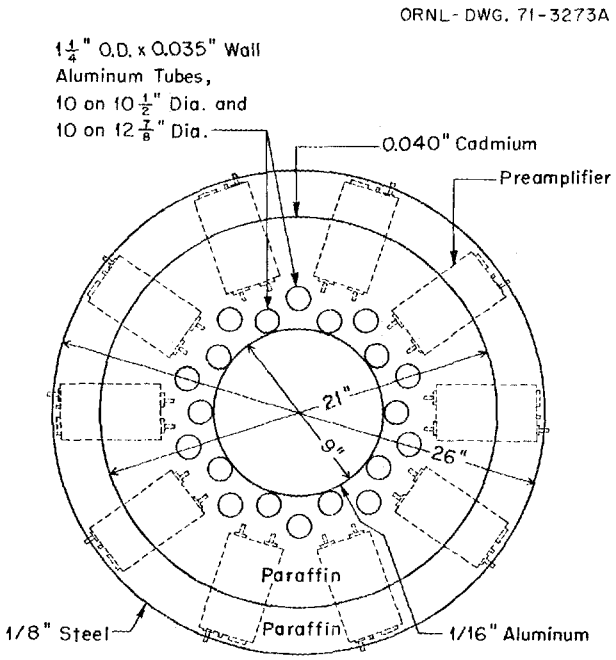

Fig. 2.39. Schematic section of neutron multiplicity counter.

statistical tests can be applied to this distribution. In addition, a printed output of time is made from the start of the count in 1000-sec intervals. The suppression of singles events in the printed output, which are primarily due to background and are $\sim 10^3$-fold greater than the multiplicity rates (only a few per day), is an operational convenience and is accomplished with a front panel selectable switch.

The output of the discriminator also feeds a separate analog circuit with independent timing which discriminates events of varying multiplicities and records them in four scalers which indicate (1) the total number of pulses, (2) the number of doubles and greater, (3) the number of triples and greater, and (4) the number of quadruples and greater. This circuitry has an independent anticoincidence and coincidence gating capability. Because of the low frequency of events of interest, dual recording provides a level of assurance against spurious events.

A limitation in making these measurements is the need to provide adequate shielding from the cosmic-ray background. The apparatus is located in the EGCR building, which currently is not otherwise used. The counter is situated some 53 ft below grade, beneath ~20 ft of concrete shielding, which appears to be adequate to eliminate the nucleonic component of the cosmic-ray spectrum, leaving contributions only from the μ-meson component. Counter backgrounds for multiplicities of $\geqslant 3$ are in the range of one to two events per day. However, massive samples of high Z increase this background by about an order of magnitude, and an anticoincidence mantle is planned to reduce background still further.

A measure of $\bar{\nu}$ can be made with the instrument by examining the distribution of multiplicities for a sample of interest. By calibrating the counter with known emitters, $\bar{\nu}$ for unknown spontaneously fissioning nuclides can be determined. In order to sharpen such measurements, a fragment detector may be placed within the sample volume of the neutron counter and its output used to gate the neutron counter for a variable time ranging from 0 to 1000 μsec.

Using a calibrated ^{252}Cf source, the single neutron efficiency of the counter was determined to be ~0.30. For the case of $\nu = 10$, the binomial distribution law leads to an efficiency of 62% for multiplicities of $\geqslant 3$ and 35% for $\geqslant 4$. If ν should be as low as 6, however, the counter efficiency can be similarly computed to be 26% for multiplicities $\geqslant 3$ and 7% for $\geqslant 4$.

---

1. The authors especially wish to acknowledge the assistance given by R. H. Ward, R. E. Druschel, O. L. Keller, and J. L. Fowler during the planning and assembly of the instrument.

2. Physics Division.
3. Instrumentation and Controls Division.
4. Reactor Division.

5. G. T. Seaborg, *Ann. Rev. Nucl. Sci.* **18**, 53 (1968).
6. A. Marinov et al., *Nature (London)* **229**, 464 (1971).
7. G. N. Flerov and W. P. Perelygin, *At. Energ.* **26**, 520 (1969).
8. N. Bhandari et al., *Nature (London)* **230**, 219 (1971).
9. E. Cheifetz et al., *Phys. Rev. C* **5**, 2017 (1971).
10. J. R. Nix, *Phys. Lett. B* **30**, 1 (1969).

FAST-CLOSING PROTECTIVE VALVE AT ORIC

R. L. Hahn J. R. Tarrant
R. L. Stone[1] L. D. Hunt
M. L. Mallory

Last year,[2] we reported the development of a fast-acting valve that was designed to protect the ORIC from contamination due to the possible rupture of radioactive targets. The valve operation depended upon a spring-loaded plate being kept out of the cyclotron beam line by an electromagnet. In case of target rupture a spark plug, acting as a pressure sensor, would fire, shorting the current to the electromagnet and causing the valve to slam shut.

When the assembly was installed in the ORIC, the valve operated satisfactorily in stopping shock-wave

progression from target to cyclotron, but only ~50% of the cyclotron beam reached the target. To improve beam transmission, the valve was rebuilt with an opening of $2\frac{1}{2}$ in. instead of the 1 in. formerly used, and with only one baffle, which was placed near the target. The new system worked completely satisfactorily. Beam transmission was effectively 100% (or comparable with our experience with no valve or baffle in place), and various tests showed that the larger valve still closed before the shock wave could reach it.

This latter result is especially important because it indicates that special baffles are not required in many situations. Apparently, pumping stations and other cavities that are routinely connected to the ORIC beam line (such as shield-wall plugs) act to slow the shock wave sufficiently to prevent contamination of the cyclotron.

---

1. Plant and Equipment Division.
2. R. L. Hahn et al., *Chem. Div. Annu. Progr. Rep. May 20, 1970,* ORNL-4581, p. 59.

3. Isotope Chemistry

FRACTIONATION OF CARBON ISOTOPES: THE CYANEX SYSTEM

L. L. Brown

The development of the CYANEX system for the fractionation of carbon isotopes continued at the bench-scale level. This chemical exchange system is based on the reaction

$$R_2C(OH)^{12}CN(org) + {}^{13}CN^-(aq) = R_2C(OH)^{13}CN(org) + {}^{12}CN^-(aq) ,$$

which has a separation factor of 1.04 at 25°C.

The previously reported objectionable mass transfer of "CN" from the aqueous to the organic phase was eliminated by the use of *p*-xylene as a solvent for the organic-phase cyanohydrin. No mass transfer occurs when xylene solutions 1.2 *M* in cyanohydrin and 3 *M* in total ketone are equilibrated with aqueous 0.9 *M* KCN solutions. Equimolar transport of "CN" in each phase was obtained by adjusting the volume flow of organic solution to three-fourths that of the aqueous phase. Reflux of both streams was readily accomplished in the modified system, and continuous integrated runs involving the simultaneous operation of the product end refluxer, the exchange column, and the waste-end refluxer were successfully performed for periods as long as 141 hr.

Inventory losses of "CN" during these extended runs amounted to about 1%/day. We believe the bulk of this loss was caused by venting of HCN through the mechanical action of the pulsers. If this view is valid, most or perhaps all of this relatively small loss can be eliminated by equipment design. An adverse consequence of the use of an inert diluent for the cyanohydrin has been a several-fold increase in the theoretical plate height. We attribute this change to an increased half-time of exchange and are presently seeking ways to minimize this effect.

PHOTOCHEMISTRY OF CHLORINE

W. H. Fletcher[1]

Investigation of the possibility of separating chlorine isotopes photochemically was concluded. Separation by this method depends upon the selective excitation of one isotopic form of Cl_2 to a discrete vibrational level in the ${}^3\Pi_0{}^+$ state and a subsequent reaction of the excited molecule with a given substrate without the formation of a radical or the release of an atom. Calculations previously reported[2] indicated that the 5145-Å radiation of an argon ion laser would excite the ${}^{37}Cl$-${}^{37}Cl$ much more effectively than the ${}^{37}Cl$-${}^{35}Cl$ or the ${}^{35}Cl$-${}^{35}Cl$ species. Subsequent studies established that CO, $CH_2{=}CF_2$, C_4F_8 (perfluorobutene-2), and C_2H_4 did not react with Cl_2 at a measurable rate in the absence of light but did react when exposed to 5145-Å radiation. In all cases, however, the photochemically initiated reactions proceeded by a chain mechanism, with quantum yields ranging from 10 to 100. The occurrence of these chain reaction mechanisms rendered these systems unsuitable for isotopic fractionation since isotopic selectivity cannot exist under these conditions.

1. Consultant; Department of Chemistry, University of Tennessee, Knoxville.
2. W. H. Fletcher, *Chem. Div. Annu. Progr. Rep. May 20, 1970*, ORNL-4581, p. 64.

OXYGEN-17 FACILITY

D. Zucker

The Oxygen-17 Facility performed satisfactorily during the past year.

The Water Distillation Cascade operated continuously; no outages of any kind were experienced. A peak ${}^{17}O$ concentration of 1.3% had been attained at the end of the report period. The peak concentration for ${}^{18}O$ was 90%. The isotopic gradient for both ${}^{17}O$ and ${}^{18}O$ is slowly increasing.

The Thermal Diffusion Cascade operated continuously since startup at the beginning of FY 1971. (Prior to this time operation of the Thermal Diffusion Cascade was interrupted for leak hunting and replacement of the sample manifold at the top of the columns.) The peak concentrations of ${}^{17}O$ and ${}^{18}O$ in the Thermal Diffusion Cascade were 20 and 99.3% respectively. During the latter portion of FY 1971, operation of the thermal diffusion columns was aimed at maximizing ${}^{18}O$

production because of the current interest in using this isotope in the synthesis of transuranic and ultimately superheavy elements.

Transfers to the Isotopes Division inventory included 49 g of H_2O containing 98.1% ^{18}O, valued at $24,500; 13.3 liters of oxygen gas containing 99% ^{18}O, valued at $21,000; and 9.5 liters of oxygen gas containing 10 to 20% ^{17}O, valued at $13,450. Also, on hand, but not transferred to inventory, were 130 liters of high-purity ^{16}O gas which contained <20 ppm ^{17}O and ^{18}O.

In March, a decision was made to terminate the operation of the facility at the end of June. Other sources of separated oxygen isotopes have made this operating facility superfluous.

MOLECULAR SPECTROSCOPY[1]

G. M. Begun

Early in the work of the Isotope Chemistry Group, it became evident that molecular spectroscopy, both infrared and Raman, was a powerful tool for the investigation of isotopic properties. Observations of the vibrational frequencies of isotopic molecules provide data for the calculation of equilibrium constants for isotopic exchange reactions, which are of interest for the chemical separation of isotopes. More recently we have used these methods to characterize new and unique compounds, such as the xenon compounds and the perbromate ion. Raman spectroscopy has become many orders of magnitude more sensitive with the development of commercial laser light sources, and research and practical applications in this field are rapidly multiplying. We previously modified our Cary-81 Raman spectrometer to use laser light sources and are continuing our research program in molecular spectroscopy as well as examining the use of lasers for the photochemical separation of isotopes.

The fractionation of isotopes in the cuprous chloride–ammonium chloride–carbon monoxide system (the COCO system)[2] results from an exchange reaction between gaseous carbon monoxide and an aqueous cuprous chloride–ammonium chloride solution. The Raman spectrum of the aqueous solution is shown in Fig. 3.1. The interesting feature of this Raman spectrum is the sharp band at 2098 cm^{-1}, which is due to the stretching vibration of the ^{12}C–O bond in the complex. In gaseous ^{12}CO this vibration occurs at 2143.24 cm^{-1}. The small band at 2050.2 cm^{-1} is due to the presence of ^{13}C–O in the complex. It is interesting that the stretching frequency, which decreases 45 cm^{-1} with the formation of the complex, has almost the same isotopic shift in the complex (Δ cm^{-1} = 47.8) as in gaseous CO (Δ cm^{-1} = 47.2). Thus nearly all the isotopic fractionation of the system is due to the primary effect of bonding of the carbon atom of the CO in the solution complex.

The Raman spectrum offers a convenient and rapid method of isotopic analysis of the solution. A very small drop in a melting-point tube may be used to obtain the spectrum; comparison of the areas of the 2098.0- and 2050.2-cm^{-1} peaks then provides the abundance data. The ratios of the areas of these peaks in Fig. 3.1 give an isotopic analysis of 13.4% ^{13}C, compared with 12.8% ^{13}C determined by mass spectrographic analysis. Isotopic analysis of production plant samples could be obtained routinely and economically by this method.

Fused salt systems are of considerable interest to ORNL in various applications, and last year[3] we reported data obtained from Raman studies of $AlCl_3$-

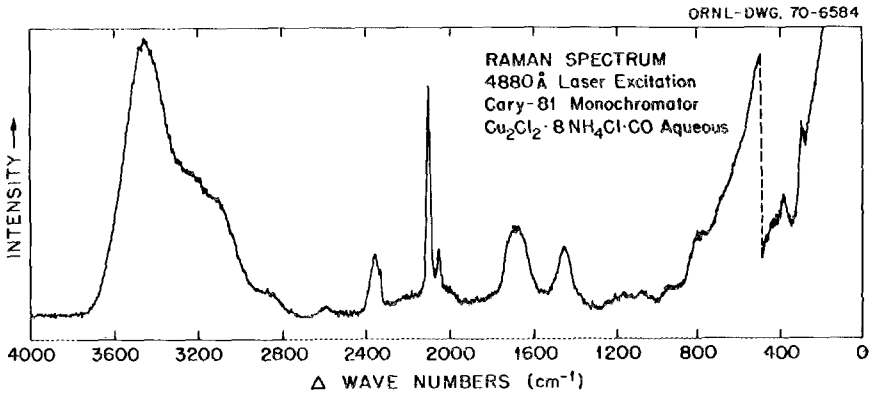

Fig. 3.1. Raman spectrum of aqueous $Cu_2Cl_2 \cdot 8NH_4Cl \cdot CO$.

NaCl melts. This work has been extended to the $AlBr_3$-NaBr and the AlI_3-CsI systems. Raman spectra were obtained for $AlBr_3$-NaBr and AlI_3-CsI melts in the region 50-50 mole % to pure aluminum halide. Figure 3.2 shows the Raman spectra of several mixtures of molten $AlBr_3$-NaBr in the concentration region 50-50 to 100-0 mole %. The data are recorded in Table 3.1. The Raman spectra for three concentrations of the AlI_3-CsI system are shown in Fig. 3.3, and the data for these melts and for polycrystalline $CsAl_2I_7$ are given in Table 3.2.

It is clear from the Raman spectra that, in the 50-50 mole % mixtures, the $AlBr_3$-NaBr and AlI_3-CsI systems are similar to the $AlCl_3$-NaCl system and that the dominant species is the tetrahedral AlX_4^- ion, where X is Cl, Br, or I. In the case of $AlBr_4^-$ and AlI_4^-, only the four characteristic Raman peaks of the tetrahedral ion are seen, and any other species present at 50-50 mole % must be in low concentrations. Table 3.3 lists the frequencies we have observed for the AlX_4^- ions and the assignments made to the vibrational modes, assuming tetrahedral symmetry.

Using the symmetry coordinates of Meister and Cleveland,[4] we calculated valence force constants for $AlCl_4^-$, $AlBr_4^-$, and AlI_4^-. The Wilson F and G matrix method[5] was used, and solutions were arrived at by a machine-iterative least-squares process similar to that of Overend and Scherer.[6] The Al-X distances were assumed to be 2.13, 2.27, and 2.55 Å for $AlCl_4^-$, $AlBr_4^-$, and AlI_4^- respectively. It was possible to fit the frequencies to within a few tenths of a wave number by various combinations of valence force constants; one of the simplest sets is given in Table 3.4. The nonzero force constants used were: f_d, stretching; f_α, bending; $f_{\alpha\alpha'}$, bend-bend interaction between opposite angles; $f_{d\alpha}$ and $f_{d\alpha'}$, stretch-bend interactions. The force

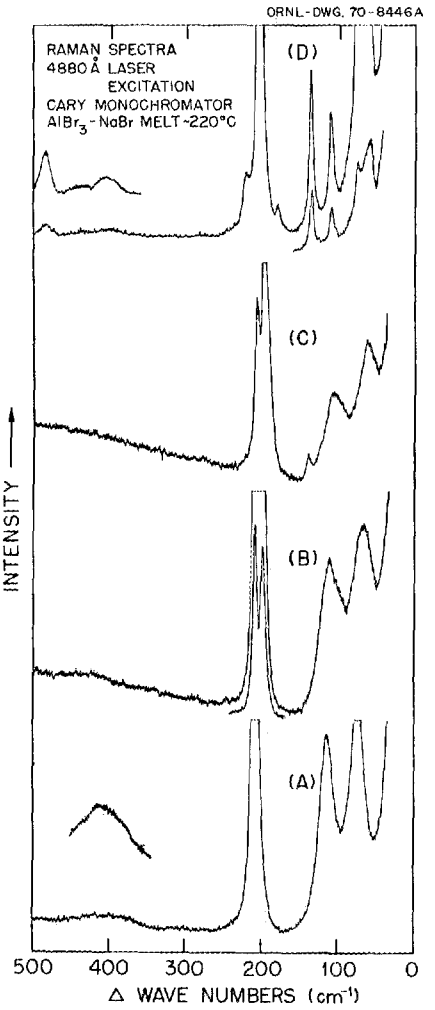

Fig. 3.2. Raman spectra of molten $AlBr_3$-NaBr at 220°C. Conditions: 4880-Å laser excitation. Composition: (*A*) 50-50 mole %; (*B*) 62-38 mole %; (*C*) 75-25 mole %; (*D*) 100-0 mole %.

Table 3.1. Raman frequencies of the $AlBr_3$-NaBr system at ~220°C

Frequency[a] (cm^{-1}) at composition (mole % $AlBr_3$-NaBr)								Polarization
50-50	52-48	54-46	62-38	67-33	75-25	80-20	100-0	
				60 m	61 m	65 m	65 s	P
75 s	73 s	73 s	71 s			80 m	79 m	D
				103 m	98 m	100 m		
114 s	114 s	113 s	108 m	109 m	109 m	112 m	113 m	D
					140 w	141 m	140 m	P
							183 w	P
			198 s	198 vs	199 vs	199 s		P
209 vs	209 vs	209 vs	209 s	209 s	208 s	208 vs	208 vs	P
						224 w	224 w	D?
409 w	408 w						405 w	?
							434 w	?
							489	D

[a]s, strong; m, medium; w, weak; v, very; P, polarized; D, highly depolarized.

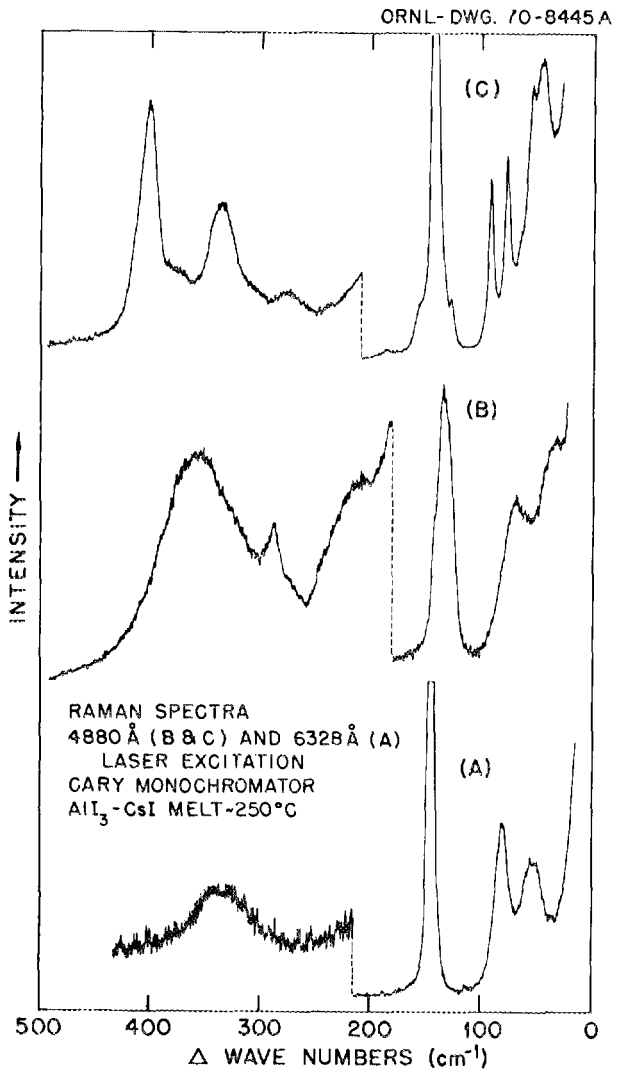

Fig. 3.3. Raman spectra of molten AlI_3-CsI at 250°C. Conditions: 6328-Å (*A*) and 4880-Å (*B* and *C*) laser excitation. Composition: (*A*) 50-50 mole %; (*B*) 67-33 mole %; (*C*) 100-0 mole %.

constants clearly illustrate the progressive weakening of the Al-X bond as the size of the halide increases.

In the fused $AlCl_3$-NaCl system, we observed Raman lines which we assigned[3] to the $Al_2Cl_7^-$ ion. Cyvin et al.[7] independently obtained similarly results and made the same interpretation. In the spectra of $AlBr_3$-NaBr and AlI_3-CsI mixtures, a similar effect may be seen with the appearance of a strong polarized line and several other weaker lines which are probably due to the $Al_2Br_7^-$ and $Al_2I_7^-$ ions respectively. This assignment is strengthened by the similarity between the spectrum of solid $CsAl_2I_7$ and that of the 67-33 mole % AlI_3-CsI melt.

Table 3.2. Raman frequencies and polarization of the AlI_3-CsI System at 250°C and of solid $CsAl_2I_7$

Frequency[a] (cm^{-1})			
Composition (mole %), AlI_3-CsI melt			Polycrystalline $CsAl_2I_7$
50-50	67-33	100-0	
	35 m		
51 m		48 m	
		57 m	56, 60, 65 w
	69 m		72 s
82 m		80 m	82 s
		95 m,P	
		132 w	
	137 s,P		142 vs
146 s,P	145 w,sh	145 s,P	
		158 w,sh	164 w
		189 w,b	183 w
	210 w,b		213, 221 w,b
		277 vw	240 m,b
	288 w,P		292 m
336 w,b		339 w	325 w
	360 m,b		370, 373, 380 m
		380 vw,sh	
		404 w,b	

[a]w, weak; m, medium; s, strong; v, very; sh, shoulder; b, broad; P, polarized.

Table 3.3. Vibrational frequencies (cm^{-1}) of aluminum tetrahalide ions

Ion	ν_1 (A_1)	ν_2 (E)	ν_3 (F_2)	ν_4 (F_2)
$AlCl_4^-$	351	121	490	186
$AlBr_4^-$	209	75	409	114
AlI_4^-	146	51	336	82

Table 3.4. Valence force constants for $AlCl_4^-$, $AlBr_4^-$, and AlI_4^- ions (millidynes/Å)

Ion	f_d	f_α/d^2	$f_{\alpha\alpha'}/d^2$	$(f_{d\alpha} - f_{d\alpha'})/d$
$AlCl_4^-$	2.58	0.14	−0.04	0.30
$AlBr_4^-$	2.06	0.10	−0.02	0.17
AlI_4^-	1.59	0.08	−0.02	0.15

In all three cases we found the strongest, polarized, symmetrical stretching vibration of the AlX_4^- ion to be very close to the similar vibration of the Al_2X_6 dimer. The greatest difference occurred with $AlCl_4^-$-Al_2Cl_6, where the two frequencies observed are 351 and 341 cm^{-1} respectively. Similar values for $AlBr_4^-$-Al_2Br_6 and AlI_4^--Al_2I_6 are 209, 208 and 146, 145 cm^{-1}. The

frequency most characteristic of the $Al_2X_7^-$ ion, a strong polarized band, is found to be lower than the symmetrical stretching frequency for either the AlX_4^- ion or the Al_2X_6 dimer. This characteristic frequency occurs at 313, 198, and 137 cm^{-1} for $Al_2Cl_7^-$, $Al_2Br_7^-$, and $Al_2I_7^-$ respectively. Table 3.5 lists the lines we have assigned to the $Al_2X_7^-$ ions in the melt. A linear Al-Cl-Al bridge with a staggered ethane-like structure (D_{3d}), as assumed by Cyvin et al.,[7] will fit the data and is more likely than a less-symmetric structure which would have more Raman-active frequencies.

Table 3.5. Vibrational frequencies[a] (cm^{-1}) for $Al_2X_7^-$ ions

$Al_2Cl_7^-$	$Al_2Br_7^-$	$Al_2I_7^-$
435 w		360 w
		288 w,P
		220 w
313 s,P	198 s,P	137 s,P
165 m	104 m	69 m
100 m	60 m	35 m

[a]P, polarized; s, strong; m, medium; w, weak.

Raman studies of several solute species in molten LiF-NaF-KF (46.5-11.5-42.0 mole %) were undertaken to obtain additional evidence for the existence of the superoxide ion O_2^- in this basic fluoride melt.[8] In addition to the spectrum of the O_2^- ion, spectra of CrO_4^{2-} and CO_3^{2-} ions were also obtained. A very simple procedure was used to obtain the Raman spectra of these melts. Samples were sealed under slightly less than 1 atm pressure of helium in quartz tubes (4 mm OD and 2 in. long). The salt was melted inside the sample compartment of the Raman spectrophotometer by passing a current through a coil of platinum wire wrapped around the section of the quartz tube which contained the sample. The temperature of the sample was ~500°C.

The Raman spectrum of O_2^- in molten LiF-NaF-KF consists of a single, strongly polarized band at 1107 cm^{-1}, as shown in Fig. 3.4. Holzer et al.[9] have reported an especially interesting series of observations of the

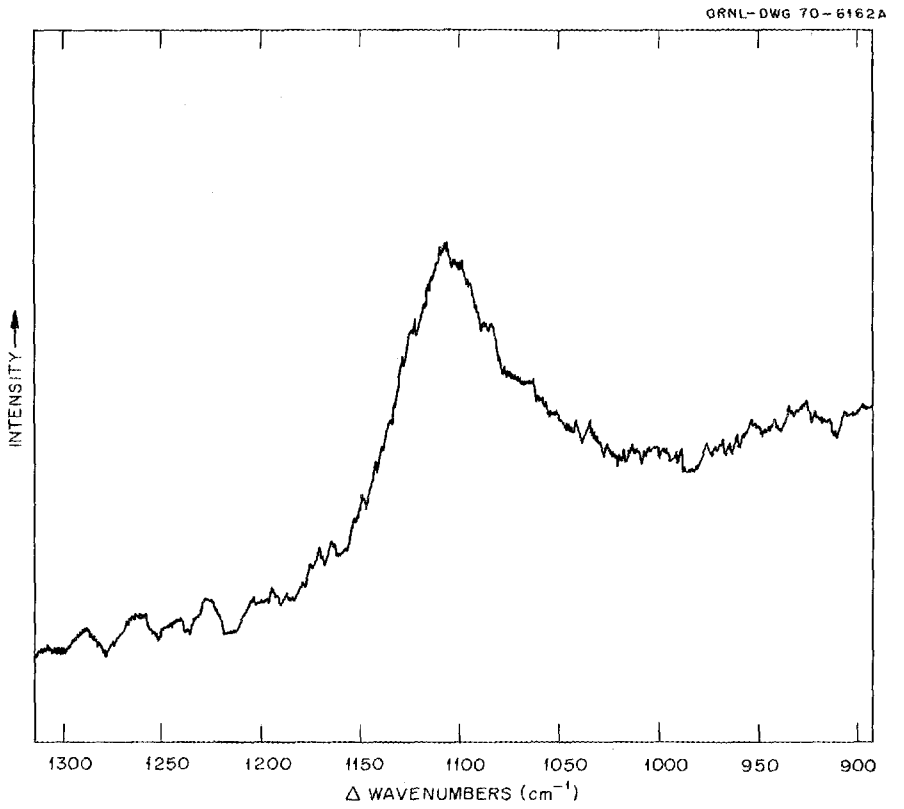

Fig. 3.4. Raman spectrum of O_2^- at 500°C in molten LiF-NaF-KF. Conditions: 4880-Å argon ion laser excitation; slit width at 4880 Å, 5 cm^{-1}.

Raman spectrum of O_2^- ion in alkali halide crystals. Here the O_2^- frequency varied from 1123 cm^{-1} in KI to 1145 cm^{-1} in KCl. It was shown that the vibrational frequency decreased with an increase in unit cell size of crystals having a common cation. By extrapolation, Holzer and co-workers estimated the frequency for an isolated O_2^- ion to be 1090 cm^{-1}. In the LiF-NaF-KF melt, the O_2^- ion would not be isolated and yet would not be subjected to the same type of rigid repulsion experienced in crystals. Thus we observe the symmetrical stretching vibration of O_2^- ion in the fluoride melt between that for the free O_2^- ion and that for the ion embedded in a crystal lattice.

The Raman spectrum of a solution of Na_2CO_3 in molten LiF-NaF-KF gave a single polarized band at 1053 cm^{-1} which we assigned to the symmetrical stretching frequency of CO_3^{2-} (ν_1). It is interesting to compare this frequency with the value for aqueous carbonate ion, which is observed at 1060 cm^{-1}. In both aqueous and molten fluoride solutions the other Raman-active bands of the CO_3^{2-} ion are difficult to observe because they are weak and broad. Maroni and Cairns[10] recently reported Raman values for the ν_1 stretching frequency of CO_3^{2-} in fused carbonates. They observed lines at 1064 and 1066 cm^{-1} in melts having the compositions Li_2CO_3-K_2CO_3-Na_2CO_3 (42-27-31 mole %) and Li_2CO_3-K_2CO_3 (59-41 mole %) respectively. For the mixture Li_2CO_3-LiBr (13-87 mole %), they obtained 1080 cm^{-1}. The large shift in the latter value was attributed to the presence of excess Li^+ ions. However, our melt contained considerable Li^+, and the shift was in the other direction. The observed shift must be due to an anion effect, since our system differed from that of Maroni and Cairns only in the use of fluoride rather than bromide salts.

Since CrO_4^{2-} ion occurs occasionally as an impurity in molten fluoride solutions, a Raman spectrum of K_2CrO_4 dissolved in LiF-NaF-KF was obtained. This spectrum is reproduced in Fig. 3.5. The band assignments and positions as seen in the present investigation are: ν_1 (A_1), 840 cm^{-1}; ν_2 (E), 348 cm^{-1}; ν_3 (F_2), 880 cm^{-1}; and ν_4 (F_2), 378 cm^{-1}. The peak at 840 cm^{-1} is polarized, and the 378-cm^{-1} band is almost hidden on the side of the 348-cm^{-1} peak. The band assignments were made in accordance with those reported by Stammreich and co-workers.[11] There is a very close agreement between our values in molten LiF-NaF-KF and the values reported for aqueous CrO_4^{2-} ion (ν_1, 847 cm^{-1}; ν_2, 348 cm^{-1}; ν_3, 884 cm^{-1}; and ν_4, 368 cm^{-1}). As in the case of CO_3^{2-} ion, we find a slight lowering of the symmetrical stretching frequency. In the absence of strong, specific interactions, ions in molten fluoride solutions seem to be analogous to ions in aqueous solutions.

A new ion, Hg_3^{2+}, has been obtained[12] in acidic chloroaluminate melts (mole ratio $AlCl_3/MCl > 1$, where M is an alkali metal) by the oxidation of mercury metal, present in excess, or by the partial reduction of Hg_2^{2+}. A solid compound containing this ion was prepared by mixing an excess of $AlCl_3$ with mercury

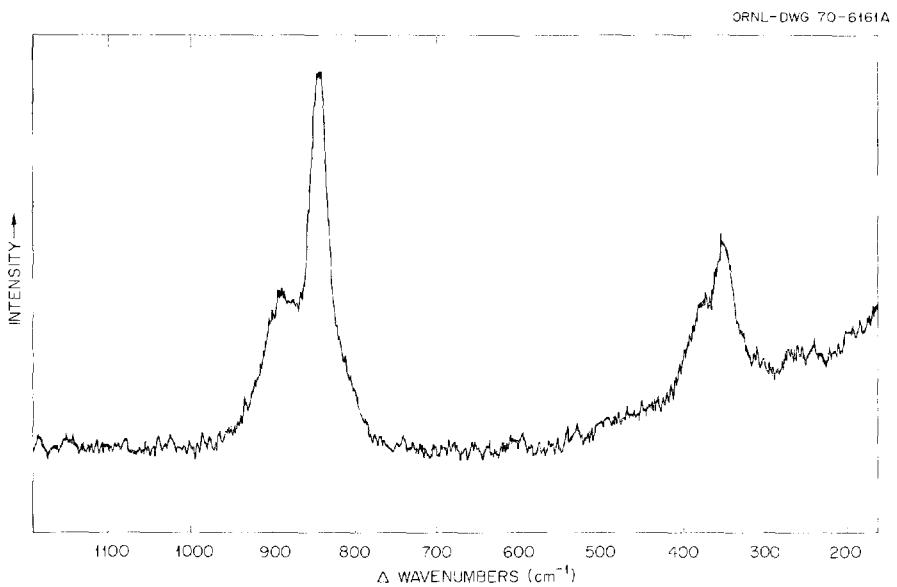

Fig. 3.5. Raman spectrum of CrO_4^{2-} at 500°C in molten LiF-NaF-KF. Conditions: 6328-Å helium-neon laser excitation; slit width at 6328 Å, 5 cm^{-1}.

and a known weight of $HgCl_2$. The mixture was sealed in a glass tube under vacuum and heated at 240°C. After the reaction (36 hr), the excess $AlCl_3$ and mercury were distilled off and condensed in one end of the tube, which was at 100°C. A yellow solid was obtained by cooling the remaining liquid slowly. The chemical analysis of this solid corresponds to the formula $Hg_3(AlCl_4)_2$.[13] Figure 3.6 reproduces the Raman spectrum of the yellow polycrystalline compound. Very strong Raman peaks were observed at 93 and 123 cm^{-1} and weaker peaks at 178, 225, 242, and 350 cm^{-1}. The spectrum shows no evidence of Al_2Cl_6 or of $Al_2Cl_7^-$, while the absence of the strong stretching vibration of Hg_2Cl_2 reported at 167 cm^{-1} indicates that no or very little Hg_2Cl_2 is present. $AlCl_4^-$ has its strongest band at 351 cm^{-1} and weaker bands at 121, 186, and 490 cm^{-1}. We would not expect to see the 490-cm^{-1} band because of its weakness, and the 121-cm^{-1} band would be hidden by the strong line at 123 cm^{-1}. A weak peak can be seen near 180 cm^{-1} in the spectrum. Therefore we assign the 350-cm^{-1} band to the $AlCl_4^-$ group. The crystalline compound Hg_2Cl_2 has its symmetric Raman-active Hg-Cl stretching frequency at 270 cm^{-1} and its infrared-active antisymmetric stretching frequency at 261 cm^{-1}. We observe bands at 225 and 242 cm^{-1}. We believe these bands to be the result of Hg-Cl stretching vibrations. Since the vibrational frequencies of $HgCl_2$ are much higher (ν_1 = 314 cm^{-1}), we conclude that the Hg to which the Cl is bonded is probably also linked to another Hg atom.

We believe the two strong Raman peaks at 93 and 123 cm^{-1} are produced by the symmetric and antisymmetric vibrations of the Hg_3 group. The vibrational frequency observed previously for molecules containing Hg-Hg bonds varies from 108 to 193 cm^{-1}. Either a nonlinear Hg-Hg-Hg grouping or a triangular three-membered ring would produce two Raman-active bands in the observed region. Preliminary x-ray crystallographic data show that the molecule contains a nearly linear Cl-Hg-Hg-Hg-Cl group with an Hg-Hg-Hg angle of ~174° and a Cl-Hg-Hg angle of ~172°. The two remaining $AlCl_3$ groups have tetrahedral angles and are attached to the Cl groups with Al-Cl-Hg angles of ~103°. Therefore we assign the mercury-mercury stretching frequencies as A_1, 93 cm^{-1} (symmetric stretch) and B_1, 123 cm^{-1} (antisymmetric stretch), in accordance with expectations for a nearly linear model. The Raman activity of the antisymmetric stretch apparently results from the lack of symmetry of the whole molecule and the deviations from linearity of the Cl-Hg-Hg-Hg-Cl chain. Thus the Raman spectrum of this new compound clearly shows the presence of $AlCl_4^-$ groups and of Hg-Cl and Hg-Hg bonds.

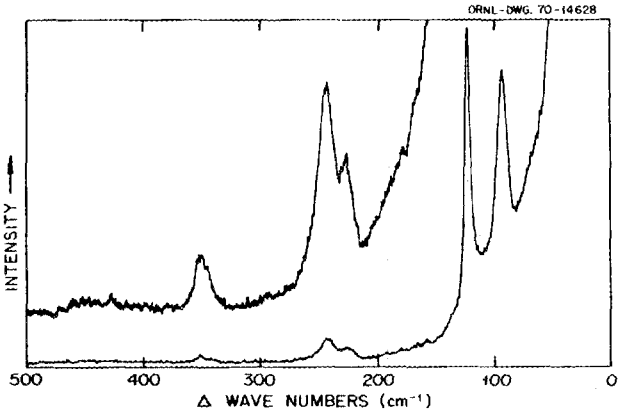

Fig. 3.6. Raman spectrum of polycrystalline $Hg_3(AlCl_4)_2$. Conditions: 5145-Å laser excitation.

1. G. Mamantov, G. Torsi, and W. Fung, Chemistry Department, University of Tennessee, Knoxville, have participated in parts of this research.
2. A. A. Palko, *Chem. Div. Annu. Progr. Rep. May 20, 1967*, ORNL-4164, p. 27.
3. G. M. Begun, *Chem. Div. Annu. Progr. Rep. May 20, 1970*, ORNL-4581, p. 65.
4. A. G. Meister and F. F. Cleveland, *Amer. J. Phys.* **14**, 13 (1946).
5. E. B. Wilson, Jr., J. C. Decius, and P. C. Cross, *Molecular Vibrations*, pp. 61 ff. McGraw-Hill, New York, 1955.
6. J. Overend and J. R. Scherer, *J. Chem. Phys.* **32**, 1289 (1960).
7. S. J. Cyvin et al., *J. Chem. Phys.* **52**, 2776 (1970).
8. F. L. Whiting, G. Mamantov, and J. P. Young, *J. Amer. Chem. Soc.* **91**, 6531 (1969).
9. W. Holzer et al., *J. Mol. Spectrosc.* **26**, 543 (1968).
10. V. A. Maroni and E. J. Cairns, *J. Chem. Phys.* **52**, 4915 (1970).
11. H. Stammreich, D. Bassi, and O. Sala, *Spectrochim. Acta* **12**, 403 (1958).
12. G. Torsi and G. Mamantov, *Inorg. Nucl. Chem. Lett.* **6**, 843 (1970).
13. See also R. D. Ellison and H. A. Levy, "Crystal and Molecular Structure of Trimercury Chloroaluminate, $Hg_3(AlCl_4)_2$," a contribution in chap. 7, this report.

ISOTOPIC MASS SPECTROMETRY

L. Landau

During this report period water samples were analyzed on a routine basis to monitor the performance of the Water Distillation Cascade. Oxygen samples were analyzed for ^{17}O, ^{18}O, N_2, Ar, and CO_2 content to maintain control over the Thermal Diffusion Cascade.

Standard O_2 samples were prepared[1] by heating $KMnO_4$ to ~250°C and collecting replicate samples of high-purity O_2.

A total of 400 samples were analyzed.

1. R. C. Brasted, *Comprehensive Inorganic Chemistry*, vol. 8, p. 255, Van Nostrand, Princeton, N.J., 1961.

COMPARATIVE ISOTOPIC CARBON ANALYSES OF CO AND CO_2

L. Landau J. S. Jones[1] L. L. Brown

This study was undertaken to determine the relative merits of analyzing CO directly for ^{13}C by mass spectrometric measurements of the relative peak heights at *m/e* 29 and 28 (method 1) or by first oxidizing the CO to CO_2 with V_2O_5 and making measurements on the *m/e* 45 and 44 peaks (method 2). V_2O_5 was chosen for the oxidant because it forms no other gaseous products, and it worked well in the oxidation of AgCN to CO_2.

The advantages of the second method include the ease of handling and purifying CO_2 because of its low vapor pressure at liquid N_2 temperature and the avoidance of mass spectrometric measurements at *m/e* 28, where CO from the filament and N_2 interfere.

Six mixtures of ^{13}CO were prepared by additions of normal CO to a sample of CO assaying 55.43% ^{13}C. Each mixture was pumped through a mixing loop for 1 hr and then divided and sealed into four sample tubes. Two of these tubes contained V_2O_5 and were heated to 500°C for 1 hr, converting the CO to CO_2 quantitatively.

Table 3.6. Analysis of carbon dioxide (method 2)

$(^{13}C/^{12}C)_{sample}/(^{13}C/^{12}C)_{reference}$

Computed from dilution procedure	Measured by mass spectrometry (duplicates)	Difference between duplicates
1.318	1.3170 ± 0.001, 1.3180 ± 0.0020	0.0010
1.249	1.2469 ± 0.0008, 1.2460 ± 0.0010	0.0009
1.133	1.1327 ± 0.0009, 1.1326 ± 0.0005	0.0001
1.041	1.0412 ± 0.0004, 1.0408 ± 0.0005	0.0004
1.020	1.0199 ± 0.0002, 1.0174 ± 0.0002	0.0025
1.012	1.0123 ± 0.0004, 1.0120 ± 0.0002	0.0003
1.000	1.0000 ± 0.0001	

Table 3.7. Analysis of carbon monoxide (method 1)

$(^{13}C/^{12}C)_{sample}/(^{13}C/^{12}C)_{reference}$

Computed from dilution procedure	Measured by mass spectrometry (duplicates)	Difference between duplicates
1.318	1.2887 ± 0.0006, 1.3091 ± 0.0002	0.0204
1.249	1.2274 ± 0.0002, 1.2428 ± 0.0003	0.0154
1.133	1.1225 ± 0.0002, 1.1284 ± 0.0002	0.0059
1.041	1.0390 ± 0.0001, 1.0397 ± 0.0001	0.0007
1.020	1.0188 ± 0.0002, 1.0187 ± 0.0003	0.0001
1.012	1.0116 ± 0.0002, 1.0114 ± 0.0002	0.0002
1.000	1.0001 ± 0.0001	

Table 3.6 compares the six mixtures with a reference sample, first as calculated from the volumes and pressures of the CO added, and then from the peak height ratios at *m/e* 45 and 44 of the mixtures and the reference. Table 3.7 shows a similar analysis of the CO mixtures measured at *m/e* 29 and 28.

The CO_2 analyses were consistent; the maximum deviation between duplicates was three parts per thousand. The CO analyses are very good for ratios near unity, but internal agreement is poor for higher ratios. The agreement with the values calculated from the dilutions is also poor.

It appears that oxidation of CO to CO_2 with V_2O_5 works very well, and the precision and accuracy of the CO_2 mass spectrometric analysis for ^{13}C are superior to those by direct CO analysis.

1. Student participant in the Great Lakes Colleges Association Science Semester, Sept. 10–Dec. 18, 1970, from DePauw University, Greencastle, Ind.

EXCHANGE OF OXYGEN BETWEEN CO_2(g) AND V_2O_5(s)

L. Landau J. S. Jones[1] L. L. Brown

V_2O_5 has been used to oxidize CO to CO_2 for ^{13}C isotopic analyses. If there were no exchange of oxygen between the CO_2 formed and V_2O_5 under the conditions for oxidation, it would be feasible to use this same reaction for ^{17}O and ^{18}O isotopic analyses also. If there were complete exchange, this reaction might still be utilized, but only if a small excess of V_2O_5 were used and if the amount were determined accurately. In

order to determine whether oxygen exchange occurs between V_2O_5 and CO_2 under conditions suitable for the oxidation of CO, the following experiments were performed.

A number of Pyrex glass tubes containing normal V_2O_5 were filled with CO_2 having a 70% ^{18}O assay. These tubes were heated at 400 or 500°C for different periods of time, the resulting CO_2 was analyzed, and the extent of oxygen exchange was calculated. Table 3.8 shows the results.

It can be seen from the table that some exchange does take place under all conditions examined, but complete exchange would take a very long time or require a very high temperature. The two measurements indicating more than 100% exchange of the available oxygen suggest either a lack of accuracy in estimating the amount of reactants used or that oxygen from the glass is entering into the reaction. In view of these results, this system does not appear promising for the analysis of oxygen isotopes.

Table 3.8. Rate of exchange of oxygen between $CO_2(g)$ and $V_2O_5(s)$

Temperature (°C)	Time (hr)	Percent exchange
400	0.3	2.0
	0.5	3.7
	2.0	7.2
500	0.3	20.2
	0.6	29.1
	1.4[a]	44.2
	1.4[b]	50.9
	2.2	51.9
	16.0	65.7
	54.2	117.0
	66.2	95.8
	120.0	115.0

[a]Small surface area of V_2O_5.
[b]Large surface area of V_2O_5.

1. Student participant in the Great Lakes Colleges Association Science Semester, Sept. 10–Dec. 18, 1970, from DePauw University, Greencastle, Ind.

4. Radiation Chemistry

OZONE FORMATION IN THE PULSE RADIOLYSIS AND FLASH PHOTOLYSIS OF OXYGEN

J. A. Ghormley J. W. Boyle
C. J. Hochanadel P. J. Ogren[1]

The formation of ozone via the reaction

$$O + O_2 + M \rightarrow O_3 + M \qquad (1)$$

following absorption of energy by a system containing oxygen is of both fundamental and practical interest. The O atoms can originate from either ionic precursors or neutral electronically excited precursors. We carried out a variety of studies aimed at determining mechanisms of O_3 formation and inhibition, including: sensitized formation in mixtures with N_2, Ar, or He; use of the electron scavenger SF_6 to evaluate the contribution to the O_3 yield from ionic and excited precursors; inhibition of O_3 formation in the above mixtures by scavengers of electrons or negative charge (O_3, SF_6) or positive charge (NH_3, toluene) and by water; the relative efficiencies of these molecules as third body, M, in reaction (1); and formation and reactions of the transients OH, HO_2, and NH in some of these systems. The results are summarized briefly.

Sensitized O_3 Formation in the Pulse Radiolysis of O_2 Mixed with N_2, Ar, or He: The Use of SF_6 to Evaluate the Yield from Ionic and Excited-State Precursors

The gas mixtures were exposed to single pulses of electrons from a Febetron at a nominal maximum energy of 2.3 MV, a current of 5000 A, and a pulse duration of 30 nsec. We observed the formation of O_3 (by its absorption at 2560 Å) which occurs after the pulse via reaction (1). Under our experimental conditions O_3 does not compete with O_2 for O atoms. Therefore back reaction is negligible, and the total O_3 yield and rate of formation can be accurately measured. Typical oscilloscope traces of O_3 formation are shown in Fig. 4.1 for pure O_2 and O_2 saturated with H_2O (3%).

The yields of O_3 in pure O_2 and in mixtures with N_2, based on the total energy absorbed by the system, are shown in Fig. 4.2. Effects of the inhibitors SF_6, H_2O, and NH_3 on O_3 yields are also shown. Similar results are shown for O_2-Ar mixtures in Fig. 4.3. Sufficient inhibitor was added to produce a limiting yield, as determined from plots such as those shown for O_2 in Fig. 4.4 and for air in Fig. 4.5. The yield of O_3 in pure O_2 was determined previously to be 13.8 molecules of O_3 per 100 eV.[2] The presence of added SF_6 lowers the yield to 7.2, indicating a yield of 6.6 from ionic precursors. Since the yield of ions is 3.1 (from the W value of 32.2 eV per ion pair), the neutralization reaction must be dissociative, O_2^+ (or O_4^+) + $O_2^- \rightarrow 2O + O_2$. Since no pressure effect was observed in the range 0.1 to 1 atm, neutralization of O_2^+ by e^-, if it occurs, is also dissociative. SF_6 eliminates formation of O atoms, and therefore O_3, from ionic precursors by scavenging

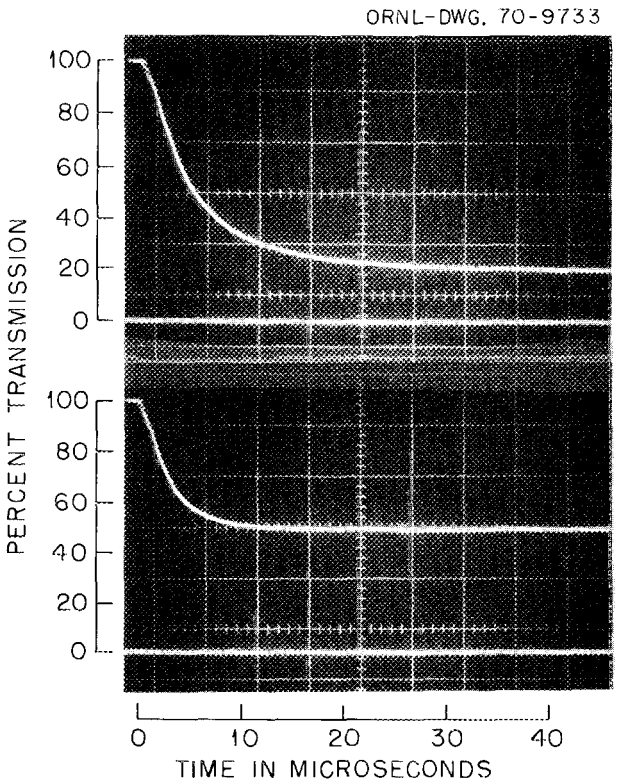

Fig. 4.1. Oscilloscope traces. Absorption by O_3 at 2560 Å following an electron pulse in O_2 (upper trace) and in O_2 saturated with H_2O (3 mole %) (lower trace).

electrons and preventing dissociative neutralization of O_2^+.[3] The ratio of the number of excited species to the number of ions, $N_{ex}/N_{ions} \simeq 1.1$, agrees with Platzman's[4] calculations for a molecular gas. The shape of the upper curve in Fig. 4.2 indicates efficient O_3 formation from ions and electronically excited states of N_2 produced initially. A simple extrapolation of the upper curve gives an O_3 yield of ~9.7 from energy initially absorbed by N_2. Measurements of the rate of formation of O_3 in the O_2-N_2 system indicate that O_2 reacts directly with N_2* and that little, if any, O_3 originates via N atom intermediates. The slow reaction $N + O_2 \rightarrow NO + O$ would lead to O_3 formation on a time scale an order of magnitude longer than that observed.

Similar extrapolations of plots for O_2-Ar and O_2-He mixtures give O_3 yields of ~10.3 and ~13.5 from energy initially absorbed by Ar or He respectively. Extrapolation of the yield curves for mixtures with added SF_6 allows an estimate of N_{ex}/N_{ions} for the rare gases. The ratio is low, in qualitative agreement with Platzman's[4] calculation, ≃0.4.

We made similar measurements of the yields (NO_2 + N_2O_3) in the pulse radiolysis of NO with and without added SF_6 and estimated this ratio for a third type of molecule, namely, one with an unpaired electron. The observed high ratio was in qualitative agreement with Platzman's[4] calculated ratio, $N_{ex}/N_{ions} \simeq 1.8$.

The high yield of O_3 from energy absorbed in He and the large effect of SF_6 indicate that reactions of He^+ and He* with O_2 produce dissociative ionization. Each He^+ or He* leads to the formation of 4 molecules of O_3 through the sequence

$$He^+ \text{ (or He*)} + O_2 \rightarrow O^+ + O\,(+\,e^-) + He\,,$$

$$O^+ + O_2 \rightarrow O + O_2^+\,,$$

$$O_2^+ + O_2^- \rightarrow 2O + O_2\,.$$

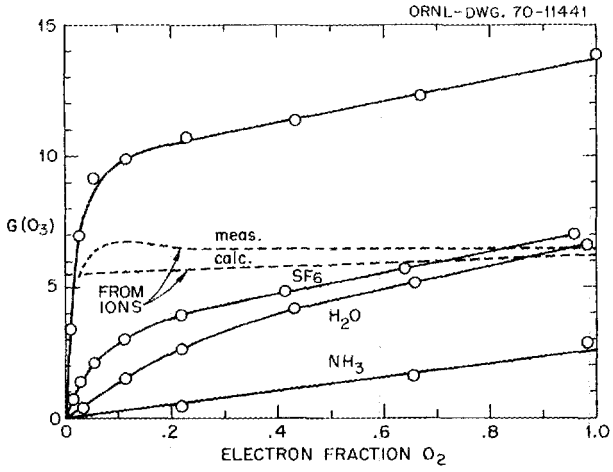

Fig. 4.2. Effects of SF_6 (1%), H_2O (3%), or NH_3 (7%) on $G(O_3)$ in O_2-N_2 mixtures.

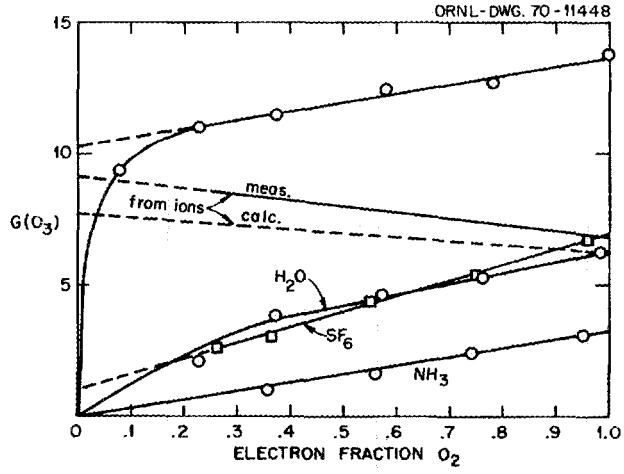

Fig. 4.3. Effects of SF_6 (1%), H_2O (3%), or NH_3 (7%) on $G(O_3)$ in O_2-Ar mixtures.

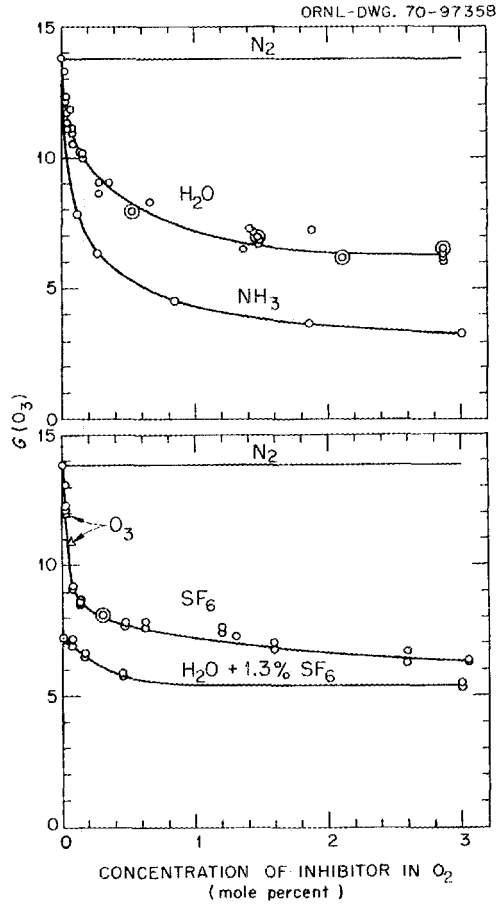

Fig. 4.4. Dependence of $G(O_3)$ on inhibitor concentration in O_2.

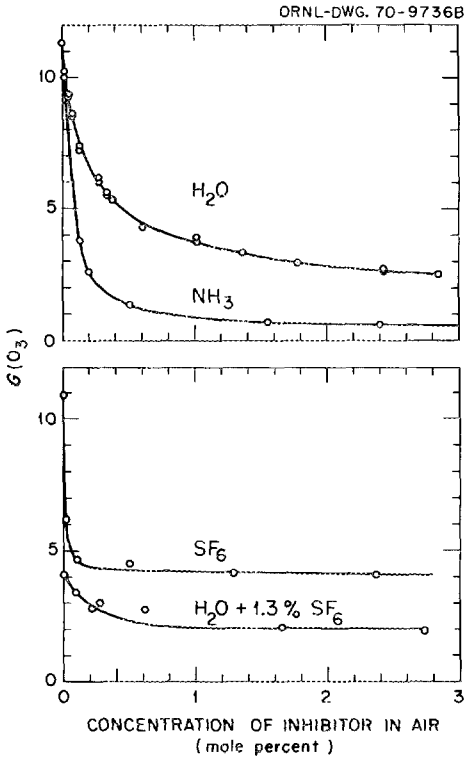

Fig. 4.5. Dependence of $G(O_3)$ on inhibitor concentration in air.

Effects of O_3, H_2O, and NH_3 on the Ozone Yield

The effects of these inhibitors on the O_3 yield are shown in Figs. 4.1–4.5. It was suggested[3] that in the steady radiolysis of O_2, the product O_3 lowers the O_3 yield by scavenging negative charge and preventing dissociative neutralization of O_2^+. We confirmed this by adding O_3 to the O_2 before pulsing (Fig. 4.4).

Water has a large effect on the O_3 yield, as shown by the figures. The addition of water to O_2 containing SF_6 produces a small additional decrease in yield (Fig. 4.4), and in air containing SF_6 it produces a greater decrease (Fig. 4.5). It is clear that H_2O eliminates O_3 formation from ionic precursors. The mechanism is likely to involve the clustering of O_2^+ by H_2O followed by the ion-molecule reaction $O_2^+ \cdot H_2O + H_2O \rightarrow H_3O^+ + OH + O_2$, as suggested by Fehsenfeld et al.[5] The neutralization reaction is probably $H_3O^+ + O_2^- \rightarrow H_2O + HO_2$. Both OH and HO_2 absorptions were observed in these systems. The additional small decrease in yield of O_3 on adding H_2O to O_2 or air containing SF_6 may indicate reaction of H_2O with O_2* or N_2*. Reaction of H_2O with N_2* may be the origin of NH observed in this system. Loss of O_3 by reaction with OH and HO_2 is also possible.

Ammonia has a very large effect on the O_3 yield. With its low ionization potential it is expected to be a positive-charge scavenger and eliminate O_3 formation from ionic precursors via the reactions $NH_3 + O_2^+ \rightarrow NH_3^+ + O_2$, $NH_3^+ + NH_3 \rightarrow NH_4^+ + NH_2$, and $NH_4^+ + O_2^- \rightarrow NH_3 + HO_2$. In oxygen, added NH_3 lowers the O_3 yield to ~3. In O_2-N_2 and O_2-Ar mixtures the O_3 yield with NH_3 present is proportional to the O_2 concentration. This indicates that NH_3 reacts with N_2* and Ar* and eliminates O_3 formation from energy initially absorbed by either N_2 or Ar. The low yield in O_2 with NH_3 present indicates a reaction stoichiometrically equivalent to $NH_3 + O_2^* \rightarrow NH_2OH + O$. However, O_2 excited in the Schumann-Runge system is thought to dissociate very rapidly either directly or via predissociation. The NH_3 presumably does not compete for O atoms, since the reaction is slow. Also, the results show that the O_3 yield reaches a limiting value (not zero) at high NH_3 concentrations.

From kinetic analysis of oscilloscope traces as shown in Fig. 4.1, we evaluated relative efficiencies as third body, M, for formation of ground-state O_3 in reaction (1) to be $O_2:N_2:H_2O:SF_6:NH_3$ = 1:2:36:44:50. From standard competition plots of results shown in Figs. 4.4 and 4.5, the ratio of rate constants for reactions of SF_6 and O_2 with electrons was 3000.

---

1. Department of Chemistry, Maryville College, Maryville, Tenn.

2. J. A. Ghormley, C. J. Hochanadel, and J. W. Boyle, *J. Chem. Phys.* **50**, 419 (1969).
3. C. Willis et al., *Can. J. Chem.* **48**, 1505, 1515 (1970).
4. R. L. Platzman, *Int. J. Appl. Radiat. Isotop.* **10**, 116 (1961).
5. F. C. Fehsenfeld and E. E. Ferguson, *J. Geophys. Res.* **74**, 2217 (1969).

ABSORPTION SPECTRUM AND REACTION KINETICS OF THE HO_2 RADICAL IN THE GAS PHASE

C. J. Hochanadel J. A. Ghormley P. J. Ogren[1]

The perhydroxyl radical, HO_2, is an important intermediate in many reaction systems in radiation chemistry, photochemistry, atmospheric chemistry, and in combustion and other thermal reactions. However, it had not been detected spectroscopically in the gas phase despite many attempts. Porter[2] suggested that the reason for this is probably very low sensitivity resulting from a diffuse and uncharacteristic spectrum caused by predissociation. Its spectrum in aqueous solution has been measured by pulse radiolysis[3] and flash photolysis and is a broad band centered at ~2300 Å.

In studies of various gaseous systems by pulse radiolysis and flash photolysis, we observed weak absorption in the far ultraviolet which could be attributed to the HO_2 radical. The best conditions[4] for measuring the spectrum were by flash photolysis of water vapor (~3%) in argon, helium, or hydrogen containing ~2% oxygen. Water is dissociated in the first continuum to H and OH, and O_2 converts the H atoms to HO_2. Hydrogen converts the OH to H ($H_2 + OH \rightarrow H_2O + H$), thereby doubling the amount of HO_2 produced. The absorption spectrum of HO_2 in the gas phase is shown in Fig. 4.6 and is characterized by a broad band centered at ~2050 Å. It is similar to the spectrum in aqueous solution but is shifted ~250 Å toward shorter wavelengths.

Evaluation of the extinction coefficients ϵ is based on analysis of the H_2O_2 produced in the H_2-H_2O-O_2 system, assuming that all radicals are converted to HO_2, which then combine to form H_2O_2 and O_2.[5] From second-order plots of HO_2 decay in the H_2-H_2O-O_2 system, we obtain a rate constant for $2HO_2 \rightarrow H_2O_2 + O_2$ of $(5.7 \pm 0.5) \times 10^9\ M^{-1}\ sec^{-1}$ at 298°K compared with reported values of 6.5×10^{10} (ref. 6) and 1.8×10^9 (ref. 7).

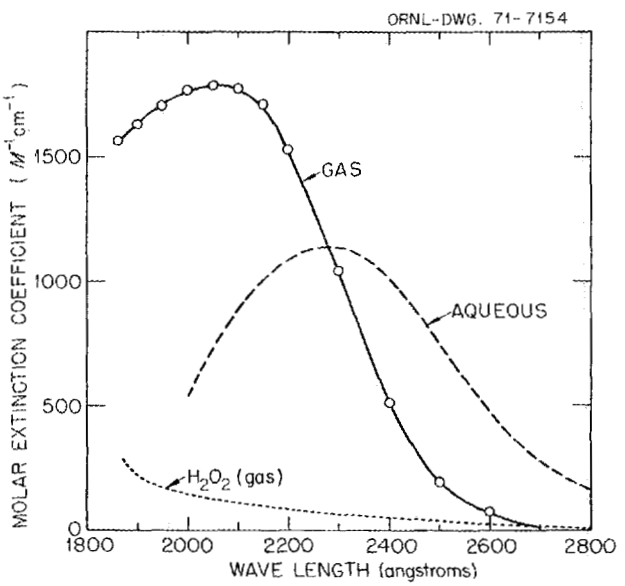

Fig. 4.6. Absorption spectrum of the HO_2 radical in the gas phase (solid curve). The spectrum of HO_2 in aqueous solution (dashed curve) is an average of five sets of data by various workers summarized by Bielski and Gebicki (ref. 3). The spectrum of H_2O_2, produced by the combination of HO_2 radicals, is also shown (taken from J. G. Calvert and J. N. Pitts, Jr., *Photochemistry*, p. 201, Wiley, New York, 1966; original references are given therein).

Absorption attributed to HO_2 was produced only with both H_2O and O_2 in the system. With only H_2O present in Ar or He, the only absorber observed was OH, and with only O_2 present, the only absorber was O_3. In the Ar-H_2O-O_2 or He-H_2O-O_2 systems the rate of HO_2 formation increased with increased O_2 concentration, and the formation time was consistent with published rate constants for $H + O_2 + M \rightarrow HO_2 + M$ (e.g., $\tau \simeq 7\ \mu sec$ for 0.5% O_2). The yield increased with increasing O_2 concentration until it reached a constant value above ~2% O_2, indicating scavenging of an intermediate, probably H, by O_2. The decay rate was independent of O_2 concentration.

Absorption by OH in the $(0, 0; A\ ^2\Sigma^+ \leftarrow X\ ^2\Pi)$ band at 3064 Å was also observed in these systems. It was produced during the flash. In the H_2-H_2O-O_2 system it decayed by pseudo-first-order reaction, giving a second-order rate constant for $H_2 + OH \rightarrow H_2O + H$ of $4 \times 10^6\ M^{-1}\ sec^{-1}$ at 298°K, in agreement with values reported by Kaufman[8] and by Greiner.[9]

---

1. Department of Chemistry, Maryville College, Maryville, Tenn.
2. G. Porter in *Photochemistry and Reaction Kinetics*, ed. by P. G. Ashmore, F. S. Dainton, and T. M. Sugden, p. 100, Cambridge Press, Cambridge, 1967.
3. Review by B. H. J. Bielski and J. M. Gebicki in *Advan. Radiat. Chem.* **2**, 191 (1970).
4. Absorption by HO_2 was also observed in the flash photolysis of NH_3 (1%) + O_2 (3%) in Ar and in the pulse radiolysis of $NH_3 + O_2$ (6%), in N_2 or Ar containing H_2O (3%) and O_2 (2%), and in $H_2 + O_2$ (1%).
5. The spectrum published here was revised in proof (July 11, 1971) after the normal report period. The original estimate of ϵ_{max} at 2050 Å was 1180 M^{-1} cm^{-1} based on O_3 formation in O_2 as actinometer. This value was uncertain because of inaccurate measurement of the relative absorption of the photolytic light by O_2 and H_2O.
6. R. H. Burgess and J. C. Robb, *Reactions of Free Radicals in the Gas Phase, Chem. Soc. London, Spec. Pub.* **9**, 167 (1957).
7. S. N. Foner and R. L. Hudson, *Advan. Chem. Ser.* **36**, 34 (1962).
8. F. Kaufman, *Can. J. Chem.* **47**, 1917 (1969).
9. N. R. Greiner, *J. Chem. Phys.* **46**, 2795 (1967).

RADIATION CHEMISTRY OF GASEOUS METHANE[1]

P. R. Reed[2] F. Schmidt-Bleek[3]

Methane in the gas phase at 700 torr and at ambient temperature was irradiated with ^{60}Co gamma rays. Hydrogen, ethane, propane, *n*-butane, *i*-butane, and *n*-pentane were the products observed by gas chromatography. Product yields from methane were investi-

gated in mixtures of methane containing acetylene, ethylene, propylene, nitric oxide, and oxygen as a function of the concentration of the additive, normally from 0.02 to 10 mole %. In those experiments using acetylene and ethylene as additives, acetylene-^{14}C and ethylene-^{14}C were added to several samples in order to distinguish products formed from methane.

The experimental hydrogen yield in pure methane was 5.48 ± 0.09 molecules per 100 eV. All hydrogen yields from methane decreased rapidly at low additive concentrations and then more slowly with increasing additive concentration. Extrapolation of the hydrogen yields at the higher additive concentrations to zero additive concentration gave a mean nonscavengeable hydrogen yield of G_{H_2} = 2.76 ± 0.04. An initial hydrogen yield, $G(H_2)^0$ = 6.54 ± 0.15, and a hydrogen atom yield, G_H = 3.78 ± 0.14, from methane were determined from a kinetic analysis of the hydrogen yields in the methane + additive mixtures. A mechanism consisting of the primary ionization processes, excitation, ion-molecule, and radical reactions was capable of accounting for the initial hydrogen, hydrogen atom, and nonscavengeable hydrogen yields in pure methane. Ratios of the rate constants for the reactions of the hydrogen atom abstraction with methane to the rate constants for hydrogen atom addition to the additive were determined.

In pure methane, $G(C_2H_6)$ was 2.16 ± 0.03. Ethane yields decreased as the concentrations of acetylene, ethylene, propylene, and nitric oxide were increased. No ethane was observed when oxygen was present in concentrations greater than 0.89 mole %.

No unsaturated products were detected in the radiolysis of pure methane. Irradiation of methane with added O_2 (0.021%), NO (0.054%), C_3H_6 (0.039%), and C_2H_2 (0.042%) gave $G(C_2H_4)$ of 0.84, 0.93, 0.83, and 1.28 respectively. Yields of ethylene decreased as the concentrations of nitric oxide and oxygen were increased, but the ethylene yields increased to a limiting value as the propylene concentration was increased. In methane + acetylene-^{14}C mixtures, ^{14}C-labeled ethylene was observed. The ethylene yield from methane in mixtures which contained 0.09, 2.1, and 9.0% acetylene accounted respectively for 34, 46, and 62% of the total ethylene yield observed. Yields of acetylene, propylene, and butene-1 in the radiolysis of pure methane were estimated by extrapolating their respective yields obtained in the methane + additive mixtures to zero additive concentration. Values of $G(C_2H_2)$ = 0.031 ± 0.003 and 0.041 ± 0.005 and $G(1\text{-}C_4H_8)$ = 0.017 ± 0.003 and 0.027 ± 0.003 were determined with ethylene and propylene as additives respectively; $G(C_3H_6)$ = 0.05 ± 0.01 and 0.021 ± 0.003 were determined with added acetylene and ethylene.

Other significant products observed during the radiolysis of methane + additives included benzene plus a yellow solid with added acetylene; propane, butane, and cyclopropane with added ethylene; methylcyclopropane with added propylene; nitrogen and nitrous oxide with added nitric oxide; and carbon dioxide with added oxygen.

---

1. Abstract of Ph.D. thesis submitted to Purdue University, Lafayette, Ind., August 1971.
2. AUA-ANL Predoctoral Fellow from Purdue University, Lafayette, Ind.
3. Chemistry Department, University of Tennessee, Knoxville.

PHOTOOXIDATION AND FLUORESCENCE OF CERIUM(III) IN AQUEOUS SULFURIC ACID SOLUTIONS

R. W. Matthews[1] T. J. Sworski

The H_2^+ radical ion,[2] H atom,[3,4] and hydrated electron[5] have been suggested as possible intermediates in the photooxidation of cerium(III) in acidic aqueous solutions. To determine the nature of the intermediate in the photooxidation of cerium(III), we conducted a kinetic study of the photooxidation and fluorescence of cerium(III) in 0.4 *M* sulfuric acid solutions containing peroxydisulfuric acid. We previously determined[6] the relative reactivities of oxygen, peroxymonosulfuric acid, and peroxydisulfuric acid with H atom by a kinetic study of the oxidation of cerium(III) by peroxysulfuric acids induced by ^{60}Co gamma radiation.

Our results are quantitatively explicable by the following reaction mechanism:

$$Ce^{III} + h\nu \rightarrow (Ce^{III})^* , \quad (1)$$

$$(Ce^{III})^* \rightarrow Ce^{III} + h\nu' , \quad (2)$$

$$(Ce^{III})^* + S_2O_8^{2-} \rightarrow Ce^{IV} + SO_4^{2-} + SO_4^- , \quad (3)$$

$$Ce^{III} + SO_4^- \rightarrow Ce^{IV} + SO_4^{2-} . \quad (4)$$

The fluorescence F for any peroxydisulfuric acid concentration is related to the fluorescence F_0 in the absence of peroxydisulfuric acid by Eq. (I):

$$F = \frac{F_0}{1 + k_3 [S_2O_8^{2-}]/k_2} . \quad (I)$$

The fluorescence at 350 nm induced by excitation at 300 nm adhered well to Eq. (I) with $k_3/k_2 = 99.0 \pm 1.5$ for 0.03 *M* cerium(III) solutions and $k_3/k_2 = 94.6 \pm 1.3$ for 0.003 *M* cerium(III) solutions.

The quantum yield of cerium(IV), $\phi(Ce^{IV})$, is related to the quantum yield of excited cerium(III), $\phi(Ce^{III})^*$, by Eq. (II):

$$\phi(Ce^{IV}) = \frac{2\phi(Ce^{III})^*}{1 + k_2/(k_3[S_2O_8^{2-}])} . \qquad \text{(II)}$$

The quantum yields of cerium(IV) for 0.03 *M* cerium(III) solutions with excitation at 300 nm adhered well to Eq. (II) with $k_3/k_2 = 98 \pm 7$ for both oxygen-free solutions and air-saturated solutions. $\phi(Ce^{III})^* = 1.0 \pm 0.2$ was determined by ferrioxalate actinometry[7] using a quantum yield of 1.24 for ferrous ion at 300 nm.

Our results show no evidence for any significant yield of either H_2^+, H atom, or hydrated electron as an intermediate in the photolysis of cerium(III) solutions at 300 nm. Our results are not inconsistent, however, with the previous alternative suggestions[2,3] that solute may react with electronically excited cerium(III) that has formed a complex with hydrogen ion.

1. Visiting scientist from the Australian Atomic Energy Commission Research Establishment, Lucas Heights, New South Wales.

2. L. J. Heidt and A. F. McMillan, *J. Amer. Chem. Soc.* **76**, 2135 (1954).
3. F. H. C. Edgecombe and R. G. W. Norrish, *Nature (London)* **197**, 282 (1963).
4. F. Hussain and R. G. W. Norrish, *Proc. Roy. Soc. Ser. A* **275**, 161 (1963).
5. A. W. Adamson et al., *Chem. Rev.* **68**, 541 (1968).
6. R. W. Matthews, H. A. Mahlman, and T. J. Sworski, *J. Phys. Chem.* **74**, 2475 (1970).
7. C. G. Hatchard and C. A. Parker, *Proc. Roy. Soc. Ser. A* **235**, 518 (1956).

REDUCTION OF CERIUM(IV) BY HYDROGEN PEROXIDE: DEPENDENCE OF REACTION RATE ON HAMMETT'S ACIDITY FUNCTION[1]

H. A. Mahlman R. W. Matthews[2] T. J. Sworski

Reduction of cerium(IV) by hydrogen peroxide in aqueous solutions was postulated[3,4] to proceed through two consecutive one-electron transfer reactions:

$$Ce^{IV} + H_2O_2 \rightarrow Ce^{III} + H^+ + HO_2 , \qquad (1)$$

$$Ce^{IV} + HO_2 \rightarrow Ce^{III} + H^+ + O_2 . \qquad (2)$$

Isotopic exchange between cerium(IV) and radioactive cerium(III), induced by reaction of cerium(IV) with hydrogen peroxide, was interpreted[5] as evidence for the reverse of reaction (1):

$$Ce^{III} + H^+ + HO_2 \rightarrow Ce^{IV} + H_2O_2 .$$

This was confirmed[6] in a kinetic study using dynamic-flow methods; at high cerium(III) concentrations, when $k_{-1}[H^+][Ce^{III}]$ is much greater than $k_2[Ce^{IV}]$, the rate of reaction adhered well to Eq. (I),

$$-d[Ce^{IV}]/dt = 2k_{obs}[Ce^{IV}]^2[H_2O_2]/[Ce^{III}] , \qquad \text{(I)}$$

in which $k_{obs} = k_1k_2/(k_{-1}[H^+])$.

We report a kinetic study of the reduction of cerium(IV) by hydrogen peroxide both in sulfuric acid solutions from 2.0 to 13.0 *M* and in ammonium bisulfate solutions from 1.0 to 5.0 *M*. The rate of reaction in all experiments adhered well to Eq. (I). Figure 4.7 shows a marked dependence of k_{obs} on both sulfuric acid and ammonium bisulfate concentrations.

Protonation of HO_2

The dependence of k_{obs} on sulfuric acid concentration from 0.4 to 8.0 *M* can be quantitatively explained

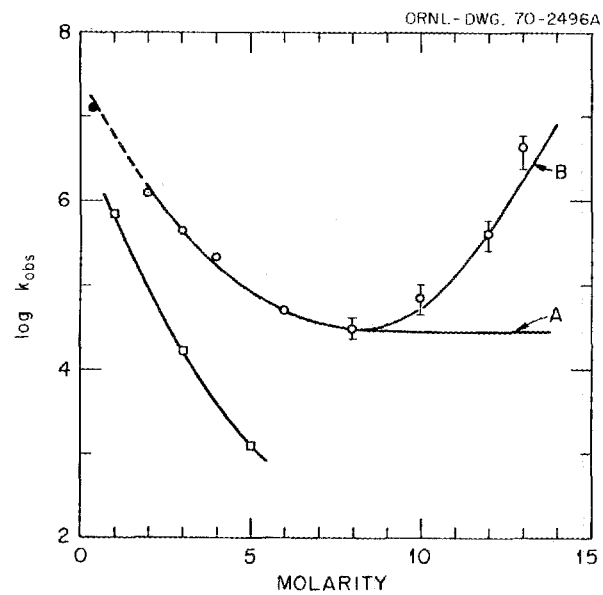

Fig. 4.7. Dependence of k_{obs} on ammonium bisulfate and sulfuric acid concentrations. □, ammonium bisulfate solutions; ○, sulfuric acid solutions, data of this paper; ●, sulfuric acid solutions, data of ref. 5; *A*, computed curve using Eq. II; *B*, computed curve using Eq. III.

by assuming virtual equilibrium between HO_2 and $H_2O_2^+$, with $K_{H_2O_2^+} = h_0[HO_2]/[H_2O_2^+]$. The function h_0 is related to Hammett's acidity function H_0 by the relationship $H_0 = -\log h_0$.[7] The data are consistent with the following reaction mechanism:

$$Ce^{IV} + H_2O_2 \rightleftharpoons Ce^{III} + H_2O_2^+ , \quad (3)$$

$$H_2O_2^+ \rightleftharpoons H^+ + HO_2 , \quad (4)$$

$$Ce^{IV} + HO_2 \rightarrow Ce^{III} + HO_2^+ , \quad (5)$$

$$HO_2^+ \rightarrow H^+ + O_2 , \quad (6)$$

$$Ce^{IV} + H_2O_2^+ \rightarrow Ce^{III} + H_2O_2^{2+} , \quad (7)$$

$$H_2O_2^{2+} \rightarrow H^+ + HO_2^+ . \quad (8)$$

$K_{HO_2^+}$ and $K_{H_2O_2^{2+}}$ are assumed to be large and reactions (5) and (7) are therefore sensibly irreversible. The rate of cerium(IV) reduction is then given by Eq. (I) with

$$k_{obs} = \frac{k_3k_7}{k_{-3}}\left(1 + \frac{k_5K_{H_2O_2^+}}{k_7h_0}\right) . \quad (II)$$

The data adhere well to Eq. (II), as indicated by computed curve A in Fig. 4.7, with $k_7k_3/k_{-3} = (2.8 \pm 0.2) \times 10^4\ M^{-1}\ sec^{-1}$ and $k_5K_{H_2O_2^+}/k_7 = (4.4 \pm 0.3) \times 10^2\ M$.

Protonation of H_2O_2

The increase in k_{obs} with further increase in sulfuric acid concentration from 8.0 to 13.0 M can be quantitatively explained by assuming virtual equilibrium between H_2O_2 and $H_3O_2^+$, with $K_{H_3O_2^+} = h_0[H_2O_2]/[H_3O_2^+]$. The data are consistent with inclusion of reactions (9)–(11) into our proposed reaction mechanism:

$$H_3O_2^+ \rightleftharpoons H^+ + H_2O_2 , \quad (9)$$

$$Ce^{IV} + H_3O_2^+ \rightarrow Ce^{III} + H_3O_2^{2+} , \quad (10)$$

$$H_3O_2^{2+} \rightarrow H^+ + H_2O_2^+ . \quad (11)$$

$K_{H_3O_2^{2+}}$ is assumed to be so large that reaction (10) is sensibly irreversible. The rate of cerium(IV) reduction is then given by Eq. (I) with

$$k_{obs} = \frac{k_3k_7}{k_{-3}}\left(1 + \frac{k_5K_{H_2O_2^+}}{k_7h_0}\right)\left(1 + \frac{k_{10}h_0}{k_3K_{H_3O_2^+}}\right) . \quad (III)$$

The data adhere well to Eq. (III), as indicated by computed curve B in Fig. 4.7, with $k_3k_7/k_{-3} = (2.6 \pm 0.3) \times 10^4\ M^{-1}\ sec^{-1}$, $k_5K_{H_2O_2^+}/k_7 = (4.8 \pm 0.6) \times 10^2\ M$, and $k_3K_{H_3O_2^+}/k_{10} = (1.1 \pm 0.2) \times 10^5\ M$.

This kinetic study provides the basis for determining the importance of hydrogen peroxide as an intermediate in the radiolysis of sulfuric acid solutions containing cerium(IV) since it would cause significant postirradiation reduction of cerium(IV) at sufficiently high radiation intensities.

1. Expanded abstract of published paper: *J. Phys. Chem.* **75**, 250 (1971).
2. Visiting scientist from the Australian Atomic Energy Commission Research Establishment, Lucas Heights, New South Wales.
3. S. Baer and G. Stein, *J. Chem. Soc. London* **1953**, 3176.
4. J. H. Baxendale, *Special Publication No. 1*, p. 40, The Chemical Society, London, 1954.
5. P. B. Sigler and B. J. Masters, *J. Amer. Chem. Soc.* **79**, 6353 (1957).
6. G. Czapski, B. Bielski, and N. Sutin, *J. Phys. Chem.* **67**, 201 (1963).
7. L. P. Hammett, *Physical Organic Chemistry*, chap. 9, McGraw-Hill, New York, 1940.

REDUCTION OF CERIUM(IV) BY NITROUS ACID IN AQUEOUS NITRIC ACID SOLUTIONS

R. W. Matthews[1] T. J. Sworski

The reduction of cerium(IV) by nitrous acid in aqueous sulfuric acid solutions was postulated[2] to occur by the following reaction mechanism:

$$Ce^{IV} + HNO_2 \rightarrow Ce^{III} + H^+ + NO_2 , \quad (1)$$

$$2NO_2 + H_2O \rightarrow NO_3^- + H^+ + HNO_2 . \quad (2)$$

The rate of reaction adhered well to Eq. (I):

$$-d[Ce^{IV}]/dt = k_1[Ce^{IV}][HNO_2] . \quad (I)$$

In sulfuric acid solutions from 0.2 to 2.0 M, k_1 was found to be inversely proportional to the sulfuric acid concentration.

The rate of reaction in nitric acid solutions also adheres well to Eq. (I). Table 4.1 shows that k_1 decreases markedly also with increase in nitric acid concentration from 6.0 to 12.0 M. The constancy of log $k_1 - 2H_0$ at high nitric acid concentrations suggests strongly the importance of protonation equilibria either between NO_2^-, HNO_2, and $H_2NO_2^+$ or between NO_2^-, HNO_2, and NO_2. Our results are consistent with the assumptions that reduction of cerium(IV) occurs only

Table 4.1. A correlation between the rate of cerium(IV) reduction by nitrous acid and the Hammett acidity function

$[HNO_3]$ (M)	$-H_0$[a]	$\log k_1$	$\log k_1 - 2H_0$
6.0	1.94	3.54 ± 0.08	7.42
7.0	2.18	3.22 ± 0.02	7.58
8.0	2.40	2.87 ± 0.03	7.67
10.0	2.80	2.07 ± 0.01	7.67
12.0	3.21	1.24 ± 0.02	7.66

[a]Interpolated from the data of J. G. Dawber and P. A. H. Wyatt, *J. Chem. Soc. London* **1960**, 3589.

through reaction with NO_2^- and that nitrous acid exists predominantly in the form of NO_2 or $H_2NO_2^+$ at high nitric acid concentrations.

This kinetic study provides the basis for determining the importance of nitrous acid as an intermediate in the radiolysis of nitric acid solutions containing cerium(IV) since it would cause postirradiation reduction of cerium(IV) at sufficiently high radiation intensities.

1. Visiting scientist from the Australian Atomic Energy Commission Research Establishment, Lucas Heights, New South Wales.

2. T. J. Sworski, R. W. Matthews, and H. A. Mahlman, *Advan. Chem. Ser.* **81**, 164 (1968).

ENERGY TRANSFER AND THE RADIOLYSIS OF ALIPHATIC CARBOXYLIC ACIDS

A. R. Jones

The gamma radiolyses of normal aliphatic carboxylic acids at 77°K lead to the production of carbon dioxide at constant rates from each individual acid. The radiolytic yields of carbon dioxide are shown as a function of the number of carbon atoms in the acids in Fig. 4.8. An informative comparison may be made by plotting simultaneously the data of Fig. 4.8 and data from irradiations of the same acids in the liquid state,[1] as is shown in Fig. 4.9. The results at 77°K are then readily seen to separate the acids into three groups: (1) C_1, C_{15}, and C_{22} acids; (2) the odd-numbered acids above and including C_{11}; and (3) the remainder of the homologs.

The singular yield of carbon dioxide from formic acid will not be discussed at this time, merely recalling the uniqueness of formic acid as the first member of the series. For example, all of the other homologs exist as dimers in the solid state; formic acid is polymeric.[2] The experimentally reproducible carbon dioxide yields from the C_{15} and C_{22} acids may be indicative of some peculiarity of structure which demands a separate discussion, but at this time they will be ascribed to impurities and will not be considered further.

Figure 4.9 shows the startling fact that for the odd-numbered acids (except C_{15}) above and including C_{11}, the carbon dioxide yields obtained by irradiating these substances in the solid state at 77°K are the same as the yields obtained by irradiating them as liquids at temperatures several hundred degrees higher, 330 and 365°K. With the exception of the isolated data points for C_1, C_{15}, and C_{22} at 77°K, the carbon dioxide yields for the remaining homologs — with special emphasis on the even-numbered acids above C_8 — are lower and decrease with increasing chain length at a slower rate than the carbon dioxide yields from the same acids irradiated as liquids.

The observed decrease of $G(CO_2)$ with increase in chain length can be interpreted by assuming that the interactions of a secondary electron with different parts of a normal carboxylic acid molecule are not equally effective in producing a particular unstable excited state. Even without a quantitative theory, one can interpret the observed change in yield with change in chain length within the framework of this assumption. Interaction with electrons of atoms farther removed from the carboxyl group is presumably less effective in exciting the molecule to the unstable state. For this reason the value of $G(CO_2)$ steadily decreases with increase in chain length. A simple description of the effectiveness of the interaction is obtained by dividing the molecule into two regions. Interaction in one region alone is assumed to be effective in exciting to the unstable state. This region would include the carboxyl group and perhaps a few nearby atoms. Since the energy absorbed by a molecule is proportional to the total number of electrons in the molecule, E, the yield of carbon dioxide should be inversely proportional to E for the longer homologs.

With this simple description one might expect for a plot of $G(CO_2)$ vs electron fraction of COOH in RCOOH that all of the data points except possibly those for a few of the smallest homologs might fall on a straight line passing through the origin. This was the case for the liquid acids when the points for formic and acetic acids were excluded.[1] The odd-numbered acids in the 77°K irradiations whose CO_2 yields fall on the liquid curve (Fig. 4.9) of course also display this same behavior. The CO_2 yields from the remaining solid acids (excluding C_1, C_{15}, and C_{22}) also produce a straight-line correlation, as is shown in Fig. 4.10.

1. A. R. Jones, *Chem. Div. Annu. Progr. Rep. May 20, 1970*, ORNL-4581, p. 76.

2. F. Holtzberg, B. Post, and I. Fankuchen, *J. Chem. Phys.* **20**, 198 (1952).

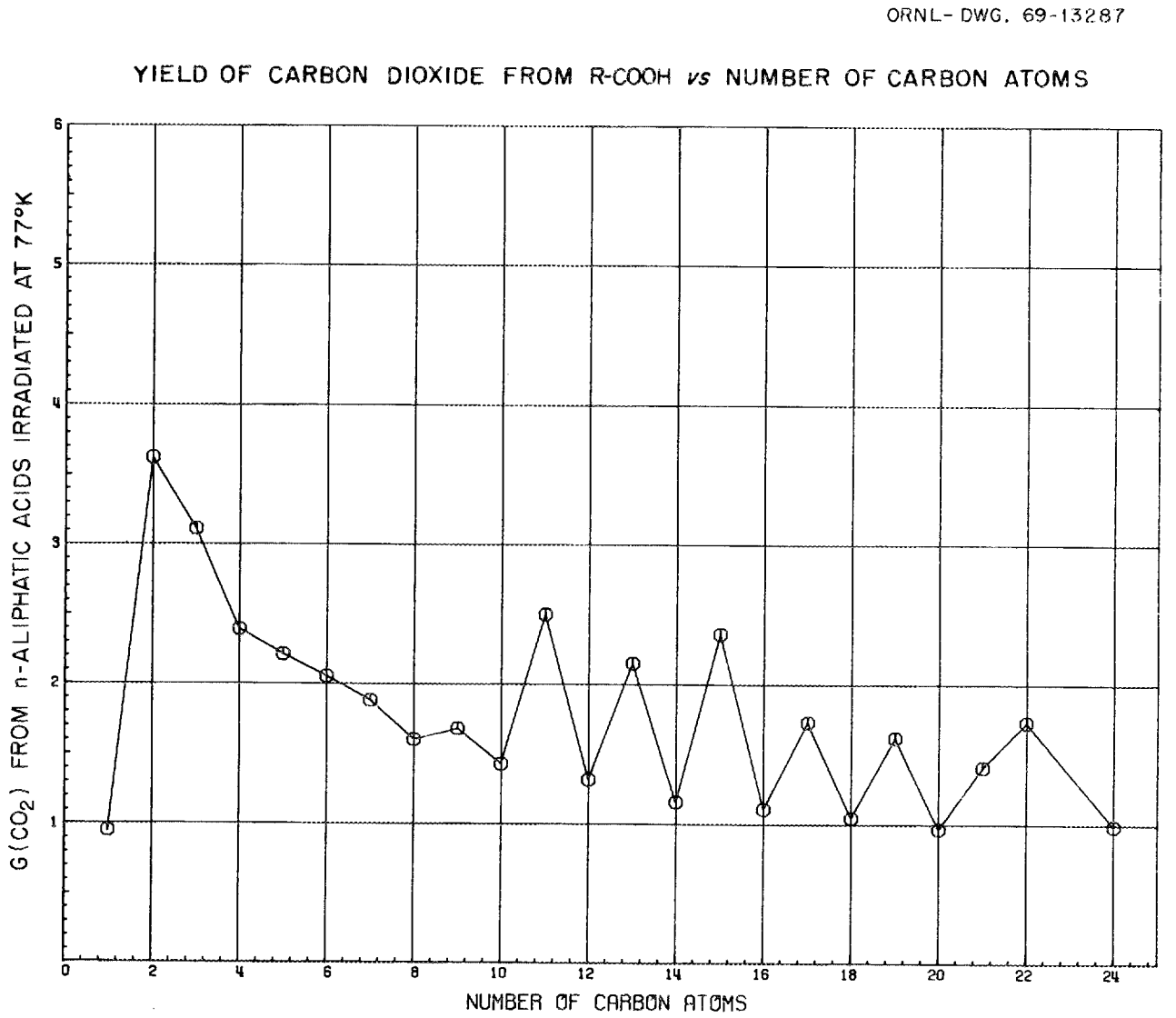

Fig. 4.8. $G(CO_2)$ from *n*-aliphatic acids irradiated at 77° K vs chain length.

ORNL-DWG. 69-13288

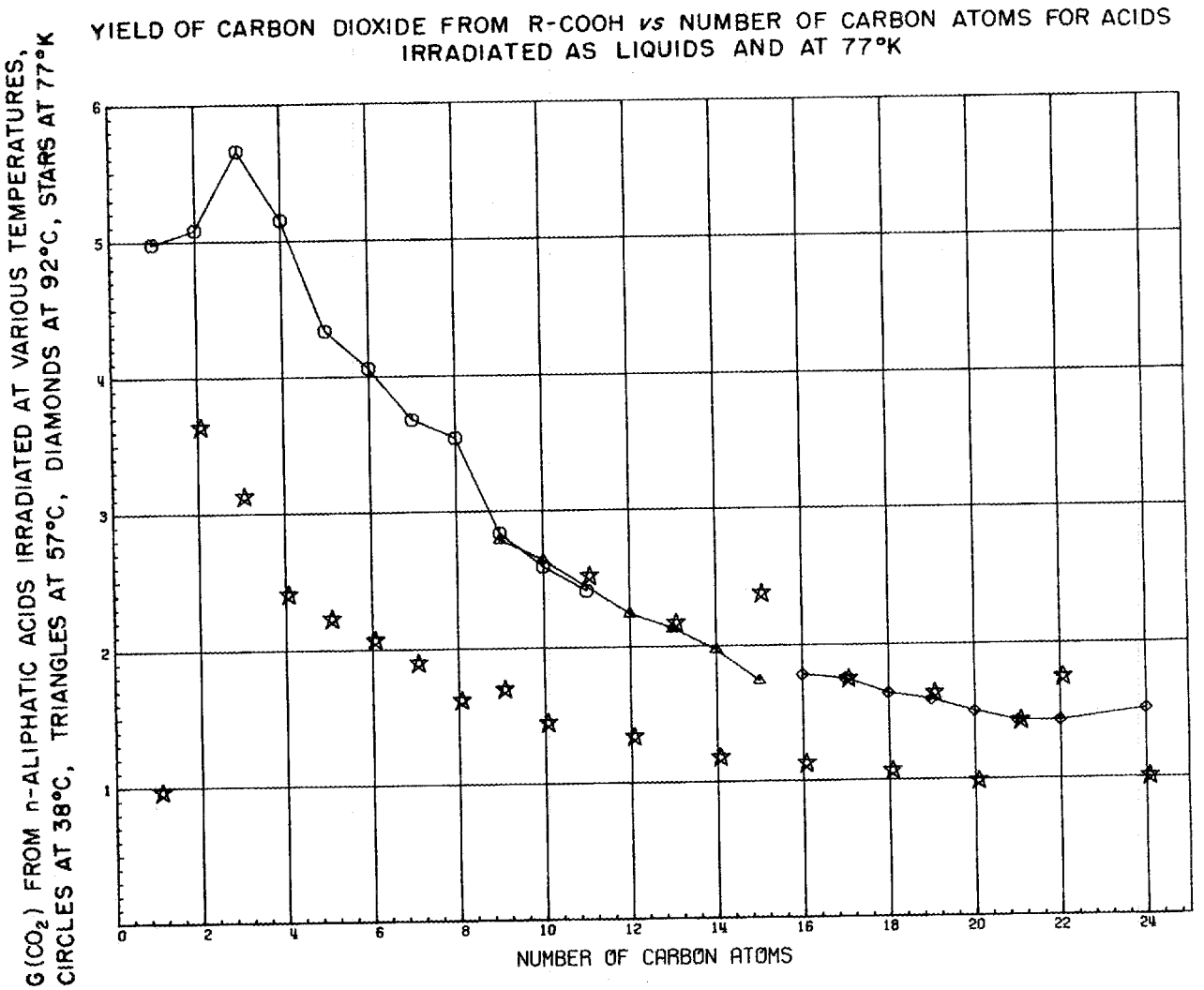

Fig. 4.9. Yields of carbon dioxide from *n*-aliphatic acids irradiated as liquids and as solids vs chain length. Solids irradiated at 77°K; liquids irradiated at various temperatures: ○, 38°C, △, 57°C, ◇, 92°C.

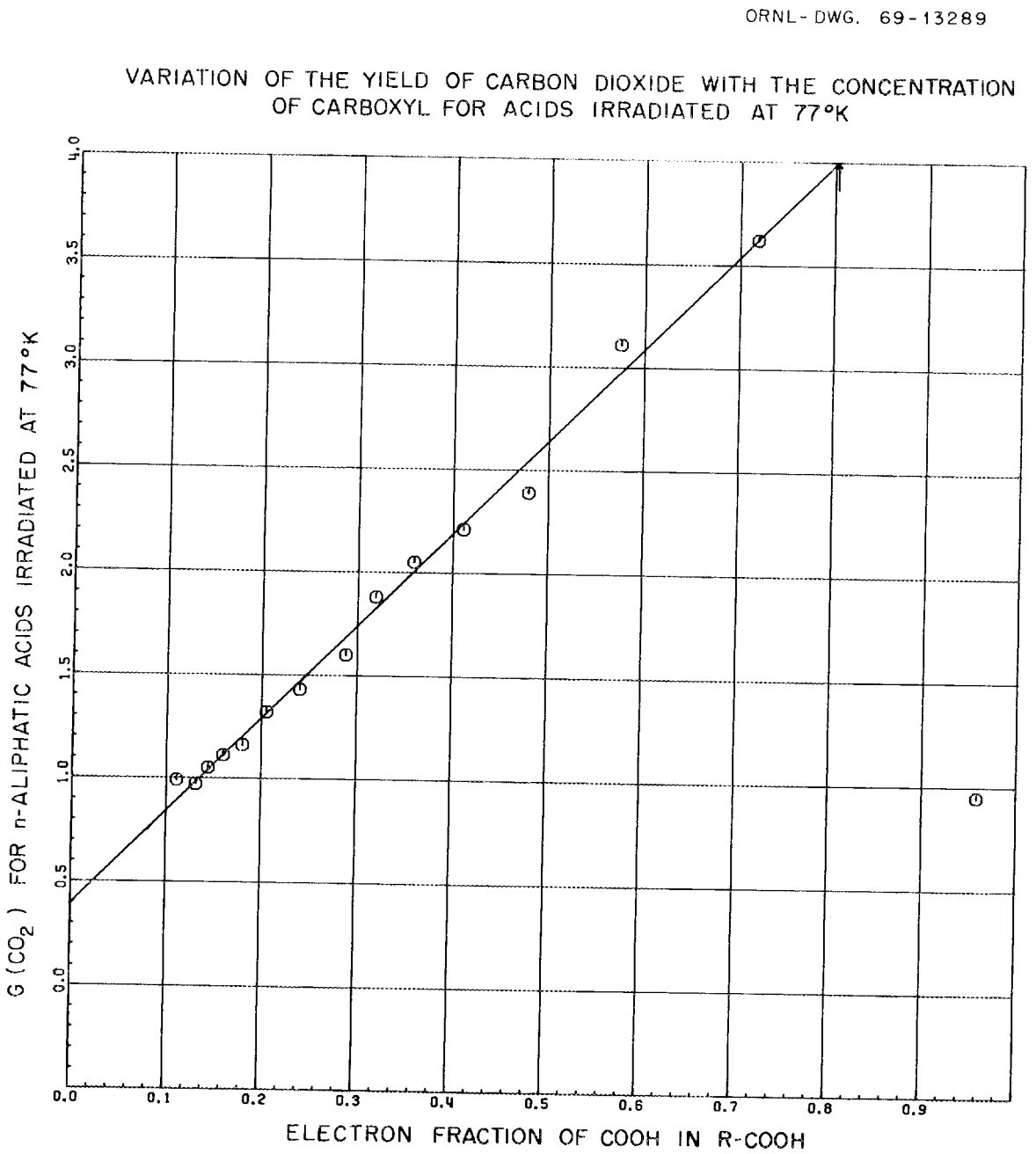

Fig. 4.10. Correlation of the yield of carbon dioxide from the gamma radiolysis of *n*-aliphatic acids irradiated at 77°K with the carboxylic electron fraction in the acid. Included in the least-squares curve are acids C_2 through C_9 and the even-numbered acids C_{10} through C_{24}. Datum point for formic acid is shown.

RADIATION AND HOT-ATOM CHEMISTRY OF INORGANIC CRYSTALLINE SOLIDS

A RAMAN SPECTRAL STUDY OF THE ^{60}Co GAMMA RADIOLYSIS OF ^{18}O-ENRICHED POLYCRYSTALLINE KNO_2

M. H. Brooker[1] G. E. Boyd[2]

The effects of an atmosphere of natural isotopic abundances of oxygen and nitrogen on the ^{60}Co gamma radiolysis of ^{18}O-enriched polycrystalline KNO_2 have been studied by Raman and infrared spectroscopy. It has been shown that atmospheric $^{16}O_2$ is incorporated into the reactant KNO_2 and into its radiolysis product KNO_3. Similar studies with ^{15}N-enriched KNO_2 have shown that atmospheric nitrogen does not exchange. Raman spectroscopy has proved to be an excellent nondestructive in situ method of detecting stable radiolytic decomposition products in solids.[3]

Oxygen-18-enriched KNO_2 (nominal 73% ^{18}O enriched) purchased from Isomet Corporation was used after treatment of its aqueous solution with Norit A decolorizing carbon and subsequent recrystallization (to remove fluorescent impurities). Raman spectra were recorded on a Jarrell-Ash model 25-300 Raman spectrometer after sample excitation with the 4880-Å line of the Coherent Radiation model 52B argon ion laser. Raman bands at 806, 787, and 767 cm^{-1} were assigned to the ν_2 bending modes of the isotopically different nitrite species $N^{16}O_2^-$, $N^{16}O^{18}O^-$, and $N^{18}O_2^-$ respectively. The Raman bands of 1056, 1036, 1016, and 996 cm^{-1} were assigned to the ν_1 symmetric stretching mode of the isotopically different nitrate species $N^{16}O_3^-$, $N^{16}O_2{}^{18}O^-$, $N^{16}O^{18}O_2^-$, and $N^{18}O_3^-$ present initially as an impurity in the KNO_2.[3] Quantitative measurements of the areas under the bands for each species indicate that the original ^{18}O enrichment of the nitrite species was 81%; however, the ^{18}O enrichment of the nitrate impurity was only 44%. Raman analysis[4] for nitrate indicated that the total nitrate impurity was 2.2 wt %. Duplicate samples of the ^{18}O-enriched KNO_2 were irradiated simultaneously in the center position of a ^{60}Co gamma-ray source. One of the samples was degassed at 200°C and sealed under vacuum in thin-walled Pyrex capillary tubes, while the other sample was left open to the atmosphere. Raman spectra were recorded for the samples in the same capillaries in which they were irradiated.

The difference between the ^{18}O enrichment of the samples irradiated in vacuo and open to the atmosphere was striking (Fig. 4.11). Atmospheric $^{16}O_2$ was rapidly incorporated into nitrite ion, as evidenced by the increase in the band intensities at 806 and 787 cm^{-1} for the open atmosphere irradiated sample. For the sample irradiated in vacuo, the ^{18}O enrichment was virtually unaltered. These results explain the relative stability of the nitrite ion to ionizing radiation previously reported.[5] Nitrite ion is not unaffected by radiation, but rather, after the absorption of energy, the excited intermediate reverts to nitrite ion. Apparently this excited intermediate can exchange oxygen readily with the atmosphere.

An increase in the intensity of the nitrate ion bands was observed with both the in vacuo and open atmosphere irradiated samples, but the amount of nitrate produced was greater for the sample irradiated open to the atmosphere (Fig. 4.11). In addition, the

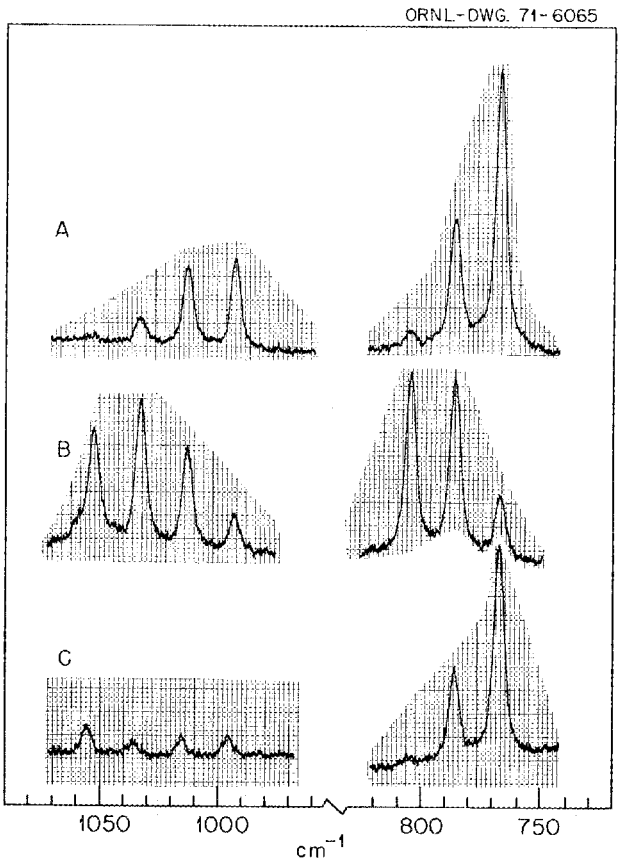

Fig. 4.11. Photograph of portions of Raman spectra of ^{18}O-enriched KNO_2. (*A*) Irradiated in vacuo, dose 1.8 × 10^{24} eV/mole; (*B*) irradiated open to atmosphere, dose 1.8 × 10^{24} eV/mole; and (*C*) unirradiated sample. Instrument conditions: slits 3.0 cm^{-1}; 5 × 10^3 counts/sec; 2-sec time constant; 4880-Å argon ion exciting line.

^{18}O enrichment of the nitrate ions in the two samples was very different. The sample irradiated in vacuo had an ^{18}O nitrate enrichment which was greater than the original starting material. This observation appears to confirm an earlier conclusion[3] that the ^{18}O-containing nitrate species are more stable toward decomposition by ^{60}Co gamma radiation than the corresponding ^{16}O species.

1. Visiting scientist, National Research Council of Canada Postdoctoral Fellow, 1969–71.
2. Director's Division.
3. M. H. Brooker and G. E. Boyd, *Chem. Div. Annu. Progr. Rep. May 20, 1970,* ORNL-4581, p. 82.
4. M. H. Brooker and D. E. Irish, *Can. J. Chem.* **46,** 229 (1968).
5. Y. A. Zakharov and V. A. Nevostruev, *Russ. Chem. Rev.* **37,** 61 (1968).

5. Organic Chemistry

PREPARATION OF VINYL ESTERS

Ben M. Benjamin Clair J. Collins

Reactions which proceed through vinyl carbonium[1] ion intermediates have recently been studied; however, the properties of the vinyl cations have not been carefully examined. Therefore we have decided to attempt to prepare selected compounds which can be induced to give stable vinyl cations when treated with super acid (such as SO_2-SbF_5-HF) at low temperatures. A nmr spectroscopic study[2] of the stable vinyl cations is expected to reveal whether the positive charge is delocalized. This information will then be compared with data obtained from the reactions of identical vinyl cations produced from the solvolysis of ^{14}C-labeled vinyl *p*-toluenesulfonates.

First we chose to synthesize triphenylvinyl acetate and triphenylvinyl tosylate by reaction of the corresponding enolate ion with the appropriate acid chloride. Conventional methods of preparation of triarylvinyl[3] esters result in partially rearranged products.

The reaction of benzhydryl phenyl ketone (1) with sodium amide, followed by treatment of the sodium enolate (2) with acetyl chloride, gave triphenylvinyl acetate (3), m.p. 105°. However, when the sodium enolate was treated with *p*-toluenesulfonyl chloride, the only products formed were 2,2-diphenyl-2-chloroacetophenone (4) and sodium *p*-toluenesulfinate. The latter reaction is thought to be general for ketones containing a tertiary hydrogen α to the carbonyl group, for example, benzhydryl *p*-tolyl ketone (5), *p*-methylbenzhydryl phenyl ketone (6), and 3-*endo*-phenylbicyclo-[2.2.1]heptanone-2 (7).

ORNL-DWG. 71-5402

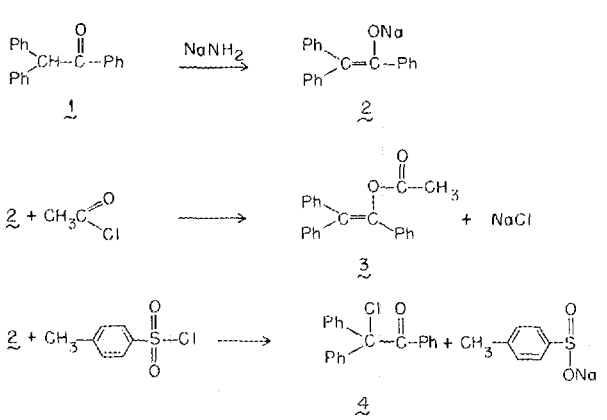

ORNL-DWG. 71-5403

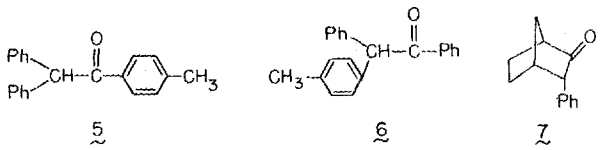

Ketones which have two hydrogens adjacent to the carbonyl react with sodium amide to give enolates, but treatment with acid chlorides gives mixtures of cleavage products and mono- and disubstituted products whose structures have not yet been confirmed. Some of these reactions will be studied further to determine their potential value in organic synthesis.

1. M. Hanack, *Accounts Chem. Res.* 3, 209 (1970).
2. The portion of this research involving the nmr investigation is being done in collaboration with Dr. John W. Larsen, University of Tennessee, Knoxville.
3. W. M. Jones and F. W. Miller, *J. Amer. Chem. Soc.* 89, 1960 (1967).

THE DEAMINATION OF 1-CYCLOPENTYLETHYLAMINE

C. J. Collins J. R. Wiersig[1] B. M. Benjamin

The deamination of alkylamines usually results in the formation of alcohols and olefins. In the case of cycloalkylamines some products are formed as a result of ring expansion. 1-Cyclopentylethylamine (1) is reported[2] to give mainly 1-cyclopentylethanol (2), 1-ethylcyclopentanol (3), *trans*-2-methylcyclohexanol (4), and a small amount of mixed olefins. We were interested to learn if compound 4 is formed partially through protonated cyclopropane intermediates[3] rather

than through conventional carbonium ion rearrangement. The two mechanisms should result in products with different ^{14}C position labels, starting with amine **1** labeled in the 1 position of the cyclopentyl ring.

1-(Cyclopentyl-1-^{14}C)-ethylamine, 0.1937 mCi/mole, was synthesized. It was deaminated using sodium nitrite in acetic acid saturated with sodium acetate. The mixture of products, as acetate esters, was treated with lithium aluminum hydride. The resulting alcohol mixture was treated with phthalic anhydride, and the phthalic acid ester of **4** was isolated by fractional crystallization. Hydrolysis of the ester gave the pure alcohol, which was then oxidized to the corresponding ketone, 2-methylcyclohexanone (**5**). Compound **5** was treated with phenylmagnesium bromide, and the product of this reaction was oxidized to benzoic acid. The radioactivity of the benzoic acid was 0.1906 mCi/mole. It is therefore concluded that no more than 1.5% of the deamination reaction proceeded through protonated cyclopropane intermediates.

1. Student participant in the Great Lakes Colleges Association Science Semester, Sept. 10–Dec. 18, 1970, from Denison University, Granville, Ohio.
2. P. A. S. Smith, D. R. Baer, and S. N. Ege, *J. Amer. Chem. Soc.* 78, 4564 (1954).
3. C. J. Collins, *Chem. Rev.* 69, 543 (1969).

SOLVOLYSIS OF 3-PHENYL-2-BROMOPROPANAL

Ben M. Benjamin Clair J. Collins

Because of our interest in molecular rearrangement, we decided to investigate the acid-catalyzed isomerization[1] of 3-phenyl-2-hydroxypropanal (**1**) to 1-phenyl-1-hydroxy-2-propanone (**2**). A mechanism for the rearrangement has not been suggested, and we experienced difficulty in proposing one.

ORNL-DWG. 71-5404

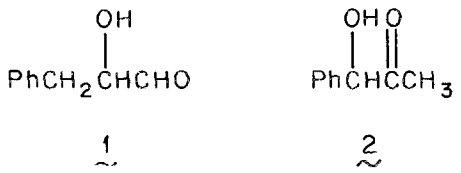

1 **2**

Aldehyde **1** is reported to have been prepared by hydrolysis of 3-phenyl-2-bromopropanal (**3**) in the presence of freshly precipitated barium carbonate. For us the procedure resulted only in the isolation of polymeric material; similar results were obtained when hydrolysis was attempted with calcium carbonate or with dilute aqueous sodium bicarbonate.

When the bromoaldehyde **3** was solvolyzed with potassium acetate in acetic acid at steam-bath temperature, it was slowly converted to 2-acetoxy-3-phenylpropanal (**4**), which could be isolated as a mixture with **3**, and another compound later identified as 1-acetoxy-3-phenyl-2-propanone (**5**). Compound **4** was detected and identified by nmr spectroscopy. Heating the acetic acid reaction mixture for a longer time or at higher temperatures resulted in good yields of **5**.

When **5** was heated with a dilute solution of sulfuric acid in ethanol the only reaction observed was hydrolysis of the acetate to give the free keto alcohol **6**. Compound **6** was unchanged after heating it with dilute sulfuric acid in a sealed tube at 135° for 8 hr.

Reduction of either **5** or **6** gave 3-phenyl-1,2-propanediol. None of the compounds actually found in this series of reactions has physical properties corresponding to those described by Danilov,[1] and we are unable to explain why.

ORNL-DWG. 71-5405

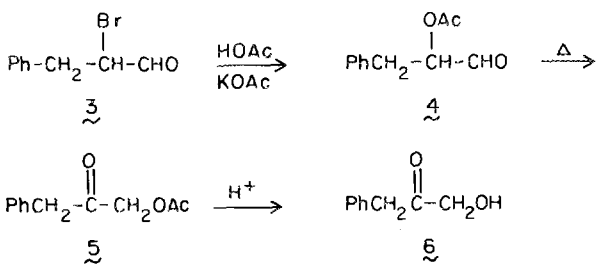

1. S. Danilov and E. Venus-Danilov, *Ber. Deut. Chem. Ges. B* 63, 2765 (1930).

THE MECHANISM OF THE DIELS-ALDER REACTION. ATTEMPTS TO PREPARE UNUSUAL HYDROCARBONS

Vernon F. Raaen Clair J. Collins

The dienophile **1** was prepared from the adduct[1] of anthracene and acetylene-dicarboxylic ester. Compound **1** was then subjected to Diels-Alder reaction conditions[1] with the unsaturated cyclic hydrocarbons **2**–**6**.[2]

ORNL-DWG. 71-5406

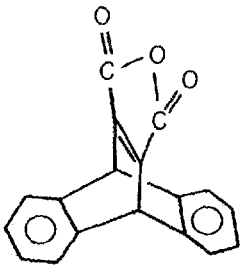

1

ORNL-DWG. 71-5407

2 3 4 5 6[2]

The adducts were prepared by prolonged heating (two to five weeks) of **1** with two or three equivalents of **2**–**6** in refluxing toluene. Thus the temperature was maintained at about 110°. Solid, crystalline, high-melting adducts were obtained from **2**, **3**, and **6**. Compounds **4** and **5** afforded dark-brown amorphous solids that were too unstable to permit further purification. The adducts of **1** with **3** and **6** on heating at 235 to 240° underwent decomposition to yield, among other products, *o*-phthalic anhydride and anthracene.

Our work in this field continues. The adducts of **1** with **3** and **6** would be expected to yield *o*-phthalic anhydride through normal reverse Diels-Alder reactions together with the production of ethylene (from the adduct of **1** with **3**), or acetylene or cyclobutadiene[3] from the adduct **1** + **6**. The adducts **1** + **2**, **1** + **4**, and **1** + **5** apparently cannot undergo normal reverse Diels-Alder reaction to yield *o*-phthalic acid and anthracene plus unsaturated hydrocarbon without proceeding through diradical fragments. It is our purpose, therefore, in continuing this work to determine (*a*) whether reverse Diels-Alder reactions are possible with these adducts; (*b*) if the adduct of **1** + **6** can be induced to add another mole of **1**, which could conceivably decompose to yield *bis*-1,4-dicyclohexadiene; and (*c*) the hydrocarbon fragment – other than anthracene – formed on decomposition of adduct **1** + **6**.

---

1. O Diels and K. Alder, *Justus Liebigs Ann. Chem.* 486, 199 (1931); ibid., 513, 150 (1934).
2. We are indebted to Dr. Berndt Zeeh and Badische Anilin- und Soda-Fabrik for a generous gift of 100 g of cyclooctatetraene.
3. L. Watts, J. D. Fitzpatrick, and R. Pettit, *J. Amer. Chem. Soc.* 87, 3253 (1965).

HEATS OF FORMATION OF 3-ARYL-2,3-DIMETHYL-2-BUTYL CATIONS IN SUPER ACIDS[1]

Vernon F. Raaen Clair J. Collins

In 1969, Olah and co-workers[2] studied the nmr spectra, in SO_2-SbF_5 solutions at −78°, of a series of compounds of general structure **1** (where X = –H, –CH_3, –OCH_3, and –CF_3; Y = Cl). From these spectra

ORNL-DWG. 71-5408

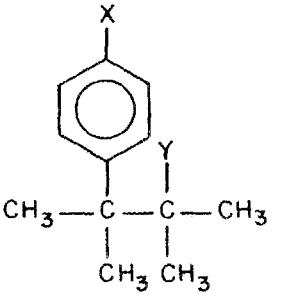

1

it was concluded that when X = H the cation formed was a phenonium ion, when X = CH_3 two cations were produced, namely, the phenonium ion and the classical ion in nearly equal proportions. All other reactants led to classical tertiary cations. We doubted[3] the conclusions of Olah and co-workers[2] and undertook a study[1] of the heats of formation of the appropriate cations from **1** (X = H, Y = OH; X = CH_3, Y = OH, and X = OCH_3, Y = OH), which should allow us to distinguish classical from nonclassical (bridged) ions. The three carbinols were prepared by known methods,[4,5] and the heats of formation of the corresponding cations are currently being studied. The calorimeter employed has been described by Arnett and co-workers.[6]

1. The work is being carried out jointly with Dr. John W. Larsen of the Chemistry Department, University of Tennessee, Knoxville.
2. G. A. Olah, M. B. Comisarow, and C. J. Kim, *J. Amer. Chem. Soc.* 91, 1458 (1969).
3. See p. 1467, footnote 29, of ref 2.
4. E. V. Heynengen, *J. Amer. Chem. Soc.* 74, 486 (1952).
5. H. C. Brown and C. J. Kim, ibid., 90, 2082 (1968).
6. E. M. Arnett, W. G. Bentrude, J. J. Burke, and P. McC. Duggleby, *J. Amer. Chem. Soc.* 87, 1541 (1965); E. M. Arnett, R. P. Quirk, and J. J. Burke, ibid., 92, 1260 (1970).

THE MECHANISM OF HYDRIDE SHIFT IN NORBORNYL CATIONS

Vernon F. Raaen Clair J. Collins
Ben M. Benjamin David Houser[1]

1-Methyl-7,2-norbornanecarbolactone (**1**) in the presence of concentrated sulfuric acid undergoes a compli-

ORNL-DWG. 71-5409

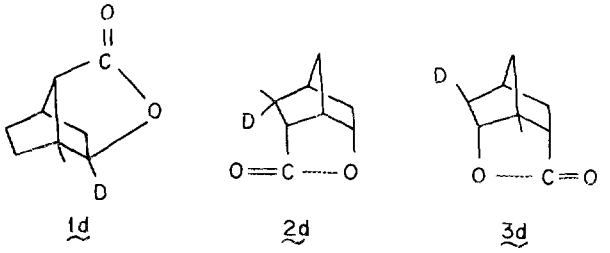

cated series of rearrangements to yield 3-*exo*-methyl-2,6-norbornanecarbolactone (**2**) and 1-methyl-2,6-norbornanecarbolactone (**3**).[2] By synthesis of compound **1d**, labeled as shown with deuterium,[3] followed by treatment with cold concentrated sulfuric acid and subsequent isolation of **2d** and **3d**, we were able to show with nmr spectroscopy that the deuterium atoms in **2d** and **3d** were predominantly in the 3-*endo*- and 5-*exo*-positions, respectively, as designated in the structures. There was no evidence for the presence of deuterium in any of the other positions of the two compounds. These results allow us to draw the following important conclusions:

1. The lactone **2d** has been formed predominantly by the sequence: 6,2-hydride shift; Wagner-Meerwein rearrangement; 6,2-deuteride shift; 3,2-hydride shift.
2. The lactone **3d** has been formed predominantly by the sequence: 3,2-hydride shift; Wagner-Meerwein rearrangement; 6,2-hydride shift; Wagner-Meerwein rearrangement; 3,2-deuteride shift.
3. In the formation of **2d** the 6,2-deuteride shift is *endo-endo,* whereas in the formation of **3d** both the 3,2-hydride and -deuteride shifts are *exo-exo.*

The foregoing conclusions offer strong support for our previous formulations of 6,2-hydride[4] and 3,2-hydride[5] migration in substituted norbornyl cations.

1. Student participant in the Great Lakes Colleges Association Science Semester, Sept. 10–Dec. 18, 1970, from De Pauw University, Greencastle, Ind.
2. H. Geiger and S. Beckmann, *Justus Liebigs Ann. Chem.* **722**, 219 (1969).
3. J. A. Berson and P. W. Grubb, *J. Amer. Chem. Soc.* **87**, 4016 (1965).
4. C. J. Collins and B. M. Benjamin, *J. Amer. Chem. Soc.* **89**, 1652 (1967); ibid., **88**, 1558 (1966); *Tetrahedron Lett.* 5477 (1966).
5. C. J. Collins and C. E. Harding, *J. Amer. Chem. Soc.* **91**, 7194 (1969); *Justus Liebigs Ann. Chem.*, in press (1971).

A DEUTERIUM TRACER STUDY OF 6,1,2-HYDRIDE SHIFT IN SUBSTITUTED NORBORNYL CATIONS

Vernon F. Raaen Ben M. Benjamin Clair J. Collins

One of the important but unanswered questions concerning the reaction of nitrous acid with primary aliphatic amines[1,2] has been[3] whether the classical ions originally formed on loss of nitrogen can survive several Wagner-Meerwein rearrangements or hydride shifts. We now have evidence that they can. We previously reported[4] that a classical *secondary* norbornyl cation survives a Wagner-Meerwein rearrangement, since the rearranged cation was attacked from the *endo* direction to produce 1.8% of *endo* product. Hückel and Kern[5] have demonstrated that both *exo*- and *endo*-fenchylamines produce *exo* and *endo* isomers of α-fenchene hydrate, thus showing that a *tertiary* classical cation can survive Wagner-Meerwein rearrangement to yield *endo* products.

In the deaminations (in acetic acid–sodium acetate) of **1**[6] and **2**[7] (Chart I) the yields of **3** and **4** (as the monoacetates)[8] are in the same ratio (1.6–1.7) from

ORNL-DWG. 70-7077A

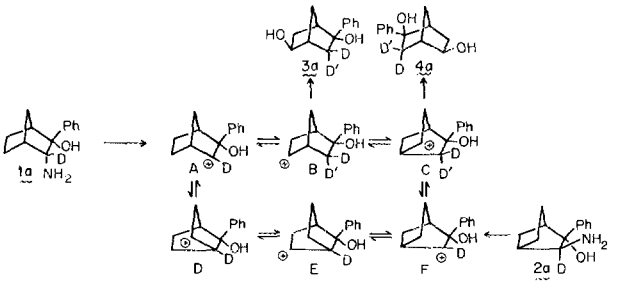

Chart I

both reactants, and this ratio is roughly the same as the ratio of **3**:**4** (1.4) observed upon the hydrolyses[9] of the secondary tosylates of **3** and of **4**. Thus B and C might

mistakenly be interpreted as a nonclassical ion, particularly since the two *exo*-amines corresponding to the two ions B and C yield the acetates of **3** and **4**, on deamination, in the ratios of 2.2:1 and 1:1.7 respectively.[10]

If both **1** and **2**, however, should prefer the same clockwise pathway and approach B ⇌ C from the "B side," then deaminations both of **1** and **2** should result in **3**:**4** > 1, even if B and C are classical. That both reactants approach the equilibrium B ⇌ C through clockwise pathways (as the intermediates are oriented in the chart) was demonstrated by means of deuterium labeling. The positions in **3** and **4** designated "D" denote where the deuterium goes via the clockwise pathways, whereas "D′" denotes the fate of deuterium when **3** and **4** result from counterclockwise pathways. The results, given in Table 5.1, show that both reactants yield **3** and **4** by predominant (77–89%) clockwise routes. The yields of **3** and **4** as determined by the isotope dilution method[11] are also given in the table. These data thus show that a comparison of the product ratios **3**:**4** from the two reactants **1** and **2** is not of itself a sufficient criterion for nonclassical character of the ions B ⇌ C.

Another important conclusion can be drawn from Chart I and Table 5.1: If B ⇌ C were in fact a single nonclassical ion, then **3** and **4** from a given single reactant should exhibit identical deuterium distributions in D and D′. That these distributions are significantly different means that even after two Wagner-Meerwein rearrangements and a hydride shift, ions B and C are best formulated as unbridged, classical ions, *which have not yet reached their equilibrium concentrations.*

In **4** containing no D, the signals for 2H at C_3 are centered at δ = 2.07 ppm (pyridine) and overlap the multiplet for the *anti*-C_7H (intensity 3.00 ± 0.02). In **4** from either **1** or **2** the intensity is 2.00 ± 0.03. There was no loss of deuterium in the other products[7,8] of deamination of **1** and **2**. Conversion of **4** to the 2-*exo*-5-*endo*-diol[7] allowed isolation of the signal (δ = 3.25 ppm) for *endo*-H at C_3. Diol **3** (no D) exhibits a quartet (δ = 2.4 ppm, pyridine) for *exo*-H at C_3 and is overlapped by H at C_4 (intensity, 2.00 ± 0.03). Integration of this signal for **3** (with D) gave the fraction of *exo*-H at C_3. On oxidation of **3** to the ketone,[4] the signal for *exo*-H at C_3 is at δ = 2.6 ppm (pyridine) and is also overlapped by H at C_4.

1. H. Söll, pp. 133–81 in Houben Weil *Methoden der organischen Chemie,* E. Müller, ed., Georg Thieme Verlag, Stuttgart XI/2, 1958.
2. J. H. Ridd, *Quart. Rev., Chem. Soc.* 15, 418 (1961).
3. P. D. Bartlett, *Nonclassical Ions,* p. 65, W. A. Benjamin, New York, 1965.
4. B. M. Benjamin and C. J. Collins, *J. Amer. Chem. Soc.* **92**, 3183 (1970).
5. W. Hückel and H.-J. Kern, *Justus Liebigs Ann. Chem.* **728**, 49 (1969).
6. C. J. Collins et al., *Justus Liebigs Ann. Chem.* **739**, 7 (1970).
7. C. J. Collins, V. F. Raaen, and M. D. Eckart, *J. Amer. Chem. Soc.* **92**, 1787 (1970).
8. The products of the deaminations of **1** and **2** have all been described before [see ref. 7, and C. J. Collins and B. M. Benjamin, ibid., **89**, 1652 (1967)].
9. B. M. Benjamin, B. S. Benjaminov, and V. F. Raaen, unpublished work.
10. C. J. Collins and B. M. Benjamin, *J. Amer. Chem. Soc.* **92**, 3182 (1970).
11. V. F. Raaen, G. A. Ropp, and H. P. Raaen, chap. 2 in *Carbon-14,* McGraw-Hill, New York, 1968.

PREPARATION AND PURIFICATION OF *p*-SEXIPHENYL

W. H. Baldwin P. T. Perdue[1]

During the study of organic crystal scintillators by Perdue and Brown,[2] it was noted in agreement with others[3–5] that *p*-sexiphenyl (Ps) would be an interest-

Table 5.1. Yields and deuterium distributions in 3 and 4 from deaminations of 1 and 2

Reactant	Product 3		Product 4	
	Yield[a] (%)	D′[b]	Yield[a] (%)	D′[b]
1	4.25 ± 0.01	0.11 ± 0.025	2.7 ± 0.01	0.175 ± 0.016
2	6.3 ± 0.02	0.145 ± 0.025	3.7 ± 0.02	0.23 ± 0.016

[a]The ± values are the reproducibilities of the ^{14}C assays.

[b]Standard error.

ORNL-DWG. 71-7577

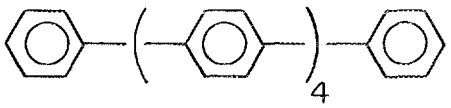

ing scintillating compound. It is expected to function as a wave shifter, to have a fast pulse decay, high light output, and excellent vacuum characteristics. Investigation of *p*-sexiphenyl in the past has suffered from difficulties in preparation and purification on the centigram scale; the compound is so insoluble that recrystallization is impractical, and the high melting point, above 450°C, indicates the refractory nature of the compound. However, in our purification scheme we take advantage of these properties; for example, continuous extraction with chloroform or dimethylformamide removes soluble impurities. The stability of the compound at high temperatures permits: (1) sublimation at 400–500°C under reduced pressure and (2) zone-melting refining.

Kovacic and Lange[6] have outlined a method for *p*-sexiphenyl production in which diphenyl or *p*-terphenyl is reacted with aluminum chloride and cupric chloride. The reaction of terphenyl has proven more satisfactory for us since the product, Ps, can be purified more easily. In general, the product from the reaction is treated with aqueous hydrochloric acid to remove metals, with water to remove acid, with ethyl alcohol to remove water, and then with chloroform and finally dimethylformamide. A preliminary sublimation removes low-molecular-weight compounds, the Ps being collected at about 500°C at 1 torr. Single crystals, 1 cm square by 8 μ thick, were grown in a special temperature gradient furnace (465–470°C) in a helium atmosphere. The completely transparent crystals have an index of refraction above 1.64, density of 1.26 g/cc, and maximum fluorescence near 450 nm. The principal mass (by mass spectrometry) is 458.6 amu (calculated for $C_{36}H_{26}$, 458.6 amu) with traces of *m/e* 534 (heptaphenyl) and 610 (octaphenyl). The infrared spectrum agrees with that reported by Cade and Pilbeam[7] for Ps. Further improvement in purity results from zone-melt refining of the sublimed material.

We are currently preparing larger quantities of this high-purity scintillator and collecting optical, physical, and chemical data on the pure product.

---

1. Health Physics Division.
2. P. T. Perdue and M. D. Brown, *Nucl. Instrum. Methods* 71, 113 (1969).
3. T. Nozaki et al., *Bull. Chem. Soc. Jap.* **33**, 1329 (1960).
4. I. B. Berlman, *Mol. Cryst.* **4**, 157 (1968).
5. H. O. Wirth et al., *Mol. Cryst.* 4, 321 (1968).
6. P. Kovacic and R. M. Lange, *J. Org. Chem.* **29**, 2416 (1964).
7. J. A. Cade and A. Pilbeam, *J. Chem. Soc. London* **1964**, 114.

6. Physical Chemistry

AQUEOUS SYSTEMS

FREE ENERGIES OF ELECTROLYTE MIXTURES

R. M. Rush J. S. Johnson, Jr. G. Scatchard[1]

Osmotic Coefficients of Mixed Perchlorate Solutions

Our studies of solutions of common inorganic electrolytes have continued to concentrate on the perchlorates, which are widely used in studies of complexing and reaction kinetics. A report of our work on mixtures involving $UO_2(ClO_4)_2$ discussed in a previous annual report[2] has been submitted for publication. Experimental work on mixtures of $Ba(ClO_4)_2$ with $HClO_4$ and $NaClO_4$ has been completed, and analysis of the data is in progress.

Osmotic coefficients for the system $HClO_4$-$Ba(ClO_4)_2$-H_2O are shown in Fig. 6.1 and for the system $NaClO_4$-$Ba(ClO_4)_2$-H_2O in Figs. 6.2 and 6.3. The system $HClO_4$-$Ba(ClO_4)_2$-H_2O illustrates the situation where the osmotic coefficients of the limiting two-component systems show a wide divergence with increasing concentration. The mixtures show a behavior intermediate between the limiting systems, as would be expected. The system $NaClO_4$-$Ba(ClO_4)_2$-H_2O represents a somewhat different behavior. The osmotic coefficients for the limiting two-component systems are relatively close together and, in fact, have a crossover point at an ionic strength of about 2. For this reason, the osmotic coefficients at low concentrations are shown in more detail in Fig. 6.3. The mixtures show a behavior intermediate between the limiting systems with an inversion of the order on either side of the crossover point.

Our results for pure $Ba(ClO_4)_2$ solutions are in poor agreement with literature values.[3] Our values for ϕ are consistently lower than the literature values; the difference varies from 0.10 at $I = 17$ to 0.02 at $I = 1.5$. At high $Ba(ClO_4)_2$ concentrations, the water fraction, obtained by difference, is low and is therefore quite sensitive to uncertainties in the solute concentration. A change of 1% in the solute concentration of the stock solution is required to bring the results into agreement.

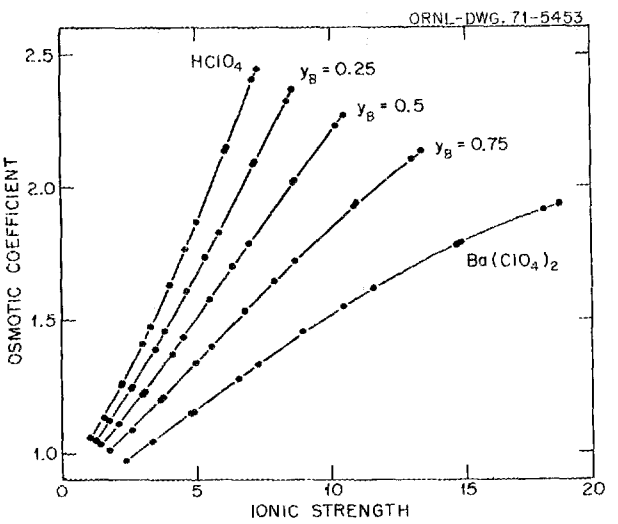

Fig. 6.1. Osmotic coefficients for the system $HClO_4$ (A)–$Ba(ClO_4)_2$ (B)–H_2O.

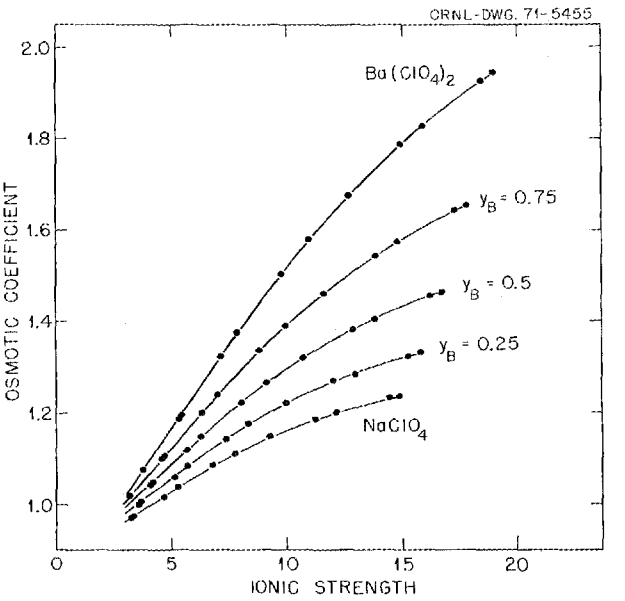

Fig. 6.2. Osmotic coefficients for the system $NaClO_4$ (A)–$Ba(ClO_4)_2$ (B)–H_2O.

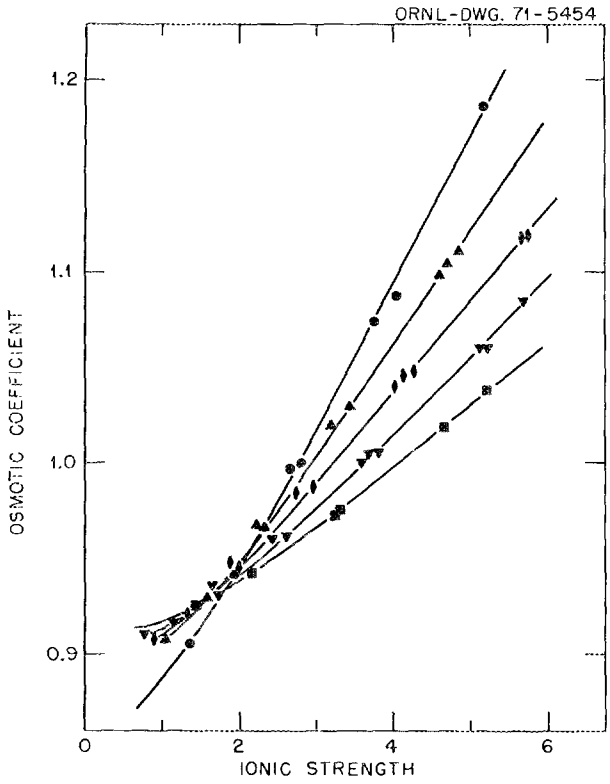

Fig. 6.3. Osmotic coefficients for the system $NaClO_4$ (A)–$Ba(ClO_4)_2$ (B)–H_2O. Values for y_B: •, 1.0; ▲, 0.75; ◆, 0.5; ▼, 0.25; ■, 0.0.

This is greater than the uncertainty in the analysis of the stock solution, and the disagreement is, at present, unexplained.

Limiting Behavior of Osmotic Coefficients at Low Concentrations

The limiting behavior of free energies in dilute solutions of mixed electrolytes is specified differently in equations developed by Scatchard[4] and in the theory developed by Friedman.[5] The disagreement is of theoretical interest and has been discussed by both Scatchard[4] and Friedman.[5] It also, however, has a practical aspect of particular importance to us in that the calculation of activity coefficients of solutes from osmotic coefficients of mixed electrolyte solutions will be affected.

The freezing point depression measurements of Scatchard and Prentiss[6] are, to our knowledge, the most accurate measurements of osmotic coefficients of mixed electrolyte solutions at low concentrations. Revised values of the osmotic coefficients have been calculated from the original data using a more recent value for the freezing point constant.[7] The results are presented in Figs. 6.4–6.7 as plots of $\Delta/y_A y_B m$ vs $\sqrt{m}$, where, for a mixture of two 1-1 type electrolytes,

$$\Delta = 2(\phi - y_A\phi_A{}^0 - y_B\phi_B{}^0)\,,$$

m is the molality, y_A and y_B are the molality fractions of components A and B, respectively, ϕ is the osmotic

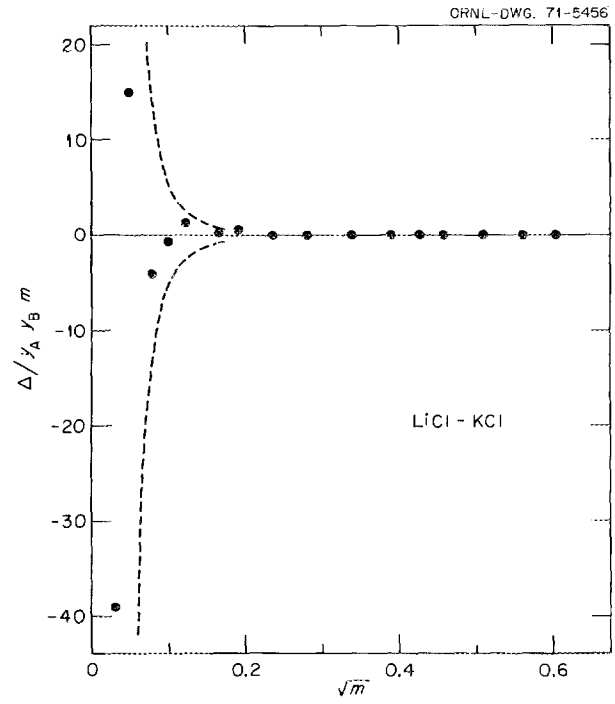

Fig. 6.4. Freezing point depression data of Scatchard and Prentiss for equimolar mixtures of LiCl and KCl; behavior at low concentrations. Dashed line represents 5×10^{-4} deg.

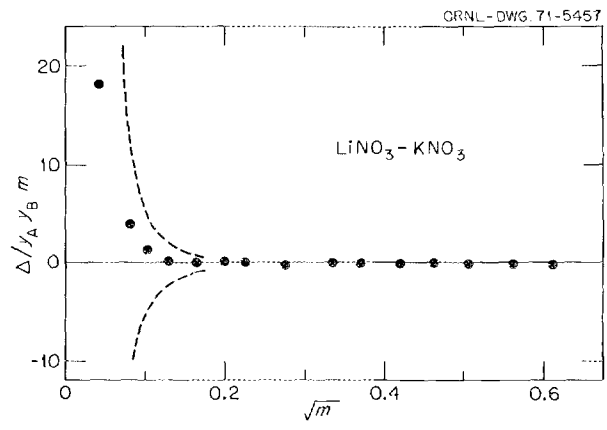

Fig. 6.5. Freezing point depression data of Scatchard and Prentiss for equimolar mixtures of $LiNO_3$ and KNO_3; behavior at low concentrations. Dashed line represents 5×10^{-4} deg.

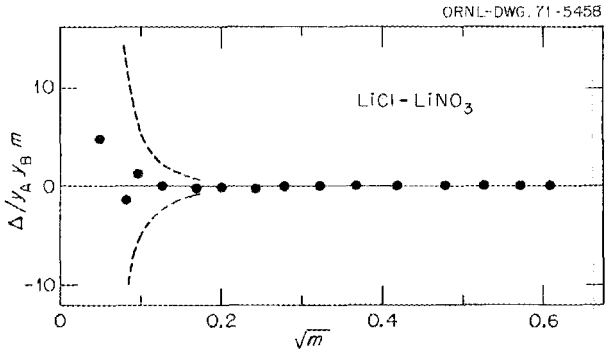

Fig. 6.6. Freezing point depression data of Scatchard and Prentiss for equimolar mixtures of LiCl and $LiNO_3$; behavior at low concentrations. Dashed line represents 5×10^{-4} deg.

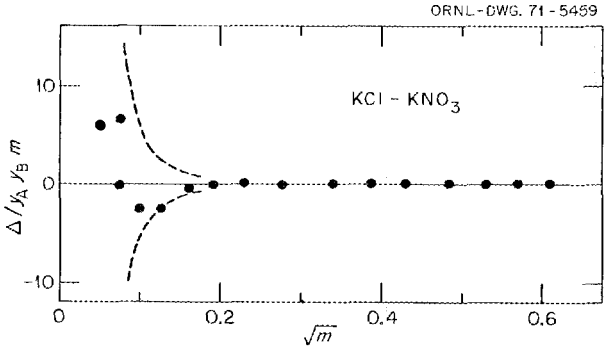

Fig. 6.7. Freezing point depression data of Scatchard and Prentiss for equimolar mixtures of KCl and KNO_3; behavior at low concentrations. Dashed line represents 5×10^{-4} deg.

coefficient of the mixed solution containing A and B, and ϕ^0 is the osmotic coefficient of the pure component at the same total molality as the mixture.

For the Scatchard treatment of equimolar mixtures of two 1-1 type electrolytes

$$\Delta/y_A y_B m = b_{AB}^{(0,1)} + b_{AB}^{(0,2)} m + b_{AB}^{(0,3)} m^2 ,$$

where the b_{AB}'s are parameters characteristic of the particular mixture. A plot of this function vs $\sqrt{m}$ should approach a finite intercept with a zero slope. Although at low concentrations, $\Delta/y_A y_B m$ is very sensitive to experimental error, the results in Figs. 6.4–6.7 indicate that the values are small and appear to approach $\sqrt{m} = 0$ with zero slope. It appears, therefore, that the Scatchard equations describe the low-concentration behavior of these mixtures within the accuracy of the best available data.

1. Consultant; Professor of Physical Chemistry, Emeritus, Massachusetts Institute of Technology, Cambridge.

2. J. S. Johnson, Jr., et al., *Chem. Div. Annu. Progr. Rep. May 20, 1970,* ORNL-4581, p. 91.
3. R. A. Robinson, C. K. Lim, and K. P. Ang, *J. Amer. Chem. Soc.* 75, 5130 (1953).
4. G. Scatchard, *J. Amer. Chem. Soc.* **83,** 2636 (1961).
5. H. L. Friedman, *Ionic Solution Theory,* Wiley, New York, 1962.
6. G. Scatchard and S. S. Prentiss, *J. Amer. Chem. Soc.* **56,** 2320 (1934).
7. We are indebted to H. Frank Gibbard for these calculations.

A SIMPLE EQUATION FOR THE PREDICTION OF THE ACTIVITY COEFFICIENT VALUE OF EACH COMPONENT IN AQUEOUS ELECTROLYTE MIXTURES

M. H. Lietzke R. W. Stoughton

In recent years there has been an upsurge of interest in the thermodynamic properties of aqueous electrolyte mixtures. Much of this interest is of a very practical nature, for example, in the fields of desalination, oceanography, and geochemistry. One of the problems in this area that has received considerable attention is the prediction of the activity coefficients of each component (electrolyte) in an aqueous solution containing several electrolytes. Some of the approaches used, for example, the ion-component treatment of Scatchard, Rush, and Johnson,[1] involve many parameters which must be estimated by least squares on a high-speed computer. The purpose of this report is to present a very simple equation which makes it possible to predict the activity coefficient of each component in a solution containing several electrolytes, in fact even in mixtures containing electrolytes of different valence types. In most cases activity coefficient values calculated with this equation are about the same as values predicted using the more elaborate ion-component treatment.

Any current method of predicting the activity coefficient of one component in an aqueous electrolyte mixture depends upon a knowledge of the activity coefficient of each component in solution in the pure state, that is, in a solution containing only one electrolyte. In the ion-component treatment the method of least squares is used to determine coefficients that may be used to express the concentration dependence of the logarithm of the activity coefficient of each electrolyte in the pure state. These coefficients are then combined in the ion-component model and used to predict the activity coefficient of any one

component in a mixture of these electrolytes. In our treatment we use directly the activity coefficient values of each electrolyte in the pure state at the total ionic strength of the mixture. The equation that we propose for combining these values to predict the activity coefficient of one component in a mixture is

$$\frac{1}{|Z^+_i Z^-_i|}\log \gamma_i = \frac{1}{|Z^+_i Z^-_i|}\log \gamma_i^0 + \sum_{\substack{j=1\\ j\neq i}}^{n} \frac{F_j}{2}\left(\frac{1}{|Z^+_j Z^-_j|}\log \gamma_j^0 - \frac{1}{|Z^+_i Z^-_i|}\log \gamma_i^0\right) . \quad (1)$$

In this equation γ_i is the activity coefficient of the ith component in a mixture containing n electrolytes, the F_j are the ionic strength fractions of each of the other electrolytes, the superscript 0 indicates activity coefficient values in the pure state at the total ionic strength of the mixture, and Z^+ and Z^- represent the charges on the cation and anion respectively. The charges have been included so that the logarithms of all the activity coefficients approach the same limiting slope at low concentrations.

For an aqueous mixture of two electrolytes, Eq. (1) becomes

$$\frac{1}{|Z^+_1 Z^-_1|}\log \gamma_1 = \frac{1}{|Z^+_1 Z^-_1|}\log \gamma_1^0 + \frac{F_2}{2}\left(\frac{1}{|Z^+_2 Z^-_2|}\log \gamma_2^0 - \frac{1}{|Z^+_1 Z^-_1|}\log \gamma_1^0\right) . \quad (2)$$

If the charges are omitted from Eq. (2) an expression is obtained which holds only for binary mixtures of electrolytes of the same valence type and which is similar to an equation given by Harned and Owen.[2] Such an equation follows from Guggenheim's treatment of the theory of specific ion interaction.[2]

One of the difficulties in discussing activity coefficients in mixtures is that the values obtained for each component are sensitive to the method of calculation. For example, values of the activity coefficient of NaCl in HCl-NaCl mixtures may differ by as much as 1.0% or more, depending upon whether they were obtained by cross-differentiation[3] or by application of the neutral-electrolyte treatment[4] to HCl-NaCl mixture data.[5] This makes it impossible to state, for example, whether the activity coefficient of NaCl at 10°C in a 50-50 mixture at I = 1.0 is 0.700 or 0.709.[5] As will be shown later, similar results are obtained when the neutral-electrolyte treatment and the ion-component treatment are applied to the same set of mixture data by the method of least squares. The differences probably result from a difference in weighting when attention is focused on the ions as components or on the electrolytes themselves. Also, the degree of statistical correlation between the parameters in the two treatments may be different.

A comparison will now be made between activity coefficient values computed using Eq. (1) and values computed in three other ways: (1) values computed from parameters obtained by fitting the ion-component model[1] to mixture data by least squares; this will be referred to as the IC(II) treatment, and these values are plotted and joined by the solid lines in Figs. 6.8 and 6.9; (2) values predicted by the ion-component treatment (ignoring any interaction terms); this will be referred to as the IC(I) treatment; and (3) values computed from parameters obtained by fitting the neutral-electrolyte model[4] to mixture data by least squares; this will be referred to as the NE treatment.

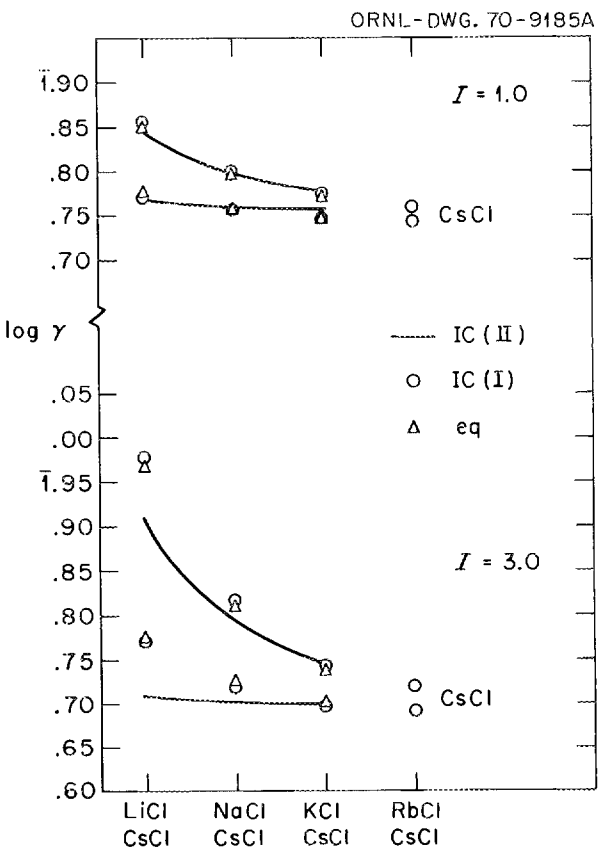

Fig. 6.8. Activity coefficient behavior in binary mixtures containing LiCl, NaCl, KCl, or RbCl with CsCl at I = 1.0 and 3.0 with X_{CsCl} = 0.5. Lower points at each ionic strength refer to CsCl.

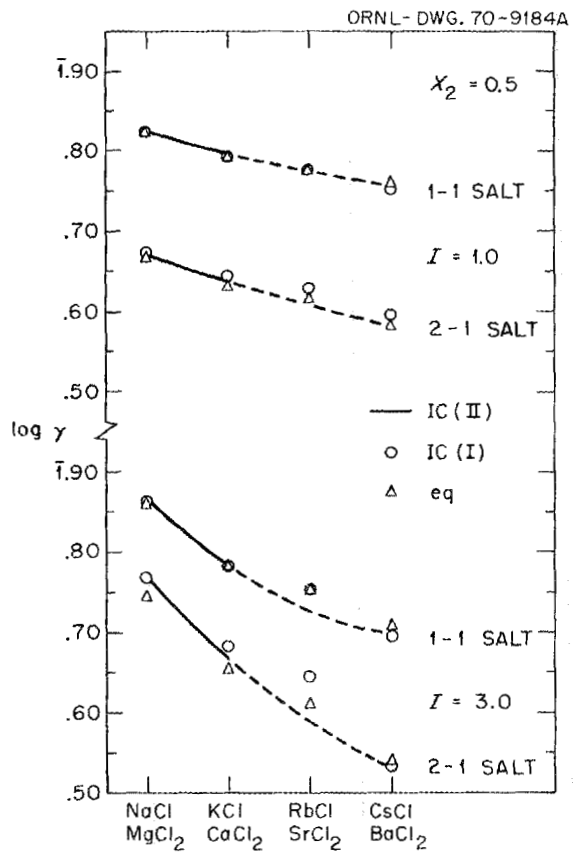

Fig. 6.9. Activity coefficient behavior in $NaCl-MgCl_2$, $KCl-CaCl_2$, $RbCl-SrCl_2$, and $CsCl-BaCl_2$ mixtures at I = 1.0 and 3.0 with the ionic strength fraction of each salt 0.5.

Results of the Calculations

First we consider mixtures containing CsCl and each of the other alkali metal chlorides as shown in Fig. 6.8. In each case each component has an ionic strength fraction X = 0.5. The data points have significance at the discrete systems shown along the abscissa; smoothed curves have been drawn through the IC(II) data points to suggest activity coefficient trends from one system to the next. The first three mixtures starting at the left have been studied isopiestically, while to our knowledge the RbCl-CsCl mixture has not been studied experimentally. Note that at both I = 1.0 and I = 3.0, log γ_{CsCl} is nearly constant, while that of the other salt decreases in going from LiCl-CsCl to RbCl-CsCl. The lower points at each ionic strength refer to the CsCl, while the upper points refer to the other salt in the mixture. At I = 1.0 both Eq. (1) and the IC(I) treatment give predictions that are comparable and that agree very well with values calculated from parameters obtained by fitting osmotic coefficient data on the mixtures by least squares using the IC(II) model. At I = 3.0, however, both methods IC(I) and Eq. (1) give relatively poor results for LiCl-CsCl mixtures, somewhat better results for NaCl-CsCl, and excellent results for KCl-CsCl mixtures as compared with the values obtained by fitting the data using the IC(II) treatment. At both total ionic strengths the predictions on RbCl-CsCl mixtures using either Eq. (1) or the IC(I) treatment are consistent with the measured values on the other systems.

All of the systems depicted in Fig. 6.9 except $RbCl-SrCl_2$ have been studied experimentally. Observe that there is very little difference in the values predicted by Eq. (1) and IC(I) at I = 1.0. It is interesting to note that Eq. (1) seems to predict a more consistent value of log γ_{SrCl_2} at I = 3.0 than does the IC(I) treatment.

Next we turn our attention to activity coefficient values of HCl and of a series of alkali metal and alkaline-earth metal chlorides in HCl–metal chloride solutions at I = 1.0 with the ionic strength fraction of each component equal to 0.5. These values are shown in Table 6.1. In columns 2 and 4 are values of log γ_{HCl} computed from coefficients obtained by fitting activity coefficient data on these systems using either the IC(II) or the neutral-electrolyte treatments. In column 3 are values predicted using the IC(I) treatment, while in column 5 are predictions made using Eq. (1). The greatest difference between values obtained by fitting mixture data and using Eq. (1) is in the case of the HCl-LiCl mixture, where the difference amounts to 4% in the activity coefficient of the HCl. The corresponding log γ_{salt} values are shown in the last three columns of Table 6.1. Here the greatest difference between a fitted value and a value predicted by Eq. (1) amounts to 4% in the activity coefficient of the $SrCl_2$ in the $HCl-SrCl_2$ mixture.

In Table 6.2 are shown values of log γ_{HCl} and log γ_{NaCl} in HCl-NaCl mixtures as a function of the ionic strength fraction of the other component at a total ionic strength of unity. Note that there is essentially no difference between log γ_{HCl} values predicted by the IC(I) treatment or by Eq. (1); as the fraction of NaCl in the mixtures increases, these predicted values become increasingly too low as compared with the fitted values [IC(II)]. The same is true of the log γ_{NaCl} values as the fraction of HCl in the mixture increases.

In Table 6.3 are shown values of log γ_{HCl} and log γ_{MgCl_2} in the $HCl-MgCl_2$ mixtures as a function of the ionic strength fraction of the other component at a total ionic strength of unity. In this system, again in

Table 6.1. Activity coefficient values of HCl and metal chlorides in HCl–metal chloride solutions at $I = 1.0$ with the ionic strength fraction of each component equal to 0.5

System	$\log \gamma_{HCl}$				$\log \gamma_{salt}$		
	IC(II)	IC(I)	NE	Eq. (1)	IC(II)	IC(I)	Eq. (1)
HCl-LiCl	$\bar{1}.886$	$\bar{1}.886$		$\bar{1}.903$	$\bar{1}.888$	$\bar{1}.888$	$\bar{1}.894$
HCl-NaCl	$\bar{1}.897$	$\bar{1}.886$	$\bar{1}.893$	$\bar{1}.885$	$\bar{1}.850$	$\bar{1}.841$	$\bar{1}.846$
HCl-KCl	$\bar{1}.880$	$\bar{1}.878$		$\bar{1}.876$	$\bar{1}.816$	$\bar{1}.816$	$\bar{1}.813$
HCl-RbCl	$\bar{1}.875$	$\bar{1}.875$		$\bar{1}.872$	$\bar{1}.798$	$\bar{1}.806$	$\bar{1}.801$
HCl-CsCl	$\bar{1}.869$	$\bar{1}.869$		$\bar{1}.865$	$\bar{1}.785$	$\bar{1}.783$	$\bar{1}.779$
HCl-$MgCl_2$	$\bar{1}.891$	$\bar{1}.884$	$\bar{1}.887$	$\bar{1}.888$	$\bar{1}.692$	$\bar{1}.696$	$\bar{1}.711$
HCl-$CaCl_2$	$\bar{1}.884$		$\bar{1}.881$	$\bar{1}.888$	$\bar{1}.682$	$\bar{1}.680$	$\bar{1}.693$
HCl-$SrCl_2$			$\bar{1}.879$	$\bar{1}.886$	$\bar{1}.668$	$\bar{1}.671$	$\bar{1}.687$
HCl-$BaCl_2$	$\bar{1}.874$		$\bar{1}.875$	$\bar{1}.883$	$\bar{1}.653$		$\bar{1}.668$

Table 6.2. Activity coefficients of HCl and NaCl in HCl-NaCl mixtures at $I = 1.0$

X_{NaCl}	$\log \gamma_{HCl}$		
	IC(II)	IC(I)	Eq. (1)
0.25	$\bar{1}.904$	$\bar{1}.897$	$\bar{1}.897$
0.50	$\bar{1}.897^a$	$\bar{1}.886$	$\bar{1}.885$
0.75	$\bar{1}.889$	$\bar{1}.875$	$\bar{1}.874$
X_{HCl}	$\log \gamma_{NaCl}$		
	IC(II)	IC(I)	Eq. (1)
0.25	$\bar{1}.834$	$\bar{1}.830$	$\bar{1}.829$
0.50	$\bar{1}.850$	$\bar{1}.841$	$\bar{1}.846$
0.75	$\bar{1}.868$	$\bar{1}.852$	$\bar{1}.851$

[a]NE value is $\bar{1}.893$.

Table 6.3. Activity coefficients of HCl and $MgCl_2$ in HCl-$MgCl_2$ mixtures at $I = 1.0$

X_{MgCl_2}	$\log \gamma_{HCl}$		
	IC(II)	IC(I)	Eq. (1)
0.25	$\bar{1}.901$	$\bar{1}.896$	$\bar{1}.899$
0.50	$\bar{1}.891^a$	$\bar{1}.884$	$\bar{1}.888$
0.75	$\bar{1}.876$	$\bar{1}.872$	$\bar{1}.882$
X_{HCl}	$\log \gamma_{MgCl_2}$		
	IC(II)	IC(I)	Eq. (1)
0.25	$\bar{1}.676$	$\bar{1}.681$	$\bar{1}.694$
0.50	$\bar{1}.692$	$\bar{1}.696$	$\bar{1}.711$
0.75	$\bar{1}.725$	$\bar{1}.710$	$\bar{1}.729$

[a]NE value is $\bar{1}.887$.

comparison with the fitted values [IC(II)], Eq. (1) predicts $\log \gamma_{HCl}$ better than IC(I) at ionic strength fractions of $MgCl_2$ equal to 0.25 and 0.5. At X_{MgCl_2} equal to 0.75 the values predicted by the two methods fall on opposite sides of the fitted value. In the case of the $\log \gamma_{MgCl_2}$ values the IC(I) predictions are better at the lower two fractions of acid, while the value predicted by Eq. (1) is better at the highest fraction of acid.

The use of Eq. (1) is not restricted to solutions containing only two electrolytes. In Fig. 6.10 are shown the results obtained in a series of mixtures, each containing HCl, an alkali metal chloride, and an alkaline-earth metal chloride. In all cases the ionic strength fraction of the HCl is 0.5, while the ionic strength fraction of each salt is 0.25. Only the HCl-NaCl-$MgCl_2$[6] and the HCl-CsCl-$BaCl_2$[7] systems have been studied experimentally. Hence $\log \gamma$ values for each component in these two systems calculated from parameters obtained by fitting the experimental data by least squares using both the neutral-electrolyte and the ion-component models are shown. Note that the values predicted by Eq. (1) are very close to the measured values in each case and about the same as the IC(I) predictions.

In the HCl-KCl-$CaCl_2$ system all three two-electrolyte systems have been studied,[8] and the squares [IC(II)] show $\log \gamma$ values predicted using these data and data on the pure components. Note that the values calculated using Eq. (1) are again very close to the fitted values [IC(II)] and to the IC(I) predictions.

In the HCl-RbCl-$SrCl_2$ system both $\log \gamma$ values shown for each component are predicted from pure component data only. Both methods of prediction,

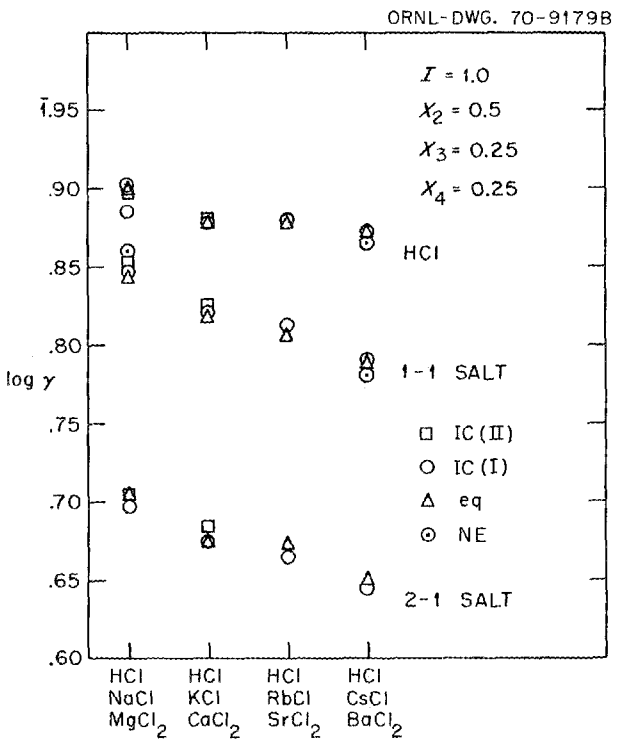

Fig. 6.10. Activity coefficient behavior in HCl-NaCl-$MgCl_2$, HCl-KCl-$CaCl_2$, HCl-RbCl-$SrCl_2$, and HCl-CsCl-$BaCl_2$ mixtures. $X_2 = X_{HCl}$, $X_3 = X_{MCl}$, $X_4 = {}_{MCl_2}$.

IC(I) and Eq. (1), give about the same log γ values for each component, and these values are consistent with the values in the adjacent systems.

Finally we consider the activity coefficients of HCl, NaCl, and $MgCl_2$ in HCl-NaCl-$MgCl_2$ mixtures at $I = 1.0$ as a function of total salt fraction in the mixtures. These results are shown in Table 6.4. Here we have a direct comparison of log γ values for each component calculated from parameters obtained by fitting the experimental data by least squares using both the neutral-electrolyte and the ion-component models. In most cases the neutral-electrolyte values are a little higher than the ion-component values. Both methods of prediction, Eq. (1) and IC(I), give comparable values for log γ_{NaCl} in the mixtures. However, in the case of both the HCl and the $MgCl_2$ the activity coefficient values predicted by Eq. (1) are closer to the fitted values [IC(II)] than are the IC(I) predicted values. This is especially striking in the case of the unsymmetrical electrolyte $MgCl_2$.

The results of the calculations show that, at least in the case of the mixtures investigated, the very simple Eq. (1) may be used to predict remarkably well the activity coefficient of each component. This is true even when the mixtures contain unsymmetrical electrolytes. In most cases the log γ values predicted by Eq. (1) are about as good as or better than values predicted using the more elaborate ion-component model.

Table 6.4. Activity coefficients of HCl, NaCl, and $MgCl_2$ in HCl-NaCl-$MgCl_2$ mixtures at $I = 1.0$

$X_3 + X_4$ ($X_3 = X_4$)	log γ_{HCl} NE	IC(II)	IC(I)	Eq. (1)
0.25	$\bar{1}.910$	$\bar{1}.903$	$\bar{1}.897$	$\bar{1}.898$
0.50	$\bar{1}.901$	$\bar{1}.894$	$\bar{1}.885$	$\bar{1}.888$
0.75	$\bar{1}.892$	$\bar{1}.884$	$\bar{1}.873$	$\bar{1}.878$
$X_3 + X_4$ ($X_3 = X_4$)	**log γ_{NaCl} NE**	**IC(II)**	**IC(I)**	**Eq. (1)**
0.25	$\bar{1}.876$	$\bar{1}.869$	$\bar{1}.854$	$\bar{1}.853$
0.50	$\bar{1}.861$	$\bar{1}.854$	$\bar{1}.844$	$\bar{1}.843$
0.75	$\bar{1}.845$	$\bar{1}.839$	$\bar{1}.834$	$\bar{1}.833$
$X_3 + X_4$ ($X_3 = X_4$)	**log γ_{MgCl_2} NE**	**IC(II)**	**IC(I)**	**Eq. (1)**
0.25	$\bar{1}.727$	$\bar{1}.731$	$\bar{1}.710$	$\bar{1}.726$
0.50	$\bar{1}.708$	$\bar{1}.704$	$\bar{1}.695$	$\bar{1}.706$
0.75	$\bar{1}.690$	$\bar{1}.684$	$\bar{1}.680$	$\bar{1}.686$

1. G. Scatchard, R. M. Rush, and J. S. Johnson, *J. Phys. Chem.* **74**, 3786 (1970).
2. H. S. Harned and B. B. Owen, *The Physical Chemistry of Electrolyte Solutions*, 3d ed., p. 607, Reinhold, New York, 1958.
3. N. Bjerrum, *Z Physik. Chem.* **104**, 406 (1923).
4. M. H. Lietzke and R. W. Stoughton, *J. Phys. Chem.* **67**, 2573 (1963).
5. M. H. Lietzke and R. W. Stoughton, *J. Tenn. Acad. Sci.* **39**, 30 (1964).
6. M. H. Lietzke and R. J. Herdklotz, *J. Inorg. Nucl. Chem.*, in press.
7. M. H. Lietzke, H. B. Hupf, and R. W. Stoughton, *J. Inorg. Nucl. Chem.* **31**, 3481 (1969).
8. M. H. Lietzke and H. A. O'Brien, Jr., *J. Phys. Chem.* **72**, 4408 (1968).

9. We thank Professor J. W. Cobble of Purdue University for encouragement and interesting discussions concerning this work.

PARAMETERS FOR CALCULATING THE ACTIVITY COEFFICIENT OF EACH COMPONENT IN HCl-RbCl, HCl-CsCl, HCl-$SrCl_2$, AND HCl-$BaCl_2$ MIXTURES TO IONIC STRENGTH 3

M. H. Lietzke M. T. Unger[1] M. D. Danford

Investigations of the activity coefficient behavior of both components in the aqueous systems HCl-RbCl,[2]

$HCl\text{-}SrCl_2$,[2] $HCl\text{-}CsCl$,[2] and $HCl\text{-}BaCl_2$[3] to total ionic strength unity ($I = 1$) have been previously reported. In these studies emf measurements of cells such as

$$Pt\text{-}H_2(p = 1)|HCl(m_2), MCl_x(m_3)|AgCl, Ag$$

were combined with literature data on the pure salt solutions to compute the activity coefficient of both components in the mixtures. Emf measurements have now been made in all of these systems at $I = 3$. These results have been combined with the previous data, and a set of parameters has been obtained describing in each case the activity coefficient behavior of both components in these mixtures to $I = 3$ as a function of temperature (from 25 to 75°C), total ionic strength, and fraction of each component in the mixtures. As before, the neutral-electrolyte treatment[2] has been used in fitting the data. In this treatment the logarithm of the activity coefficient of the HCl is given by

$$\log \gamma_{HCl} = \frac{-\mathring{A}_T\sqrt{I}}{1 + 1.5\sqrt{I}} + 2I\left[B_{22}(1 - x_3) + \frac{B_{23}}{a}x_3\right] + 3I^2\left[C_{222}(1 - x_3)^2 + 2\frac{C_{223}}{a}x_3(1 - x_3) + C_{233}\left(\frac{x_3}{a}\right)^2\right], \quad (1)$$

while that of the salt is given by

$$\log \gamma_{salt} = \frac{-|Z_+Z_-|\mathring{A}_T\sqrt{I}}{1 + 1.5\sqrt{I}} + bI\left[B_{23}x_2 + \frac{B_{33}}{a}(1 - x_2)\right] + cI^2\left[C_{223}x_2^2 + 2\frac{C_{233}}{a}x_2(1 - x_2) + C_{333}(1 - x_2)^2\right]. \quad (2)$$

In these equations x_2 and x_3 are the ionic strength fractions of the acid and salt respectively. The values of a, b, and c for the various systems are shown in Table 6.5. The value of the limiting slope $\mathring{A}_T$, which is temperature dependent, was computed as before.[2] The temperature dependence of the B_{2j} coefficients was expressed as

$$B_{2j} = B'_{2j} + B''_{2j}/T + B'''_{2j}\left[\frac{T - T_0}{T} - \ln\frac{T}{T_0}\right] \quad (3)$$

Table 6.5. Values of a, b, and c for Eqs. (1) and (2)

System	a	b	c
HCl-RbCl, HCl-CsCl	1	2	3
$HCl\text{-}SrCl_2$, $HCl\text{-}BaCl_2$	3	4/3	2

Table 6.6. Parameters of the B and C coefficients of Eqs. (1) and (2)

HCl-RbCl		
$B'_{22} = 0.0835367$	$B''_{22} = -10.9595$	$B'''_{22} = 0.458531$
$B'_{23} = 0.572793$	$B''_{23} = -150.032$	$B'''_{23} = 2.44348$
$C'_{222} = 0.0264948$	$C''_{222} = -6.74428$	
$C'_{223} = -0.0839013$	$C''_{223} = 23.7117$	
$C'_{233} = -0.0075937$	$C''_{233} = -0.0030340$	
HCl-CsCl		
$B'_{22} = 0.0268850$	$B''_{22} = 8.33017$	$B'''_{22} = 0.131204$
$B'_{23} = 0.313654$	$B''_{23} = -71.7526$	$B'''_{23} = 0.996197$
$C'_{222} = -0.00285759$	$C''_{222} = 1.18733$	
$C'_{223} = -0.0199082$	$C''_{223} = 4.00433$	
$C'_{233} = -0.0230773$	$C''_{233} = 2.97280$	
$HCl\text{-}SrCl_2$		
$B'_{22} = 0.0615335$	$B''_{22} = -1.83625$	$B'''_{22} = 0.345937$
$B'_{23} = 0.920589$	$B''_{23} = -253.727$	$B'''_{23} = 1.55010$
$C'_{222} = -0.00405709$	$C''_{222} = 1.55710$	
$C'_{223} = -0.0885162$	$C''_{223} = 29.1768$	
$C'_{233} = -0.358096$	$C''_{233} = 108.938$	
$HCl\text{-}BaCl_2$		
$B'_{22} = 0.0672304$	$B''_{22} = -4.30355$	$B'''_{22} = 0.38324$
$B'_{23} = 0.163624$	$B''_{23} = -33.1578$	$B'''_{23} = 0.574580$
$C'_{222} = -0.00802180$	$C''_{222} = 2.87953$	
$C'_{223} = 0.00102184$	$C''_{223} = -0.303276$	
$C'_{233} = -0.0886089$	$C''_{233} = 41.2068$	

At 25°C only

	B_{33}	C_{333}
HCl-RbCl	−0.0253282	0.00607747
HCl-CsCl	−0.0428693	0.00781711
$HCl\text{-}SrCl_2$	0.104545	0.006354318
$HCl\text{-}BaCl_2$	0.1707873	0.06586335

and that of the C_{2jk} coefficients as

$$C_{2jk} = C'_{2jk} + C''_{2jk}/T. \quad (4)$$

The rationale of the form of these terms has been discussed previously[2] and will not be repeated here. The B_{33} and C_{333} coefficients, which refer in each case to solutions containing only the salt in water, were determined at 25°C only.

Values of the parameters for the B_{2j} and C_{2jk} coefficients as determined by least squares are shown in Table 6.6. The parameters are valid in the temperature range 25 to 75°C to $I = 3$.

1. Oak Ridge Associated Universities summer student trainee from Huntington College, Huntington, Ind., Summer 1970.
2. M. H. Lietzke and H. A. O'Brien, Jr., *J. Phys. Chem.* **72**, 4408 (1968).
3. M. H. Lietzke and R. W. Stoughton, *J. Phys. Chem.* **70**, 756 (1966).

OSMOTIC AND ACTIVITY COEFFICIENTS FOR MIXTURES OF CESIUM CHLORIDE AND BARIUM CHLORIDE IN WATER AT 25°

S. Lindenbaum[1] R. M. Rush

The free energies in the system $CsCl$-$BaCl_2$-H_2O have been investigated by the isopiestic method. Activity coefficients were obtained by both the Scatchard treatment and the McKay-Perring treatment. "Trace" activity coefficients (activity coefficient of one component in a pure solution of the other component) calculated by the two methods differ by as much as 0.04 in log γ (10% in γ) at high concentrations (ionic strength ca. 3). This difference is greater than that expected from the experimental error and cannot be readily explained. A report of these results has been submitted for publication.[2]

1. Director's Division.
2. Submitted to *J. Chem. Thermodyn.*

ESTIMATION OF SOLUTE ACTIVITY COEFFICIENTS IN DILUTE AQUEOUS MIXTURES AT 25°: COMPARISONS WITH PREDICTIONS FROM THE GUGGENHEIM THEORY OF SOLUTIONS[1]

G. E. Boyd[2] S. Lindenbaum[2] R. A. Robinson[3]

Mean molal solute activity coefficients, $\gamma_\pm$, in *dilute* aqueous electrolyte mixtures were predicted with Guggenheim's theory[4] of solutions for the system $NaBr$-$ZnBr_2$-H_2O. The predicted $\gamma_\pm$ were compared with values derived by applying the McKay-Perring equation[5] to experimentally measured isopiestic concentrations for the same ternary mixtures. The concentration dependence of $\gamma_\pm$ for NaBr (B) and $ZnBr_2$ (C) in mixtures of constant total ionic concentration

$$m = m_B + 1.5m_C$$

is described quantitatively by the equations:

$$\log \gamma_B = \log \gamma_{B(0)} - \alpha_B m_C - \beta_B m_C^2 \quad (1)$$

and

$$\log \gamma_C = \log \gamma_{C(0)} - \alpha_C m_B - \beta_C m_B^2 \quad (2)$$

respectively. The absolute values of α_B and α_C increase strongly as m decreases (Fig. 6.11, in which $m \approx M_B$) and the quadratic interaction coefficients, $\beta_B = -0.20$ and $\beta_C = -0.23$, are independent of m and surprisingly large. Agreement between the activity coefficients predicted by

$$\log \gamma_B = \log \gamma_{B(0)} - F_C[(2/3) \log \gamma_{B(0)} - (3/8) \log \gamma_{C(0)} + (1/12) \log \gamma^{st}] \quad (3)$$

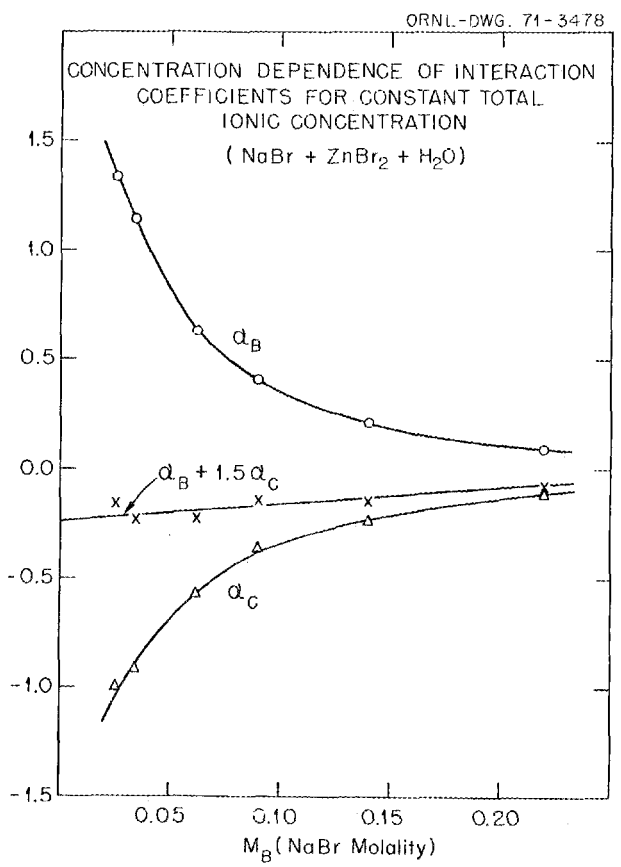

Fig. 6.11. Concentration dependence of Harned interaction coefficients for ternary $NaBr$-$ZnBr_2$-H_2O mixtures at 25° and constant total ionic concentration.

Table 6.7. Comparison of predicted (G) and observed (MKP) solute activity coefficients for NaBr and $ZnBr_2$ present at trace concentrations in their aqueous mixtures at 25°C

$I = 3m_C$	$-\log \gamma_{NaBr}{}^{G}$, Eq. (3)	$-\log \gamma_{NaBr}{}^{MKP}$, Eq. (1)	Δ
0.0543	0.0803	0.0856	−0.0053
0.0737	0.0889	0.0968	−0.0079
0.1346	0.1068	0.1128	−0.0060
0.1937	0.1176	0.1192	−0.0016
0.3011	0.1305	0.1292	+0.0013
0.4645	0.1410	0.1338	+0.0072
$I = m_B$	$-\log \gamma_{ZnBr_2}{}^{G}$, Eq. (4)	$-\log \gamma_{ZnBr_2}{}^{MKP}$, Eq. (2)	Δ
0.0253	0.1220	0.1343	−0.0123
0.0341	0.1364	0.1450	−0.0086
0.0620	0.1681	0.1757	−0.0076
0.0896	0.1892	0.1995	−0.0103
0.1401	0.2159	0.2224	−0.0065
0.2196	0.2430	0.2271	+0.0159

and

$$\log \gamma_C = \log \gamma_{C(0)} - (1 - F_C)[(1/4) \log \gamma_{C(0)} - (2/3) \log \gamma_{B(0)} + (1/6) \log \gamma^{st}] , \quad (4)$$

where F_C is the ionic strength fraction of electrolyte C (=$ZnBr_2$) in the mixture of total ionic strength I, and those derived from experiment [i.e., Eqs. (1) and (2)] is better than 2% for $I \leqslant 0.45$ (cf. Table 6.7). The quantity γ^{st} in Eqs. (3) and (4) is defined by

$$\log \gamma^{st} = -z_i^2 A I^{1/2}/(1 + 1.5 I^{1/2}) , \quad (5)$$

where z_i is the charge on the ith ion and $A = 0.5171$ is the Debye-Hückel constant.

1. Expanded abstract of paper accepted for publication in *J. Phys. Chem.* (1971).
2. Director's Division.
3. Visiting Professor of Chemistry, University of Florida, Gainesville.
4. E. A. Guggenheim, *Phil. Mag.* 19, 588 (1935).
5. H. A. C. McKay and J. K. Perring, *Trans. Faraday Soc.* 49, 163 (1953).

HEATS OF DILUTION OF AQUEOUS SOLUTIONS OF SODIUM SALTS OF CARBOXYLIC ACIDS[1]

Siegfried Lindenbaum[2]

Many studies of solution properties of tetraalkylammonium salts in aqueous solution have been reported in recent years.[3-5] The results have been interpreted in terms of the effect the hydrocarbon chains have on the solvent. Just as pure hydrocarbons dissolved in water cause increased hydrogen bonding in the solvent, so do hydrocarbon chains attached to a central nitrogen promote increased structure in water as suggested by the thermodynamic properties of aqueous solutions of tetraalkylammonium salts.[3] Large exothermic heats of dilution of these salts have been reported, and it has been suggested that these heats are a measure of the increase in structure or hydrogen bonding in the solvent on dilution.[6,7] It was the purpose of this study to determine whether a similar structure-making effect could be observed with a salt of an ion having hydrocarbon chains attached to a negatively charged atom. A good anionic analog of a tetraalkylammonium cation is not available in that no water-soluble negatively charged ion having hydrocarbon chains attached on four sides has been reported. Sodium salts of carboxylic acids were chosen for this study because they are water soluble and provide the means whereby the effect of the interaction of long hydrocarbon chains with solvent may be observed. A brief summary of some of these results was reported recently.[8]

The values of the heat of dilution, ϕ_L, determined in this study of aqueous solutions of sodium butyrate (C_4), valerate (C_5), heptylate (C_7), and pelargonate (C_9) were combined with the osmotic and activity coefficient data of Smith and Robinson[9] to calculate excess apparent molal thermodynamic functions according to the following equations:[10]

$$H^{EX} \equiv \phi_L , \quad (1)$$

$$G^{EX} = 2RT(1 - \phi + \ln \gamma) , \quad (2)$$

$$TS^{EX} = H^{EX} - G^{EX} , \quad (3)$$

where ϕ and γ are the osmotic and activity coefficients, respectively, and S^{EX}, H^{EX}, and G^{EX} are the excess apparent molal entropy, enthalpy, and free energy. These quantities are plotted as a function of concentration in Fig. 6.12. The values of ϕ_L for sodium acetate (C_2) were obtained from the compilation of Parker.[11]

The excess entropy and enthalpy functions increase as the number of carbon atoms in the anion increases. At high concentrations for the longer chain carboxylates, TS^{EX} and H^{EX} level off, and for C_9 there is even a maximum. It is believed for these longer-chain carboxylates that aggregation or micelle formation is responsible for this leveling effect. The increase of

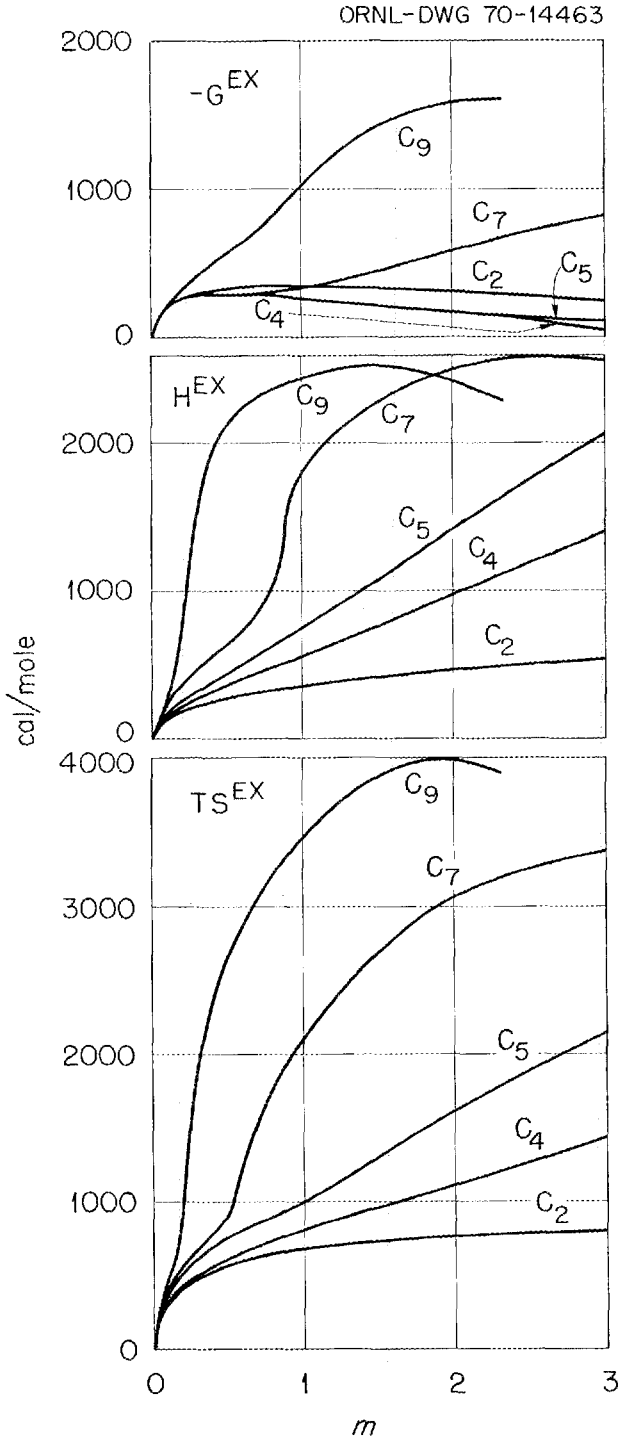

Fig. 6.12. Excess apparent molal thermodynamic functions for aqueous solutions of sodium salts of carboxylic acids at 25°C. C_2, C_4, C_5, C_7, and C_9 represent sodium acetate, butyrate, valerate, heptylate, and pelargonate respectively.

TS^{EX} and H^{EX} with the number of carbon atoms on the carboxylate chain is similar to the behavior found for the tetraalkylammonium salts. In both cases, the larger the number of methylene groups introduced into the solvent, the larger the values of H^{EX} and TS^{EX}. This suggests that in both cases the hydrophobic alkyl chains cause increased solvent hydrogen bonding of the water molecules.

---

1. Expanded abstract of paper accepted for publication in *J. Chem. Thermodyn.* (1971).
2. Director's Division.
3. H. S. Frank and W-Y. Wen, *Discuss. Faraday Soc.* **24**, 133 (1957).
4. J. E. Prue, A. J. Read, and G. Romeo, *Hydrogen-Bonded Solvent Systems,* ed. by A. K. Covington and P. Jones, Taylor and Francis, London, 1968.
5. F. Franks, ibid.
6. S. Lindenbaum, *J. Phys. Chem.* **70**, 914 (1966).
7. R. H. Wood et al., ibid. **71**, 2149 (1967).
8. S. Lindenbaum, ibid. **74**, 3027 (1970).
9. E. R. B. Smith and R. A. Robinson, *Trans. Faraday Soc.* **38**, 70 (1942).
10. H. L. Friedman, *J. Chem. Phys.* **32**, 1351 (1960).
11. V. B. Parker, *Thermal Properties of Aqueous Uni-Univalent Electrolytes,* NSRDS-NBS 2, National Bureau of Standards, Washington, D.C., 1965.

THERMODYNAMICS OF AQUEOUS SOLUTIONS OF TETRABUTYLAMMONIUM CARBOXYLATES. MODEL SYSTEMS FOR THE HYDROPHOBIC INTERACTION IN PROTEINS[1]

Siegfried Lindenbaum[2]

Studies of thermodynamic and other properties of aqueous solutions of tetraalkylammonium salts[3-6] and salts of carboxylic acids[7-9] have suggested that these electrolytes, possessing hydrophobic moieties in their structure, cause increased hydrogen bonding of the solvent. This apparent increased solvent structure in aqueous solutions has been most pronounced for solutions of salts which also form crystalline clathrate hydrates. Tetra-*n*-butylammonium fluoride, for example, forms a clathrate hydrate with composition $Bu_4NF \cdot 32.8H_2O$.[10] Thermodynamic studies of aqueous solutions of Bu_4NF[5,11] have strongly supported the suggestion[6] that tetrabutylammonium ions increase hydrogen bonding in the solvent. Further evidence that this interpretation is correct comes from recent x-ray scattering measurements on aqueous solutions of Bu_4NF.[12] The radial distribution function determined in this study was accurately fitted by a model in which it was assumed that the fluoride ion was

indistinguishable from an oxygen atom. The fluoride ion apparently does not interfere, or interferes only minimally, in the formation of the hydrogen-bonded water cage around the hydrophobic tetrabutylammonium ion. The larger halide ions interfere in this hydrophobic structure formation to an increasing extent.[13] This structure formation, as measured by apparent molal heat content,[4] is greatest for tetrabutylammonium fluoride and diminishes as the size of the halide ion increases and becomes less compatible with the water structure.

The purpose of this study was to determine how the hydrophobic nature of tetraalkylammonium ions would manifest itself in the thermodynamic properties of aqueous solutions if the negatively charged counterion also possessed hydrophobic properties.

Exothermic heats of dilution increasing with hydrocarbon chain length[8,9] were measured for sodium salts of carboxylic acids. Straight-chain carboxylate ions are also apparently effective in increasing the hydrogen bonding of water. It was therefore of great interest to determine the effect on aqueous solvent thermodynamic properties of solutions of tetraalkylammonium carboxylates, salts in which both cationic and anionic moieties have hydrophobic water-structure-enhancing properties. Some of these salts, for example, tetra-*n*-butylammonium butyrate and tetra-*n*-butylammonium valerate, also form crystalline clathrate hydrates,[14] suggesting that in aqueous solution these salts will also increase the hydrogen bonding of the solvent. Since both the cation and anion contribute to the hydrophobic solvent hydrogen bonding or "hydration of the second kind,"[15] it might be speculated that the heats of dilution of these solutions would be more negative than those of tetrabutylammonium fluoride.

However, it has also been suggested that a special "water-structure-enforced ion pairing"[16] occurs when both cation and anion are large and hydrophobic. If this interaction persisted in dilute solutions of these salts, the net interaction with the solvent would be diminished, and the enthalpy of dilution would be smaller than that observed for tetrabutylammonium fluoride.

Apparent molal heat contents, ϕ_L, and osmotic and activity coefficients at 25° were determined in this investigation for aqueous solutions of Bu_4N butyrate, Bu_4N valerate, Bu_4N heptylate, Bu_4N pelargonate, and Bu_4N caprate. These data were used to calculate excess enthalpies, H^{EX}, free energies, G^{EX}, and entropies, S^{EX}, according to the following equations:[17]

$$H^{EX} = \phi_L \,, \tag{1}$$

$$G^{EX} = 2RT(1 - \phi + \ln \gamma) \,, \tag{2}$$

$$TS^{EX} = H^{EX} - G^{EX} \,. \tag{3}$$

A plot of the concentration dependence at 25° of these three thermodynamic excess properties is given in Fig. 6.13 for five tetrabutylammonium carboxylates and also for tetrabutylammonium fluoride to serve as a basis for comparison. The osmotic and activity coefficients required for the calculation of G^{EX} for Bu_4NF were taken from the paper of Wen, Saito, and Lee.[11] The apparent molal heat contents of aqueous solutions of Bu_4NF have also been reported.[5]

The apparent molal heat contents of aqueous solutions of tetrabutylammonium carboxylates are larger than those of any other 1-1 electrolyte reported in the literature. These exothermic heats of dilution are attributed to the formation of more complete hydrogen-bonded water cages as water is added in the dilution process. The increase of ϕ_L with concentration for tetraalkylammonium halides has been attributed[18,19] to an increase in the overlap of the hydration cages with concentration. This overlap is even greater for tetrabutylammonium carboxylates since both cations and anions compete for the available water molecules to form hydration spheres. For this reason,

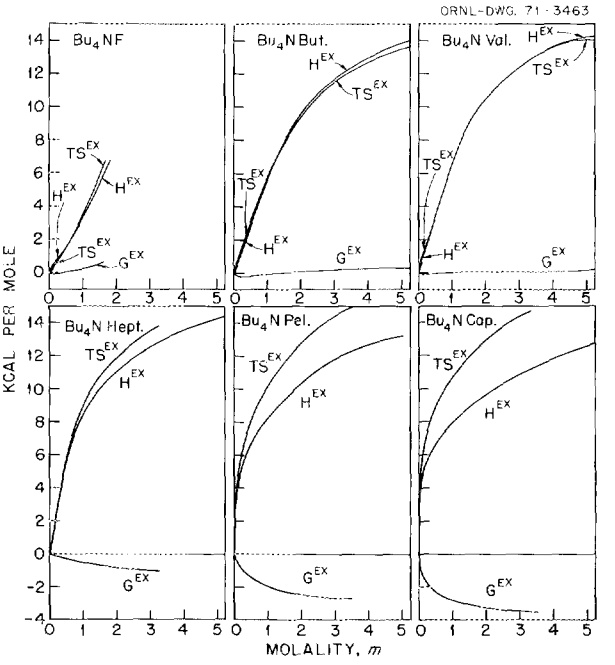

Fig. 6.13. Excess thermodynamic functions vs molality for aqueous solutions of tetrabutylammonium carboxylates at 25°.

ϕ_L for Bu_4NBut at a given molality is far greater than the sum of ϕ_L for Bu_4NF[4] and ϕ_L for NaBut[9] at the same molality.[8]

These large values of ϕ_L or H^{EX} (Fig. 6.13) are also paralleled by large values of TS^{EX}. This change in entropy on dilution is a measure of the increased structure or order in the solution per mole of solute for the transition from the overlap (disorder) condition in concentrated solution to the completed hydrophobic hydration sphere (ordered) condition at infinite dilution.

The magnitude of TS^{EX} increases with the carboxylate chain length over the entire concentration range. H^{EX} is almost identical with TS^{EX} for Bu_4NBut and Bu_4NVal over the concentration range studied. In concentrated solution, H^{EX} decreases with increasing carboxylate chain length, and G^{EX} becomes more negative. These lower values for G^{EX} at higher concentrations also suggest increased association or overlap as the size of the anion increases.

Hydrophobic Bonding

The interaction between hydrophobic species in aqueous solutions may be compared to the interaction between neighboring nonpolar groups in the native conformation of proteins. It has been suggested by Kauzmann[20] that the hydrophobic moieties are attracted and stabilized in the native conformation because of the unfavorable negative entropy change accompanying the interaction of these unfolded hydrophobic groups with the solvent. This solvent-induced stabilization has been referred to as "hydrophobic bonding" or, more correctly, the "hydrophobic interaction." Theoretical calculations[21-23] and thermodynamic studies[23] have tended to support this mechanism.

Our interpretation of the thermodynamics of dilution of aqueous solutions of tetrabutylammonium carboxylates is similar to the "hydrophobic interaction" interpretation of protein denaturation. Concentrated solutions of Bu_4NBut, for example, with extensive overlap of hydration spheres or possibly ion association, may be compared to a protein in its native configuration. The dilution process for Bu_4NBut solutions is accompanied by a loss in entropy due to the formation or completion of hydration spheres; this process is analogous to the denaturation process in which nonpolar groups on a protein are exposed to the solvent, leading to the formation of hydrogen-bonded water cages. The thermodynamics of dilution of Bu_4N carboxylate solutions and the denaturation of proteins suggest a disorder-order transition. Aqueous solutions of tetrabutylammonium carboxylates may therefore serve as model systems for proteins stabilized in their native configuration by the "hydrophobic interaction."

1. Expanded abstract of paper submitted for publication in *J. Phys. Chem.* (1971).
2. Director's Division.
3. S. Lindenbaum and G. E. Boyd, *J. Phys. Chem.* **68**, 911 (1964).
4. S. Lindenbaum, ibid. **70**, 814 (1966).
5. S. Lindenbaum, ibid. **73**, 4334 (1969).
6. H. S. Frank, *Z. phys. Chem. (Leipzig)* **228**, 367 (1965).
7. H. Snell and J. Greyson, *J. Phys. Chem.* **74**, 2148 (1970).
8. S. Lindenbaum, ibid. **74**, 3027 (1970).
9. S. Lindenbaum, *J. Chem. Thermodyn.*, accepted for publication.
10. R. K. McMullan, M. Bonamico, and G. A. Jeffrey, *J. Chem. Phys.* **39**, 3295 (1963).
11. W-Y. Wen, S. Saito, and C. Lee, *J. Phys. Chem.* **70**, 1244 (1966).
12. A. H. Narten and S. Lindenbaum, *J. Chem. Phys.* **51**, 1108 (1969).
13. (*a*) J. E. Desnoyers et al., *J. Phys. Chem.* **73**, 3346 (1969); (*b*) A. H. Narten, ibid. **74**, 765 (1970).
14. G. Beurskens, G. A. Jeffrey, and R. K. McMullan, ibid. **39**, 3311 (1963).
15. H. G. Hertz and M. D. Zeidler, *Ber. Bunsenges. Phys. Chem.* **68**, 82 (1964).
16. R. M. Diamond, *J. Phys. Chem.* **67**, 2153 (1963).
17. H. L. Friedman, *Ionic Solution Theory*, Interscience, New York, 1962.
18. R. H. Wood et al., *J. Phys. Chem.* **71**, 2149 (1967).
19. R. H. Wood and H. L. Anderson, ibid. **71**, 1871 (1967).
20. W. Kauzmann, *Advan. Protein Chem.* **14**, 1 (1959).
21. G. Nemethy and H. A. Scheraga, *J. Phys. Chem.* **66**, 1773 (1962).
22. G. Nemethy, *Angew. Chem. Int. Ed. Engl.* **6**, 195 (1967).
23. J. F. Brandts and L. Hunt, *J. Amer. Chem. Soc.* **89**, 4826 (1967).

THE EFFECT OF DIMETHYL SULFOXIDE (DMSO) ON HYDROPHOBIC INTERACTIONS: HEATS OF DILUTION OF TETRABUTYLAMMONIUM BROMIDE IN THE MIXED SOLVENT SYSTEM WATER-DMSO

M. J. Mastroianni[1] M. J. Pikal[1] S. Lindenbaum[2]

The physical properties of aqueous and nonaqueous solutions containing large organic ions, especially tetraalkylammonium ions,[3-7] have suggested that these ions "promote structure" via increased hydrogen bonding in these solvents. One would then expect mixed solvents that consist of water and some aprotic solvent to have inherently less structure than pure water, and thus the effect of tetraalkylammonium ions would not be as

pronounced in such mixed solvents. The purpose of this study was to determine the effect of increasing DMSO concentration on the heats of dilution of tetrabutylammonium bromide in DMSO-H_2O solvent systems. We are eventually interested in comparing the effect of a poor protein denaturant (DMSO) with the effect of a good denaturant (i.e., urea).

We have measured the heats of dilution of several mixed solvent solutions of tetrabutylammonium bromide at 25°C. The correction term to infinite dilution is given by

$$\Delta H^{\circ}{}_{D} = -\frac{2}{3}\delta_H \sqrt{m}\,, \tag{1}$$

where $\Delta H^{\circ}{}_{D}$ is the correction to infinite dilution, m is the molality, and δ_H is the Debye-Hückel limiting law slope, which may be calculated. The measured heats of dilution were then corrected to infinite dilution to yield apparent molal heat contents ϕ_L. Data for ϕ_L at one aquamolal Bu_4NBr vs mole fraction DMSO are given in Fig. 6.14. Aquamolality, m_a, is defined by

$$m_a = \frac{n_2}{n_{01}}\,\frac{1000}{M_0}\,, \tag{2}$$

where n_2 is moles of solute, M_0 is molecular weight of water, and n_{01} is the total number of moles of mixed solvent. The limiting law slopes, δ_H, vs mole fraction DMSO are given in Fig. 6.15. The Debye-Hückel limiting law slope, δ_H, is given by

$$\delta_H = -\frac{3}{2}RT^2\left[\frac{\pi N_0 e^6}{1000}\right]^{1/2}\left[\frac{\Sigma \nu_i z_i^2}{kDT}\right]^{3/2} \times \rho^{1/2}\left[\frac{1}{D}\frac{\partial D}{\partial T} + \frac{1}{3V}\frac{\partial V}{\partial T} + \frac{1}{T}\right], \tag{3}$$

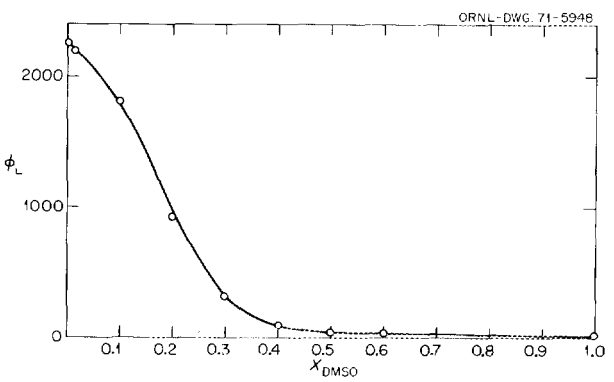

Fig. 6.14. Apparent molal heat contents of aquamolal tetrabutylammonium bromide in the mixed solvent system H_2O-DMSO at 25°C.

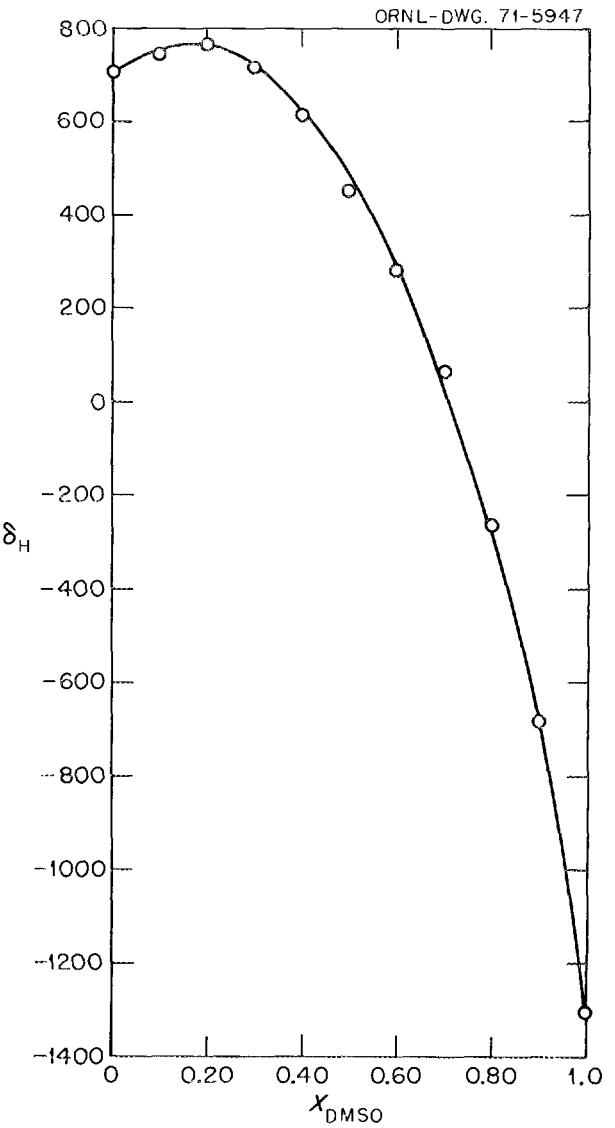

Fig. 6.15. Theoretical Debye-Hückel limiting slope in the mixed solvent system H_2O-DMSO at 25°C.

where ν_i is the number of ions put into solution by the solute, z_i the respective charges on cations and anions, ρ the density of the solvent, D the dielectric constant, and V the molal volume of the solvent. The other terms have their usual meanings.

It should be noted that these are the first negative Debye-Hückel slopes to be reported.[8] This negative slope is caused by the small negative value of $\partial D/\partial T$ for this system; most other systems have a highly negative $\partial D/\partial T$, which gives rise to a positive δ_H.

The ϕ_L data shown in Fig. 6.14 fall off quite rapidly up to ~0.35 mole fraction DMSO and remain fairly

constant (and small) at the higher DMSO concentrations. The 0.35 mole fraction region is where a 2:1 water:DMSO complex probably exists; the existence of this complex is supported by:

1. the fact that the point of greatest deviation from a straight line connecting the density of pure water with that of pure DMSO occurs at $X_{DMSO} = 0.33$;
2. the viscosity maximum and the point of greatest deviation from a straight line between the pure solvents occur at $X_{DMSO} = 0.3 \rightarrow 0.4$;
3. the heat of mixing per mole of solution has an exothermic maximum between $X_{DMSO} = 0.3$ and 0.4;
4. the thermodynamic excess function, $T\ \Delta S^{EX}$, is negative for all DMSO-water solutions and passes through a minimum value at $X_{DMSO} = 0.3$ to 0.4;
5. finally, the temperature coefficient $d \ln D/dT$ for the temperature range 15 to 35° is relatively insensitive to solvent change until $X_{DMSO} \sim 0.35$.[9]

We may interpret the ϕ_L data as follows: DMSO disrupts water structure only slightly at low DMSO levels ($X_{DMSO} \sim 0.05$). However, above $X_{DMSO} \sim 0.1$, the "degree of water structure" decreases rapidly as the DMSO level is increased until $X_{DMSO} = 0.33$. Here, the water is "bound" with DMSO, the "water structure" is completely destroyed, and the hydrophobic $(Bu)_4N^+$ ion can no longer "increase water structure."

The interpretation is consistent with the fact that DMSO is a poor protein denaturant. According to popular concepts, much of the stability of a protein in its native state arises because of the unfavorable entropy change which would result if denaturation took place (i.e., if hydrophobic chains were exposed to an aqueous environment, thereby causing an increase in water structure). Thus, a denaturant will be good if addition of a small amount of it will modify (or destroy) the water structure such that hydrophobic groups in the "aqueous" environment will no longer increase the water structure. In this case, ΔS for denaturation will no longer be unfavorable, and the denatured state will be thermodynamically stable. From the data presented here, we conclude that *large* amounts of DMSO are needed to prevent hydrophobic groups (butyl groups) from increasing the "structure" in the aqueous environment. Thus, from this interpretation, one would predict that DMSO would be a poor denaturant — in agreement with observation.

The next steps to be followed are (1) to look at the heat of dilution of an electrostrictive ion such as Li^+ in these solvents and (2) to look at heats of dilution of tetrabutylammonium bromide in a water–good-denaturant medium as a function of $X_{denaturant}$.

---

1. Visiting scientist from the Department of Chemistry, University of Tennessee.
2. Director's Division.
3. H. S. Frank and W-Y. Wen, *Discuss. Faraday Soc.* **24**, 133 (1957).
4. S. Lindenbaum and G. E. Boyd, *J. Phys. Chem.* **68**, 911 (1964).
5. S. Lindenbaum, ibid. **70**, 814 (1966).
6. R. L. Kay et al., ibid. **70**, 2336 (1966).
7. M. J. Mastroianni and C. M. Criss, ibid., to be published.
8. It appears that above 40°C, dimethylformamide also has a negative δ_H; private communication, C. M. Criss.
9. R. K. Wolford, *J. Phys. Chem.* **68**, 3392 (1964). This reference summarizes most of the work on DMSO-H_2O systems and contains conclusions and specific references.

TRACER DIFFUSION COEFFICIENTS OF HTO AND $^{36}Cl^-$ IN CATION EXCHANGERS

M. J. Pikal[1]

Tracer diffusion coefficients for the species HTO and $^{36}Cl^-$ were determined in sodium-form sulfonated polystyrene type (i.e., Dowex 50) cation exchangers of nominal 1.7, 4, and 8% divinylbenzene (DVB) at 25°C. A batch technique[2,3] was used for the diffusion measurements. The external aqueous phase was 0.22 *N* $NaNO_3$.

The purpose of this study is to provide diffusion data in sodium-form Dowex 50 type ion exchangers which may be directly compared with diffusion data in aqueous solutions of sodium *p*-ethylbenzenesulfonate,[4] a "model electrolyte" for exchangers of the Dowex 50 type.

The diffusion coefficients of HTO and $^{36}Cl^-$ in sodium *p*-ethylbenzenesulfonate (NapEBS) are compared with the corresponding data in the ion exchange resins in Fig. 6.16. The concentrations N_w are "weight normalities," or "molalities" (i.e., units of equivalents per kilogram of H_2O). It should be noted that diffusion of water (HTO) and co-ion ($^{36}Cl^-$) proceed slightly faster in the electrolyte solution (NapEBS) than in the ion exchanger at concentrations where the data overlap. However, the differences between the NapEBS data and the ion exchanger data are fairly small, particularly for $N_w \geqslant 3.0$. Moreover, the NapEBS and ion exchanger curves seem to approach one another as the concentration increases.

One feature of the ion exchange data which is not mirrored by the model electrolyte is the curious lack of dependence of D_{Cl^-} on concentration in the region

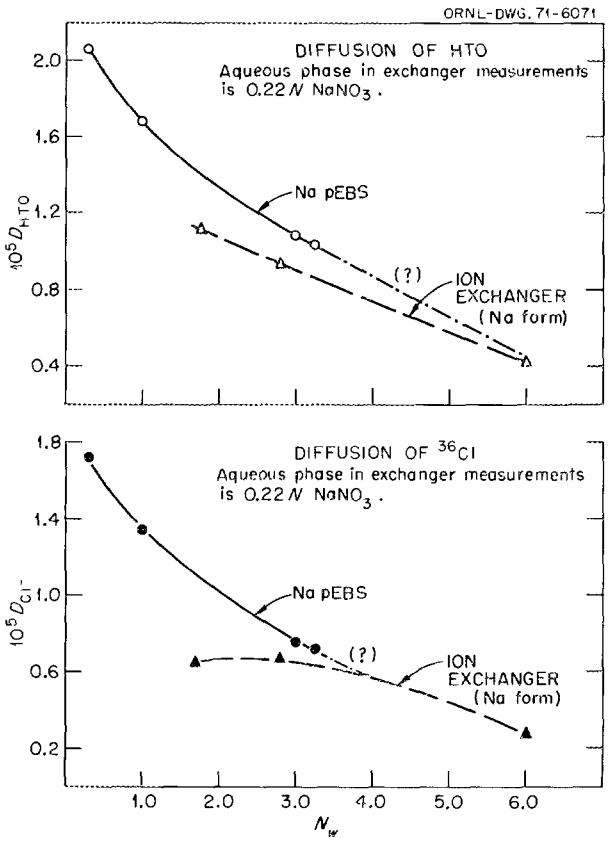

Fig. 6.16. Tracer diffusion coefficients for HTO and $^{36}Cl^-$ in sodium *p*-ethylbenzenesulfonate and in Dowex-50-type ion exchangers at 25°C.

between 1.5 and 3.5 *m*. Although this feature is believed to be real, no satisfactory theoretical explanation can be offered at present. Very careful equivalent water content measurements are currently in progress in an attempt to reduce the uncertainty in the N_w values for the ion exchangers. However, it is very unlikely that more accurate N_w data will alter the basic characteristics shown in Fig. 6.16.

1. Visiting scientist from the Department of Chemistry, University of Tennessee, Knoxville.

2. G. E. Boyd and B. A. Soldano, *J. Amer. Chem. Soc.* **75**, 6091 (1953).

3. G. E. Boyd and B. A. Soldano, ibid. **75**, 6105 (1953).

4. M. J. Pikal, *Chem. Div. Annu. Progr. Rep. May 20, 1970*, ORNL-4581, p. 100.

THEORY OF THE POROUS-FRIT METHOD OF MEASURING SELF-DIFFUSION CONSTANTS[1]

Lawrence Dresner

Nelson and co-workers[2–4] have developed a radiometric variant of the porous-frit method[5] of measuring self-diffusion constants. A porous frit is equilibrated with a solution containing a radioactive tracer. A solution of identical composition but not containing any tracer is then flowed past the surface of the frit. The radioactive tracer diffuses out of the frit into the flowing stream, while an equal amount of its nonradioactive counterpart diffuses in. The total activity of the frit decreases with time in a way that depends on the self-diffusion constant $\mathcal{D}$ of the tracer species in the solution.

The frits used by Nelson et al. are rectangular parallelepipeds much thinner than they are long or wide, and it is tempting to treat them as homogeneous slabs infinite in two directions. The tracer eluted from the slab is assumed to be swept away as soon as it appears at the surface of the frit. Under these assumptions, after an initial transient, the activity remaining in the frit decreases exponentially with a half-time $t_{1/2}$ related to $\mathcal{D}_{eff}$, the effective self-diffusion coefficient of the tracer in the frit, as follows:

$$\mathcal{D}_{eff} = \frac{\ln 2}{\pi^2} \frac{c^2}{t_{1/2}}, \qquad (1)$$

where c is the frit thickness.

Equation (1) is inaccurate for at least two reasons. First, the frit is not an infinite slab, but has a finite length and width which are, however, large compared with its thickness. The practical effect of this on Eq. (1) is to change the numerical constant slightly; detailed formulas for correcting the constant are given in the full report.[1] Second, the tracer eluted from the slab is not swept away as soon as it appears at the surface of the frit but (roughly speaking) must diffuse through an adherent layer of liquid into the main stream before being swept away. This increases the observed half-time above the value that should be inserted in Eq. (1) by an amount that depends on the hydrodynamic conditions near the frit. The necessary correction to the observed half-time has been calculated for a variety of laminar and turbulent flows, both for developing and fully developed concentration distributions. In addition, the effective self-diffusion coefficient of the tracer in the frit is smaller than the self-diffusion coefficient of the tracer in the eluting solution owing to the obstruction of the diffusing tracer by the solid parts of the frit. The extent of this obstruction effect has been estimated. Finally, the application of the equations to membranes instead of frits is indicated.[1]

1. Research jointly sponsored by the ORNL-NSF Environmental Program and by the Office of Saline Water, U.S. Department of the Interior, under Union Carbide Corporation's

contract with the U.S. Atomic Energy Commission. A full report of this work under the same title was published as ORNL-4667 in March 1971.

2. F. Nelson, *J. Polym. Sci.* **40**, 563 (1959).

3. F. Nelson and K. A. Kraus, pp. 191–213 in *Production and Use of Short-Lived Isotopes from Reactors*, vol. I, IAEA, Vienna, 1962.

4. A. E. Marcinkowsky, F. Nelson, and K. A. Kraus, *J. Phys. Chem.* **69**, 303 (1965).

5. F. T. Wall, P. F. Grieger, and C. W. Childers, *J. Amer. Chem. Soc.* **74**, 3562 (1952).

MASS TRANSPORT STUDIES[1]

F. Nelson R. J. Raridon
H. O. Phillips A. J. Shor[2]
K. A. Kraus[3]

During this year a variety of mass transport studies have been carried out. These included:

1. development of extrapolation procedures for measurement of self-diffusion coefficients by the porous-frit method,
2. effect of temperature on the calibration of the porous-frit method,
3. development of extrapolation procedures and general confirmation of hydrodynamic theory for self-diffusion coefficient measurements with porous tubes,
4. measurement of self-diffusion coefficients of simple ions in water-organic mixtures (Na^+ in glycerol triacetate and in polyacrylic acid),
5. development of techniques and evaluation of the hydrodynamic aspects of measurement of self-diffusion coefficients of counterions in ion exchange membranes under conditions where distribution coefficients are large,
6. hydrodynamic aspects of trace metal deposition in tubular systems [deposition of Hg(II) on copper tubes].

Several of these topics are briefly described below.

Development of the Porous-Frit Method – Effect of Temperature

In the porous-frit method for measurement of self-diffusion coefficients, a rectangular porous frit saturated with a solution containing a tracer of interest is placed into the center of a tube through which an identical solution not containing tracer is pumped. The rate of removal of the radioactive tracer is monitored, and diffusion coefficients are calculated, after appropriate calibration with a tracer of known diffusion coefficients. A flow regime has to be selected under which diffusional resistance in the boundary layer is small and reproducible, or extrapolation procedures to "infinite circulation velocities" need to be used. In many of our earlier studies, the former technique was applied; during this year, more emphasis was placed on development of extrapolation procedures. With proper extrapolations, it was hoped to increase the precision of the method and make it more broadly applicable, for example, to systems with widely differing viscosities, to systems with widely differing temperatures, and to systems such as thin adsorbing membranes where the resistance in the boundary layer is difficult to eliminate at reasonable pumping velocities. For all the extrapolation techniques, the equations developed by Dresner[4] were used. In the more difficult hydrodynamic cases, it appeared that a significant improvement in precision could be obtained by modifying the porous-frit technique by using instead of a suspended rectangular frit, a tubular system containing a snugly fitting cylindrical, hollow porous body. A few of the experiments carried out with this geometry are described in the following subsection.

In the extension of the porous-frit method to measurements as a function of temperature, one would expect that the frit constant, which is essentially the ratio of diffusion coefficients in the frit to those in a simple solution, would be independent of temperature, and that the temperature effect would be restricted to the boundary layer and hence could be eliminated by proper extrapolation procedures. In a series of self-diffusion experiments with Na^+ in ca. 0.1 and 1 *m* NaCl, it appeared that the diffusional half-lives vary linearly with $1/\sqrt{u}$, where u is the circulation velocity (see Fig. 6.17), as suggested by theory. From the intercepts at $1/\sqrt{u} = 0$ (corresponding to extrapolation to $u = \infty$), the apparent diffusion coefficients were computed as a function of temperature, using the 1 *m* NaCl point at 25°C for calibration.

For the 0.1 *m* NaCl series, the computed diffusion coefficients are compared in Table 6.8 with those computed from limiting ionic conductances through the Nernst equations ($\mathcal{D}_N$). The ratios $\mathcal{D}/\mathcal{D}_N$ are somewhat less than unity, qualitatively as expected from the dependence of self-diffusion coefficients on ionic strength. Correcting the "infinite dilution" diffusion coefficients for the effect of finite salt concentration by the method of Gosting and Harned[5] ($\mathcal{D}_{GH}$) yields values of $\mathcal{D}/\mathcal{D}_{GH}$ (see Table 6.8) approximately equal to unity. It thus appears that the assumption of invariance of the frit constant with temperature is valid

within experimental error. Under this assumption, self-diffusion coefficients of Na^+ in NaCl solutions were computed for the temperature range 15 to 85°C from the experimentally determined diffusional half-lives. The results are summarized in Table 6.9.

Mass Transport and Diffusion in Tubular Ion Exchange Systems

We have reported[6] previously on certain hydrodynamic aspects of adsorption of ions by cation exchange membranes under conditions where adsorbability of the ions was large, and hence the back reaction, diffusion from the membrane to the solution, negligible. The observed mass transfer rates as a function of tube length and solution flow rate were in excellent agreement with theory.[7]

During the current year we have investigated the more complex mass-transfer problem in which not only the hydrodynamic environment in the solution phase is important, but where also diffusion from the membrane to the solution must be considered. The tubular systems were made by lining small glass tubes with thin ion exchange membranes. The rates of exchange of radioactive sodium (^{24}Na) from the sodium form of the cation exchange membranes to contacting NaCl solutions were measured as a function of flow rate, aqueous salt concentration, membrane type, and membrane length. The salt concentration range was 0.08 to 5 M, which corresponds to a range of volume distribution coefficients D_v (amount per cubic centimeter of membrane/amount per cubic centimeter of solution) between 15 and 0.3. The membranes used were of the

Table 6.8. Comparison of measured diffusion coefficients ($\mathcal{D}$) for Na^+ in 0.1 m NaCl with those computed from conductance data ($\mathcal{D}_N$ and $\mathcal{D}_{GH}$)

Temperature (°C)	$\mathcal{D}/\mathcal{D}_N$	$\mathcal{D}/\mathcal{D}_{GH}$
15	0.957	1.020
25	0.938	1.000
40	0.928	0.994
60	0.915	0.984
85	0.944	1.019

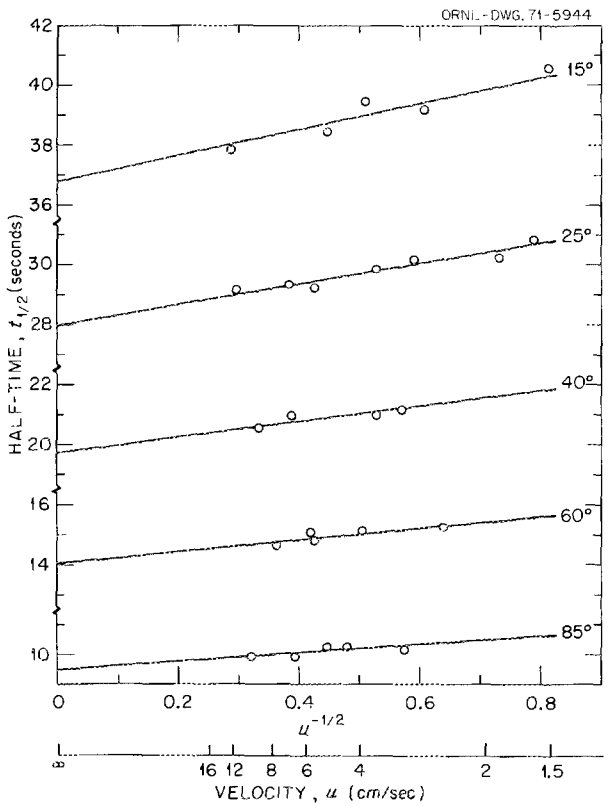

Fig. 6.17. Half-times for self-diffusion of Na^+ in 1.022 m NaCl as a function of temperature and circulation velocity.

Table 6.9. Self-diffusion coefficients of Na^+ in NaCl solutions

Temperature (°C)	0.10 m NaCl			1.022 m NaCl		
	$\mathcal{D} \times 10^5$ (cm²/sec)	Viscosity, η (cP)	$\mathcal{D}\eta \times 10^5$	$\mathcal{D} \times 10^5$ (cm²/sec)	Viscosity, η (cP)	$\mathcal{D}\eta \times 10^5$
15	0.98 ± 0.2[a]	1.147	1.13	0.94 ± 0.01[a]	1.232	1.16
25	1.25 ± 0.01	0.898	1.12	1.234[b]	0.977	1.21
40	1.76 ± 0.03	0.659	1.16	1.75 ± 0.04	0.725	1.27
60	2.54 ± 0.02	0.472	1.20	2.46 ± 0.06	0.524	1.29
85	3.84 ± 0.11	0.338	1.30	3.65 ± 0.04	0.378	1.38

[a]Standard error calculated from least-squares fit of data.
[b]Value taken from R. Mills, *J. Amer. Chem. Soc.* 77, 6116 (1955).

sulfonated polyethylene-polystyrene type (AMF C-60, Rust-Mason CC-60). In 0.1 M NaCl, these had a thickness of 0.32 and 0.070 mm, respectively, and capacities of ca. 0.9 and 1.25 meq per cubic centimeter of water-swollen membrane. Water contents, estimated from manufacturers' data, were ca. 29 and 50% of their water-swollen weights. Most of the exchange rates were measured under laminar flow conditions.

Typical data for the AMF C-60 membranes in 0.1 and 1 M NaCl are shown in Fig. 6.18, where the half-time for exchange, $t_{1/2}$, is plotted against $(l/u)^{1/3}$ (l = membrane length in centimeters, and u = linear flow velocity in centimeters per second). As expected from simplified theory,[4] $t_{1/2}$ varies linearly with $(l/u)^{1/3}$. Experiments with two different lengths of membrane, 1.52 and 5.00 cm, show that the rate of exchange depends on $l^{1/3}$. In these cases, extrapolation to $l/u = 0$ appears to permit meaningful estimation of $(t_{1/2})_\infty$ and hence of the diffusion coefficient in the membrane. The latter can be obtained from the equation for an infinite slab sealed on one face: $\mathcal{D} = 0.281d^2/t_{1/2}$, where d is thickness of the membrane. Values of $\mathcal{D}$ for this membrane were: 1.1, 0.95, and 0.38 $\times$ 10^{-6} cm^2/sec for the membrane immersed in 0.1, 1.0, and 5.0 M NaCl respectively.

As shown in Fig. 6.18, at a given flow rate the rate of exchange decreases rapidly with decreasing NaCl concentration and hence with increasing distribution coefficient. This is at least qualitatively in agreement with theory.

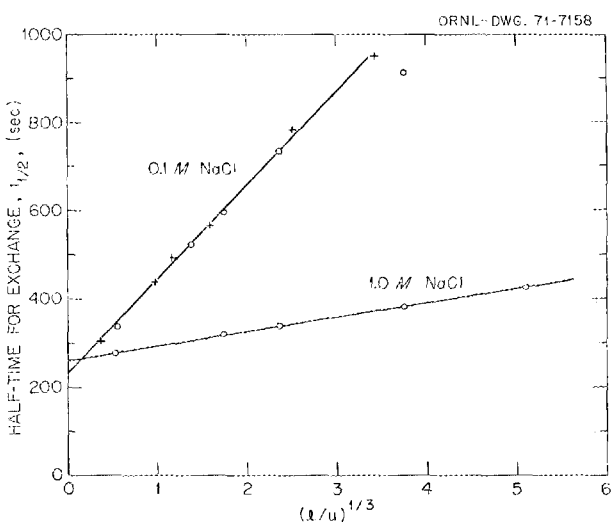

Fig. 6.18. Dependence of self-exchange of Na^+ in tubular cation exchange membranes on flow rate (u, cm/sec) and length (l, cm). Experimental conditions: AMF-C-60 membrane (0.30 mm); tube radius, 0.26 cm; 25°C. l = 1.52 cm, +; l = 5.00 cm, ○.

Mass transfer data were also obtained for the thinner and more swollen CC-60 membrane in 0.08, 0.3, and 1 M NaCl. As with the AMF C-60 membrane, $t_{1/2}$ varied linearly with $u^{-1/3}$ and was markedly dependent on D_v. At the higher distribution coefficients, mass transfer in these systems was largely controlled by film diffusion with diffusional half-lives being well over an order of magnitude larger than the extrapolated value at infinite velocity. In these cases, determination of $\mathcal{D}_{Na}$ in the membrane would thus be difficult and subject to large uncertainties.

The experiments dramatically demonstrate that extreme caution is necessary in the determination of diffusion coefficients in membranes when distribution coefficients are large.

Adsorption of Hg(II) on Metal Tubes

In connection with studies on the removal of traces of mercury from aqueous streams,[8] it is of interest to establish the extent to which mercury losses might occur by adsorption or deposition on walls of containers. Monitoring of the buildup of tracer on the walls during flow of radioactive tracer through tubes seemed to be a particularly simple method of obtaining quantitative information.

Some experiments were carried out with type 304 stainless steel tubes 5 cm long and 0.5 cm in diameter. Using ca. 1.25 $\times$ 10^{-5} M Hg(II) solutions in 1 M NaCl, essentially negligible adsorption was found during 3 hr of circulation. With copper tubes, on the other hand, significant "adsorption" occurred. The copper tube studied had a diameter of 0.48 cm; length varied between 2 and 15 cm. Rates of adsorption were studied over the linear flow velocity range 0.1 to 160 cm/sec, corresponding to Reynolds numbers of ca. 6 to 9000. In the laminar flow regime, adsorption of Hg(II) varied with the $^2/_3$ power of tube length and the $^1/_3$ power of flow rate, as expected from the Levich equation for a reaction which is essentially diffusion controlled. In the turbulent flow region, the rate of adsorption varied approximately linearly with tube length as was expected.

Although one cannot expect that liquid diffusion control for deposition of mercury will hold when large amounts of mercury are to be removed from solution (in that case, presumably, the rate-limiting step will be diffusion of copper through the deposited mercury layer), these results imply that small amounts of mercury could be removed by flowing contaminated streams through small-diameter tubes of appropriate metals, including copper, or through screens or packed

beds of metal particles. From the Levich equation and its extension by Posey[9] to a region of large percentage removal, one can estimate that with tubes ca. 1 ft long and with cross-sectional area ca. 1 mm^2, removal of mercury at trace concentrations should be well over 95% at flow rates of several centimeters per minute.

---

1. Research jointly sponsored by the Office of Saline Water, U.S. Department of the Interior, by the ORNL-NSF Environmental Program, and by the U.S. Atomic Energy Commission under Union Carbide Corporation's contract with the U.S. Atomic Energy Commission.
2. On loan from the Reactor Chemistry Division.
3. Director's Division.
4. L. Dresner, *Theory of the Porous-Frit Method of Measuring Self-Diffusion Constants*, ORNL-4667 (March 1971) and the preceding contribution, this report.
5. L. J. Gosting and H. S. Harned, *J. Amer. Chem. Soc.* 73, 159 (1951).
6. F. Nelson, *Chem. Div. Annu. Progr. Rep. May 20, 1970*, ORNL-4581, p. 103.
7. V. G. Levich, *Physiochemical Hydrodynamics*, p. 112, Prentice-Hall, Englewood Cliffs, N.J., 1962.
8. See, for example, F. Nelson and M. D. Danford, "Adsorption of Cd(II) and Hg(II) on Anion Exchangers from Chloride Solutions," the following contribution, this report.
9. K. A. Kraus et al., *Chem. Div. Annu. Progr. Rep. May 20, 1967*, ORNL-4164, p. 86.

ADSORPTION OF Cd(II) AND Hg(II) ON ANION EXCHANGERS FROM CHLORIDE SOLUTIONS

F. Nelson M. D. Danford

Two elements known to be toxic pollutants, mercury and cadmium, have received considerable public attention because of their widespread occurrence in waters and because of their high toxicity at low concentrations. Methods of removing these elements from sources of contamination, for example, industrial effluents, and from other aqueous media in which they occur apparently will become increasingly important. Ion exchange methods appear particularly promising.

To extend previous information on the anion exchange behavior of Cd(II) and Hg(II) in HCl solutions,[1] we have measured their adsorption on an anion exchanger (Dowex 1-X10) from other chloride solutions (NaCl, LiCl, $AlCl_3$) containing a small amount of acid (10^{-2} *M* HCl).

The observed distribution coefficients, D_v (amount per cubic centimeter of resin/amount per cubic centimeter of solution) at tracer loading of the resin, measured radiometrically (^{197}Hg, ^{109}Cd) are shown in Fig. 6.19. As expected from earlier anion exchange studies of Zn(II),[2] adsorbabilities were significantly greater from the salt solutions than from HCl solutions.

Methods of eluting Cd(II) and Hg(II) after their adsorption from chloride media were also investigated. Although moderately concentrated H_2SO_4 (2 to 4 *M*) and HNO_3 (2 to 6 *M*) may be used to elute these elements, the elution bands, particularly those of Hg(II), tail badly, and regeneration of columns to the chloride form after removal of Cd(II) and Hg(II) is difficult.

A systematic study of the elution behavior of Cd(II) and Hg(II) with 1 to 5 *M* NaCl solutions containing small amounts of ethylenediaminetetraacetic acid (EDTA) showed that this complexing agent, at an appropriate pH, is an effective eluent. Easy removal of the elements under these conditions is consistent with an earlier observation[3] that anionic EDTA complexes of many metals are weakly adsorbed by anion exchangers in moderately concentrated chloride solutions.

In addition, Cd(II) and Hg(II) may be sequentially eluted through pH control of the NaCl-EDTA solutions. A typical separation is shown in Fig. 6.20. After adsorbing and concentrating the elements from 5 *M* NaCl on a small anion exchange column, Cd(II) and Hg(II) were eluted in well-separated, sharp bands with 1 *M* NaCl–0.1 *M* EDTA solutions adjusted with NaOH to pH 5.5 and 12.0 respectively. Since the selectivity of the anion exchanger is small for EDTA, the column remains predominantly in the chloride form, and only minor pretreatment is required prior to the next adsorption cycle.

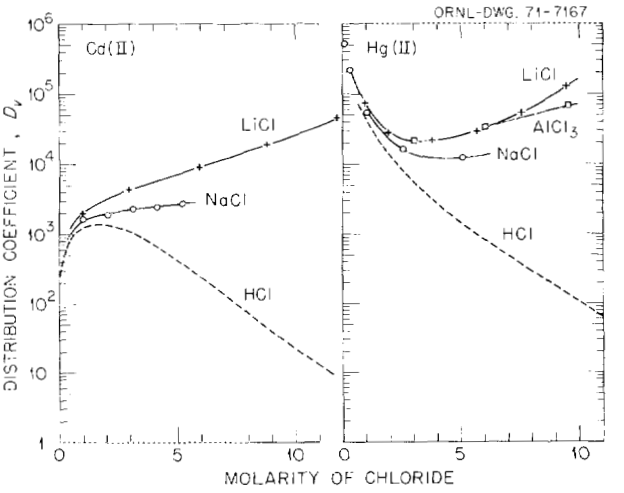

Fig. 6.19. Adsorption of Cd(II) and Hg(II) in chloride solutions. Dowex 1-X10, 25°C; HCl data from ref. 1.

1. K. A. Kraus and F. Nelson, *Proc. Int. Conf. Peaceful Uses At. Energy* 7, 113 (1955).
2. K. A. Kraus and F. Nelson, *American Society for Testing Materials Special Technical Publication No. 195* (1958).
3. F. Nelson, R. A. Day, Jr., and K. A. Kraus, *J. Inorg. Nucl. Chem.* 15, 140 (1960).

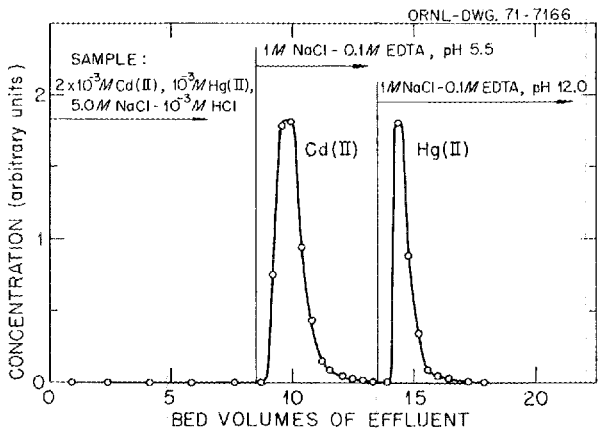

Fig. 6.20. Concentration of Cd(II) and Hg(II) from 5 *M* NaCl; selective elution with 1 *M* NaCl–0.1 *M* EDTA solutions. Dowex 1-X10, 200–400 mesh, 0.25 cm^2 × 4 cm column, 25°C.

ACTIVITY COEFFICIENTS OF NaCl IN WATER-ORGANIC MIXTURES[1,2]

R. J. Raridon K. A. Kraus[3]

Activity coefficients of NaCl in water mixtures of low-molecular-weight diols, Cellosolves, and Carbitols at 25°C were calculated from solubility measurements made previously. The compounds included in this study can be classified under the types R″OR′OH or R″OR′OROH where R and R′ range from -C_2H_4- to -C_6H_{12}- and R″ ranges from -H to -C_4H_9.

For the straight chain compounds, the solubility of NaCl at a given water content decreases as molecular weight increases in a homologous series, as we had observed previously with glycols and glycol monomethyl ethers. Branching has a measurable effect on solubility, but, as might be expected, the effect becomes less pronounced as the chain length increases. For example, at water contents less than 15%, the solubilities of NaCl in the propanediols differ by a factor of 2 or more, while for the 1,3- and 1,4-butanediols the solubilities are nearly the same over the entire composition range. Comparison of the results for the 5-carbon diols (pentane-1,5-diol and 2,2-dimethylpropane-1,3-diol) shows that branching not involving functional groups can also result in a higher NaCl solubility at low water contents.

It is of interest to compare the activity coefficient of NaCl, $\gamma_\pm{}^*$, in aqueous solutions of the different compounds. The results (at 5% water content) are shown in Fig. 6.21 as a function of N_{CH}/N_O where N_{CH} is the number of carbon-hydrogen bonds and N_O is the number of oxygen atoms present in the molecule. The compounds are identified in Table 6.10. The previously determined value for ethylene glycol is also included. The logarithm of the activity coefficients for these two series (R″OR′OH and R″OR′OROH) increases roughly linearly with this ratio. The equation for the dashed line in Fig. 6.21 is $\log \gamma_\pm{}^* = -1.8 + 0.53N_{CH}/N_O$.

Activity coefficients in some of the higher members of the polymer series of polyethylene glycols and their monomethyl ethers[4] also fall near this straight line. The activity coefficients in the dimethyl ethers and the highest-molecular-weight members of the other two polymer series, however, are far above those predicted from Fig. 6.21. Thus, although the relationship can be used to estimate activity coefficients for other members

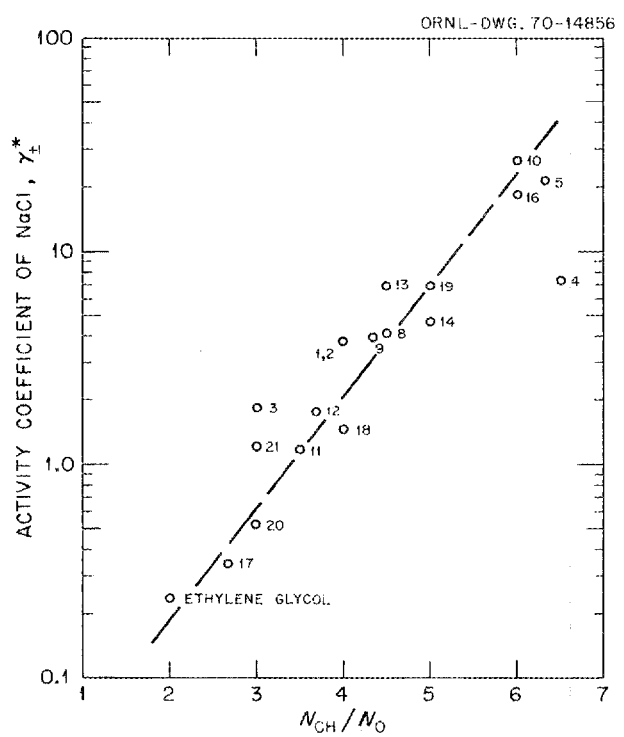

Fig. 6.21. Activity coefficients of sodium chloride at saturation in solutions of some oxy-oxa compounds containing 5% water. N_{CH} = number of carbon-hydrogen bonds, N_O = number of oxygen atoms; compounds identified in Table 6.10.

Table 6.10. Identification of compounds studied

Number	Compound
1	1,3-Butanediol
2	1,4-Butanediol
3	2-Butene-1,4-diol
4	2-Butoxyethanol
5	Butoxyethoxypropanol
6	1-Butyne-1,4-diol
7	2,2-Dimethyl-1,3-propanediol
8	2-Ethoxyethanol
9	2-(β-Ethoxyethoxy)ethanol
10	2,5-Hexanediol
11	2-Methoxyethanol
12	2-(β-Methoxyethoxy)ethanol
13	2-Methoxypropanol
14	2-(β-Methoxypropoxy)propanol
15	2-Methyl-2-ethylpropanediol
16	2-Methyl-2,4-pentanediol
17	2,2'-Oxydiethanol
18	2,2'-Oxydipropanol
19	1,5-Pentanediol
20	1,2-Propanediol
21	1,3-Propanediol

of the series studied here, it should not be used for widely differing series.

1. Research sponsored by the Office of Saline Water, U.S. Department of the Interior, under Union Carbide Corporation's contract with the U.S. Atomic Energy Commission.
2. Expanded abstract of a paper in *J. Chem. Eng. Data* **16**, 241 (1971).
3. Director's Division.
4. W. H. Baldwin, R. J. Raridon, and K. A. Kraus, *J. Phys. Chem.* 73, 3417 (1969).

DENSITY OF WATER-ORGANIC MIXTURES AT 25°C[1]

R. J. Raridon K. A. Kraus[2]

As part of the Water Research Program we have measured the densities of a large number of water-organic solutions. The solutions were prepared by weight and had water contents of ca. 5, 15, 25, 50, and 75%. The pycnometers (2 ml) were equilibrated in a water bath.

The density data have been fitted to an empirical equation so that the results might be readily available. We first calculated an excess density function,

$$\Delta\rho = \rho - x_1\rho_1 - x_3\rho_3 \ , \qquad (1)$$

where ρ is the density and x is the weight fraction. The subscripts refer to water (1) and organic (3). This $\Delta\rho$ function was then fitted by a least-squares routine to

$$\Delta\rho = Ax_1x_3 + Bx_1x_3(x_1 - x_3) \ . \qquad (2)$$

With the values of A and B thus obtained for a specific compound, the density for any given organic-water composition can be calculated as follows:

$$\rho = x_1\rho_1 + x_3\rho_3 + Ax_1x_3 + Bx_1x_3(x_1 - x_3) \ . \qquad (3)$$

The computed values of A and B for some 40 organic compounds, plus the measured values of ρ_3, are listed in Table 6.11. The values of A are positive in all cases. A measure of the accuracy of a computed density can be obtained from the data in the last two columns, the maximum deviation between computed and measured values, and the maximum standard error. A value of 10×10^{-4} for either quantity would correspond to an error of ca. 0.1% in the density. Thus it appears that densities can be computed for water mixtures of most of these organic compounds with a maximum error of less than 0.1%.

1. Research sponsored by the Office of Saline Water, U.S. Department of the Interior, under Union Carbide Corporation's contract with the U.S. Atomic Energy Commission.
2. Director's Division.

HYPERFILTRATION WITH DYNAMICALLY FORMED MEMBRANES

W. H. Baldwin A. J. Shor[1]
J. Csurny C. G. West
L. L. Fairchild[1] C. G. Westmoreland
N. Harrison J. T. Day[3]
C. E. Higgins P. H. Wadia[3]
J. S. Johnson J. Acosta[3]
K. A. Kraus[2] J. B. Cabellon[3]
D. C. Michelson J-P. Jacks[3]
R. E. Minturn A. K. Padia[3]
G. E. Moore S. Ruben[3]
L. E. Whitesides[3]

Water Research Program efforts supported by the Office of Saline Water, U.S. Department of the Interior, have been focused on development of hydrous Zr(IV) oxide–polyacrylate membranes. Last year,[4] we reported that exposure of a hydrous oxide membrane to an acidic solution containing polyacrylate resulted in a

Table 6.11. Parameters for calculating densities of water-organic mixtures at 25°

$$\rho = x_1\rho_1 + x_3\rho_3 + Ax_1x_3 + Bx_1x_3(x_1 - x_3)$$

x_1 = weight fraction water
x_3 = weight fraction organic compound
ρ_1 = density of water = 0.99707 g/cm^3
ρ_3 = density of pure organic compound

Compound	ρ_3	A	B	Maximum deviation	Maximum standard error
		$\times 10^{-1}$	$\times 10^{-1}$	$\times 10^{-4}$	$\times 10^{-4}$
Acetone	0.7855	1.0577	0.0932	15	7
Acetonitrile	0.7781	0.2798	−0.4982	8	6
2-Aminoethanol	1.0112	0.6044	0.4869	12	8
1,3-Butanediol	1.0003	0.7093	0.4239	6	5
1,4-Butanediol	1.0122	0.4981	0.4008	8	4
Butoxyethanol	0.8973	0.4838	0.0567	5	4
Diethanolamine	1.0946	0.5062	0.4281	8	6
Diethylene glycol	1.1153	0.5669	0.3137	15	8
Diethylene glycol monobutyl ether	0.9504	0.7683	0.1468	8	6
Diethylene glycol monoethyl ether	0.9860	1.1349	0.2664	12	9
Diethylene glycol monomethyl ether	1.0170	1.0335	0.3666	10	9
Dimethylformamide	0.9470	0.9196	0.4751	19	11
Dimethyl sulfoxide	1.0951	0.9219	0.8151	12	7
Dioxane	1.0314	0.7715	0.1126	11	8
Dipropylene glycol	1.0189	1.0262	0.3460	11	8
Dipropylene glycol monomethyl ether	0.9600	1.2138	0.2610	12	9
2-Ethoxyethanol	0.9253	1.1251	0.1051	15	10
Ethanol	0.7856	0.7712	−0.0370	5	4
Ethylene glycol	1.1094	0.3696	0.2276	2	2
Ethylene glycol monoacetate	1.1047	0.4698	0.1005	2	2
Ethyl lactate	1.0274	0.9237	−0.0655	13	10
Formamide	1.1300	0.1364	−0.1042	3	2
Glycerol monoacetate	1.204	0.2691	0.0442	1	2
Glycerol diacetate	1.1751	0.2718	0.1586	5	4
2,5-Hexanediol	0.958	0.6819	0.2072	5	4
1,2,6-Hexanetriol	1.1053	0.3614	0.2745	6	4
4-Hydroxy-4-methyl-2-pentanone	0.9334	1.1643	0.8377	16	12
Methanol	0.7877	0.7902	0.1982	11	6
2-Methoxyethanol	0.9599	1.0685	0.2767	14	9
N-Methylformamide	0.9999	0.7143	−0.0287	8	9
2-Methyl-2,4-pentanediol	0.9186	1.1123	0.2095	11	9
N-Methyl-2-pyrrolidone	1.0282	0.9826	0.8808	15	10
1,5-Pentanediol	0.9877	0.4494	0.2810	7	4
1,2-Propanediol	1.0326	0.7697	0.2892	10	6
1,3-Propanediol	1.0498	0.4130	0.3096	10	5
1-Propanol	0.8005	0.3300	−0.1586	13	10
2-Propanol	0.7815	0.6229	−0.2850	10	8
Propylene glycol monomethyl ether	0.9193	1.1986	0.1528	16	12
Tetraethylene glycol	1.1211	0.7008	0.4930	9	8
Tetrahydropyran-2-methanol	1.0229	0.7945	0.1673	3	3
2,2′-Thiodiethanol	1.1784	0.0724	0.1333	5	3

composite having favorable salt rejections for feeds of composition typical of low-salinity natural waters. We have since been trying to delineate formation and operating conditions for the best performance. We have also attempted to identify porous supports on which membranes of adequate performance can be formed, and which are cheap enough to be promising for use in practical modules. Additives other than carboxylates and hydrous oxides have also been tried for dynamic membrane formation, although relatively less effort has gone into this than in previous years.

With support by the National Science Foundation under the ORNL-NSF Environmental Program, we have initiated fundamental studies of dynamic membranes and of transport in hyperfiltration through ion exchange membranes, the class to which most dynamic membranes belong. We have also looked in a preliminary way at the technical feasibility of treating by hyperfiltration waste solutions generated in the dyeing of textiles and in kraft pulp manufacture.

Hydrous Zr(IV) Oxide–Polyacrylate Membranes — Formation and Operating Variables

Among the variables investigated were the degree of aggregation of hydrous oxide and polyacrylate additives; the concentration of additive and salt and the pH of the solution during membrane formation; and the pressure, the circulation velocity past the membrane, the temperature, and the pore size of the support. All these influence membrane properties, and their effects are frequently interdependent. Although much more work will be necessary to establish optimum conditions, certain trends have become evident; we shall illustrate these with two examples.

In our earlier work with dual-layer membranes, we usually made the polyacrylic acid (PAA) addition at pH 3 to 4. Recently, higher acidities were tested, and a pH about 2 appears to yield membranes of good performance more reliably. In 5 runs, in which 15 membranes were formed on 0.22- or 0.45-μ supports, rejections of 0.05 M NaCl were from 90 to 95% after bringing the solution pH to 7–8. Fluxes through 12 membranes were between 100 and 170 gal per square foot per day (gpd/ft^2); through the other 3, fluxes were 80 to 100 gpd (950 psig, 35 fps circulation velocity, 25°C). Although performance in this range has been observed on occasion with our earlier procedures, the consistency of these results, particularly the high fluxes obtained, is impressive.

The effect of molecular weight of the polyacrylic acid is significant. Figure 6.22 summarizes hyperfiltration properties of membranes having similar histories, including exposure to a typical brackish water composition, but formed with different polycarboxylic acids of nominal molecular weights of 5000 to 10^7. Initial exposure of the hydrous oxide layer to the organic polyelectrolytes was at pH 3. Highest rejections appear to be attained when the molecular weight is about 100,000.

In Fig. 6.33 of last year's report,[4] performance of dual-layer membranes was shown to be superior to single-layer polyacrylate membranes in hyperfiltration of natural water compositions. Such waters usually contain polyvalent counterions [for polyacrylate membranes, Mg(II) and Ca(II) would be most important], which, in general, affect deleteriously the performance of ion exchange membranes. Figure 6.23 indicates that the improvements in properties with NaCl feeds attained by modifications in formation procedures are reflected in performance with natural water compositions. In this test, the synthetic Coalinga feed, initially about 2000 ppm dissolved solids, was reduced to a ninth of its original volume by discarding product. Since solute was lost, primarily because of incomplete rejection, final concentrations were only five to seven times the initial values. The performance was considerably better than that reported a year ago — fluxes were two to four times higher. In another experiment

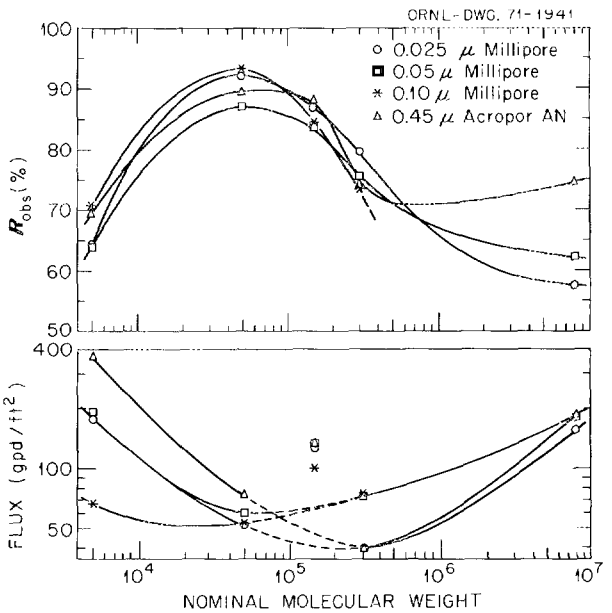

Fig. 6.22. Hyperfiltration of 0.05 M NaCl by dual-layer hydrous Zr(IV) oxide membranes with different molecular weight polycarboxylates, after exposure to Coalinga water. 1000 psig, pH ~7, 35 fps.

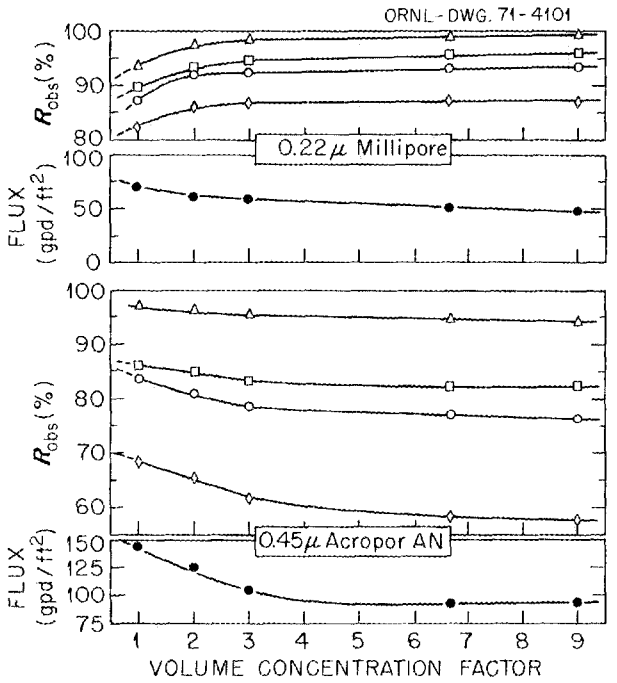

Fig. 6.23. Hyperfiltration of Coalinga water by dual-layer hydrous Zr(IV) oxide–Acrysol A-3 PAA membranes as a function of volume concentration factor. 950 psig, 35 fps, 25°C. ○ conductivity, △ Mg(II) + Ca(II), ◇ Cl^-, □ total anion.

with Coalinga feed, we collected product and subjected it to a second hyperfiltration. Fluxes in the second stage were about 100 gpd/ft^2 for a membrane on 0.22-μ Millipore and about 125 gpd/ft^2 for 0.45-μ Acropor; these values were about half again as high as in the first stage. Rejections were also higher in the second stage, values being 96% or higher for chloride, Mg(II) + Ca(II), and total anion. Product of the second stage contained less than 25 ppm total dissolved solids.

Search for Practical Porous Supports

The experiments so far described were carried out with membranes formed on filter sheets, whose pores were usually 0.5 μ or less, wrapped around the outside of metal tubes having pores usually 5 μ or greater. This configuration provides a well-defined surface for membrane formation and minimizes pressure drop not associated with transport through the membrane and fouling layer. It is conceivable that similar supports could be developed for practical applications, but costs of components and fabrication make wrapped metal tubes unattractive for the immediate future. As membrane performance improves, the search for supports which can be adapted to practice at an early date becomes more urgent.

Two of the materials examined in the past year look particularly promising. Carbon tubes have been used previously.[5] Dual-layer membranes on a 6C carbon tube, which is more porous than those we previously employed, have had rejections comparable with wrapped metal tubes; fluxes are inferior but still favorable. Figure 6.24 illustrates properties during addition of base, with PAA in the solution. Two tubes were used in the test, one of which had the extrusion skin machined off.[6] Rejections of about 95% for 0.05 *M* NaCl were attained at neutral pH, with fluxes of about 100 gpd/ft^2. The temperature was about 60°C, and the fluxes are estimated to be about twice what they would be at room temperature. Feed velocity past the membrane was 8 fps, considerably lower than in the other tests reported and a value well in the range for practical operation. Removal of the extrusion skin significantly improved performance.

We have attained comparable performance with ceramic tubes of about 0.3 μ pore size manufactured by the Flotronics Division, Selas Corporation.

Hyperfiltration of Waste Streams

Figure 6.25 summarizes results in a test of Zr(IV)-PAA membranes in processing of waste solutions

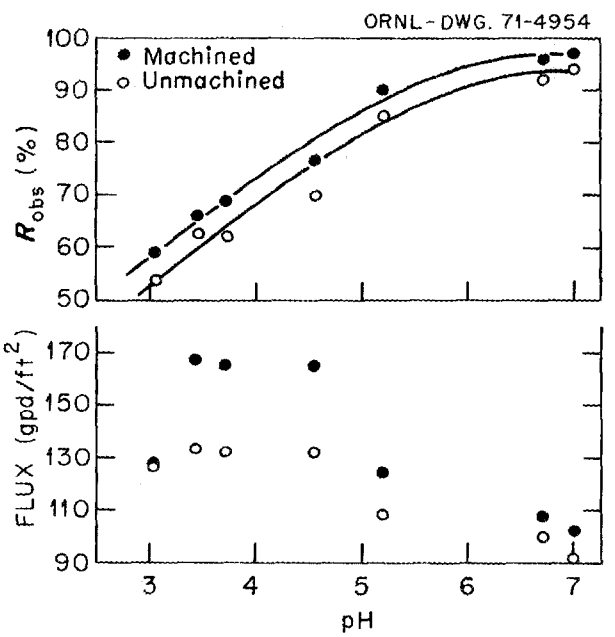

Fig. 6.24. Formation curves for Zr(IV)-PAA hyperfiltration membranes on machined and unmachined 6C carbon tubes. Acrysol A-3 PAA, 0.05 *M* NaCl, 900 psig, ~60°C, 8 fps.

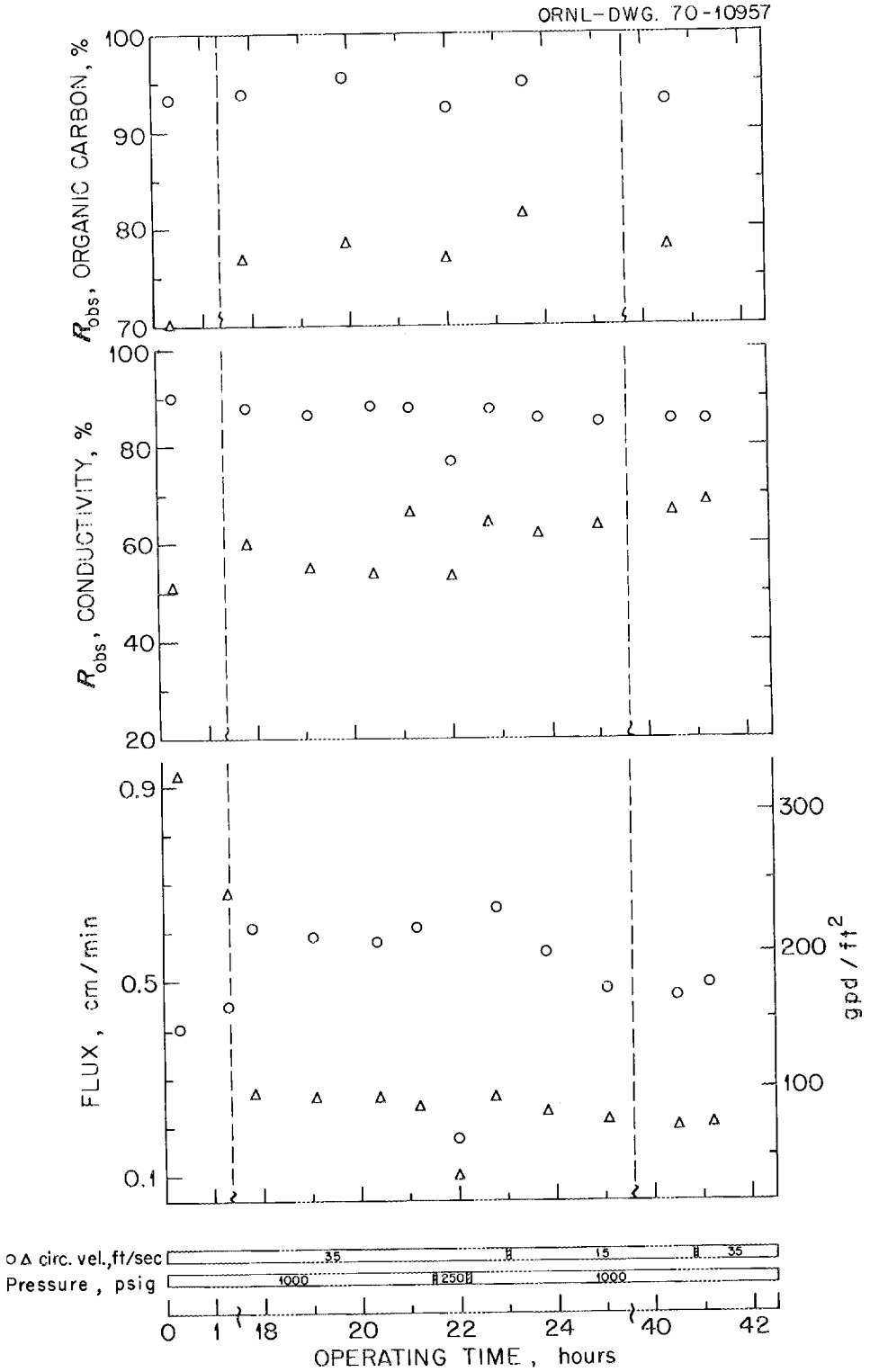

Fig. 6.25. Hyperfiltration of waste solution from dyeing of synthetic fabric. 0.45-μ Acropor AN. ○ hydrous Zr(IV) oxide–PAA membrane, △ membrane dynamically formed from feed constituents.

(1400 to 16,000 ppm total solids, 200 to 3000 Pt-Co color units) generated in dyeing of synthetic fabrics.[7] The product was essentially clear and colorless, and a large fraction of organic contaminants was removed at high production rates. Dual-layer membranes performed better in both rejection and flux than a membrane formed of feed constituents simultaneously tested. This run was at room temperature. In other experiments at the temperature of the dyeing operation, above 50°C, we found that flux was higher, with little, if any, penalty in rejection. Purification of waste streams at process temperatures would be a substantial advantage if product water were to be recycled in the process.

Waste streams are generated at several points in the kraft pulping process, and we have looked into treatment of several.[8] Particularly large volumes originate in the bleaching process, and Fig. 6.26 summarizes performance in an experiment in which such waste was concentrated. The acidity of the solution was too high for a polyacrylate layer to be expected to improve performance, and a simple hydrous Zr(IV) oxide membrane was used. Color and organic carbon were largely removed, but chloride rejection was probably too low for recycle of filtrate in a single-stage operation. Tests and evaluation of our methods for this and other kraft waste streams are, however, not completed.

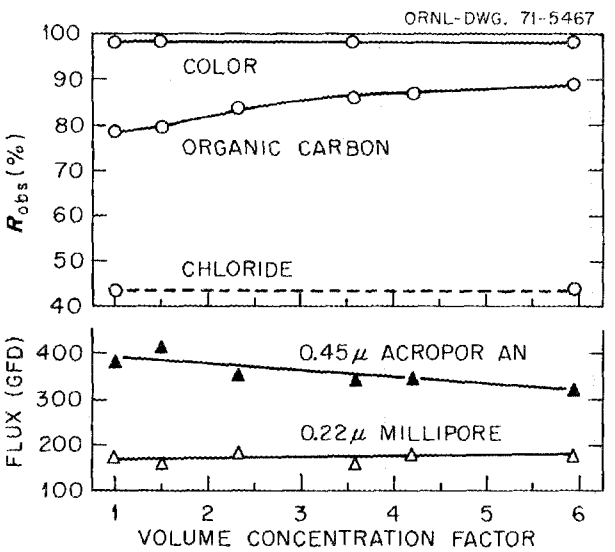

Fig. 6.26. Rejection and flux vs volume concentration factor in hyperfiltration of kraft bleach effluent by dynamic hydrous Zr(IV) oxide membranes. Rejections shown are typical of membranes on both supports. 950 psig, 35°C, 35 fps, pH ~2.

1. On loan from the Reactor Chemistry Division.
2. Director's Division.
3. Massachusetts Institute of Technology School of Chemical Engineering Practice: J. T. Day, Director, and P. H. Wadia, Assistant Director, of the Oak Ridge Station.
4. *Chem. Div. Annu. Progr. Rep. May 20, 1970,* ORNL-4581, p. 108.
5. K. A. Kraus, A. J. Shor, and J. S. Johnson, *Desalination* 2, 243 (1967). We thank L. M. Litz of Union Carbide Corporation, Tarrytown, N.Y., for supplying these tubes.
6. W. R. Mixon, M.S. thesis, University of Tennessee, Knoxville; ORNL-TM-2150 (March 1969).
7. Work with dye wastes was in collaboration with C. Aurich and K. Turner of the Gaston County Dyeing Machine Co., Stanley, N.C., and C. A. Brandon of Clemson University, Clemson, S.C.
8. Tests were carried out in cooperation with K. J. Brown and R. L. Calleton of the International Paper Company, Tuxedo Park, N.Y.

ORGANIC POLYELECTROLYTES FOR HYPERFILTRATION TESTS[1]

W. H. Baldwin Neva Harrison C. E. Higgins

Polyelectrolytes remain among the organic polymers considered for hyperfiltration membranes. At this time we are considering three organic polyelectrolytes. Chitosan, poly(glucosamine), is a weak base resulting from deacetylation of chitin, poly(*N*-acetylglucosamine), which is a naturally occurring component of the exoskeleton of some insects and marine animals. Chitin is obtained commercially from crab shells. We have been able to cast a self-membrane of chitosan and have used acid solutions for the formation of dynamic membranes.

The controlled sulfonation of poly(phenylene oxide) has yielded polymers of varying exchange capacity that have been tested for dynamic membrane formation.

Another class of strong anion exchangers is being tested. Polyaminoresins will react with some cations forming coordination compounds analogous to the simpler adducts such as $Cu(NH_3)_4^{2+}$ and $Co(NH_3)_6^{3+}$. The resulting complexes are highly ionized salts that we are incorporating into polymers for evaluation in hyperfiltration.

Chitosan Membrane

Chitosan, a weak base, is soluble in aqueous acid and in glacial acetic acid solution. We have been able to cast a self-membrane from glacial acetic acid on glass plates. Although the film that remained after drying adhered firmly to the plate, it could be detached by soaking the plate and film in sodium hydroxide solution.

Rejection of sodium chloride from 0.05 *M* NaCl at 1500 psi was 30 to 40% with fluxes around 5 gpd/ft^2. These observations were made at pH 7.6 and at 10.3; at pH 3.0 the membrane dissolved. Dynamic membranes formed in situ by deposition from solution of pH 4 showed higher fluxes but much lower rejections.

Sulfonation of Poly(Phenylene Oxide)

Rejections of sodium chloride by hyperfiltration through cast poly(phenylene oxide sodium sulfonate), SPPO, membranes[2] have been encouraging enough for us to test SPPO as a dynamic membrane. Poly(phenylene oxide) in chloroform at −40°C was treated with chlorosulfonic acid. The product, resulting from evaporation of solvent, was washed with ether and was found to contain up to 5.7 meq of ion exchange capacity per gram of dry solid, depending upon the amount of chlorosulfonic acid used. Alcohol that is present in reagent-grade chloroform as a preservative will react with chlorosulfonic acid at the expense of product. Plummer, Kimura, and La Conti[2] chose to add extra chlorosulfonic acid to react with the alcohol, but we elected to wash the alcohol from the chloroform with water and to dry the chloroform batchwise with calcium chloride, and, for final drying, passage through a column of Drierite.

Polymers with desirably high exchange capacities also contained sufficient cross-linking to be insoluble in water and did not provide satisfactory material for dynamically formed hyperfiltration membranes. We are continuing tests to overcome these problems of cross-linking and membrane formation.

Insolubilized PEI Polymers

Poly(ethylene imine) prepared from aziridine

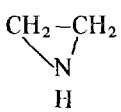

by ring cleavage and addition contains the repeating unit

$$[\text{-}CH_2CH_2N\!<]\ ,$$

where the nitrogen is distributed in the ratio of one primary to two secondary to one tertiary amine group. The homopolymer is water soluble and is a weak base. The amine groups may undergo further reactions that are typical of amines, such as alkylation and acylation. The usual polyfunctional reagents such as α,ω-dihalohydrocarbons, diesters, or diacyl halides have been employed to cross-link PEI and thus render it insoluble. We have found a new method for insolubilizing PEI. Amines when heated with methyl acrylate react in two ways: the usual acylation of amine to amide and the addition of another amine molecule to the conjugated double bond.

$$2R_2NH + CH_2 = CHCOOMe \rightarrow R_2NCH_2CH_2CONR_2 + MeOH$$

The advantages of this reaction include low cost (methyl acrylate is cheap), low temperature of reaction (refluxing methanol), the mixture of reagents is stable at room temperature, reaction takes place only on heating, and ease of isolation and purification.

The repeating unit can also be considered to be a substituted ethylene diamine,

$$>NCH_2CH_2N<\ ,$$

the ligand that has been used so successfully to prepare chelates of transition metals. In fact, the chelated derivatives of some metals with insolubilized PEI have been studied[3] as anion exchange resins, but certain obvious advantages of these have been overlooked: in the chelated polymer the metal-nitrogen cation is a strong polyvalent base. We will continue studies of these polymers.

---

1. Research jointly sponsored by the ORNL-NSF Environmental Program and by the U.S. Atomic Energy Commission under Union Carbide Corporation's contract with the U.S. Atomic Energy Commission.

2. C. W. Plummer, G. Kimura, and A. B. LaConti, *Development of Sulfonated Poly(Phenylene Oxide) Membranes for Reverse Osmosis*, OSW Research and Development Progress Report No. 551 (1970).

3. S. Nonogaki, S. Makishima, and Y. Yoneda, *J. Phys. Chem.* **62**, 601 (1958).

SOME REMARKS ON THE INTEGRATION OF THE EXTENDED NERNST-PLANCK EQUATIONS IN THE HYPERFILTRATION OF MULTICOMPONENT SOLUTIONS[1]

Lawrence Dresner

Schlögl,[2] among others, has described ionic transport in ion exchange membranes using an extension of the Nernst-Planck equations that includes convection. These extended Nernst-Planck equations (ENPE) are

attractive candidates for a phenomenological description of ionic transport in membranes. They take into account the three main mechanisms of ionic transport in membranes – diffusion, migration in an electric field, and convection – while neglecting the complicated and largely unknown details of short-range ion-ion interaction. (Ions do have long-range interactions through the electric field.) In spite of their simplicity from the physical point of view, the ENPE are highly complicated from a mathematical point of view because they are nonlinear. Thus in trying to decide just how well they describe ionic transport, we are faced with the difficult problem of solving them or at least of getting information about their solutions.

I studied a slightly more general form of the ENPE than that used by Schlögl. Schlögl treated the water-ion interaction by assuming the ions acted as though they were dissolved in the water in the membrane. He took the convective contribution to the transport velocity of the ions to be that of the water. I have allowed for a difference in these two velocities by introducing a convective coupling coefficient for each ion, defined as the ratio of the convective part of the ionic transport velocity to the water flow velocity. The convective coupling coefficients are phenomenological coefficients that take into account differences in the ion-membrane and water-membrane interactions.

For the purposes of simplifying his investigations, Schlögl took all activity coefficients equal to unity. I restrict myself in this regard, too, but not as severely. I take each activity coefficient to be constant in each phase, but permit it to change across phase boundaries.

The only problem of hyperfiltration for which a solution of the ENPE in terms of elementary functions is known is the hyperfiltration of two-component solutions (water plus one binary electrolyte).[2-4] The ENPE may always be dealt with by finite differences, but this is time consuming and laborious; furthermore, numerical treatments often fail to reveal in an obvious way important general properties. Several approximate methods of handling the ENPE have been suggested, but all have serious shortcomings as indicated in a detailed discussion in the paper on which this summary is based.[1]

A new method of obtaining from the ENPE the *asymptotic rejections* of the solutes in a multicomponent solution is employed in this work. The new method rests on the assumption of good coion exclusion. In hyperfiltration this assumption does not impose a serious restriction since the most interesting situations are those in which there is good coion exclusion. Results obtained with the new method compare well with exact results obtained by finite differences. The new method has the advantage of requiring only a modest amount of calculation, even when several ions are present.

The new method has uncovered some interesting circumstances, hitherto unnoticed, under which negative rejection of a solute may occur. In the limit of asymptotic rejections (high permeation rates), only one counterion accompanies the coions through the membrane, the one with the largest ratio of convective coupling coefficient to practical mobility (penetrating counterion). All other counterions are completely rejected. (It should be remembered that this conclusion is based on an approximate integration of the ENPE; in actuality we might expect that the rejection of other counterions would be close to 100% and that the coions would be accompanied mostly by the penetrating counterion. Finite difference calculations have borne this out.) If the concentration of the penetrating counterion is low enough in the feed, the filtrate may be more concentrated in it than the feed (negative rejection).

Although the diffusion and convective coupling coefficients of ions in membranes are not yet known, it is reasonable to assume that the proton is more mobile than any other cation. R. B. Bevan has observed negative rejections of Na^+ at low concentration in solutions ~0.05 *M* in acid with both dynamic and detachable membranes. Most striking was with a prefabricated ion exchange membrane (AMF CC-60). For example, in solutions of NaCl in 0.05 *M* HCl, negative rejection of Na^+ is observed at Na^+ concentrations below 3×10^{-5} *M* (e.g., –110% at 10^{-5} *M* Na^+). In solutions of $NaNO_3$–0.05 *M* HNO_3, again using the AMF CC-60, negative rejection of Na^+ of 400% was observed at $Na^+ = 10^{-4}$ *M*. In other cases in which negative rejection of the less mobile of two counterions would be expected, it was not observed. For example, in the systems $MgCl_2$–0.01 *M* KCl and $Mg(NO_3)_2$–0.01 *M* HNO_3, negative rejection of Mg^{2+} was predicted but not observed using either dynamically formed polystyrene sulfonate membranes or the AMF membrane.

---

1. Research jointly sponsored by the ORNL-NSF Environmental Program and by the Office of Saline Water, U.S. Department of the Interior, under Union Carbide Corporation's contract with the U.S. Atomic Energy Commission. Submitted for publication to *Desalination*.

2. R. Schlögl, *Stofftransport durch Membranen*, Dr. Dietrich Steinkopff Verlag, Darmstadt, 1964.

3. R. Schlögl, *Ber. Bunsenges. Phys. Chem.* **70**, 400 (1966).

4. E. Hoffer and O. Kedem, *Desalination* **2**, 25 (1967).

GEOMETRIC EFFECTS IN PIEZODIALYSIS THROUGH CHARGE-MOSAIC MEMBRANES[1]

Lawrence Dresner

Charge-mosaic membranes are made up of alternating patches of anion and cation exchangers. When such a membrane is placed in a hyperfiltration cell, the permeate may be enriched in salt compared with the feed.[2-4] This process has been called piezodialysis. If the salt enrichment of the permeate were great enough, piezodialysis could represent an interesting membrane process for the desalination of brackish water.

Piezodialysis is one of many possible processes involving transport through composite membranes, that is, membranes made of patches of different materials. An elaborate general theory of such membranes has been given by Kedem and Katchalsky,[5] but it ignores geometric effects arising from the heterogeneity of the membrane. These geometric effects arise because the ions being transported through different patches of membrane leave the feed bath at different points and also arrive in the permeate bath at different points. In the theory of Kedem and Katchalsky, this "mixing"-"unmixing" is treated as though it takes place instantaneously, whereas in fact it does not. In the work on which this summary is based,[1] an explicit but highly schematic theory of the effect of the geometric heterogeneity of charge-mosaic membranes on piezodialysis is given. The effect is always to reduce the salt flux through the membrane. The factor of reduction, ϵ, has been calculated for two geometric arrangements of the parts of the mosaic membrane, namely, alternating strips and a checkerboard of squares (see Fig. 6.27).

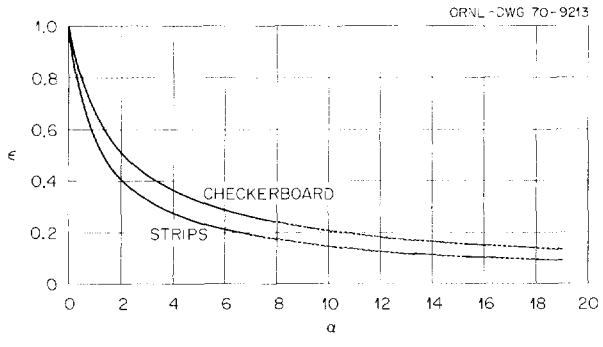

Fig. 6.27. The factor of reduction, ϵ, for the strip and checkerboard membranes. $\alpha = \frac{h}{2\pi l}\frac{\sigma_m(\sigma_f + \sigma_p)}{\sigma_p \sigma_f}$, where h is the width of an ion exchange strip or the side of an ion exchange square, l is the membrane half thickness, σ_m is the membrane conductivity, σ_p is the conductivity of the permeate, and σ_f is the conductivity of the feed.

---

1. Research jointly sponsored by the ORNL-NSF Environmental Program and by the Office of Saline Water, U.S. Department of the Interior, under Union Carbide Corporation's contract with the U.S. Atomic Energy Commission. Submitted for publication in *Desalination.*
2. U. Merten, *Desalination* **1**, 297 (1966).
3. J. N. Weinstein and S. R. Caplan, *Science* **161**, 70 (1968); ibid. **169**, 296 (1970).
4. F. B. Leitz, S. S. Alexander, and A. S. Douglas, *Research on Piezodialysis,* OSW Research and Development Progress Report No. 452 (July 1969).
5. O. Kedem and A. Katchalsky, *Trans. Faraday Soc.* **59**, 1918, 1931, 1941 (1963).

CROSS-FLOW FILTRATION OF SEWAGE EFFLUENTS[1]

H. A. Mahlman K. A. Kraus[2] W. G. Sisson[3]

In hyperfiltration, maintaining a flow of the stream to be treated past the membrane surface is necessary to control concentration polarization. It also inhibits fouling of the membrane surface. A cross flow may also be helpful in ordinary filtration of particulates and in ultrafiltration of colloids by limiting the rate of filter cake thickening and consequent flux decline. For the past year, we have been investigating this technique for filtration of primary sewage effluent after treatment with a clarifying agent (a salt of a hydrolyzable inorganic ion) and/or powdered carbon.

Cross-flow velocity indeed aids the maintenance of product flux, at least in short-term operation, as Fig. 6.28 indicates. The filtering surface was a fire-hose jacket slipped over a perforated metal tube. Sewage effluent, treated with an Fe(III) salt, is pumped through an annulus between the jacket and a transparent outer jacket. Fluxes are higher at higher circulation velocities.

However, cross-flow velocity is not the only factor; there are materials in sewage which tend to form low-flux membranes dynamically.[4] These need to be made inoperative. Figure 6.29 compares performance at different levels of Fe(III) additive with internal and external flow past the filter and indicates the ameliorating effects of the clarifying agent; both flux and organic carbon removal improve with ferric ion addition.

Although these results demonstrate that flux decline in filtration can be to some extent controlled by circulation velocity and additive, regeneration of the

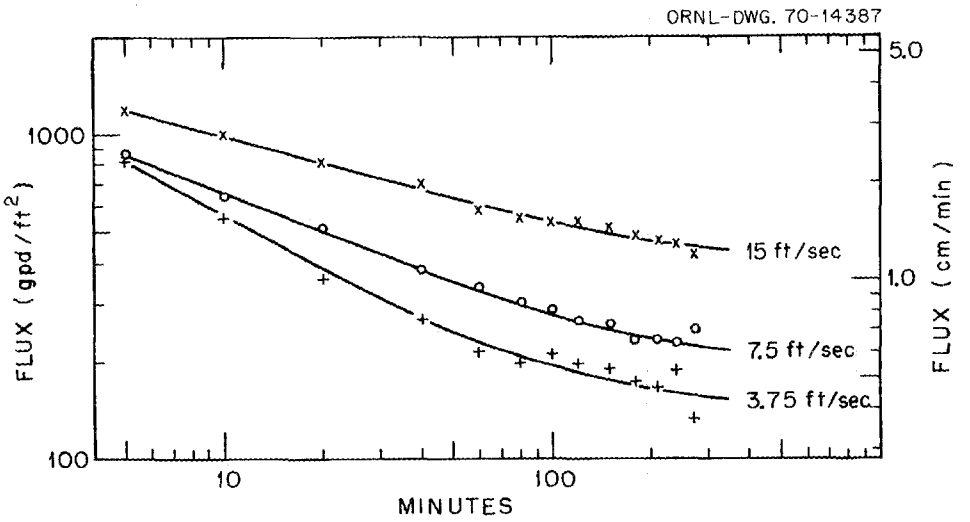

Fig. 6.28. Clarification of Oak Ridge primary sewage effluent by cross-flow filtration. Fe(III)/(total organic carbon) = 1.1; 30 psi.

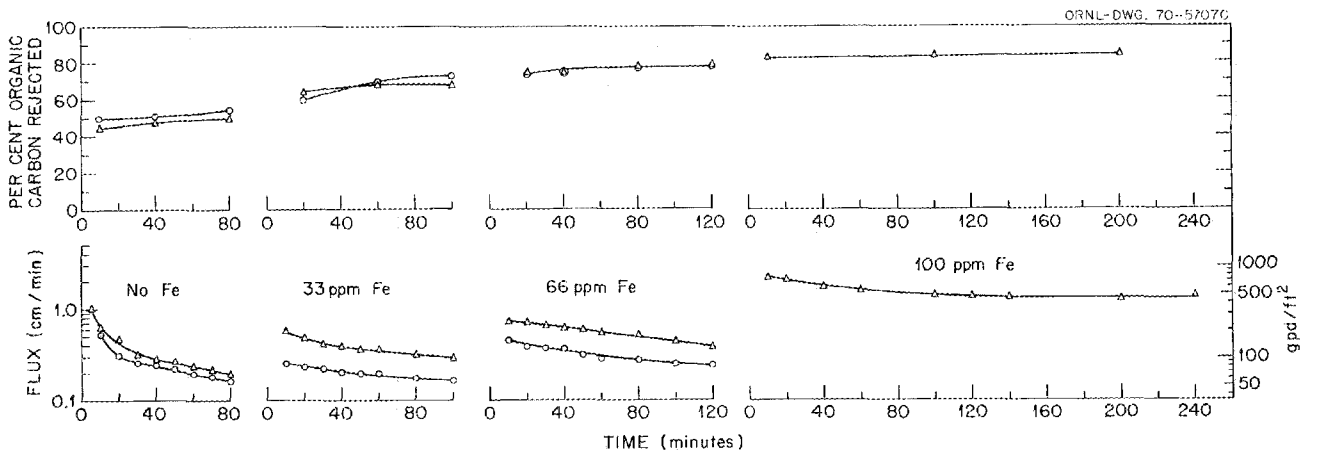

Fig. 6.29. Effect of Fe(III) concentration on cross-flow filtration of effluent from primary treatment of municipal sewage. Conditions: 50 psi, 15 fps. Feed inside, ○; outside, △.

filters will probably be necessary. Chemical treatment, electrical pulses, or backwashing by reversal of pressure are possible methods for regeneration. At present backwashing seems the most promising approach; Fig. 6.30 illustrates flux recovery by this technique. In other experiments, fine-mesh screens appeared to be regenerated more effectively than fire-hose jackets.

The purification of primary sewage by cross-flow filtration using additives under the better operating conditions so far delineated is comparable with that by combined conventional secondary and tertiary treatment. Turbidity of filtrate is about that of tap water, organic carbon content about 10 ppm, and phosphate less than 1 ppm. Longer-term tests carried out in a mobile unit at an Oak Ridge sewage plant have confirmed the results of the short-term tests described here. Problems which must be overcome to bring the technique into full-scale operation have been better defined.

---

1. Research sponsored by the Water Quality Office of the Environmental Protection Agency under Union Carbide Corporation's contract with the U.S. Atomic Energy Commission.
2. Director's Division.
3. Chemical Technology Division.
4. H. C. Savage et al., *Water Sewage Works* **116**, 102 (1969).

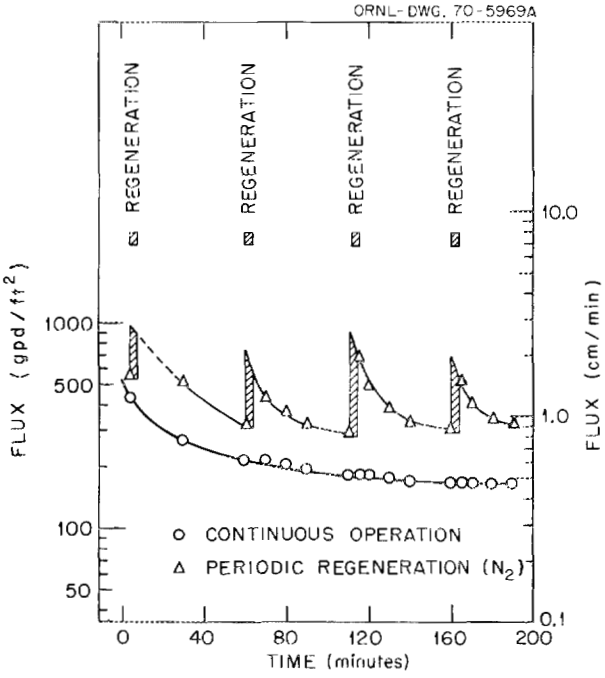

Fig. 6.30. Cross-flow filtration of primary sewage effluent: comparison of continuous operation and periodic regeneration. Conditions: 50 psi, 150 ppm Fe(III), 15 fps.

MOLTEN SALTS AND RELATED NONAQUEOUS SYSTEMS

A REFERENCE ELECTRODE SYSTEM FOR USE IN FLUORIDE MELTS[1]

H. R. Bronstein

A knowledge of the chemical and thermodynamic properties of molten fluoride mixtures is of great importance to the technology of molten-salt power reactors. The measurement of equilibrium potentials of galvanic cells is in principle one of the most direct means of obtaining much of this information. However, as an example, the galvanic cell

$$\mathrm{Be}\left|\begin{matrix}\mathrm{LiF}(x)\\ \mathrm{BeF_2}(1-x)\end{matrix}\right|\mathrm{HF\ (g), H_2\ (g), Pt}\ ,$$

though yielding excellent results, illustrated the difficulties in the use of the Pt, H_2 (g), HF (g),$|F^-$ reference electrode.[2] A new reference electrode system was developed[3–5] in an attempt to provide a more versatile and convenient reference electrode (Fig. 6.31). The electrical potential is poised by the couple $Ni|NiF_2$-saturated melt [10^{-3} mole fraction in $LiF\text{-}BeF_2$ (67-33 mole %)]. The single-crystal LaF_3, by means of its mobile fluoride ion (virtually 100% F^- ion transport), provides the exclusive ionic transport between the reference melt and the test melt.

Further study of the galvanic cell comprised of this reference electrode system and the half-cell $Be|LiF\text{-}BeF_2$ (67-33 mole %) led to findings believed to be of considerable interest and significance.

Deterioration of the initial cell voltage with time as reported previously[5] now has been found to be caused by the depletion of the small NiF_2 content of the reference half-cell through its conversion into an equivalent amount of finely dispersed nickel metal. An impurity in the static atmosphere of highly purified argon or helium gas maintained in the quite-limited volume of the apparatus could not be responsible for the consumption of NiF_2. Subsequent experiments established the actual mechanism involved.

The potential deteriorated even with all external measuring circuits disconnected. Loss of NiF_2 due to beryllium metal transport in the vapor phase was ruled out since beryllium has no measurable vapor pressure at 600°C. It was concluded that an *internal* "short" in the cell supplied the electrons for $NiF_2 + 2e^- \rightarrow Ni^0 + 2F^-$. Obviously, beryllium, the only reductant present, reached the NiF_2 in some manner. This required not only transport through the salt melt, either by dis-

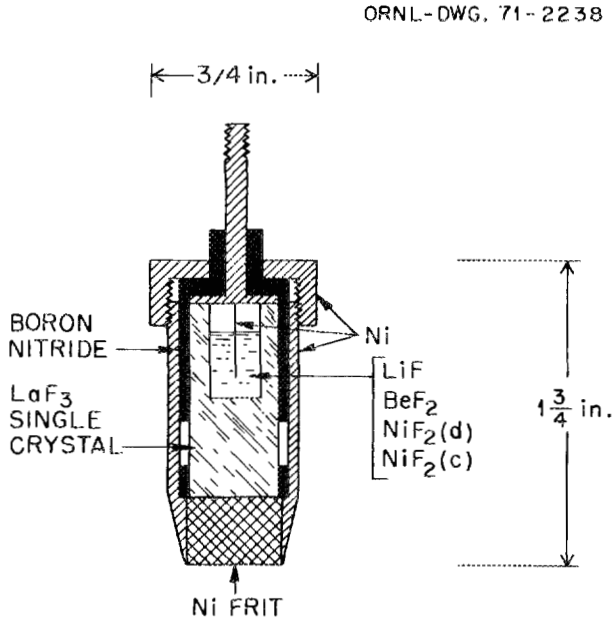

Fig. 6.31. Bronstein-Manning reference-electrode system for use in fluoride melts.

solution or by the so-called "chunking effect,"[6,7] but also electron transport through the LaF_3. The beryllium arriving at or in the nickel frit would act as metallic beryllium if the "chunking effect" were valid or, if dissolved, perhaps as a subvalent Be^+ or Be_2^{2+} ion. This would be followed by transport of the electrons from these species through the LaF_3 and thence by the reaction $2e^- + Ni^{2+} \rightarrow Ni^0$, with equivalent fluoride ions moving in the opposite direction. The overall reaction is then simply Be + NiF_2 (from the electrodes) to give nickel metal in the LaF_3 cup and beryllium fluoride in the main melt.

A series of experiments was conducted to verify this mechanism. First, a beryllium electrode was mounted through an inverted BeO crucible. Since solid beryllium metal is less dense than the melt, any solid metal detached from the electrode by "chunking" would rise to, and be trapped at, the melt surface within the crucible. Dissolved metal, on the other hand, would still reach the reference electrode. The observation was that under these conditions the NiF_2 in the LaF_3 cup was still transformed into Ni metal.

Second, with the same crucible-encapsuled beryllium electrode, the reference electrode assembly was modified by cutting the LaF_3 crystal below the cup portion and placing a thin disk of CaF_2 $^1/_{16}$ in. thick between the two portions of the LaF_3. It was believed that the CaF_2 crystal would perhaps have slight or no electronic conduction and so act as a filter of electrons. This cell maintained the theoretical voltage for a period five times longer than the single-crystal LaF_3 before onset of deterioration. The CaF_2 apparently had some small intrinsic electronic conductance.

A third and definitive experiment was made with the original reference electrode assembly (Fig. 6.31). To the main melt NiF_2 was added as a "getter" for dissolved beryllium. The beryllium electrode was immersed in pure LiF-BeF_2 melt, contained in, and separated from the main melt by, a BeO crucible whose porosity allowed ion migration. Any dissolved metal entering the main melt is immediately oxidized by the Ni^{2+} ions. By this means the theoretical cell potential was maintained for a period of three days. Termination of the experiment apparently was caused by loss of ion migration through the BeO crucible walls, which had become plugged by the deposition of nickel metal.

The voltage recorded in all these cells before onset of deterioration was 2.045 ± 0.003 V. According to the compilation of Baes[8] for the free energy of formation of NiF_2 and of BeF_2 in BeF_2-LiF (33-67 mole %), this cell should yield 2.041 ± 0.003 V at 600°C.

These experiments have established that beryllium does dissolve in the LiF-BeF_2 (67-33 mole %) melt to some small undetermined extent and that, somewhat surprisingly, the conductance in LaF_3 has a small electronic component.

The results of these experiments when compared with those of the U^{4+}/U^{3+} system,[9] where no reduction of NiF_2 occurs, suggest a reaction of the LaF_3 crystal with the Be-BeF_2-LiF melt leading to the formation of some lanthanum metal, according to

$$3\text{Be (dissolved in LiF-BeF}_2\text{ melt)} + 2\text{LaF}_3 = 3\text{BeF}_2\ (\text{LiF-BeF}_2) + 2\text{La (in LaF}_3).$$

Calculation of the activity of lanthanum from the free energies of formation of LaF_3 and of BeF_2 in LiF-BeF_2 (67-33 mole %) gives a value of 10^{-9}. This activity of lanthanum would contribute an *n*-type electronic conduction to the LaF_3 crystal.[10] While this electronic conduction initially is low enough not to affect the measured voltage of the cell, its magnitude seems to increase with time, as reflected in the steady decrease in the measured voltage. The electronic conduction causes eventually the complete reduction of the NiF_2. The formation of lanthanum from the U^{4+}/U^{3+} couple is virtually nonexistent ([La] = 10^{-29}), as would be expected since the free energy per equivalent is much less negative than the Be|BeF_2 couple.

With this knowledge, the technique described will be employed to obtain reliable thermodynamic data on a variety of systems of interest.

The validity of the value for the free energy of formation, ΔG°_f, of NiF_2, our standard, is of interest. We consider the following solid-state cells:[11-13]

	Electromotive force (V) at 600°C	
Ni,NiF_2|CaF_2|AlF_3,Al	−1.720 ± 0.003	(1)
Ni,NiF_2|CaF_2|MgF_2,Mg	−2.343 ± 0.003	(2)
Mg,MgF_2|CaF_2|ThF_4,Th	+0.310 ± 0.005	(3)
Th,ThF_4|CaF_2|AlF_3,Al	+0.310 ± 0.003	(4)
Th,ThF_4|CaF_2|NiF_2,Ni	+1.980 ± 0.005	(5)

Combination of cells 1 and 2 and of cells 3 and 4 yields emf values for the cell Mg,MgF_2|CaF_2|AlF_3,Al. The emf from cells 1 and 2 (Ni|NiF_2 electrode) is +0.623 V, in good agreement with the value +0.620 V from cells 3 and 4 (Th|ThF_4 electrode). Furthermore, these values agree satisfactorily with the value calculated from *calorimetric* data[14] for the reaction

$$^1/_3\text{Al} + {}^1/_2\text{MgF}_2 = {}^1/_3\text{AlF}_3 + {}^1/_2\text{Mg}$$

using free energies of formation at 600°C: MgF_2, $\Delta G^\circ_f = -232.4 \pm 0.6$ kcal and AlF_3, $\Delta G^\circ_f = -306.5 \pm 0.7$ kcal.

$$\Delta G^\circ = \tfrac{1}{3}(-306.5 \pm 0.7 \text{ kcal}) - \tfrac{1}{2}(-232.4 \pm 0.6 \text{ kcal}) = +14.0 \pm 0.5 \text{ kcal},$$

which is equivalent to $+0.608 \pm 0.022$ V for the cell

$$Mg, MgF_2|CaF_2|AlF_3, Al.$$

It is obvious that the emf of the $Ni|NiF_2$ couple of cells 1 and 2 was very reproducible. On using the above value of ΔG°_f for MgF_2 and -2.343 V from cell 2, ΔG°_f for NiF_2 at 600°C is -124.3 kcal, equivalent to 2.694 V. From data of Baes,[8] Blood,[15] and this investigation, one obtains 2.692 V.

The emf of cell 2, -2.343 ± 0.003 V, is in poor agreement with -2.290 ± 0.01 V from combining cells 3 and 5. No obvious reason is apparent as to why the results of cell 5, ref. 13, may be in error.

1. A portion of this work will appear in *MSR Program Semiannu. Progr. Rep. Feb. 28, 1971*, ORNL-4676.

2. B. F. Hitch and C. F. Baes, Jr., *Inorg. Chem.* **8**, 201 (1969); B. F. Hitch and C. F. Baes, Jr., *MSR Program Semiannu. Progr. Rep. Aug. 31, 1968*, ORNL-4344, p. 167.

3. H. R. Bronstein and D. L. Manning, *MSR Program Monthly Rep. December 1969 and January 1970*, MSR-70-10, p. 28 (internal memorandum).

4. D. L. Manning and H. R. Bronstein, *MSR Program Semiannu. Progr. Rep. Feb. 28, 1970*, ORNL-4548, p. 184.

5. H. R. Bronstein, *Chem. Div. Annu. Progr. Rep. May 20, 1970*, ORNL-4581, p. 119.

6. *The Encyclopedia of Electrochemistry*, ed. by C. A. Hampel, pp. 44–51, Reinhold, New York, 1964.

7. H. Aida, J. Apelboin, and M. Garreau, *J. Electrochem. Soc.* **118**, 243 (1971).

8. C. F. Baes, Jr., *Nuclear Metallurgy*, vol. 15, *AIME Symposium on Reprocessing of Nuclear Fuels*, pp. 615–44 (1969).

9. D. L. Manning, *MSR Program Semiannu. Progr. Rep. Aug. 31, 1970*, ORNL-4622, p. 115.

10. C. Wagner, *J. Electrochem. Soc.* **115**, 933 (1968).

11. T. L. Markin, R. J. Bones, and V. J. Wheeler, *Proc. Brit. Ceram. Soc.* **8**, 51 (1967); T. L. Markin, p. 91 in *Electromotive Force Measurements in High Temperature Systems*, Proceedings of a Symposium, Imperial College, London, ed. by C. B. Alcock, April 1967.

12. N. F. Lofgren and E. J. McIver, UKAEA report AERE-R-5169 (1966).

13. R. J. Heus and J. J. Egan, *Z. Phys. Chem. (Frankfurt am Main)* **49**, 38 (1966).

14. E. Rudzitis, H. M. Feder, and W. N. Hubbard, *J. Phys. Chem.* **68**, 2978 (1964).

15. C. M. Blood, private communication, September 1961.

FREE ENERGY OF FORMATION OF LANTHANIDE HALIDES

A. S. Dworkin

The free energy of formation of a compound at elevated temperatures is frequently calculated from thermochemical data since this information is usually easier to obtain than emf and reaction equilibria data. This thermochemical method entails the measurement of the room-temperature heat of formation, the entropy derived from low-temperature heat capacities, and high-temperature enthalpies. The free-energy values for the lanthanide halides which now appear in the literature are for the most part derived from a confused tangle of estimates, contradictory measured data, inconsistent standard states, and errors resulting from transposing from one collection of data to another. In connection with our previous measurement of the high-temperature enthalpies of the lanthanide halides and our proposed measurements of their low-temperature heat capacities, we have made a critical assessment of the literature in order to determine the best sources of data now available for free-energy calculations.

We conclude that none of the free-energy compilations in current use gives reliable values for the lanthanide halides. However, the literature now contains more of the thermochemical data necessary to calculate these free energies of formation than those used in the compilations. However, the low-temperature heat capacities of the lanthanide halides (with the exception of CeF_3) remain unmeasured. There are also no measured room-temperature heats of formation for the lanthanide bromides, while those for the iodides are questionable.

Our high-temperature enthalpy measurements of lanthanide halides[1] indicate the possibility of hitherto unpredicted structure-dependent differences in their room-temperature entropies. We propose to measure low-temperature heat capacities beginning with selected lanthanide chlorides to clarify this point, as well as to obtain the necessary data to generate a reliable free-energy compilation. We will then extend the measurements to the fluorides, bromides, and iodides. If necessary at that time, we will begin measurements of room-temperature heats of formation of the lanthanide bromides and iodides.

1. A. S. Dworkin and M. A. Bredig, *High Temp. Sci.* **3**, 81 (1971).

ENTHALPY OF URANIUM TETRAFLUORIDE FROM 298 TO 1400°K: ENTHALPY AND ENTROPY OF FUSION[1]

A. S. Dworkin

The high-temperature thermochemical behavior of UF_4 described in the literature is open to some question. King and Christensen[2] have reported the surprisingly low values for the enthalpy and entropy of melting for UF_4 of 10.2 kcal and 7.7 eu respectively. These values, however, were derived from high-temperature enthalpy measurements which included only two points in the liquid region slightly above the melting temperature. The low enthalpy of fusion, then, could possibly be the result of a low value for the enthalpy of liquid UF_4. On the other hand, Khripin and co-workers,[3] employing differential thermal analysis, have reported a polymorphic solid transition in UF_4 about 200° below its melting point with an enthalpy of transition of about 3.4 kcal. They claim this to be the reason for the low entropy of melting. However, neither the calorimetric study[2] nor the many reported phase diagrams involving UF_4[4] have shown any indication of such a transition. A recent DTA study by Gilpatrick[5] also failed to show the transition. We have, therefore, remeasured the enthalpy of UF_4 from room temperature up into the liquid phase with our copper block drop calorimeter in an attempt to clarify this matter.

The UF_4 was sealed in an inner nickel liner to prevent attack on the Inconel capsules especially designed for our enthalpy measurements. Platinum was not used because King and Christensen[2] reported that their platinum-rhodium capsules leaked due to attack by liquid UF_4.

The following equations represent our measured enthalpy data for UF_4 in calories per mole:

$$H_T - H_{298} = -9650 + 29.53T + 1.15 \times 10^{-3} T^2 + 2.21 \times 10^5 T^{-1} \quad (298\text{–}1309°K),$$

$$\Delta H_{fusion} = 11{,}230 \text{ cal/mole} \quad ;$$

$$\Delta S_{fusion} = 8.6 \text{ eu } (1309°K),$$

$$H_T - H_{298} = -9420 + 39.57T \quad (1309\text{–}1400°K).$$

Our enthalpy values are in fair agreement with those of King and Christensen.[2] They are about 1% higher from room temperature to about 900°K; they agree within a few tenths of a percent from 900°K to about 1200°K and are about 1% lower from there to the melting point. Our enthalpy values for the liquid are a little more than 1% higher than those in ref. 2. The fact that our enthalpy for the solid does not increase as rapidly just below the melting point and is somewhat higher in the liquid than in ref. 2 leads to an enthalpy of melting somewhat but not significantly (i.e., about 1 kcal) higher than that found by King and Christensen.

Our results give no indication of a transition. Khripin and co-workers report this transition in studies of the UF_4-UCl_4,[6] UF_4-UO_2,[7] and UF_4-UF_3[8] systems, but it has not been reported by any other investigators with the exception of Nekrasova et al.[9] in a study of the UF_4-CaF_2 system. However, they report the transition temperature to be 910°C (about 70° higher than that reported by Khripin), which is almost identical with the eutectic temperature reported for the UF_4-UO_2 system[7] and is almost certainly due to oxygen impurity in the UF_4 used in ref. 9. Although Khripin et al. eliminate oxygen as a cause for their observation of a halt at about 840°C, they say nothing about cation impurities. It is of interest to note in this connection that the eutectic halt in the UF_4-CaF_2 system[9] was found at 843°C.

Table 6.12 shows a comparison of the entropies for the isostructural (monoclinic) compounds ZrF_4, UF_4, and ThF_4. The entropy of melting for ZrF_4 of 12.7 eu is considerably larger than that of 8.6 eu for UF_4. However, the absolute entropy of UF_4 at 1400°K is larger than that for ZrF_4 by about 7 eu. This is approximately what would be expected considering the differences in size, mass, and magnetic characteristics of the cations.

An attempt was also made to measure the enthalpy of fusion of ThF_4. However, experimental difficulties were encountered, and the measurements were terminated. Enough qualitative data were obtained, however,

Table 6.12. Comparison of entropies of ZrF_4, UF_4, and ThF_4

	T_M (deg K)	Entropy (eu/mole)			
		ΔS_M	$S°_{298}$	$S°_{1400} - S°_{298}$	$S°_{1400}$
ZrF_4	1205	12.7[a]	25.0[b]	59.7[c]	84.7
UF_4	1309	8.6	36.3[d]	56.0	92.3
ThF_4	1383		34.0[e]		

[a]Reference 10.
[b]Reference 11.
[c]Calculated from ref. 10.
[d]Reference 12.
[e]Reference 13.

to indicate that, as expected, the fusion behavior of ThF_4 approximates that of UF_4 rather than that of ZrF_4. No further enthalpy measurements of ThF_4 are planned with our present apparatus.

---

1. This work also has been reported in the *MSR Program Semiannu. Progr. Rep. Feb. 28, 1971,* ORNL-4676.

2. E. G. King and A. U. Christensen, *U.S. Bur. Mines Rep. Invest.* 5909 (1961).

3. L. A. Khripin, Y. V. Gagarinski, and L. A. Lukyanova, *Izv. Sib. Otd. Akad. Nauk SSSR, Ser. Khim. Nauk* No. 3 (1), 14 (1965).

4. R. E. Thoma, ed., *Phase Diagrams of Nuclear Reactor Materials,* ORNL-2548 (1959).

5. L. O. Gilpatrick, *MSR Program Semiannu. Progr. Rep. Feb. 28, 1970,* ORNL-4548, p. 148.

6. L. A. Khripin et al., *At. Energ.* **19**, 437 (1965).

7. L. A. Khripin and L. A. Lukyanova, *Izv. Sib. Otd. Akad. Nauk SSSR, Ser. Khim. Nauk* No. 3 (1), 131 (1966).

8. L. A. Khripin, S. A. Poduzova, and G. M. Zadneprovskii, *Russ. J. Inorg. Chem.* **13**(10), 1439 (1968).

9. N. P. Nekresova et al., *At. Energ.* **22**, 293 (1967).

10. R. A. McDonald, G. C. Sinke, and D. R. Stull, *J. Chem. Eng. Data* **7**, 83 (1962).

11. E. F. Westrum, Jr., *J. Chem. Eng. Data* **10**, 140 (1965).

12. J. H. Burns, D. W. Osborne, and E. F. Westrum, Jr., *J. Chem. Phys.* **33**, 387 (1960).

13. H. R. Lahr, D. W. Osborne, and E. F. Westrum, Jr., *J. Amer. Chem. Soc.* **76**, 3837 (1954).

ENTHALPY OF LITHIUM FLUOROBORATE FROM 298 TO 700°K: ENTHALPY AND ENTROPY OF FUSION

A. S. Dworkin

We have examined the effect of the differences in structure and cation size on the enthalpy and entropy of fusion and transition in the alkali fluoroborates sodium through cesium.[1] Lithium fluoroborate, with its much smaller cation, differs from the other fluoroborates in that it has at room temperature a hexagonal structure type, probably that of SiO_2.[2] One recent paper[3] reports that there is no transition in $LiBF_4$ between room temperature and the melting point, while another[4] reports a transition at about 115°C. We, therefore, have measured the enthalpy of $LiBF_4$ from room temperature to about 40° above its melting temperature to complete our thermochemical studies of the alkali metal fluoroborates.

We found no evidence for a transition either in the enthalpy measurements or in a separate thermal analysis experiment. $LiBF_4$ is hygroscopic and must be handled in a dry, inert atmosphere as it was in our work and in that of ref. 3. However, this was not the case in the work reported in ref. 4, where in fact the $LiBF_4$ was ground to a fine powder in the open and even heated in an open system for the differential thermal analysis experiments.

The following equations represent our measured enthalpy data for $LiBF_4$ in calories per mole:

$$H_T - H_{298} = -11{,}570 + 32.02T + 1.19 \times 10^{-3} T^2 + 5.72 \times 10^5 T^{-1} \quad (298\text{–}577°K),$$

$$\Delta H_{fusion} = 3550 \text{ cal/mole};$$

$$\Delta S_{fusion} = 6.16 \text{ eu } (577°K),$$

$$H_T - H_{298} = -11{,}300 + 40.1T \; (577\text{–}700°K).$$

Table 6.13 compares the enthalpies and entropies of fusion and transition for the alkali metal fluoroborates. The high-temperature forms of the fluoroborates of sodium through cesium acquire considerable entropy at the transition temperature, probably due to anionic rotational or librational disorder.[1] Their entropy of melting, therefore, is lower than that for $LiBF_4$, although the sum of the entropy of transition and melting ($\Delta S_m + \Delta S_{tr}$) is higher than that for $LiBF_4$. $NaBF_4$ differs in both high- and low-temperature structure from the other fluoroborates as well as from

Table 6.13. Heats and entropies of melting and transition of alkali metal fluoroborates

	T_m (°K)	ΔH_m (kcal/mole)	ΔS_m (eu/mole)	T_{tr} (°K)	ΔH_{tr} (kcal/mole)	ΔS_{tr} (eu/mole)	$\Delta S_m + \Delta S_{tr}$ (eu/mole)
$LiBF_4$	577	3.55	6.16				6.2
$NaBF_4$	679	3.25	4.78	516	1.61	3.1	7.9
KBF_4	843	4.30	5.10	556	3.30	5.9	11.0
$RbBF_4$	855	4.68	5.5	518	2.86	5.5	11.0
$CsBF_4$	828	4.58	5.5	443	1.94	4.4	9.9

$LiBF_4$. This is reflected in its intermediate value for $\Delta S_m + \Delta S_{tr}$. The different structure, lack of transition, and lower $\Delta S_m + \Delta S_{tr}$ for $LiBF_4$ most likely may be attributed to the small size of the lithium ion.

1. A. S. Dworkin and M. A. Bredig, *J. Chem. Eng. Data* 15, 505 (1970).

2. G. Brunton, private communication, 1971.

3. S. Cantor, D. P. McDermott, and L. O. Gilpatrick, *J. Chem. Phys.* 52, 4600 (1970).

4. R. J. Marano and E. R. Shuster, *Thermochimica Acta* 1, 521 (1970).

HIGH-TEMPERATURE CRYSTAL CHEMISTRY OF TETRAFLUOROBORATES AND STRUCTURALLY RELATED COMPOUNDS[1]

M. A. Bredig

After construction of a simple heating attachment to a Buerger precession camera, a high-temperature x-ray powder pattern of $NaBF_4$ was obtained. It confirmed my recent criticism[2] of an alleged monoclinic crystal structure proposed earlier.[3] The structure found now makes $NaBF_4$ di-isotypic with $CaSO_4$, namely, orthorhombic at room temperature, hexagonal above the transition temperatures of 241 and 1100°C respectively. The hexagonal lattice constants of $NaBF_4$, $a_0 = 5.00 \pm 0.02$ Å and $c_0 = 7.75 \pm 0.03$ Å at 265°C, are very similar to 4.98 ± 0.02 and 7.67 ± 0.03 Å of $CaSO_4$ at 1200°C.[4] Thus far, attempts to derive atomic positions from the intensities of the powder patterns were not successful; efforts are under way to prepare and study a single crystal of $NaBF_4$.

A high degree of rotational disorder of the BF_4^- ion is indicated by the rapid decrease in intensities with x-ray diffraction angle as well as by the relatively large transition entropy.[5] The presence of such disorder may also reconcile the hexagonal symmetry with the observation of optical isotropy[6] and apparent degeneracies in the Raman spectrum.[7]

An x-ray powder pattern of $CsBF_4$ at 212°C yielded $a_0 = 7.88 \pm 0.03$ Å for the face-centered cubic high-temperature modification, quite in line with $a_0 = 7.612$ Å for $RbBF_4$ and 7.40 ± 0.03 Å for KBF_4 obtained in good agreement with existing measurements.

Relative volume expansions, $\Delta V/V_0$, from room temperature to slightly above the temperatures of the transition orthorhombic-cubic in three of the alkali metal tetrafluoroborates $M(I)BF_4$ and perchlorates $M(I)ClO_4$, M(I) = K, Rb, Cs, and two of the alkaline-earth sulfates, $M(II)SO_4$, M(II) = Sr, Ba, were computed from the x-ray data. These relative expansions show a decrease with increasing cation size, from salts with small cations, for example, Sr^{2+}, $r = 1.13$ Å, to salts with large ones, for example, Cs^+, $r = 1.69$ Å. As the compounds with the smallest cations, Na^+ and Ca^{2+}, $r \approx 1.0$ Å, differ in both their low- and high-temperature structures from those of the larger ones, it is not surprising that they do not fit the trend above. At least for $NaBF_4$ and KBF_4, however, a Clausius-Clapeyron calculation of ΔV_{tr} at T_{tr} from ΔS_{tr} and dT_{tr}/dp indicates it to be similar, 4.6 and 5.6 cm^3/mole. Therefore, the difference in $\Delta V/V_0$ is mainly due to the difference in the thermal expansion of the two different orthorhombic low-temperature structures of these two compounds. A similar expansion behavior is exhibited by $NaNO_3$ and KNO_3.

1. Summarized from a similar contribution in the *MSR Program Semiannu. Progr. Rep. Feb. 28, 1971,* ORNL-4676.

2. A. S. Dworkin and M. A. Bredig, *Chem. Div. Annu. Progr. Rep. May 20, 1970,* ORNL-4581, p. 116.

3. C. W. F. T. Pistorius, J. C. A. Boeyens, and J. B. Clark, *High Temp.–High Pressures* 1, 41 (1969).

4. M. A. Bredig, *Chem. Div. Annu. Progr. Rep. May 20, 1968,* ORNL-4306, p. 129.

5. A. S. Dworkin and M. A. Bredig, *J. Chem. Eng. Data* 15, 505–7 (1970).

6. G. D. Brunton, private communication.

7. A. S. Quist, J. B. Bates, and G. E. Boyd, private communication, and *MSR Program Semiannu. Progr. Rep. Feb. 28, 1971,* ORNL-4676; also "Raman Spectra of the High-Temperature Phase of Polycrystalline $NaBF_4$," a following contribution in this section, this report.

EXCESS FREE ENERGY IN SOME BINARY MOLTEN-SALT MIXTURES WITH A COMMON CATION

M. A. Bredig

LiF-Li_2BeF_4

Very accurate measurements of the LiF liquidus in the LiF-BeF_2 system which included the finding that Li_2BeF_4 melts congruently[1] suggested an attempt to interpret this liquidus in terms of mixing F^- and BeF_4^{2-} anions in the presence of the common cation, Li^+, instead of the more common model of mixing Li^+ and Be^{2+} cations in the presence of a common anion, F^-.[2] The partial molar free energy of LiF, calculated according to the Temkin model, was compared with that represented by the LiF liquidus in LiF-Li_2BeF_4 and also in the systems LiF-Li_2SO_4[3] and LiF-

Li_2WO_4,[4] expected to be quite analogous. The ideal liquidus was computed from

$$\ln a(\mathrm{LiF}) = \frac{\Delta H_m}{R}(T_m^{-1} - T^{-1}) + \frac{\Delta C_p}{RT}(T_m - T) - \frac{\Delta C_p}{R}\ln(T_m/T),$$

with $\Delta H_m = 6470$ cal per mole of LiF and $\Delta C_p = 5.87 - 4.78 \times 10^{-3} T$, derived from the JANAF tables.

The observed LiF liquidus in LiF-Li_2SO_4 deviates somewhat negatively, but that in LiF-Li_2WO_4 not perceptibly, from the calculated one (Fig. 6.32). It is surprising to see ions as different in size (crystal radius r), charge (z), polarizability (α), and composition as F^- and WO_4^{2-} seemingly mix ideally according to the Temkin model. Significantly, however, the ionic field strengths are similar, z/r for $F^- \approx -1/1.36 = -0.73$ and z/r for $WO_4^{2-} \approx -2/(2 \times 1.40) = -0.71$.

In LiF-Li_2BeF_4, up to approximately 45 mole % Li_2BeF_4, departure from ideality is hardly noticeable. The increasing positive deviation with further decrease in excess LiF over $2LiF \cdot BeF_2$ (= Li_2BeF_4) probably is best attributed to what may well be the first stage of polymerization,[5] a dimer, from $2BeF_4^{2-} = F^- + Be_2F_7^{3-}$. By analogy with the known $Si_2O_7^{6-}$, $Be_2F_7^{3-}$ would consist of two fluoride tetrahedra sharing one corner. Direct evidence for this particular species ought to be sought from a comparison of the Raman spectrum of a melt 60 LiF–40 BeF_2 with the spectrum of solid and molten $Na_2LiBe_2F_7$ or $RbLi_2Be_2F_7$, proof of the actual existence of $Be_2F_7^{3-}$ in the solid compounds to be obtained by x-ray analysis.

Fluoride-Iodide Mixtures with a Monovalent Common Cation

The systems LiF-LiI and NaF-NaI contain an anion, I^-, similar in size to, yet much more polarizable than, the ions ZX_4^{2-} above. New liquidus data were recently reported,[6] yet without reference to thermodynamic relationships. I examined them with the following results.

In the vicinity of the melting points of LiF and NaF, the liquidus curves as drawn by the investigators (dotted lines, Fig. 6.33) are in error. They would

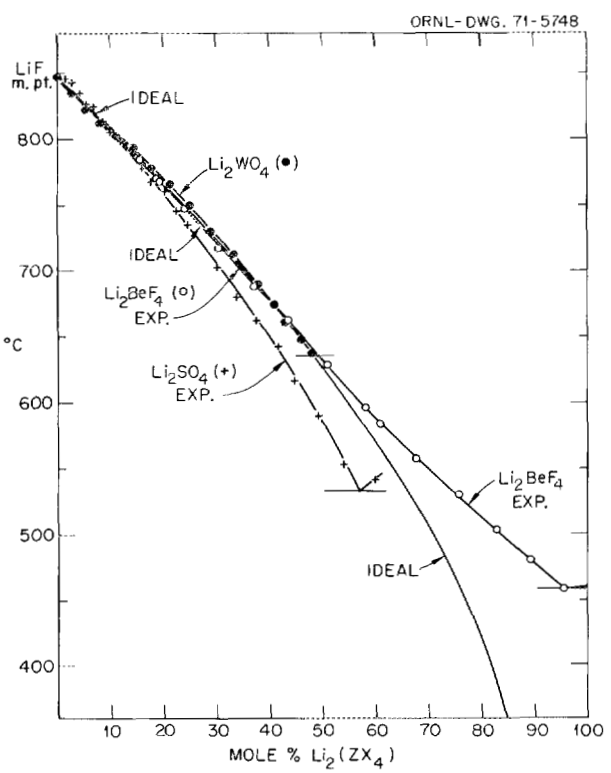

Fig. 6.32. LiF liquidus, experimental and Temkin-ideal, in the systems LiF-Li_2BeF_4, LiF-Li_2WO_4, and LiF-Li_2SO_4.

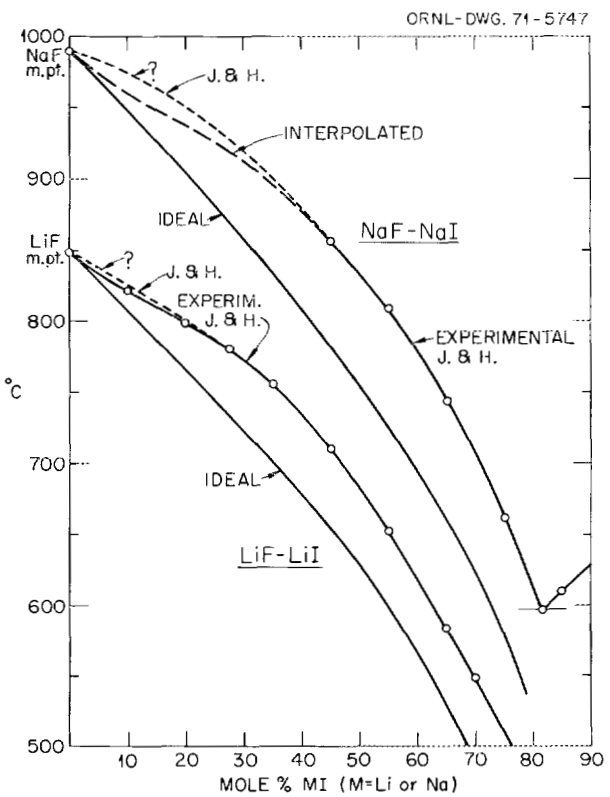

Fig. 6.33. LiF and NaF liquidus curves, experimental and Temkin-ideal, in the LiF-LiI and NaF-NaI systems.

indicate solid solution, that is, a mixing of F^- and I^- in solid fluoride to a degree highly improbable considering their difference in size and polarizability. The reasonable alternative, an ideal liquidus for small iodide additions, with no solid solution, is actually indicated by the experimental point at 10 mole % LiI (Fig. 6.33); in NaF-NaI no data exist for the lower iodide concentrations. However, the most significant aspect of these phase diagrams is the pronounced nonideality of the LiF and NaF liquidus at higher iodide concentrations. Not surprisingly, the positive excess free energy (μ^E) of mixing thus indicated for the mixing of the smallest (F^-) with the largest (I^-) halide ion is larger than in any other simple binary alkali halide system investigated, that is, as high as 650 cal/mole for $\mu^E{}_{NaF}$ near 30 mole % NaF.

Fluoride-Iodide Mixtures with a Divalent Cation

We compare the case of CaF_2-CaI_2 mixtures with the preceding ones. In a discussion of the phase diagram,[7] my calculation of the ideal CaF_2 liquidus (Fig. 6.34) was used to point out the large deviation from the Temkin model. At the eutectic, $\mu^E{}_{CaF_2}$ is 615 cal/equiv, quite similar to the maximum $\mu^E{}_{NaF}$ in NaF-NaI. At low CaI_2 concentrations (high temperatures), where direct measurements were not made, extrapolation (dashed line, Fig. 6.34) gives maximal values for the liquidus temperatures, that is, maximal values of $\mu^E{}_{CaF_2}$ that are by as much as a factor of 3 smaller than those for NaF in NaF-NaI. The difference may perhaps be explained as follows.

The overall positive excess free energy results from the large difference in polarizability and its effect upon van der Waals interaction between anions, F^- and I^-. However, in fluoride-rich melts a negative component, apparently not previously recognized, may arise from the enhancement in the polarization of I^- by Ca^{2+} in cation-anion-anion configurations, such as $Ca^{2+}I^-F^-$, over that in $Ca^{2+}I^-I^-$ of pure CaI_2. The greater field strength of F^-, $z/r = -0.73$, compared with I^-, $z/r = -0.46$, leads to an enhancement of the field gradient that the I^- in $Ca^{2+}I^-F^-$ encounters. The effect is greater in mixtures with a divalent common cation than with a monovalent one (NaF-NaI, above) for two reasons: the higher field strength of the cation and the greater anion:cation ratio resulting in greater frequency of configurations MIF. Other examples, such as MgF_2-MgI_2, ZnF_2-ZnI_2, and AgF-AgI, are being considered for further study which will also allow assessing the influence of high temperatures (above 1000°C), not taken into account as yet.

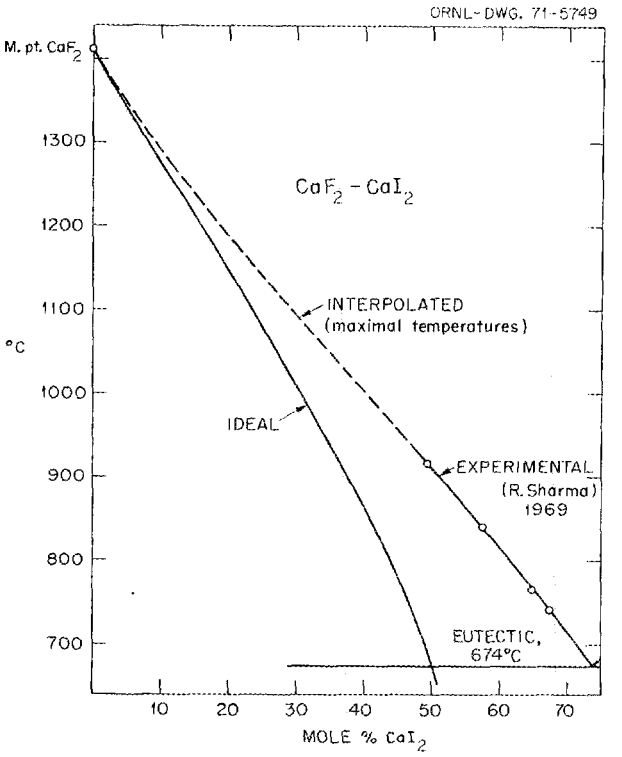

Fig. 6.34. CaF_2 liquidus, experimental, interpolated, and Temkin-ideal, in CaF_2-CaI_2.

Comparison of LiF-Li_2BeF_4 and LiF-LiI Mixtures

It has been suggested[8] that small positive enthalpy changes on mixing NaBr with $NaNO_3$ or NaCl are explainable by ion "packing" or "short-range repulsion" effects — not a change in van der Waals dispersion forces between anions. It would seem, however, that for the much larger free-energy change in mixing relatively rigid F^- with I^- of high polarizability the difference in dispersion forces, which are proportional to the square of the polarizability, $\alpha^2(I^-):\alpha^2(F^-) = 65!$, is the dominant factor. This seems to follow also from the observed near ideality, up to high $BeF_4{}^{2-}$ concentrations (Fig. 6.32), of mixing F^- with $BeF_4{}^{2-}$, where the size difference is as large as with I^-, yet the difference in dispersion forces is much smaller, $\alpha^2(BeF_4{}^{2-}):\alpha^2(F^-) = 12$. The same holds for the highly ideal LiF-Li_2WO_4 system (Fig. 6.32), where the polarizability ratio $WO_4{}^{2-}:F^-$ is also smaller than for $I^-:F^-$, as well as for the similarly ideal MgF_2-$MgCl_2$,[9] with $\alpha^2(Cl^-):\alpha^2(F^-) \approx 13$. Of course, in the case of LiF-Li_2SO_4 a factor, unknown as yet, other than the (intermediate) difference in polarizability [$\alpha^2(SO_4{}^{2-}):\alpha^2(F^-) = 35$], must be responsible for the observed

negative excess free energy of mixing; interestingly, $NaF\text{-}Na_2BeF_4$ exhibits a very similar behavior.

Solid Solutions in Alkali Metal Iodide-Chloride Systems

Examination of additional alkali halide phase diagrams from ref. 6 in terms of fusion entropies led to the finding that the liquidus curves in LiI-LiCl and NaI-NaCl, as was to be expected, definitely demonstrate the existence of considerable mutual solid solubility through the considerable positive deviation of the liquidus temperatures *even at the smallest solute concentrations.* At the eutectic temperatures my estimates are 13 mole % NaCl in solid NaI and 6 mole % NaI in solid NaCl, 5 mole % LiCl in solid LiI and 2 mole % LiI in solid LiCl. Thus, the statement[6] that the three fields of crystallization in the ternary systems Li(F, Cl, I) and Na(F, Cl, I) are those of the "pure" components is in need of modification. Because of this solid solubility, interpretation of the liquidus in terms of excess free energy of mixing is, of course, not possible.

---

1. K. A. Romberger and J. Braunstein, *MSR Program Semiannu. Progr. Rep. Feb. 28, 1970,* ORNL-4548, p. 161.
2. J. Braunstein also is considering the problem (private communication).
3. E. I. Speranskaya and A. G. Bergman, *Izv. Sekt. Fiz. Khim. Anal., Inst. Obshch. Neorg. Khim., Akad. Nauk SSSR* **26,** 180 (1955).
4. A. I. Kiselova, V. I. Posypaiko, and A. G. Bergman, *Zh. Fiz. Khim.* **29,** 359 (1955).
5. See also the discussion of BeF_2 polymerization by C. F. Baes, *J. Solid State Chem.* **1,** 159 (1970).
6. C. E. Johnson and E. J. Hathaway, *J. Electrochem. Soc.* **118,** 631 (1971).
7. R. A. Sharma, *High Temp. Sci.* **1,** 423 (1969).
8. O. J. Kleppa and S. V. Meschel, *J. Phys. Chem.* **67,** 668 (1963).
9. R. A. Sharma and I. Johnson, *J. Amer. Ceram. Soc.* **52,** 612 (1969).

"ThOF": TRIVALENT THORIUM?

M. A. Bredig

In spite of the preparation, by a number of investigators, of a few thorium compounds such as "ThI_3" of a stoichiometry suggesting Th^{3+}, the existence of this chemical valency has not been accepted. According to Scaife and Wylie,[1] "It is not clear whether the observations of Clark and Corbett[2] as to high resistance and qualitative diamagnetism apply to thorium triiodide or to a mixed phase with I/Th $\leqslant$ 3.4 . . . ." Hayek et al.[3] state (in translation): ". . . including thorium in the actinide group . . . does not make good sense."

Contradicting the latter statement are the results of two publications by Lucas and Rannou[4,5] that describe preparation and properties of what is claimed to be an oxyfluoride "ThOF." Its grayish-white (!) color would make it appear to be analogous to the truly actinide-type oxyfluorides AcOF, PuOF, and CfOF. In connection with observation here at ORNL of a certain, if very small, solubility of Th metal in $LiF\text{-}ThF_4$ melts,[6,7] I have examined this evidence for "ThOF" with the following results.

1. Lucas and Rannou give 5.68 Å as the lattice constant of a fluorite-type cubic face-centered unit cell containing four molecules of "ThOF." This corresponds to a molar volume of 27.6 cm^3/mole. Figure 6.35 shows the very large deviation of more than 10%, that is, more than 20 times the experimental error, from the value 30.8 cm^3/mole which one reads off the line connecting the molar volumes of AcOF, PuOF, and CfOF (dashed line). For comparison Fig. 6.35 also shows the complete regularity (which includes CeOF) of the corresponding molar volumes for the lanthanide oxyfluorides.

2. The lattice constant reported for "ThOF," 5.68 Å, is identical with 5.674 Å of the saturated solution of ThF_4 (25 mole %) in solid ThO_2 (5.600 Å without ThF_4).[8] The product of the reaction of $2ThO_2$ with

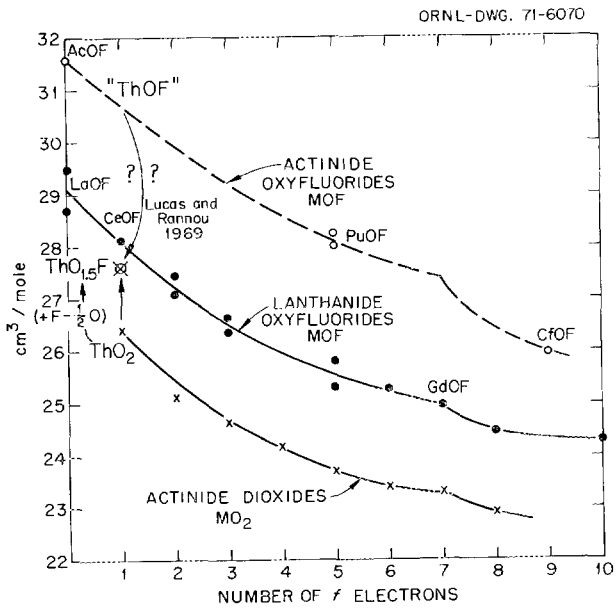

Fig. 6.35. Molar volumes of actinide oxyfluorides, lanthanide oxyfluorides, and actinide dioxides. ⊗ is the molar volume of "ThOF" as well as of the solid solution of ThF_4 in ThO_2.

$1ThF_4$ and 1Th observed by Lucas and Rannou, then, in all probability was not 4ThOF, but $2ThO_{1.5}F$ (the solid solution) + $1ThOF_2$ + 1Th (unreacted). No attempt at chemical or mechanical separation of "ThOF" was reported; thus the analysis simply could not be expected to give anything but the initial composition! On titration with permanganate the unreacted thorium metal was, of course, not distinguishable from its equivalent in "4ThOF." Why no metal was said to have been found in the x-ray pattern of the reaction product might be explained if segregation took place on screening the powder in preparing the x-ray sample, as observed by us in similar cases. The absence of the very numerous and therefore much weaker reflections of the 25 mole % $ThOF_2$ (of low crystal symmetry), which I assume to have been present, seems also understandable, especially in samples of high x-ray absorption.

3. After a tentative reference to "antiferromagnetism,"[4] "ThOF" was reported to be paramagnetic but *not* to obey the Curie-Weiss law.[5] This greatly favors the presence of thorium metal over that of a Th^{3+} ion.

One concludes that the evidence for "ThOF" is unsatisfactory and that it remains highly questionable to include thorium among the true actinide elements.

1. D. E. Scaife and A. W. Wylie, *J. Chem. Soc. London* **1964**, 5450.

2. R. J. Clark and J. D. Corbett, *Inorg. Chem.* **2**, 460–63 (1963).

3. E. Hayek, Th. Rehner, and A. Frank, *Monatsh. Chem.* **82**, 575–87 (1951); see also G. T. Seaborg in *The Actinide Elements*, pp. 750–51, McGraw-Hill, New York, 1954.

4. J. Lucas and J.-P. Rannou, *Compt. Rend. Acad. Sci., Ser. C* **266**, 1056–58 (1968).

5. J. P. Rannou and J. Lucas, *Mater. Res. Bull.* **4**, 443–50 (1969).

6. C. J. Barton and H. H. Stone, *Reduction of Iron Dissolved in Molten LiF-ThF4*, ORNL-TM-2036 (Nov. 2, 1967).

7. H. R. Bronstein and M. A. Bredig, *Chem. Div. Annu. Progr. Rep. May 20, 1969*, ORNL-4437, pp. 101–2.

8. R. W. M. D'Eye, *J. Chem. Soc. London* **1958**, 196.

POLARIZABILITY CHANGE FOR HALIDE IONS (X^-) ON FORMING COMPLEX IONS (BF_4^-) OR MOLECULES ZX_n[1]

M. A. Bredig

The polarizability of the negative ion is one of the fundamental parameters determining the properties of a salt. For example, the large difference in the polarizabilities of Cl^- and F^-, 3.48 Å^3 vs 0.95 Å^3 (K. Fajans) leads to a practically useful reversal in relative chemical stabilities of halides of lithium, thorium, uranium, protactinium, and rare earths, and thus is implicitly the basis of the "metal transfer process" using a chloride melt for separations in processing the fluoride-based fuel of the molten-salt breeder reactor.

Unfortunately, considerable confusion exists with respect to the use of proper standards for ion polarizabilities in evaluating changes on compound formation. I have examined the problem as applied (1) to the tetrafluoroborate ion, BF_4^-, (2) to halides of some polyvalent elements similar to boron, and (3) to some apparently "anomalous" behavior which may be attributed to mutual interaction of halide ions.

The Tetrafluoroborate Ion

Measured polarizabilities, α_m, of crystalline alkali metal tetrafluoroborates, MBF_4,[2] were used together with those of the free (gaseous) cation, α_+,[3] to derive $\alpha_- \equiv \alpha_m - \alpha_+$ for BF_4^- in the crystals.

As expected, for M = Na to Cs, $\alpha_- = 3.06 \pm 0.04$ Å^3 shows no systematic variation: the weak field of M^+ ($z/r \approx 1.05$ to 0.06, as compared with $z/r \approx 15$ for B^{3+}) contributes very little to the tightening of the F^- electron shells by B^{3+}, $\Delta\alpha_{F^-} = [\alpha_- - (\alpha_{B^{3+}} + 4\alpha_{F^-})]/4 = (3.06 - 3.90)/4 = -0.21$ Å^3 (~21%) per F^- ion.

An apparent trend for α_-, from 2.87 Å^3 in $NaBF_4$ to 2.29 Å^3 in $CsBF_4$, reported earlier[2] resulted merely from the misleading nature of *average* solid-state cation polarizabilities[4] used, which are inconsistent with established distinct systematic deviations from additivity of polarizability even in the alkali halides.

Test of Recent Theoretical Set of Halide Ion Polarizabilities, Especially F^-

In the preceding, the value used for α_{F^-} was 0.95 Å^3 derived by Fajans, not very different from 1.06 Å^3 given by Pauling. A recent calculation based on a simple classical model led to a much larger value, 1.56 Å^3 (model II, Wilson and Curtis) or even 1.83 Å^3 (their model I).[5] Earlier, quantum-mechanical calculations had also yielded 1.56 Å^3.[6] I have chosen as a simple test of validity the relative change in the reciprocal of polarizability, that is, the increase in "rigidity" of the electron shell $(\alpha_{HX}^{-1} - \alpha_{X^-}^{-1})/\alpha_{X^-}^{-1} \equiv \Delta(\alpha^{-1})/\alpha^{-1}$, on formation of the hydrogen halides from the gaseous ions, $X^- + H^+ \rightarrow HX$ (introduction of a proton into X^-).[7] Among the mole refractivities used[8] was a fairly recent value for liquid HF.[9] Figure 6.36 shows a

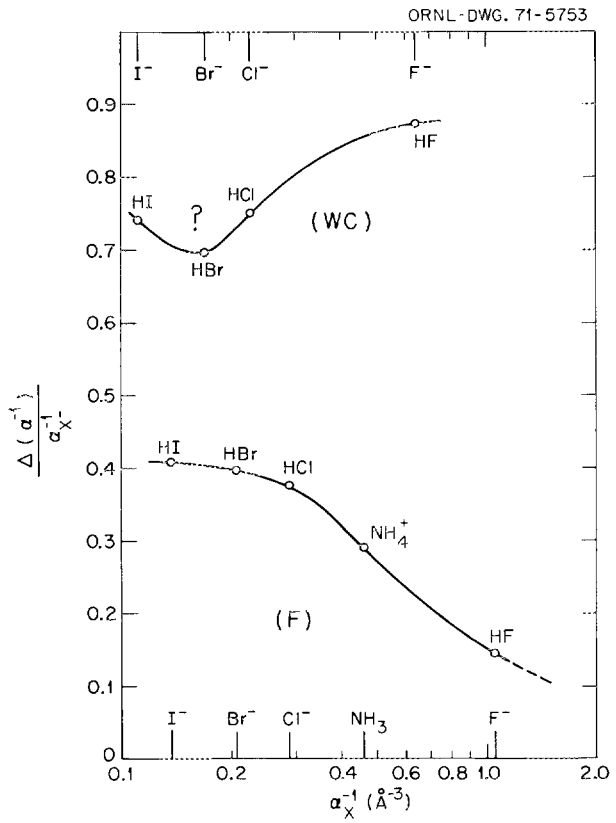

Fig. 6.36. Test of Wilson-Curtis model II (1970) vs Fajans free halide ion polarizabilities. Relative increase in electron shell rigidity, $\Delta(\alpha^{-1})/\alpha^{-1}$, for the process $X^- + H^+ \rightarrow HX$.

comparison of the two rather different sets of polarizabilities, Fajans (F) vs Wilson-Curtis model II (WC). The latter gives a complicated and unreasonable dependence of $\Delta(\alpha^{-1})/\alpha^{-1}$ on the original "rigidity," α^{-1}. Curve F, on the other hand, shows the smooth, monotonic *de*crease with increasing "rigidity" of X^-, which one expects for the simple process involved. Significantly, it also gives a perfect fit to an experimental point for the introduction of a proton into NH_3, that is, a molecule other than a halide ion (cf. ref. 11, pp. 133 ff.). One concludes, as Fajans did in another way (namely, by applying his method of inequalities of quotients[10]), that the newly proposed free-ion polarizabilities[5] are in disagreement with basic principles and experimental facts and that there is no reason to revise the well-proven set, especially $\alpha = 0.95$ Å^3 for the fluoride ion.

Halide Interaction Effect on Polarizability in Halides BX_3, AlX_3, CX_4, and SiX_4

An anomaly appears to exist in the polarizability decrease (electron shell tightening) of free halide ions, X^-, in the strong Coulomb field of Z^{n+} on forming ZX_n molecules (or ions) such as the boron trihalides, BX_3. Figure 6.37 shows that in contrast to the monotonic change of $-\Delta\alpha/\alpha$ as a function of α_X for the hydrogen halides, above, a maximum occurs in $-\Delta\alpha/\alpha \equiv [\alpha_{ZX_n} - (\alpha_{Z^{n+}} + n\alpha_{X^-})]/n\alpha_{X^-}$ between α_{F^-} and α_{Cl^-} in the tri- and tetrahalides shown. This has led me to suggest, it seems for the first time, that in molecular compounds ZX_n ($n \geqslant 3$) "crowding" of X^- ions, resulting in mutual interaction (deformation, "loosening") of their electron shells, may be a significant factor. An attempt was made to evaluate the magnitude of this effect by comparison with linear triatomic molecules, ZY_2 or ZXY, in which the geometry may be taken to minimize interaction between the two Y^{2-}, or Y^{2-} and X^-. In the absence of data for suitable boron compounds, for example, BOF, the carbon tetrahalides were studied first by comparison with carbon dichalcogenides for which such data exist.

Curve CY_2 in Fig. 6.38 represents the relative decrease, $-\Delta\alpha/\alpha$, of polarizability per Y^{2-} ($\alpha \equiv \alpha_D$ for $\lambda = 589$ nm) on formation of the triatomic molecules CO_2, COS, CS_2, and CSe_2 from $C^{4+} + 2Y^{2-}$ as a function of $\alpha_{Y^{2-}}$. The refractivities of free O^{2-}, S^{2-}, and Se^{2-} were taken as 6.95, 22.7, and 28.8 cm^3/mole respectively.[3] With $-\Delta\alpha/\alpha$ taken as 0 for $\alpha = 0$,[11] the observations can be fitted to an expression

$$-\Delta\alpha/\alpha = 0.535\,(1 - e^{-1.16\alpha}), \qquad (1)$$

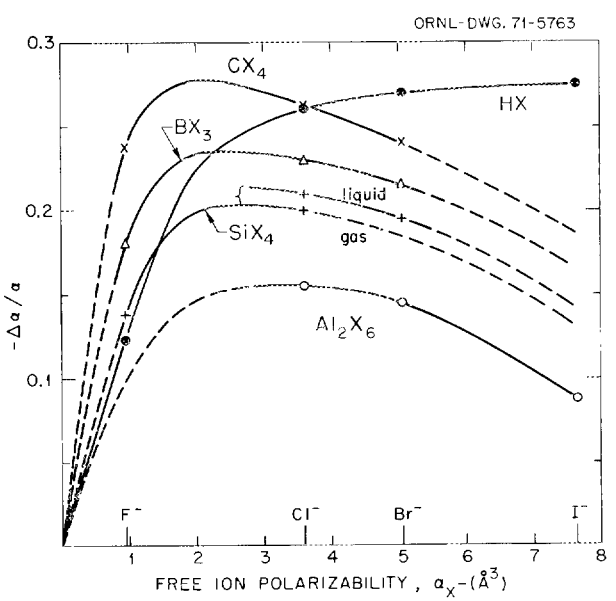

Fig. 6.37. Relative decrease in polarizability of X^-, $\Delta\alpha/\alpha$, in the process $Z^{n+} + nX^- \rightarrow ZX_n$ for Z = B, C, Al, and Si.

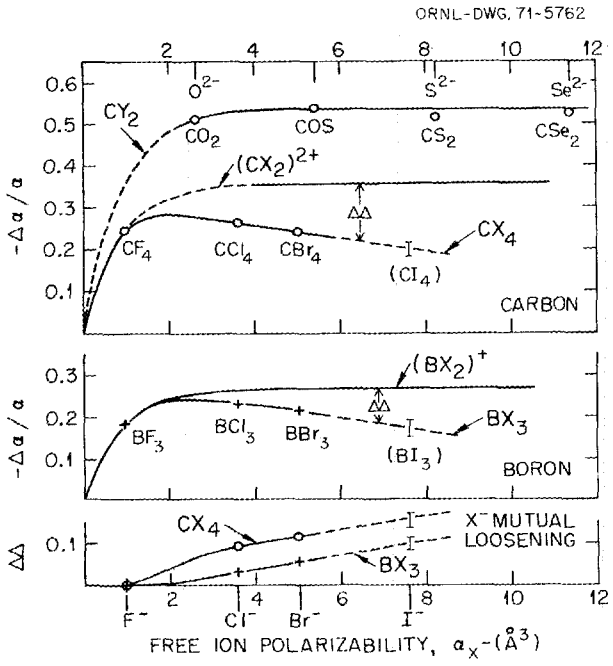

Fig. 6.38. Effect of X^- mutual deformation upon decrease in polarizability for $B^{3+} + 3X^- \rightarrow BX_3$ and $C^{4+} + 4X^- \rightarrow CX_4$.

identical in form to one given by Fajans for a variety of ions and molecules, F^-, OH^-, Cl^-, H_2O, NH_3, etc., on forming the respective molecules or ions, HF, H_2O, HCl, H_3O^+, NH_4^+, etc.[7,11] For comparison of CY_2 with CX_4, an adjustment for the double charge on Y^{2-} must first be made. A factor 1.5 is seen to hold for the ratio $-\Delta\alpha/\alpha = 0.360$, on the curve CY_2 at $\alpha = 0.97$ Å^3 (for F^-), to $-\Delta\alpha/\alpha = 0.240$ for CF_4 (experimental), where, because of the small size and low polarizability of F^- in the strong field of C^{4+}, the mutual deformation of the F^- is here neglected. Dividing Eq. (1) by 1.5 we obtain

$$-\Delta\alpha/\alpha = 0.360\,(1 - e^{-1.16\alpha}) \qquad (2)$$

to represent the tightening of X^- in a hypothetical linear CX_2^{2+} (Fig. 6.38), where mutual deformation of the $2X^-$, if any, is again neglected. Curve CX_4 for the formation of CX_4 from $C^{4+} + 4X^-$ would coincide with curve CX_2^{2+} if the larger X^- (Cl^-, Br^-, I^-) would not interfere with (i.e., "loosen") each other. The difference between the two curves is taken to represent just that interaction (bottom of Fig. 6.38).

To estimate the effect in the boron trihalides, curve BX_2^+ was obtained by reducing 0.360, in Eq. (2), to 0.270, that is, in proportion to the charges on B^{3+} and C^{4+}. This procedure reflects the effect of charge[11] on refractivity in the series SiO_4^{4-}, PO_4^{3-}, SO_4^{2-}, and ClO_4^-, where I find it to be approximately proportional to the charges of Si^{4+} to Cl^{7+}. The other parameter in the equation, 1.16 Å^{-3}, was taken over from Eqs. (1) and (2), as its variation has little effect, especially at higher values of α.

We see, then (bottom of Fig. 6.38) that the mutual deformation of X^- in BX_3 is considerably smaller than in CX_4, as indeed might be expected. For instance, it amounts for BBr_3 to 20% and for CBr_4 to 31% of the tightening effect estimated for no mutual deformation [curves BX_2^+ and CX_2^{2+}].

---

1. Modified from *MSR Program Semiannu. Progr. Rep. Aug. 31, 1970*, ORNL-4622, pp. 85–88.
2. S. Cantor, D. P. McDermott, and L. O. Gilpatrick, *J. Chem. Phys.* **52**, 4600 (1970); **53**, 4121 (1970).
3. N. Bauer and K. Fajans, *J. Amer. Chem. Soc.* **64**, 3023 (1942), and earlier papers by K. Fajans and co-workers.
4. J. R. Tessman, A. H. Kahn, and W. Shockley, *Phys. Rev.* **92**, 890 (1953).
5. J. N. Wilson and R. M. Curtis, *J. Phys. Chem.* **74**, 184 (1970); includes extensive literature references to other theoretical work.
6. H. D. Cohen, *J. Chem. Phys.* **45**, 10 (1966).
7. K. Fajans and N. Bauer, *J. Chem. Phys.* **10**, 410 (1942).
8. Appropriate volumes of Gmelin, 8th ed.
9. A. J. Perkins, *J. Phys. Chem.* **68**, 654 (1964).
10. K. Fajans, private communication and *J. Phys. Chem.* **74**, 3407 (1970).
11. K. Fajans, *Z. Phys. Chem. Abt. B* **24**, 103 (1934).

MAGNETIC SUSCEPTIBILITY OF TITANIUM(II) TETRACHLOROALUMINATE

A. S. Dworkin

J. Brynestad and co-workers of the Metals and Ceramics Division have succeeded in preparing and characterizing $Ti(AlCl_4)_2$,[1] in which titanium is stabilized in its divalent state by the Lewis acid $AlCl_3$. The compound was characterized by means of chemical analysis, crystal structure determinations, and absorption spectra measurements. We were asked to measure its magnetic susceptibility in order to confirm the expectation that the compound is magnetically dilute, that is, that its paramagnetic susceptibility is due to two unpaired *d* electrons.

The magnetic measurements were made by the Gouy method. Briefly, the apparatus consists of a Varian 9-in. magnet (V-3401), a Varian field-regulated magnet

power supply (Fieldial Mark I), and an Ainsworth semimicro recording balance. Cylindrical pole caps 9 in. in diameter were fabricated, and a pole gap width of 2 in. was used. The large pole gap allows for possible future high-temperature measurements. The apparatus was checked with both a diamagnetic sample (H_2O) and a paramagnetic sample (concentrated $CuCl_2$ solution).

Seven inches of powdered $Ti(AlCl_4)_2$ sealed in a 14- by ½-in. glass tube was supplied by J. Brynestad. Measurements were made at room temperature at field strengths of from 2 to 10 kG. The susceptibility remained constant to a few tenths of a percent over this range. An absolute accuracy of a few percent was attained, with the largest uncertainties involving the powder density of the compound in the tube and the cross-sectional area of the tube. Obviously, much greater accuracy in these measurements can be achieved if necessary.

The molar susceptibility of $Ti(AlCl_4)_2$, χ_M, was found to be 3530×10^{-6} cgs. The effective Bohr magneton number, μ_{eff}, calculated from $\mu_{eff} = 2.84 \times \sqrt{\chi_M T}$ is approximately 2.9, in good agreement with that expected from two unpaired electrons, $\mu_{eff} = \sqrt{n(n+2)} = 2.83$.

1. J. Brynestad et al., *Inorg. Nucl. Chem. Lett.* 6, 889 (1970).

RAMAN SPECTRA OF THE HIGH-TEMPERATURE PHASE OF POLYCRYSTALLINE $NaBF_4$[1]

Arvin S. Quist[2] John B. Bates[2]
George E. Boyd[2]

At a temperature of 245 ± 1°C,[3] orthorhombic $NaBF_4$ undergoes a phase change to a crystal structure first reported as a monoclinic[4] but later as a hexagonal structure with disordering of the fluoride ion positions in the lattice.[5] The Raman spectrum of this high-temperature form has now been measured to provide additional information regarding the lattice symmetry.

Static and dynamic field effects on the vibrational modes of BF_4^- in the orthorhombic $NaBF_4$ structure have been established by previous studies.[6,7] In this crystal, all components of the doubly degenerate ν_2 mode and of the triply degenerate ν_3 and ν_4 modes are observed. An increase in site symmetry of the BF_4^- ion in the high-temperature form may result in a collapse of the splitting, and only one frequency for each of the vibrational modes might be expected; thus the presence or absence of such effects would establish the symmetry of the effective field about the BF_4^- in the high-temperature lattice and, perhaps, might resolve the existing conflict in the x-ray data.

Raman spectra were measured with the equipment and techniques described previously.[8,9] The only innovation was the addition of a 20-mm-diam, 22-mm focal-length double-convex Pyrex lens positioned within the side port of the furnace to collect and collimate the scattered light. In the current studies, only the splitting of the ν_2 and ν_4 modes were examined in detail since the intensities of the ν_3 modes are quite weak. Figure 6.39 gives a comparison of the spectra of the ν_2 and ν_4 bands of polycrystalline $NaBF_4$ at temperatures of 240 and 254°C (a few degrees below and above the transition point of 245°C). This figure clearly shows the abrupt change in the Raman spectrum of crystalline $NaBF_4$ as the solid undergoes a phase transition. Below 245°C the two components of ν_2 shifted from 344 and 369 cm^{-1} at 25°C to 347 and 364 cm^{-1} at 240°C. Of

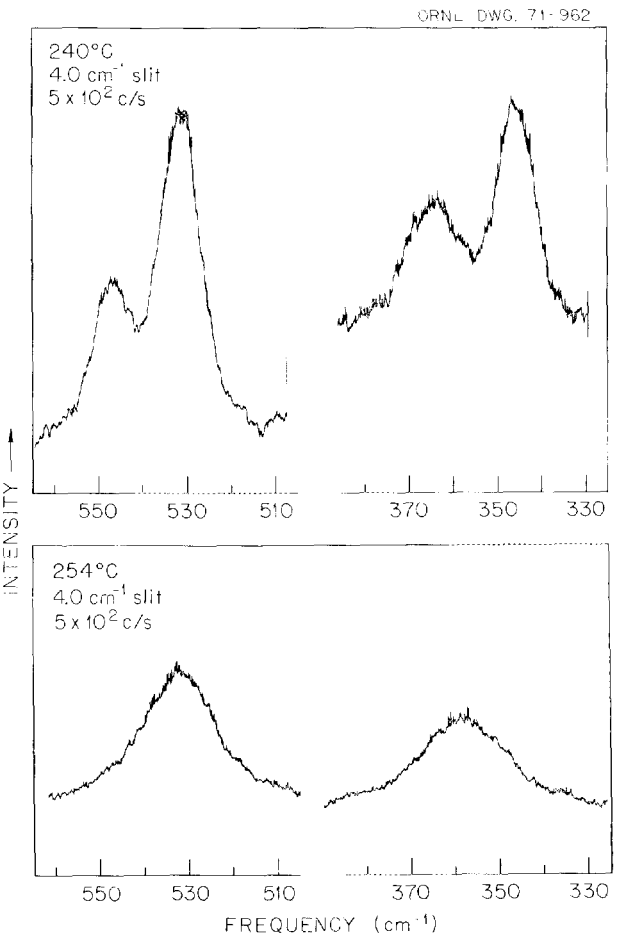

Fig. 6.39. Raman spectra of the ν_2 and ν_4 regions of polycrystalline $NaBF_4$ at 240 and 254°C. A phase transition occurs at 245°C.

the three components of ν_4, the two observed at 532 and 534 cm^{-1} at 25°C had coalesced into one band at 531 cm^{-1} at 240°C. The other component of this vibrational mode decreased from 554 cm^{-1} at 25°C to 547 cm^{-1} at 240°C. Above the transition temperature only single bands at 358 and 532 cm^{-1} were observed for ν_2 and ν_4 respectively. Essentially the same frequencies were observed previously with the molten salt.[9]

The Raman spectra indicate that the effective environment about the BF_4^- ion in the high-temperature crystalline phase of $NaBF_4$ has tetrahedral (or higher) symmetry. This observation is consistent with the recent x-ray results which lead to a hexagonal structure if complete disordering of all fluoride positions is assumed. With this complete disordering, the effective field experienced by a BF_4^- ion would be highly symmetric and would account for the lack of splitting of the ν_2 and ν_4 bands in the Raman spectra. The disordered structure also explains the similarity between the Raman spectra of the high-temperature crystalline phase and that of the melt; as a result of the disorder in the solid phase, a given BF_4^- ion "sees" an average, symmetric field similar to that experienced in the melt.

---

1. Expanded abstract of paper accepted for publication in *J. Chem. Phys.*

2. Director's Division.

3. C. J. Barton et al., *J. Inorg. Nucl. Chem.* 33, 337 (1971).

4. C. W. F. T. Pistorius, J. C. A. Boeyens, and J. B. Clark, *High Temp.—High Press.* 1, 41 (1969).

5. M. A. Bredig, *MSR Program Monthly Rep. December 1970 and January 1971*, MSR-71-13, p. 21 (internal memorandum).

6. J. B. Bates, A. S. Quist, and G. E. Boyd, *J. Chem. Phys.* 54, 124 (1971); *Chem. Div. Annu. Progr. Rep. May 20, 1970*, ORNL-4581, p. 168.

7. J. B. Bates, *Chem. Div. Annu. Progr. Rep. May 20, 1970*, ORNL-4581, p. 161; *J. Chem. Phys.* (1971).

8. A. S. Quist, *Appl. Spectrosc.* **25**, 80, 82 (1971); *Chem. Div. Annu. Progr. Rep. May 20, 1970*, ORNL-4581, pp. 171, 172.

9. A. S. Quist, J. B. Bates, and G. E. Boyd, *Chem. Div. Annu. Progr. Rep. May 20, 1970*, ORNL-4581, p. 168; *J. Chem. Phys.* 54, 4896 (1971).

RAMAN SPECTRA OF BeF_4^{2-} IN MOLTEN LiF AND NaF TO 686°C[1]

Arvin S. Quist[2] John B. Bates[2]
George E. Boyd[2]

The proposed solvent for UF_4 and ThF_4 in the molten-salt breeder reactor will contain approximately 22 mole % BeF_2 and 78 mole % LiF; the coolant may be a melt of composition Li_2BeF_4. It has been of interest, therefore, to measure the vibrational spectra of molten LiF-BeF_2 mixtures to characterize the bands caused by Be-F interactions and to identify the complexes present in solution. Additionally, the BeF_4^{2-} ion is of interest as the first member of the isoelectronic triad BeF_4^{2-}, BF_4^-, and CF_4, in which the number of valence electrons (8) remains constant and the nuclear charge of the central atom increases progressively by unity. All of the four normal modes of vibration of the tetrahedral BeF_4^{2-} anion are Raman active; hence, Raman spectral measurements are particularly well suited for investigations on this anion.

The captive-liquid or "windowless" cell used to contain the melts has been described[3,4] as has the furnace[5] and optical system for focusing and collecting the Raman scattered light.[3–5] Spectra were recorded with a Jarrell-Ash model 25-300 spectrophotometer (Jarrell-Ash Company, Waltham, Massachusetts) and 4880-Å radiation from an argon ion laser for excitation.

Although Li_2BeF_4 melts are the ones of greatest practical interest currently, an Na_2BeF_4 melt also was studied to obtain information on "cation effects" on the vibrational spectra of BeF_4^{2-}. Molten Li_2BeF_4 and Na_2BeF_4 contain no more than the minimum fluoride ion concentration necessary for complete 4-coordination of beryllium; therefore it was of interest to measure the spectrum of BeF_4^{2-} in an excess of F^-. Binary LiF-BeF_2 and NaF-BeF_2 systems containing less than 20 mole % BeF_2 exhibit melting points above 700 and 800°C respectively; hence a ternary system of LiF-NaF-BeF_2 (30-53-17 mole %) melting near 550°C was studied. Additional measurements were made at 25°C on an aqueous $(NH_4)_2BeF_4$ solution with excess NH_4F and on solid Li_2BeF_4 (where x-ray measurements have indicated that beryllium is 4-coordinated).

The Raman spectrum of molten Na_2BeF_4 at 616°C is shown in Fig. 6.40. The spectra of molten Li_2BeF_4[6] and of the LiF-NaF-BeF_2 mixture are similar in appearance except that the half bandwidth of ν_1 for Li_2BeF_4 (100 cm^{-1}) is about twice that observed in Na_2BeF_4 (50 cm^{-1}). The corresponding value for the LiF-NaF-BeF_2 mixture is about 65 cm^{-1} and for aqueous BeF_4^{2-}, about 40 cm^{-1}. The Be-F vibrational frequencies observed in the above systems and their assignments are given in Table 6.14.

The frequencies of the BeF_4^{2-} vibrations observed from Raman spectral measurements on the solutions listed in Table 6.14 are relatively insensitive (within experimental error) to temperature and composition. The frequency of the symmetric, ν_1, vibrational mode

does not vary appreciably in going from the molten state (for several compositions and temperatures) to aqueous $(NH_4)_2BeF_4$. The most significant change observed in the Raman spectra of BeF_4^{2-} was the broadening of ν_1 on substituting Li for Na in the melts. The origin of this effect would appear to be cation dependent, as any significant change in anion-anion interaction should be observed as a frequency shift of ν_1.

The Raman spectrum of solid Li_2BeF_4 shows the expected splitting of the triply degenerate ν_3 and ν_4 modes and of the doubly degenerate ν_2 mode. This is

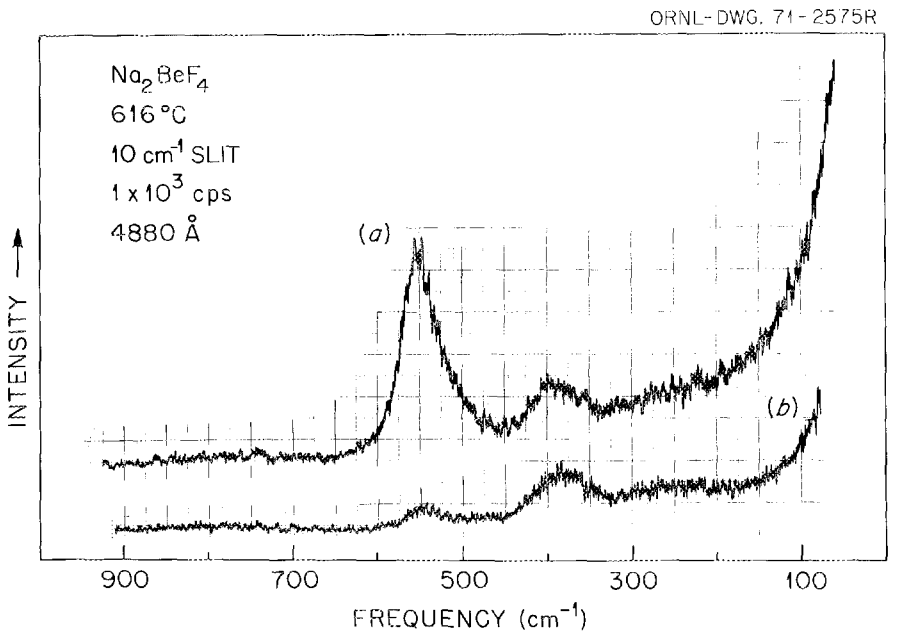

Fig. 6.40. Raman spectrum of molten Na_2BeF_4 at 616°C. (*a*) Incident light polarized perpendicular to plane containing slit and laser beam; (*b*) parallel polarization.

Table 6.14. Vibrational frequencies (cm^{-1}) observed in the Raman spectra of BeF_4^{2-} in melts, in solid Li_2BeF_4, and in aqueous solutions

Li_2BeF_4 melts			Molten Na_2BeF_4, 616°C	NaF-LiF-BeF_2 (53-30-17 mole %), 645°, 686°C	2.5 *M* $(NH_4)_2BeF_4$ in 2 *M* NH_4F, 25°C	Li_2BeF_4(s), 25°C		Assignment
487°C	533°C	640°C				Raman	Infrared	
255	240	260	265	255		257 295		$\nu_2(e)$
385	390	390	385	380	380	348 377 402	360 372 405	$\nu_4(f_2)$
						440 475	435 463 500	*a*
547	550	545	550	552	548	563		$\nu_1(a_1)$
800	800	800	800	800	795	775 795 850	775 805 860	$\nu_3(f_2)$

[a]Vibrations assigned to the Li^+ sublattice moving against the F^- sublattice.

consistent with a lowering of the T_d symmetry of the BeF_4^{2-} ion in the hexagonal unit cell lattice of Li_2BeF_4.[7] The weak bands observed near 125, 165, and 210 cm^{-1} are probably caused by external lattice modes. The weak bands at 440 and 475 cm^{-1} correspond to strong infrared bands which have been measured at 435, 463, and 500 cm^{-1}. These bands may be due to vibrations of the Li^+ sublattice against the sublattice of F^-. Analogous bands in the 400-to-550-cm^{-1} frequency region of the infrared spectrum of solid Li_2CO_3 were assigned to Li-O vibrations.[8]

The force constants of the general valence force field of BeF_4^{2-} were calculated by the approximation method of Krebs et al.[9] using the ν_1, ν_2, ν_3, and ν_4 frequencies observed in molten Li_2BeF_4 at 487°C. The Be-F bond distance of 1.56 Å used in calculating the G matrix was taken from the crystallographic data of ref. 7. The symmetrized force constants, F_{11}, F_{22}, F_{33}, F_{34}, and F_{44}, were calculated to be 3.342, 0.242, 3.115, 0.689, and 0.355 millidyne/Å respectively. The bond stretching constant, f_d, for Be-F was computed to be 3.17 millidyne/Å based on the values of F_{11} and F_{33} and the formula $f_d = \frac{1}{4}(F_{11} + 3F_{33})$.[8]

The results from this investigation indicate that the BeF_4^{2-} ion retains its tetrahedral symmetry in all the solutions examined. Additionally, the tetrafluoroberyllate anion appears to occur as a "free" entity in the molten salts studied; there are no frequency shifts to indicate detectable corner sharing of BeF_4^{2-} tetrahedra to form dimers such as $Be_2F_7^{3-}$.[10] Small concentrations of dimers might be present in stoichiometric Li_2BeF_4 and Na_2BeF_4, but their Raman spectrum would be too weak to be observed under the present conditions.

---

1. Expanded abstract of paper to be submitted to *J. Phys. Chem.*

2. Director's Division.

3. A. S. Quist, *Appl. Spectrosc.* **25**, 80 (1971); *Chem. Div. Annu. Progr. Rep. May 20, 1970,* ORNL-4581, p. 172.

4. A. S. Quist, J. B. Bates, and G. E. Boyd, *J. Chem. Phys.* **54**, 4896 (1971).

5. A. S. Quist, *Appl. Spectrosc.* **25**, 82 (1971); *Chem. Div. Annu. Progr. Rep. May 20, 1970,* ORNL-4581, p. 171.

6. A. S. Quist, J. B. Bates, and G. E. Boyd, *Chem. Div. Annu. Progr. Rep. May 20, 1970,* ORNL-4581, p. 166.

7. J. H. Burns and E. K. Gordon, *Acta Crystallogr.* **20**, 135 (1966); also, *Reactor Chem. Div. Annu. Progr. Rep. Jan. 31, 1965,* ORNL-3789, p. 30.

8. P. Tarte, *Spectrochim. Acta* **20**, 238 (1964).

9. B. Krebs, A. Müller, and A. Fadini, *J. Mol. Spectrosc.* **24**, 198 (1967).

10. M. A. Bredig, *MSR Program Monthly Rep. April 1971,* MSR-71-49, p. 27 (internal memorandum).

RAMAN SPECTRAL STUDIES OF MOLTEN LITHIUM NITRATE–LITHIUM PERCHLORATE MIXTURES[1]

M. H. Brooker[2] A. S. Quist[3] G. E. Boyd[3]

One of the fundamental goals in the interpretation of data from molten-salt systems is to determine the nature and extent of the ordering forces. It is known from neutron and x-ray diffraction studies that the long-range periodicity of crystals is lost when they melt. Atom-pair correlation functions derived from diffraction data show peaks characteristic of near-neighbor interactions and indicate charge alternation in successive shells about any ion. Significantly, positional correlation appears to be lost about 8 Å from any given starting point. Although these facts lend partial support to an irregular or distorted lattice model for molten salts, they also set a practical upper limit on possible long-range correlation of vibrational modes.

Within the confines of this limited order, the extent to which motions of molecules are correlated in the liquid phase has remained a matter of interest and speculation. The vibrational spectra of ionic nitrate melts have been studied by many workers in an effort to resolve this problem, but the results are still inconclusive.[4–9] Dynamical coupling between identical vibrations of nitrate molecules has been proposed.[7] Low-frequency infrared and Raman bands have been observed for melts in the same regions where external lattice mode bands are found for solids. Presence of these bands has prompted speculation that the vibrational spectrum of melts can be interpreted in terms of phonons, much like that of the solid.[7,9] However, there are many reasons for doubting the existence of nonlocalized modes in liquids. In a previous publication,[8] we proposed that the vibrational spectrum from molten $NaNO_3$ could be generated without invoking a species consisting of more than one nitrate ion. Bands in the low-frequency region have been observed for many polar liquids, and they are not unusual.[10,11] Although their origin is uncertain, dilution studies[10,11] have clearly shown that the band structure does not collapse and disappear as might be expected if long-range phase-related motions were dominant factors in their origin. Dilution studies with ionic nitrate melts also should give information about the nature of interactions in fused salts.

Raman spectra from molten $LiNO_3$, $LiClO_4$, and mixtures of the two molten salts have been obtained for a wide range of temperatures. Molten $LiClO_4$ proved to be an excellent diluent because it has no Raman bands which overlap those of the NO_3^- ion in either the

internal or external regions. In addition, the low melting point of $LiClO_4$ meant that spectra of the molten mixtures could be recorded at the same temperature as for pure molten $LiNO_3$. Complications to the spectra from hot bands, temperature broadening effects, and thermal emission were thus minimized.

The Raman frequencies observed with molten $LiNO_3$, $LiClO_4$, and a mixture of 5.3 mole % $LiNO_3$ and $LiClO_4$ at temperatures near the melting points are collected in Table 6.15 together with recently reported infrared frequencies of $LiNO_3$.[7] Portions of the Raman spectra from the 5.3 mole % $LiNO_3$ + $LiClO_4$ melt are shown in Fig. 6.41. Similar results were obtained for the other mixtures. Temperature changes of as much as 130°C caused only small variations in the measured spectra.

The significant observation of this work is the virtual insensitivity of the frequencies in the Raman spectrum of the molten mixtures to anion concentration (Table 6.15). Most dramatic is the presence of the low-frequency band and the two components in the ν_3 region in a melt containing only 5.3 mole % nitrate ions (Fig. 6.41). Two weak bands are also visible in the ν_4 region (Table 6.15). If the low-frequency mode and the doublet structure of the degenerate ν_3 and ν_4 modes were the result of order that required specific phase-related motions of nitrate ions (dynamical coupling) similar to that found in a lattice, it would be expected that as dilution proceeded, the band at 145 cm^{-1} would disappear and the doublet structure of the ν_3 and ν_4 modes would collapse to give single components. It would appear that dynamical coupling does not effect the vibrational spectrum of the molten nitrates. Bands of the nitrate ion apparently arise from "species" which contain only a single nitrate group. This is not to suggest that the nitrate ion does not feel the repulsive forces of other ions of like charge, but rather that one nitrate does not know if the next nearest neighbor is a nitrate or a perchlorate ion.

The semiqualitative description of ions vibrating in a cavity proposed by Edgell et al.[11] appears to present an extremely attractive pictorial representation of the motions involved in the generation of low-frequency modes. Translational motions of an ion vibrating in a cage formed by its counterions can give rise to a large dipole moment change and an infrared band. These infrared bands should be strongly dependent on the mass of the caged particle.[11] Hindered rotational

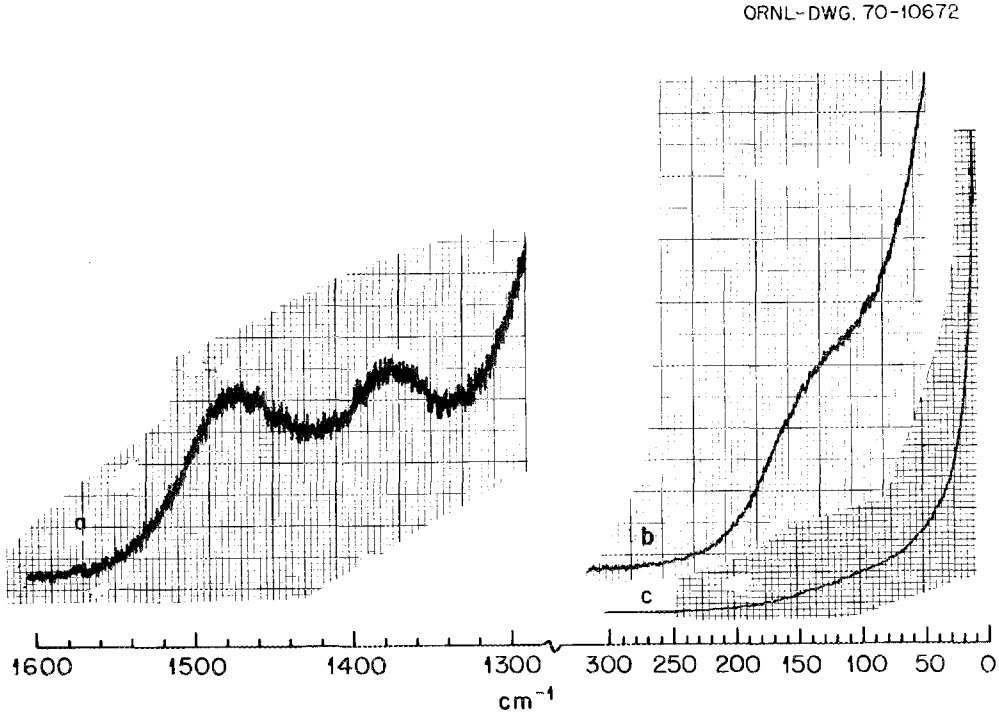

Fig. 6.41. Portions of Raman spectra from molten salts. Conditions: (*a*) 5.33 mole % $LiNO_3$ in $LiClO_4$, 257°C, 6.0-cm^{-1} slits, 1 × 10^3 counts/sec; (*b*) sample as in (*a*), 4.0-cm^{-1} slits, 2 × 10^4 counts/sec; (*c*) pure $LiClO_4$, 256°C, 4.0-cm^{-1} slits, 2 × 10^4 counts/sec. For *b* and *c* the perchlorate bands at 462 and 633 cm^{-1} have comparable intensities.

Table 6.15. Vibrational frequencies (cm^{-1}) obtained from $LiNO_3$-$LiClO_4$ melts

$LiNO_3$ (258°C)		5.33 mole % $LiNO_3$ in $LiClO_4$ (257°C), Raman	$LiClO_4$ (256°C), Raman[b]	Assignments (free ion notation)
Infrared[a]	Raman[b]			
	145 (dp)	145		
343[c]				
		462	462	ν_2 ClO_4^-
		633	633	ν_4 ClO_4^-
	718 (dp)	714		ν_4 NO_3^-
~742	746 (dp)	748		
819				ν_2 NO_3^-
827	823 (dp)			
		925	925 (sh)	$2\nu_2$ ClO_4^-
		954	954	ν_1 ClO_4^-
1053	1064[d] (p)	1064[d]		ν_1 NO_3^-
		1118	1118	ν_3 ClO_4^-
			1180 (vw, sh)	
1345				
1424	1360 (dp)[e]	1370		ν_3 NO_3^-
	1465 (dp)[e]	1475		
	1641[f] (p)	1638[f]		$2\nu_2$ NO_3^-

[a]Obtained from ref. 7.

[b]dp = depolarized, p = polarized, sh = sharp, and vw = very weak.

[c]Obtained from ref. 4.

[d]Slightly asymmetric on the low-frequency side.

[e]Analysis of the ν_3 band contour revealed four bands: 1355, 1380, 1445, 1480 cm^{-1}.

[f]Slightly asymmetric on the high-frequency side.

motions will give rise to a polarizability change and a Raman-active band if the rotator has anisotropic symmetry (i.e., NO_3^- but not ClO_4^-, Li^+, etc.). Raman band frequencies will depend on the interaction between the cage and the rotating ion such that the greater the interaction (smaller cavity size), the higher the rotational barrier and the greater the force constant and frequency. The insensitivity of the $LiNO_3$ spectrum to the amount of added $LiClO_4$ would indicate that the NO_3^- ion librates in a cavity created by Li^+ ions. The size of the cavity would be of the order of the Li^+-Li^+ distances in the fused salts, ca. 4 Å. For the molten $NaNO_3$, the cavity would be slightly larger and the barrier to rotation smaller; consequently, the corresponding band should be at lower frequencies. This band has been reported at 115 cm^{-1} in molten $NaNO_3$.[7,8]

The internal modes of the nitrate ion also can be rationalized on the hypothesis of a cage formed by the nearest-neighbor ions. Selection rules for the nitrate group will be determined by the symmetry of the field and not by the "free ion" selection rules. Asymmetry of the cage may be responsible for the infrared activity of ν_1 and the Raman activity of ν_2. Field asymmetry also may have lifted the degeneracies of the $\nu_3(E)$ and $\nu_4(E)$ modes causing the doublet structure in these regions, but the possibility that more than one type of cage can exist about a nitrate ion must be considered. A second type of cage would have the effect of doubling the number of vibrational bands. The two bands ca. 720 and 740 cm^{-1} in molten $LiNO_3$ and the $LiNO_3$ + $LiClO_4$ mixtures are reminiscent of similar bands in aqueous nitrate systems which have been used successfully to measure quantitatively the free and bound nitrate concentrations respectively.[12] In addition, if we allow for the possibility of hindered rotation to explain low-frequency modes, it might be expected that this rotational motion would also complicate the region of

the internal modes. It has been shown that even in liquids, damped rotational motions of molecular groups can couple with internal vibrational motions to cause spectral features similar to those found for the nitrate ion in aqueous solution and certain melts.[13]

---

1. Summary of published paper; *Chem. Phys. Lett.* 9, 242 (1971).
2. Visiting scientist, National Research Council of Canada Postdoctoral Fellow, 1969–71.
3. Director's Division.
4. J. K. Wilmshurst and S. Senderoff, *J. Chem. Phys.* 35, 1078 (1961).
5. S. C. Wait, A. T. Ward, and G. J. Janz, ibid. 45, 133 (1966).
6. D. W. James and W. H. Leong, ibid. 51, 640 (1969).
7. J. P. Devlin, P. C. Li, and G. Pollard, ibid. 52, 2267 (1970); J. P. Devlin, D. W. James, and R. Frech, ibid. 53, 4394 (1970).
8. M. H. Brooker, A. S. Quist, and G. E. Boyd, *Chem. Phys. Lett.* 5, 357 (1970).
9. G. H. Wegdam, R. Bonn, and J. Van Der Elsken, ibid. 2, 182 (1968).
10. B. J. Bulkin, *Helv. Chim. Acta* 52, 1348 (1969).
11. W. F. Edgell et al., *J. Amer. Chem. Soc.* 92, 2240 (1970).
12. D. E. Irish, A. R. Davis, and R. A. Plane, *J. Chem. Phys.* 50, 2262 (1969); D. E. Irish and A. R. Davis, *Can. J. Chem.* 46, 943 (1968).
13. P. V. Huong, M. Couzi, and M. Perrot, *Chem. Phys. Lett.* 7, 189 (1970).

CALORIMETRY

LOW-TEMPERATURE HEAT CAPACITY OF ^{7}Li HYDRIDE AND ^{7}Li DEUTERIDE

R. H. Busey R. B. Bevan, Jr.

Lithium hydride is an ionic compound with a face-centered cubic structure and is unique among all ionic crystals in that both of its ions have the helium electronic configuration. Crystalline lithium hydride, with four electrons per primitive unit cell, has been the subject of many experimental and theoretical studies because of its simple electronic structure. A comprehensive study of the lattice dynamics of lithium hydride has been made by Verble, Warren, and Yarnell,[1] who also list references to earlier experimental and theoretical work. They measured the phonon dispersion curves along the three high-symmetry directions in a single crystal of ^{7}LiD using the techniques of coherent inelastic scattering of thermal neutrons. Dispersion curves and frequency distribution curves were calculated for ^{7}LiD and ^{7}LiH based upon a seven-parameter shell-model fit of the data. Jaswal and Hardy,[2] using the data of Verble et al.[1] (along with other data) and a deformation-dipole model, have computed phonon dispersion curves and frequency distribution curves for LiH and LiD which have longitudinal optical branches consistently higher than those calculated by Verble et al. Both models give approximately the same transverse optical branches and are in agreement with infrared reflection[3] and absorption[4,5] spectra.

Other properties of lithium hydride have been tabulated and discussed by Pretzel et al.[6]

We report here briefly results of measurements of the low-temperature heat capacities of ^{7}LiH and ^{7}LiD. These data should provide important additional information on the lattice dynamics of probably the simplest of ionic solids. The only previous heat capacity measurements at low temperatures are those of Kostryukov[7] on normal lithium hydride made from naturally occurring lithium and hydrogen. Our measurements are the first on lithium hydride made from isotopically pure starting materials.

Calorimetric samples of ^{7}LiH and ^{7}LiD were provided by the late F. E. Pretzel of Los Alamos Scientific Laboratory. The samples were encapsulated in gold along with a small amount of helium to facilitate rapid heat transfer. The encapsulated samples required a special calorimeter whose whole top could be removed to receive the capsule. The heat capacity measurements on the full and "empty" calorimeter were made in our liquid-hydrogen-cooled calorimeter cryostat described previously.[8] The preparation and probable purity[9] of the samples are described by Pretzel et al.[6]

The data will be presented by deriving from it the contribution to the heat capacity of the optical vibrational modes and the acoustical vibrational modes. Lithium hydride, with the sodium chloride type crystal structure, has two ions contained in the primitive unit cell. For 1 mole there are $6N$ degrees of freedom, N being Avogadro's number. These vibrational degrees of freedom are divided into $3N$ acoustical vibrational modes and $3N$ optical vibrational modes. Each of the acoustical and optical modes is further divided into transverse and longitudinal modes.[10]

For the treatment of the heat capacity data of ^{7}LiH and ^{7}LiD, we will make the considerable simplifying assumption that the transverse optical mode frequencies may be represented by a twofold degenerate average frequency, $\bar{\nu}_{TO}$, and the longitudinal optical mode frequencies by a nondegenerate average frequency, $\bar{\nu}_{LO}$. The heat capacity arising from the optical lattice modes is then given by the equation:

$$C_{opt} = E\left(\frac{\theta_{LO}}{T}\right) + 2E\left(\frac{\theta_{TO}}{T}\right) , \qquad (1)$$

where the first term on the right side represents the Einstein heat capacity function for one degree of freedom and θ_{LO} is the Einstein theta (characteristic temperature) corresponding to $\bar{\nu}_{LO}$, and similarly for the second term.

The difference in heat capacity between ^{7}LiD and ^{7}LiH is due almost exclusively to the difference in that portion of the heat capacity due to the optical vibrational modes, that is, to ΔC_{opt} (Eq. 1). Below 50°K there is no detectable difference in the experimentally observed heat capacities of the two compounds, but above approximately 50°K the heat capacity of ^{7}LiD increases at a faster rate with temperature than that of ^{7}LiH. At 150°K the heat capacity of ^{7}LiD is 15% greater than that of ^{7}LiH; above 210°K the percentage difference exceeds 20%, with a maximum percentage difference of 20.9% at 240°K. At sufficiently high temperatures, of course, this difference disappears as the classical contribution of R (gas constant) for each vibrational degree of freedom is reached.

In the frequency distribution curves,[1,2] the two branches of the optical branch (transverse and longitudinal vibrations) are well separated from each other and from the acoustical branch. For our purposes it is thus possible to extract from each of these curves an average frequency which is a weighted average where the weight given a particular frequency is directly proportional to the intensity at that frequency. From the curves of Verble et al.[1] the following averages were obtained, the frequencies being given in wave numbers (reciprocal wavelength) all in units of cm^{-1}: ^{7}LiD, $\bar{\omega}_{TO}$ = 554, $\bar{\omega}_{LO}$ = 690; ^{7}LiH, $\bar{\omega}_{TO}$ = 784, $\bar{\omega}_{LO}$ = 956. From the curves of Jaswal and Hardy[2] the following averages were obtained: LiD, $\bar{\omega}_{TO}$ = 570, $\bar{\omega}_{LO}$ = 820; LiH, $\bar{\omega}_{TO}$ = 800, $\bar{\omega}_{LO}$ = 1125. When these values are substituted into Eq. (1) (with θ_{TO} = $1.4387\bar{\omega}_{TO}$, etc.) and $\Delta C_p = C_{opt}(^7\text{LiD}) - C_{opt}(^7\text{LiH})$ is calculated, the curves given in Fig. 6.42 result. The points in Fig. 6.42 are experimental heat capacity differences taken from smooth curves through the experimental heat capacity data and represent $\Delta C_p = C_p(^7\text{LiD}) - C_p(^7\text{LiH}) = C_{opt}(^7\text{LiD}) - C_{opt}(^7\text{LiH})$. It is seen that the curve derived from Verble et al. (solid line, Fig. 6.42) is consistently above the experimental data, whereas that of Jaswal and Hardy (dashed line) is consistently below.

If frequencies which are averages between those obtained from Verble et al.[1] and Jaswal and Hardy[2] are employed in the calculation outlined above, there results the theoretical curve shown in Fig. 6.43. The curve shown is based upon the following: ^{7}LiD, $\bar{\omega}_{TO}$ = 562 cm^{-1}, $\bar{\omega}_{LO}$ = 755 cm^{-1}; ^{7}LiH, $\bar{\omega}_{TO}$ = 792 cm^{-1}, $\bar{\omega}_{LO}$ = 1040 cm^{-1}. The theoretical curve reproduces the experimental data quite well, and, in what follows, these frequencies will be employed with Eq. (1) to calculate that portion of the heat capacity of ^{7}LiD and ^{7}LiH arising from the optical vibrational modes.

To extract from the heat capacity data that portion which arises from the acoustical vibrational modes, it is necessary to have, in addition to the contribution due to the optical modes evaluated above, a measure of the

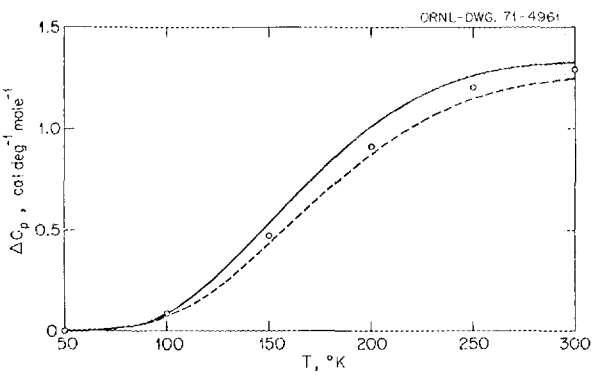

Fig. 6.42. Low-temperature heat capacity differences of lithium hydride. The points represent the experimental difference in molar heat capacity, $\Delta C_p = C_p(^7\text{LiD}) - C_p(^7\text{LiH})$, taken from smooth curves. The curves are theoretical ones for the difference in the optical-mode vibrational heat capacities based upon the frequency distribution curves of Verble et al. (ref. 1) (solid curve) and Jaswal and Hardy (ref. 2) (dashed curve).

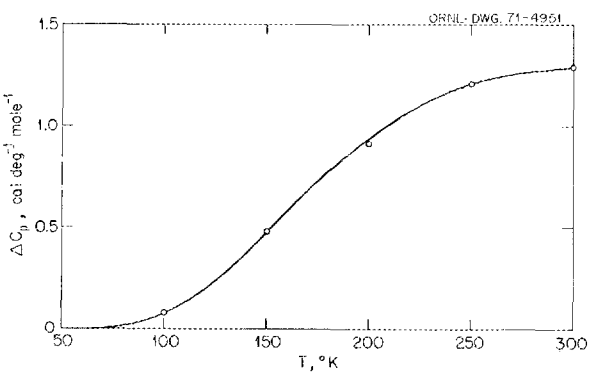

Fig. 6.43. Theoretical average (curve) and smoothed experimental (points) heat capacity differences of lithium hydride. The points represent the experimental difference in molar heat capacity, $\Delta C_p = C_p(^7\text{LiD}) - C_p(^7\text{LiH})$, taken from smooth curves. The curve is a theoretical one for the difference in the optical-mode vibrational heat capacities based upon four frequencies which represent averages of the optical branches of the frequency distribution curves of Verble et al. (ref. 1) and Jaswal and Hardy (ref. 2).

dilation correction, $C_p - C_v$, to place the heat capacity data on a constant volume basis. The dilation correction is given by the thermodynamic relation: $C_p - C_v = \alpha^2 VT/\beta$, where α is the volume coefficient of thermal expansion, V is the molar volume, and β is the isothermal compressibility, all at temperature T. For the temperature dependence of the correction, the relation $C_p - C_v = ATC_p^2$ was used, where A is a constant based upon the Grüneisen relation[10] for α. The value of A for each salt was evaluated from α, V, and β at room temperature; the α's were taken from Brückner et al.,[11] the molar volumes from Anderson et al.,[12] and the compressibilities from Stephens and Lilley.[13] These data give $A = 2.083 \times 10^{-5}$ and 1.826×10^{-5} mole cal^{-1} for ^{7}LiH and ^{7}LiD respectively. Below approximately 100°K, the correction is negligible and amounts to about 4.5% at room temperature.

The heat capacity attributable to the acoustical vibrational modes, C_{acoust}, was obtained by applying the equation:

$$C_{acoust} = C_p - ATC_p^2 - C_{opt} , \qquad (2)$$

where C_p is the experimental heat capacity at temperature T, the second term is the dilation correction term discussed above, and the last term is evaluated by Eq. (1) using the adopted average optical frequencies. The Debye approximation for heat capacity is applicable to the acoustical heat capacity;[10] consequently the C_{acoust} results were used to calculate the Debye theta (characteristic temperature), θ_D, as a function of temperature from the equation

$$C_{acoust} = 3D\left(\frac{\theta_D}{T}\right) ,$$

where $D(\theta_D/T)$ represents the Debye heat capacity function for a single degree of freedom. The results are presented in Fig. 6.44.

The θ_D(acoust) curves of Fig. 6.44 exhibit several interesting features. The overall agreement of the two curves confirms the frequency distribution curves of Verble et al.,[1] namely, that the two compounds have quite similar acoustical branches or vibrational frequencies.[14] Second, the θ_D is remarkably constant over the temperature range 100 to 300°K, which indicates that the Debye approximation of the acoustical frequency branch is quite good in this temperature region. A single average value of θ_D(acoust) = 593 ± 5° for ^{7}LiH and 603 ± 3° for ^{7}LiD reproduces the heat capacities on the average to 0.6 and 0.4% respectively. Finally, the rapid rise of θ_D below ~80°K is typical,

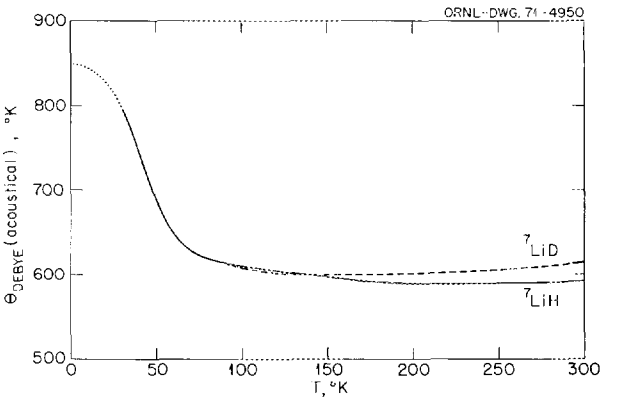

Fig. 6.44. The Debye characteristic temperature vs temperature, derived from the acoustical-mode vibrational heat capacities (three degrees of freedom) of ^{7}LiH (solid curve) and ^{7}LiD (dashed curve). The dotted portion of the curve below 30°K is an extrapolation.

the behavior in the low-temperature region being dependent on the low-frequency modes of the acoustical branch.[15]

If the Debye heat capacity function is used to represent the total heat capacity at constant volume, that is, $C_v = C_{opt} + C_{acoust} = C_p - ATC_p^2 = 6D(\theta_D/T)$, then the temperature dependence of θ_D is that given in Fig. 6.45. The variation with temperature is unusually large, especially for ^{7}LiH (~35% between maximum and minimum). Examination of the frequency distribution curve[1] of the latter reveals the explanation for this behavior, namely, that there exists in the distribution curve a large gap between the acoustical and optical branches where no lattice vibrational frequencies occur, and consequently the simple distribution function of the Debye theory is a very poor approximation for this frequency distribution.

In spite of the approximate nature of the Debye theory, there are occasions in solid-state theory where a mean calorimetric value of the Debye characteristic temperature is useful. The mean Debye characteristic temperatures, computed from the θ_D vs T curves of Fig. 6.45 using the equation

$$\bar{\theta}_D = \frac{1}{T}\int_0^T \theta_D \, dT ,$$

are: $\bar{\theta}_D(^7\text{LiH}) = 953$°K and $\bar{\theta}_D(^7\text{LiD}) = 878$°K. Earlier estimates for LiH and LiD (normal lithium ~^{7}Li) by Ubbelohde[16] are 815 and 611°K respectively. Gibb and Messer[17] estimated $\bar{\theta}_D$(LiH) to be as high as 920°, which is seen to be a good estimate. From the

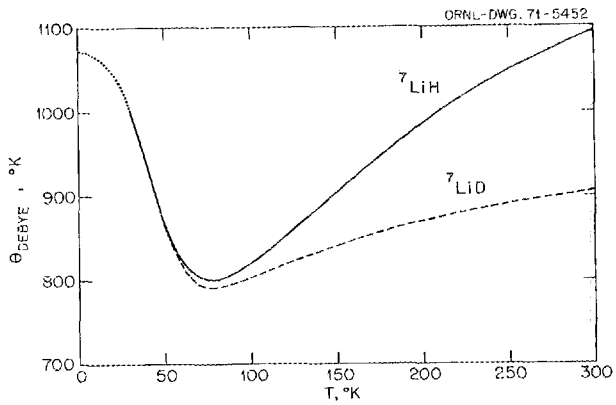

Fig. 6.45. The Debye characteristic temperature vs temperature, derived from the heat capacities at constant volume (six degrees of freedom) of ^{7}LiH (solid curve) and ^{7}LiD (dashed curve). The dotted portion of the curve below 30°K is an extrapolation.

heat capacity data of Kostryukov,[7] $\bar{\theta}_D$(LiH) = 936°K was calculated. His curve of θ_D vs T agrees reasonably well with ours above 70°K, but below this temperature there is a large disagreement, his θ_D curve rising only slightly below 70° to give θ_D(0°K) = 850°K.

The entropies of the two compounds at 298.15°K are calculated by the third law of thermodynamics to be: $S^\circ_{298.15}(^7\text{LiD})$ = 5.645 cal deg^{-1} mole^{-1} and $S^\circ_{298.15}(^7\text{LiH})$ = 4.871 cal deg^{-1} mole^{-1}. The entropies of formation are −18.642 and −17.721 cal deg^{-1} mole^{-1} respectively. Entropies of H_2(g), D_2(g), and Li(c) required were taken from the JANAF Tables,[18] the value given for lithium being increased by 0.032 cal deg^{-1} mole^{-1} to take into account the mass difference between normal lithium and ^{7}Li. The most reliable enthalpies of formation for the two compounds may be obtained from the data of Gunn and Green.[19] They have determined, for normal lithium, the results: ΔH°_f(LiD) = −21,784 cal/mole and ΔH°_f(LiH) = −21,666 cal/mole. It is assumed that the difference between these results and those that would be obtained using isotopically pure ^{7}Li is negligible. The free energies are, therefore, $\Delta F^\circ_f(^7\text{LiD})$ = −16,226 cal/mole and $\Delta F^\circ_f(^7\text{LiH})$ = −16,382 cal/mole at 298.15°K.

1. J. L. Verble, J. L. Warren, and J. L. Yarnell, *Phys. Rev.* 168, 980 (1968).
2. S. S. Jaswal and J. R. Hardy, *Phys. Rev.* 171, 1090 (1968).
3. M. H. Brodsky and E. Burstein, *J. Phys. Chem. Solids* 28, 1655 (1967).
4. W. B. Zimmerman and D. J. Montgomery, *Phys. Rev.* 120, 405 (1960).
5. D. J. Montgomery and J. R. Hardy, p. 491 in *Lattice Dynamics*, ed. by R. F. Wallis, Pergamon, Oxford, 1965.
6. F. E. Pretzel et al., *J. Phys. Chem. Solids* 16, 10 (1960).
7. V. N. Kostryukov, *Russ. J. Phys. Chem.* 35, 865 (1961).
8. R. H. Busey, *A Combination Isothermal-Adiabatic Low Temperature Calorimeter*, ORNL-1828 (Jan. 26, 1955).
9. Analytical determination of the purity of the samples is in process. Previous preparation experience (ref. 6 above) ensures a very high-purity product.
10. C. Kittel, *Introduction to Solid State Physics*, 3d ed., Wiley, New York, 1968.
11. W. Brückner, K. Kleinstück, and G. E. R. Schulze, *Phys. Status Solidi* 14, 298 (1966).
12. J. L. Anderson et al., *J. Phys. Chem. Solids* 31, 613 (1970).
13. D. R. Stephens and E. M. Lilley, *J. Appl. Phys.* 39, 177 (1968).
14. Below 50°K our measurements do not distinguish any difference in the heat capacities of the two compounds. The relatively small samples of ^{7}LiH and ^{7}LiD, with their very low C_p (high θ_D) at low temperatures, combine in an unfavorable manner making our measurements below 30°K of limited value.
15. M. Blackman, "The Specific Heat of Solids," in *Handbuch der Physik*, vol. 7(1), p. 325, ed. by S. Flügge, Springer-Verlag, Berlin, 1955.
16. A. R. Ubbelohde, *Trans. Faraday Soc.* 32, 525 (1936).
17. T. R. P. Gibb, Jr., and C. E. Messer, *A Survey Report on Lithium Hydride*, Tufts University report NYO-3957 (May 2, 1954); Supplement 1954–1957, Tufts University report NYO-8022 (Aug. 31, 1957).
18. D. R. Stull, ed., *JANAF Thermo-Chemical Tables*, The Dow Chemical Co., Midland, Mich.
19. S. R. Gunn and L. G. Green, *J. Amer. Chem. Soc.* 80, 4782 (1958).

ENTHALPIES OF ORTHORHOMBIC AND CUBIC LEAD DIFLUORIDE. THE ORDER-DISORDER TRANSITION IN THE CUBIC PHASE

R. A. Gilbert R. H. Busey

Last year[1] mention was made of the errors discovered in the enthalpies of the lead halides due to the use of Nichrome V capsules even though these capsules were made from the *same* bar. The additional measurements referred to, using platinum–10% rhodium capsules to obtain the necessary corrections, have been completed.

With the help of C. W. Nestor of the Mathematics Division, equations have been developed for the heat capacity of the cubic form of PbF_2 using exponential functions which when integrated lead to a fit of the enthalpy data to an accuracy of 0.2%. It, of course, was necessary to develop separate equations for the data above and below the order-disorder transition temperature (711°K). These equations were extremely useful in making corrections for the capsule error to the orthorhombic data. Data above the transition temperature had been obtained which, since the transition is highly

irreversible, could be treated as cubic data. These data on the cubic phase could thus be compared with those obtained from the above-mentioned equations and the necessary corrections for the capsule error determined and applied. The orthorhombic data could therefore be reconciled and an equation developed for the enthalpy of this form up to the transition temperature.

Although this procedure did not change the previously determined temperatures of the orthorhombic-to-cubic transition (583 ± 1°K) and the melting point (1103°K), it did make some minor changes in the values of the transition enthalpies. The heat of transition was revised to 365 cal/mole and the heat of fusion to 3490 cal/mole. The entropies of transition and fusion then become 0.63 and 3.16 cal deg^{-1} mole^{-1} respectively. The new data on the cubic PbF_2 agree within about 0.4% with the previous data. The heat capacity derived agrees quite well with the previously derived curve;[2] the extensive equations mentioned above employed to fit the data are available but will not be presented here. The following enthalpy equations were developed to fit the remaining data on PbF_2. Orthorhombic phase (273.15 – 583°K):

$$H_T - H_{273.15} = 3.0718 \times 10^{-3} T^2 + 15.819T - 4550.2 .$$

Liquid phase (1103 – 1150°K):

$$H_T - H_{273.15} = 23.366T - 3403 .$$

A previous estimate[2] of the entropy change associated with the order-disorder transition exhibited by cubic PbF_2 was made by the "eyeball and spline" technique to estimate the "normal" heat capacity. Raman[3,4] and infrared[4] spectral data are now available giving information on the lattice vibrational optical modes of cubic PbF_2. These data, together with other information available in the literature, permit a superior and unbiased estimate to be made of the normal heat capacity through the region of interest.

The symmetries of the normal modes of the vibration of the three atoms in the primitive cell of cubic PbF_2 are given by the irreducible representations $2F_{1u} + F_{2g}$. One of the triply degenerate F_{1u} representations corresponds to the acoustical branch, and the other F_{1u} species is split into a doubly degenerate transverse optical mode, ω_{TO}, and a nondegenerate longitudinal optical mode, ω_{LO}. The mode of symmetry F_{2g} is a triply degenerate Raman-active vibration with frequency ω_R. The optical frequencies have been observed to be:[3,4] $\omega_{TO} = 106$ cm^{-1}, $\omega_{LO} = 338$ cm^{-1}, and $\omega_R = 257$ cm^{-1}, or 152, 486, and 370°K respectively.

For 1 mole of PbF_2 (single crystal) there are $9N$ vibrational modes (N = Avogadro's number) distributed among $3N$ acoustical modes and $6N$ optical modes. For the purpose of calculating the heat capacity at constant volume, C_v, we will assume (1) that the frequency distribution of the $3N$ acoustical modes may be represented by the simple Debye frequency distribution giving a term $3D(\theta_D/T)$ in the heat capacity, where $D(\theta_D/T)$ represents the Debye heat capacity function for one degree of freedom with a Debye characteristic temperature θ_D, and (2) that the $6N$ optical mode frequencies may be represented by the three optical frequencies ω_{TO}, ω_{LO}, and ω_R (with degeneracies 2, 1, and 3 respectively), giving in the expression for the heat capacity the terms $2E(\theta_{TO}/T) + E(\theta_{LO}/T) + 3E(\theta_R/T)$, where $E(\theta_{TO}/T)$ represents the Einstein heat capacity function for one degree of freedom with θ_{TO} (Einstein characteristic temperature) being the above-mentioned frequency in degrees Kelvin, etc.

To obtain the heat capacity at constant pressure, C_p, which is the experimentally observed quantity, it will be necessary to include in addition to the above harmonic contributions the anharmonic correction term $C_p - C_v = \alpha^2 VT/\beta$, where α is the volume coefficient of expansion, V the molar volume, and β is the isothermal compressibility, all at temperature T. At room temperature the term was evaluated using $\alpha = 8.64 \times 10^{-5}$ deg^{-1},[5] $V = 31.55$ ml,[5] and $\beta = 1.64 \times 10^{-12}$ cm^2/dyne calculated from the elastic constants.[6] Above room temperature the correction $C_p - C_v = AT(C_v)^2$ was used, where A is a constant based upon the Grüneisen relation for α and was evaluated from the $C_p - C_v$ correction at toom temperature, giving $A = 1.255 \times 10^{-5}$ mole/cal.

Using for the Debye characteristic temperature $\theta_D = 221$°K, based upon the elastic constants,[6] the heat capacity equation for cubic PbF_2 thus becomes

$$C_p = 1.225 \times 10^{-5} T(C_v)^2 + 3D\left(\frac{221}{T}\right) + 3E\left(\frac{370}{T}\right) + 2E\left(\frac{152}{T}\right) + E\left(\frac{486}{T}\right), \quad (1)$$

where C_v in the first term on the right is equal to the sum of the last four terms. The equation reproduces the heat capacity derived from the enthalpy determinations to within 0.5% over the temperature range 273.15 to 400°K. Since the experimental heat capacities are not known any better than this, the fit is considered excellent. The equation gives $C_p = 22.15$ cal deg^{-1} mole^{-1} at the melting point (1103°K), the calculated heat capacity curve being slightly concave downward.

The entropy of the order-disorder transition may now be estimated based upon the experimental entropy change for the temperature interval of interest and the calculated entropy change for the same interval based upon Eq. (1), or an equivalent one for entropy utilizing Debye and Einstein entropy functions. From the experimental enthalpy data on cubic PbF_2, we have derived $S_{1103} - S_{273.15} = 30.34$ cal deg^{-1} mole^{-1}; the calculated entropy with no transition is 26.96 cal deg^{-1} mole^{-1} for the same interval, which leads to $\Delta S_{trans} = 3.38$ cal deg^{-1} mole^{-1}.

The order-disorder transition in cubic PbF_2 giving rise to a cooperative-type heat capacity anomaly[2] arises from a positional disordering of the fluoride ions within the lattice. Reference here is to an essentially complete disorder, not to intrinsic defects or disorder such as Schottky and Frenkel defects which are treated theoretically by the Schottky-Wagner theory[7] where the assumption is made that the number of disordered ions or particles is small compared with their total number. The existence of the cooperative heat capacity anomaly in PbF_2 precludes application of this theory. We wish to consider what configurational entropy to expect if the fluoride ions become disordered by being distributed between their normal site positions in the fluorite structure, $\pm(1/4, 1/4, 1/4)$; F. C., and the vacant site positions $(1/2, 1/2, 1/2)$; F. C., with no disordering of the lead ions at (0, 0, 0); F. C. positions. Two degrees of disordering are considered:

1. In the unit cell of the ordered state, there are eight fluoride ions and four vacancies, or for every pair of fluoride ions there is a vacancy. If in the disordered state we limit the disorder to the extent that a vacancy is always associated with a pair of fluoride ions, then a given pair of ions may be distributed over the three sites in three ways, the next pair in three ways, etc., giving for N pairs (N is Avogadro's number) a total of 3^N configurations. The configurational entropy in this case is, then, $k \ln 3^N = R \ln 3 = 2.18$ cal deg^{-1} mole^{-1}.

2. If the above restriction is removed, then the number of configurations is considerably increased. Thus the number of ways that $2N$ fluoride ions and N vacancies can be distributed over $3N$ lattice sites is $(3N)!/(2N)!N!$. The configurational entropy is then $k \ln [(3N)!/(2N)!N!]$, and making use of Stirling's approximation, this becomes $k(3N \ln 3N - 2N \ln 2N - N \ln N) = k(3N \ln 3 - 2N \ln 2) = R \ln (27/4) = 3.79$ cal deg^{-1} mole^{-1}.

It would seem that this latter disordered state (2) would not ever be fully developed because of the highly energetic configurations that are counted.

The entropy of transition, $\Delta S_{trans} = 3.38$ cal deg^{-1} mole^{-1}, contains, in addition to the configurational entropy of disorder, contributions from a change in entropy associated with an alteration of the lattice vibrational frequency spectrum[8] and from a change in entropy attributable to an abnormal variation in compressibility, coefficient of expansion, and/or volume which would be reflected in the dilation term $(C_p - C_v)$. Staveley and Linford[9] have recently demonstrated that even for a first-order transition at low temperature (~100°K) an alteration in the lattice vibrational spectrum at such a transition could in itself make an important contribution to the entropy of transition. In light of these considerations the difference of 1.20 cal deg^{-1} mole^{-1} between the estimated entropy of transition and the configurational entropy of $R \ln 3$ could well be the entropy associated with the above entropy increments; and consequently, the disordering of the fluoride ions in PbF_2 is most probably that described in (1) above.

1. C. W. Linsey, R. A. Gilbert, and R. H. Busey, *Chem. Div. Annu. Progr. Rep. May 20, 1970*, p. 122.
2. C. W. Linsey, R. A. Gilbert, and R. H. Busey, *Chem. Div. Annu. Progr. Rep. May 20, 1969*, p. 111.
3. N. Krishnamurthy and V. Soots, *Can. J. Phys.* **48**, 1104 (1970).
4. P. Denham et al., *Proc. Roy. Soc. Ser. A* **317**, 55 (1970).
5. P. Pascal, ed., *Nouveau Traité de Chimie Minérale*, vol. VIII, Masson and Cie, Paris, 1963.
6. J. H. Wasilik and M. L. Wheat, *J. Appl. Phys.* **36**, 791 (1965).
7. See, e.g., W. Jost, *Diffusion in Solids, Liquids, Gases*, chap. 2, Academic, New York, 1952.
8. A. A. Maradudin, *Rep. Progr. Phys.* **28**, 331 (1965).
9. L. A. K. Staveley and R. G. Linford, *J. Chem. Thermodyn.* **1**, 1 (1969).

ELECTROCHEMISTRY

HYDROUS OXIDES OF TECHNETIUM IN ITS LOWER VALENCIES

G. H. Cartledge

As was reported previously,[1] when elementary technetium is electrochemically coated with a film of $Tc(OH)_4$ and placed in H_2SO_4, a reversible electrode potential is established briefly. From the measured potential over a wide range of pH values and an indirectly evaluated free energy of formation of $Tc(OH)_4$, it was established that the potential corresponds to the couple

$$Tc + 4H_2O \rightleftharpoons Tc(OH)_4 + 4H^+ + 4e^- ,$$

from which the free energy of formation of $Tc(OH)_4$ may be calculated directly. The normalized result obtained from numerous electrodes gave -199.7 ± 0.6 kcal/mole, which may be compared with the value -202 kcal/mole obtained by combining the heat of

Table 6.16. Free energy of formation of various technetium compounds

Compound	ΔF°_f (kcal/mole)
TcOH	−56.0
$Tc(OH)_2$	−110.1
Tc_3O_4	−206.1
$Tc(OH)_3$	−157.3
Tc_4O_7	−316.6 (?)[a]
$Tc(OH)_4$	−199.7

[a]Uncertainty in identification of observed couples.

combustion of technetium to pertechnic acid[2] with the electrode potential of the couple[3]

$$Tc(OH)_4 \rightleftharpoons TcO_4^- + 4H^+ + 3e^- .$$

Continuation of the investigation disclosed other stationary or pseudostationary potentials which it was possible to identify by use of an empirical relation between the free energy of formation of oxides of a given metal in different valence states and the valence of the cation. By this means, 15 characteristic normal potentials were established, from which the compounds shown in Table 6.16 were identified in films, and their free energies of formation were calculated. The results provide a direct means for referring free energies of other technetium compounds to the element. The details of the measurements and their interpretation have been published.[4]

1. G. H. Cartledge, *Chem. Div. Annu. Progr. Rep. May 20, 1970,* ORNL-4581, p. 124.
2. J. W. Cobble, W. T. Smith, Jr., and G. E. Boyd, *J. Amer. Chem. Soc.* **75**, 5777 (1953).
3. G. H. Cartledge and W. T. Smith, Jr., *J. Phys. Chem.* **59**, 1111 (1955).
4. G. H. Cartledge, *J. Electrochem. Soc.* **118**, 231 (1971).

ELECTROCHEMISTRY OF TECHNETIUM AND OF IRON CONTAINING TECHNETIUM

G. H. Cartledge

The electrochemical behavior of elementary technetium has been investigated by means of cathodic and anodic polarization in sulfuric acid. The electrodes were either a fused bead of technetium or the metal plated over platinum or gold and freed of oxide by various reduction procedures. Cathodic evolution of hydrogen on such electrodes was found to give a Tafel line having a slope approximating −40 mV/decade, with an exchange current density of 10^{-4} to 10^{-3} A/cm^2, depending on the type of electrode used. Under anodic polarization, the current density remained $\leqslant 10^{-6}$ A/cm^2 over a 650-mV span from the reversible hydrogen potential to ca. +450 mV (S.C.E.). At that point, the current density began to rise rapidly as soluble $HTcO_4$ was formed and increased by four orders of magnitude in the next 200 mV.

The behavior of iron containing 0.1 wt % technetium was also studied. Such an alloy has a surface concentration of the order of 10^{12} atoms of technetium per square centimeter. Before being polarized, the electrodes were treated with ammoniacal hydrogen peroxide to remove any extractable technetium or its compounds and then etched briefly in HCl. Upon cathodic polarization of such "clean" electrodes in 1 *N* H_2SO_4, hydrogen was evolved with almost the same Tafel slope as that observed with pure iron. The corrosion potential and corrosion current density also were essentially normal.

Decided deviations from the behavior of pure iron were observed in anodic polarization, however. After the anodic overvoltage had been increased to perhaps 50 mV, the electrode became almost unpolarizable in that, as anodic dissolution proceeded at a potentiostatically fixed potential, the open-circuit, or corrosion, potential steadily ennobled. The effective overvoltage consequently decreased as corrosion proceeded. It was shown analytically that this effect arose from the steady increase in the concentration of technetium on the surface. At the end of a conventional anodic polarization, the amount of technetium extractable by ammoniacal peroxide was of the order of 10^{16}–10^{17} atoms/cm^2, instead of the original 10^{12}.

When an electrode having such an enrichment in technetium was next polarized cathodically, the Tafel slope was numerically smaller and the overvoltage for a specified current density was reduced by about 70 mV. Both changes correspond to the shift of the surface conditions in the direction of pure technetium.

In studies of the passivation of the iron alloy, it was found that the presence of technetium makes anodic passivation somewhat more difficult than that of pure iron and that the "passive" corrosion current density above the passivating potential is of the order of 10^{-3} A/cm^2, or some 250 times greater than that of pure iron. It is believed that this difference is due to the fact that formation and further oxidation of technetium hydrous oxides begin to occur in just the region of potentials in which normal passivation of iron occurs. Such processes should be expected to interfere with the formation and supercharge[1] of the pore-free film associated with full passivation.

The results of these studies have been submitted for publication.

1. G. H. Cartledge, *Corrosion* **24**, 223 (1968); *Chimia* **23**, 450 (1969).

ELECTROCHEMICAL BEHAVIOR OF TITANIUM

E. J. Kelly

The effect of electrode potential on the current density corresponding to the steady-state rate of dissolution of titanium to form Ti^{3+} ions in H_2-saturated acidic sulfate solutions was described in an earlier report.[1] For comparative purposes, typical results obtained in 1 N H_2SO_4 are shown in curve A of Fig. 6.46. Titanium undergoes spontaneous active-state dissolution in this medium at a corrosion potential of −0.740 V vs S.C.E. As the potential is made increasingly positive, the anodic current density corresponding to the dissolution reaction rises to a maximum (i_m) at the "critical potential" (E_m) and then decreases as the metal is transformed from the active to the passive state.

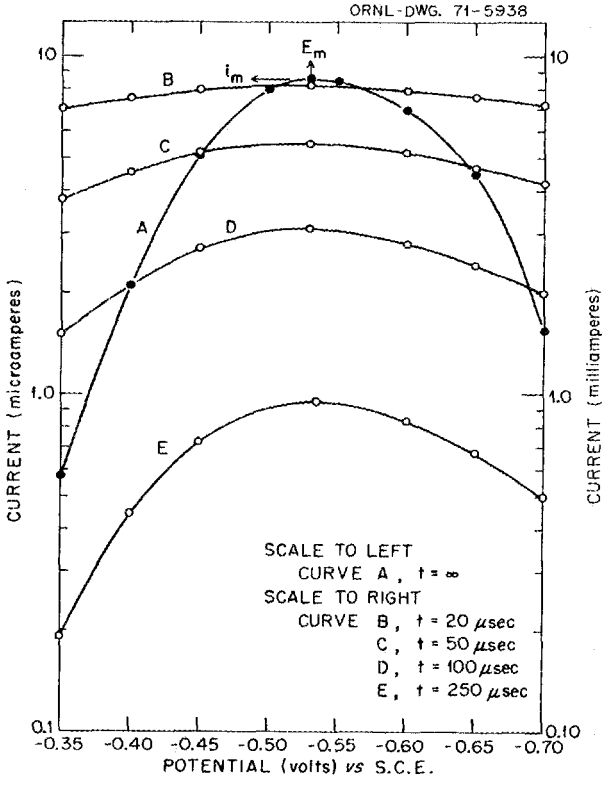

Fig. 6.46. Anodic polarization current for titanium dissolution as a function of time at constant potential in 1 N H_2SO_4. T = 30°C.

On the basis of the form of the steady-state polarization curve (A), the effect of pH on the curve (in particular, the observed effects of pH on i_m and E_m),[1] the effects of added halide ions, the absence of stirring effects, etc., a reaction mechanism for titanium dissolution analogous to that observed for other metals (such as Fe, Co, and Ni) which undergo active-state dissolution in acid media may be proposed. The mechanism of active-state dissolution of iron in acidic sulfate solutions is represented by Eqs. (1) and (2),

$$Fe + H_2O \rightleftharpoons (FeOH)_{ad} + H^+ + e^- , \quad (1)$$

$$(FeOH)_{ad} \rightarrow (FeOH)_s^+ + e^- \text{ (rate-determining)} , \quad (2)$$

where the oxidation process consists of a series of one-electron charge-transfer reactions, with the subvalent Fe^+ existing only as an adsorbed reaction intermediate.[2] It is proposed that the dissolution of titanium follows the same general reaction scheme as iron (Co, Ni, etc.), with the metal being oxidized in a sequence of one-electron charge-transfer reactions resulting in the formation of an adsorbed intermediate for each of the lower valence states of titanium (Ti^+, Ti^{2+}) and, in the last step, Ti^{3+} ions in solution. Although such a mechanism is consistent with the observed steady-state data, the latter alone do not permit exclusion of all other mechanistic possibilities. Consequently, a complementary study of the transient polarization behavior of titanium was inititated during the past year.

In the transient polarization studies, the potential of a titanium electrode relative to a reference electrode E is suddenly (<2 μsec) shifted from an original steady-state value to a second constant value by means of a fast-rise potentiostat. The time-dependent current at the new potential is displayed on an oscilloscope and recorded on film. A typical current-time transient is shown in Fig. 6.47. In this particular example, the titanium was initially in a steady state at E_m (cf. Fig. 6.46), and the potential was then suddenly changed by +40 mV. Although it has not been possible to analyze completely such a complex transient (for reasons which will become apparent), considerable progress toward this end has been achieved. Let i_f represent the current corresponding to the titanium dissolution reaction, that is, the so-called Faradaic or charge-transfer current. The observed current, i, is given by

$$i = i_f + i_c , \quad (3)$$

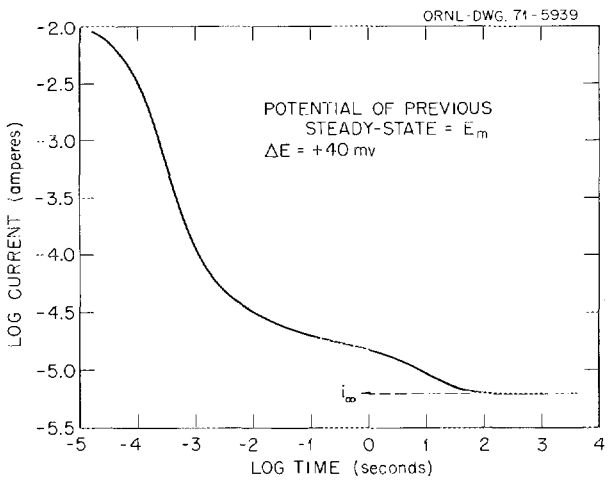

Fig. 6.47. Potentiostatic current-time transient for titanium in 1 N H_2SO_4.

where i_c, the current associated with charging of the electrical double layer at the metal-solution interface, is given by

$$i_c = C(dV/dt) \,. \tag{4}$$

In Eq. (4), C is the double-layer capacity and V is the interfacial potential difference. The potential of the titanium electrode with respect to the reference electrode, E, is given by

$$E = V + iR_s + \beta \,, \tag{5}$$

where R_s is the resistance of the solution between the titanium and the reference electrode probe and β is a constant. A third electrode, the "counter electrode," serves only as a return for i. The electrochemical behavior of titanium is described by Eqs. (3) to (5). Under potentiostatic conditions, $dE/dt = 0$ and the relationship of i to t is given by

$$\frac{d^2 i}{dt^2} + \frac{1}{R_s C}\frac{di}{dt} = \frac{1}{R_s C}\frac{di_f}{dt} \,. \tag{6}$$

If i_f were constant, for example, Eq. (6) could be solved immediately for i as an explicit function of t. Unfortunately, i_f depends on the particular reaction mechanism and is a function not only of V but also of the concentrations of the surface intermediates. Thus, an analysis of a transient such as that shown in Fig. 6.47 in the sense of solving Eq. (6) is not possible for a complex reaction such as titanium dissolution. Instead one must attempt to break down the overall transient curve on the basis of the wide differences in the rate constants for the various reactions involved in the dissolution process.

It should be emphasized that it is only E which can be measured (or, in the potentiostatic case, controlled), whereas it is V (interfacial potential difference) which affects the rates of electrode reactions. The latter may be expressed in terms of E by making the iR_s correction indicated by Eq. (5). To determine R_s, one notes that since $(\Delta V)_{t=0} = 0$,

$$R_s = \Delta E/(\Delta i)_{t=0} \,. \tag{7}$$

The current at $t = 0$, following a change (ΔE) in E, may be readily obtained by extrapolation of the current-time curve to $t = 0$. The ability to obtain current-time data in the microsecond region makes this an attractive method for determining R_s. Moreover, since $R_s = k/L$, where L is the specific conductance of the solution and k is a constant which depends only on the system geometry (a cell constant), one may use the potentiostatic voltage-step technique to measure specific conductance,

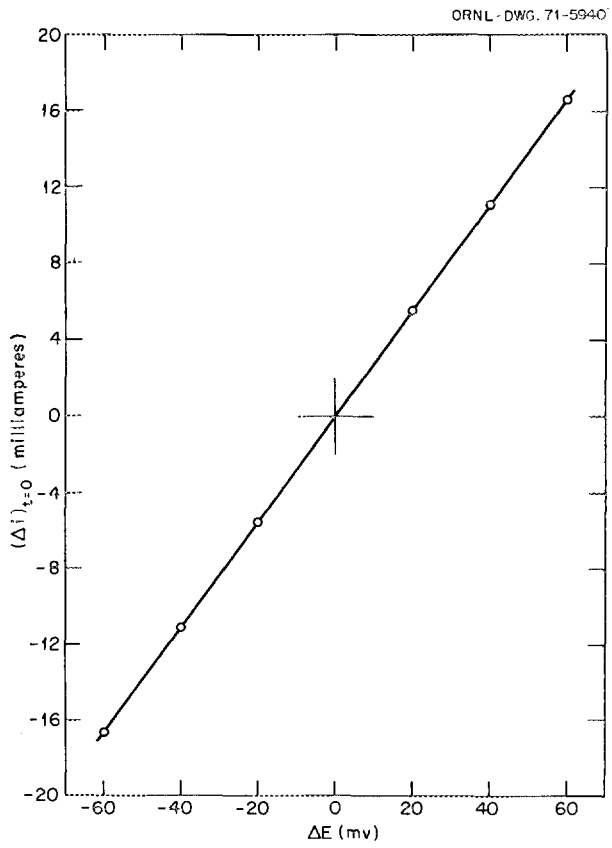

Fig. 6.48. Test of Eq. (7) for the determination of solution resistance.

k being determined by measuring R_s for a standard KCl solution. The development of this technique as an alternative to the usual ac-bridge method for measuring specific conductance is described in the following report.[3] According to Eq. (7), $(\Delta i)_{t=0}$ should be a linear function of ΔE. This is shown to be the case by the data presented in Fig. 6.48. Figure 6.49 shows the initial portions of current-time curves for transients in which the states prior to the shift in E (+40 mV in all cases) corresponded to steady states at various potentials along curve A of Fig. 6.46. Since R_s and ΔE were the same in each case, $\Delta i_{t=0}$ ($\cong i_{t=0}$) is seen to be constant, in agreement with Eq. (7).

A second point to be emphasized is that it is i_f and not i which is the relevant current in the analysis of the reaction mechanism. In the steady state, $dV/dt = 0$, and, according to Eqs. (3) and (4), $i = i_f$. During a transient this is not the case, and one encounters the problem of extracting i_f from i. One may determine V as a function of t as described above and, from the slope of V vs t, determine i_c and i_f if C is known. In the present studies, i_c becomes insignificant for $t > 1$ msec.

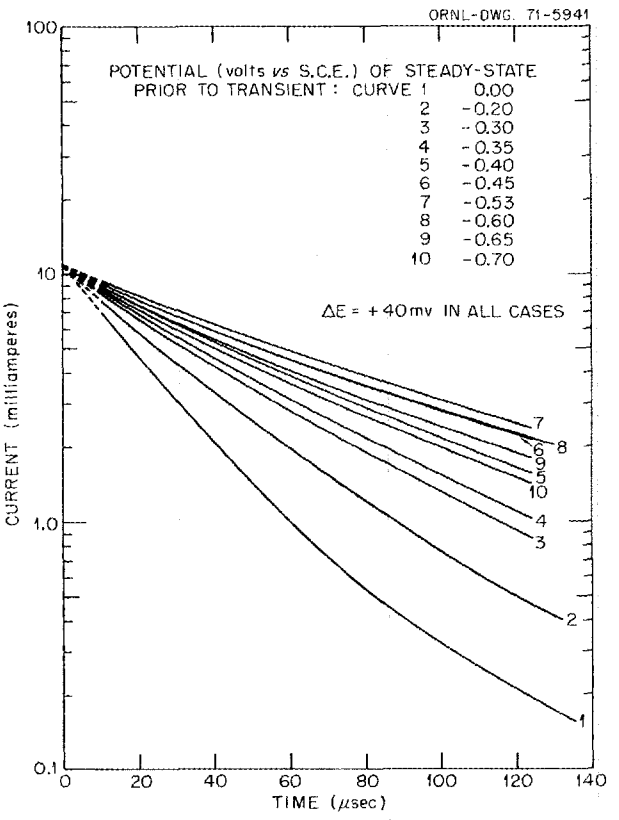

Fig. 6.49. Effect of initial steady state on potentiostatic current-time transients for titanium in 1 N H_2SO_4.

For $t < 1$ msec, both i_c and i_f are significant parts of i. Curves B, C, D, and E in Fig. 6.46 correspond to the currents shown in Fig. 6.49 at $t = 20$, 50, 100, and 250 μsec respectively. The appearance of a maximum in these curves at E_m demonstrates that a very fast Faradaic process is occurring at a significant rate simultaneously with the double-layer charging process. While it has been possible to analyze the latter stages of the current-time transients in terms of the proposed reaction mechanism, it has not yet been possible to isolate and analyze this initial fast process. The effect of pH on the current-time curves may aid in the analysis. Finally, it should be noted that the current-time transients have been found to be independent of stirring from $t = 0$ to steady states; consequently, rate control by mass transport in the solution phase is not a factor in the transients for titanium, in contrast to those for iron.

---

1. E. J. Kelly, *Chem. Div. Annu. Progr. Rep. May 20, 1970*, ORNL-4581, p. 125.
2. E. J. Kelly, *J. Electrochem. Soc.* 115, 1111 (1968).
3. E. J. Kelly and H. R. Bronstein, "Potentiostatic Method for the Determination of Specific Conductance," the following contribution, this report.

POTENTIOSTATIC METHOD FOR THE DETERMINATION OF SPECIFIC CONDUCTANCE

E. J. Kelly H. R. Bronstein

A study of the transient electrochemical polarization behavior of titanium, in which a three-electrode potentiostatic voltage-step technique was employed, is described in the preceding contribution[1] (hereinafter referred to as I). During the course of that study, it soon became apparent that the same technique could be used to measure the specific conductance of an electrolyte. In the potentiostatic method, the potential of a test electrode with respect to a reference electrode is suddenly changed from an initial value (E_1) to a second, constant value (E_2), and the resulting current-time transient at E_2 is displayed on an oscilloscope and recorded on film. From an extrapolation of the current-time curve in the microsecond time region to $t = 0$, one obtains the quantity $(i_2)_{t=0}$, the current at the potential E_2 for $t = 0$. As shown in I, the resistance of the electrolyte between the test and reference electrodes, R_s, is given by

$$R_s = \frac{E_2 - E_1}{(i_2)_{t=0} - i_1} = \frac{\Delta E}{(\Delta i)_{t=0}} . \qquad (1)$$

Since $R_S = k/L$, where L is the specific conductance of the solution and k is a constant which depends only upon the geometry of the system, one may determine the specific conductance from measured values of R_S and k. The cell constant, k, is determined by measuring R_S for a reference electrolyte, usually a standard KCl solution; alternatively, of course, one could employ a known geometry to determine k.

In addition to certain tests described in I, the potentiostatic method was tested by determining the equivalent conductances of aqueous KCl solutions at 25°C in the concentration range from approximately 10^{-3} to 10^{-1} M and comparing the results with the generally accepted value obtained by use of the usual ac-bridge method.[2] The 0.2% maximum deviation in the results obtained by the two methods (Fig. 6.50) is entirely within the limitations imposed by the oscilloscope employed in the studies and does not reflect an inherent error in the potentiostatic method. The latter method has certain distinct advantages over the conventional ac-bridge method, such as elimination of ambiguous "frequency effect" corrections resulting from the Faradaic component of the current, that is, from electrode polarization effects, and elimination of the need to use platinized platinum electrodes; indeed, corroding titanium electrodes worked equally well.

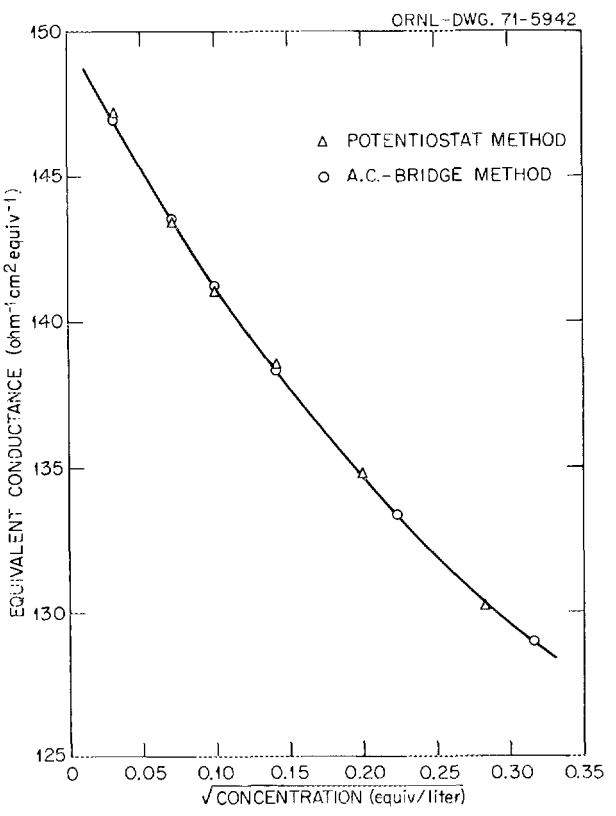

Fig. 6.50. Equivalent conductance of aqueous KCl solutions vs square root of concentration at 25°C.

In view of its simplicity, as well as the advantages cited above, the potentiostatic method should prove to be of special value in determining specific conductances of molten salts. To test its applicability to such systems, the specific conductance of molten KNO_3 at 353°C was measured and found to be 0.679 Ω^{-1} cm^{-1}, in agreement with the results obtained by the ac-bridge and dc methods.[3,4] Measurements at higher temperatures showed an error arising from the enhanced conductivity of the soft glass of the conductance cell. A quartz cell will be used in future studies to eliminate this error.

The potentiostatic method requires evaluation of the quantity $(i_2)_{t=0}$ by extrapolation of the current-time curve at the potential E_2 to $t = 0$. Since the rise time of the potentiostat is ~2 μsec, a problem arises if the current decay is too rapid. If Eq. (6) of I is solved for the case where $(dV/di_f) = R_f$, a constant Faradaic resistance, the current transient is described by

$$i - i_\infty = (i_0 - i_\infty) \exp\left[-(R_S + R_f)t/R_f R_S C\right] , \quad (2)$$

where i_∞ is the current in the new steady state ($t \to \infty$) and $i_0 = (i_2)_{t=0}$ is the current at $t = 0$. It is evident from this equation that, for a capacity (C) of 20 μF, a solution resistance less than 1 Ω results in too rapid a current decay. Specific conductances are very high in molten-salt systems, and consequently a capillary is used to increase R_S and thus obtain a suitably slow current decay.

---

1. E. J. Kelly, "Electrochemical Behavior of Titanium," the preceding contribution, this report.
2. G. Jones and B. C. Bradshaw, *J. Amer. Chem. Soc.* **55**, 1780 (1933).
3. G. D. Robbins and J. Braunstein, *J. Electrochem. Soc.* **116**, 1218 (1969).
4. L. A. King and F. R. Duke, *J. Electrochem. Soc.* **111**, 712 (1964).

HYDROGEN PRODUCTION WITH A SUSPENSION ELECTRODE IN A FLOW CELL[1]

R. E. Meyer P. M. Lantz F. A. Posey

Some preliminary experiments on the properties of the suspension electrode as an efficient device for production or oxidation of hydrogen in aqueous media were presented in a previous report.[2] In addition, a simplified theoretical model was developed which ex-

plains a number of the principal experimental observations.[3] A suspension electrode consists of a finely divided, conducting catalytic material (Pt or Pd black, Raney Ni, etc.) suspended in a solution of strong electrolyte. The catalyst particles are charged by intermittent contact with a stationary electrode or array of electrodes. Contact may be effected either by stirring the suspended particles or by flow of the suspension past charging electrodes fixed in a channel. It has been found that certain electrode processes may be carried out on a suspension electrode with high current output at modest overvoltages. Some of the important parameters which affect current output are the amount of catalyst material suspended in the electrolyte and the rate and mode of stirring, which influences the rate of particle impact with the charging electrode.[2] More recently we have investigated the operation of a flow cell designed for relatively high current output. This cell contains an array of charging electrodes through which the suspension can be pumped at various velocities. A description of the cell and its operation and some of the principal observations are presented below.

A schematic diagram of the flow system constructed for use with the suspension electrode is shown in Fig. 6.51. The slurry, consisting of particles of Raney nickel catalyst suspended in 1 *N* KOH, was pumped through the two compartments of the flow cell (*A* in Fig. 6.51) by use of magnetic impeller plastic centrifugal pumps (*B*). After passage upward through the cell (details described below) the suspension was discharged into vented glass reservoirs (*H*) located several feet above the cell. Continuous recycling of the suspension was accomplished by connecting the reservoirs to the intakes of the pumps. The flow rate of the suspension through the cell half which contained nickel charging electrodes was controlled by means of a bypass line and clamp (*E*) and by a resistance control on the pump motor. The flow rate of the suspension was monitored by use of calibrated glass standpipes containing a number of holes (*I*) and incorporated into the reservoirs. Constant temperature of the suspension entering the cathode side of the cell was controlled by use of a glass condenser (*D*). In order to expedite removal of dissolved atmospheric oxygen at the start of an experiment, hydrogen gas (*F*) was bubbled through the suspension in the reservoir and discharged through a water trap (*G*).

Current was supplied by a regulated-voltage power supply (160 V, 4 A). Saturated calomel reference electrodes (*C*) bridged into the cathode and anode streams in the cell were used to monitor the potential of the charging electrodes. Electrode potentials were measured by use of an electrometer, and applied current and electrode potential were recorded on a strip-chart recorder.

Details of the flow cell are shown in Fig. 6.52. The two halves of the cell were machined from Lucite with a $4\frac{1}{2} \times \frac{1}{2} \times \frac{1}{8}$ in. depression milled into each half. The ends of the depressions were tapered to match inlet and outlet tubes ($\frac{3}{16}$ in. diameter) which entered obliquely at each end of the cell. Seven electrodes [nickel for the cathode side (*A*) and platinum for the anode side (*D*)] passed through each cell half perpendicular to the direction of flow (cf. *F* and *G* in Fig. 6.52) and were sealed into the cell halves with epoxy cement. The electrodes, 0.041 in. in diameter, were spaced $\frac{3}{8}$ in. apart in the channel. The compartments were separated with a 0.004-in.-thick membrane (*C*) of

ORNL-DWG. 70-4171

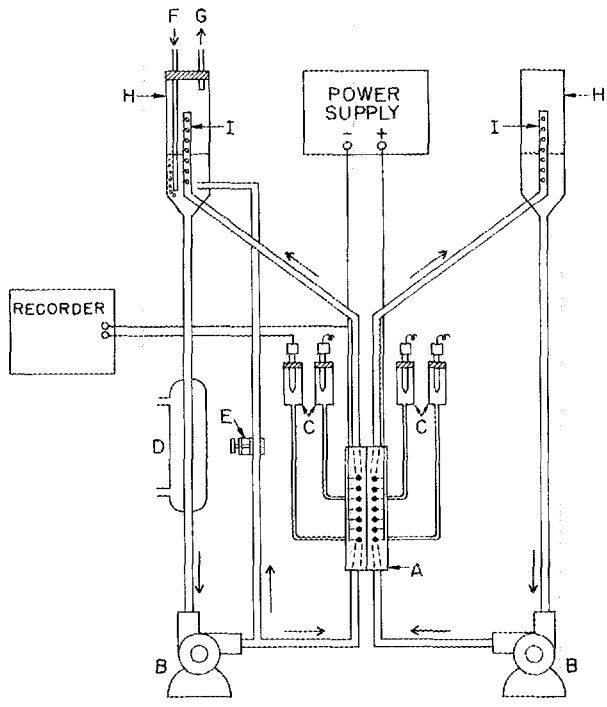

SCHEMATIC DIAGRAM OF FLOW SYSTEM FOR SUSPENSION ELECTRODE

A, Flow cell. B, Pumps. C, Reference electrodes and chambers. D, Heat exchanger. E, Bypass line clamp for flow control. F, Inlet for H_2 gas. G, Gas outlet. H, Slurry reservoirs. I, Flow monitors.

Fig. 6.51. Schematic diagram of flow system for suspension electrode. *A*, flow cell; *B*, pumps; *C*, reference electrodes and chambers; *D*, heat exchanger; *E*, bypass line clamp for flow control; *F*, inlet for H_2 gas; *G*, gas outlet; *H*, slurry reservoirs; *I*, flow monitors.

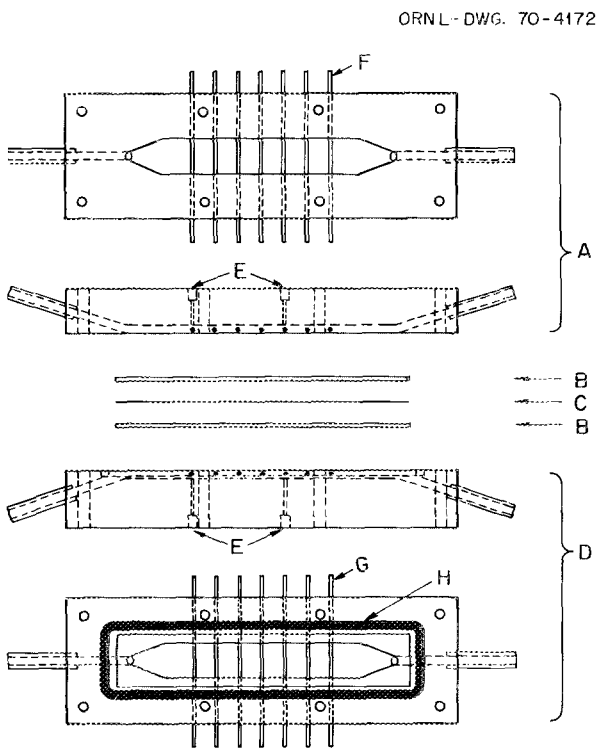

FLOW CELL FOR SUSPENSION ELECTRODE

A, Half cell with nickel wire electrodes.
B, Rubber gaskets. C, Dacron membrane.
D, Half cell with platinum wire electrodes.
E, Ports to reference electrodes (S.C.E.).
F, Nickel electrodes. G, Platinum electrodes.
H, "O"-ring gasket.

Fig. 6.52. Flow cell for suspension electrode. *A*, half-cell with nickel wire electrodes; *B*, rubber gaskets; *C*, Dacron membrane; *D*, half-cell with platinum wire electrodes; *E*, ports to reference electrodes (S.C.E.); *F*, nickel electrodes; *G*, platinum electrodes; *H*, O-ring gasket.

Webril, a nonwoven Dacron (The Kendall Company, Walpole, Massachusetts). Thin rubber gaskets (*B*) were used to seal the membrane into the cell, and a rubber "O"-ring gasket (*H*) was used in assembly of the cell. Two reference electrode capillaries (*E*) were provided in each cell half. These capillaries terminated within $^1/_{16}$ in. of the surfaces of electrodes 1 and 5, counting from the inlet ends of each half. The capillaries were connected with tubing to separate compartments containing saturated calomel reference electrodes (cf. *C* in Fig. 6.51).

Previously it was found that, of several finely divided catalytically active metals, Raney nickel was most effective as a suspension material in the enhancement of the hydrogen evolution reaction in 1 *N* KOH. This property may be due principally to the large internal surface area of the porous particles of Raney nickel.[2,3] Activated Raney nickel catalyst was prepared from sized particles (>350 mesh) of nickel-aluminum alloy powder and stored in refrigerated absolute ethanol until needed.

Fig. 6.53 shows a number of current-voltage curves for the hydrogen evolution reaction on the suspension electrode. The total geometrical surface area of the seven nickel wire electrodes used in the cathode compartment of the flow cell was ca. 2.9 cm^2. One notes that at the highest catalyst content (70 g of Raney Ni in 275 ml of 1 *N* KOH at 25°C) the current output of the cell is greater than 1 A/cm^2 (ca. 10^3 A/ft^2), calculated with respect to the area of the charging electrodes, at only 300 mV overvoltage. Thus the flow-cell configuration of the suspension electrode

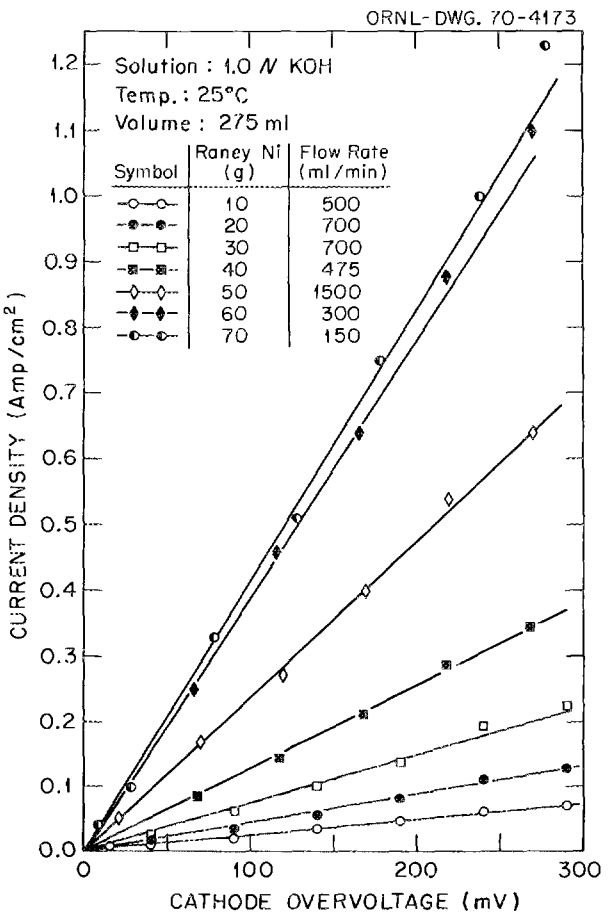

Fig. 6.53. Effect of overvoltage and catalyst content on output of suspension electrode at optimum flow rate.

is a very efficient device for the generation of electrolytic hydrogen. Still greater current output could be obtained by use of a more concentrated electrolyte (e.g., 6 *N* KOH), with higher catalyst contents, and by operation at elevated temperatures.

The data of Fig. 6.53 represent the enhancement of the output current due to addition of Raney Ni catalyst. A background current, due to the hydrogen evolution on the nickel charging electrodes in the absence of the catalyst, was subtracted from all the data of Fig. 6.53. Precise determination of the background current presents certain difficulties, however. Impingement of catalyst particles upon the charging electrodes erodes the surfaces and increases the surface area and therefore the background current with time. More consistent results are obtained, particularly at low catalyst contents, by use of charging electrodes which have been exposed previously to the flow of suspended particles for a considerable length of time.

It may be seen from the data in Fig. 6.53 that current output appears not to be a linear function of catalyst content. There are a number of reasons for this. First of all, there exists for each amount of catalyst an optimum flow rate for which the current output is a maximum. The data in Fig. 6.53 represent the maximum current output obtainable from our cell configuration as a function of catalyst content. Maximum current output implies maximum frequency and efficiency of contact of suspended particles with the charging electrodes. Some of the factors which affect contact frequency are the hydrodynamic conditions within the cell, the presence of an appreciable void fraction of hydrogen gas bubbles in the liquid phase due to the great rate of hydrogen production, and the existence of a "clumping" phenomenon with respect to the catalyst particles. After operation of the suspension electrode for some time, the nickel particles tend to agglomerate in clusters, thus probably affecting the efficiency of contact with the charging electrodes. Because of this phenomenon reproducible data were difficult to obtain with catalyst contents less than about 10 g/275 ml. Under conditions where gas evolution is not so vigorous and where clumping of catalyst particles is not too significant, the current output is roughly proportional to catalyst content.

When the current output of the individual nickel charging electrodes was examined, it was found that the outputs of all electrodes downstream from the first were quite similar. Current output of the first electrode was at least 25% higher than the others. This suggests that the overall performance of the cell could be increased even further by appropriate arrangement and spacing of the nickel charging electrodes.

1. Research jointly sponsored by the Office of Saline Water, U.S. Department of the Interior, and by the U.S. Atomic Energy Commission under contract with Union Carbide Corporation.

2. R. E. Meyer, P. M. Lantz, and F. A. Posey, *Chem. Div. Annu. Progr. Rep. May 20, 1969*, ORNL-4437, p. 90.

3. F. A. Posey and R. E. Meyer, *Chem. Div. Annu. Progr. Rep. May 20, 1969*, ORNL-4437, p. 93.

ELECTROCHEMICAL PRETREATMENT OF SEAWATER FOR pH CONTROL AND BICARBONATE REMOVAL[1]

A. A. Palko R. E. Meyer F. A. Posey

Several areas of present or potential technological importance require pH adjustment of process streams in order to optimize the performance of treatment processes, to avoid deposition of scales or layers of substances found in waters on process equipment, or to minimize corrosion of materials of construction. Present industrial practice depends heavily upon the use of reagents such as sulfuric acid, lime, etc. Such procedures usually involve considerable cost and inconvenience in transportation, storage, handling, and dispensing of chemicals. We have begun an investigation of theoretical and experimental aspects of the use of electrochemical techniques in the generation of acid or base for pH control of process streams without the necessity of using additional reagents.

Initial efforts during the past year were devoted to design and construction of a prototype device for simultaneous removal of bicarbonate and acidification of seawater. The device, based on the suspension electrode principle, promises a more efficient means of pH control than other known electrochemical methods. In the present prototype acid generator, the cell, of concentric cylindrical geometry, has a central anode compartment separated from the surrounding cathode compartment by a porous barrier. The anode assembly makes use of a high-efficiency suspension electrode in which a suspension or slurry of palladium black catalyst particles is forced to impinge upon a large array of charging electrodes. Incoming seawater enters the surrounding cathode compartment and is circulated through a loop consisting of the cathode compartment and a settling tank. The reaction at the stainless steel cathodes is production of hydrogen gas and hydroxide ions. The latter first react with Mg^{2+} ions in the seawater and would ordinarily tend to form a tight coating of $Mg(OH)_2$ on the cathode surfaces which would soon prevent further reaction and lead to greatly increased voltage requirements. However, the cathode surfaces are kept clean by means which allow continuous, efficient operation of the cathode reaction.

Continued production of hydroxide ions raises the pH of the solution in the cathode loop until conversion of bicarbonate ions to carbonate causes precipitation of $CaCO_3$, with subsequent removal in the settling tank. Essentially carbonate-free seawater from the cathode loop is forced into the anode compartment through the porous separator, where acidification takes place due to the anodic reaction, oxidation of hydrogen to hydrogen ions. The hydrogen for the anode reaction is the product of the cathodic process and is extracted from the cathode loop and fed into the solution in the anode loop. The output of the cell – decarbonated, acidified seawater – is taken from the suspension anode loop and may then be used for acidification pretreatment of larger volumes of seawater. This mode of operation, based upon a hydrogen feedback cycle, circumvents the old problem of anode attrition in electrolysis of seawater and chloride solutions and allows operation at greatly reduced cell voltages and therefore modest power requirements. In addition, the use of expensive membrane materials and catalyzed electrode structures, as in some acid generators,[2] is avoided.

1. Research jointly sponsored by the Office of Saline Water, U.S. Department of the Interior, and by the U.S. Atomic Energy Commission under contract with Union Carbide Corporation.

2. L. H. Shaffer and R. A. Knight, *J. Electrochem. Soc.* 116, 1595 (1969).

ELECTROCHEMICAL METHOD FOR ANALYSIS OF DISSOLVED OXYGEN IN THE PARTS-PER-BILLION RANGE[1]

R. E. Meyer P. M. Lantz F. A. Posey

A continuing need has existed for a reliable, sensitive method of on-line analysis of the dissolved oxygen content of various waters and process streams in the parts-per-billion range. The classical method for determination of the dissolved oxygen content of solutions is the Winkler method, or its several modifications, in which exacting and time-consuming chemical operations are required. In recent years, measurement devices which use a membrane-electrode assembly have been developed. These so-called polarographic oxygen sensors are convenient in operation but require relatively frequent and uncertain calibration, undergo deterioration of membrane properties, and possess mass-transport limitations on sensitivity. In addition, the measured quantity is a diffusion-limited current which depends significantly upon temperature, and, therefore, reliable measurements at low oxygen contents require careful technique.

As a result of our previous experience with coupled electrochemical and hydrodynamic systems, we have designed and constructed a device, which promises to overcome many of the limitations of the polarographic oxygen sensors, for measuring the dissolved oxygen content of aqueous streams in the parts-per-billion range. Our device, like the polarographic oxygen sensors, uses a membrane and electrode assembly but, unlike them, is not limited in sensitivity by mass transport of oxygen through the membrane which separates the measurement system from the stream to be analyzed. The measurement device incorporates an exchange section in which dissolved oxygen in the test stream penetrates a commercial copolymeric membrane (high permeability to gases but none to ions) and equilibrates with an internal solution. The path length and rate of flow in the exchange section assure essentially complete oxygen equilibration of the internal solution. Subsequently, the equilibrated internal electrolyte flows through a porous sensor electrode maintained at a constant electrode potential and so constructed and operated that all of the oxygen contained in the internal electrolyte is reduced by a four-electron process. Knowledge of the reduction current and of the volume flow rate then allows the oxygen concentration of the internal solution to be calculated from Faraday's law; this, of course, is also the oxygen concentration of the test stream because of the equilibrium conditions. The boundary value problem pertaining to steady-state operation of the device was solved by use of various approximations, and the results were used in establishing the dimensions and operating conditions of the exchanger-sensor electrode system. This method of measurement depends only indirectly on the permeability of the membrane, and thus there is no temperature dependence of the measured quantity as in conventional membrane probes. Although there is a small background current on the sensor electrode, there are no calibration constants involved in the measurement, and sensitivity is quite adequate even at the parts-per-billion level.

1. Research jointly sponsored by the Office of Saline Water, U.S. Department of the Interior, and by the U.S. Atomic Energy Commission under contract with Union Carbide Corporation.

7. Chemical Physics

NEUTRON AND X-RAY DIFFRACTION

THE CRYSTAL AND MOLECULAR STRUCTURE OF THE "ANOMALOUS ACETATE" OF KATONIC ACID. A SEVERELY TWISTED CARBON-CARBON DOUBLE BOND

W. E. Thiessen H. A. Levy

In recent years compounds containing many types of strained double bonds have been prepared and studied, and particular interest has been given to rotation about a double bond, so-called "torsional strain."[1] Such compounds are usually highly reactive and require special synthetic methods for their preparation. We report here results related to preparation (under acidic conditions) of an unreactive compound containing a double bond under considerable torsional strain.

King and Morgan[2] reported that the triterpene katonic acid (1) undergoes normal acetylation with acetic anhydride and pyridine, but, when treated with acetic anhydride containing a catalytic amount of perchloric acid, it yields a neutral ketoacetate, for which structure 2 was proposed. They noted that the

ORNL-DWG. 71-4949

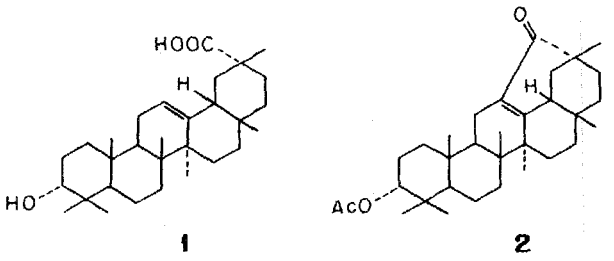

ultraviolet (uv) absorption maximum at 273 nm (ϵ 8900) was well outside the normal limits of 225 to 252 nm for α,β-unsaturated ketones.[3] This anomalous acetate was also reported to take up 2 moles of hydrogen to yield a product in which the keto group has been replaced by a methylene (uv maximum 217 nm, ϵ 5400). They also prepared, by lithium aluminum hydride reduction, a dihydro product with uv maximum 224 nm (ϵ 5200). Dauben, Beasley, and Cox[4] have confirmed this latter result and also have obtained an isomeric dihydro alcohol by lithium-ammonia reduction with uv maximum 229 nm (ϵ 5180).[5] These spectral properties, remarkable for compounds containing a lone carbon-carbon double bond, led us to undertake a crystal structure analysis of the anomalous acetate.

Crystals of the acetate, $C_{32}H_{48}O_3$, are monoclinic with the symmetry of space group $P2_1$; the unit cell containing 2 molecules has parameters a = 14.6934(8) Å, b = 12.7735(8) Å, c = 7.5595(3) Å, and $\cos\beta$ = −0.19662(5).[6] The structure was solved from 2183 x-ray reflections measured on the Oak Ridge computer-controlled diffractometer by a search of the Patterson function followed by tangent-formula phase refinement. It was assumed that the 16-carbon fragment containing C1 through C11, C14, and C23 through C26 has the configuration of the corresponding fragment in crystalline adiantol B bromoacetate.[7] The Patterson search procedure of Braun, Hornstra, and Leenhouts[8] yielded the orientation and position of the fragment in the unit cell; the corresponding atomic coordinates were used to calculate initial phase values for 218 selected[9] reflections. Tangent-formula refinement yielded phase values for all 416 reflections with normalized structure factor $|E| > 1.5$; the corresponding E map[10] displayed 34 of the 35 true carbon and oxygen positions among the 41 strongest peaks. The current value of the conventional discrepancy index $R(F)$ for all reflections is 0.04.

The result of the crystal-structure analysis, presented in Fig. 7.1, shows unequivocally that structure 2 is correct[11] and reveals the structural feature responsible for the large bathochromic shifts cited above. Closure of the sixth ring has forced the six carbon atoms associated with the double bond to depart from a common plane. The C11, C12, C29 plane makes an angle of 26° with the C14, C13, C18 plane. The distortion is mostly but not entirely a torsion about the double bond; while atom C12 lies nearly in the C14, C13, C18 plane, atom C13 is 0.16 Å away from the C11, C12, C29 plane, corresponding to a slightly

ORNL DWG. 71-4947

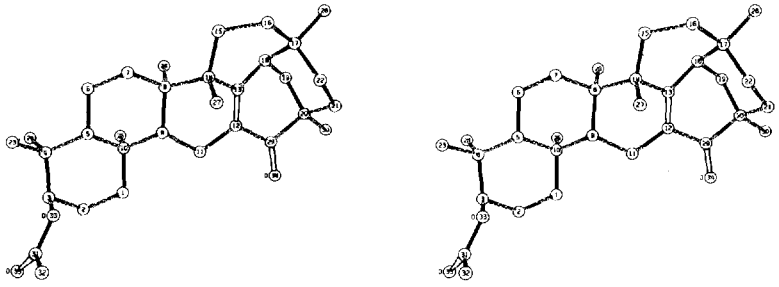

Fig. 7.1. Stereoscopic drawing of the molecule (excluding hydrogen atoms) viewed approximately along b. The a axis is horizontal. Atoms linked by double bonds are connected by two lines.

pyramidal configuration at C12. The overall geometry is most readily appreciated from the conformation angles about the C12 → C13 direction.

ORNL-DWG. 71-4840

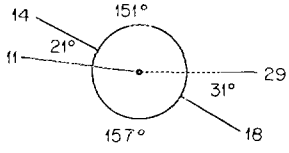

This distortion from coplanarity decreases the π-electron overlap from that normally present in a double bond and causes a mutual approach of the energy levels of the ground and excited electronic states, qualitatively accounting for the observed spectra.[12] As expected, the optical rotatory dispersion (o.r.d.) curve for the alcohol shows a large negative Cotton effect (Φ_{240} = −9500). The sign follows the rules of Scott.[13] The o.r.d. of the enone 2 also shows a negative Cotton effect; the molecular amplitude of rotation ($\Delta\Phi$) of 222,000 is the largest yet reported for this chromophore.[14] The unusual weakness of the Raman band at 1690 cm^{-1} assigned to the tetrasubstituted double bonds in the alcohols indicates a diminished polarizability ascribable to the reduced π-electron overlap.[15]

These materials do not display the high reactivity reported for simpler compounds containing strained carbon-carbon double bonds.[16] It is of particular interest that only the carbonyl group of enone 2 is reduced in a lithium-ammonia reaction. This observation and the lack of reactivity of all the compounds toward hydroxylic solvents indicate that addition reactions at the double bond offer no appreciable relief of strain in this complex ring system. Attempts to reverse the acylation reaction to yield the starting material, katonic acid, have not been successful;[4] this most likely reflects the same lack of reactivity of the olefinic linkage.

---

1. For a general review of strained double bonds, see N. S. Zefirov and V. I. Sokolov, *Russ. Chem. Rev.* **36,** 87 (1967).
2. F. E. King and J. W. W. Morgan, *J. Chem. Soc. London* **1960,** 4738.
3. For a survey of ultraviolet spectra of unsaturated compounds, see A. I. Scott, *Interpretation of Ultraviolet Spectra of Natural Products,* Macmillan, New York, 1964.
4. Certain chemical reactions and electronic spectral measurements cited here were carried out by W. G. Dauben, G. H. Beasley, and D. A. Cox, Department of Chemistry, University of California, Berkeley. We thank these workers for providing the crystals for this investigation and Professor Dauben for suggesting the problem to us.
5. Both alcohols upon oxidation yielded the same enedione.
6. The numbers in parentheses, corresponding to the least significant digits of the parameters, are estimated standard derivations from a least-squares analysis.
7. H. Koyama and H. Nakai, *J. Chem. Soc.* B 546 (1970).
8. P. B. Braun, J. Hornstra, and J. I. Leenhouts, *Philips Res. Rep.* **24,** 85 (1969). For an example of a structure solution by this method, see *Acta Crystallogr., Sect. B* **26,** 352 (1970).
9. J. Karle, *Acta Crystallogr., Sect. B* **24,** 182 (1968).
10. J. Karle and I. L. Karle, "Phase Determination for Centrosymmetric Crystals by Probability Methods," chap. 17 in *Computing Methods in Crystallography,* J. S. Rollett, ed., Pergamon, Oxford, 1965.
11. B. Tursch, J. Leclercq, and G. Chiurdoglu [*Tetrahedron Lett.,* 4161 (1965)] reported the preparation of a similar ketone from the triterpene mesembryanthenoidigenic acid; and, since their material was shown by nmr spectroscopy to contain one vinyl proton, they suggested that a reinvestigation of structure 2 was warranted. In view of the present results, a study of their ketone would be interesting.
12. For a complete discussion of spectral effects, see ref. 1.
13. A. I. Scott and A. D. Wrixon, *Tetrahedron* **26,** 3695 (1970).
14. The authors are indebted to Dr. J. Fried and Dr. Lewis J. Throop of Syntex Research for measurement of the optical rotatory dispersions.

15. The authors wish to thank Dr. J. R. Scherer of the U.S.D.A. Western Regional Research Laboratory, Albany, Calif., for obtaining the Raman spectrum.

16. J. R. Wiseman, H.-F. Chan, and C. J. Ahola, *J. Amer. Chem. Soc.* **91**, 2812 (1969); P. M. Lesko and R. B. Turner, *ibid.* **90**, 6888 (1968); T. A. Marshall and H. Faubl, ibid. **89**, 5965 (1967).

THE CRYSTAL STRUCTURE OF 3-HYDROXYXANTHINE DIHYDRATE, A TUMOR-INDUCING CHEMICAL AGENT

W. E. Thiessen

Many low-molecular-weight compounds having widely disparate structures but sharing the property of inducing tumors have been lumped together under the general heading of chemical carcinogens or, more properly, chemical oncogens.[1] Several of the most potent of these are, or are transformed in vivo into, aromatic nitrogen compounds capable of electrophilic attack upon cell components to initiate the process of oncogenesis.[2] Examples are 2-*N*-hydroxyacetylaminofluorene[3] and 4-hydroxylaminoquinoline-*N*-oxide.[4]

Dr. G. B. Brown and his co-workers at the Sloan-Kettering Institute for Cancer Research have found[5] that certain *N*-hydroxypurines, characterized as adenine-1-oxide (**1**),[6] guanine-3-oxide (**2**), and 3-hydroxyxanthine (**3**),[7] have oncogenic properties. (The ring-

ORNL-DWG. 71-6792

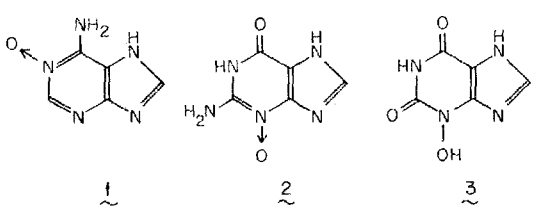

system numbering is given in Fig. 7.2). Compounds **2** and **3** undergo facile rearrangement to 8-hydroxy derivatives in the course of acetylation and of other reactions[8] and, in consequence, were initially thought to be 7-*N*-oxides.[9] From samples of these compounds kindly provided by Dr. Brown, the dihydrate of 3-hydroxyxanthine was chosen for initial investigation because the crystals as supplied were suitable for intensity data collection and because the assigned structure **3** contains a hydroxamic acid grouping and no detailed study of the molecular geometry of this functional group had, to our knowledge, been carried out.

ORNL-DWG. 71-6072

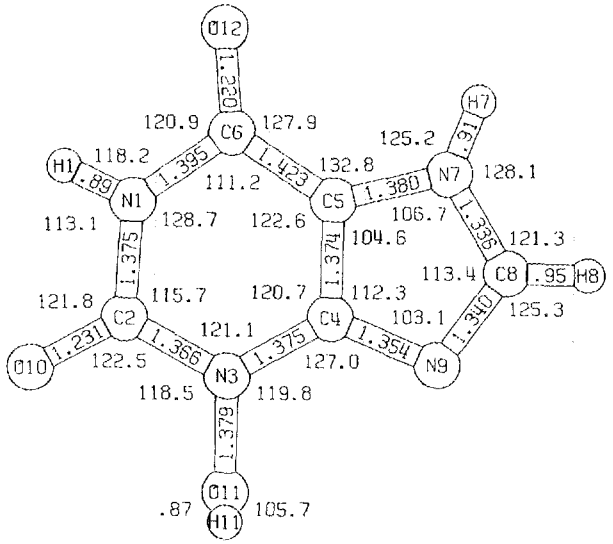

Fig. 7.2. The ring number system, bond lengths (Å), and valence angles (deg) in the 3-hydroxyxanthine molecule.

Crystals of 3-hydroxyxanthine dihydrate,

$$C_5H_4N_4O_3 \cdot 2H_2O\ ,$$

are triclinic. The unit cell containing 2 molecules has parameters a = 7.8383(1) Å, b = 8.4054(2) Å, c = 7.4408(1) Å, cos α = −0.41039(2), cos β = −0.32227(3), cos γ = 0.40919(3).[10] The methods used in obtaining these parameters and in the subsequent data collection were very similar to those described in previous reports.[11,12] The distribution of the normalized structure factors, E, indicates[13] that the crystal is centrosymmetric.

Structure solution using Long's computer program[14] for reiterative application of Sayre's equation[15] was straightforward and led to an E map[16] showing the expected 14 nonhydrogen atoms as the 14 largest peaks. Full-matrix least-squares refinement, eventually including the hydrogen atoms with individual isotropic temperature factors and the nonhydrogen atoms with anisotropic temperature factors, leads to a value of $R(F)$ = 0.037 for all 2411 reflections measured (including duplicate measurements). In the final difference Fourier map, 10 of the 11 highest peaks (0.4 to 0.2 electron/Å^3) are located near the midpoints of the ring bonds, indicating that a model which does not take into account bonding-electron density is inadequate. Investigation of this aspect of the problem is continuing.

The structure analysis confirms the postulated 3-hydroxyxanthine structure (Fig. 7.2) and reveals that

this compound, like purine[17] and 6-mercaptopurine,[18] exists as the N(7)–H tautomer. Although purine chemists seem to use N(7)–H and N(9)–H tautomers interchangeably when writing structural formulas (sometimes even in the same paper[5]), crystallographic results consistently indicate the N(7)–H tautomer to be the more stable.

The most striking feature of the molecular geometry is that O(11) lies 0.189 Å from the best plane through all the atoms of the ring system except N(1) (see Table 7.1); the deviations of N(1) and O(10) from the plane are also significant. A plausible explanation in terms of molecular bonding follows.

It is well known[19] that the five atoms of a carboxylic acid fall, at least roughly, in a common plane, reflecting delocalization of the π electrons above and below the plane of the carboxyl group.

ORNL-DWG. 71-6793

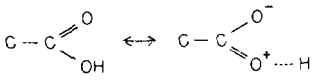

In the hydroxamic acid under discussion here, the angle between the C(2)–N(3)–C(4) plane and the N(3)–O(11)–H(11) plane is 90°. There being no appreciable delocalization of the oxygen lone-pair electrons into the ring, the hydrogen atom evidently takes up a position convenient for hydrogen bonding to a neighboring water molecule. A dipole is thus set up having a large component normal to the ring plane in the direction of the oxygen lone pairs. An induced dipole then displaces the polarizable π electrons of the neighboring ring nitrogen atom, making its configuration pyramidal in the direction observed in the crystal structure, that is, with O(11) and H(11) on opposite sides of the plane of the molecule. The slight tipping of the N(1)–C(2)–O(10) plane is in the expected direction for maximum π bonding between C(2) and N(3).[20]

ORNL-DWG. 71-6794

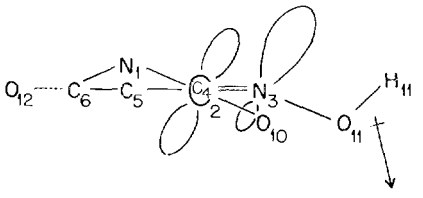

A similar, but smaller, effect seems to be operative in crystalline 2,4,6-trinitrophenetole[21] and is apparently to be expected wherever an oxygen atom *exo*cyclic to

Table 7.1. Distances (Å) of atoms from a least-squares plane fitted to all the ring atoms except N(1) in the 3-hydroxyxanthine molecule

Atoms in the right-hand column were not used to determine the plane

Atom	Distance	Atom	Distance	Atom	Distance
C(2)	0.000	C(6)	0.000	N(1)	0.015
N(3)	0.003	N(7)	0.001	O(10)	−0.011
C(4)	−0.001	C(8)	0.002	O(11)	−0.189
C(5)	−0.002	N(9)	−0.003	O(12)	0.003

an aromatic ring (or other planar system) has its second substituent out of the plane. We plan crystal structure investigations of guanine-3-oxide and adenine-1-oxide which may be pertinent here since the assumption that these substances exist in the *N*-oxide form is based on uv spectral correlations[7] which do not seem conclusive and do not rule out the reasonable alternative *N*-hydroxy forms **1′** and **2′**.

ORNL-DWG. 71-6795

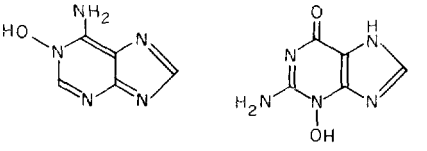

1′ **2′**

Finally, the direct pathway for the 3-oxy → 8-oxy rearrangement proposed by Wölcke et al.[8]

ORNL-DWG. 71-6796

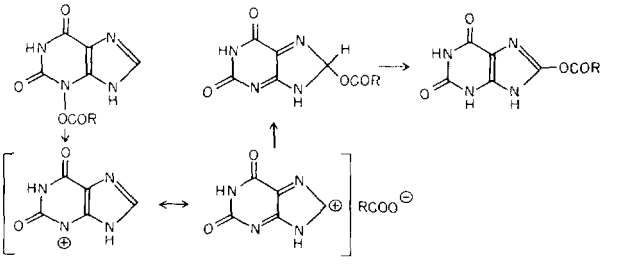

is not applicable to the N(7)–H tautomer found in the crystal. It is quite possible, of course, that the reaction in solution proceeds through N(9)–H intermediates, but an appealing alternative is an intermediate "dehydroxanthine" (**4**).

ORNL-DWG. 71-6797

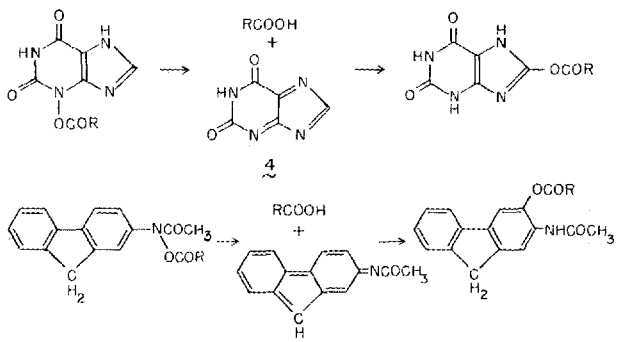

It is interesting that an analogous $4n$ π-electron intermediate, **5**, can be written for the known rearrangement of 2-hydroxylaminofluorene esters.

1. G. Stöhrer and G. B. Brown, *Science* **167**, 1622 (1970), hold that "The more common term 'carcinogenic' should be restricted to agents that induce carcinomas. Oncogenic is an inclusive term for agents that induce any form of neoplasia."
2. J. A. Miller and E. C. Miller, *Progr. Exp. Tumor Res.* **11**, 273 (1969).
3. (*a*) E. C. Miller, J. A. Miller, and H. A. Hartmann, *Cancer Res.* **21**, 815 (1961); (*b*) J. A. Miller, M. Enomato, and E. C. Miller, ibid. **22**, 1381 (1962).
4. Y. Shirasu, *Proc. Soc. Exp. Biol. Med.* **118**, 812 (1965).
5. K. Sugiura et al., *Cancer Res.* **30**, 184 (1970).
6. M. A. Stevens and G. B. Brown, *J. Amer. Chem. Soc.* **80**, 2759 (1958).
7. U. Wölcke and G. B. Brown, *J. Org. Chem.* **34**, 978 (1969).
8. U. Wölcke et al., *J. Org. Chem.* **34**, 981 (1969).
9. T. J. Delia and G. B. Brown, *J. Org. Chem.* **31**, 178 (1966).
10. Changes in these parameters were noted during data collection and were assumed to be due to radiation damage.
11. G. M. Brown and W. E. Thiessen, *Chem. Div. Annu. Progr. Rep. May 20, 1969*, ORNL-4437, p. 129.
12. H. A. Levy, W. E. Thiessen, and G. M. Brown, *Chem. Div. Annu. Progr. Rep. May 20, 1970*, ORNL-4581, p. 135.
13. D. Rogers, "Statistical Properties of Reciprocal Space," chap. 15 in *Computing Methods in Crystallography*, J. S. Rollett, ed., Pergamon, Oxford, 1965.
14. R. E. Long, Ph.D. dissertation, University of California, Los Angeles, 1965.
15. D. Sayre, *Acta Crystallogr.* **5**, 60 (1952).
16. J. Karle and I. L. Karle, "Phase Determination for Centrosymmetric Crystals by Probability Methods," chap. 17 in *Computing Methods in Crystallography*, J. S. Rollett, ed., Pergamon, Oxford, 1965.
17. D. G. Watson, R. M. Sweet, and R. E. Marsh, *Acta Crystallogr.* **19**, 573 (1965).
18. G. M. Brown, *Acta Crystallogr., Sect. B* **25**, 1338 (1969).
19. J. Donohue, *Acta Crystallogr., Sect. B* **24**, 1558 (1968).
20. Dr. H. A. Levy must share the credit (or the blame) for this explanation of the observed molecular geometry.
21. C. M. Gramaccioli, R. Destro, and M. Simonetta, *Acta Crystallogr., Sect. B* **24**, 129 (1968).

PRECISE X-RAY CRYSTAL-STRUCTURE ANALYSIS OF DECACHLORORUTHENOCENE

George M. Brown

Molecular structural parameters are reported here from a precise x-ray analysis of crystalline decachlororuthenocene, $Ru(C_5Cl_5)_2$, one of a number of metallocenes polysubstituted with electronegative substituents which were recently synthesized for the first time.[1] This is the first structure determination of a decasubstituted metallocene of any kind.

Crystals of decachlororuthenocene were found to be triclinic with unit-cell parameters as follows: a = 8.5193(3) Å, b = 13.8812(5) Å, c = 7.3770(3) Å, α = 95.839(3)°, β = 101.063(3)°, γ = 89.216(3)°, where the numbers in parentheses, corresponding to the least significant digits of the parameters, are estimated standard deviations. There are two formula units per cell, and the space group is the centrosymmetrical group $P\bar{1}$. Intensities of 6181 independent reflections were recorded with Mo $K\alpha$ radiation using the Oak Ridge automatic computer-controlled diffractometer. The intensities were corrected for absorption, and the observed structure-factor square F^2_{obsd} was calculated for each reflection in the usual way.

The solution for the structure was achieved with textbook simplicity by inspection of a three-dimensional Patterson map. The refinement, by the method of least squares, was straightforward. Anisotropic thermal parameters were refined for all atoms; corrections for an almost negligible degree of extinction were applied. The final discrepancy factor R (defined as $\Sigma\,|\,|F_{obsd}| - |F_{calc}|\,|/\Sigma|F_{obsd}|$) is 0.048. The excursions of electron density in a final difference map correspond roughly to the excursions in a skew-density map.[2,3] The estimated standard errors of the structure parameters are substantially lower than those from determinations of other metallocenes known to the author, except two other determinations also done in this laboratory.[4,5]

From the scaled drawings of the molecule shown in Fig. 7.3 and the numerical data included in them, it is clear that the molecule nearly has the symmetry of point group D_{5h}, even though its environment in the crystal of $P\bar{1}$ symmetry is totally asymmetric. The D_{5h} symmetry is the symmetry the molecule must have in isolation if its equilibrium conformation is the eclipsed one. The eclipsing in the crystal is exact, within the errors of the determination. It is interesting that the eclipsed conformation seems to be a characteristic feature of ruthenocene[6] and its derivatives[7] in the crystalline state.

The symmetry of the ruthenium-carbon framework is essentially perfect in all respects. No carbon atom deviates by more than 0.001 Å from the best plane through its ring as established by the method of least squares, using equal weights for all ring atoms. The best planes of the two rings of carbon atoms are inclined to each other by about 0.3°, not significantly different from 0°. The distance between the centroids of the two rings is 3.598 Å, the same, of course, as the average distance C ... C′ between opposing carbon atoms across the sandwich. The two Ru-to-plane distances are 1.800 and 1.798 Å.

The chlorine atoms are displaced from the planes of the rings to which they are attached, in each case in the direction away from the opposing chlorine atom, by from 0.094 to 0.126 Å, or by an average of 0.106 Å

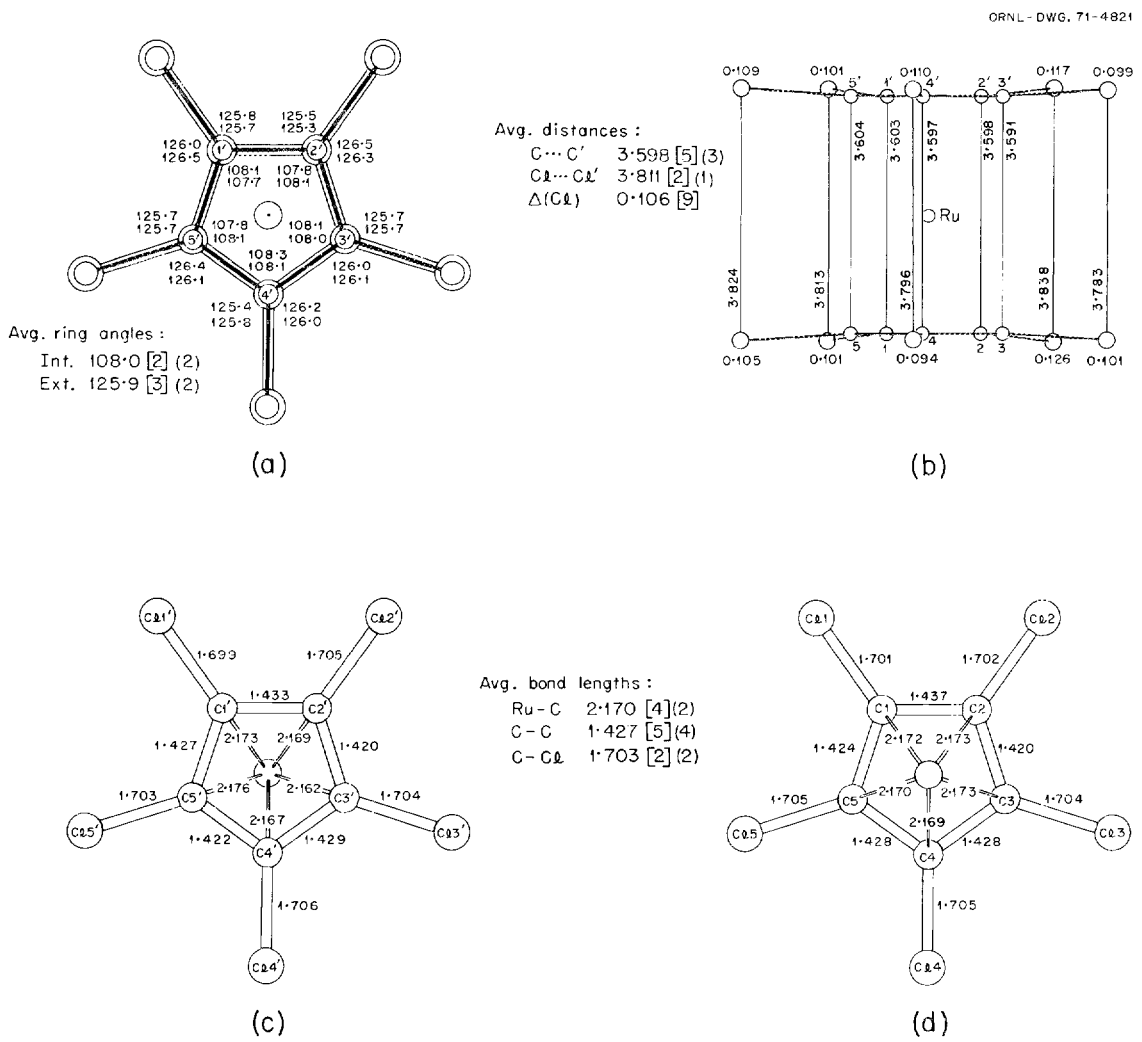

Fig. 7.3. Geometry of the decachlororuthenocene molecule. (*a*) A view of the molecule along the line (see trace marked by the dot within the circle representing Ru) connecting the mean of the atomic positions for one group C_5Cl_5 to that of the other, showing the nearly perfect eclipsing. Bonds Ru–C are omitted. The top group (primed atoms) is represented with smaller circles and thinner bonds than the bottom group (unprimed atoms, not labeled in this part of the figure). The numerical values of the interior angles C–C–C and exterior angles C–C–Cl are given for both groups C_5Cl_5; the top and bottom numbers of each pair refer to $C'_5Cl'_5$ and C_5Cl_5 respectively. (*b*) A view of the molecule perpendicular to that of *a*, showing the numerical values (Å) of the deviations of the chlorine atoms from the ring planes. The distances C ... C′ and Cl ... Cl′ between opposing atoms across the sandwich are also specified. Bonds Ru–C are omitted. (*c*) Bond lengths (Å) in the top half of the molecule. (*d*) Same for the bottom half of the molecule. The numbers in brackets associated with the average values of parameters specified in the figure correspond to the least significant digits of the averages and express the root-mean-square deviations from the averages; similarly, the numbers in parentheses express the estimated standard errors of individual parameters as derived from the least-squares covariance matrix.

(root-mean-square deviation, 0.009 Å). These highly significant displacements, which correspond to bending the C–Cl bonds out of plane by from 3.15 to 4.21°, constitute one of the most interesting features of the molecular structure.

Such displacements may conceivably arise either as a manifestation of directed valence or from repulsion between the atoms opposing each other across the sandwich. However, in this case repulsion can hardly be important, for the average Cl ... Cl′ distance of 3.811 Å between opposing atoms is substantially more than twice the usually accepted value[8] of 1.80 Å for the van der Waals radius of chlorine. Moreover, there are 25 intermolecular Cl ... Cl contacts less than 3.838 Å, the greatest Cl ... Cl′ distance. Of these, 10 are less than 3.70 Å, 4 are between 3.61 and 3.64 Å, and 1 is at 3.33 Å. It seems clear that the chlorine atoms are held out of the ring planes by valence forces, not by repulsion.

The average Ru–C and C ... C′ distances in decachlororuthenocene of 2.170 and 3.598 Å are to be compared with corresponding distances of 2.21 and 3.68 Å from the x-ray analysis of ruthenocene.[6] The comparison is complicated by the fact that the standard errors of the Ru–C and C ... C′ distances from the ruthenocene determination are, characteristic of an earlier stage of development of x-ray analysis, six to ten times those of the perchloro compound. However, there is almost certainly a slight effect of tightening of the Ru-to-ring bonding as a result of the multiple substitution by chlorine atoms. Comparison of our results with those from the x-ray analysis of bisindenylruthenium[9] suggests a smaller effect than the comparison above; the Ru–C distances in bisindenylruthenium range from 2.165 to 2.211 Å, averaging 2.190 Å. In this case the standard errors are about three to four times ours.

The average C–C distance of 1.427 Å in the cyclopentadienyl rings is not significantly different from the averages in ruthenocene and bisindenylruthenocene. The average C–Cl distance of 1.703 Å agrees with the value 1.70 ± 0.01 given by Sutton[10] as the average from a number of chlorine derivatives of aromatic compounds, in which the carbon atoms are also in the sp^2 state of hybridization.

The packing of the molecules is shown in the stereoscopic drawing of Fig. 7.4, in which atoms are represented by their 50% probability ellipsoids.[11] The very short Cl ... Cl van der Waals contact at 3.33 Å mentioned above is indicated in the figure. The molecules pack in layers parallel to the (001) plane. The stacking of these layers along the direction of the reciprocal axis c^* puts each group C_5Cl_5 of one layer in contact with a group $C'_5Cl'_5$ of an adjacent layer, but with an offset parallel to (001) so that the two rings of carbon atoms only partly overlap. The perpendicular distance from one ring plane to the centroid of the other ring is 3.559 Å, slightly less than the intramolecular ring spacing.

I thank Drs. F. L. Hedberg and H. Rosenberg of the Air Force Materials Laboratory, Wright-Patterson Air Force Base, for suggesting the problem and supplying crystals. Thanks are due also to Dr. P. K. Sen Gupta for some assistance in collecting and preliminary processing of data.

1. F. L. Hedberg and H. Rosenberg, *J. Amer. Chem. Soc.* **92**, 3239 (1970).
2. C. K. Johnson, *Acta Crystallogr., Sect. A* **25**, 187 (1969).
3. C. K. Johnson, chap. 9 in *Thermal Neutron Diffraction*, ed. by B. T. M. Willis, Oxford University, Oxford, 1970.
4. L. H. Hall and G. M. Brown, *Acta Crystallogr., Sect. B* **27**, 81 (1971).

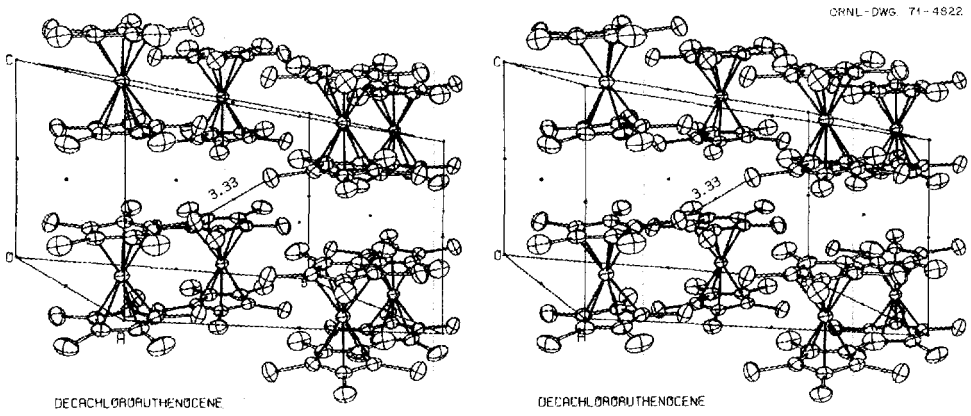

Fig. 7.4. Stereoscopic drawing showing the packing of the molecules in the decachlororuthenocene crystal. The short Cl ... Cl distance between two atoms Cl(3′) related by inversion through the symmetry center at ½, ½, ½ is indicated.

5. G. M. Brown, "Precise X-Ray Crystal-Structure Analysis of 1,1′-Diethoxyoctachloroferrocene," the following contribution, this report.

6. G. L. Hardgrove and D. H. Templeton, *Acta Crystallogr.* **12,** 28 (1959).

7. P. J. Wheatley, in *Perspectives in Structural Chemistry,* vol. 1, ed. by J. D. Dunitz and J. A. Ibers, Wiley, New York, 1967.

8. L. Pauling, *The Nature of the Chemical Bond,* 3d ed., p. 260, Cornell, Ithaca, N.Y., 1960.

9. N. C. Webb and R. E. Marsh, *Acta Crystallogr.* **22,** 382 (1967).

10. L. E. Sutton, ed., *Tables of Interatomic Distances and Configuration in Molecules and Ions,* p. S17s, Special Publication No. 18, supplement, The Chemical Society, London, 1965.

11. C. K. Johnson, *OR TEP: A Fortran Thermal Ellipsoid Plot Program for Crystal-Structure Illustrations,* ORNL-3794 (2d rev.) (1970).

PRECISE X-RAY CRYSTAL-STRUCTURE ANALYSIS OF 1,1′-DIETHOXYOCTACHLOROFERROCENE

George M. Brown

In continuation of studies on polysubstituted metallocenes initiated by the x-ray analysis of decachlororuthenocene,[1] the structure of crystalline 1,1′-diethoxyoctachloroferrocene was determined.

Crystals of 1,1′-diethoxyoctachloroferrocene are triclinic with unit-cell parameters as follows: a = 9.9094(10) Å, b = 12.7356(13) Å, c = 8.9512(9) Å, α = 109.492(8)°, β = 113.660(8)°, γ = 81.127(9)°. There are two formula units per cell, and the space group is $P\bar{1}$. The collection of intensity data (for 5546 independent reflections) and the derivation from the data of the refined structure followed procedures essentially identical to those used in the work on decachlororuthenocene, except that the solution of the phase problem was obtained by the direct-method program of Long.[2] Approximate locations, chemically sensible, were found for all of the hydrogen atoms of the molecule. The final discrepancy factor R is 0.049. The scaled drawings of Fig. 7.5 and the numerical data included in them show the principal results of the structure analysis.

In this compound the presence of the two ethoxy groups instead of the ninth and tenth chlorine atoms causes the C_5 rings of the molecule to depart significantly from exact pentagonal symmetry. There is slightly more spread of values for each type of distance in the molecule and considerably more spread in the angles of a given type than in the case of decachlororuthenocene. However, the FeC_{10} framework does not deviate greatly from D_{5h} symmetry.

There is a twist of one ring with respect to the other of about 1.3° around the line joining the ring centroids. This twist, which is discernible in Fig. 7.5, is significant in relation to the errors of the determination but not chemically significant. Generally the chlorine atoms follow closely the twist of the rings and are also nearly totally eclipsed. The torsion or conformation angle[3] of O and O′ about the axis of ring centroids is −3.95°, and the oxygen atoms are farther from the totally eclipsed condition than the chlorine atoms.

No ring carbon atom deviates by more than 0.008 Å from the least-squares best plane of its ring. The best planes of the two different rings are inclined to each other at 0.8°. The chlorine atoms are displaced from the best planes, in each case in the direction away from the opposing chlorine atom, by from 0.080 to 0.147 Å, or by an average of 0.110 Å. These displacements correspond to bending the C–Cl bonds by from 2.293 to 4.83°. The two oxygen atoms are displaced from their respective ring planes by 0.097 and 0.346 Å, corresponding to bending the C–O bonds by 1.25 and 4.06°.

The intramolecular distances Cl ... Cl′ between opposing chlorine atoms, which are in the range 3.467 to 3.531 Å, include the closest nonbonded contacts Cl ... Cl in the crystal. The two closest intermolecular Cl ... Cl contacts are at 3.515 and 3.534 Å, and there are only four others less than 3.600 Å. Nevertheless, the average out-of-plane displacement of the chlorine atoms is almost the same as in decachlororuthenocene, where the average Cl ... Cl′ distance is 3.811 Å, suggesting that the chlorine atoms are held out of plane mainly by valence forces, as already concluded for decachlororuthenocene.

There is no suggestion, contrary to the case of decachlororuthenocene, that the multiple substitution of hydrogen atoms by negative groups leads to shortening of the average Fe–C and Fe-to-plane distances. These distances are 2.047 and 1.650 Å, respectively, virtually identical with the averages given by Wheatley[4] from a number of cyclopentadienyl complexes with iron and also close to the values 2.033 and 1.645 Å found in *N*-formylaminomethylferrocene.[5] It is possible that there is a tendency toward contracting the Fe–C bonds which is countered by repulsion between the carbon atoms opposing each other across the sandwich. The opposing carbon atoms, at the average separation of 3.301 Å, are much closer than in decachlororuthenocene and in fact a little closer than twice the usually quoted value[6] of 1.70 Å for the half-thickness of an aromatic ring.

The average ring C–C distance of 1.424 Å and the average C–Cl distance of 1.709 Å are nearly the same as the averages found in decachlororuthenocene.

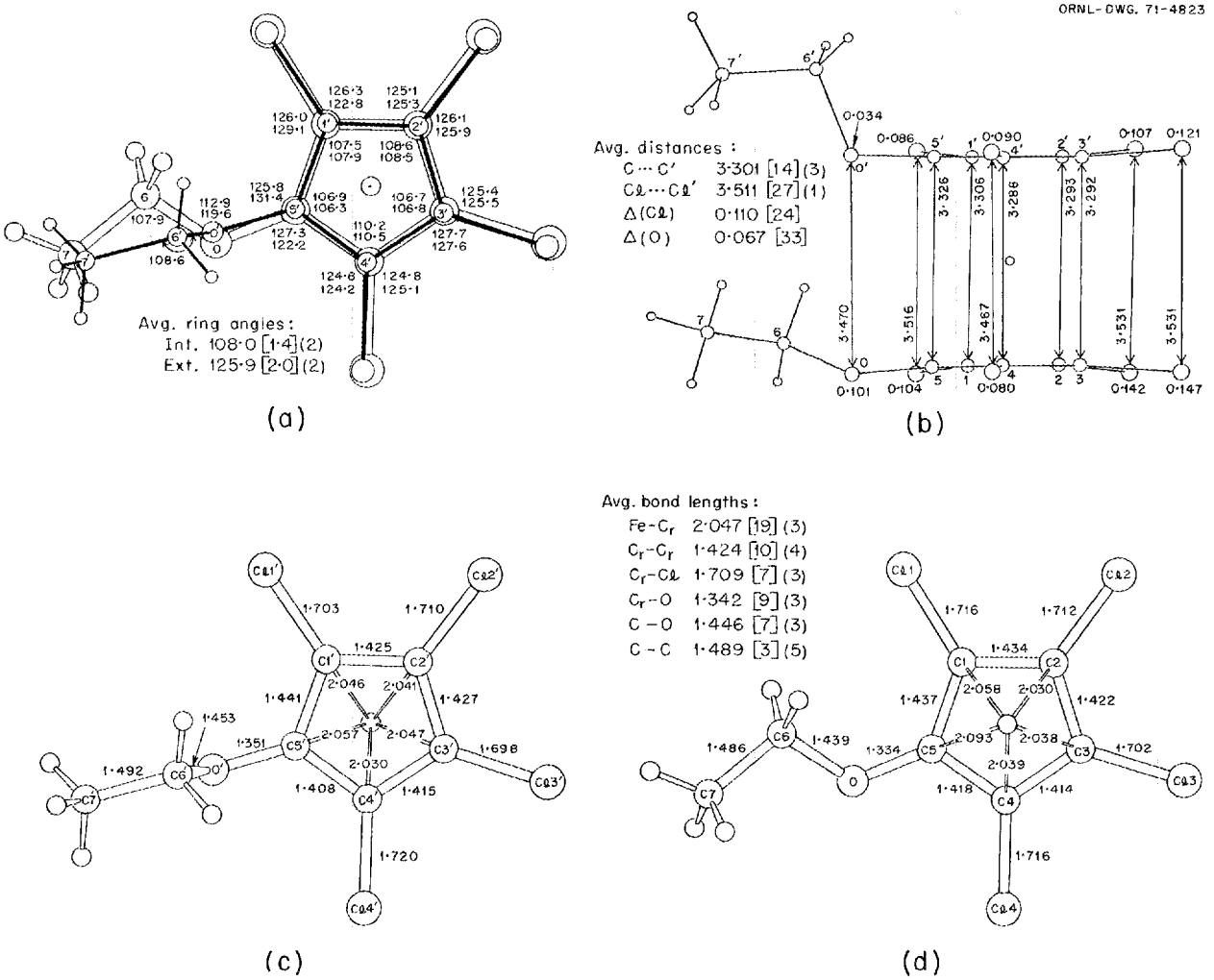

Fig. 7.5. Geometry of the 1,1′-diethoxyoctachloroferrocene molecule. (*a*) A view of the molecule along the line (see trace marked by the dot within the circle representing Fe) connecting the mean of the atomic positions for one ring C_5 to that of the other, showing the slight departure from total eclipsing of the rings. Bonds Fe–C are omitted. The top group $C_5Cl_4OC_2H_5$ (primed atoms) is represented with smaller circles and thinner bonds than the bottom group (unprimed atoms, not labeled in this part of the figure). The numerical values of the angles C–C–C, C–C–Cl, C–O–C, and C–C–O are given for both groups; the top and bottom numbers of each pair refer to the top and bottom groups respectively. (*b*) A view of the molecule perpendicular to that of *a*, showing the numerical values (Å) of the deviations of the chlorine and oxygen atoms from the ring planes. The distances C ... C′, Cl ... Cl′, and O ... O′ between opposing atoms across the sandwich are also specified. Bonds Fe–C are omitted. (*c*) Bond lengths (Å) in the top half of the molecule. (*d*) Same for the bottom half of the molecule. The numbers in brackets associated with the average values of parameters specified in the figure correspond to the least significant digits of the averages and express the root-mean-square deviations from the averages; similarly, the numbers in parentheses express the estimated standard errors of individual parameters as derived from the least-squares covariance matrix.

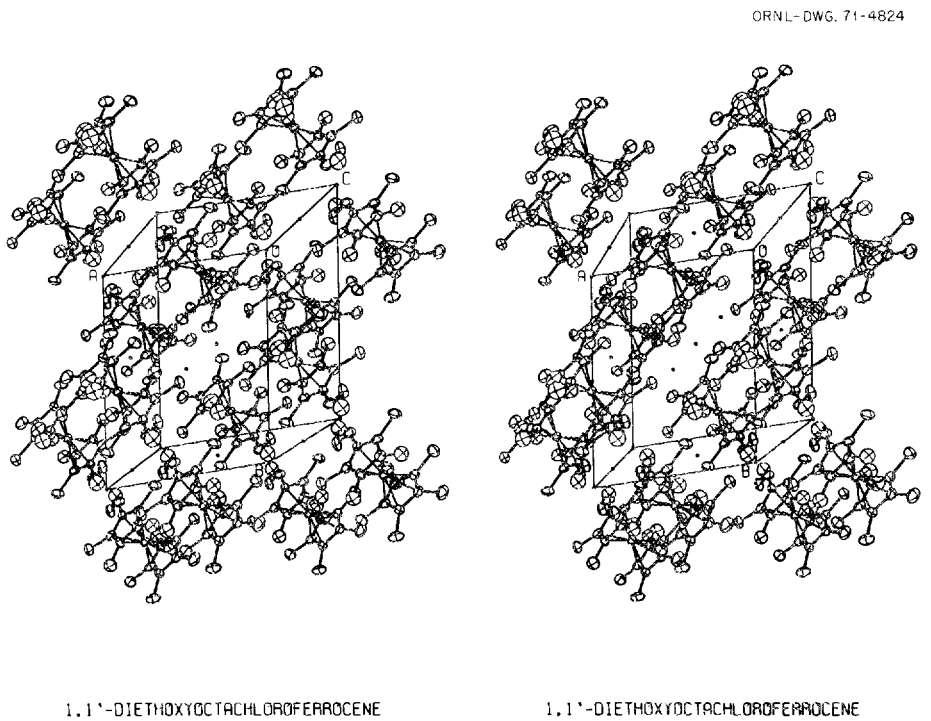

Fig. 7.6. Stereoscopic drawing showing the packing of molecules in the crystal of 1,1′-diethoxyoctachloroferrocene.

The packing of the molecules is shown in the stereoscopic drawing of Fig. 7.6, in which the atoms are represented by their ellipsoids of 50% probability.

I thank Drs. F. L. Hedberg and H. Rosenberg of the Air Force Materials Laboratory, Wright-Patterson Air Force Base, for suggesting this work and for supplying crystals. Thanks are due also to Dr. P. K. Sen Gupta for some assistance in collecting and preliminary processing of data.

1. G. M. Brown, "Precise X-Ray Crystal-Structure Analysis of Decachlororuthenocene," the preceding contribution, this report.
2. R. E. Long, Ph.D. dissertation, University of California, Los Angeles, 1965. See Appendix: "Program for Sign Determination by Reiterative Application of Sayre's Equation."
3. W. Klyne and V. Prelog, *Experientia* **16**, 521 (1960).
4. P. J. Wheatley, in *Perspectives in Structural Chemistry*, vol. 1, ed. by J. D. Dunitz and J. A. Ibers, Wiley, New York, 1967.
5. L. H. Hall and G. M. Brown, *Acta Crystallogr., Sect. B* **27**, 81 (1971).
6. L. Pauling, *The Nature of the Chemical Bond*, 3d ed., p. 260, Cornell, Ithaca, 1960.

CRYSTAL AND MOLECULAR STRUCTURE OF α,α'-TREHALOSE DIHYDRATE

George M. Brown

In continuation of structure analyses in this laboratory of sugars and of crystalline hydrates, the structure of α,α'-trehalose dihydrate was determined. α,α'-Trehalose ($C_{12}H_{22}O_{11}$, more properly named α-D-glucopyranosyl-α-D-glucopyranoside) is a nonreducing disaccharide composed of two α-D-glucosyl units bridged by an oxygen atom. Known also as mycose and as mushroom sugar, it is widespread in nature, where it is found in fungi, bacteria, insect blood, algae, lichens, and in some higher plants.[1]

Crystals of α,α-trehalose dihydrate are orthorhombic with the following unit-cell parameters: a = 12.230(4) Å, b = 17.902(6) Å, c = 7.598(2) Å, where the numbers in parentheses are the estimated standard deviations times 10^3. The space group is $P2_12_12_1$, and there are four formula units $C_{12}H_{22}O_{11}\cdot 2H_2O$ per cell. The calculated density is 1.511 g/cc, and the observed[2] is 1.512 g/cc. The collection of intensity data for 3328 independent reflections and the preliminary processing

followed the same procedures used for decachlororuthenocene.[3] The solution of the phase problem was achieved quite easily by direct methods; the tangent-formula refinement procedure[4] was used with the 258 normalized structure factors of magnitude greater than 1.66, starting with four phases fixed to specify origin and enantiomorph and seven others for which preliminary values were indicated with acceptable probability by a calculation with the sigma-1 formula.[5] Approximate coordinates were eventually found for all the hydrogen atoms. In the final least-squares refinement cycles the parameters adjusted were: a scale factor on the calculated structure-factor magnitudes, three coordinates for each atom, six anisotropic thermal parameters for each carbon and oxygen atom, and an isotropic thermal parameter for each hydrogen atom. There was no evidence for extinction. The final discrepancy index R is 0.057.

Figure 7.7, which is labeled with numerical values of the bond lengths, valence angles, and conformation angles[6,7] of most interest, shows the geometry of the molecule.

The ring conformation angles fall in the range of magnitudes 48.0 to 62.4° for one ring (unprimed atoms) and 49.5 to 59.6° for the other. These ranges are wider than the range (54.9 to 56.0°) found for the same ring structure in sucrose[7] but not much different from that (51.3 to 62.3°) found in α-D-glucose.[8] The variations in the ring conformation presumably arise because of the differing intramolecular and intermolecular environment from one crystalline compound to another; they show a degree of flexibility of the pyranose ring in chair form.

The conformation angles about the bonds C(1)–O(1) and C′(1)–O(1) of the bridge between the two rings are about those which would be expected to minimize repulsion between neighboring atoms of the two rings. Atoms C(1) and C′(2) are in *anti* positions about bond C′(1)–O(1), and atoms C′(1) and C(2) are in *anti* positions about bond C(1)–O(1).

The minimum, mean, and maximum bond lengths C–C are 1.513, 1.522, and 1.535 Å, nearly identical with the corresponding values for α-D-glucose and sucrose. The minimum, mean, and maximum bond lengths C–O are 1.406, 1.422, and 1.434 Å, also close to the corresponding values for sucrose and glucose. The bonds C(5)–O(5) and C′(5)–O′(5) are slightly longer than the adjacent bonds O(5)–C(1) and O′(5)–C′(1). This kind of effect was first observed in sucrose[7] and has since been observed in a number of pyranosides.[9]

The average C–H and O–H apparent bond lengths of 0.96 and 0.75 Å are typical values for determinations of these bonds from x-ray analyses, showing the usual

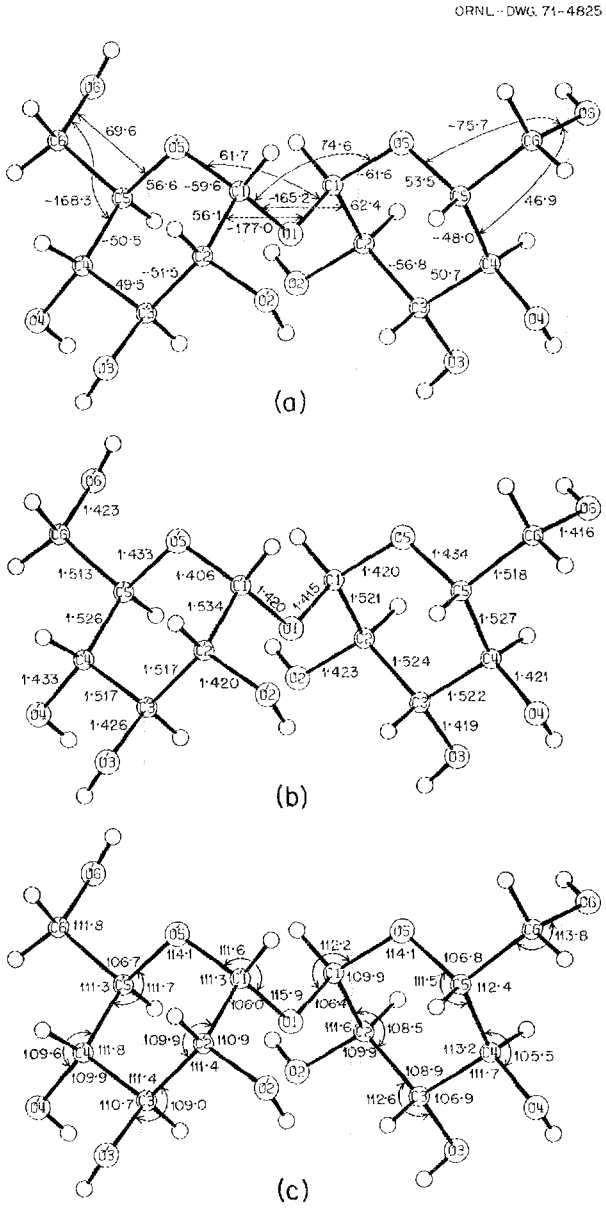

Fig. 7.7. Molecular geometry of the α,α′-trehalose molecule with numerical values of the molecular structural parameters of most interest. (*a*) Conformation angles (deg). For each ring bond the conformation angle of the two adjacent ring bonds is written along the bond. Angles about other specific bonds are defined by lines pointing in each case to two bonds attached at opposite ends of a central bond. (*b*) Lengths (Å) of bonds C–C and C–O. (*c*) Bond angles (deg) involving carbon and oxygen atoms.

shortening relative to the values 1.10 and 0.97 Å obtained in neutron analyses of sucrose and α-D-glucose.

The average interior ring angle at carbon is 110.9°, to be compared with 110.7° in α-D-glucose and 110.3° in the α-D-glucosyl moiety of sucrose. The angle of 115.9° at O(1) is in the normal range for glycosidic linkages, and the two angles of 114.1° at O(5) and O′(5) are similarly normal for ring oxygens in pyranosides.

The trehalose and water molecules are held together in the crystal structure by a complex system of 12 crystallographically independent hydrogen bonds O–H···O (see Fig. 7.8). Each hydroxyl group of the sugar molecule is a donor and an acceptor in hydrogen bonding. The ring atom O(5) is an acceptor; atoms O′(5) and O(1) are not involved in the hydrogen bonding. Each water molecule is a donor for two different bonds; one is an acceptor for two and the other for one. The hydrogen-bond parameters are in the normal ranges; the minimum, mean, and maximum O···O′ distances are 2.70, 2.79, and 2.91 Å, and the O–H···O angles range from 151 to 174°.

By coincidence, the crystal structure of α,α′-trehalose dihydrate has also been determined independently and concurrently in two other laboratories.[2,10] Comparison of the structure parameters shows that the agreement among the three sets is about as good as is ever achieved for independent determinations but that the standard errors may have been underestimated by a factor of 2 or 3, probably because of systematic errors. The standard errors of the Oak Ridge determination are about two-thirds of those of the better of the other two determinations. A joint paper from the three laboratories is now in preparation.

1. G. G. Birch, p. 201 in *Advances in Carbohydrate Chemistry*, vol. 18, ed. by M. L. Wolfrom and R. S. Tipson, Academic, New York, 1963.

2. C. A. Beevers, R. O. Gould, and R. Simpson, University of Edinburgh, private communication.

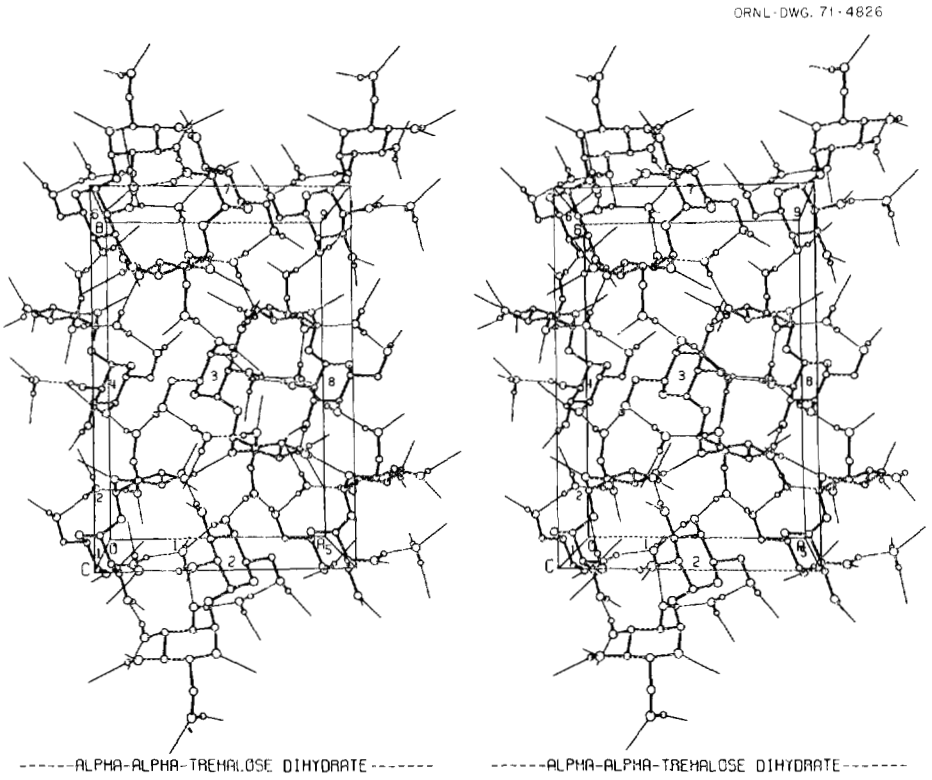

Fig. 7.8. Stereoscopic view of the packing of the sugar and water molecules in α,α′-trehalose dihydrate. Hydrogen atoms attached to carbon atoms are not shown. The thin lines connecting hydrogen atoms and oxygen atoms show the hydrogen bonding. The nine sugar molecules included in the drawing are labeled *1, 2, ... , 9* within the rings of primed atoms in Fig. 7.7. Two crystallographically independent water molecules are labeled *1* and *2*.

3. G. M. Brown, "Precise X-Ray Crystal-Structure Analysis of Decachlororuthenocene," a previous contribution in this section, this report.
4. J. Karle and I. L. Karle, *Acta Crystallogr.* **21**, 849 (1966).
5. J. Karle and H. Hauptman, *Acta Crystallogr.* **9**, 635 (1956).
6. W. Klyne and V. Prelog, *Experientia* **16**, 521 (1966).
7. G. M. Brown and H. A. Levy, *Science* **141**, 921 (1963).
8. G. M. Brown and H. A. Levy, *Science* **146**, 1038 (1965).
9. H. Berman, S. S. C. Chu, and G. A. Jeffrey, *Science* **157**, 1576 (1967).
10. D. Rohrer and B. Berking, University of Pittsburgh, private communication.

CHARACTERIZATION OF THE THERMAL MOTION IN TRISACETYLACETONATOCHROMIUM(III)

C. K. Johnson R. C. Thomas[1]

An x-ray diffraction crystal-structure analysis by Morosin[2] showed that one of the three acetylacetonato ligands (i.e., ligand A) in $Cr(CH_3COCHCOCH_3)_3$ undergoes unusually large thermal displacements along the **b** axis of the monoclinic crystal. The abnormal thermal motion makes this crystal a good candidate for the evaluation of various methods for determining thermal motion.

In order to test the hypothesis that the large displacements are caused by a dynamic thermal effect and not by static disorder, a preliminary study of thermal-diffuse scattering of x rays was made. The results of that study, summarized in the caption to Fig. 7.9, led us to conclude that the hypothesis is true.

A neutron-diffraction structure analysis of the crystal was undertaken to permit a proper characterization for the thermal displacements of the hydrogen atoms on the six different methyl groups. A total of 2829 unique neutron Bragg-diffraction data were collected at the High Flux Isotope Reactor using a 40.2-mg crystal[3] held at −5°C by a cold air stream. The large thermal motion caused the intensities to diminish rather rapidly with increasing 2θ, and an extended data set was collected later at −40°C; however, the preliminary results presented below are from the data collected at −5°C. The diffraction data were corrected for absorption.

For the least-squares refinement, the starting parameters for the heavy atoms were taken from the x-ray results of Trus and Marsh,[4] and the starting hydrogen parameters were determined by Fourier methods. The refined methyl-group conformations, illustrated in Fig. 7.10, show no preference for any particular eclipsed or staggered intramolecular configuration and, in fact, appear to be influenced principally by intermolecular packing considerations. The unweighted R factor based on F^2 for the refinement with anisotropic temperature factors is 13.4% for all data. This rather high R value does not reflect the quality of the data but rather indicates that the normal model is inadequate when large-amplitude curvilinear thermal motions are present. More elaborate models, including the orthogonalized series-expansion model described in last year's report,[5] will be adjusted to the neutron data set collected at −40°C.

The average bond lengths (Å) derived from the present refinement, along with the corresponding values corrected for thermal motion by the segmented-body model,[6,7] are: Cr–O bonds, 1.970 (1.986); terminal C–C bonds, 1.507 (1.518); internal C–C bonds with partial double-bond character, 1.396 (1.406); C–O bonds, 1.257 (1.269); and C–H bonds, 1.070 (1.169) [or 1.030 (1.148) omitting ligand A]. The C–H distances tend to be overcorrected and indicate that a more rigorous model[8] should be used for correcting interatomic distances when large-amplitude curvilinear motions are present.

The orientations of the thermal ellipsoids in Fig. 7.10 indicate the presence of internal molecular torsional motion for the methyl groups on ligands B and C. This motion can be approximated with the segmented-body model[7] by letting each methyl group ride on the rigid body of the parent ligand with freedom of motion about the adjacent C–C bond. The internal torsional amplitudes derived in this manner are 27.4, 24.1, 32.2, and 26.6° for methyl groups 1B, 5B, 1C, and 5C respectively.

The large thermal motion of the A ligands is illustrated in Figs. 7.11 and 7.12. Some of the hydrogen atoms have rms displacements of nearly 1 Å. An interpretation which is consistent with the thermal-ellipsoid drawings and the diffuse-scattering results is that the A ligands in a given column parallel to the **b** axis are moving in phase cooperatively over an extended distance along **b**, and the corresponding motion in adjacent columns is independent.

Raman spectroscopic studies of an oriented single crystal of trisacetylacetonatoaluminum(III) were carried out by J. B. Bates (Director's Division). This crystal is isostructural with the Cr derivative and has more favorable optical properties. A polarization analysis of the particularly strong band at 17 cm^{-1} indicates that a librational lattice vibration exists with large projected displacements in the crystallographic *ab* plane, which is the principal plane for motion of ligand A. Further collaborative studies along this line are under way.

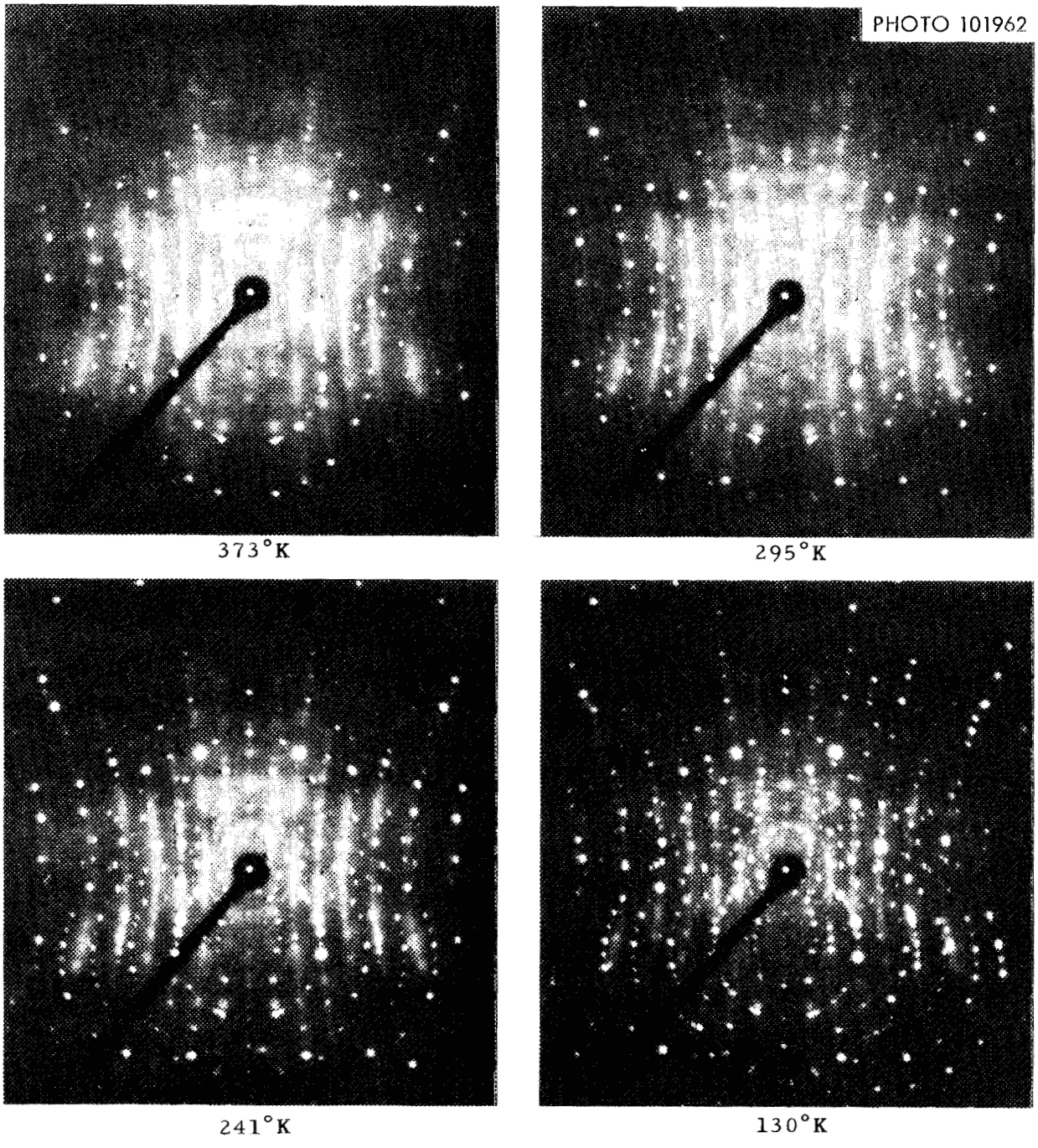

Fig. 7.9. Stationary-crystal flat-film x-ray photographs from a single crystal of trisacetylacetonatochromium(III) at four different temperatures. The [30$\bar{1}$] axis is vertical, and the [010] axis is horizontal and points to the right. These 1-hr exposures to zirconium-filtered x rays from a molybdenum-target tube were recorded with a Polaroid cassette containing a fluorescent intensifying screen. The sharp spots are Laue reflections from the polychromatic x-ray continuum, and the broad streaks are diffuse scattered intensities from the monochromatic Mo $K\alpha$ line. The continuous temperature dependence of the diffuse scattering rules out the possibility of extensive static disorder in the crystal.

ORNL-DWG. 70-15287

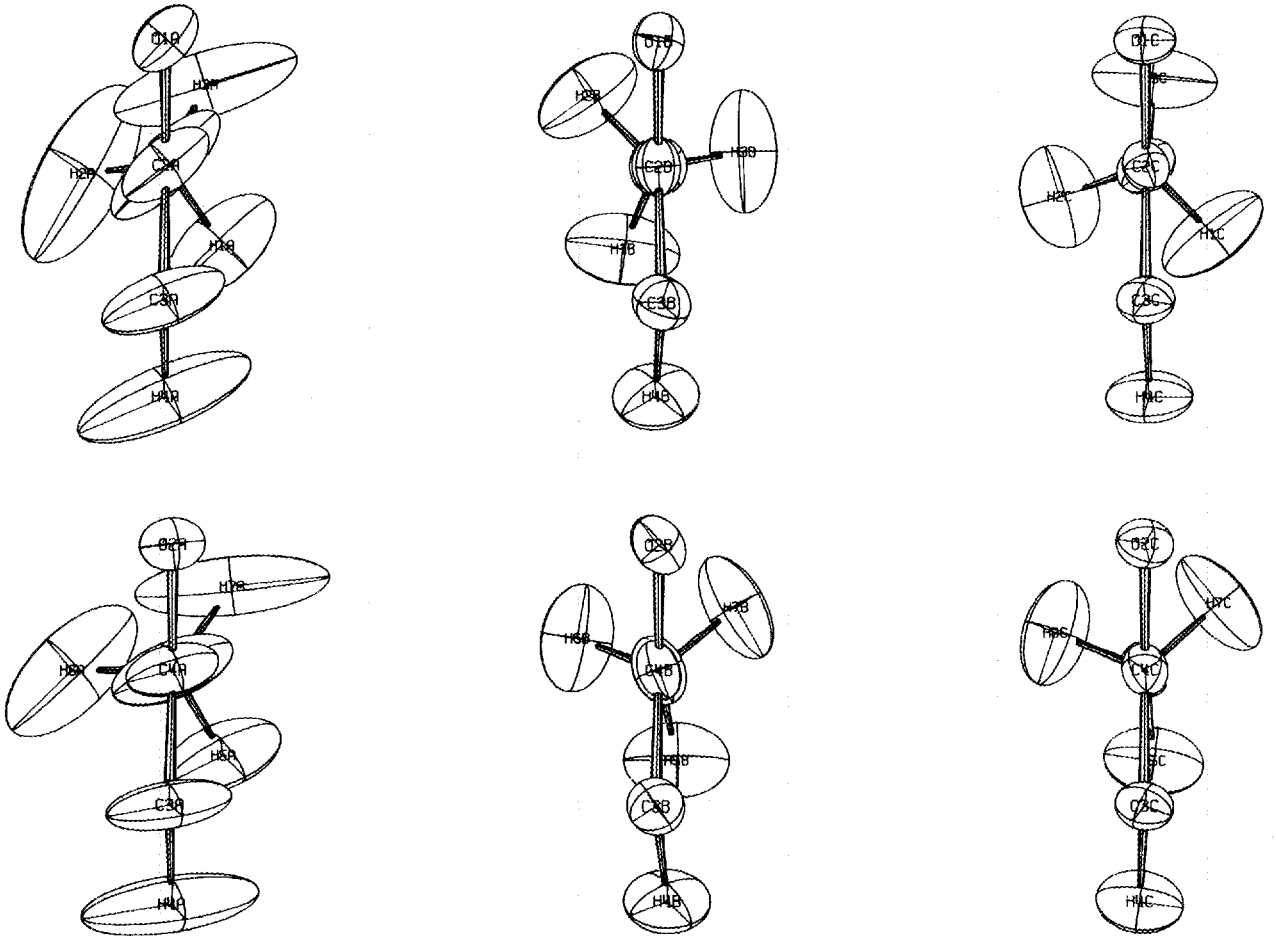

Fig. 7.10. Thermal ellipsoids for the six different methyl groups and their neighboring atoms in trisacetylacetonatochromium(III). Each group is viewed along a terminal C–C bond. The ellipsoids enclose 20% probability.

ORNL-DWG. 70-15289

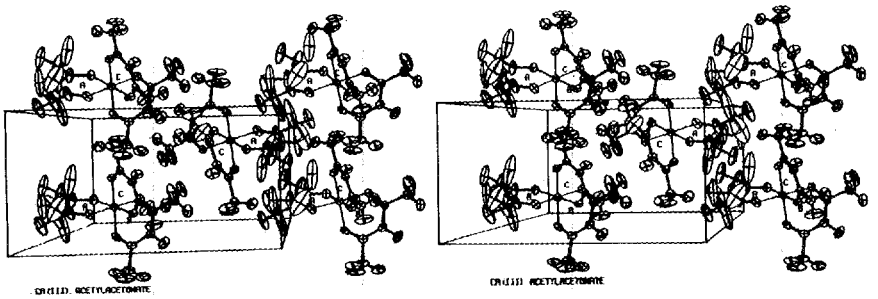

Fig. 7.11. Stereoscopic view of trisacetylacetonatochromium(III) showing the 20% probability level for the thermal ellipsoids. The **a** axis is horizontal, and the **b** axis is vertical. Note how the acetylacetonato ligands A pack together to form two-dimensional sheets through the crystal.

1. Student participant in the Great Lakes Colleges Association Science Semester Sept. 10–Dec. 18, 1970, from Albion College, Albion, Mich.
2. B. Morosin, *Acta Crystallogr.* **19**, 131 (1965).
3. The crystal used in this study was prepared by R. A. Bell at the California Institute of Technology.
4. B. L. Trus and R. E. Marsh, *Abstr. Amer. Crystallogr. Ass.*, Seattle Meeting, p. 30 (1969).
5. C. K. Johnson, *Chem. Div. Annu. Progr. Rep. May 20, 1970,* ORNL-4581, p. 133.
6. C. K. Johnson, p. 220 in *Crystallographic Computing,* F. R. Ahmed, ed., Munskgaard, Copenhagen, 1971.
7. C. K. Johnson, chap. 9 in *Thermal Neutron Diffraction,* B. T. M. Willis, ed., Oxford, London, 1970.
8. C. K. Johnson, *Acta Crystallogr., Sect A* **25**, S29 (1969).

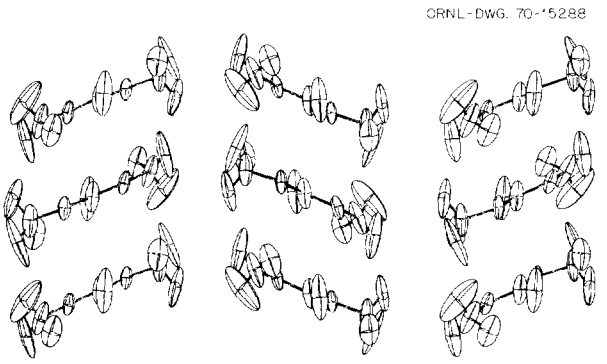

Fig. 7.12. Thermal-ellipsoid drawing illustrating the two-dimensional sheet formed by adjacent columns of A ligands. The c axis is horizontal, and the b axis is vertical. The ligands shown are related by inversion centers and twofold screw axes. The ellipsoids are scaled to enclose 20% probability.

CRYSTAL AND MOLECULAR STRUCTURE OF TRIMERCURY CHLOROALUMINATE, $Hg_3(AlCl_4)_2$

R. D. Ellison H. A. Levy

Yellow needle-shaped crystals of the new compound $Hg_3(AlCl_4)_2$ were furnished by Dr. K. W. Fung and Prof. G. Mamantov of the University of Tennessee, who have reported its preparation[1] and, with G. M. Begun of this Division, have characterized the compound.[2] Because the crystals are highly hygroscopic, all manipulations were carried out in a dry box (<2 ppm H_2O). A specimen about 0.05 × 0.10 × 0.40 mm sealed in a glass capillary was used to obtain all x-ray diffraction measurements (Mo $K\alpha$ radiation). Measurements of the dimensions, shape, and orientation of the specimen were refined by the method of least squares in a novel procedure[3] to permit calculation of absorption corrections.

The crystals are monoclinic, space group $P2_1/c$, with 4 molecules per unit cell of dimensions a = 7.1321(2) Å, b = 15.0468(3) Å, c = 14.1771(4) Å, β = 99.05(1)° (the numbers in parentheses are least-squares standard errors corresponding to the least significant digit of the associated quantity). The structure was solved by inspection of a Patterson function prepared from 4391 symmetry nonequivalent reflections. Subsequent refinement by the method of least squares yielded the atomic parameters listed in Table 7.2 [discrepancy index R_F = 0.082 for $|F|^2 \geqslant \sigma(F^2)$].

The molecule, illustrated in Fig. 7.13, contains Hg–Hg bonds averaging 2.56 Å and Hg–Cl bonds averaging 2.54 Å in length and is well isolated from neighboring molecules, for which the closest approach is a contact Hg ··· Cl of 3.21 Å. The central skeleton is nearly linear with angles Cl(7)–Hg(2)–Hg(1) = 176.6(1)°, Cl(11)–Hg(3)–Hg(1) = 172.8(1)°, and Hg(2)–Hg(1)–Hg(3) = 174.42(4)°. Coordination of Cl atoms around both Al atoms is nearly that of a regular tetrahedron, the angles ranging from 104.5 to 113.3°. The bonds from Al to bridging Cl atoms average 2.18 Å, longer by 0.06 Å than the average of those to terminal Cl atoms. There is an approximation to twofold rotational symmetry about an axis through the central Hg atom.

The Hg_3 group has been found also in a study[4] of the compound $Hg_3(AsF_6)_2$, which came to our attention after completion of the present work; in this case the group is required by site symmetry to be linear and symmetric, and the Hg-Hg bond length of 2.55 Å is in good agreement with the value 2.56 Å found in $Hg_3(AlCl_4)_2$. These values are somewhat larger than those in the range 2.49 to 2.54 Å reported for the

Table 7.2. Fractional atomic coordinates of the crystal structure of $Hg_3(AlCl_4)_2$

Atom	x	y	z
Hg 1	−0.1804	0.1370	0.1099
Hg 2	−0.0072	0.2597	0.0360
Hg 3	−0.3684	0.0251	0.1960
Al 4	0.3942	0.3180	−0.0949
Cl 5	0.3181	0.3280	−0.2447
Cl 6	0.4061	0.1842	−0.0448
Cl 7	0.1763	0.3832	−0.0271
Cl 8	0.6460	0.3911	−0.0471
Al 9	−0.8050	−0.1023	0.2232
Cl 10	−0.8462	−0.2379	0.1896
Cl 11	−0.5123	−0.0878	0.2983
Cl 12	−0.9946	−0.0630	0.3154
Cl 13	−0.8245	−0.0214	0.0988

Hg-Hg bond lengths in several halide[5] and other salts[6-11] of the mercurous ion Hg_2^{2+}. The increase is in accord with expectation for the lower average oxidation state of mercury in Hg_3^{2+}.

The average Hg–Cl bond length of 2.54 Å in $Hg_3(AlCl_4)_2$, in which the Cl atom is a bridge between Hg and Al, is significantly greater than the recently reported[5] value of 2.43 Å in Hg_2Cl_2, in which no bridging occurs. The Al–Cl distances, 2.106 to 2.185 Å, are similar to those reported[12] for $Co(AlCl_4)_2$, 2.105 Å for the terminal Cl atoms and 2.151 to 2.188 Å for the bridging Cl atoms. The distances[13] in $NaAlCl_4$, all to nonbridging Cl atoms, are also similar, 2.11 to 2.16 Å.

Significant contacts between $Hg_3(AlCl_4)_2$ molecules are all between Hg and Cl and range in length from 3.21 to 3.80 Å. The arrangement may be visualized as consisting of double chains along the crystal **a** axis as illustrated in Fig. 7.14. The chains are linked to neighboring chains by Hg ··· Cl contacts which form a net of molecules in the (102) planes of the crystal as shown in Fig. 7.15.

Although the Hg–Cl bond length of 2.54 Å in the crystal is somewhat greater than one might predict for a covalent bond (one-half the Hg–Hg distance plus the covalent radius of Cl, e.g., yields 2.28 Å), it is much shorter than an expected ionic contact (~3.1 Å).

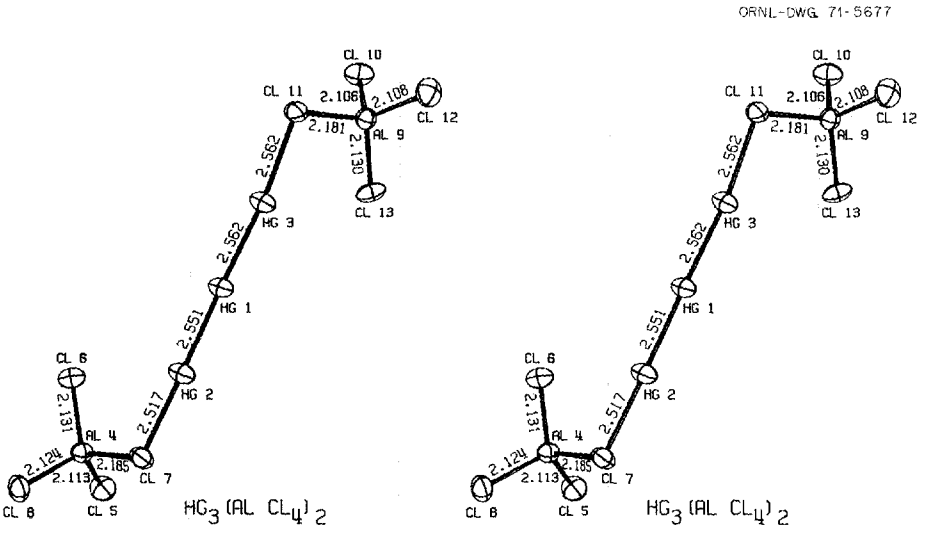

Fig. 7.13. Stereoscopic illustration of the molecular structure of $Hg_3(AlCl_4)_2$. Atoms are represented by 50% probability thermal ellipsoids. Interatomic distances (Å) are shown; their precision is Hg–Hg, 0.001; Hg–Cl, 0.004; Al–Cl, 0.006.

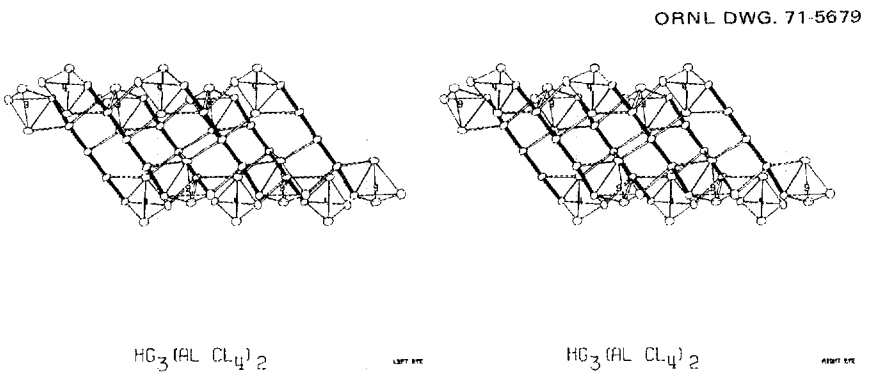

Fig. 7.14. Stereoscopic illustration of the packing of $Hg_3(AlCl_4)_2$ molecules into chains. Three repeating units are shown. The $AlCl_4^-$ tetrahedra are outlined with single light lines, and nonbonded Hg ··· Cl contacts are indicated by double lines. The **a** axis of the crystal is horizontal.

ORNL DWG. 71-5678

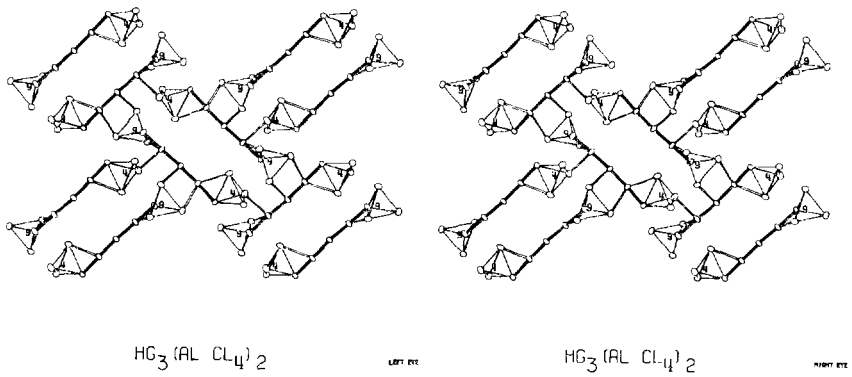

Fig. 7.15. Stereoscopic illustration of the net of $Hg_3(AlCl_4)_2$ molecules parallel to (102) planes of the crystal. The view direction is along the normal to (102); the **b** axis is vertical, and the [201] zone axis is horizontal.

Furthermore, since the distances from Al to bridging Cl atoms are significantly longer than the distances to nonbridging Cl atoms, it is clear that the Hg atoms compete effectively with Al for the valence electrons of Cl. Hence an ionic formulation implying separate Hg_3^{2+} and $AlCl_4^-$ species does not appear to be an appropriate description of this structure.

1. G. Torsi, K. W. Fung, G. M. Begun, and G. Mamantov, *Inorg. Chem.* (1971), in press.
2. G. M. Begun, "Molecular Spectroscopy," a contribution in chap. 3, this report.
3. H. A. Levy and R. D. Ellison, "Least-Squares Refinement of Measurements for Crystal Absorption Corrections," another contribution in this section, this report.
4. C. G. Davies, P. A. W. Dean, R. J. Gillespie, and P. K. Ummat, *Chem. Commun.* (1971), in press; private communication of August 1971.
5. E. Dorm, *Chem. Commun.*, No. 9, 466 (1971).
6. D. Grdenić, *J. Chem. Soc.* 1312 (1956).
7. G. Johansson, *Acta Chem. Scand.* **20**, 553 (1966).
8. E. Dorm, *Acta Chem. Scand.* **21**, 2834 (1967).
9. B. Lindh, *Acta Chem. Scand.* **21**, 2743 (1967).
10. R. C. Elder, J. Halpern, and J. S. Pond, *J. Amer. Chem. Soc.* **89**, 6877 (1967).
11. E. Dorm, *Acta Chem. Scand.*, **23**, 1607 (1969).
12. J. A. Ibers, *Acta Crystallogr.* **15**, 967 (1962).
13. N. C. Baenziger, *Acta Crystallogr.* **4**, 216 (1951).

X-RAY AND NEUTRON DIFFRACTION STUDY OF XENON HEXAFLUORIDE

P. A. Agron H. A. Levy

In spite of extensive study by several investigators, the detailed atomic arrangement in crystalline xenon hexafluoride is as yet elusive. The substance exists in several crystalline modifications,[1] each of which is subject to disorder. We report here conclusions drawn from x-ray and neutron diffraction studies of the room-temperature monoclinic modification (Phase I).

The space group $P2_1/m$ and arrangement of Xe atoms at the vertices of a nearly regular tetrahedron, loosely bridged by fluorine atoms situated outside the tetrahedron faces, was reported earlier.[2] Starting with this partial structure and utilizing successive Fourier syntheses alternated with least-squares refinements, a model of the remainder of the structure has been derived. This model contains five additional fluorine atoms bonded to each xenon atom: one, designated as the "polar" fluorine, lies along the approximate trigonal axes of the tetrahedron, and four, designated as "waist fluorines," lie in planes approximately perpendicular to the pseudotrigonal axes. The waist positions do not conform to space-group symmetry; in fact, any attempt to place the requisite number of fluorine atoms in accord with the mirror plane required by the space group leads to unacceptably short F ··· F contacts. The model is therefore described as disordered, with the mirror plane present only in the statistical sense. One of the disordered configurations is shown in Fig. 7.16. Least-squares refinement of the model (190 parameters, 590 neutron diffraction data) yielded the measure of fit

$$R(F^2) \equiv \Sigma|F_o^2 - F_c^2|/\Sigma F_o^2 = 0.13 .$$

This fit, although not as satisfactory as is usually achieved, is good enough to suggest the essential correctness of the main features of the model. However, the large root-mean-square thermal displacements required for the fluorine atoms (0.6 Å average), the excessively large range of equivalent distances, and the

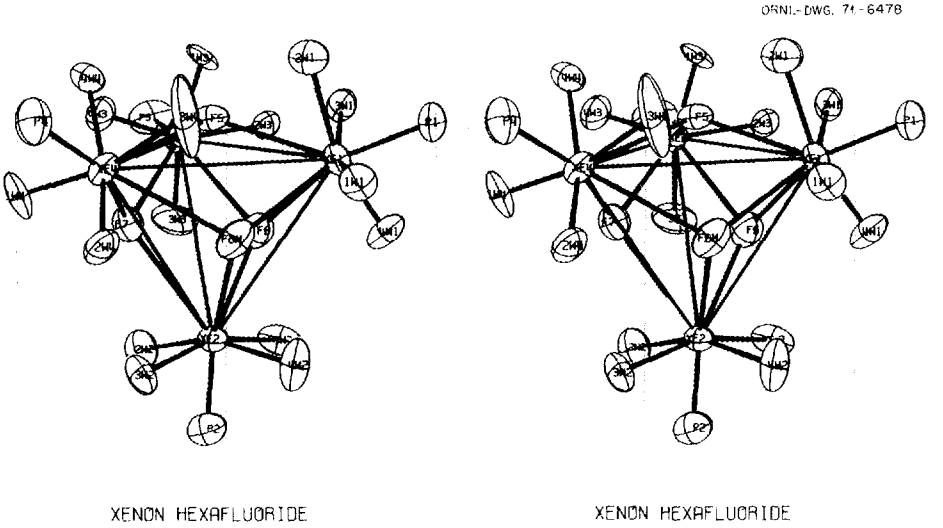

Fig. 7.16. Stereoscopic drawings of one formula unit of the xenon hexafluoride tetramer. The atoms are represented by 20% probability thermal ellipsoids. Xe 1, 2, 3, 4 – xenon atoms at the corners of the tetrahedron; F 5, 6, 6M, 7 – bridging fluorine atoms; P 1, 2, 3, 4 – polar fluorine atoms bound to their respective xenon atoms; W – waist fluorine atoms.

strange orientations of the thermal ellipsoids suggest that the fine details of the model are specious.

Attempts to reach a better and more satisfactory model in the polar space group $P2_1$ were fruitless. Attempts to describe the present model in terms of disordered arrangements of more symmetric molecular models also failed; in this study, idealized models with point symmetries of $\bar{4}3m$, $2mm$, $\bar{4}2m$, and $\bar{4}$ were examined.

The model shown in Fig. 7.16 has approximately the symmetry $\bar{4}$. The crystallographic mirror plane bisects the Xe3-Xe4 edge and passes through the Xe1 and Xe2 vertices. The disordered superposition thus has approximate $\bar{4}2m$ symmetry. The separations of the Xe atoms range from 4.17 to 4.24 Å. The distances from Xe to bridging fluorine atoms range between 2.20 and 2.80 Å. Remaining Xe to F distances range between 1.65 and 2.00 Å. No attempt has been made to estimate separations corrected for thermal motion, but these corrections could be of considerable magnitude. The extent of displacement of waist fluorine atoms toward the polar fluorine positions is indicated by the range of angles F(polar)–Xe–F(waist), which is 78.0 to 88.5°.

1. G. R. Jones and R. Burbank, *Science* **168**, 248 (1970); G. R. Jones, R. D. Burbank, and W. E. Falconer, *J. Chem. Phys.* **52**, 6450 (1970); ibid., **53**, 1605 (1970); and H. A. Levy and P. A. Agron, *Chem. Div. Annu. Progr. Rep. May 20, 1970*, ORNL-4581, p. 150.

2. P. A. Agron, C. K. Johnson, and H. A. Levy, *Inorg. Nucl. Chem. Lett.* **1**, 145 (1965).

A COMPUTER PROGRAM TO AID IN THE UNDERSTANDING OF INTERATOMIC FORCES IN MOLECULES AND CRYSTALS

W. R. Busing

Extensive modifications have been made to a computer program which was described previously[1] so that it is now capable of manipulating static and dynamic models of crystals or isolated molecules and calculating their energies from interatomic potential functions. The main features of this program are described here, and some applications of the program are illustrated in accompanying reports.[2,3]

The models under consideration may be built up of rigid molecules which may rotate or translate, molecules composed of rigid segments but with internal rotation about certain bonds, or individual atoms with positions which can change independently. These units may be used to describe either crystals or isolated molecules, and the model may be constrained to conform to any desired crystal or molecular symmetry. The parameters which describe the structure include the crystal-lattice parameters and the translations and orientations of the rigid units.

The energy calculated for the model may include the following contributions: (1) Coulomb energy, (2) inverse-sixth-power van der Waals attraction, (3) exponential repulsion in the form suggested by Gilbert,[4] (4) a quadratic potential $\frac{1}{2}k(r_{ij} - r_0)^2$ associated with a covalent bond, (5) a quadratic potential of similar form

associated with an intramolecular bond angle, and (6) an energy associated with a torsional strain about a covalent bond. In calculating the first two terms for crystals the Ewald-Bertaut-Williams method[5,6] is used, so that convergence errors can be virtually eliminated.

Several types of calculations may be made with this program. One may wish to adjust the structural parameters to minimize the energy; three different techniques are available for this purpose. In Newton's method the second derivatives of the energy with respect to the parameters are used to solve for the configuration in which the first derivatives are zero. This method is useful only when the trial structure is already near a relative minimum. Alternatively, the program can use the method of steepest descents, which uses only first derivatives, or a modified Rosenbrock search,[7] which requires no derivatives.

The program can also calculate the vibrational frequencies and normal coordinates for any structure at an energy minimum. The basic coordinates of this calculation are the structural parameters of the model (excluding the lattice parameters); these may be constrained to conform to any desired symmetry. In this way it is possible to study the internal modes of an isolated molecule, the lattice modes of rigid molecules in a crystal, or the interaction of lattice modes and internal modes of flexible molecules in a crystal.

Another scheme of operation may be used to adjust parameters of the potential functions using the method of least squares. Observations for this calculation may include known structural parameters and experimental lattice energies, and it is possible to use information from several substances to adjust potential parameters common to them. These observations may be appropriately weighted.[8]

A mapping option is also available which calculates the energy over an array of points in parameter space. Up to three structural or energy parameters may be stepped through specified ranges for this calculation.

In all of these calculations where first and second derivatives are needed, they are obtained numerically. This greatly simplifies the application of constraints and increases the flexibility of the program.

---

1. W. R. Busing, *Chem. Div. Annu. Progr. Rep. May 20, 1968*, ORNL-4306, p. 139.
2. W. R. Busing, "The Calculation of Potential-Energy Parameters from the Vibrational Frequencies of Ethane," another contribution in this section, this report.
3. W. R. Busing and W. E. Thiessen, "A Method for Predicting the Conformation of the Isolated Molecule of an Organic Compound from Its Crystal Structure," the following contribution, this report.
4. T. L. Gilbert, *J. Chem. Phys.* **49**, 2640 (1968).
5. F. Bertaut, *J. Phys. Radium* **13**, 499 (1952).
6. D. E. Williams, *Trans. Amer. Crystallogr. Ass.* **6**, 21 (1970).
7. H. H. Rosenbrock, *Comput. J.* **3**, 175 (1960).
8. W. R. Busing, *Trans. Amer. Crystallogr. Ass.* **6**, 57 (1970).

A METHOD FOR PREDICTING THE CONFORMATION OF THE ISOLATED MOLECULE OF AN ORGANIC COMPOUND FROM ITS CRYSTAL STRUCTURE

W. R. Busing W. E. Thiessen

Crystal structure determinations, especially of organic compounds, are often performed for the principal purpose of determining the molecular geometry rather than for any interest in the crystal structure itself. When a feature of this geometry appears to be unusual the question arises as to whether it should be considered to be a property of the molecule or whether it is a result of intermolecular forces in the crystal. An example of such a feature is the orientation of the isopropyl group, C(12), C(13), and C(14), in nor-β-cubebone[1] as shown in Fig. 7.17.

According to a simple model[2] the configuration of the C(7) and C(12) hydrogen atoms would be expected to be *anti*, whereas in fact a *gauche* arrangement is found.[3] We have calculated the intramolecular and intermolecular nonbonded interaction energy for this compound using a computer program described in another report[4] to show in a preliminary way that the configuration found in the crystal is probably the stable one for the isolated molecule as well.

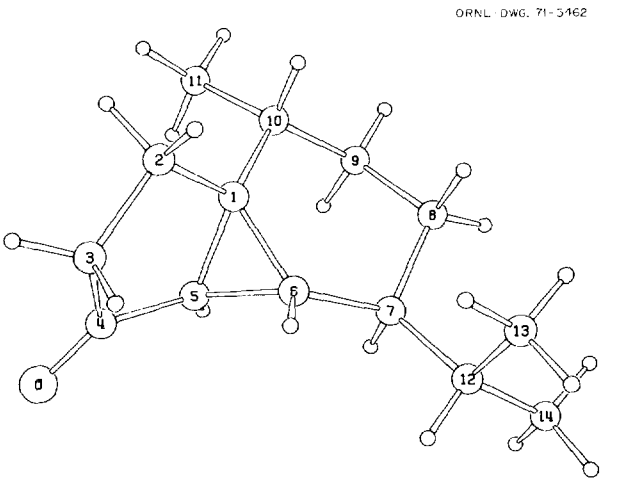

Fig. 7.17. Perspective drawing of the nor-β-cubebone molecule. The isopropyl group appears at the right.

The energy is assumed to have the form

$$W = \frac{1}{2}\sum_i \sum_j \left[-\frac{D_i D_j}{r_{ij}} + (B_i + B_j) \times \exp\left(\frac{A_i + A_j - r_{ij}}{B_i + B_j}\right)\right] + \sum_{k=1}^{3} \frac{V_0}{2}(1 - \cos 3\phi_k),$$

where the terms represent van der Waals attraction, nonbonded repulsion, and a contribution from the three mean torsion angles ϕ_k. Parameters D_i and B_i for C, H, and O were fixed at values derived from those reported by others,[5,6] and the A_i's and V_0 were adjusted by the method of least squares to make the arrangement with minimum energy reproduce the experimental crystal structure. In minimizing the energy, 12 degrees of freedom were permitted: the 3 parameters of the orthorhombic lattice, the 6 rotations and translations of the molecule, and 3 internal rotations. The latter were the rotation of the isopropyl group about the C(7)–C(12) bond and the rotations of the methyl groups about the C(12)–C(13) and C(12)–C(14) directions. All bond distances and angles were held constant. The largest discrepancies between the predicted and experimental structures are 2.0% for the lattice parameters, 0.04 Å for the molecular translations, and 1.4° for molecular or intramolecular rotations.

Next, a relative energy minimum was found for the isolated molecule using only the three internal rotations as degrees of freedom. The maximum rotation of a group from the position predicted in the crystal was only 0.05°.

The energy minimization was performed twice more for the isolated molecule, starting with the isopropyl group rotated 120 and 240° from its experimental position. Local minima were found near these starting positions with calculated energies 0.8 and 0.9 kcal/mole higher than that calculated for the observed configuration. We conclude, therefore, that the arrangement found in the crystal would also be the stable one for the isolated molecule. We regard our calculations as preliminary, however, because the groups were constrained to be rigid. We are proceeding with efforts to remove this restriction and also to study other aspects of the molecular geometry which may be of interest.

1. W. E. Thiessen, *Chem. Div. Annu. Progr. Rep. May 20, 1970,* ORNL-4581, p. 140.

2. E. L. Eliel, *Stereochemistry of Carbon Compounds,* chap. 6, McGraw-Hill, New York, 1962.

3. For other examples of this configuration, see M. G. B. Drew, D. H. Templeton, and A. Zalkin, *Acta Crystallogr., Sect. B* **25**, 261 (1969), and R. Parthasarathy et al., *Tetrahedron* **26**, 4705 (1970). An *anti* arrangement also has been found: E. Höhne, *Collect. Czech. Chem. Commun.* **28**, 3128 (1963).

4. W. R. Busing, "A Computer Program to Aid in the Understanding of Interatomic Forces in Molecules and Crystals," the preceding contribution, this report.

5. D. E. Williams, *Trans. Amer. Crystallogr. Assoc.* **6**, 21 (1970).

6. D. A. Buckingham et al., *J. Amer. Chem. Soc.* **92**, 3617 (1970).

THE CALCULATION OF POTENTIAL-ENERGY PARAMETERS FROM THE VIBRATIONAL FREQUENCIES OF ETHANE

W. R. Busing

Several authors[1–4] have described calculations which predict the configuration of an isolated molecule by minimizing its energy, and we are proceeding to make similar calculations for molecular crystals.[5]

The energy is calculated from a model which includes terms to represent van der Waals attraction and exponential repulsion between nonbonded atoms, contributions of the form $\frac{1}{2}k(r_{ij} - r_0)^2$ for bond-length deformation, analogous terms in the bond angles, and contributions which depend on the conformation angles. Previous authors have set r_0 at the usual bond distance and taken the force constant k directly from the results of vibrational spectroscopy. However, since the spectroscopic values were derived without taking into account nonbonded interactions, it seems reasonable to rederive these energy parameters from the known geometry and observed vibrational frequencies of a simple molecule. We have chosen to make these calculations for ethane, CH_3CH_3, because its frequencies and geometry are well known.

Fixing nonbonded repulsion and van der Waals parameters at values consistent with the crystal structure of a large organic molecule,[5] we have used the program described in another report[6] to adjust the other energy parameters to reproduce exactly the geometry of ethane and to approximate its vibrational spectrum. The agreement between observed and calculated frequencies is not good enough to indicate that the result is an accurate model for the potential energy of ethane, but these parameters should be better than those previously used for the calculation of molecular conformation.

1. J. B. Hendrickson, *J. Amer. Chem. Soc.* 83, 4537 (1961).
2. K. B. Wiberg, *J. Amer. Chem. Soc.* 87, 1070 (1965).
3. R. H. Boyd, *J. Chem. Phys.* 49, 2574 (1968).
4. D. A. Buckingham et al., *J. Amer. Chem. Soc.* 92, 3617 (1970).
5. W. R. Busing and W. E. Thiessen, "A Method for Predicting the Conformation of the Isolated Molecule of an Organic Compound from Its Crystal Structure," the preceding contribution, this report.
6. W. R. Busing, "A Computer Program to Aid in the Understanding of Interatomic Forces in Molecules and Crystals," a previous contribution in this section, this report.

A CONVENIENT WAY OF APPLYING CONSTRAINTS IN A CRYSTALLOGRAPHIC LEAST-SQUARES REFINEMENT

W. R. Busing

A crystallographic least-squares program adjusts parameters p_i to make the calculated structure factors $F_{\mathbf{h}}$ agree with those observed. The derivatives $\partial F_{\mathbf{h}}/\partial p_i$ needed to set up the normal equations are calculated analytically for each reflection with indices **h**.

It is often desirable to apply various constraints to the parameters being adjusted, and one way of doing this is to choose certain parameters p_j' as independent and to require other parameters to have values which depend on them. The derivatives needed for the constrained refinement are then

$$\partial F_{\mathbf{h}}/\partial p'_j = \sum_i (\partial F_{\mathbf{h}}/\partial p_i)(\partial p_i/\partial p'_j) .$$

Users of our least-squares program[1] have been required in the past to write two subroutines: subroutine RESETP, to set the dependent variables p_i in terms of the independent ones p'_j, and subroutine CSTRAN, to set the derivatives $\partial F_{\mathbf{h}}/\partial p'_j$ in terms of the $\partial F_{\mathbf{h}}/\partial p_i$ which are calculated by the program.

Preparation of this last routine has now been eliminated by the inclusion of a general CSTRAN routine which uses subroutine RESETP to determine numerically the coefficients $\partial p_i/\partial p'_j$ and automatically calculates the revised derivatives. The numerical differentiation needs to be performed only at the start of each cycle, because the coefficients are the same for every $F_{\mathbf{h}}$. This modification, which is described in more detail elsewhere,[2] greatly facilitates the application of complicated constraints.

1. W. R. Busing, K. O. Martin, and H. A. Levy, *OR FLS, a Fortran Crystallographic Least-Squares Program,* ORNL-TM-305 (1962).
2. W. R. Busing, submitted for publication in *Acta Crystallogr.*

LEAST-SQUARES REFINEMENT OF MEASUREMENTS FOR CRYSTAL ABSORPTION CORRECTIONS

H. A. Levy R. D. Ellison

One step in the reduction of diffraction data in preparation for crystal-structure determination is the correction for absorption of radiation within the crystal specimen. This correction is often evaluated by a numerical integration over the volume of the specimen,[1] a procedure which requires a quantitative description of the size, shape, and orientation of the specimen.

A widely used computer program for this purpose, ORABS,[2] requires this information in the form of the coefficients of the equations describing the set of plane faces of the specimen. A modified version of ORABS in current use calls for input of this information in the form of the directions and lengths of a set of vectors, one for each plane face of the specimen, which lie perpendicular to the faces of the specimen and extend from a fixed origin to the point of intersection with the face or extension thereof. These data, estimated by means of an optical microscopic examination of the specimen, are subject to experimental error, particularly if the crystal faces are not sharply defined and easily visible. When the specimen must be enclosed during the examination, these errors can be serious.

This report describes a procedure whereby a set of approximate measurements may be improved by a least-squares procedure utilizing x-ray measurements of integrated intensities of equivalent Bragg reflections. In cases in which the present method is of value, differences in observed values among such equivalent reflections arise principally from absorption effects; the method adjusts the specimen parameters to produce corrected intensities as nearly equal as possible.

The quantity minimized in this procedure is

$$\sum_{i,j} w_i(C_{ij}^o - C_j T_i)^2 ,$$

where C_{ij}^o and w_i represent the observed x-ray integrated intensity and weight for an observation i of a reflection j, T_i is the transmission factor for the observation, and C_j is the absorption-free intensity for the reflection. The quantities C_j are independent of crystal orientation, whereas the observed quantities C_{ij}^o depend, through the transmission factors T_i, on orientation. If measurements of a reflection are made for more than one orientation (several C_{ij}^o for each C_j), either by utilization of symmetry-equivalent reflections or by

variation of the azimuthal angle of the crystal in one Bragg setting, the quantities C_j may be considered parameters to be adjusted, along with the size, shape, and orientation parameters. This procedure has been implemented for the IBM 360, utilizing modifications of the general FORTRAN least-squares program ORGLS[3] and the crystal absorption program ORABS.[2]

As a demonstration of the method, we present an application to data from the crystal[4] $Hg_3(AlCl_4)_2$. The observations consisted of the integrated intensities of 34 sets of four symmetry-equivalent general reflections from the monoclinic crystal. Initial measurements of the crystal faces were obtained by the usual optical examination but were considered of less than usual precision because of difficulties introduced by the glass capillary surrounding the specimen. Parameters for the description of the crystal included the orientation angles and distance parameters for seven faces; those parameters judged to be of minor importance in determining the transmission were held fixed to avoid indeterminacy in the solution of the normal equations. In the present case, these fixed parameters included chi angles of all faces (for small and intermediate scattering angles in the bisecting mode of measurement, chi coordinates describe approximately the rotation of the specimen around the primary and scattered x-ray beams and are thus of little effect for absorption) and all parameters for the end faces of the needle-shaped specimen. Three distance parameters were necessarily fixed to establish the origin of coordinates.

In all, six parameters describing the crystal and 34 absorption-free intensity values were adjusted against 4 observations for each of the 34 reflections. The standard error of fit fell from an initial value of 10.1 to a final value of 0.97 (weights corresponded to a constant relative standard error of 4%).

Use of the improved absorption corrections in least-squares refinement of the structure yielded a standard error of fit of 1.055, which may be compared with the value 1.34 with the original absorption corrections. Corresponding values of the conventional discrepancy index R_F ($|F|^2 \geqslant \sigma$) are 0.106 and 0.082.

Figure 7.18 shows the shape and orientation of the crystal specimen as originally estimated and as refined by the least-squares procedure.

1. W. R. Busing and H. A. Levy, *Acta Crystallogr.* **10**, 180 (1957).

2. D. J. Wehe, W. R. Busing, and H. A. Levy, *ORABS, a Fortran Program for Calculating Single Crystal Absorption Corrections*, ORNL-TM-229 (April 1962).

3. W. R. Busing and H. A. Levy, *ORGLS, a General Fortran Least-Squares Program*, ORNL-TM-271 (June 1962).

4. R. D. Ellison and H. A. Levy, "Crystal and Molecular Structure of Trimercury Chloroaluminate, $Hg_3(AlCl_4)_2$," a previous contribution in this section, this report.

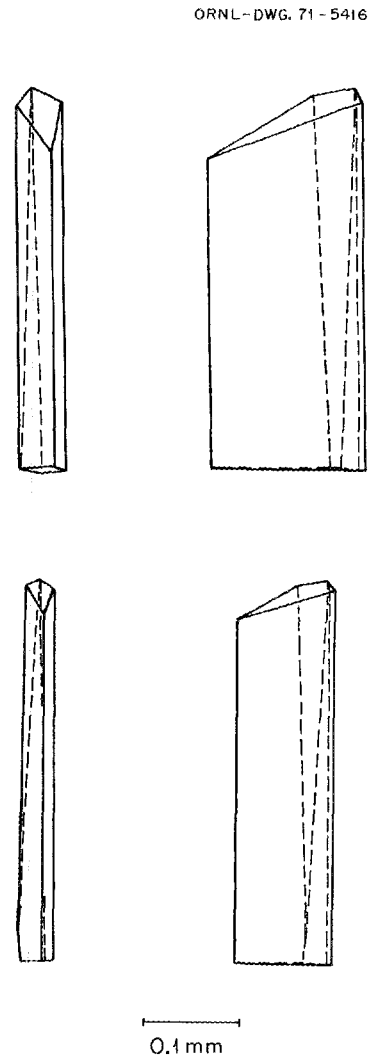

Fig. 7.18. Shape and orientation of the crystal specimen of $Hg_3(AlCl_4)_2$ as given by optical examination (above) and as improved by the least-squares procedure (below).

A NEW FORMULISM FOR REPORTING THE PRECISION OF CRYSTAL STRUCTURE PARAMETERS

C. K. Johnson

The results of a crystal structure determination conventionally are reported as three positional parameters x^i (i = 1,2,3) and six anisotropic thermal-motion parameters b^{ij} (i,j = 1,2,3; $i \leqslant j$) per atom, with

standard deviations for all parameters. An unfortunate aspect of this practice is that the reported standard deviations alone do not characterize adequately the precision of the positional and thermal parameters. In particular, they do not permit the calculation of the estimated standard error for a derived quantity, such as an interatomic distance corrected for thermal motion. The standard deviation for a parameter is obtained from the appropriate diagonal element of the inverted least-squares matrix corrected for degrees of freedom (i.e., the covariance matrix). A full characterization of the precision for a crystal structure would require the reporting of the complete covariance matrix; however, such a procedure is not practical. An abridged formulism for precision using eight parameters (sometimes just five parameters) per atom is presented here. Six of the eight parameters are taken directly from the covariance matrix to define completely the symmetric matrix of covariances for the positional parameters, $||\mathrm{cov}(x^i, x^j)||$, for an atom. The remaining two parameters, μ and λ, are scalar quantities, invariant to the choice of coordinate system, in the equation

$$\begin{aligned}\mathrm{cov}(b^{ij}, b^{kl})_{\mathrm{obs}} &\approx \mathrm{cov}(b^{ij}, b^{kl})_{\mathrm{calc}} \\ &\equiv \mu\,\mathrm{cov}(x^i, x^k)\,\mathrm{cov}(x^j, x^l) + \mu\,\mathrm{cov}(x^i, x^l)\,\mathrm{cov}(x^j, x^k) \\ &\quad + \lambda\,\mathrm{cov}(x^i, x^j)\,\mathrm{cov}(x^k, x^l)\,. \qquad (1)\end{aligned}$$

Equation (1) is a tensor equation defining the calculated covariances for the thermal-motion coefficients b^{ij} in terms of observed covariances for the positional parameters x^i. Since the covariances transform as tensors, we can always transform to a new coordinate system where $||\mathrm{cov}(x^i, x^j)||$ is an identity matrix. In this positional unit-variance system of coordinates, designated by carets, we may write the covariances of b^{ij} in matrix form as

$$\hat{C}_{\mathrm{calc}}{}^{IJ} \equiv \widehat{\mathrm{cov}}(b^{ij}, b^{kl})_{\mathrm{calc}}$$

$$\equiv \begin{pmatrix} 2\mu+\lambda & \lambda & \lambda & 0 & 0 & 0 \\ \lambda & 2\mu+\lambda & \lambda & 0 & 0 & 0 \\ \lambda & \lambda & 2\mu+\lambda & 0 & 0 & 0 \\ 0 & 0 & 0 & \mu & 0 & 0 \\ 0 & 0 & 0 & 0 & \mu & 0 \\ 0 & 0 & 0 & 0 & 0 & \mu \end{pmatrix}, \qquad (2)$$

where the correspondence between tensor indices i, j, k, l and matrix indices I, J is $ij = 11, 22, 33, 12, 13, 23$ for $I = 1, 2, 3, 4, 5, 6$.

As a numerical example, we examine atom H9 in the crystal structure of the triclinic photodimer of isophorone.[1] The matrix of the transformed observed covariances of b^{ij} in a positional unit-variance system of coordinates is

$$\hat{C}_{\mathrm{obs}}{}^{IJ} = \begin{pmatrix} 272 & -77 & -73 & -2 & -2 & -7 \\ -77 & 311 & -71 & 12 & -4 & 3 \\ -73 & -71 & 271 & -1 & -16 & 11 \\ -2 & 12 & -1 & 172 & -3 & -7 \\ -2 & -4 & -16 & -3 & 163 & 0 \\ -7 & 3 & 11 & -7 & 0 & 174 \end{pmatrix} \times 400\pi^4\,. \qquad (3)$$

If we define

$$S_1 = \sum_{I=1}^{3} \hat{C}^{II}\,, \quad S_2 = \sum_{I=4}^{6} \hat{C}^{II}\,, \quad S_3 = \sum_{I,J=1}^{3} \hat{C}^{IJ}\,,$$

we find from Eqs. (2) and (3) that

$$\mu = \frac{1}{30}(3S_1 + 6S_2 - S_3) = 174 \times 400\pi^4$$

and

$$\lambda = \frac{1}{9}(S_3 - 6\mu) = -70 \times 400\pi^4$$

to give the result

$$\hat{C}_{\mathrm{calc}}{}^{IJ} = \begin{pmatrix} 278 & -70 & -70 & 0 & 0 & 0 \\ -70 & 278 & -70 & 0 & 0 & 0 \\ -70 & -70 & 278 & 0 & 0 & 0 \\ 0 & 0 & 0 & 174 & 0 & 0 \\ 0 & 0 & 0 & 0 & 174 & 0 \\ 0 & 0 & 0 & 0 & 0 & 174 \end{pmatrix} \times 400\pi^4\,.$$

The disagreement factor,

$$R = \left[\frac{\sum_{i,j,k,l} (\hat{C}_{\mathrm{obs}}{}^{IJ} - \hat{C}_{\mathrm{calc}}{}^{IJ})^2}{\sum_{i,j,k,l} (\hat{C}_{\mathrm{obs}}{}^{IJ})^2} \right]^{1/2}, \qquad (4)$$

has the numerical value 0.09 for atom H9. The average disagreement factor for the 24 atoms in the photodimer is 0.08; the minimum and maximum values are 0.03 and 0.13. This is a rather remarkable agreement for such a simple approximation as Eq. (1).

An interesting correlation of anisotropy exists often between the positional error ellipsoid derived from the matrix $||\mathrm{cov}(x^i, x^j)||$ and the thermal-motion ellipsoid derived from the matrix $||b^{ij}/2\pi^2||$. In the triclinic photodimer of isophorone, the correlation is sufficiently exact that we need present only five error parameters for each atom [μ, λ, and the square roots of the three eigenvalues of $||\mathrm{cov}(x^i, x^j)||$], since eigen-

vectors for $||\mathrm{cov}(x^i, x^j)||$ are approximated well by those from $||b^{ij}/2\pi^2||$. The size and anisotropy of a positional-error ellipsoid appear to be determined by two independent random processes: (1) the thermal motion and static disorder in crystal space and (2) the intensity errors in diffraction (reciprocal) space. If a sphere of intensities is measured and if the measurement errors are isotropic, then the anisotropy of the positional error ellipsoid will follow that of the thermal-motion ellipsoid. Further work is under way to develop a statistical model to explain the observed correlations.

Linear combinations of the coefficients μ and λ derived by resolving the covariances of b^{ij} along an orthonormal set of isotropic tensor bases[2] provide a convenient physical interpretation for the coefficients. The quantity $2\sqrt{5}\mu$ is a measure of the shape uncertainty of the thermal ellipsoid, and the quantity $3\lambda + 2\mu$ is a measure of the size uncertainty. The quantities μ and $3\lambda + 2\mu$ must always be greater than zero because the least-squares matrix is positive definite.

Assuming we have neutron data from a crystal with space group $P\bar{1}$, a simplified analysis of the equations for a block-diagonal crystallographic least-squares matrix with one atom per block shows that μ is proportional to the square of the atomic scattering amplitude and to the reciprocal square root of the determinant $|b^{ij}/\pi^2|$. The analysis also predicts the value 5.59 (i.e., $5\sqrt{5}/2$) for the ratio of shape uncertainty to size uncertainty, $S = 2\sqrt{5}\mu/(3\lambda + 2\mu)$. After full-matrix least-squares refinement, the average experimental values for S are 4.73 and 5.57 for the nonhydrogen and hydrogen atoms, respectively, in the triclinic photodimer. When full-matrix refinement is used with x-ray data, the ratio S is diminished considerably for a heavy atom in the presence of lighter atoms, as shown by the average values 1.48, 5.07, and 5.53 found for the Ru, Cl, and C atoms, respectively, in decachlororuthenocene.[3] The mean disagreement factor R, Eq. (4), for the 21 atoms in decachlororuthenocene is 0.064, and the correlation of eigenvectors for the positional-error ellipsoids and the thermal-motion ellipsoids is extremely good.

1. C. K. Johnson and A. Vos, *Chem. Div. Annu. Progr. Rep. May 20, 1968*, ORNL-4306, p. 160.
2. D. C. Gazis, I. Tadjbakhsh, and R. A. Toupin, *Acta Crystallogr.* **16**, 917 (1963).
3. G. M. Brown, "Precise X-Ray Crystal-Structure Analysis of Decachlororuthenocene," a previous contribution in this section, this report.

ORTEP-II: A CRYSTAL-STRUCTURE GRAPHICS PROGRAM WITH ELIMINATION OF OVERLAP

C. K. Johnson

The computer program ORTEP[1] (Oak Ridge Thermal Ellipsoid Plot program) is used widely to prepare illustrations for crystal-structure papers. A shortcoming of the original version is that the drawings produced by the plotter often require manual retouching to eliminate the portions of atoms and bonds which should be hidden behind other atoms and bonds. A new version of the program, ORTEP-II, eliminates most of the retouching tasks by solving the overlap problem analytically. Since the general graphical representation for an atom is a quadratic surface (i.e., a thermal ellipsoid) with internal structure such as principal axes and octant shading, the solution of the hidden-line problem is nontrivial and is described briefly.

The overlap calculation in ORTEP-II involves three steps. In the first step, the projected outlines of the thermal ellipsoids and the interatomic bonds are stored as ellipses and quadrangles respectively. As a consequence of this projection, the major calculations in the succeeding steps can be performed in two dimensions rather than three.

The second step, the area-overlap search step, is executed just before each atom or bond is drawn. A search of the projected ellipses and quadrangles is made to detect all elements which intersect the projected atom or bond which is to be drawn. The quadrangle-quadrangle intersections are found by solving linear equations, and the ellipse-quadrangle intersections are found by solving quadratic equations. The ellipse-ellipse intersections could be found by solving quartic equations; however, in this step we are concerned only in detecting the existence of intersections, and this problem can be solved by examining the coefficients and roots of a cubic equation.[2] Once an intersection is found, the question of whether the interfering atom or bond is above or below the object to be drawn is resolved by three-dimensional vector analysis.

The final step of the overlap calculation is carried out just before each straight line segment in the graphical representation of an atom or bond is drawn. A list of intersections between the line segment and the interfering ellipses and quadrangles found in the second step is compiled and sorted by distance along the segment. The sequence of intersections is then analyzed to determine which parts of the line segment are hidden, and the remaining visible portions are drawn. An important feature of this scheme is that all graphical details, including chemical symbols inside an atom and bond-

distance labels inside a bond, are automatically corrected for overlap.

Most crystal-structure illustrations are oriented to minimize the number of overlaps; however, partially hidden atoms and bonds often aid in giving a three-dimensional appearance to an illustration. An example of such a case is shown in Fig. 7.19. Other examples of unretouched ORTEP-II drawings are shown in Fig. 7.20 and in other contributions included in this section of this report.

1. C. K. Johnson, *ORTEP: A Fortran Thermal-Ellipsoid Plot Program for Crystal Structure Illustrations*, ORNL-3794 (2d rev.) (June 1965).

2. The cubic equation is $|\mathbf{a} + \lambda\mathbf{b}| = 0$, where **a** and **b** are the 3-by-3 matrices in the equations for the ellipses $\mathbf{y}'\,\mathbf{a}\,\mathbf{y} = 0$ and $\mathbf{y}'\,\mathbf{b}\,\mathbf{y} = 0$ with $\mathbf{y}' \equiv (x, y, l)$. This is a Euclidean specialization of a result from classical projective geometry. See C. E. Springer, *Geometry and Analysis of Projective Spaces*, chap. 8, Freeman and Co., 1964.

ORNL-DWG. 71-747

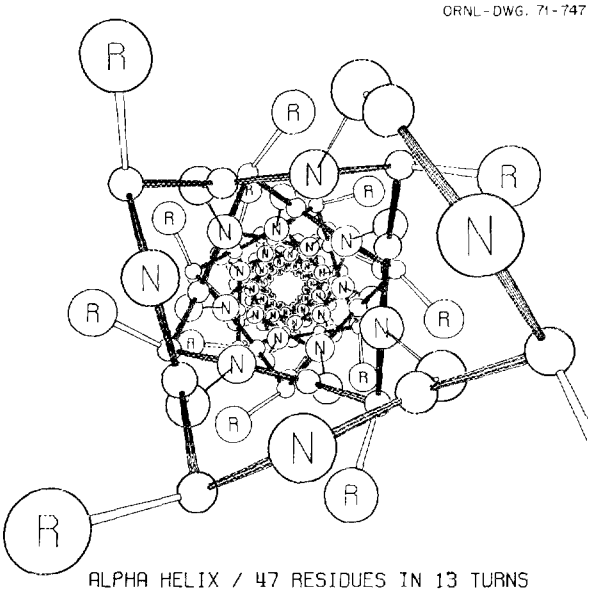

Fig. 7.19. An unretouched ORTEP-II drawing showing the end-on view of a 70-Å length of alpha helix. There are 47 residues in 13 turns of this alpha helical model for poly-*L*-alanine. The symbol *R* represents a methyl group. The atomic parameters are taken from A. Elliott and B. R. Malcolm, *Proc. Roy. Soc., Ser. A* **249**, 30 (1959).

ORNL-DWG. 71-746

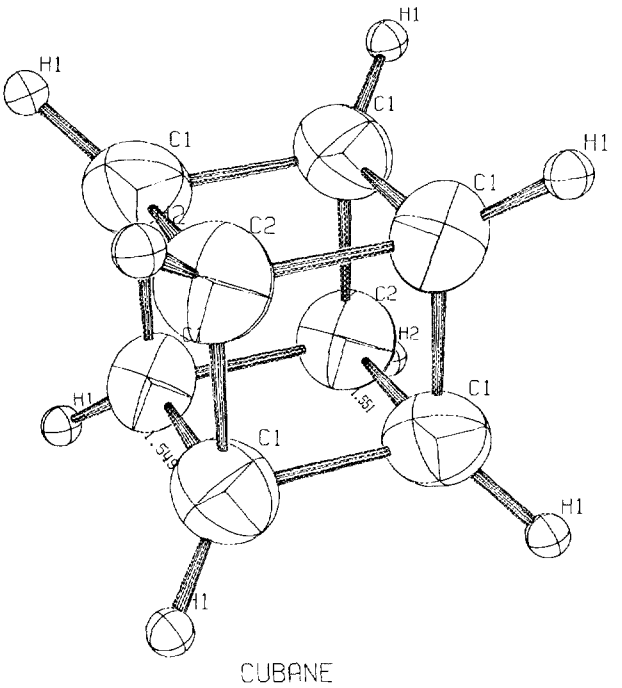

Fig. 7.20. An unretouched ORTEP-II drawing of the novel molecule cubane [E. B. Fleischer, *J. Amer. Chem. Soc.* 86, 3889 (1964)]. The width of the white strip between overlapping elements is under program control and may be changed by the user.

COMPUTER-CONTROLLED NEUTRON DIFFRACTOMETER FOR THE STUDY OF LIQUIDS

A. H. Narten W. R. Busing H. A. Levy

The diffractometer,[1] located at the lower level of HB-4 at the ORR, was extensively modified for automatic data collection over the long periods of time necessary in the study of liquid samples.

The diffractometer consists of a monochromator crystal, banks of collimator slits, a monitor counter (BF_3) in the primary beam, a detector (BF_3) arranged to scan the diffracted beam out to scattering angles $2\theta \simeq 120°$, and a PDP-8S computer interfaced to the counters and to a stepping motor driving the detector arm of the instrument. Neutrons of wavelength $\lambda = 1.101$ Å are selected by reflection from the (311)

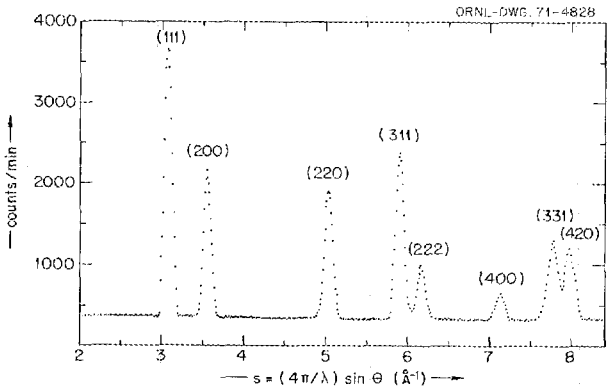

Fig. 7.21. Neutron diffraction pattern of polycrystalline nickel.

planes of a germanium crystal. The samples are contained in thin-walled cylinders ($\leqslant$50 mm long, $\leqslant$10 mm diameter) of vanadium or vitreous quartz. In the present configuration, the accessible range of scattering angles 2θ is such that $0.5 < s \equiv (4\pi/\lambda) \sin\theta < 10$ Å^{-1}.

The interface of the diffractometer to the computer is identical to that described[2] for the triple-axis instruments in use at ORNL, and existing programs can be used with only minor modifications.

Figure 7.21 shows the diffraction pattern of polycrystalline nickel in a vanadium container (7 mm OD, 0.3-mm wall). From the width of the Bragg peaks the resolution of the instrument (half width at half height) may be estimated as $\Delta s < \pm 0.05$ Å^{-1} at low angles, increasing to $\Delta s < \pm 0.08$ Å^{-1} at high angles; these values are comparable with the resolution obtained in x-ray diffraction experiments.

---

1. P. C. Sharrah and G. P. Smith, *J. Chem. Phys.* **21**, 228 (1953).
2. W. R. Busing et al., *The Oak Ridge Computer Controlled X-Ray Diffractometer*, ORNL-4143 (1968).

LIQUID GALLIUM: COMPARISON OF X-RAY AND NEUTRON DIFFRACTION DATA

A. H. Narten

Liquids have been studied with x rays since 1916 and with thermal neutrons since 1950. The first quantitative comparison of the two methods was made in 1968 for liquid lead and thallium,[1] and sizable discrepancies between the x-ray and neutron data measured in different laboratories remain unexplained. Liquid gallium (melting point 29.8°C) has been extensively studied with both x rays and neutrons, and again the results of the two most recent studies[2,3] differ by as much as 20%. Since gallium is easily supercooled to ~0°C, it can be studied at room temperature, and we have measured the diffraction pattern of liquid gallium at 20°C with both x rays and neutrons.

In a diffraction experiment an integrated intensity is measured at a given scattering angle 2θ. The integration over the energy transfer, $\hbar\omega$, is performed by the detector so that an effective differential scattering cross section is measured. The observed intensity, corrected for background and absorption and scaled to the scattering from an average independent atom, may be written

$$I(s) = f_c^2 [1 + h^*(s)] + f^{*}_i{}^2 + \Delta . \qquad (1)$$

The variable $s = (4\pi/\lambda) \sin\theta$ measures the momentum transfer, $\hbar s$, in the case of elastic scattering, f_c and f^*_i are the static coherent and effective incoherent atomic scattering amplitudes (isotropic for neutrons but angle dependent for x rays), and Δ denotes the multiple scattering terms. The quantity $h^*(s)$ is, for x rays, equal to the static structure function

$$h(s) = \int_0^\infty 4\pi r^2 \rho_0 [g(r) - 1] \frac{\sin(sr)}{sr} dr , \qquad (2)$$

with $g(r)$ the pair correlation function and ρ_0 the bulk density. For neutrons of ~1 Å, the scattering is centered around the elastic value since the incident energy (~0.085 eV) is much larger than the energy transfer ($\lesssim$0.01 eV). Placzek[4] has shown that for this case the effective quantities in Eq. (1) are related to the static values by the approximate expressions

$$h^*(s) = h(s) + p(s) ,$$
$$f^*_i = f_i [1 + p(s)] . \qquad (3)$$

The function $p(s)$ can be calculated[4] from the incident neutron energy, the neutron mass, and the mass and average kinetic energy of the atoms in the liquid; for gallium the function $p(s)$ is a low-frequency term of magnitude <0.01 in the observed intensity function. All quantities needed for the evaluation of Eqs. (1) and (3) are either negligibly small or known with good accuracy, and thus the structure function $h(s)$ can be derived from the scattering data.

Structure functions for liquid gallium from x-ray (λ = 0.71 Å) and neutron (λ = 1.10 Å) data are compared in Fig. 7.22. The neutron experiment[5] was done in transmission mode, and reflection geometry was used in

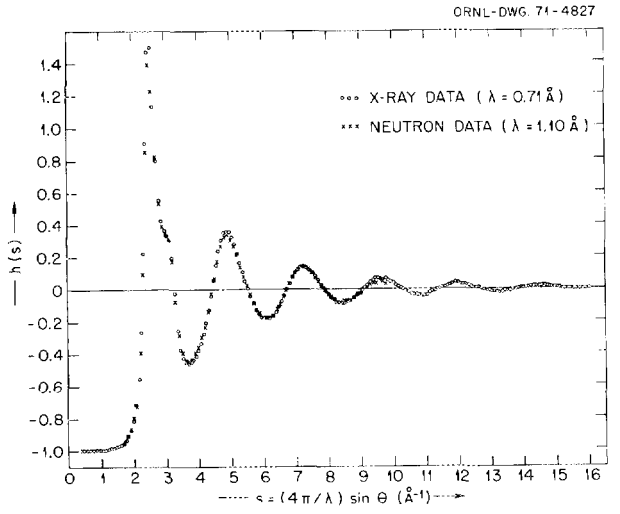

Fig. 7.22. Comparison of x-ray and neutron diffraction data on liquid gallium at 20°C.

the x-ray experiment.[6] The two data sets are of comparable accuracy (<1%) and cover the same range of scattering angles, $4° \lesssim 2\theta \lesssim 120°$. There is no significant difference between the x-ray and neutron data, and hence the equivalence of the two methods has been established, for the first time, with high precision.

1. D. M. North, J. E. Enderby, and P. A. Egelstaff, *Proc. Phys. Soc., London, Solid State Phys.* [2] 1(4), 1075 (1968).
2. S. E. Rodriguez and C. J. Pings, *J. Chem. Phys.* **42**, 2435 (1965).
3. P. Ascarelli, *Phys. Rev.* **143**, 36 (1966).
4. G. Placzek, *Phys. Rev.* **86**, 377 (1952).
5. A. H. Narten, W. R. Busing, and H. A. Levy, "Computer-Controlled Neutron Diffractometer for the Study of Liquids," the preceding contribution, this report.
6. H. A. Levy, M. D. Danford, and A. H. Narten, *Data Collection and Evaluation with an X-Ray Diffractometer Designed for the Study of Liquid Structure,* ORNL-3960 (1966).

THE MEAN SPHERICAL MODEL: SOLUTION OF AN INTEGRAL EQUATION FOR THE STRUCTURE OF LIQUID METALS

L. Blum[1] A. H. Narten

The equilibrium properties of simple monatomic liquids are described, in good approximation, by the potential $\phi(r)$ and the pair correlation function $g(r)$, the latter being accessible from scattering experiments. Ornstein and Zernike[2] (1914) introduced a direct correlation function $c(r)$ through the integral equation

$$h(r) = c(r) + \rho_0 \int c(\mathbf{r} - \mathbf{r}')\, h(\mathbf{r}')\, d\mathbf{r}' , \qquad (1)$$

which may be regarded as the definition of $c(r)$ in terms of the total correlation function $h(r) \equiv g(r) - 1$, with ρ_0 the bulk number density.

Of the many existing theories for predicting correlation functions from potentials, the Percus-Yevick (PY) approximation[3] has been the most successful one. It assumes that the direct correlation function has the form

$$c(r) = g(r)\ \{1 - \exp[\phi(r)/kT]\}, \qquad (2)$$

and the PY integral equation is obtained by eliminating $c(r)$ from Eqs. (1) and (2). The PY approximation [Eq. (2)] describes the fluid noble gases well but cannot be expected to yield valid results for liquids interacting with relatively long-range forces.

The mean spherical model (MSM) proposed by Lebowitz[4] assumes that the PY approximation [Eq. (2)] remains valid for radial distances $r < \sigma$ but that outside the hard-sphere diameter σ the relationship between potential and direct correlation function is

$$c(r) = -\phi(r)/kT , \qquad r > \sigma . \qquad (3)$$

Waisman and Lebowitz[5] have shown that the MSM, applied to 1-1 electrolyte solutions, predicts excess energies and osmotic coefficients in close agreement with experimental values.

To test the usefulness of this model for systems of particles interacting with long-range forces, we have calculated correlation functions from two potentials for liquid sodium.

The Ornstein-Zernike equation (1) may be written in bipolar coordinates as

$$r\,\eta(r) = 2\pi\rho_0 \int_0^r u\, c(u)\, du \int_{|r-u|}^{r+u} t\, h(t)\, dt , \qquad (4)$$

with $\eta(r) \equiv h(r) - c(r)$. A trial function $\eta_{in}(r)$ was used to calculate a value $\eta_{out}(r)$ from Eqs. (2), (3), and (4). The two values were then "mixed" according to $\alpha\eta_{in} + (1 - \alpha)\eta_{out}$ to yield a new trial function $\eta_{in}(r)$, and the iteration was repeated until convergence was obtained. Our results for Paskin and Rahman's[6] potential LRO2 and for Schiff's[7] potential V3 are in good agreement with those obtained by these authors from molecular dynamics studies.

It seems likely that the MSM may be usefully applied to other liquids. We plan to use the model to extract potential functions from the diffraction data on gallium[8] and water.[9]

1. Oak Ridge Associated Universities research participant from the University of Puerto Rico, summer 1970.
2. L. S. Ornstein and F. Zernike, *Proc. Acad. Sci. (Amsterdam)* 17, 793 (1914).
3. J. K. Percus and G. J. Yevick, *Phys. Rev.* **110**, 1 (1958).
4. J. L. Lebowitz and J. Percus, *Phys. Rev.* **144**, 251 (1966).
5. E. Waisman and J. L. Lebowitz, *J. Chem. Phys.* **52**, 4307 (1970).
6. A. Paskin and A. Rahman, *Phys. Rev. Lett.* **16**, 300 (1966).
7. D. Schiff, *Phys. Rev.* **186**, 151 (1969).
8. A. H. Narten, "Liquid Gallium: Comparison of X-Ray and Neutron Diffraction Data," the preceding contribution, this report.
9. A. H. Narten and H. A. Levy, "Liquid Water: Molecular Correlation Functions from X-Ray Diffraction," the following contribution, this report.

LIQUID WATER: MOLECULAR CORRELATION FUNCTIONS FROM X-RAY DIFFRACTION

A. H. Narten H. A. Levy

The scattering of x rays or neutrons from molecular liquids can always be analyzed to yield atom-pair correlation functions from which the molecular structure and positional or orientational correlations between pairs of molecules can be inferred. Additional information may be extracted for nearly spherical molecules: the scattering from these liquids yields correlation functions for molecular scattering centers, from which the intermolecular potential and hence many thermodynamic properties can often be calculated through molecular theory.

Many nonspherical molecules have a very nearly spherical distribution of electron density; for these, x-ray rather than neutron scattering seems likely to yield information on the radial dependence of the molecular correlation functions.

In the case of liquid water, orientational correlation between neighboring molecules must be expected to play an important role, but it is scarcely detectable with x rays. The x-ray scattering amplitude of a water molecule has been calculated[1] from the known molecular structure and the atomic scattering amplitudes of oxygen and hydrogen (free atom approximation), and from the molecular scattering amplitudes defined by Steele and Pecora[2] and evaluated by Blum[3] from the SCF-MO expansions of Moccia[4] (SCF-MO approximation). Both approximations yield very nearly the same result. Comparison of the average scattering from one independent molecule, $\langle F^2 \rangle$, and the average scattering from a molecule of random orientation with respect to any other molecule, $\langle F \rangle^2$, shows that $\langle F^2 \rangle \cong \langle F \rangle^2$, within $<1\%$. This means that orientational correlation between molecules in water cannot be detected with x rays, and the formalism descriptive of spherical molecules may be applied to x-ray scattering data from water.

We have deconvoluted the x-ray scattering data on liquid water[1] and calculated positional correlation functions, $G_M(r)$, descriptive of molecular centers. A comparison with previously derived atom-pair correlation functions, $G(r)$, is shown in Fig. 7.23. The two sets of curves differ significantly in the region of radial distances $r \lesssim 3.5$ Å. The maximum around 1 Å, characteristic of the intramolecular O–H interactions, is absent in the molecular correlation functions $G_M(r)$ through their inclusion in the molecular scattering amplitudes. The peak around 2.8 Å is sharper in the molecular correlation functions because it represents true molecular pair interactions, while in the atomic

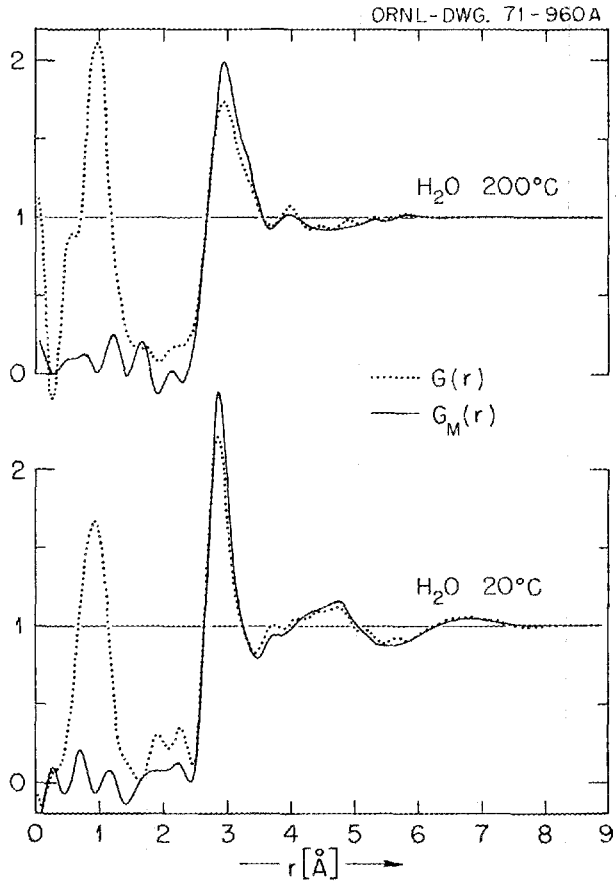

Fig. 7.23. Comparison of correlation functions for liquid water at two temperatures. The functions $G(r)$ represent superposition of modified atom-pair correlation functions for O–O, O–H, and H–H interactions. The functions $G_M(r)$ represent correlation functions for x-ray scattering centers (oxygen atoms).

$G(r)$ curves this peak shows the residual broadening of the inherent electron distribution.

The molecular correlation functions for water are sufficiently accurate to provide a sensitive test for future work on a molecular theory of liquid water. Alternatively, the data may be used to test proposed potential functions in computer experiments.

1. A. H. Narten and H. A. Levy, *J. Chem. Phys.*, in press.
2. W. A. Steele and R. Pecora, *J. Chem. Phys.* **42**, 1863 (1965).
3. L. Blum, *J. Comput. Phys.* 7, 592 (1971).
4. R. Moccia, *J. Chem. Phys.* **40**, 2186 (1964).

X-RAY DIFFRACTION STUDY OF THE SYSTEM BeF_2-LiF

A. H. Narten F. Vaslow

We have resumed studies of molten salts by x-ray diffraction in support of spectroscopic investigations of these materials. Initial studies were devoted to glasses of pure BeF_2 and of composition 15 mole % LiF in BeF_2, both at 25°C. Polycrystalline LiF was studied for comparison because it is very difficult to obtain noncrystalline solid samples containing more than 15 mole % LiF. Correlation functions[1] for these three materials, obtained from x-ray scattering experiments, are compared in Figs. 7.24 and 7.25.

As a consequence of the long-range order in the crystalline phase, the function $G(r)$ for LiF (Fig. 7.25) deviates from the asymptotic value $G(\infty) = 1$ to very large radial distances. In contrast, the correlation functions for the noncrystalline materials, typical of liquids, showed no significant deviations from a uniform distribution of interatomic distances beyond about 8 Å. On the other hand, the peaks at 1.55 and 2.54 Å in the glasses, representing near-neighbor Be–F and F–F distances, show no significant broadening compared with the Li–F (2.01 Å) and F–F (2.85 Å) peaks in crystalline LiF.

We have shown[2] that glasses of pure BeF_2 and of SiO_2 contain BeF_4 (SiO_4) tetrahedra joined at the corners so that one anion is common to two tetrahedra. The packing of these tetrahedra is very similar to that found in the crystalline modifications[3] of BeF_2 and SiO_2, and a model based on the quartz structure describes the diffraction data quantitatively. The quartz model has also been shown[4] to predict the vibrational spectra of noncrystalline BeF_2 and SiO_2 in close agreement with experiment. The diffraction data on the noncrystalline sample containing 15 mole % LiF in BeF_2 have not yet been completely analyzed, but a comparison with the curve for pure BeF_2 (Fig. 7.24) shows no indication of deviations from the packing scheme typical of all solid phases of BeF_2, namely, corner sharing of BeF_4 tetrahedra.

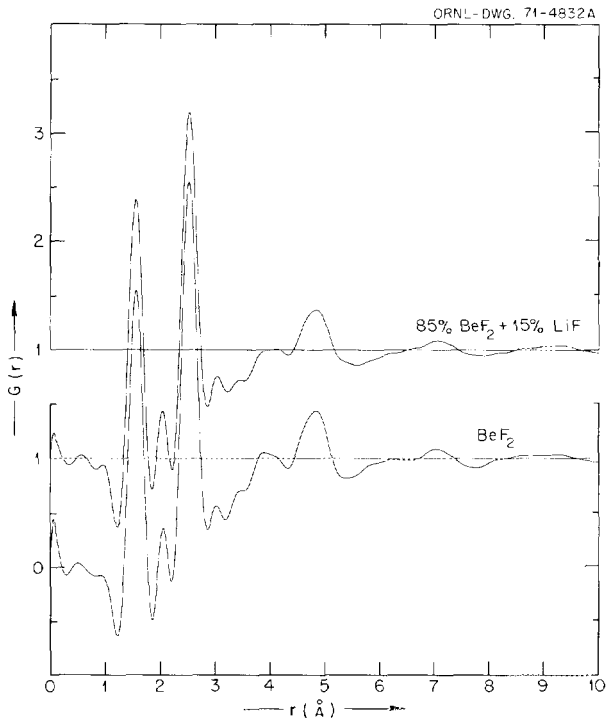

Fig. 7.24. Atom-pair correlation functions (ref. 1) for noncrystalline solid BeF_2 and 15 mole % LiF in BeF_2.

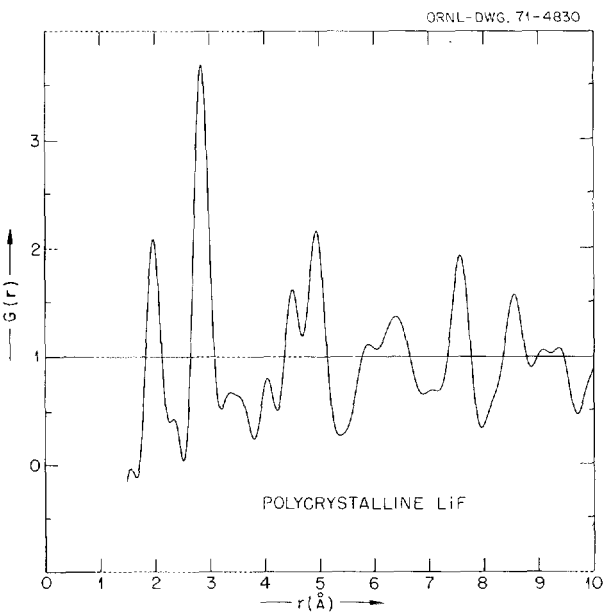

Fig. 7.25. Atom-pair correlation functions (ref. 1) for polycrystalline LiF.

The structure of these solid noncrystalline materials may be regarded as a "snapshot" of the structure in the corresponding melts in the sense that all relaxation processes occur on a time scale large compared with that of most experiments. In Fig. 7.26 correlation functions for two molten samples of different composition are presented. These curves have not yet been analyzed, but some qualitative statements may be made.

The peaks (Fig. 7.26) characteristic of near-neighbor interactions occur at very nearly the same radial distances found in the solid phases, but they are considerably broadened in the melts. This broadening might have been expected because in the liquids sizable instantaneous deviations from the average near-neighbor configurations must occur. The distance ratio for the maxima in the correlation functions (Fig. 7.26) which correspond to Be–F and F–F interactions indicates that the *average* deviation from ideal tetrahedral coordination of the F^- ions around the Be^{2+} ions must be quite small.

We plan to study the system BeF_2-LiF over wide ranges of composition and temperature using both x-ray and neutron diffraction. The diffraction work, when combined with results from thermodynamic, spectroscopic, and possibly computer studies on these melts, may be expected to yield results of both fundamental and practical interest for the Molten Salt Reactor Project.

1. The functions $G(r)$ represent superpositions of modified atom-pair correlation functions.

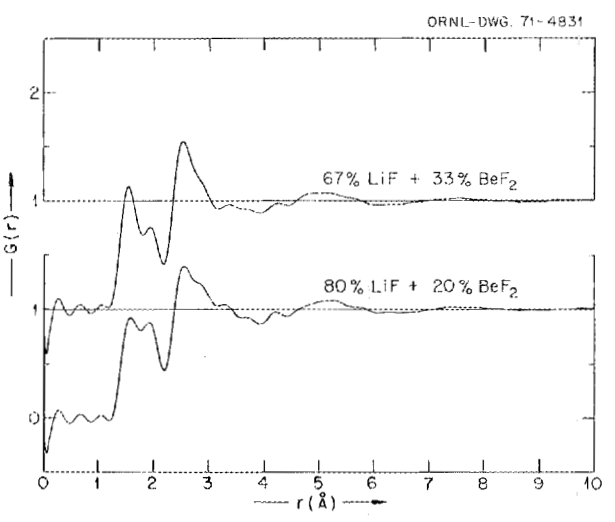

Fig. 7.26. Atom-pair correlation functions (ref. 1) for molten solutions of BeF_2 in LiF.

2. A. H. Narten, *J. Chem. Phys.*, in press.
3. R. W. G. Wyckoff, *Crystal Structures*, vol. 1, pp. 312–19, Interscience, New York, 1960.
4. J. B. Bates, *J. Chem. Phys.*, in press; also, "Dynamics of β-Quartz Structures of Vitreous SiO_2 and BeF_2," another contribution in this chapter, this report.

DIFFRACTION STUDIES ON AQUEOUS ELECTROLYTE SOLUTIONS

F. Vaslow A. H. Narten

In the interpretation of the thermodynamic properties of aqueous electrolyte solutions, some quantities and concepts of major importance are the mean distance of the ions from nearest-neighbor water molecules and from each other, the number of nearest-neighbor water molecules around the ions, and the effect of the solute ions on the general structure of water. These are matters which can be effectively studied with x-ray and neutron diffraction.

Such studies are currently being carried out. At present experimental x-ray diffraction measurements at 25°C are available for four solutions of LiCl ranging from 3.6 to 18.5 *m*. Neutron diffraction studies of corresponding solutions of ^7LiCl in D_2O are in progress.

Although only a preliminary analysis of the x-ray data has been made, there are some general conclusions which are worth noting. These conclusions are discussed in terms of the four correlation functions calculated from the x-ray measurements and the curves for water[1] and fused LiCl[2] from previous work, all shown in Fig. 7.27.

A prominent feature of all four solution curves is the peak at 3.17 Å, which is assigned to the separation of first-neighbor Cl and O atoms. A second peak at 2.0 Å, marginal in the 3.43 *m* solution but reasonably clear in the others, probably represents the Li–O nearest-neighbor distance. The preliminary least-squares analyses indicate that the peaks are consistent with four oxygen neighbors for the Li^+ ions and six neighbors for the Cl^- ions. The distances given are based on least-squares analysis.

For the 13.83 and 18.53 *m* solutions, peaks at 2.4 and 3.7 Å appear which probably represent the Li–Cl and Cl–Cl distances. These distances suggest ion-ion contacts as in the fused LiCl, where the corresponding distances (based on a different method of analysis[2]) are 2.47 and 3.85 Å, the latter probably involving several interactions. The fused salt, however, shows positional correlation (i.e., structure) to at least 15 Å, while the solutions have little structure beyond 6 Å, the 3.43 and

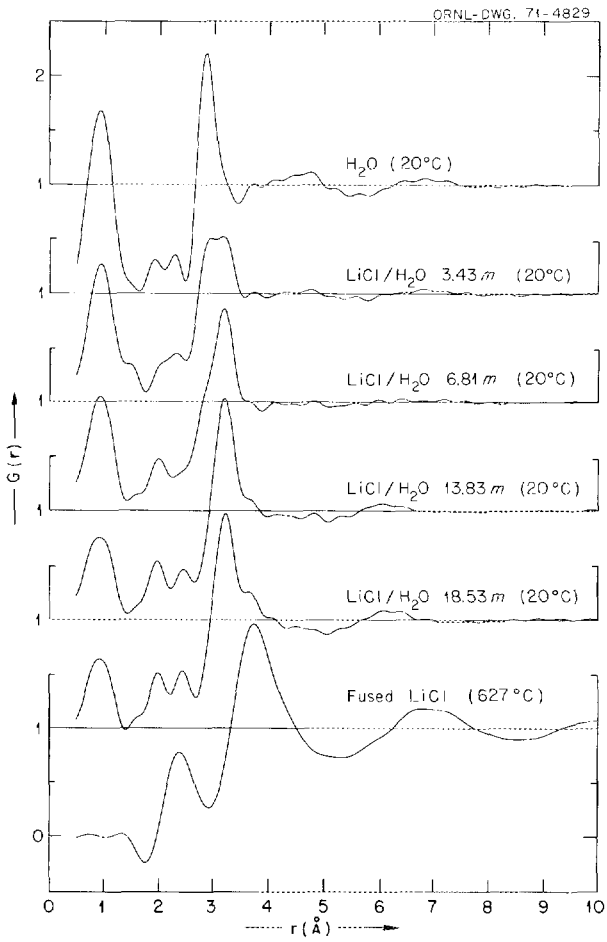

Fig. 7.27. X-ray correlation functions for water, four LiCl solutions, and fused LiCl.

6.81 *m* solutions in fact having little structure beyond about 3.5 Å. The 13.83 and 18.53 *m* solutions both show a broad peak around 6.2 Å which may possibly be ascribed to Cl^- ion pairs separated by a water molecule. Each of the above distances corresponds fairly well to sums of Pauling radii for the Li^+, Cl^-, and O^{2-} ions. A prominent peak near 1 Å for the water and the solutions arises from the intramolecular H–O distance.

In several respects addition of LiCl disrupts very strongly the original water structure. The peaks around 2.8, 4.5, and 7 Å in the correlation function for water have almost disappeared in that for the 6.81 *m* solution, while in contrast, in the case of a 6.5 *m* NH_4Cl solution, these peaks are almost unaffected. Even in the 3.43 *m* solution the water peaks are sharply diminished, and the O–O distance in each of the four solutions appears to be close to 3.0 Å rather than 2.84 Å, as in pure water.

1. A. H. Narten, *X-Ray Diffraction Data on Liquid Water in the Temperature Range 4–200°C*, ORNL-4578 (1970).
2. H. A. Levy et al., *Ann. N.Y. Acad. Sci.* 79, 762 (1970). We are indebted to Dr. M. D. Danford for making available tabulated data for this system.

INFRARED AND RAMAN SPECTROSCOPY

EFFECTS OF DENSITY AND STATE ON THE PROFILES AND INTEGRATED INTENSITIES OF NEAR-INFRARED ABSORPTION BANDS OF H_2O

W. C. Waggener A. J. Weinberger R. W. Stoughton

Our studies of the familiar, broad 0.96- and 1.15-μ absorption bands of orthobaric liquid water from 0 to 250°C[1] have been augmented by the data in Table 7.3, which show the effects of density and state on the integrated intensities of these composite bands near 254°C. The effects on the band profiles are shown by plotting four of the data sets of Table 7.3 in Fig. 7.28. The gas-phase spectra were calculated and drawn by computer from data sets taken with the digitized Cary 14. A special 0–0.2 absorbance-unit slide-wire was used, and the base lines were run with Ar replacing H_2O vapor at the same pressure and temperature in the sample cell. The ranges of the sample beam attenuation were 30, 19, and 7% for curves *B*, *C*, and *D*, respectively, in Fig. 7.28.

The data for the liquid phase were obtained earlier, including calculation of the areas of the band composites with due allowance for the overlap of nearby bands.[1]

It is apparent from Table 7.3 that at a constant temperature the intensities of both the (111) and (201) vibrational band composites of H_2O increase in going from the liquid to the gaseous state and with decreasing density. The increases in the integrated intensities of the (111) band composite (8000–9600 cm^{-1}) and the (201) band composite (9600–11,625 cm^{-1}) in going from the saturated liquid to the saturated vapor state at 254° are 34 and 78% respectively. The associated decrease in density is about 37-fold.

The integrated intensities of both bands continue to increase about 6 or 7% in going from saturated to superheated steam with a two- to fourfold decrease in vapor density.

The effect of density upon vibrational absorption band intensities is qualitatively similar to that which we have previously observed in our study of the near-

ORNL-DWG. 70-6591A

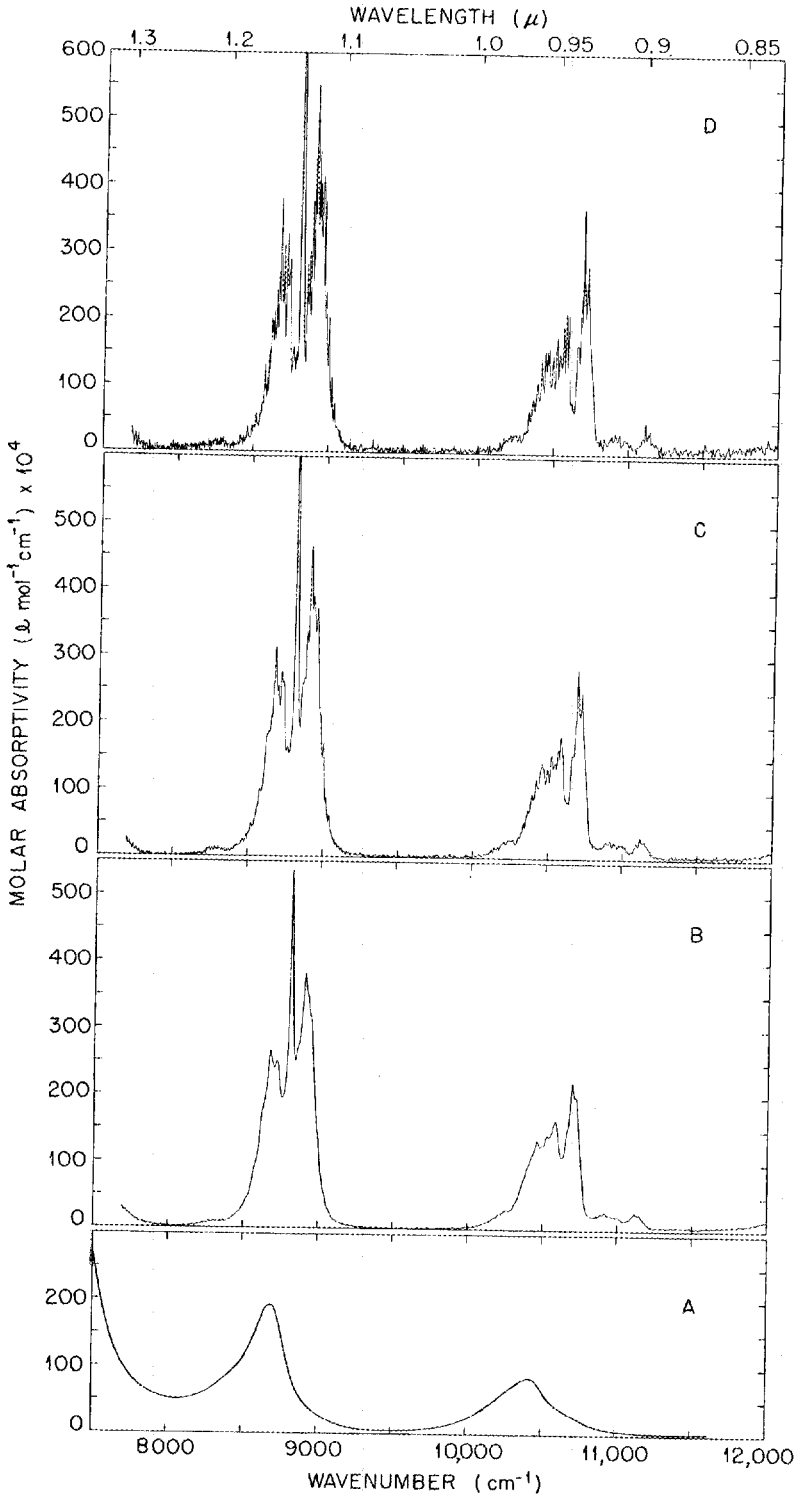

Fig. 7.28. The effect of density and state on the molar absorptivities of the two bands of fluid H_2O near 254°C in the 0.85–1.3 μ region. *A*, saturated liquid, 41.8 atm; *B*, ~ saturated vapor, 41.4 atm; *C*, superheated vapor, 21.1 atm; *D*, superheated vapor, 10.3 atm.

Table 7.3. Effect of density and state on the integrated molar absorptivities of the two bands of fluid H_2O near 254°C in the 0.85-to-1.3-μ region

	Curve in Fig. 7.28	Temperature (°C)	Pressure (atm)	Density (g/cm^3)	Area (liters mole^{-1} cm^{-2})	
					8000–9600 cm^{-1}	9600–11,625 cm^{-1}
Saturated liquid	*A*	253.8	41.8	0.7935	9.01	4.21
Nearly saturated vapor		254.3	42.2	0.02152	12.07	7.69
Nearly saturated vapor	*B*	254.3	41.4	0.02104	12.18	7.49
Superheated vapor	*C*	254.3	21.1	0.00953	12.55	7.59
Superheated vapor		254.3	20.7	0.00933	12.54	7.26
Superheated vapor	*D*	254.3	10.3	0.00447	12.86	7.97

infrared spectra of CO_2 at 25°,[2] and may also be explained using the Lorentz theory of band broadening.

1. W. C. Waggener, A. J. Weinberger, and R. W. Stoughton, *Chem. Div. Annu. Progr. Rep. May 20, 1969*, ORNL-4437, p. 107.

2. W. C. Waggener, A. J. Weinberger, and R. W. Stoughton, *J. Phys. Chem.* 71, 4320 (1967).

SPECTROPHOTOMETRY OF LIQUIDS AND SOLUTIONS OVER WIDE RANGES OF TEMPERATURE AND PRESSURE

W. C. Waggener W. H. Fletcher[1]
A. J. Weinberger R. W. Stoughton

Measurements of the $3\nu_1^{C\text{-}H}$ band of $CHBr_3$ and $CHCl_3$ and of both the $3\nu_1^{C\text{-}H}$ and $(2\nu_1 + 2\nu_4)^{C\text{-}H}$ bands of CHF_3 in the orthobaric liquid state were completed. Bromoform and chloroform were studied at intervals from their respective freezing points, 8.5 and −63°, up to the point where thermal decomposition was detectable in each liquid, 150 and 225° respectively. Orthobaric liquid fluoroform, which was studied earlier at 19 and at −48° in both the orthobaric gas and liquid states,[2] was measured at −92 and at −123°C. Useful measurements could not be made at lower temperatures down to the freezing point (−165°) due to the development of turbidity. Since the samples were rigorously dried using a molecular sieve, we believe the cloudiness was most probably caused by freezing out of traces of a fluorocarbon contaminant.

It is apparent for these haloforms that (1) the bands are complex and have a distinct asymmetry, (2) the band intensities of CHF_3 are the order of a tenth of those for $CHCl_3$ and $CHBr_3$, (3) the effect of density changes upon the band positions for CHF_3 is opposite and an order of magnitude greater than that observed for $CHCl_3$ and $CHBr_3$, and finally (4) the effect of density changes upon the bandwidths for $CHBr_3$ is opposite those observed for $CHCl_3$ and CHF_3.

The bands appear generally to be skewed toward the high-energy side. This is true for $CHCl_3$ at low temperatures; however, a moment analysis of the $3\nu_1^{C\text{-}H}$ for $CHCl_3$ indicated that its asymmetry decreases with increasing temperature, is essentially zero near 140°, and increases at still higher temperatures. At the higher temperatures the band is skewed toward the low-energy side. Both CHF_3 bands exhibit nearly linear negative shifts in position, of the order of −0.48 cm^{-1}/°C, with increasing temperature in the range from −123 to 20°. The shift observed for the $CHBr_3$ band also is essentially linear but positive, 0.1 cm^{-1}/°C, over the temperature range from 8.5 (fp) to 150°. In contrast, the shift of the $CHCl_3$ band is nonlinear. It is positive but very small (<0.03 cm^{-1}/°C) at −63° (fp) but increases to the order of 0.1 cm^{-1}/°C above 200°. The $3\nu_1^{C\text{-}H}$ band of liquid CHF_3 has an estimated half bandwidth of 103 cm^{-1} at −123°. It decreases only slightly with increasing temperature to 100 cm^{-1} at −92° and 97 cm^{-1} at −48°, then more rapidly to about 73 cm^{-1} at 20°. Similarly, the half bandwidth of $3\nu_1^{C\text{-}H}$ for liquid $CHCl_3$, which is between 59 and 60 cm^{-1} at −63° (fp), narrows with increasing temperature to about 52 cm^{-1} at 80°. Between 80 and 140° the half bandwidth reaches a minimum of 51 cm^{-1} and at higher temperatures appears to broaden slightly. In contrast, the half bandwidth of $3\nu_1^{C\text{-}H}$ for liquid $CHBr_3$, which is 49 cm^{-1} at 8.5° (fp), is relatively insensitive to temperature change but does broaden slowly and nonlinearly with rising temperatures to 51 cm^{-1} in the region of 150°C.

These observations point up the fact that these spectra reflect in a complex way both the internal structure and the environment of these relatively simple molecules. Assuming that a major factor causing the asymmetry and change in apparent position of the

$CHCl_3$ and $CHBr_3$ bands is overlapping "hot bands," we are attempting to analyze the band profiles by least-squares fitting, using mixed Gauss-Lorentzian distribution functions which are introduced in accord with the positions and intensities of the main band and the predicted hot bands. The initial trials indicate that a fit can be obtained with a reasonable number (two or three) of hot bands.

The bands of CHF_3 are apparently perturbed by these same factors, but a larger effect is produced by hydrogen bonding, which causes the bands to broaden and shift to lower frequencies as the temperature is increased.

The relative breadth and band broadening observed in the three liquid haloforms are correlated with increasing intermolecular association in going from $CHBr_3$ to CHF_3. The $3\nu_1$ band is narrowest for $CHBr_3$ and it broadens slowly and monotonically with increasing temperature. The band for $CHCl_3$ first narrows and then broadens with temperature, indicating that at the lower temperatures the effect of hydrogen bonding is overriding the effect of kinetic broadening which should occur in the absence of specific interaction. In the case of CHF_3 the $3\nu_1$ band is extremely broad, and the observation that the band narrows monotonically as the temperature of the orthobaric liquid is raised to within a few degrees of the critical point indicates relatively strong intermolecular association.

---

1. Department of Chemistry, University of Tennessee, Knoxville.

2. W. C. Waggener, A. J. Weinberger, and R. W. Stoughton, *Chem. Div. Annu. Progr. Rep. May 20, 1970,* ORNL-4581, p. 153.

MEASUREMENT OF INFRARED EMISSION SPECTRA OF MOLTEN SALTS BY FOURIER TRANSFORM SPECTROSCOPY

J. B. Bates[1] G. E. Boyd[1]

Infrared spectra of molten salts have been measured with transmission[2] and reflection[3,4] methods as well as with emission techniques.[5] There are serious problems and disadvantages characteristic of each of these methods which are due partly to the system being studied but also, to a greater extent, to the inherent deficiencies of conventional grating spectrophotometers. The large absorption coefficients of ionic melts such as the alkali metal nitrates[2] require that very thin samples be used in transmission measurements; otherwise insufficient energy is received by the detector. The attenuated total reflection method (ATR)[4] appears to offer a somewhat improved technique, but the ATR reflection elements must not react with the molten salt since they are in direct contact with the melt. For corrosive melts such as $NaBF_4$, the cost of a suitable ATR element such as diamond would be considerable. Both transmission and reflection spectra of molten salts will contain uncorrected contributions from emission, which will distort the measurements to an extent which depends on the melt temperature. (The higher the temperature, the stronger the emission from the melt.) Infrared emission spectroscopy[5] provides an alternative method in which the sampling problems discussed above are avoided.

The selection rules for infrared activity in emission spectra are the same as those for the absorption of infrared radiation. Since the intensity of the observed emission is dependent on the population of upper vibrational states, however, stronger emission can be achieved by increasing the temperature of the sample. The sensitivity of the instrument employed to measure emission spectra thus sets a lower limit to the temperature at which a measurement can be made. In conventional infrared spectrophotometers, the spectrum is recorded by measuring the intensity of one spectral element ($\Delta\nu$) at a time, where $\Delta\nu$ is defined by the spectral slit width. The energy in the remainder of the spectrum is thrown away (dispersed) by the monochromator.

A Fourier transform spectrophotometer (FTS) operates on an entirely different principle. Briefly, the FTS is constructed around a rapid-scan Michelson interferometer. The interferometer produces an interference or fringe pattern in a beam of light by varying the path length for one of the components of a split beam and then recombining the two beams. The fringe pattern, or interferogram, which is measured by an infrared detector is sampled as a function of the path length differences (δ), and the values of δ and the recorded intensity are stored in a small on-line computer. The infrared emission spectrum is recovered by taking the Fourier transform of the interferogram. Thus, all spectral elements are sampled at the same time. The resolution is determined by the maximum distance from $\delta = 0$ over which the interferogram is sampled. Defining a spectral element, N, by $N = (\nu_H - \nu_L)/\Delta\nu$, where ν_H and ν_L are the highest and lowest frequencies, respectively, to be recorded and $\Delta\nu$ is the resolution, a conventional grating infrared spectrophotometer will require a total time of NT to record the spectrum, where T is the response time of the detector. Since in an FTS all elements in the range $\nu_H - \nu_L$ fall on the detector at the same time, the FTS can record

the spectrum N times faster for an equivalent signal-to-noise ratio. (The response times of the detectors are the same in both cases.) For an equivalent scanning time, the signal-to-noise ratio can be improved by a factor of $\sqrt{N}$ compared with the grating instrument.

Emission spectra of molten $KClO_3$, $LiNO_3$, and a mixture of $LiNO_3$ in $KClO_3$ were measured at about 500°C using a Digilab model 14 FTS.[6] The spectra shown in Fig. 7.29 were observed by collecting the emission from thin films of each material spread over the surface of an aluminum sheet placed on top of a hot plate. For a resolution of 8 cm^{-1}, the interferogram of each molten salt was recorded in 8 sec (16 scans). Computation and plotting required an additional 50 sec. Thus, each spectrum shown in Fig. 7.29 was recorded in less than 1 min. The computation time also includes subtracting the background due to blackbody emission from the aluminum plate and absorption due to atmospheric water vapor.

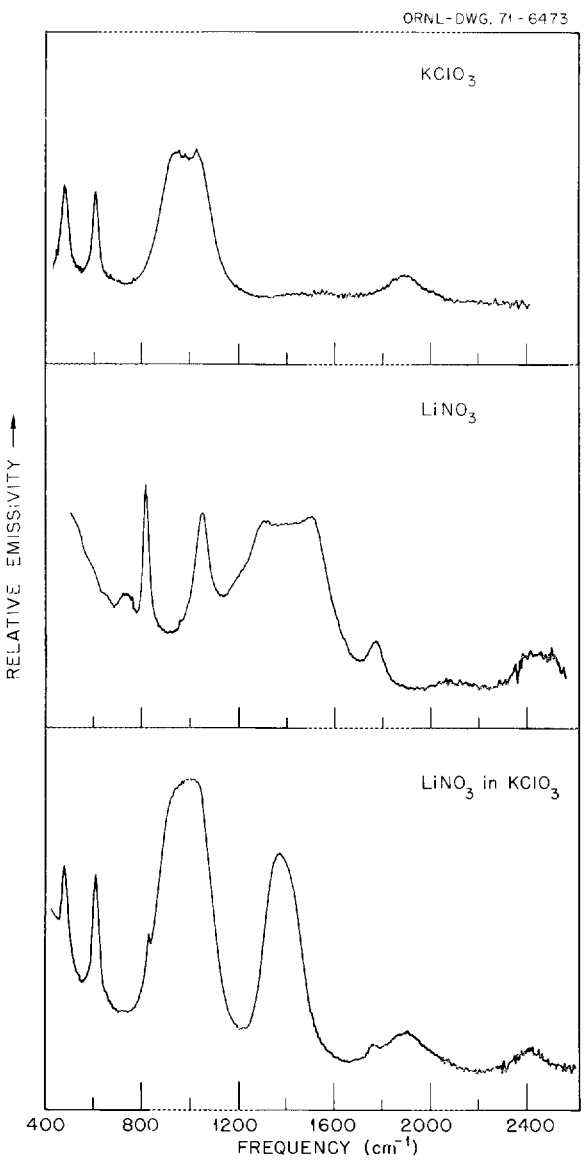

Fig. 7.29. Emission spectra of molten salts measured by Fourier transform infrared spectroscopy. $KClO_3$, $LiNO_3$, and about 20 mole % $LiNO_3$ in $KClO_3$. All spectra measured at about 500°C.

The quality of the molten-salt infrared spectra shown in Fig. 7.29, in terms of signal/noise ratio and band shapes, is equal to, or better than, that of the spectra previously reported[2–5] for the same molten salts. The simplicity of the experimental setup and the speed at which these spectra were recorded indicate that infrared spectra of molten salts of current interest to the Molten-Salt Reactor Program can be obtained quite readily from measurements of the emission spectra using an FTS system.

1. Director's Division.
2. R. E. Hester and K. Krishman, *J. Chem. Phys.* **47,** 1747 (1967).
3. J. K. Wilmhurst and S. Senderoff, ibid. **35,** 1078 (1961).
4. A. Bandy et al., *Rev. Sci. Instrum.* **35,** 1206 (1964).
5. T. R. Kozlowski, *Appl. Opt.* **7,** 795 (1968).
6. The FTS-14 was made available through the courtesy of Digilab, Inc.

POLARIZED RAMAN SPECTRA OF β-QUARTZ[1]

J. B. Bates[2] A. S. Quist[2]

The polymorphs of SiO_2 have been subjected to many thorough spectroscopic investigations. Much of the work on these materials reported prior to 1970 has been reviewed recently by Wong and Angell.[3] Polarized Raman spectra of α-quartz were measured by Scott and Porto,[4] and all $k = 0$ modes of the D_3 (trigonal) lattice were assigned on the basis of the polarization measurements. At 573°C, α-quartz undergoes a phase transition to the β-phase in which the lattice symmetry is reported to be D_6^4 ($P6_222$). Using infrared and Raman frequencies taken from early studies of β-quartz, the authors of ref. 4 proposed an assignment of the $k = 0$ modes of β-quartz based on a correlation with the frequencies and symmetry types determined for the room-temperature structure.

Our interest in the vibrational spectrum of β-quartz stems from recent studies of the dynamics of β-quartz models of vitreous SiO_2 and BeF_2.[5] To correlate the frequencies observed in SiO_2 with those of β-quartz, it was necessary to know the correct assignments for the

optical modes for the latter. Preliminary calculations indicated that several of the assignments proposed in ref. 4 are incorrect.

A small cylinder of single-crystal quartz with the cylinder axis parallel to the crystallographic z axis was placed in the high-temperature furnace described previously.[6] The crystal was aligned such that the scattering geometries described by $z(ij)\bar{y}$, $i = x$ or $\bar{y}$ and $j = x$ or z, could be obtained, where $\bar{y}$ is perpendicular to z and x, z and $\bar{y}$ indicate the directions of the incident and scattered light, respectively, and i and j denote the polarization of the incident and scattered light respectively. In going from the α- to the β-phase, the z axis remains invariant while the x and y axes are retained in the original xy plane. The optical modes of β-quartz are described by

$$\Gamma(D_6) = a_1 + 2\,a_2 + 3\,b_1 + 2\,b_2 + 4\,e_1 + 4\,e_2 \ .$$

The a_1, e_1, and e_2 modes are Raman active, while the b_1 and b_2 modes are both infrared and Raman inactive. The correlation diagram given in Table 7.4 shows the relationship between the symmetry species of the D_3 factor group of α-quartz and the D_6 factor group of β-quartz. The table shows that the modes in α-quartz which have e symmetry give rise to modes in β-quartz which have either e_1 or e_2 symmetry. Table 7.4 also shows that the e_1 modes of β-quartz are polarized in the yz and xz planes, while the e_2 modes are polarized in the xy planes. Thus, the e_1 and e_2 modes can be readily distinguished using the crystal orientation and scattering geometry described above: e_1 modes are active in $z(\bar{y}z)\bar{y}$ and $z(xz)\bar{y}$ spectra, while the e_2 modes are active in $z(\bar{y}z)\bar{y}$ and $z(xx)\bar{y}$ spectra. Modes having a_1 symmetry in β-quartz should appear only in the $z(xx)\bar{y}$ spectra.

The polarized Raman spectra of β-quartz measured at about 610°C are shown in Figs. 7.30–7.32. The frequencies and assignments of the observed fundamental modes are collected in Table 7.5. The appearance of theoretically forbidden bands in certain of the polarized spectra in the table is the result of errors both in alignment of the crystal and in the initial cutting of the quartz cylinder. The 462-cm^{-1} band, which should not appear in spectra due to changes in off-diagonal polarizability tensor elements, exhibits a residual band of appreciable intensity in the $z(\bar{y}x)\bar{y}$ spectrum (Fig.

Table 7.4. Correlation diagram relating the symmetry species of the factor groups for α- and β-quartz

	α-Quartz, D_3	β-Quartz, D_6	
$x^2 + y^2, z^2$	A_1	A_1	$x^2 + y^2, zz$
		A_2	z
z	A_2	B_1	
		B_2	
x,y		E_1	$x,y;\ yz,xz$
$x^2 - y^2,\ xy;\ yz,xz$	E	E_2	$x^2 - y^2,\ xy$

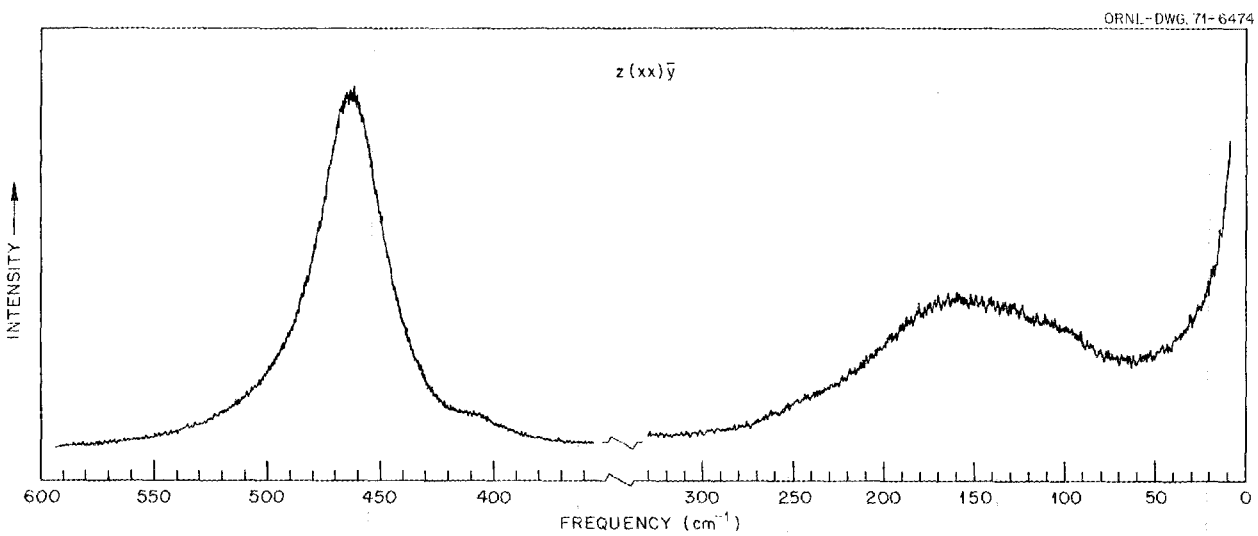

Fig. 7.30. $z(xx)\bar{y}$ **Raman scattering from β-quartz at 610°C.**

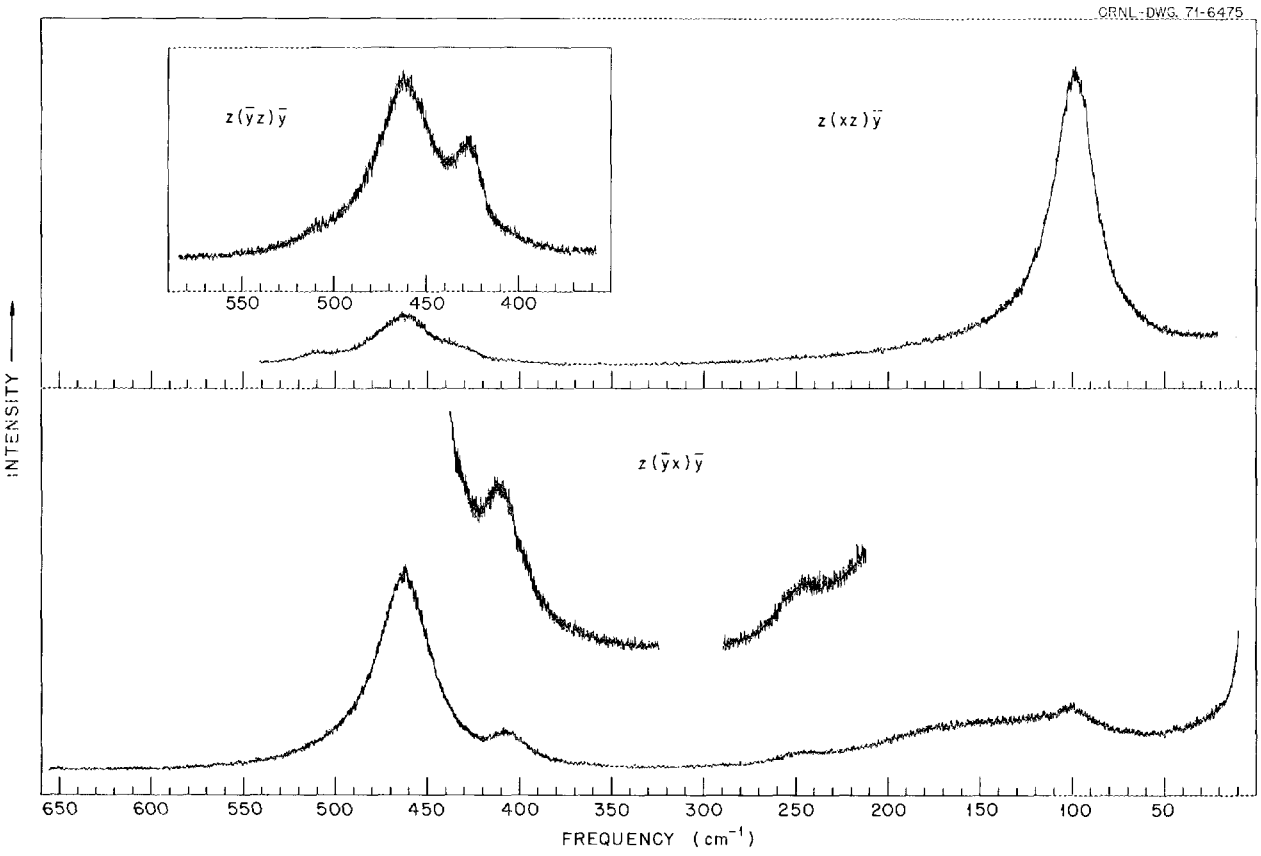

Fig. 7.31. $z(\bar{y}z)\bar{y}$, $z(xz)\bar{y}$, and $z(\bar{y}x)\bar{y}$ Raman scattering from β-quartz in the region below 600 cm^{-1} at 610°C.

Table 7.5. Bands observed in polarized Raman spectra of β-quartz at 610°C

Frequency (cm^{-1})	Intensity[a]				Assignment, D_6
	$z(xx)\bar{y}$	$z(xz)\bar{y}$	$z(\bar{y}z)\bar{y}$	$z(\bar{y}x)\bar{y}$	
1173				m	e_2
1067		m	m		e_1
788		m	m		e_1
688				m	e_2
462	vs	w	w	m	a_1
428		m	m		e_1
409	vw			m	e_2
245				w	e_2
99		s	s		e_1

[a]vs = very strong, s = strong, m = medium, w = weak; blanks indicate no measurable intensity observed.

7.31 and Table 7.5). In this case, a large contribution from $z(xx)\bar{y}$ scattering occurred due to alignment errors cited above. The appearance of this band in other spectra can be similarly accounted for by noting that the a_1 mode at 462 cm^{-1} will exhibit strong components in yy and zz scattering as well as in xx scattering.

Additional bands were observed in the Raman spectra of β-quartz that are not cited in Table 7.5. The band at ~165 cm^{-1} in $z(xx)\bar{y}$ spectra does not appear to be due to first-order Raman scattering. This region of the spectrum of quartz exhibits unusual features a few degrees below the phase transition. We studied this region as a function of temperature both above and below the phase transition. A discussion of the results of these measurements is beyond the scope of this report and will be presented elsewhere.[1]

1. Abstracted from a paper to be submitted for publication.
2. Director's Division.
3. J. Wong and C. A. Angell, *Appl. Spectrosc. Rev.* **4**, 155 (1971).
4. J. F. Scott and S. P. S. Porto, *Phys. Rev.* **161**, 903 (1967).
5. J. B. Bates, "Dynamics of β-Quartz Structures of Vitreous SiO_2 and BeF_2," another contribution in this section, this report.
6. A. S. Quist, *Appl. Spectrosc.* **25**, 82 (1971).

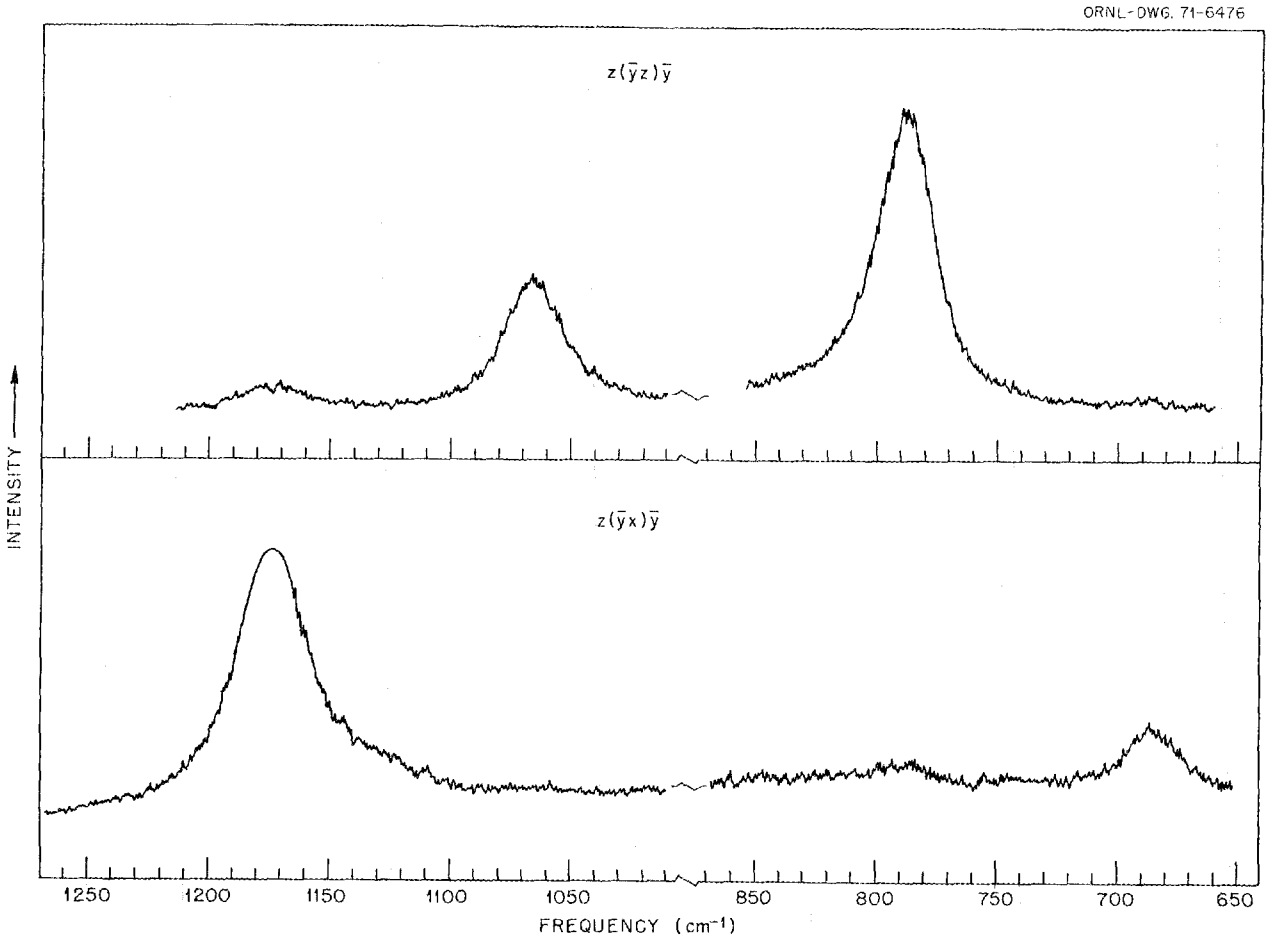

Fig. 7.32. $z(\bar{y}z)\bar{y}$ **and** $z(\bar{y}x)\bar{y}$ **Raman scattering from β-quartz in the region above 600 cm^{-1} at 610°C.**

DYNAMICS OF β-QUARTZ STRUCTURES OF VITREOUS SiO_2 AND BeF_2[1]

John B. Bates[2]

One of the major difficulties encountered in interpreting the vibrational spectra of glassy materials is the lack of structural models from which selection rules can be derived and which provide the framework for dynamical calculations. Recent x-ray scattering experiments by Narten[3] have shown that the β-quartz structure is the best model of all the known crystalline polymorphs of SiO_2 for interpreting the observed diffraction patterns of vitreous SiO_2 and BeF_2. Previous calculations of the vibrational modes of glassy SiO_2 and BeF_2 were based on random network models and on the α-quartz structure. Apparently there have been no previous attempts to correlate the observed vibrational spectra of SiO_2 and BeF_2 with a model based on the structure of β-quartz.

The β-quartz lattice has the space group symmetry given by D_6^4 ($P6_222$).[4] The Si (or Be) atoms occupy D_2 sites, and the O (or F) atoms occupy sites of C_2 symmetry. The irreducible representation for the 24 optically active ($k = 0$) modes of SiO_2 and BeF_2 is given by:

$$\Gamma(D_6)^{op} = a_1 + 2\,a_2 + 3\,b_1 + 2\,b_2 + 4\,e_1 + 4\,e_2 \,.$$

This can be compared with $\Gamma(D_3)^{op}$ for α-quartz, which is given by $\Gamma(D_3)^{op} = 4\,a_1 + 4\,a_2 + 8\,e$. Thus the β-quartz selection rules determined by $\Gamma(D_6)^{op}$ predict only one totally symmetric mode, $\nu_1(a_1)$, compared with the four a_1 modes predicted by the α-quartz selection rules.

The vibrational frequencies observed from infrared and Raman spectral studies on β-quartz and vitreous SiO_2 and BeF_2 are given in Table 7.6.[5–10] The frequencies observed in α-quartz which can be correlated

Table 7.6. Observed frequencies (cm^{-1}) of crystalline α- and β-quartz and vitreous SiO_2 and BeF_2

p = polarized; dp = depolarized

α-Quartz[a] (D_3)	β-Quartz[b] (D_6)	SiO_2[c]	BeF_2[d]
464 (a_1)	462 (a_1)	432 p	280 p
1080 (a_2)	(a_2)		
364 (a_2)	(a_2)		
1085 (a_1)	Inactive (b_1)		
356 (a_1)	Inactive (b_1)		
778 (a_2)	Inactive (b_2)		
495 (a_2)	Inactive (b_2)		
1162 (e)	1067 (e_1)	1065 dp	910
795 (e)	788 (e_1)	800 dp	770
394 (e)	428 (e_1)	400 dp	410
128 (e)	99 (e_1)	60 dp	105[e]
1072 (e)	1173 (e_2)	1200 dp	805 dp
697 (e)	688 (e_2)		
450 (e)	409 (e_2)		379
265 (e)	245 (e_2)		

[a]Reference 5.
[b]Reference 6.
[c]Reference 7.
[d]References 3 and 4.
[e]Reference 10.

Table 7.7. Calculated frequencies for crystalline β-quartz and vitreous SiO_2 and BeF_2

Symmetry type	Calculated frequency (cm^{-1})			Assignment[a]	
	β-Quartz	SiO_2	BeF_2	SiO_2	BeF_2
a_1	473	465	329	θ_2, θ_3	Φ
a_2	1274	1317	770	R	R
	333	351	417	θ_2	θ_2
b_1	1067	1066	689	R	R
	306	330	209	(θ_2, θ_3)	(θ_2, θ_3)
b_2	728	713	966	R	R, Φ
	443	401	315	(θ_2, θ_3)	Φ, R
e_1	1069	1063	915	R	R
	770	779	751	R	R
	427	413	368	(θ_2, θ_3)	$\Phi, (\theta_2, \theta_3)$
	96	62	90	$\Phi, (\theta_2, \theta_3)$	(θ_2, θ_3)
e_2	1157	1184	821	R	R
	724	735	532	R	R
	389	398	300	$\theta_1, (\theta_2, \theta_3)$	Φ
	262	240	269	$(\theta_2, \theta_3), \theta_1$	$\theta_1, (\theta_2, \theta_3)$

[a]Determined from the potential energy distribution; R, θ_1, θ_2, θ_3, and Φ refer to the symmetrically equivalent sets of internal coordinates.

with those of the β structure are also included in the table.[5] The assignments (Table 7.7) proposed for SiO_2 were based on near frequency coincidence with the corresponding modes of β-quartz; the assignments for BeF_2 were made by comparison of relative band intensities and assuming an ordering of frequencies similar to that for SiO_2.

The observation of only one strong polarized band in each of the Raman spectra of vitreous SiO_2 and BeF_2 is strong supporting evidence in favor of the β-quartz model for these glasses. The polarization characteristics for the remaining bands listed in Table 7.6 are also consistent with a structure having D_6 symmetry.

The vibrational frequencies of SiO_2 and BeF_2 were calculated at $k = 0$ (assuming ordered lattice structures) by the GF matrix method applied to crystal vibrations. Thirty-six internal coordinates were employed consisting of five symmetrically equivalent sets: 12 Si-O (Be-F) stretching coordinates, 18 O-Si-O (F-Be-F) bending coordinates (3 sets of 6 coordinates each), and 6 Si-O-Si (Be-F-Be) bending coordinates. The frequencies for β-quartz were also computed by refining the parameters of a modified valence force field (MVFF) to give the best fit to the frequencies observed from polarized Raman experiments at 610°C.[6]

Table 7.8. Calculated force constants and mean vibrational amplitudes for β-quartz and vitreous SiO_2 and BeF_2

Coordinate or interaction	Force constant (millidynes/Å)		
	β-Quartz	SiO_2	BeF_2
R	4.905	4.765	2.260
θ_1	0.428	0.550	0.222
$\theta_2 = \theta_3$	0.304	0.324	0.132
Φ	0.103	0.022	0.145
R, R'	0.791	0.713	0.578
R, θ_1	−0.592	−0.697	0.176
R, θ_3	0.330	0.236	0.254

	Mean amplitudes: $\langle \Delta r_{ij}^2 \rangle^{1/2}$ (Å)		
	Calculated		X-ray diffraction,[a] SiO_2
	β-Quartz	SiO_2	
Si–O	0.045	0.045	0.042
O–O	0.089	0.088	0.092
Si–Si	0.054	0.069	0.100
	BeF_2		BeF_2
Be–F	0.064		0.083
F–F	0.073		0.103
Be–Be	0.074		0.132

[a]Reference 3.

The results of the calculations are collected in Tables 7.7 and 7.8. Good agreement between observed and calculated frequencies is achieved using a seven-parameter MVFF. The computed mean vibrational amplitudes for SiO_2 and BeF_2 also agree reasonably well with the mean amplitudes derived from x-ray scattering data.[3] The assignments for each mode of SiO_2 and BeF_2 given in Table 7.7 are based on the potential energy distribution. The coordinate set listed first indicates the primary contributor: R denotes the Si-O (Be-F) stretching coordinates, θ_1 and (θ_2, θ_3) denote the three types of O-Si-O (F-Be-F) bending coordinates, and Φ denotes the Si-O-Si (Be-F-Be) bending coordinates.

The results of the calculations given in Tables 7.7 and 7.8, when correlated with the observed vibrational spectra of vitreous SiO_2 and BeF_2, support the conclusion[3] that the structures of these materials are best described by the β-quartz lattice model. Conversely, this conclusion, based on the x-ray scattering experiments,[3] provided a model from which vibrational calculations could be made and from which optical selection rules could be derived. Additional details will be given elsewhere.[1]

---

1. Abstracted from a paper submitted for publication in *J. Chem. Phys.*
2. Director's Division.
3. A. H. Narten, *MSR Program Semiannu. Progr. Rep. Feb. 28, 1971,* ORNL-4676; also submitted for publication in the *Journal of Chemical Physics.*
4. R. W. G. Wyckoff, *Crystal Structures,* vol. I, p. 313, Interscience, New York, 1960.
5. J. F. Scott and S. P. S. Porto, *Phys. Rev.* **161**, 903 (1967).
6. J. B. Bates and A. S. Quist, "Polarized Raman Spectra of β-Quartz," the preceding contribution, this report.
7. M. Hass, *J. Phys. Chem. Solids* **31**, 415 (1970).
8. A. S. Quist, J. B. Bates, and G. E. Boyd, *Chem. Div. Annu. Progr. Rep. May 20, 1970,* ORNL-4581, p. 166.
9. L. R. Batsanova, G. S. Yur'ev, and V. P. Doronia, *J. Struct. Chem. USSR* **9**, 63 (1968).
10. A. J. Leadbetter and A. C. Wright, *J. Non-Cryst. Solids* **3**, 239 (1970).

RAMAN AND INFRARED SPECTRAL STUDIES OF ANHYDROUS Li_2CO_3 AND Na_2CO_3[1]

M. H. Brooker[2] John B. Bates[3]

Recently, Dubbeldam and De Wolff[4] reported the (average) crystal structure of anhydrous Na_2CO_3 and suggested a modulated structure that could be explained by assuming an ordered arrangement of the CO_3^{2-} ions over two nonequivalent orientations within the primitive cell. The effects of this unusual structure should be apparent in the vibrational spectrum of Na_2CO_3. Inasmuch as Li_2CO_3 belongs to the same crystal class[5] as Na_2CO_3 but has only *one* carbonate orientation, it may serve to give a convenient normal vibrational spectrum with which Na_2CO_3 may be compared. The Raman spectra of Li_2CO_3 and Na_2CO_3 have not previously been reported; however, Buijs and Schutte[6] and Tarte[7] have reported results from thin-film infrared transmission measurements on crystalline Li_2CO_3 and Na_2CO_3. Buijs and Schutte[6] analyzed their data in terms of static field effects, but no evidence was reported that would indicate the unusual crystal structure of Na_2CO_3. Hence, a further study of the vibrational spectrum of these crystals appeared to be desirable.

Infrared and Raman spectra of polycrystalline Li_2CO_3 and Na_2CO_3 have been measured at room and liquid-nitrogen temperatures. The observed frequencies are given in Tables 7.9 and 7.10. The spectra for Li_2CO_3 and Na_2CO_3 are different in two significant ways: (1) For Li_2CO_3, except for the ν_4 region near 700 cm^{-1}, all of the internal modes of the CO_3^{2-} ion are single bands, whereas for Na_2CO_3, two bands are present in the regions of each fundamental (Tables 7.9 and 7.10; Figs. 7.33 and 7.34). (2) Raman bands caused by external lattice modes are sharp and intense for Li_2CO_3 (Fig. 7.33) but broad and diffuse for Na_2CO_3 (Fig. 7.34). Both 1 and 2 suggest substantially different crystal structures; (2) suggests that the Na_2CO_3 lattice is not as well ordered as the Li_2CO_3 lattice. Bands observed in the vibrational spectra of Li_2CO_3 were assigned according to the C_{2h} factor group symmetry. The doublet structure observed for each of the internal modes in the spectra of Na_2CO_3 was interpreted in terms of an ordered arrangement of CO_3^{2-} ions over two nonequivalent orientations within the primitive cell, in agreement with the proposed crystal structure.

Multiple internal reflection (MIR) and polarized specular reflectance (PSR) techniques were used to determine the transverse optical (TO) and longitudinal optical (LO) mode frequencies for the ν_2 and ν_3 carbonate ion vibrations in Li_2CO_3 and Na_2CO_3 (Table 7.11). Contributions from LO modes had been observed previously in the thin film transmission studies but were incorrectly assigned.[6] The general applicability of MIR techniques for determination of TO modes[8] and PSR techniques for the determination of LO modes[9] was reaffirmed.

Table 7.9. Vibrational frequencies (cm^{-1}) for Li_2CO_3[a]

Raman		Infrared		Assignment
300°K	77°K	MIR, 300°K	Transmission, 77°K	
95 (1.25)	96			
126 (0.16)	129			
156 (0.50)	160			
192 (0.48)	196			
		~380 (sh)	~360 (sh)	
		410 (m)	410 (m)	
		440 (w,sh)	440 (w,sh)	
		500 (s)	498 (s)	
711 (0.038)	712			$A_g + B_g$ } ν_4
748 (0.051)	748			
		713 (w)	713 (w)	$A_u + B_u$ } ν_4
		740 (m)	740 (m)	
		847 (w,sp)	847 (w,sp)	$^{13}CO_3^{2-}$ } ν_2
		859 (m,sp)		B_u (TO) } ν_2
n.o. (<0.0001)	n.o.			B_g } ν_2
			867 (m)	B_u (TO + LO) } ν_2
		1088 (m)	1089 (m)	A_u (TO) } ν_1
1091 (1.0)	1092			A_g } ν_1
		1420 (br)	1430 (br)	$A_u + B_u$ (TO) } ν_3
1459 (0.041)	1460			$A_g + B_g$ } ν_3
			~1500 (br)	$A_u + B_u$ (TO + LO) } ν_3
			1606[b]	$A_u + B_u$ (LO) } ν_3
~1720 (vw)				$2\nu_2$
			1805 (w)	$\nu_1 + \nu_4$ (713 + 1091)
			1837 (w)	$\nu_1 + \nu_4$ (748 + 1091)

[a]Raman intensities relative to the ν_1 band taken as unity are given in parentheses. Abbreviations: w, weak; m, medium; s, strong; sh, shoulder; sp, sharp; br, broad; n.o., not observed; v, very.

[b]Taken from polarized specular reflectance data.

ORNL-DWG. 70-10673

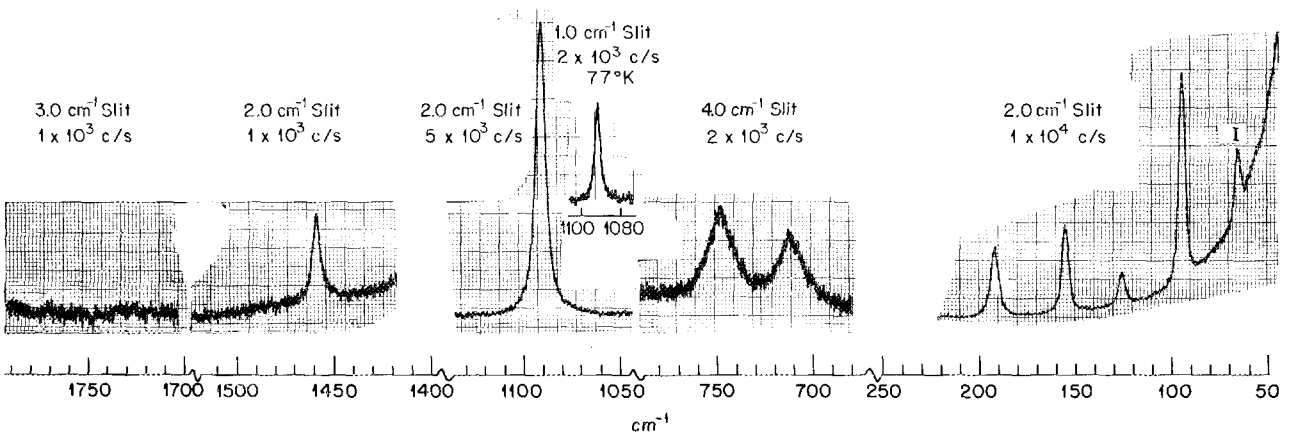

Fig. 7.33. Portions of Raman spectra of Li_2CO_3. Samples were at 300°K except where noted. *I* denotes instrumental band.

Table 7.10. Vibrational frequencies (cm^{-1}) for Na_2CO_3[a]

Raman		Infrared		Assignment
300°K	77°K	MIR, 300°K	Transmission, 77°K	
	133 (w)			
146 (0.06)	156			
172 (0.25)	182			
185 (0.40)	195			
	201			
220 (0.02)	228			
		694 (m)	694 (m)	
698 (0.025)	698			
		701 (m)	701 (m)	ν_4
702 (0.035)	702			
		706 (vw)	706 (vw)	?
		852 (w,sp)	852 (w,sp)	$^{13}CO_3^{2-}$
n.o. (<0.0001)	n.o.	880 (s)	880 (s)	ν_2
		886 (sh)	886 (sh)	
1079 (0.70)	1079	n.o.	n.o.	
1083 (0.30)	1084	n.o.	n.o.	ν_1
		1413 (sp)	1413	
1422 (0.016)	1423			
		1425 (sp)	1425	ν_3
1431 (0.019)	1432			
			1500 (s,sh)	TO + LO
			1543[b]	LO
1760 (0.0009)	1760			
1771 (0.0011)	1771			$2\nu_2$
		1775 (w)	1775 (w)	$\nu_1 + \nu_4$

[a]Raman intensities relative to the ν_1 band taken as unity are given in parentheses. Abbreviations: w, weak; m, medium; s, strong; sh, shoulder; sp, sharp; br, broad; n.o., not observed; v, very.

[b]Taken from polarized specular reflectance data.

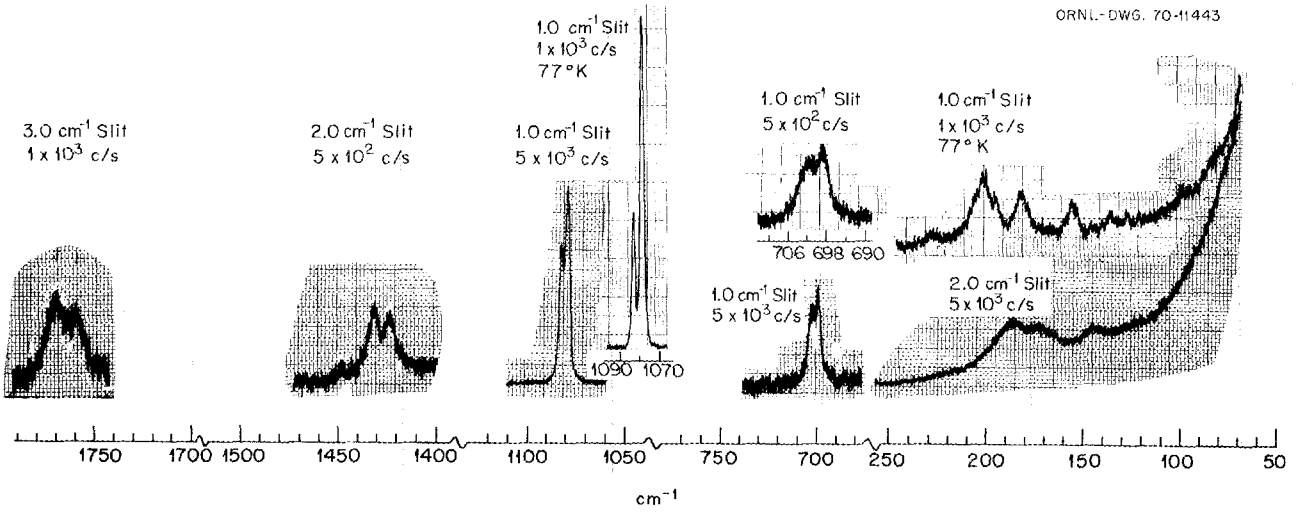

Fig. 7.34. Portions of Raman spectra of Na_2CO_3. Samples were at 300°K except where noted.

1. Expanded abstract of published paper: *J. Chem. Phys.* **54**, 4788 (1971).
2. Visiting scientist, National Research Council of Canada Postdoctoral Fellow, 1969–71.
3. Director's Division.
4. G. C. Dubbeldam and P. M. De Wolff, *Acta Crystallogr., Sect. B* **25**, 2665 (1969).
5. V. J. Zemann, ibid. **10**, 664 (1957).
6. K. Buijs and C. J. H. Schutte, *Spectrochim. Acta* **17**, 917, 921, 927 (1961).
7. P. Tarte, ibid. **20**, 238 (1964); **21**, 313 (1965).
8. M. H. Brooker, *J. Chem. Phys.* **53**, 4100 (1970).
9. J. B. Bates and M. H. Brooker, *J. Phys. Chem. Solids* (in press); also, "Determination of Longitudinal Optical Mode Frequencies by Polarized Specular Reflectance (PSR) Infrared Spectroscopy," the following contribution, this report.

Table 7.11. Longitudinal optical and transverse optical mode frequencies (cm^{-1}) determined by PSR methods[a]

Li_2CO_3		Na_2CO_3		Assignment	
P	S	P	S		
846 (w)	846 (w)	852 (w)	852 (w)	$^{13}CO_3^{2-}$	ν_2
	860 (sp)	880 (m)	880 (m)	TO	
867 (sp)				LO	
			1415 (w)		ν_3
				TO	
1420 (br)	1420 (br)	1435 (br)	1430 (w)		
1606 (sp)	~1600 (sp)	1543 (sp)	1540 (sp)	LO	

[a]P and S refer to polarization parallel and perpendicular, respectively, to the plane of incidence.

DETERMINATION OF LONGITUDINAL OPTICAL MODE FREQUENCIES BY POLARIZED SPECULAR REFLECTANCE (PSR) INFRARED SPECTROSCOPY[1]

J. B. Bates[2] M. H. Brooker[3]

Longitudinal optical (LO) mode frequencies in crystalline materials have been previously determined by five techniques:

1. measurements of ω_t (TO mode frequency), ϵ_0, and ϵ_∞ (ϵ = dielectric constant at low and high frequency), and use of the Lyddane-Sachs-Teller relation, $\omega_l = \omega_t(\epsilon_0/\epsilon_\infty)^{1/2}$;
2. varying ω_l (LO mode frequency) to obtain the best fit to reststrahlen reflectance data;
3. determination (by reflectance) of the frequency at which the real part of ϵ vanishes;
4. inelastic neutron scattering experiments;
5. polarized Raman spectra of single crystals.

Methods 1 to 4 are difficult to perform and are often subject to large errors or uncertainties in the frequencies obtained. LO modes can be accurately determined from Raman experiments, but this technique is limited to the modes that are both infrared and Raman active in acentric crystals, and the measurements should be made on single crystals. Berreman's[4] demonstration that the LO mode in LiF can be observed from absorption or polarized reflectance measurements on thin films using oblique angles of incidence indicated that this additional technique might be generally applied to other crystals. Polarized infrared reflectance spectra measured at near normal incidence have been used in this laboratory to determine the polarization characteristics of strong infrared transitions in single crystals of materials such as $NaBF_4$[5] and $KClO_3$.[6] It was shown in these studies that by limiting the maximum deviation from normal incidence of the infrared beam to about 15°, the observed frequencies agreed within experimental error (± 1 cm^{-1}) with those measured by transmission which were taken to be the transverse optical (TO) modes of the internal crystal vibrations.

Our initial PSR measurements using angles of incidence varying between 40 and 75° were made on thin films of alkali metal carbonates[7] which had been evaporated onto stainless steel substrates. The PSR spectra qualitatively resembled the polarized absorption and reflectance spectra of LiF inasmuch as reflection maxima were obtained at frequencies which corresponded to the LO mode frequencies determined by other techniques. To verify our apparent observations of LO modes in PSR spectra of the carbonates, we subsequently investigated the spectra of polycrystalline surfaces of various metal oxides, nitrates, and chlorates. The utility of PSR spectra in determining LO mode frequencies will be illustrated by discussing the spectra of those materials for which the LO modes of certain crystal vibrations have been determined by different means in independent studies.

Polarized specular reflectance (PSR) spectra and multiple internal reflectance (MIR) spectra were measured on a Perkin-Elmer 621 infrared spectrophotometer equipped with an AgBr polarizer. The steel plate with the deposited smooth dried sample was mounted on the optical bench of a Wilks model 9 MIR attachment. The angle of incidence as measured from the normal to the surface could be varied between 15 and 75° by moving both the sample and the mirrors. Although bands due to LO modes could be observed with incident angles as small as 30° from the normal, an incident angle of 75° was employed throughout these measurements to ob-

tain a maximum intensity from the LO modes. Reflectance spectra were measured with the polarizer set at 0 and 90° with respect to the plane of incidence. These two polarizations will be denoted by p and s respectively. Multiple internal reflectance spectra were obtained from finely powdered samples pressed against the surface of a KRS-5 prism with a face angle of 60°, placed in the Wilks model 9 MIR attachment. Peak frequencies measured from the MIR and PSR spectra are accurate to ±2 cm^{-1}.

The s and p polarized reflectance spectra and the MIR spectra of ZnO, CaO, and MgO and of $NaNO_3$ and $NaClO_3$ measured at 300°K are shown in Figs. 7.35 and 7.36 respectively. The results from these measurements are collected in Table 7.12 along with the LO and TO mode frequencies for the specified transitions previously reported. The LO mode frequencies for CaO and MgO reported by Wilkinson[8] were determined by noting the position at which the real part of the dielectric constant vanished (Drude's method[4]) as derived from reflection spectra; the frequencies and assignments for the optical modes of ZnO and $NaClO_3$ were based on single-crystal Raman data of Arguello et al.[9] and Hartwig et al.,[10] respectively, and the LO and TO modes of the ν_3 vibration in $NaNO_3$ were determined from analysis of single crystal reflection data of Ketelaar et al.[11]

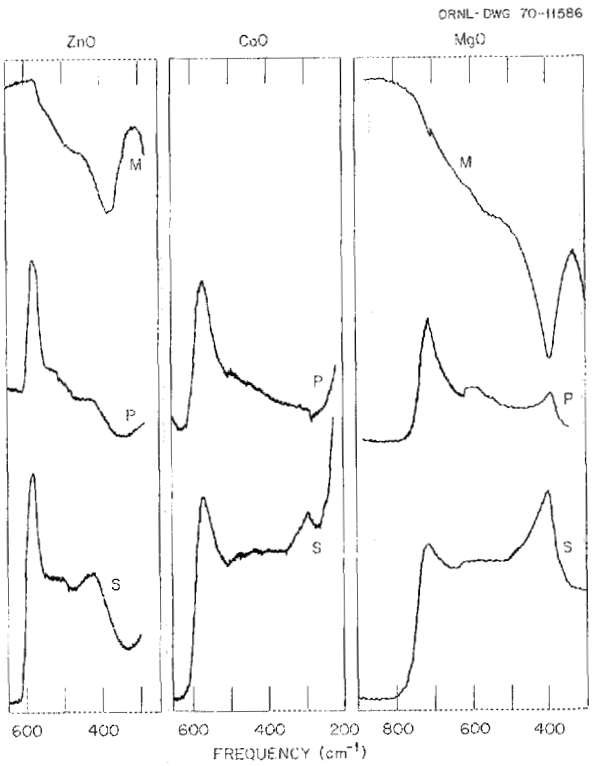

Fig. 7.35. MIR (M) and *p* and *s* polarized specular infrared reflectance spectra of ZnO, CaO, and MgO polycrystalline surfaces.

Fig. 7.36. MIR (M) and *p* and *s* polarized specular infrared reflectance spectra of $NaNO_3$ and $NaClO_3$ polycrystalline surfaces.

The data collected in Table 7.12 show remarkable agreement between the LO modes measured in our PSR spectra and the LO modes observed by other techniques. In the case of CaO, MgO, and $NaNO_3$, we believe that our measurements are more accurate than those previously reported. For materials such as $NaClO_3$ or ZnO in which several LO and TO modes occur in close proximity, an unambiguous assignment of the observed bands cannot be made from PSR data alone. However, for crystals which have only one optical mode (CaO and MgO) or in which the optical modes occur in isolated spectral regions ($NaNO_3$), the results of our measurements show that the PSR technique provides a simple method for determining LO mode frequencies. We also measured the PSR spectra of

Table 7.12. LO and TO mode frequencies as measured by PSR and MIR compared with the frequencies and assignments previously reported

All measurements at 300°K

Material	Frequency (cm^{-1}) PSR p	PSR s	MIR	Other	Assignment
ZnO	585	585		585*	LO, quasi A_1, E_1
		413		413	TO, E_1
			385	380	TO, A_1
CaO	575	568		577†	LO
		290	‡	286	TO
MgO	725	718		717†	LO
		402	396	403	TO
$NaNO_3$	1458	1458		1450*	LO } $\nu_3(E_u)$
		1355	1350	1353	TO } $\nu_3(E_u)$
$NaClO_3$	1030	1025		1030*	LO $\nu_3{}^a(F)$
			995		$2\nu_4$
			988	988	TO $\nu_3{}^a(F)$
	978			983	LO $\nu_3{}^b(F)$
		970	970		?
			962	965	TO $\nu_3{}^b(F)$
	939	938		940	LO ν_1
			936	936	TO ν_1
	629	626		629	LO ν_2
			623	623	TO ν_2
	486			490	LO ν_4
		483	482	489	TO ν_4

*Polarized Raman.
†Analysis of infrared reflection spectra.
‡TO mode of CaO below the low-frequency limit of MIR measurements.

both evaporated thin films and pressed surfaces of LiF. Our results qualitatively agree with those of Berreman,[4] although the peak position of the LO mode appears to shift to a maximum of 684 cm^{-1} as the angle of incidence is increased from 45 to about 60°. The frequency reported by Berreman was 669 cm^{-1} for an incident angle of 34°.[4]

The MIR spectra measured for the materials listed in Table 7.12 gave no evidence of absorption due to the LO components. Weak absorption around 500 cm^{-1} is mostly due to the KRS-5 prism (Figs. 7.35 and 7.36). It has been previously demonstrated[1,2] that the MIR technique is a superior method for measuring infrared TO mode frequencies. This contention is further supported by the results of the present investigations and from recent studies of crystalline carbonates.[7] It thus appears that a combination of PSR and MIR measurements provides simple and convenient means for determining LO and TO mode frequencies in polycrystalline materials.

1. Abstracted from a paper to be published in *J. Phys. Chem. Solids* (1971).
2. Director's Division.
3. Visiting scientist, National Research Council of Canada Postdoctoral Fellow, 1969–71.
4. D. W. Berreman, *Phys. Rev.* **130,** 2193 (1963).
5. J. B. Bates, *J. Chem. Phys.* (1971).
6. J. B. Bates, *J. Chem. Phys.* (1971); also, "Polarized Vibrational Spectra of Potassium Chlorate," the following contribution, this report.
7. M. H. Brooker and J. B. Bates, *J. Chem. Phys.* (1971).
8. G. R. Wilkinson in *Molecular Spectroscopy – Proceedings of a Conference Held at Brighton, England, 7–19 April 1968,* ed. by P. Hepple, The Institute of Petroleum, London, 1968.
9. C. A. Arguello, D. L. Rousseau, and S. P. S. Porto, *Phys. Rev.* **181,** 1351 (1969).
10. C. M. Hartwig, D. L. Rosseau, and S. P. S. Porto, ibid. **188,** 1328 (1969).
11. J. A. A. Ketelaar, C. Haas, and J. Fahrenfort, *Physica (Utrecht)* **20,** 1259 (1954).
12. M. H. Brooker, *J. Chem. Phys.* **53,** 4100 (1970).

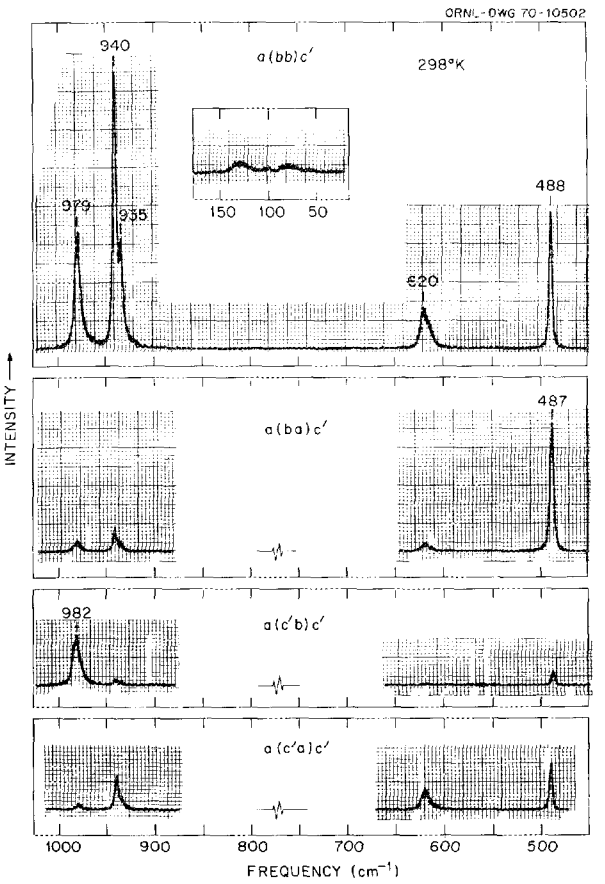

Fig. 7.37. Polarized Raman spectra of $KClO_3$ at 298°K.

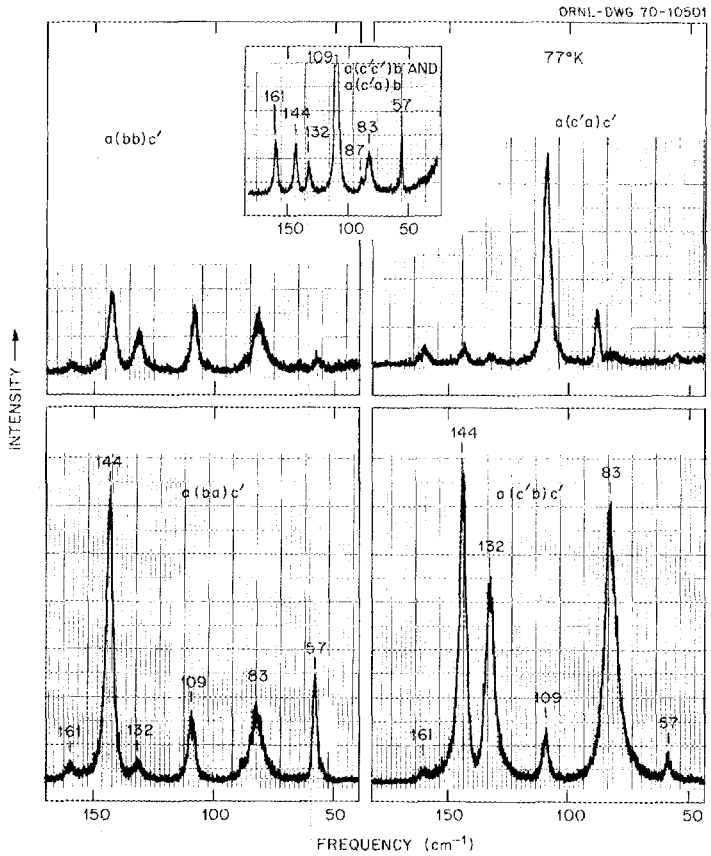

Fig. 7.38. Low-frequency polarized Raman spectra of $KClO_3$ at 77°K.

POLARIZED VIBRATIONAL SPECTRA OF POTASSIUM CHLORATE[1]

J. B. Bates[2]

The Raman spectra of a single crystal of $KClO_3$ were measured in the region above 30 cm^{-1} at 298 and 77°K. Spectra measured at 298°K in the internal mode region are shown in Fig. 7.37, and spectra measured in the external mode region at 77°K are shown in Fig. 7.38. Polarized infrared spectra in the internal mode region were measured at 298°K by specular reflection using an angle of incidence of 15°. The results of these measurements are shown in Fig. 7.39.

Assignments for all the crystal vibrations that are derived from correlation field splitting of the (internal) ClO_3^- modes were made from the results of the polarization measurements. These assignments are given in Fig. 7.40. The $KClO_3$ crystal lattice has space group symmetry C_{2h}^2 $(P21/m)$, with two equivalent ClO_3^- ions in the unit cell located on C_s sites. The ν_1 (A_1), ν_2 (A_1), ν_3 (E), and ν_4 (E) fundamental modes of the ClO_3^- ion which has C_{3v} symmetry give rise to $4\,A_g + 2\,B_g + 2\,A_u + 4\,B_u$ internal C_{2h} optical $(k = 0)$ modes in the crystal lattice. Estimates of the site state frequencies (Fig. 7.40) were made by taking the average value of the frequencies of each pair of factor group states which arise from a common site state.

The ν_1 frequency of $^{37}Cl^{16}O_3^-$ ion was observed at 935 cm^{-1} at 298°K (Fig. 7.37). The ν_1 modes of the $^{35}Cl^{16}O_2{}^{18}O^-$ and $^{37}Cl^{16}O_2{}^{18}O^-$ species were found to be split with components at 922 and 920 cm^{-1} and at 914 and 912 cm^{-1} respectively. The origin of this splitting was ascribed to an orientational effect in the crystal lattice. Similar effects have been observed for the HOD modes in hydrated crystals in which the water molecules occupy sites of C_1 symmetry.[3]

The $k = 0$ lattice modes of $KClO_3$ derived from motions of the K^+ and ClO_3^- sublattices are described

by $\Gamma(C_{2h}) = 5\ A_g + 4\ B_g + 3\ A_u + 3\ B_u$. From the low-temperature polarized Raman spectra (Fig. 7.38), 3 A_g + 4 B_g lattice modes were observed in the region below 200 cm^{-1}. The bands at 109 and 87 cm^{-1} and at 144, 132, and 83 cm^{-1} were assigned as librational-type modes having A_g and B_g symmetry respectively. The bands at 160 and 57 cm^{-1} having A_g and B_g symmetry, respectively, were assigned as due to translatory-type motion of the K^+ sublattice moving against the ClO_3^- sublattice.

1. Abstracted from a paper to be published in *J. Chem. Phys.* (1971).
2. Director's Division.
3. J. B. Bates and R. K. Khanna, *Inorg. Chem.* 9, 1376 (1970).

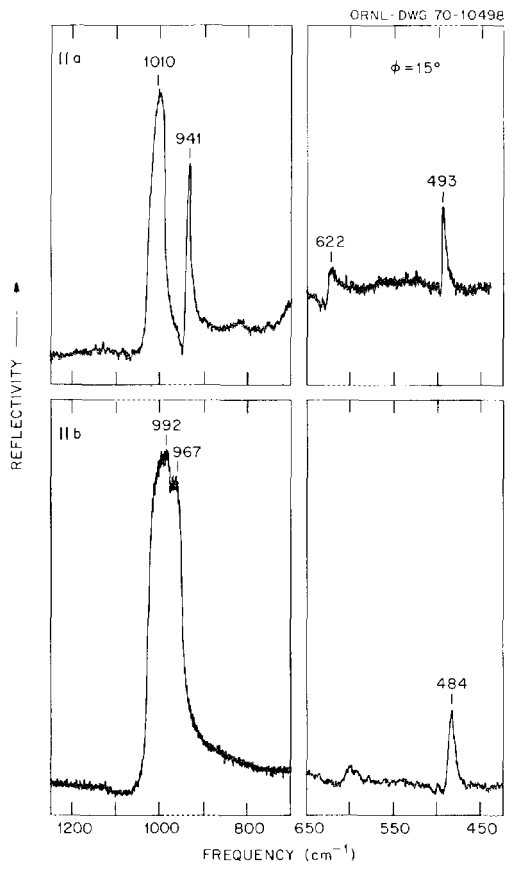

Fig. 7.39. Polarized infrared reflection spectra of $KClO_3$ at 298°K using an angle of incidence of 15°.

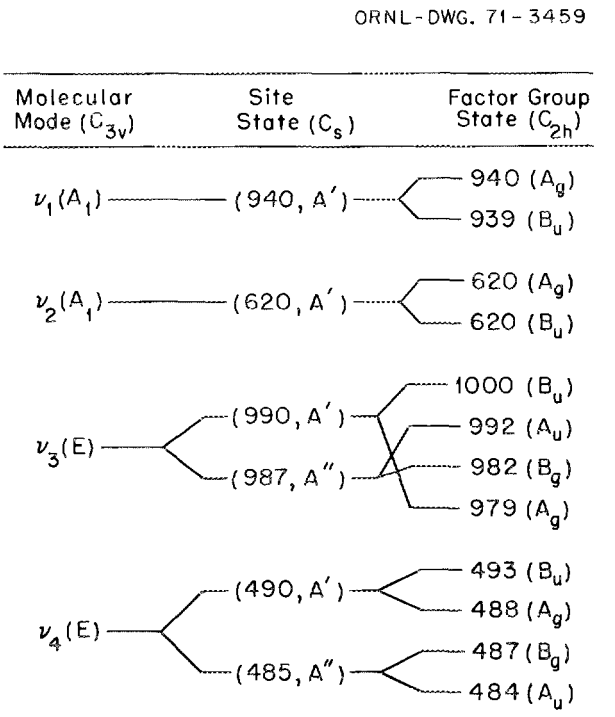

Fig. 7.40. Site and correlation field splitting of the internal ClO_3^- modes in $KClO_3$. Frequencies in cm^{-1}. Site state frequencies estimated by averaging the pair of c.f. components originating from a common site state.

THE CRYSTAL STRUCTURE OF $Sr(NO_3)_2$, $Ca(NO_3)_2$, $Ba(NO_3)_2$, AND $Pb(NO_3)_2$: AN INFRARED AND RAMAN STUDY

M. H. Brooker[1] John B. Bates[2]

The nitrates of strontium, calcium,[3] barium, and lead have long been considered to crystallize as isomorphous cubic crystals with cubic symmetry and space group T_h^6.[4,5] Recently, Birnstock[6] concluded from a neutron diffraction study that the space group for $Ba(NO_3)_2$ was T^4, which means that the crystal would not have a center of symmetry. Birnstock also concluded that the nitrate group was no longer planar but pyramidal with the nitrogen being 0.1 Å above the oxygen plane. Previous infrared and Raman measurements on these salts agree with a factor group analysis based on the T_h^6 structure,[7,8] although attempts have been made to force the infrared and Raman data to fit the T^4 structure.[9]

The presence of a center of symmetry is not easily determined by infrared and Raman spectroscopy, but

Table 7.13. Vibrational frequencies (cm^{-1}) for $Ba(NO_3)_2$

Infrared[a] Transmission 77°K	Infrared[a] Transmission 300°K	PSR,[c] 300°K	Raman[b] 77°K	Raman[b] 300°K	Assignments based on T_h factor group	
	33[d]				F_u	
	38[d]				F_u	
	49[d]				F_u	
			80	80	F_g	
	81[d]				F_u	
	97[d]				F_u	
			103		F_g	
			133	127	E_g	
			137	133	F_g	
	139[d]				F_u	
			147	141	E_g	
			149		F_g	
	157[d]				F_u	
729.0					TO F_u^1	
730.3	731[e]				TO F_u^2	
		730			LO $(F_u^1 + F_u^2)$	ν_4
			732.0	730.5	E_g	
			734.0	732.0	F_g (2)	
818	817[e]				TO F_u	
		817			LO F_u	
			818		F_g	ν_2
			821	820	A_g	
	1047[e] (vw)				F_u	
			~1048	1047.5	F_g	ν_1
			1048.5	1048.5	A_g	
1345	1345[e]				TO F_u^3	
		1389			LO F_u^4	
1415	1415[e]				TO F_u^4	
		1437			LO F_u^3	ν_3
			1358	1357	E_g	
			1391	1388	F_g	
			1410	1405	F_g	
1462	1462[e]	1463				$2\nu_4$
			1462		A_g	
			1634	1634	A_g	$2\nu_2$
			1639	1638	A_g	

[a]Infrared measurements performed with powdered samples.
[b]Raman measurements performed with oriented single crystals.
[c]Polarized specular reflection data, angle of incidence ca. 75° from the normal to the surface.
[d]Data from D. Bloor, *Spectrochim. Acta* **21**, 133 (1965).
[e]Combined transmission and MIR data. Frequency agreement between the two measurements was ±1 cm^{-1} or better. vw = very weak.

two criteria can be used: (1) noncoincidence of infrared and Raman bands, that is, the rule of mutual exclusion, and (2) failure to observe longitudinal optical (LO) modes in the Raman spectrum, although this method is less certain since the LO modes may be too weak to be observed in some cases. LO modes occur due to the interaction of the electromagnetic field of the incident radiation with the field associated with the polar vibrational modes of the crystal. The intensity of LO modes and the separation of the LO mode with its associated TO (transverse optical) mode are related to the magnitude of the dipole moment change. For centrosymmetric crystals, there is no dipole moment associated with Raman bands, so that TO and LO modes are coincident (the LO mode will still be observed in the infrared spectrum).

Hartwig et al.[10] have recently reported the infrared and Raman spectra of single-crystal $NaClO_3$ which has the T^4 space group and a structure very similar to that proposed for $Ba(NO_3)_2$ by Birnstock. These authors readily observed the LO mode associated with the strong ν_3 vibration of ClO_3^- ion at 1030 cm^{-1} in both the infrared and Raman spectra. The band is quite intense in the Raman spectrum. We have recorded the Raman spectrum of polycrystalline $NaClO_3$ and find this mode to be as intense as the TO modes with which it is associated. It is logical to assume that if the above nitrate crystals have the acentric structure proposed by Birnstock, then the LO mode should appear in the ν_3 region of NO_3^- in the Raman spectrum and should correspond to the infrared LO mode frequency.

Infrared spectra have been recorded for each of the anhydrous polycrystalline nitrates at 300 and 77°K. Multiple internal reflection (MIR) and polarized specular reflection (PSR) measurements have been employed to measure accurately the TO and LO mode frequencies in the infrared.[11] Raman spectra have been recorded for polycrystalline samples for each salt and for oriented single crystals of $Sr(NO_3)_2$, $Ba(NO_3)_2$, and $Pb(NO_3)_2$ at 300 and 77°K.

Once the LO mode frequencies had been determined from PSR infrared measurements, the same region of the Raman spectrum was scanned with very high sensitivity. No evidence of the LO modes in the Raman spectra could be detected. In addition, many of the infrared and Raman bands were found to be noncoincident. Both these facts are in accord with a centrosymmetric structure for these salts. Depolarization measurements on the oriented single crystals were in excellent agreement with a factor group analysis based on the T_h^6 space group. Infrared and Raman frequency data for $Ba(NO_3)_2$ are collected in Table 7.13; the data for strontium and lead nitrates will be presented elsewhere.[12]

---

1. Visiting scientist, National Research Council of Canada Postdoctoral Fellow, 1969–71.
2. Director's Division.
3. $Ca(NO_3)_2$ undergoes phase transitions below room temperature. See M. H. Brooker, "Raman and Infrared Spectra of Anhydrous $Zn(NO_3)_2$, $Cd(NO_3)_2$, and $Ca(NO_3)_2$: A Study of the Phase Changes in $Ca(NO_3)_2$," the following contribution, this report.
4. W. C. Hamilton, *Acta Crystallogr.* **10**, 103 (1957).
5. G. Lutz, *Z. Kristallogr. Kristallgeometrie Kristallphys. Kristallchem.* **114**, 232 (1960).
6. R. Birnstock, ibid. **124**, 310 (1967).
7. M. H. Brooker, D. E. Irish, and G. E. Boyd, *J. Chem. Phys.* **53**, 1083 (1970).
8. L. D. Vinh and P. Majou, *C. R. Acad. Sci., Ser. B* **270**, 1341 (1970).
9. C. J. H. Schutte, *Z. Kristallogr. Kristallgeometrie Kristallphys. Kristallchem.* **126**, 397 (1968).
10. C. M. Hartwig, D. L. Rousseau, and S. P. S. Porto, *Phys. Rev.* **188**, 1328 (1969).
11. J. B. Bates and M. H. Brooker, *J. Phys. Chem. Solids* (in press); also "Determination of Longitudinal Optical Mode Frequencies by Polarized Specular Reflectance (PSR) Infrared Spectroscopy," another contribution in this section, this report.
12. M. H. Brooker and J. B. Bates, to be submitted to *J. Chem. Phys.*

RAMAN AND INFRARED SPECTRA OF ANHYDROUS $Zn(NO_3)_2$, $Cd(NO_3)_2$, AND $Ca(NO_3)_2$: A STUDY OF THE PHASE CHANGES IN $Ca(NO_3)_2$

M. H. Brooker[1]

The nitrate ion has been successfully employed as a "probe" in vibrational spectroscopic studies of solids, molten salts, and aqueous solutions.[2] In this technique, the spectrum generated by the nitrate ion in an unknown environment is interpreted by comparisons with spectra of the ion in known environments. Therefore, it is desirable to obtain Raman and infrared spectra for the nitrate ion in as wide a range of environments as possible. In this study infrared and Raman spectra have been obtained for anhydrous polycrystalline $Ca(NO_3)_2$, $Cd(NO_3)_2$, and $Zn(NO_3)_2$. The vibrational spectrum of $Ca(NO_3)_2$ at room temperature is well known and is in accord with the reported crystal structure.[3] Comparison of the vibrational spectra of $Ca(NO_3)_2$ at 300°K with those of $Ca(NO_3)_2$ at 200 and 77°K, and of $Cd(NO_3)_2$ and $Zn(NO_3)_2$ at 300 and 77°K yields information about the structural differences between these salts.

Until recently the measurement of Raman spectra of solids was a difficult and unrewarding process, but development of laser Raman spectroscopy has simplified the situation so that in many cases it is now easier to obtain Raman than infrared spectra. Laser Raman techniques are especially valuable for difficult anhydrous materials since the samples may be readily sealed in vacuo in quartz or Pyrex tubes with a minimum of sample handling. Laser Raman spectra have been recorded for anhydrous $Ca(NO_3)_2$ at 77, 200, and 300°K (Fig. 7.41) and for $Cd(NO_3)_2$ and $Zn(NO_3)_2$ at 77 and 300°K (Figs. 7.42–7.44). Samples were sealed in vacuo in thin-walled capillary tubes.[4] Sample excitation was achieved with the 4880-Å line of a Coherent Radiation 52B gas laser, and spectra were recorded on the Jarrell-Ash model 25-300 Raman spectrometer. Infrared spectra also have been recorded for the three anhydrous salts, with results similar to those previously reported.[5] Generally, the Raman spectra were easier to obtain and gave greater definition than the infrared spectra. This is most obvious in the region of the symmetric stretching vibration, ca. 1050 cm^{-1}, where the bands are very intense in the Raman spectra but weak or absent in the infrared.

Very little structural evidence is available for any of these salts. X-ray diffraction studies by Weigel et al.[6] indicate the space group T_h^6 for $Cd(NO_3)_2$. The room-temperature form of $Ca(NO_3)_2$ is also considered to have the T_h^6 space group, and this premise is supported by infrared and Raman studies of the isostructural salts $Sr(NO_3)_2$, $Ba(NO_3)_2$, and $Pb(NO_3)_2$.[3] In view of the many differences between the Raman spectrum of $Ca(NO_3)_2$ at room temperature (Fig. 7.41) and the Raman spectra of $Ca(NO_3)_2$ below room temperature (Fig. 7.41), and $Cd(NO_3)_2$ and $Zn(NO_3)_2$ (Figs. 7.42–7.44), it would appear that the salts have different structures in each case. Vibrational frequencies of $Ca(NO_3)_2$ at room temperature are in excellent agreement with a factor group analysis based on the T_h^6 space group.[3] Below room temperature,

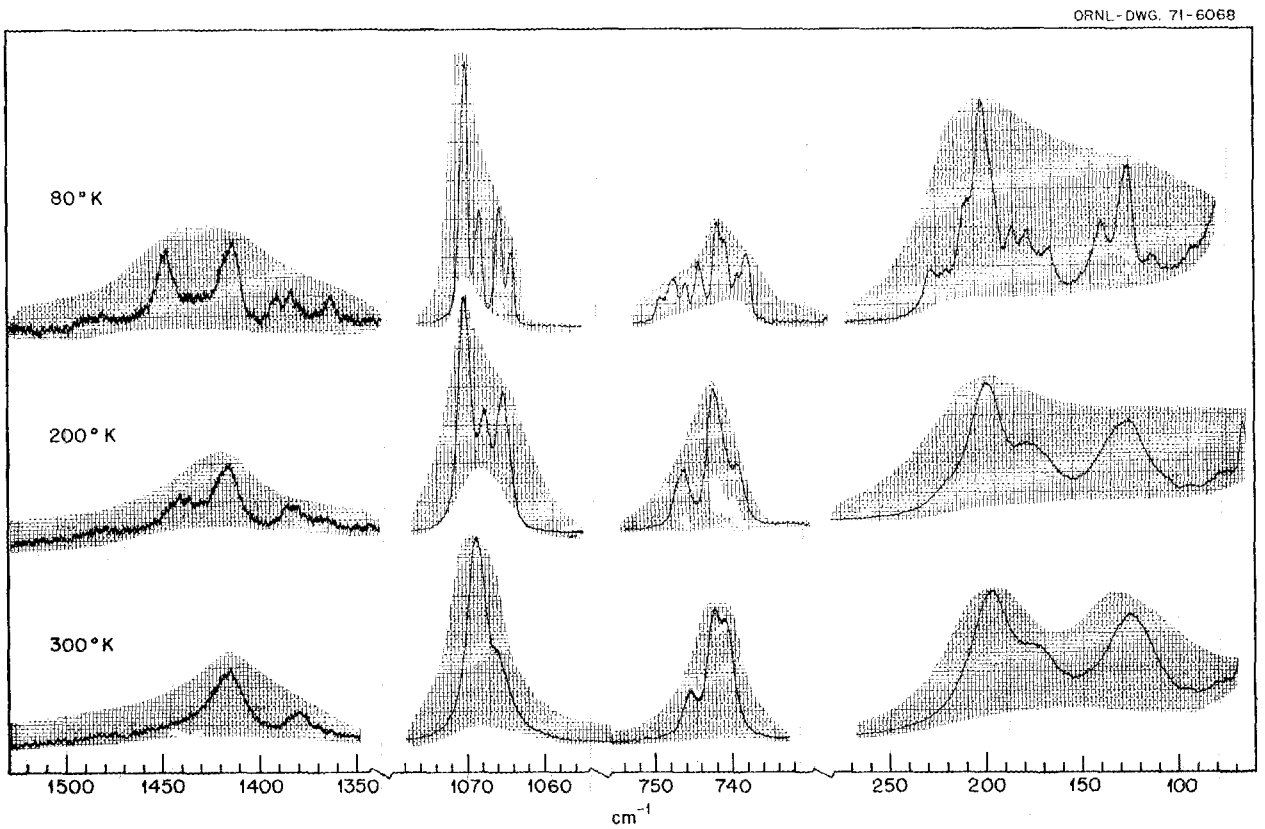

Fig. 7.41. Photograph of portions of the Raman spectra of anhydrous $Ca(NO_3)_2$ at 77, 200, and 300°K. Instrument conditions: 0–200 cm^{-1}: 2.0-cm^{-1} slit, 1×10^4 counts/sec, 2-sec time constant. 700-cm^{-1} region: 1.0-cm^{-1} slit, 2×10^3 counts/sec, 2-sec time constant. 1050-cm^{-1} region: 1.0-cm^{-1} slit, 1×10^4 counts/sec, 0.5-sec time constant. 1400-cm^{-1} region: 2.0-cm^{-1} slit, 2×10^3 counts/sec, 2-sec time constant.

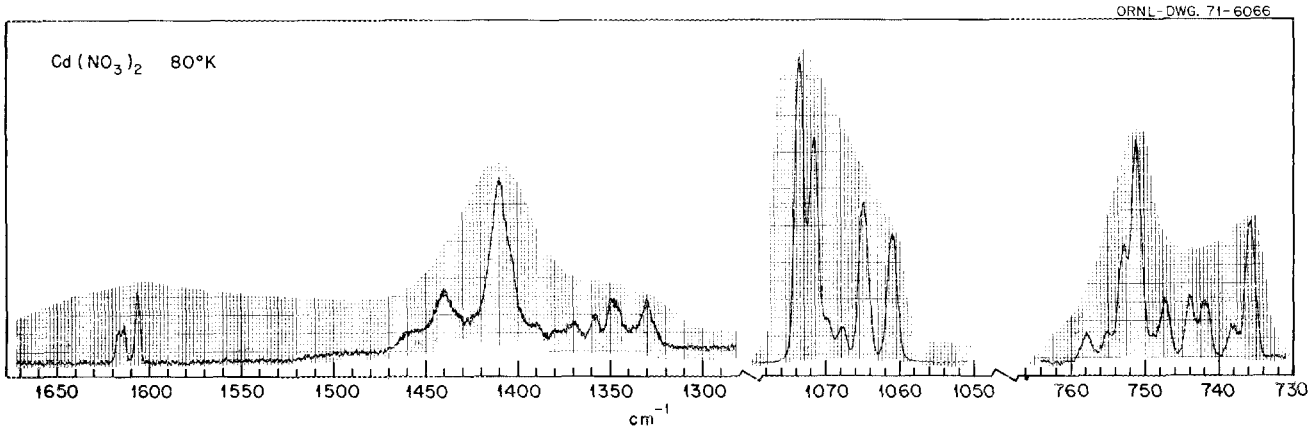

Fig. 7.42. Photograph of portions of the Raman spectrum of anhydrous $Cd(NO_3)_2$ at 77°K. Instrument conditions: 700-cm^{-1} region: 1.0-cm^{-1} slit, 2×10^3 counts/sec, 2-sec time constant. 1000-cm^{-1} region: 1.0-cm^{-1} slit, 1×10^4 counts/sec, 0.5-sec time constant. 1400-cm^{-1} region: 2.0-cm^{-1} slit, 5×10^3 counts/sec, 2-sec time constant.

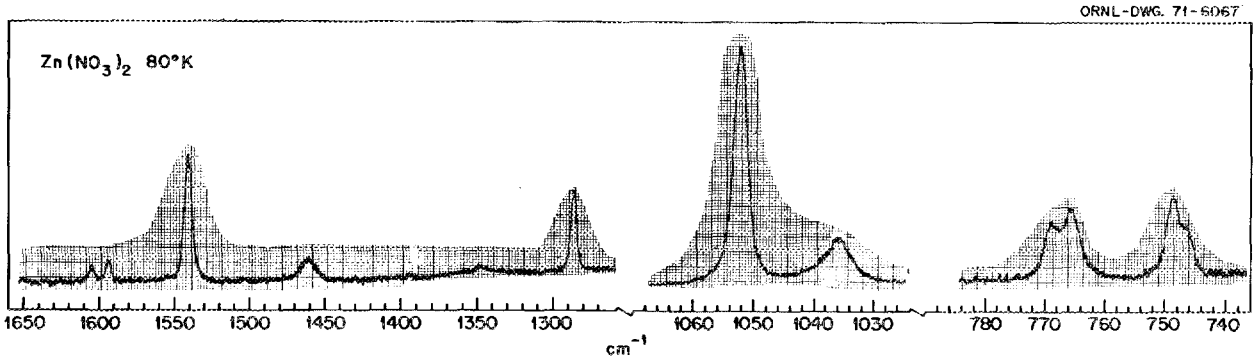

Fig. 7.43. Photograph of portions of the Raman spectrum of anhydrous $Zn(NO_3)_2$ at 77°K. Instrument conditions as in Fig. 7.42.

new bands appear which indicate that $Ca(NO_3)_2$ undergoes two phase changes between 77 and 300°K. Shomate and Kelley[7] detected humps in heat capacity data at 88.5 and 287.8°K which presumably are the transition temperatures of the phase changes. $Cd(NO_3)_2$ and $Zn(NO_3)_2$ do not appear to undergo phase changes between 300 and 77°K.

In the room-temperature form of $Ca(NO_3)_2$, the calcium atom is surrounded by 12 equivalent oxygens from 6 equivalent nitrate groups. The new band which is present at 1066.1 cm^{-1} at 200°K is characteristic of a nitrate ion in a new site closer to the calcium atom. On the basis of relative intensities, it would appear that two nitrate ions are now closer to the calcium atoms than the other four. A distorted octahedron with the two axial groups having metal-oxygen distances less than the four equatorial groups is suggested. However, the similarity of the Raman and infrared spectra at 200 and 300°K, except in the 1050-cm^{-1} region, indicates that the phase change at 287.8°K is very subtle, and the actual differences between the nitrate groups in this phase are expected to be small. The phase change at 88.5°K is much more pronounced: Two distinct sets of bands (1071.0, 1068.7 cm^{-1} and 1066.3, 1064.6 cm^{-1}) are apparent in the symmetric stretching region with approximate intensity ratios of 2:1. Arrangement of the nitrate groups into two nonequivalent sets is now complete. The coupling of the vibrational modes of the nitrate ions is greatly altered, as indicated by the increase in the number of bands in the region of each nitrate fundamental.

The similarity of the Raman spectrum of $Ca(NO_3)_2$ at 77°K to the $Cd(NO_3)_2$ spectra suggests like structures. Even for $Zn(NO_3)_2$, the separation of the symmetric stretching region into two distinct sites indicates that the nitrate groups are arranged into two

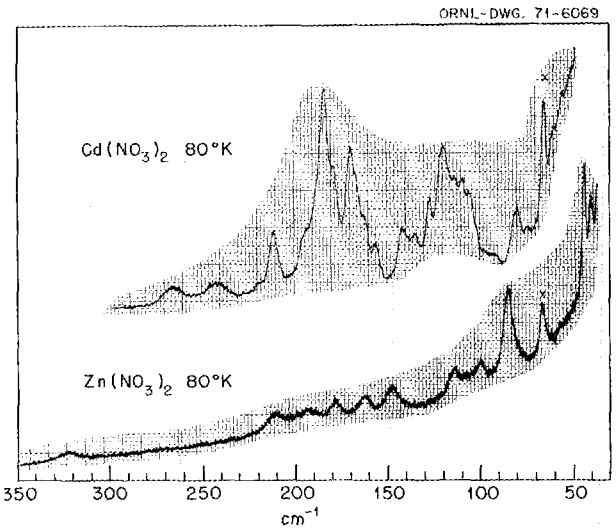

Fig. 7.44. Photograph of the low-frequency portion of the Raman spectra of $Cd(NO_3)_2$ and $Zn(NO_3)_2$ at 77°K. Instrument conditions: $Cd(NO_3)_2$: 2.0-cm^{-1} slit, 5×10^3 counts/sec, 2-sec time constant. $Zn(NO_3)_2$: 2.0-cm^{-1} slit, 1×10^4 counts/sec, 0.5-sec time constant.

groups: four equatorial and two axial. The relative simplicity of the $Zn(NO_3)_2$ spectrum, however, indicates that the nitrate groups are coupled in a more symmetric manner in this compound than in $Cd(NO_3)_2$ and $Ca(NO_3)_2$ at 77°K.

Finally, it is worth noting the presence of weak bands in the lattice region at frequencies somewhat higher than is usual for lattice modes: $Ca(NO_3)_2$ at 77°K, 229 cm^{-1}; $Cd(NO_3)_2$ at 77°K, 242 and 266 cm^{-1}; $Zn(NO_3)_2$ at 77°K, 322 cm^{-1}. These bands are probably associated with vibrational modes of weak metal-oxygen vibrations.

1. Visiting scientist, National Research Council of Canada Postdoctoral Fellow, 1969–71.

2. D. E. Irish, chap. 9 in vol. 2 of *Ionic Interactions: From Dilute Solution to Molten Salts*, ed. by S. Petrucci, Academic, New York, 1971.

3. M. H. Brooker, D. E. Irish, and G. E. Boyd, *J. Chem. Phys.* **53**, 1083 (1970), and references therein; *Chem. Div. Annu. Progr. Rep. May 20, 1970*, ORNL-4581, p. 156.

4. Anhydrous $Cd(NO_3)_2$ and $Zn(NO_3)_2$ were prepared by D. E. LaValle, Analytical Chemistry Division.

5. C. C. Addison and B. M. Gatehouse, *J. Chem. Soc. London* **1960**, 613.

6. D. Weigel, B. Imelik, and M. Prettre, *Bull. Soc. Chim. Fr.* 2600 (1964).

7. C. H. Shomate and K. K. Kelley, *J. Amer. Chem. Soc.* **66**, 1490 (1944).

MICROWAVE AND RADIO-FREQUENCY SPECTROSCOPY

PARAMAGNETIC RESONANCE STUDIES OF LIQUIDS DURING PHOTOLYSIS

Ralph Livingston Henry Zeldes
Jürgen K. Dohrmann[1]

Paramagnetic resonance spectra of a variety of short-lived radicals formed by photolysis of solutions of alloxan and of parabanic acid have been studied. Photoreduction of alloxan in aqueous solutions containing small amounts of isopropyl alcohol and acetone and at pH values greater than 2 gives a spectrum of 7 lines ascribed to the anion **1**. At very low values of pH, this radical is protonated to give the neutral radical **2**, and

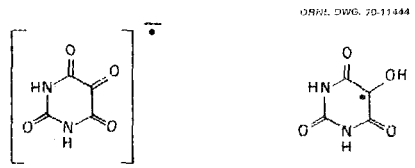

1 **2**

the 7-line spectrum becomes a 15-line spectrum. At intermediate pH's a rapid-exchange average of the two spectra is observed as a consequence of fast equilibration. The p*K* of the protonated species is 0.5. Aqueous solutions of parabanic acid containing isopropyl alcohol behave similarly. Above a pH of 3 a 15-line spectrum is obtained from anion **3**. It protonates at very low pH's to give a different 15-line spectrum from neutral radical **4**. The p*K* is 1.7. At intermediate pH values, a single

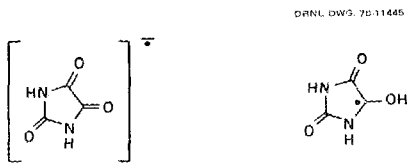

3 **4**

spectrum appears which is the result of rapid exchange between the two radicals. Photolysis of solutions of alloxanic acid formed by rearrangement of alloxan gives the same radicals that are formed from parabanic acid. If parabanic acid is photolyzed in isopropyl alcohol solution, radicals **3** and **4** are produced, but the

exchange rate becomes very slow, and a mixture of the two spectra is present. The effect on the exchange rate of adding water and acid has been studied. Similar radicals have also been formed from *N*-methylparabanic acid. More details of this work will appear elsewhere.[2]

Paramagnetic resonance spectra of short-lived free radicals made from uracil, orotic acid (uracil-6-carboxylic acid), iso-orotic acid (uracil-5-carboxylic acid), and thymine have been studied upon photolysis of solutions near room temperature. When these pyrimidines are photolyzed in hydrogen-donating solvents (isopropyl alcohol, ethyl alcohol, and *p*-dioxane), they abstract a hydrogen from the solvent, and two different radicals are observed due to the addition of hydrogen to the pyrimidine and to the loss of hydrogen from the solvent molecule. Addition appears to be at the 5 position for uracil and unequivocally at the 5 position for orotic acid. In iso-orotic acid the hydrogen addition is to the oxygen at the 4 position. When these pyrimidines are photolyzed in aqueous solutions containing hydrogen peroxide, ·OH is formed which then produces radicals from the pyrimidines by addition. In the case of aqueous uracil over the pH range of 1 to 7, the predominant process is addition of ·OH at the 5 position, but there is also a small yield of the radical from addition at the 6 position. At high pH (8 to 10) an anion radical is formed. Similarly, ·OH adds at the 5 position in orotic acid, and an anion radical is present at high values of pH. In iso-orotic acid the two radicals formed by addition at the 5 position and at the 6 position are observed. The spectra and chemical behavior of many of the radicals depend upon pH, and dynamic exchange phenomena are present. Hyperfine couplings and *g* values have been measured. Further details will appear elsewhere.[3]

The light source for the photolytic work has now been provided with a rotating sector that chops the light so that direct physical measurement of radical lifetimes can be made. This equipment has been applied to the study of spectra from tartaric acid in aqueous solution. As explained earlier,[4,5] upon photolysis of aqueous tartaric acid a carboxyl group is split off, leaving HOOCCH(OH)$\dot{C}$H(OH), radical A. This radical converts to an aldehyde form, HOOC$\dot{C}$HCHO, by an acid-catalyzed reaction. At high acidity, where the conversion is rapid, the mean life of radical A is of the order of a microsecond, and its spectrum appears entirely in emission. At low acidity, where the mean life becomes long, the Zeeman states achieve thermal equilibrium, and the spectrum is, as normally expected, an absorption spectrum. Initially it was felt that the rotating sector would be far too slow for a valid study of radical A. For example, when this radical is present at low acidity, where the spectrum is in absorption at steady state, we would expect that when the light is first switched on by the sector a line of the spectrum would initially appear in emission but within several microseconds would reverse and grow as an absorption line, quickly reaching steady state. Unexpectedly, we found upon switching the light on that the signal grew as an emission line, taking an appreciable fraction of a millisecond to achieve a maximum in emission. Over the next few milliseconds the signal reversed sign and grew to steady state as an absorption signal. More unexpectedly, upon switching the light off, the signal did not simply decay, but the intensity of absorption increased to a new peak in an appreciable fraction of a millisecond before decaying. These findings suggest that there is a precursor for radical A with a lifetime of an appreciable fraction of a millisecond. Moreover, the precursor produces radical A in an emitting state. The likely precursor is a triplet state of tartaric acid. The studies have also shown that there is an induction period for the formation of the aldehyde radical. There is a similar induction period for the decay when the light is switched off. This delay is consistent with there being a relatively long-lived precursor for radical A.

Computer programs are being developed which will be useful in analyzing complex electron paramagnetic resonance spectra encountered in the study of liquids. The programs calculate energies to second-order perturbation theory for any number of groups of equivalent nuclei in a radical. Any number of nuclei with any spin may be in each group. As an option the second-order structure produced by any group may be treated as single lines, each located at the center of gravity of the corresponding second-order structure. One program receives trial parameters for a radical and outputs ordered resonance fields and the corresponding line strengths, second-order corrections, and the total spin and total magnetic quantum number of each group of equivalent nuclei. This program optionally receives experimental data consisting of line positions in the spectrum and their resonance fields and frequencies. It then calculates the best parameters describing the data for a prescribed (as described by input) number of groups of equivalent nuclei with prescribed numbers of nuclei and nuclear spins. A least-squares criterion is used. An error analysis is also given. A second program gives plots which simulate experimental spectra. Any number of radicals, each with any Lorentzian width, may be in the spectrum. Any number of spectra may be drawn one above the other with a common field axis for ease of comparison. Experimental data and stick

spectra (made up of vertical lines) may also be plotted. This program also gives a printout describing the spectra. The programs are now being tested and refined. They have been very helpful in analyzing complex spectra under study in solutions containing pyridine during photoylsis.

1. Visiting scientist from Institut für Physikalische Chemie der Freien Universität Berlin.

2. J. K. Dohrmann, R. Livingston, and H. Zeldes, "Paramagnetic Resonance Study of Liquids during Photolysis. XII. Alloxan, Parabanic Acid, and Related Compounds," accepted for publication in the *Journal of the American Chemical Society.*

3. J. K. Dohrmann and R. Livingston, "Paramagnetic Resonance Study of Liquids during Photolysis. XIII. Uracil and Derivatives," accepted for publication in the *Journal of the American Chemical Society.*

4. R. Livingston, H. Zeldes, and J. K. Dohrmann, *Chem. Div. Annu. Progr. Rep. May 20, 1970,* ORNL-4581, p. 176.

5. R. Livingston and H. Zeldes, *J. Chem. Phys.* 53, 1406 (1970).

PARAMAGNETIC RESONANCE STUDIES OF GAMMA-IRRADIATED INORGANIC SINGLE CRYSTALS AT LOW TEMPERATURE

R. W. Holmberg

An electron paramagnetic resonance (EPR) study of the radicals formed when single crystals of $KHCO_3$ are gamma irradiated at 77°K has been completed. Hyperfine and g tensors for the various line groups have been evaluated, and the tentative identifications of the radicals reported earlier[1] have been placed on a firmer basis. Most of the radiation damage as seen by EPR can be accounted for by an electron-excess radical $\dot{C}O_3^{3-}$ and an electron-deficient radical $(HCO_3)_2\cdot^-$ which are formed and stably trapped in the crystal in roughly equal amounts. When the crystal is warmed to 130°K, both radicals undergo simultaneous and irreversible decay, suggesting that they disappear by a mechanism involving the transfer of an electron from $\dot{C}O_3^{3-}$ to $(HCO_3)_2\cdot^-$. It would seem, however, that only part of the decay is attributable to such a mechanism, for after a few hours at 130°K, although all of the $(HCO_3)_2\cdot^-$ disappears, substantial amounts of $\dot{C}O_3^{3-}$ remain.

Lesser amounts of a species which has been identified as the neutral bicarbonate radical $HCO_3\cdot$ were also found at 77°K. This radical was previously[1,2] believed to be $\dot{C}O_3^-$. Its identification as $HCO_3\cdot$ is based primarily on the observation of a small proton hyperfine splitting in its EPR spectrum that was not noted earlier, and is consistent with the large deviation from axial symmetry of its g tensor and with measured ^{17}O hyperfine splittings.[3] The radical is trapped in two physically different, non-symmetry-related sites in the crystal. On warming to ca. 150°K, EPR lines characteristic of one site disappear, while those of the other increase in strength. Apparently the $HCO_3\cdot$ reorients at this temperature to the more stable form. Details of this work will appear elsewhere.[4]

EPR studies have shown that $\dot{N}O_3^{2-}$ and $NO_3\cdot$ are major products in the low-temperature radiolysis of sodium and potassium nitrates, but only $\dot{N}O_3^{2-}$ has been observed in strontium and barium nitrates (see, e.g., ref. 5). An investigation of these latter salts has been undertaken in an attempt to stably trap $NO_3\cdot$ at lower temperatures. When these salts were irradiated at ca. 64°K and ESR observations made at this temperature, spectra characteristic of $NO_3\cdot$ were seen. The hyperfine and g tensors for this radical have been determined in $Ba(NO_3)_2$. Both tensors were found to be axially symmetric with $g_{\parallel} = 2.0075$, $g_{\perp} = 2.0242$, $A_{\parallel} = 4.3$ G, and $A_{\perp} = 3.4$ G and to have a common principal direction parallel to the crystallographic (111) direction. This direction is perpendicular to NO_3^- planes in the crystal and indicates that $NO_3\cdot$ is trapped in the nitrate position. When the crystals were warmed to 77°K, the $NO_3\cdot$ lines disappeared. This behavior is remarkably similar to that observed with the alkali nitrates, in which $NO_3\cdot$ was found to be only transiently stable at 77°K.

1. R. W. Holmberg, *Chem. Div. Annu. Progr. Rep. May 20, 1970,* ORNL-4581, p. 176.

2. G. W. Chantry et al., *Mol. Phys.* 5, 589 (1962).

3. S. Peller, Z. Luz, and B. L. Silver, *Isr. J. Chem. Proc.*, 7, 48p (1969).

4. R. W. Holmberg, "An ESR Study of Gamma-Irradiated Potassium Bicarbonate at 77°K," accepted for publication in the *Journal of Chemical Physics.*

5. Yu. A. Zakharov and V. A. Nevostruev, *Russ. Chem. Rev.* 37, 61 (1968).

ELECTRON SPECTROSCOPY

The use of electron spectroscopy for studying chemical problems has been exploited in a number of different areas over the past year by employing a double-focusing electrostatic instrument located in the Physics Division[1] and another in the Transuranium Research Laboratory modified to study radioactive materials, especially the transuranium elements.[2] With the former instrument, the photoelectron spectra using an He I (546-Å) source have been determined for GeF_4, $C(CH_3)_4$, $Si(CH_3)_4$, $Ge(CH_3)_4$, $Si(CH_3)_4$ $Pb(CH_3)_4$,[3] and for ClF, ClF_3, ClF_5, $SOCl_2$, and $CrOCl_2$;[4] the

angular distribution of photoelectrons as a method for determining the nature of molecular orbitals has been extended to CO, O_2, NO, CO_2, CS_2, H_2O, H_2S, CH_4, and benzene;[5] and finally, we have pursued the application of photoelectron spectroscopy to biological systems[6] and systems of environmental interest.[7] At TRL we have obtained preliminary results on binding energies of the *N*, *O*, *P*, and *Q* electrons of americium — first results in the program of determining binding energies of electrons in elements beyond plutonium.[2]

1. For description of the equipment, see B. P. Pullen, T. A. Carlson, W. E. Moddeman, G. K. Schweitzer, W. E. Bull, and F. A. Grimm, *J. Chem. Phys.* **53**, 768 (1970).
2. M. O. Krause and F. Wuilleumier, "Electron Spectrometry of Actinides and Actinide Compounds," a contribution in chap. 2, this report.
3. A. E. Jonas, T. A. Carlson, F. A. Grimm, and G. K. Schweitzer, to be published.
4. C. P. Anderson, J. C. Carver, T. A. Carlson, F. A. Grimm, W. E. Moddeman, W. E. Bull, and G. Mamantov, to be published.
5. T. A. Carlson, *Chem. Phys. Lett.* **9**, 23 (1971); T. A. Carlson, G. E. McGuire, A. E. Jonas, C. P. Anderson, and K. L. Cheng, to be published.
6. L. D. Hulett and T. A. Carlson, *Clin. Chem.* **16**, 677 (1970).
7. L. D. Hulett, T. A. Carlson, B. R. Fish, and J. L. Durham, *Proc. Symp. on Air Quality, Los Angeles, April 1971*, Plenum, Washington, D.C., in press.

STUDY OF CHEMICAL BONDING IN TRANSITION METAL COMPOUNDS BY USE OF PHOTOELECTRON SPECTROSCOPY[1]

J. C. Carver[2] L. C. Cain[2]
T. A. Carlson G. K. Schweitzer[3]

A new method for studying the nature of the *d* orbital in the bonding of transition metal compounds has been recently pointed out by Fadley and Shirley[4] using photoelectron spectroscopy. This method utilizes the multiplet splitting that occurs between coupling of partially filled *d* orbitals with an inner-shell orbital out of which an electron has been ejected by a soft x ray. Using Al $K\alpha$ and Mg $K\alpha$ x rays, a systematic study of about 40 different transition metal compounds was undertaken. Data were collected on both simple salts (halides, oxides, and sulfides) and hexacoordinated complexes (cyano- and fluoro-) of Cr^{3+}, Mn^{2+} and Mn^{3+}, Fe^{2+} and Fe^{3+}, and Co^{3+}. Selected second- and third-row transition-metal compounds were also investigated. The observed multiplet splittings are listed in Table 7.14.

From the photoelectron spectrum, the binding energies of the orbitals in an atom or a molecule are obtained. If the molecule is paramagnetic, then several final states can occur upon ejecting a core electron, causing a splitting in the observed spectrum.[4] Several final states occur as the result of Russell-Saunders coupling of the inner-shell vacancy formed by photoejection with unpaired valence electrons.[5] For the transition metal compounds, the uncoupled electrons are in the *d* level. We were particularly interested in an inner-shell vacancy created in the penultimate *s* shell since (1) the electronic coupling yields only two final states[5] and (2) the interaction between levels is greatest when the principal quantum number is the same. For example, iron(III) fluoride (FeF_3) has five unpaired 3*d* electrons. If a hole is made in the 3*s* shell, then two final states can occur corresponding to a ^7S state and to a ^5S state.

Our experimental results were correlated with spin-unrestricted Hartree-Fock (SUHF) free-ion calculations.

Table 7.14. Multiplet splitting observed from the photoelectron spectra of the penultimate 3*s* shell in transition metal compounds

Compound	$\Delta\epsilon$ (eV)
CrF_3	4.2
$CrCl_3$	3.9
$CrBr_3$	3.1
Cr_2O_3	4.1
Cr_2S_3	3.2
$K_3Cr(SCN)_6$	<0.3
$K_3Cr(CN)_6$	<0.3
MnF_2	6.3
$MnCl_2$	6.0
$MnBr_2$	4.5
MnO	5.5
MnS	5.3
Mn_2O_3	5.4
MnN	5.5
MnF_3	5.6
FeF_2	6.0
$FeCl_2$	5.6
$FeBr_2$	4.2
FeS	6.3
$K_4Fe(CN)_6$	<0.3
FeF_3	6.5
$FeCl_3$	5.3
$FeBr_3$	3.0
Fe_2O_3	7.3
K_3FeF_6	6.7
Na_3FeF_6	7.0
CoF_3	5.3
$K_3Co(C_2O_4)_3$	<0.3
$Co(NH_3)_6Cl_3$	5.0
$K_3Co(CN)_6$	<0.3

For a hole in the s level, the two final states are separated in energy by the exchange integral between the $3s$ and $3d$ orbitals (G^2),

$$G^2(3s, 3d) = C^2(0,0,2,0) \int_0^\infty \int_0^\infty R_{3s}(r_1) \times R_{3d}(r_2) R_{3s}(r_2) R_{3d}(r_1) \frac{r_<^2}{r_>^3} dr_1\, dr_2 \,, \quad (1)$$

where R_{3s} and R_{3d} are the radial wave functions for the respective $3s$ and $3d$ orbitals and $C^2(0,0,2,0)$ is the Clebsch-Gordan coefficient. The calculations for free ions always predict an energy separation larger than that found in molecular systems. This difference can be explained in two ways: (1) the d orbital of the metal ion which is involved in chemical bonding can be delocalized, giving rise to a decrease in the overlap between the s and d orbitals, and (2) strong ligand field effects can cause the uncoupled electron to couple (see Fig. 7.45).[6] Pairing occurs when $D_q > nP$ (Fig. 7.45), where P = energy necessary for electrons to pair and n = number of electrons which pair.

Free-ion calculations indicate correct trends on comparisons of one transition metal with another. The calculations predict the splitting for MnF_2 and FeF_2 to be about the same although the separation for CrF_3 should be about 25% smaller. Figure 7.46 illustrates that experimentally the predicted trends are correct. For $K_4Fe(CN)_6$ there is no observed splitting, which is expected since all electrons are believed to be paired.[6]

If one considers compounds of Cr^{3+} (d^3) in an octahedral environment, the electron configuration will always be $t_{2g}{}^3 e_g{}^0$ no matter how strong the ligand field is. Therefore the effects of delocalization can be observed clearly. From Fig. 7.47 it is obvious that for more covalent-type ligands, the splitting is less, that is, $\Delta\epsilon_{(Cr_2S_3)} < \Delta\epsilon_{(Cr_2O_3)}$ and $\Delta\epsilon_{(CrCl_3)} < \Delta\epsilon_{(CrF_3)}$. From other studies it is found that CN^- coordinates to a metal through extensive π bonding.[6] $K_3Cr(CN)_6$ is indicative of this type of bonding since only a single peak occurs (Fig. 7.47).

Selected compounds were examined containing metal ions from the second transition metal series. The observed splitting for Rh_2O_3 and RuO_2 appeared to be about 4 eV, but the analysis was difficult due to an increase in the natural width of the peaks and to a decrease in the peak intensity. Free-ion Hartree-Fock calculations indicate that the splittings should be about the same as or slightly lower than those of first row transition metal ions with the same number of unpaired electrons.

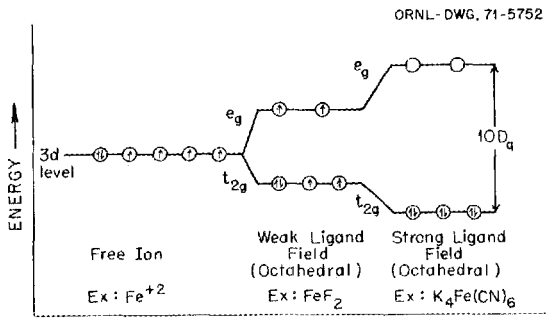

Fig. 7.45. The ligand field effect on a d^0 octahedral ion using Fe^{2+} as an example. As the ligand field is imposed, the degenerate d orbital is resolved into three degenerate t_{2g} orbitals and two degenerate e_g orbitals. If the ligand field is increased [as it is in going from FeF_2 to $K_4Fe(CN)_6$] the ligand field splitting, D_q, increases so that the electrons will be paired in the lower-energy state.

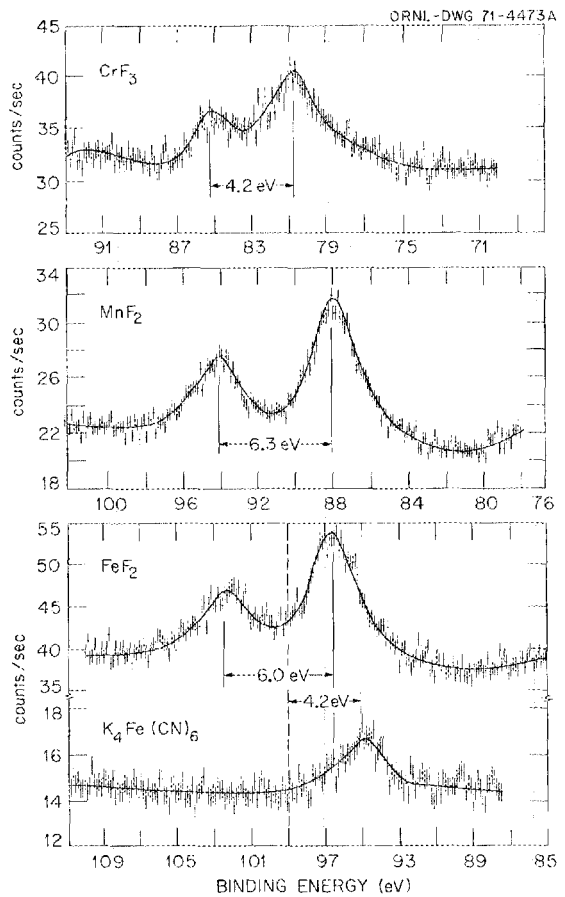

Fig. 7.46. Photoelectron spectra of $3s$ shell for CrF_3, MnF_2, FeF_2, and $K_4Fe(CN)_6$ using Al $K\alpha$ x rays. The error bars indicate the counting statistics. The dashed line indicates the weighted center of the $3s$ level. In each spectrum the multiplet splitting is indicated by an arrow between the centers (which was determined by deconvolution) of the two peaks. For $K_4Fe(CN)_6$ there is no multiplet splitting.

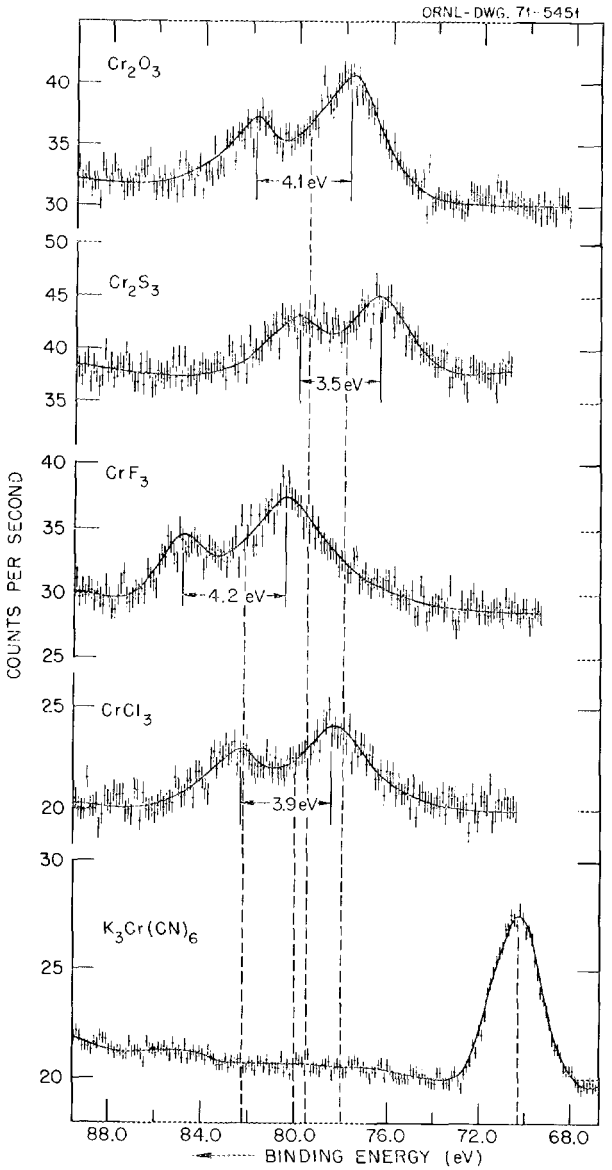

Fig. 7.47. Photoelectron spectra of the 3*s* shell for Cr_2O_3, Cr_2S_3, CrF_3, $CrCl_3$, and $K_3Cr(CN)_6$ using Al *Kα* x rays. The error bars indicate the counting statistics. The dashed lines indicate the weighted center of the 3*s* level. In each spectrum the multiplet splitting is indicated by an arrow between the centers (which was determined by deconvolution) of the two peaks. For $K_3Cr(CN)_6$ there is no multiplet splitting.

The shift in the inner-shell binding energies as a function of the chemical environment can be observed by comparing the weighted centers of the peak (the dashed lines in Fig. 7.47). These shifts agree with the chemical shifts for subshells of the metal ions in which the multiplet splitting is negligible. The chemical shifts reflect the change in overall electronic environment: the greater the density, the lower the inner-shell binding energies. Such data on the chemical shifts in the inner shells form the heart of ESCA (Electron Spectroscopy for Chemical Analysis).[7] From the photoelectron spectra of the transition metal compounds one can learn about both the specific nature of the *d* orbital (from core splitting) and about the change in the overall electron density surrounding the metal ions (from the inner-shell chemical shifts).

It is hoped that an extension of the calculations can be pursued by making the wave functions used in the exchange integral [Eq. (1)] more molecular in nature. Comparisons with other methods of measuring the nature of the *d*-orbital bonding interaction, such as neutron diffraction, NMR, ESR, and Mössbauer spectroscopy, will be made.

---

1. Work carried out jointly with the Physics Division.
2. Graduate student from the University of Tennessee, Knoxville, supported by NSF grant.
3. Department of Chemistry, University of Tennessee, Knoxville.
4. C. S. Fadley and D. A. Shirley, *Phys. Rev. A* **2**, 2 (1970).
5. J. C. Slater, *Quantum Theory of Atomic Structure*, vol. II, McGraw-Hill, 1960.
6. L. E. Orgel, *An Introduction to Transition-Metal Chemistry*, Wiley, New York, 1966.
7. Siegbahn et al. *ESCA: Atomic, Molecular, and Solid State Structure Studied by Means of Electron Spectroscopy*, Almqvist and Wiksells Boktryckeri A.B., Uppsala, 1967.

MANIFESTATION OF ATOMIC DYNAMICS THROUGH THE AUGER EFFECT[1,2]

M. O. Krause T. A. Carlson
W. E. Moddeman[3]

Using the neon Auger spectrum as an example, we show how Auger spectra yield detailed information on the interaction of radiation or particles with atomic electrons and on the mechanics of electron-electron interaction of the inner-shell-ionized atom. Processes such as simple ionization, simple excitation, double ionization, excitation-ionization, etc., can be distinguished and studied by Auger electron spectrometry. In accordance with the underlying physical process we present a classification of the some 90 lines of the neon spectrum, obtained by both photon and electron excitation. Relative energies and intensities of the lines within the various categories are given and are compared with theory and data from different sources. Dependence of spectral intensities on excitation conditions is discussed.

1. Work carried out jointly with the Physics Division.
2. Abstract of published paper: *J. Phys.* **C2**, 29 (1971), and in *Colloques Internationaux du C.N.R.S.*
3. Graduate student from the University of Tennessee, Knoxville, supported by a National Aeronautics and Space Administration research grant; address: Vanderbilt University, Nashville, Tenn.

EXCITATION ACCOMPANYING PHOTOIONIZATION IN ATOMS AND MOLECULES AND ITS RELATIONSHIP TO ELECTRON CORRELATION[1,2]

Thomas A. Carlson Manfred O. Krause
W. E. Moddeman[3]

If electron correlation is neglected, the photoelectric effect requires that only one electron be ejected from an atom. Experimentally, however, it is found in the photoionization process that there is a high probability for simultaneous excitation or ionization of a second electron in the same atom. This extra excitation can be explained by electron correlation: in some cases implicitly through the use of single-electron wave functions as in electron shake-off calculations, and in other cases through the use of wave functions that explicitly include correlation. We have utilized two recently constructed high-resolution electron spectrometers to measure satellite lines in the photoelectron spectra of both the inner and valence shells of the rare gases (He, Ne, and Ar) and some simple gaseous molecules (CO, CO_2, O_2, and N_2). These satellite lines are interpreted in terms of transitions to excited states of the singly charged ion and are used to form a broader basis for the understanding of simultaneous excitation as the result of the photoelectron process.

1. Work carried out jointly with the Physics Division.
2. Abstract of published paper: *J. Phys.* **C2**, 102 (1971), and in *Colloques Internationaux du C.N.R.S.*
3. Graduate student from the University of Tennessee, Knoxville, supported by a National Aeronautics and Space Administration research grant; present address: Vanderbilt University, Nashville, Tenn.

DETERMINATION OF THE *K-LL* AUGER SPECTRA OF O_2, N_2, CO, NO, H_2O, AND CO_2[1,2]

W. E. Moddeman[3] B. P. Pullen[4]
Thomas A. Carlson W. E. Bull[5]
Manfred O. Krause G. K. Schweitzer[5]

A double-focusing electrostatic electron spectrometer has been used to measure the *K-LL* Auger spectra resulting from electron impact for each of the elements in the gaseous molecules O_2, N_2, CO, NO, H_2O, and CO_2. An energy resolution of 0.09% FWHM was normally employed. A method for analyzing these complex spectra, which involves the identification of normal and satellite lines, has been worked out. Normal lines are those arising from single electron ionization from the *K* shell without additional excitation, followed by an Auger process in which one electron fills the vacancy while a second goes into the continuum, and where all the other electrons remain in their same orbitals. Satellite lines result when extra excitation occurs either in the initial formation of the *K* vacancy or in the subsequent Auger process. To aid in the identification of these satellite lines, auxiliary experiments have been performed such as the study of discrete energy losses in photoionization due to electron shakeup and the comparison of Auger spectra produced by monoenergetic x rays. Analyses of the Auger spectra have provided information on the nature of initial excitation processes, such as the transition of a *K* electron into excited discrete states, and on monopole excitation, and the identification of the energy and nature of the ground and excited states of the doubly charged molecular ions. The second ionization potential was obtained for each of the molecules, and in one case, N_2, the third ionization potential was estimated. Finally, the possible use of high-resolution electron spectroscopy in molecular, as well as elemental, analysis has been considered.

1. Work carried out jointly with the Physics Division.
2. Abstract of paper to appear in the *Journal of Chemical Physics* (August 1971).
3. Graduate student from the University of Tennessee, Knoxville, supported by National Aeronautics and Space Administration Research grant NGL 43-001-021, Supplement 3. Present address: Vanderbilt University, Nashville, Tenn.
4. Oak Ridge Graduate Fellow from the University of Tennessee, Knoxville, under appointment with Oak Ridge Associated Universities. Present address: Southeastern Louisiana State College, Hammond.
5. Department of Chemistry, University of Tennessee, Knoxville.

RESONANCE *K* EXCITATION AND AUGER DECAY OF THE NITROGEN MOLECULE

M. O. Krause F. Wuilleumier[1]

In previous studies[2,3] Auger electrons more energetic than those which leave the doubly charged molecule N_2^{2+} in its ground state were found under electron bombardment; and, on the basis of energy considerations and excitation conditions, these electrons were ascribed to Auger processes that follow the excitation of a *K* electron into the $(\sigma 1s)^{-1}(\pi_g 2p)$, $^1\Pi$ state. By a rare coincidence, namely, the coincidence of the Ti $L\eta$

x-ray energy [E = 401.3 eV and ΔE = 2.7 eV (FWHM)] with the excitation energy of this state [E = 400.8 eV and ΔE = 2 eV (FWHM)], we are now able to positively identify and classify these energetic lines. We also show that the appearance of an Auger spectrum can change radically with the choice of excitation source. In fact, the accidental resonance absorption reported here produces a lopsided Auger spectrum in which usually weak satellites assume a prominent position. We also obtain an indication of the overlap of the wave functions of the excited $\pi_g 2p$ electron and of the other valence electrons from the intensities of the various Auger processes which either involve or do not involve the excited electron. Finally, a rough estimate can be made for the oscillator strength of the transition $\sigma 1s \rightarrow \pi_g 2p$ in N_2.

We performed the experiment with our 15-cm electrostatic energy analyzer which was operated in the usual manner. Auger electrons were produced by bombarding N_2 either with Al $K\alpha$ x rays transmitted through 12 μm of Be or with Ti L x rays transmitted through 0.2 μm of polystyrene. The high-energy parts of the resulting Auger spectra, matched at the line $B4$ after subtraction of the underlying background, are shown in Fig. 7.48. The difference is striking; with Al $K\alpha$ x-ray excitation,

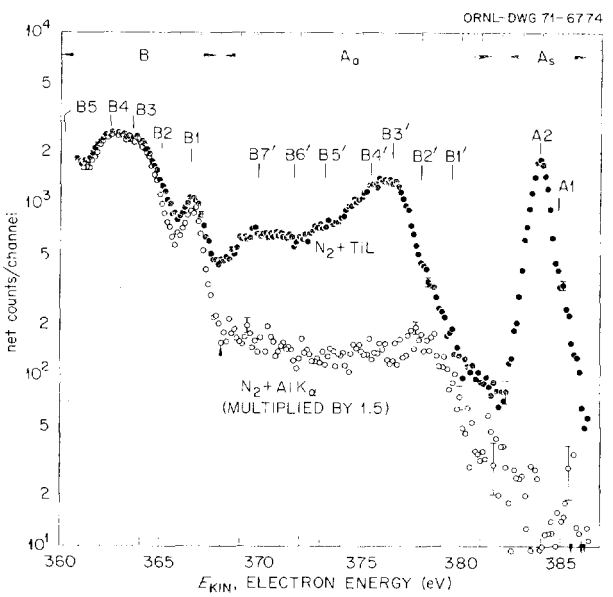

Fig. 7.48. High-energy part of K Auger spectrum of N_2 excited by Ti L x rays (solid circles) or by Al $K\alpha$ x rays (open circles). Spectra are matched at $B4$ after subtraction of background. $\Delta E/E$ = 0.16%. The greater portion of the B region is presented in ref. 3, and the total Auger spectrum in ref. 2. The series B'_1 to B'_7 corresponds to the series B_1 to B_7 shifted by 12.8 eV into the region A_a.

no lines are observed in region A_s and only a weak structure in region A_a, while with Ti L x-ray excitation intense lines and bands appear in these regions. The absence or presence of this feature in the Auger spectrum depends entirely on whether or not photons of energy 400 eV $\lesssim E \lesssim$ 402 eV are incident on N_2, since only photons of this energy can create the $(\sigma 1s)^{-1}(\pi_g 2p)$, $^1\Pi$ state by resonance absorption, the state which in the subsequent decay produces Auger electrons in regions A_s and A_a. The Ti $L\eta$ line has the correct energy; and no other autoionization states are created which could cause ambiguities. Normal Auger processes, due to K ionization by Ti $L\alpha$ x rays and by bremsstrahlung, occur at energies below 367 eV, that is, in region B; some of the Auger satellites that are due to initial double vacancies may occur in region A_a. These satellites can be seen in the Al $K\alpha$ excited spectrum, but are expected to be negligible in the Ti L excited spectrum. For, although a portion of the bremsstrahlung spectrum can ionize N_2 simultaneously in K and valence shells, Ti $L\alpha$ x rays are too close to this ionization threshold to cause much double ionization according to shake-off theory.[4]

Owing to these "clean" excitation conditions, we can assign peaks A_1 and A_2 to Auger processes in which the excited electron, $\pi_g 2p$, participates as actor, and the structure in regions A_a to Auger processes in which the excited electron does not participate but rather remains a spectator. The latter case resembles the normal Auger processes except that the escaping electrons will suffer additional repulsion by the spectator electron. In accord with this simple picture, bands B_1 to B_7 repeat themselves when shifted by +12.8 eV, as indicated in Fig. 7.48 by the symbols B'_1 to B'_7. However, structuring is less pronounced, probably due to an increase in the number of final states of this more complex configuration. Calculating the areas under the contours of A_a and A_s, we find that the excited electron participates in the decay events about 13% of the times and remains spectator 87% of the times. This frequent participation[5] of the electron in the Auger decay of N_2^{K*} indicates a relatively strong overlap of its wave functions with those of the other valence electrons.

We can use the Ti L excited Auger spectrum[6] to derive, within a factor of about 2, a value for the oscillator strength of the transition $\sigma 1s \rightarrow \pi_g 2p$, which has not been measured so far. To repeat, Auger processes in regions A_a and A_s are indicators of K excitation by Ti $L\eta$ x rays, and the corresponding Auger processes in region B are indicators of K ionization by Ti $L\alpha$. Thus we get for the oscillator

strength of the $\sigma 1s \rightarrow \pi_g 2p$ transition

$$f(\sigma 1s \rightarrow \pi_g 2p)_{N_2} = K \frac{I(A)}{I(B)} f'(1s \rightarrow \epsilon p)_{N_2} ,$$

where $I(A)$ and $I(B)$ are the Auger intensities residing in regions A and B (B_1 to B_7), respectively, and $f(1s \rightarrow \epsilon p)$ is the known oscillator strength of the continuum transition[7] at E = 452 eV. The constant K contains a number of relative correction and normalization factors, which are the following: dispersion of apparatus, multiplier 0.9; window transmission, 1.1; intensity ratio of $L\alpha/L\eta$ lines, 4 as determined in an auxiliary experiment; contribution of bremsstrahlung continuum to ionization relative to ionization by Ti $L\alpha$, 2 as estimated; and partial overlap of Ti $L\eta$ line with the "Nakamura" resonance absorption band,[8] 1.5. With $I(A)/I(B) = 0.7$ we obtain a value of 7×10^{-2} for $f(\sigma 1s \rightarrow \pi_g 2p)$ of the nitrogen *molecule.* This value, though of limited accuracy because of the estimate of the bremsstrahlung contribution, is somewhat smaller than Bearden and Wheeler's theoretical result[9] of $f(1s \rightarrow 2p) = 0.18$ for the nitrogen *atom.* The theoretical value for the atom is probably quite reliable since the same theory yields for neon $f(1s \rightarrow 2p) = 0.29$ in agreement with experiment,[10] $f(1s \rightarrow 2p) = 0.29$. That the oscillator strength of the discrete transition is only about one-fifth of the theoretical prediction might be attributed to delocalization of $2p$ orbitals in the molecule and to a change in screening. In terms of the atom, the $\pi_g 2p$ orbital can be placed between the $2p$ and $3p$ levels but closer to the $2p$ level, which results in a decrease of the oscillator strength. By comparison, $f(1s \rightarrow 3p) = 5 \times 10^{-3}$ for neon is smaller by two orders of magnitude than $f(1s \rightarrow 2p) = 0.29$.

To conclude, we note that what at first glance had appeared to be an auspicious showing of high-energy Auger lines in the N_2 spectrum has turned out, in retrospect, to be a necessary consequence of a normal behavior of the oscillator strength for the resonance absorption of Ti $L\eta$ x rays.

---

1. Guest scientist from Laboratoire de Chimie Physique de la Faculté des Sciences de Paris, Paris, France.

2. P. Stalherm et al., *Z. Naturforsch. a* **24**, 1728 (1969); Siegbahn et al., *ESCA Applied to Free Molecules,* North-Holland, Amsterdam-London, 1969.

3. T. A. Carlson et al., *Chem. Phys. Lett.* **5**, 390 (1970).

4. T. A. Carlson, W. E. Moddeman, and M. O. Krause, *Phys. Rev. A* **1**, 1406 (1970); M. O. Krause, *J. Phys.* **C2**, 273 (1971).

5. In the analogous case of neon the excited $3p$ electron participates only 3% of the times.

6. Radiative decay can be neglected.

7. B. L. Henke and R. L. Elgin, *Advances in X-Ray Analysis,* vol. 13, Plenum, New York, 1969. We doubled the value quoted for N.

8. M. Nakamura et al., *Phys. Rev.* **178**, 80 (1969); M. J. Vander Wiel, Th. M. El Sherbini, and C. E. Brion, *Chem. Phys. Lett.* **7**, 161 (1970). The latter authors find a much smaller width for the absorption resonance at 400.8 eV than Nakamura et al. This would somewhat decrease the overlap with Ti $L\eta$. With our f value 99% of resonance photons are absorbed over an 8-cm path length in Nakamura's experiment; thus "total" absorption occurs over 45 cm.

9. J. A. Bearden and J. A. Wheeler, *Phys. Rev.* **46**, 755 (1934).

10. F. Wuilleumier, thesis, Paris (1969), unpublished.

CALCULATIONS USING ATOMIC WAVE FUNCTIONS

T. A. Carlson C. W. Nestor, Jr.[1]
C. C. Lu[1] T. C. Tucker[1]
F. B. Malik[2]

To support our experimental programs in charge spectroscopy and, more recently, electron spectroscopy, a relativistic Hartree-Fock-Slater program was set up for calculating atomic wave functions.[3] In addition to calculations relating to specific experimental work, comprehensive computations have been made on a variety of atomic properties of general interest to scientists both inside and outside the Laboratory. During the last year ionization potentials have been published[4] for all the elements up to Z = 103 for all states of ionization. These calculations were based on a very simple model using eigenvalues and mean radii from the Dirac solution of the neutral atom. The average deviation of the calculated ionization potentials from available experimental values was about 5%. These calculations have proved to be most valuable for predicting charge states in the production of heavy ions.

A second publication was the complete listing[5] of the eigenvalues, radial expectation values, and potentials for free atoms from Z = 2 to 126 as calculated from our Relativistic Hartree-Fock-Slater Atomic Wave Function program. This program, which includes a finite size nucleus and provision for a Wigner-Seitz boundary, was written for the IBM 7091 computer and can be obtained from the authors upon request.

The third application of our wave-function program was in the calculation[6] of K x-ray intensities for elements from Z = 92 to 126. With the help of these values and the previously calculated x-ray energies, one may use x-ray spectra arising from K vacancies of the heavy and superheavy elements as an unambiguous means for identifying these elements.

1. Mathematics Division.
2. Consultant, University of Indiana, Bloomington.
3. T. C. Tucker, L. D. Roberts, C. W. Nestor, Jr., T. A. Carlson, and F. B. Malik, *Phys. Rev.* **178**, 998 (1969).
4. T. A. Carlson, C. W. Nestor, Jr., N. Wasserman, and J. D. McDowell, *Atomic Data* **2**, 63 (1970).
5. T. A. Carlson, C. C. Lu, T. C. Tucker, C. W. Nestor, Jr., and F. B. Malik, *Eigenvalues, Radial Expectation Values, and Potentials for Free Atoms from Z = 2 to 126 as Calculated from Relativistic Hartree-Fock-Slater Atomic Wave Functions*, ORNL-4614 (December 1970); C. C. Lu, T. A. Carlson, F. B. Malik, T. C. Tucker, and C. W. Nestor, Jr., *Nuclear Data* (in press).
6. C. C. Lu, F. B. Malik, and T. A. Carlson (submitted to *Nuclear Physics*).

ATOMIC AND MOLECULAR COLLISIONS

IONIZING COLLISIONS OF FAST ALKALI ATOMS WITH Cl_2, Br_2, AND O_2

N. Kashihira[1] H. F. Krause
F. Schmidt-Bleek[2] S. Datz

Collisional ionization of alkali atoms (M) with diatomic molecules (X_2) has recently been a subject for intensive study at several laboratories. Most of the effort has been in the measurement of positive- and negative-ion yields as a function of velocity in the energy region from thermal to 3 keV with the intention of determining the separate excitation functions for possible processes such as:

$$M + X_2 \rightarrow M^+ + X_2^- , \qquad (a)$$

$$\rightarrow M^+ + X + X^- , \qquad (b)$$

$$\rightarrow M^+ + X_2 + e , \qquad (c)$$

$$\rightarrow M^+ + X + X + e . \qquad (d)$$

Moreover, each of these processes can proceed by several mechanisms (i.e., transitions between several alternate potential energy surfaces), and it is clear that yield information alone is not sufficient to make this differentiation. For this reason, we have undertaken a study of the inelastic energy loss accompanying chemi-ionizing collisions.

In the present work, we have used time-of-flight techniques to measure energies of K^+ and Cs^+ ions formed by collision of 50- to 300-eV K^0 and Cs^0 atoms with Cl_2, Br_2, O_2, and N_2. The time-of-flight technique and the apparatus used in this work have been described previously.[3] In this experiment, a pulse (~1 μsec wide) of velocity-selected M^+ ions is passed through a cell containing M vapor, and fast neutrals are produced by resonant charge exchange. The fast M atoms pass through a 3-cm cell containing the diatomic molecular gas, where they can undergo ionizing collisions. Ions produced in a direction parallel to the incident atom beam (±1°) can leave the cell and, after passage through a flight tube, strike an electron-multiplier detector. By comparing the flight-time differences of the M^+ ions produced in collision with primary M^+ ions coming from the source (without resonant charge exchange), the energy loss of ions formed in the reaction cell can be calculated.

Some typical yield measurements are shown for the case K + Cl_2 and K + O_2 in Fig. 7.49. They are

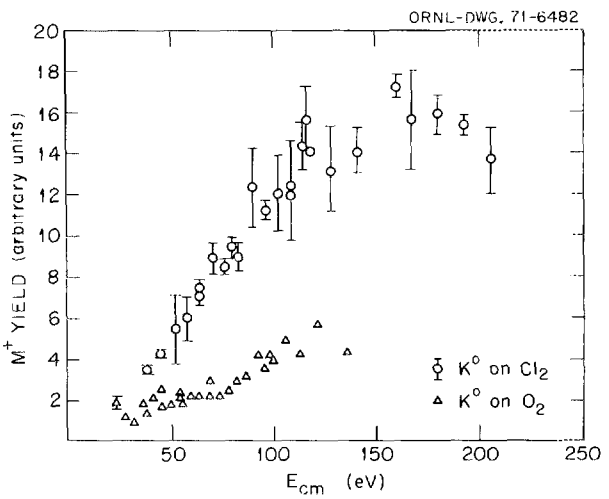

Fig. 7.49. Dependence of alkali-ion yield on relative collision energy for potassium atoms with chlorine and oxygen.

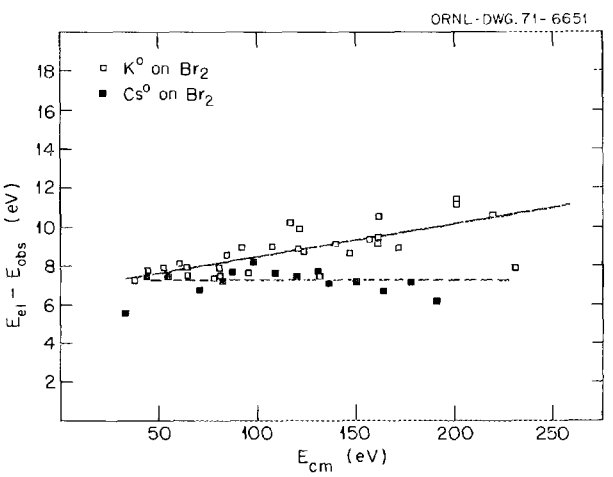

Fig. 7.50. Dependence of inelastic energy loss ($\Delta E = E_{elastic} - E_{observed}$) on relative collision energy for chemi-ionization of alkali atoms with bromine.

characterized by a rapid rise followed by a leveling off and a slight decline. At the maximum the cross sections for both K and Cs on Cl_2 and Br_2 are of the order of 100 $Å^2$, while those for O_2 and N_2 are of the order of 30 and 1 $Å^2$ respectively. The principal difference between Cs and K is that the yield curves for the former are shifted toward lower energies by ca. 20 eV.

The inelastic energy losses observed with the K + Br_2 and Cs + Br_2 systems are shown in Fig. 7.50. The curves for Cl_2 as a target are almost indistinguishable. From the magnitude of the energy loss ($\Delta E_{min} \sim 7$ eV), it is apparent that the halogen molecule must be excited to a dissociative state. The maximum energy that can be absorbed in a collision producing alkali and molecular ions is determined simply by the ionization potential of the alkali I(M), the electron affinity of the halogen atom E(X), and the dissociation energy of the halogen molecule $D^\circ_0(X_2)$; ΔE_{max} (nondissociative) = I(M) — E(X) + $D^\circ_0(X_2)$ = 2.83 and 2.4 eV, respectively, for K and Cs on Br_2.

Thus process *a* is not energetically allowed (into electronic ground states), but process *b* is. Process *c* requires a minimum inelastic loss of I(M) = 4.3 eV for K and 3.9 eV for Cs, but X_2 (if in its electronic ground state) will dissociate (process *d*) if the energy loss exceeds I(M) + $D^\circ_0(X_2)$ = 6.33 eV for K on Br_2 and 5.9 eV for Cs on Br_2. Dissociative ionization is therefore strongly indicated in these cases and is supported by the observation that X^- is the predominant negative-ion species observed in this energy region.

The most intriguing features of the energy loss measurement are the sharpness of the inelastic peak and the relative constancy of the loss with initial relative collision energy. The former feature is not expected on the basis of simple three-body breakup, and the latter indicates the formation of an intermediate in a definite excited state. We therefore postulate that the predominant process is a transition into a repulsive state of X_2^- with an energy of ca. 4 eV above the ground state of the X_2 molecule.

In the case of K or Cs and O_2 the situation is significantly different (Fig. 7.51). Although the magnitudes of the energy losses are comparable with the halogen cases, the energetics are not. The principal difference is in the binding energy of the O_2 molecule [$D^\circ_0(O_2)$ = 5.2 eV]. The minimum inelastic loss required for process *b* is 8.0 eV for K + O_2 and 7.6 eV for Cs + O_2. In the case of K + O_2, there is sufficient energy loss for this to occur, while for Cs + O_2 the loss appears too small. It would appear, therefore, that in the case of Cs + O_2 the product is excited O_2^-. From a consideration of the known states of O_2^- (Fig. 7.52), it appears that the most likely transition is to the $^2\Pi_u$ level. In the case of K + O_2 the transition is close to vertical, while for the slower Cs atom the transition may be totally adiabatic, leaving the O_2^- in the bound portion of the $^2\Pi_u$ state.

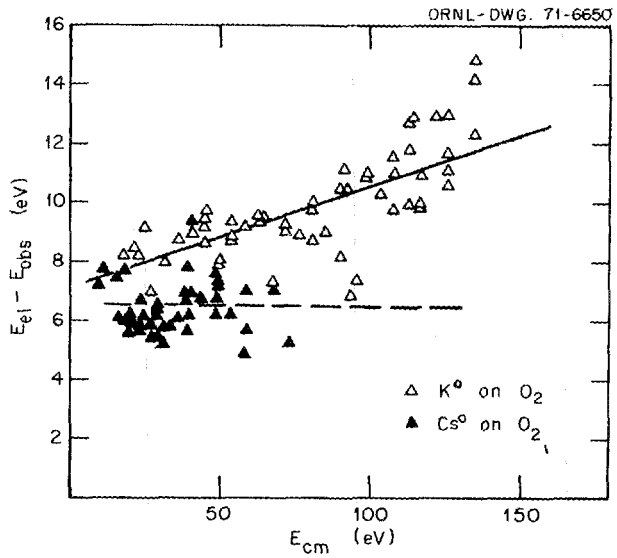

Fig. 7.51. Dependence of inelastic energy loss on relative collision energy for chemi-ionization of alkali atoms with oxygen.

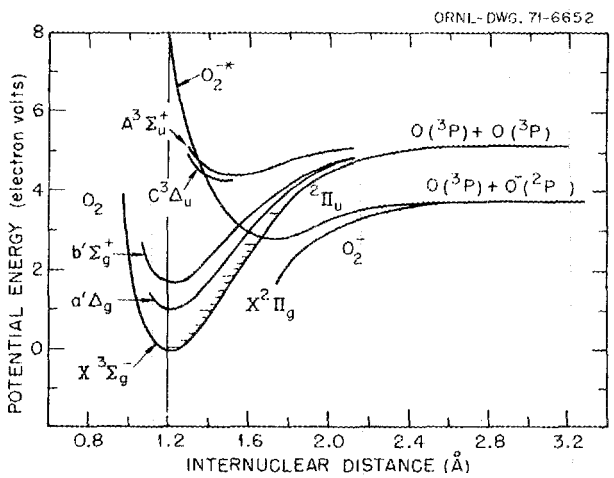

Fig. 7.52. Potential energy diagram for low-lying states of O_2 and O_2^-.

1. Graduate student from Purdue University, Lafayette, Ind.
2. Consultant; Department of Chemistry, University of Tennessee, Knoxville.
3. P. F. Dittner and S. Datz, *J. Chem. Phys.* 54, 4228 (1971).

DIFFERENTIATION IN L SUBSHELL VACANCY PRODUCTION IN IODINE IONS BY ATOMIC COLLISIONS AT 15 TO 60 MeV

S. Datz B. R. Appleton[2]
C. D. Moak[1] T. A. Carlson

Recent work on x-ray emission induced by heavy-ion–atom collisions has demonstrated a strong dependence of the production cross section on matching of energy levels in the collision partners.[3,4] It has also been demonstrated that energy shifts in the x-ray lines occur for projectiles of $Z > 2$ and that these shifts are attributable to high ionization states of the x-ray-emitting ions.[5,6] These data complement the results on inelastic energy loss, multiple ionization, and Auger electron ejection obtained from experiments on violent ion-atom collisions.[7] Taken together, all these results appear to be best explained by theories involving electron promotion through level crossing in a united atom model,[8–10] but a quantitative description of the excitation and relaxation processes has not yet been carried out.

We present the results of a systematic study of the L x-ray spectrum of iodine arising from collisions of 15- to 60-MeV iodine ions with target atoms ranging from carbon to lead (Z_2 = 6 to 82). The iodine ion beams, obtained from the Oak Ridge EN Tandem Van de Graaff accelerator, were directed at thick targets positioned in a Faraday cup at 45° to the beam direction and the x rays detected by a lithium-drifted silicon detector (resolution ~ 190 eV) placed at 90° to the beam direction.

Some typical iodine L x-ray spectra obtained at 38.4 MeV are shown in Fig. 7.53 and compared with a spectrum obtained with 5-MeV alpha particles on NaI. Two striking differences are immediately apparent. First, all the lines are shifted to higher energy than the alpha-particle-induced spectrum (note, however, that the shifts are independent of Z_2), and, second, the relative spectral intensities are drastically different. An analysis of the data has shown that the principal difference is in the relative probabilities of forming $2p_{3/2}$ and $2p_{1/2}$ vacancies and that the branching ratio for filling a given vacancy is invariant with Z_2. The branching ratio for the decay of a $2p_{3/2}$ vacancy as determined from the intensity ratios of $L_l(2p_{3/2} \rightarrow 3s_{1/2})/L_\alpha(2p_{3/2} \rightarrow 3d_{3/2,5/2})$ and $L_{\beta 2}(2p_{3/2} \rightarrow 4d_{3/2,5/2})/L_\alpha$ were 0.07 ± 0.01 and 0.165 ± 0.02, respectively, over the entire range of Z_2 and energy. Similarly, the $2p_{1/2}$ branching ratio $L_{\gamma 1}(2p_{1/2} \rightarrow 4d)/L_{\beta 1}(2p_{1/2} \rightarrow 3d)$ was 0.15 ± 0.05. The intensity ratio of the lines arising from $2p_{1/2}$ vacancies to those from $2s_{1/2}$ vacancies was also constant, that is, $[L_{\gamma 2}(2s_{1/2} \rightarrow 3p)/L_{\beta 1}]$ = 0.16 ± .03. The principal difference comes about in the ratio of $2p_{3/2}$ to $2p_{1/2}$ (or $2s_{1/2}$) vacancies in the iodine ion and can be studied simply by measuring the relative intensities of L_α and $L_{\beta 1}$. Figure 7.54 shows some spectra obtained using targets in the range Z_2 = 34 to 47. (Note here that correction of these intensities for x-ray absorption in the target does not significantly affect the spectral shape and that there are no absorption edges in this wavelength region for this set of target elements.) The $L_{\beta 1}/L_\alpha$ ratio also varies considerably with ion energy for a given target as shown In Fig. 7.55. But this decline with decreasing energy is by no means universal (e.g., the reverse is true for Cr and Ni). Figure 7.56

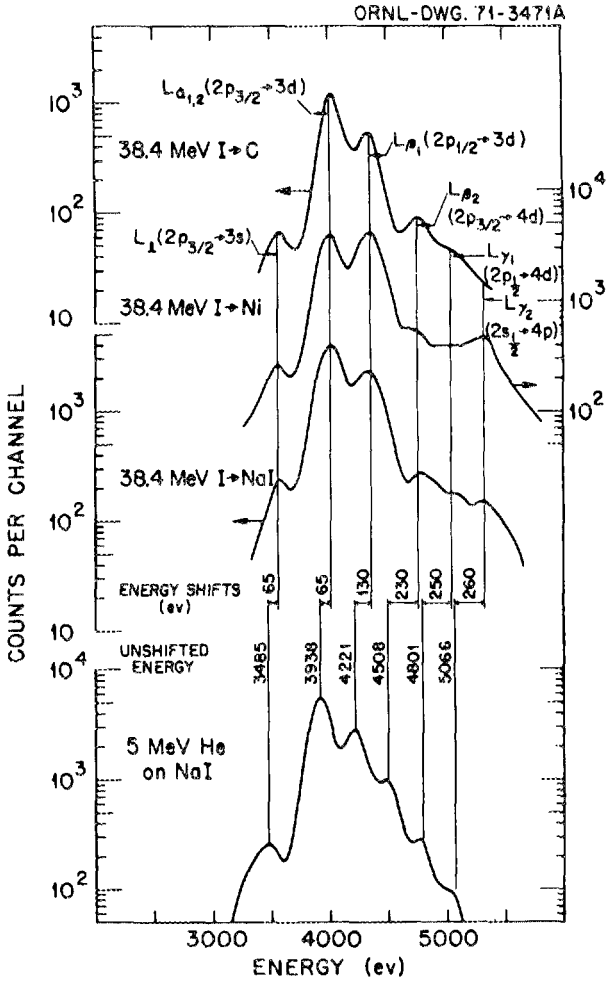

Fig. 7.53. Iodine L x-ray spectra produced by 5-MeV He ion bombardment of NaI compared with iodine L x-ray spectra produced by 38.4-MeV iodine ion bombardment of NaI, Ni, and C.

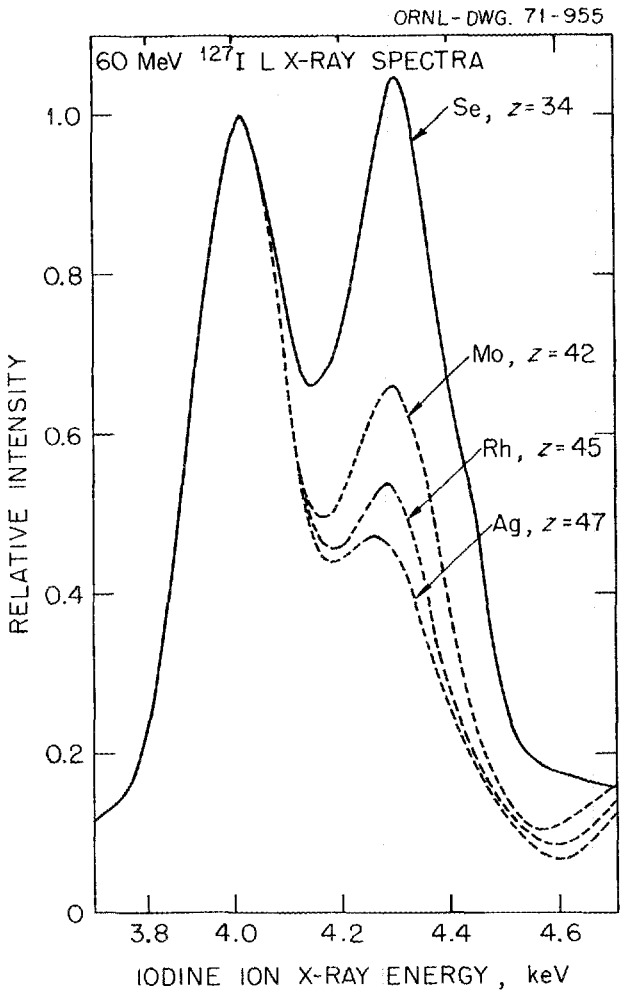

Fig. 7.54. Iodine L x-ray spectra produced by 60-MeV iodine ions incident on Se, Mo, Rh, and Ag.

summarizes the $L_{\beta 1}/L_{\alpha}$ intensity ratios obtained from computer Gaussian analysis of the spectra taken at four incident ion energies. The ratio varies from 1.4 to 0.2, depending on Z_2 and energy, and displays two maxima and two minima. These variations correspond to a differentiation in the relative cross sections for the production of $2p_{3/2}$ vis-à-vis $2p_{1/2}$ and vacancies.

Although measurements of all the absolute cross sections for iodine L x-ray production are not yet complete, we know that they are large ($\sim 10^{-19}$ cm^2) in the region $Z = 43$ (ref. 11) to 52 (ref. 12), and there is evidence that they rise in the region $Z_2 = 30$ to 50.[3] The decline of the $L_{\beta 1}/L_{\alpha}$ ratio in this region implies that the $2p_{3/2}$ vacancy production cross section is rising more rapidly than that for $2p_{1/2}$ or $2s_{1/2}$ vacancies. In this region the binding energy of the L electrons of the target atom is approaching the binding energy of the iodine L-shell electrons from below as Z_2 increases, which means an ever-closer match first with the more loosely bound $2p_{3/2}$ electrons. However, the downward trend in the ratio is reversed (at cadmium, $Z = 48$) before an exact match in binding energy is attained (i.e., iodine, $Z = 53$). In this argument we have been referring to the binding energies characteristic of neutral iodine. The L-electron binding energies of the highly charged incident iodine ion (equilibrium charge 11+ at 15 MeV and 23+ at 60 MeV) are significantly higher, that is, ~700 eV at 23+. But this effect would tend to raise rather than lower the Z_2 at which level matching is achieved. Similar minima in the $L_{\beta 1}/L_{\alpha}$ ratio are observed at sulfur ($Z_2 = 16$) prior to target K-shell energy level matching and at lead ($Z = 82$) prior to target M-shell matching with iodine L-shell levels.

The observed energy shifts are given in Table 7.15. Since no significant differences were observed with changing Z_2, the tabulated numbers are averages taken from those spectra where the target x rays did not interfere. For the L_{α} and $L_{\beta 1}$ lines the values are

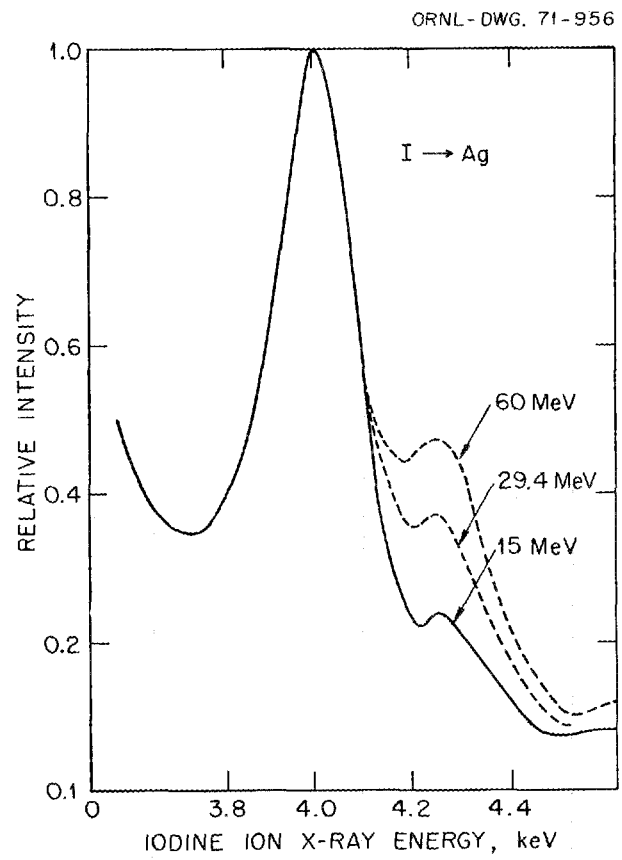

Fig. 7.55. Iodine L x-ray spectra produced by 60-, 29.4-, and 15-MeV iodine ions incident on Ag.

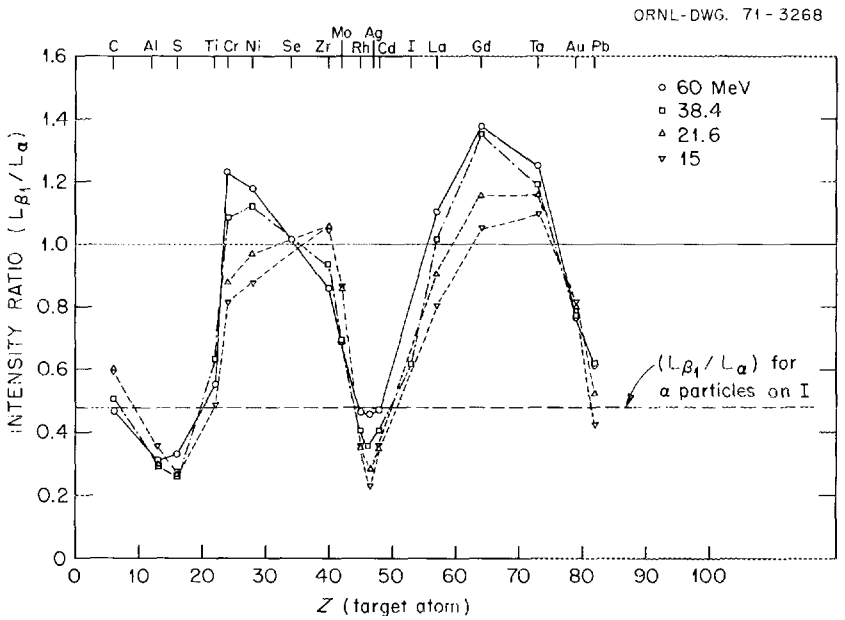

Fig. 7.56. Ratio of iodine $L\beta_1/L\alpha_{1,2}$ x-ray intensities produced by 15- to 60-MeV iodine ions incident on targets ranging from carbon to lead.

Table 7.15. Energy shifts of L iodine x rays

X ray	L_l	L_α	$L_{\beta 1}$	$L_{\beta 2}$	$L_{\gamma 1}$	$L_{\gamma 2}$
Unshifted energy (eV)	3485	3938	4221	4508	4801	5066
Transition	$2p_{3/2} \rightarrow 3s$	$2p_{3/2} \rightarrow 3d$	$2p_{1/2} \rightarrow 3d$	$2p_{3/2} \rightarrow 4d$	$2p_{1/2} \rightarrow 4d$	$2s \rightarrow 4p$
Shift (eV) for ion energy of:						
15.0 MeV	53	53	128	216	(170)	204
21.6 MeV	65	67	134	232	(224)	228
38.4 MeV	75	84	142	262	(244)	273
60.0 MeV	101	116	166	297	(250)	295
Number of elements	(8)	(16)	(16)	(14)	(10)	(11)

comparable with those reported by Mokler.[13] These shifts are caused by ionization and excitation of the emitting ion.[5] We have carried out nonrelativistic Hartree-Fock calculations for electron binding energies in ground-state and excited ions and relativistic Hartree-Fock-Slater calculations to determine differences between $2p$ subshell shifts. From these calculations we conclude:

1. Koopman's theorem gives only 15% differences with adiabatic calculations,
2. *LLM* Coster-Kronig transitions as a mechanism for the redistribution of initially formed L vacancies are not possible for any ionization state in iodine,
3. energy shifts in $2p_{3/2}$ and $2p_{1/2}$ lines should be identical within a few electron volts for the same ionic configuration,
4. removal of each $3d$ or $3p$ or $3s$ electron causes a line shift of ~13 eV in *LM* lines and 45 eV in *LN* lines,
5. removal of each $2p$ or $2s$ electron causes a line shift of 90 eV for *LM* lines and ~100 eV for *LN* transitions.

Consider first the possible configurations which could account for all line shifts (except $L_{\beta 1}$; see below). A double vacancy in the L shell gives too large a shift even if the ion were otherwise neutral. Removal of all electrons in the O and N shells without perturbing

M-shell electrons would give too small a shift [$\Delta E(L_\alpha)$ = 42 eV for ground-state 25+ ions]. The only satisfactory fit occurs when vacancies in the M shell are postulated. For example, for a base configuration of 15+ and three M-shell electrons removed (total ion charge of 18+), $\Delta E(L_\alpha) = \Delta E(L_l) = 60$ eV and $\Delta E(L_{\gamma 2}) = \Delta E(L_{\beta 1}) = \Delta E(L_{\gamma 2}) = 210$ eV, in good agreement with the data at 15 MeV. However, equally good agreement is achieved with two M-shell vacancies in a 20+ ion (total ionic charge = 22+). At best we can estimate that at 15 MeV a collision which causes an L-shell vacancy also creates an average of two to four M-shell vacancies. (Because of our limited energy resolution, the line we observe is probably an envelope covering a distribution of several lines, each attributable to a specific ionic state.) At 60 MeV similar agreement is obtained for an average of five to seven M-shell vacancies for a collision which creates a single L-shell vacancy.

Of the six lines observed, the $L_{\beta 1}$ line is the most enigmatic. The shifts are significantly larger (~50 eV) at all energies. This effect could imply that the ions emitting this radiation are, on the average, in higher excited states at the time their vacancies ($2p_{1/2}$) are relaxed than ions with $2p_{3/2}$ vacancies. This is unlikely because (1) it would require a minimum of three additional M-shell vacancies and (2) in this configuration $L_{\gamma 1}$ would have to be shifted an additional 200 eV. An alternative explanation could be interference of the unresolved $L_{\beta 4}(2s_{1/2} \rightarrow 3p_{1/2})$ and $L_{\beta 3}(2s_{1/2} \rightarrow 3p_{3/2})$ lines, which lie 50 and 100 eV above $L_{\beta 1}$. If $L_{\beta 4}$ and $L_{\beta 3}$ were comparable in magnitude with $L_{\beta 1}$, we would observe a composite line with a centroid shift of 50 eV. However, this would require a drastic change in relative transition probabilities for filling a $2s_{1/2}$ vacancy. $L_{\beta 4}$ and $L_{\beta 3}$ would normally be expected to be about the same intensity as $L_{\gamma 2}$, which is an order of magnitude lower than the line identified with $L_{\beta 1}$. Unresolved adjacent lines of this magnitude cannot possibly shift the peak of the $L_{\beta 1}$ line. Whatever the reason for this anomalous shift, it does not affect the observation of gross differences in $2p_{3/2}$ vis-à-vis $2p_{1/2}$ and $2s_{1/2}$ vacancy formation probabilities.

In summary, the $2p_{1/2}$, $2p_{3/2}$, and $2s_{1/2}$ subshell binding energies in iodine differ by only 250 eV out of a total binding energy of ~5 keV, and we are studying violent collisions at energies up to 60 MeV. Yet there is a strong differentiation with slight changes in Z_2 for the formation of vacancies in the subshells. This selectivity implies that some form of pseudomolecular interaction must be involved, but it is not clear whether energy-matching arguments are sufficient or whether differences in curve-crossing mechanisms due to spin-orbit differences between the two p subshells must be considered.

---

1. Physics Division.
2. Solid State Division.

3. H. J. Specht, *Z. Phys.* **185**, 301 (1965).
4. T. M. Kavanagh et al., *Phys. Rev. Lett.* **25**, 1473 (1970).
5. D. Burch and P. Richard, *Phys. Rev. Lett.* **25**, 983 (1970).
6. A. R. Knudson et al., *Phys. Rev. Lett.* **26**, 1149 (1971).
7. Q. C. Kessel, p. 593 in *Case Studies in Atomic Collision Physics I*, E. W. McDaniel and M. R. C. McDowell, eds., North-Holland, 1969.
8. U. Fano and W. Lichten, *Phys. Rev. Lett.* **14**, 627 (1965).
9. W. Lichten, *Phys. Rev.* **164**, 131 (1967).
10. W. Brandt and R. Laubert, *Phys. Rev. Lett.* **24**, 1037 (1970).
11. R. Laubert et al., *Bull. Amer. Phys. Soc.* **16**, 73 (1971).
12. H. J. Stein et al., *Phys. Rev. Lett.* **24**, 701 (1970).
13. P. H. Mokler, *Phys. Rev. Lett.* **26**, 811 (1971).

CHARGE-CHANGING COLLISIONS OF CHANNELED OXYGEN IONS IN GOLD

S. Datz C. D. Moak[2]
F. W. Martin[1] B. R. Appleton[3]
L. B. Bridwell[4]

When fast ions in a given charge state enter a medium, they undergo a series of charge capture and loss collisions. As the charge on the ion increases, the probability for electron capture increases relative to electron loss and ultimately an "equilibrium" charge-state distribution is attained. The most probable charge state is characterized by equal cross sections for electron capture and loss. Typically, this dynamic equilibrium stage is easily achieved within a hundred atom layers in a polycrystalline solid medium. However, when the ion is channeled in a thin single crystal, it is constrained to large impact parameter collisions with the atoms in the solid, and the cross sections for capture and loss of electrons by the ions may be affected by the density and velocity of the electrons they encounter. Earlier investigations have shown differences in the average charge for ions emerging in channeling directions and in "random" directions and have indicated departures from equilibrium. In the present work we have studied charge-state distributions of oxygen ions (4.45 to 40 MeV) in gold under conditions where it is possible to specify the trajectory of the transmitted ions and as a function of input charge and path length through the channel. By analyzing the forward exiting component of the channeled beam, we obtained group energy-loss spectra and measured the charge-state distribution for each energy-loss group. Using our previous work which correlated

channeled energy loss with ion trajectory, we obtained charge-state distributions as a function of oscillation amplitude. At higher energies (20 to 40 MeV) we find no true equilibrium even for 6000-Å path lengths. Instead, we find quasi equilibrium for charge states up to 6+ and strongly path-length-dependent charge fractions for the injection of 7+ and 8+ ions. The set of charge-transfer cross sections educed from the data shows a sharp drop at the 7 to 6 capture cross section and the 6 to 7 loss cross section. The data are interpreted in terms of velocity matching between the *K* electrons of oxygen and the outer electrons of the gold. A complete description of the results and theoretical interpretation will appear in *Radiation Effects.*

1. Physics Department, University of Maryland, College Park.
2. Physics Division.
3. Solid State Division.
4. Physics Department, Murray State University, Murray, Ky.

MASS SPECTROMETRY AND RELATED TECHNIQUES

THE RADIOLYSIS OF METHANE IN THE ELECTRIC-FIELD SOURCE

P. S. Rudolph R. Baldock

The electric-field source[1] (EFS) has been modified and now gives consistent and reproducible data; *m/e*'s 26, 28, and 30 resulting from stable products produced by electron bombardment of CH_4 in the EFS have been studied over a two-order-of-magnitude range of pressure in the EFS. Since higher masses have not yet been studied, the intensities at these *m/e*'s have not been corrected for contributions from higher hydrocarbons (HC); hence, in this report intensities at *m/e*'s 26, 28, and 30 do not accurately represent the parent ions ($C_2H_2^+$, $C_2H_4^+$, and $C_2H_6^+$). For example, the fragment ion *m/e* = 28 from C_2H_6 represents 44.7% of all the ions from C_2H_6, whereas the parent ion (*m/e* = 30, $C_2H_6^+$) represents only 11.7% of the ions.[2]

The intensities of the ions studied as a function of the CH_4 pressure in the EFS are shown in Fig. 7.57. All data were taken using a 100-eV electron beam in the EFS and with electrode 1 positive with respect to electrode 2.[1] This polarity repels the positive ions formed in the electron beam so that as they migrate toward the negative electrode 2 they react with CH_4 in the reaction volume between the electrodes. Only stable products reach the standard analytical source of the mass spectrometer as the EFS is separated from it by two molecular leaks and 18 cm of 13-mm tubing.

The intensities of *m/e*'s 26 and 28 are independent of pressure up to about 4×10^{-3} torr; then both curves break sharply with a slope of 1.5. The curve for *m/e* = 28 maintains this slope, but the *m/e* = 26 curve breaks again at about 10^{-2} torr to a slope of 2.8. The curve for *m/e* = 30 shows increasing intensity from the lowest pressure to about 2.5×10^{-3} torr with a slope of 0.65. From this pressure to the highest pressure studied the slope is 2.1.

The slope of the log-log plot should give the order of the reaction with respect to the CH_4 concentration. Since there is little contribution to *m/e* = 30 from higher HC, the slope of 2.1 is probably nearly correct.

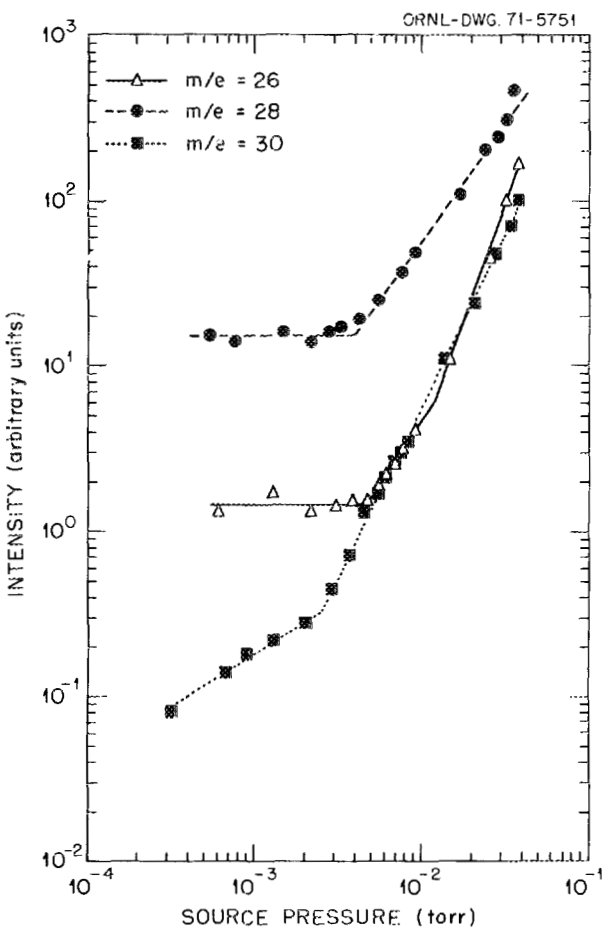

Fig. 7.57. Intensity of ions as a function of the pressure of CH_4 in the electric-field source. The stable products formed by the electron bombardment of CH_4 in the electric-field source were analyzed in the normal analytical mass spectrometer source. All *m/e*'s were studied under identical conditions (except pressure); thus, the intensities are directly comparable.

One mechanism that may explain this slope is

$$CH_4 \rightsquigarrow CH_4^+ + e\,, \quad (1)$$

$$CH_4^+ + CH_4 \longrightarrow CH_5^+ + \cdot CH_3\,, \quad (2)$$

$$\cdot CH_3 + \cdot CH_3 \longrightarrow C_2H_6^*\,, \quad (3)$$

$$C_2H_6^* + M \longrightarrow C_2H_6 + M\,, \quad (4)$$

$$CH_5^+ + e \longrightarrow CH_4 + H\,. \quad (5)$$

The overall reaction due to the above sequence of reactions would be second order with respect to the methane concentration. Of course, simultaneous competing and side reactions complicate the picture and may explain the fractional orders observed.

Figure 7.58 shows the variation in percent of ion-molecule reactions (I-M Rx) as a function of EFS pressure. The techniques for calculating the percent of I-M Rx have been previously described.[1] Figure 7.58 shows that as the pressure increases the percents I-M Rx for m/e's 26 and 28 decrease until they reach limiting values of about 43 and 37% respectively. These values have not been corrected for contributions from higher HC. The values previously reported[1] were 27 and 41% for C_2H_2 and C_2H_4 respectively.

The data for $m/e = 30$ suggest that the percent I-M Rx for this ion is independent of pressure over the range studied; the average value was (49 ±3)%. This is in good agreement with the previously reported[1] value of 45% for C_2H_6.

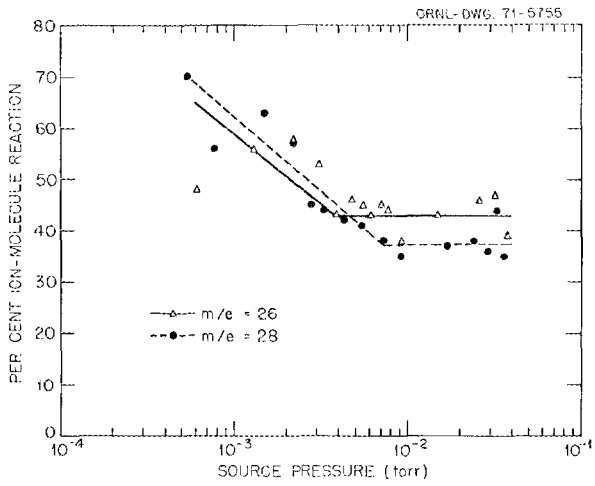

Fig. 7.58. Percent of ion-molecule reactions as a function of the methane pressure in the electric-field source.

Both the intensity and percent I-M Rx for $m/e = 30$ vs pressure differ from those for $m/e = 26$ and 28. The differences may be due to the fact that $m/e = 30$ is the "cleanest" ion studied (i.e., it has little contribution from higher HC), but further speculation is not warranted until a complete investigation of all parent ions (i.e., up to $C_4H_{10}^+$) is made.

---

1. P. S. Rudolph, p. 101 in *Radiation Chemistry II, Advan. Chem. Ser.* No 82 (1968).
2. American Petroleum Institute Research Project 44, *Catalog of Mass Spectral Data* (Texas A & M University, College Station), Serial No. 2.

CHARACTERIZATION OF VOLATILE AND NONVOLATILE SOLIDS OBTAINED FROM THE GAS PHASE RADIOLYSIS OF PENTABORANE-9[1]

J. W. Pinson[2] P. S. Rudolph
R. Baldock

Little information is available on the radiolysis of the hydrides of boron, silicon, and germanium even though they appear to be interesting compounds. One interesting aspect of these hydrides is their analogy to the paraffins, for example, diborane or boroethane (B_2H_6); they polymerize when irradiated as do the paraffins.

Work on the benzene-soluble fraction of the nonvolatile polymeric solids produced by the gamma-ray radiolysis of gaseous pentaborane-9 (B_5H_9) was previously reported.[3] Thermal-probe mass-spectral analyses (TMA) of this fraction[4] indicated several families of peaks, including one in the $m/e = 210$ region, suggesting that $B_{18}H_{22}$ might be a product, albeit a minor one.

A sample of pure octadecaborane ($B_{18}H_{22}$) was obtained, and its melting point was found to be 177 to 179°C. TMA's were made[4] on a portion of this sample. The same conditions as used in the analysis of the benzene-soluble fraction were used on this sample so

Table 7.16. Correlation of mass spectral data taken at 150°C and 15-eV energy

m/e	Relative abundance	
	Benzene-soluble fraction	$B_{18}H_{22}$
212	93	73
211	82	100
210	100	100
209	85	95

that the TMA results would be comparable. A comparison of the mass-spectral data is given in Table 7.16.

Differential thermal analyses (DTA) were made[5] on another portion of the $B_{18}H_{22}$. The thermograms from the $B_{18}H_{22}$ were very similar to those from the benzene-soluble fraction.

From the intercomparison of the TMA and DTA data, it appears that $B_{18}H_{22}$ is a component of the benzene-soluble fraction of the polymeric solids produced by the irradiation of B_5H_9.

Three 3-liter flasks filled with B_5H_9 at 200 torr were irradiated with ^{60}Co gamma rays[6] to produce larger quantities of the radiation-produced polymers for further characterization.

1. Research sponsored jointly with the University of Southern Mississippi, Hattiesburg.

2. Department of Chemistry, University of Southern Mississippi, Hattiesburg.

3. (*a*) J. W. Pinson and P. S. Rudolph, abstract PHYS-100, 159th National Meeting, American Chemical Society, Houston, Tex., Feb. 23–27, 1970; (*b*) J. W. Pinson, P. S. Rudolph, and R. Baldock, *Chem. Div. Annu. Progr. Rep. May 20, 1970,* ORNL-4581, p. 180.

4. Performed by W. T. Rainey, Jr., Analytical Chemistry Division.

5. The DTA's on $B_{18}H_{22}$ were in part performed by J. A. Solomon, undergraduate research student in chemistry at the University of Southern Mississippi, Hattiesburg.

6. We are indebted to W. W. Parkinson, Jr., Reactor Chemistry Division, for permission to use the 20,000-Ci ^{60}Co source and his help in its use.

Publications

NUCLEAR CHEMISTRY

A. C. Rester,[1,2] J. H. Hamilton,[1] A. V. Ramayya,[1] and N. R. Johnson, "Decay of ^{72}As to the Levels of ^{72}Ge," *Nucl. Phys. A* **162**, 481 (1971).

A. V. Ramayya,[1] B. Van Nooijen,[1,2] J. H. Ford,[1] D. Krmpotic,[1,3] J. H. Hamilton,[1] J. J. Pinajian,[4] and N. R. Johnson, "Energy Levels in ^{86}Sr from the Decay of 14.6-h ^{86}Y," *Phys. Rev. C* **2**, 2248 (1970).

J. R. Van Hise,[5,6] M. C. Kelley,[5,7] R. G. Lanier,[8,9] and N. R. Johnson, "Search for the 0^+ Member of the Two-Phonon Triplet in ^{110}Cd," *Phys. Rev. C* **1**, 1861 (1970).

L. L. Riedinger,[10] N. R. Johnson, and J. H. Hamilton,[1] "Studies of the Radioactive Decays of ^{152}Eu and ^{154}Eu," *Phys. Rev. C* **2**, 2358 (1970).

K. S. Toth[11] and R. L. Hahn, "α Decay from High-Spin Isomers in ^{153}Ho and ^{154}Ho," *Phys. Rev. C* **3**, 854 (1971).

K. S. Toth[11] and R. L. Hahn, "Search for New α-Emitters with $N = 86$ and $N = 87$," *Proc. Int. Conf. on the Properties of Nuclei Far from the Region of Beta-Stability*, CERN, Geneva, 1970, p. 533.

K. S. Toth,[11] R. L. Hahn, M. A. Ijaz,[12] and W. M. Sample,[12] "Production of Rare-Earth α-Emitters with Energetic ^{3}He Particles; New Isotopes, ^{151}Er, ^{156}Yb, and ^{157}Yb," *Phys. Rev. C* **2**, 1480 (1970).

J. H. Hamilton,[1] A. V. Ramayya,[1] P. E. Little,[1] and N. R. Johnson, "New Band-Mixing Anomalies in ^{178}Hf," *Phys. Rev. Lett.* **25**, 946 (1970).

G. D. Benson,[1] A. V. Ramayya,[1] R. G. Albridge,[1] and G. D. O'Kelley, "The Decay of ^{194}Au to the Levels of ^{194}Pt," *Nucl. Phys. A* **150**, 311 (1970).

Subcommittee on Radiochemistry, Committee on Nuclear Science, NAS-NRC (including G. D. O'Kelley), *Source Material for Radiochemistry*, National Academy of Sciences Report 42, 1970.

Lunar Sample Preliminary Examination Team (including P. R. Bell,[13] J. S. Eldridge,[14] V. A. McKay,[15] G. D. O'Kelley, and R. T. Roseberry,[15] *Apollo 12 Preliminary Science Report*, National Aeronautics and Space Administration Report SP-235 (1970).

---

1. Vanderbilt University, Nashville, Tenn.
2. Present address: Technological University of Delft, Department of Physics, Delft, Netherlands.
3. Present address: Boris Kidric Institute of Nuclear Science, Belgrade, Yugoslavia.
4. Isotopes Division.
5. Chemistry Department, Andrews University, Berrien Springs, Mich.
6. Present address: Tri-State College, Angola, Ind.
7. Present address: Lawrence Radiation Laboratory, University of California, Berkeley.
8. U.S. Atomic Energy Commission Postdoctoral Fellow under appointment with Oak Ridge Associated Universities.
9. Present address: Lawrence Radiation Laboratory, University of California, Livermore.
10. Oak Ridge Graduate Fellow from Vanderbilt University, Nashville, Tenn., under appointment with Oak Ridge Associated Universities. Present address: University of Notre Dame, Notre Dame, Ind.
11. Electronuclear Division.
12. Physics Department, Virginia Polytechnic Institute, Blacksburg.
13. Formerly of the NASA Manned Spacecraft Center, Houston, Tex., now of the Director's Division.
14. Analytical Chemistry Division.
15. Instrumentation and Controls Division.

CHEMISTRY AND PHYSICS OF TRANSURANIUM ELEMENTS

R. L. Hahn and O. W. Hermann,[16] "Inclusion of Fission and Charged-Particle Emission in Calculations of Nuclear Reactions; Computed Energies, Angles, and Ranges of Recoil Nuclei," ORNL-TM-3179 (April 1971).

M. R. Schmorak,[17] C. E. Bemis, Jr., M. Zender,[18] P. E. Coffman,[1] A. V. Ramayya,[1] and J. H. Hamilton,[1] "Evidence for a Two-Phonon Octupole Vibrational Band in ^{240}Pu," *Phys. Rev. Lett.* 24, 1507 (1970).

C. E. Bemis, Jr., R. J. Silva, J. E. Bigelow,[19] and A. M. Friedman,[20] "Search for a Long-Lived Spontaneous Fission Isomer of ^{241}Pu," *Inorg. Nucl. Chem. Lett.* **6**, 747 (1970).

R. J. Silva, R. L. Hahn, K. S. Toth,[11] M. L. Mallory, C. E. Bemis, Jr., P. F. Dittner, and O. L. Keller, "New Isotopes ^{241}Cf and ^{240}Cf," *Phys. Rev. C* 2, 1948 (1970).

C. E. Bemis, Jr., R. E. Druschel, and J. Halperin, "Effective Capture and Fission Cross Sections for ^{253}Cf," *Nucl. Sci. Eng.* **41**, 146 (1970).

P. F. Dittner, C. E. Bemis, Jr., D. C. Hensley,[11] R. J. Silva, and C. D. Goodman,[11] "Identification of the Atomic Number of Nobelium by an X-Ray Technique," *Phys. Rev. Lett.* **26**, 1037 (1971).

O. L. Keller, Jr., "Predicted Properties of Elements 113 and 114," *Chemistry* **43**, 8 (1970).

L. J. Nugent, R. D. Baybarz,[19] G. K. Werner,[21] and H. A. Friedman,[19] "Intramolecular Energy Transfer and Sensitized Luminescence in an Einsteinium β-Diketone Chelate and the Lower Lying Electronic Energy Levels of Es(III)," *Chem. Phys. Lett.* 7, 179 (1970).

L. J. Nugent, "Theory of the Tetrad Effect in the Lanthanide(III) and Actinide(III) Series," *J. Inorg. Nucl. Chem.* **32**, 3485 (1970).

L. J. Nugent, P. G. Laubereau,[22] G. K. Werner,[21] and K. L. Vander Sluis,[21] "Noncovalent Character in the Chemical Bonds of the Lanthanide(III) and Actinide(III) Tricyclopentadienides," *J. Organometal. Chem.* 27, 365 (1971).

J. H. Burns and J. R. Peterson,[23] "Refinement of the Crystal Structure of $AmCl_3$," *Acta Crystallogr., Sect. B* **26**, 1885 (1970).

J. H. Burns and J. R. Peterson,[23] "The Crystal Structures of Americium Trichloride Hexahydrate and Berkelium Trichloride Hexahydrate," *Inorg. Chem.* **10**, 147 (1971).

M. D. Danford, J. H. Burns, C. E. Higgins, J. R. Stokely, Jr.,[14] and W. H. Baldwin, "Preparation and Properties of Some Rare Earth and Americium Chelates," *Inorg. Chem.* **9**, 1953 (1970).

J. R. Peterson,[23] J. A. Fahey,[24,25] and R. D. Baybarz,[19] "The Preparation and Some Properties of Berkelium Metal," *Proc. 4th Int. Conf. on Plutonium and Other Actinides,* Santa Fe, N.M., Oct. 5–9, 1970; *Nucl. Met.* **17** (I), 20 (1970).

R. L. Hahn, R. L. Stone,[26] J. R. Tarrant, and L. D. Hunt, "A Fast-Closing Valve to Protect an Accelerator from Radioactive Contamination," *Nucl. Instrum. Methods* **86**, 331 (1970).

---

16. Mathematics Division.
17. Nuclear Data Project.
18. Oak Ridge Associated Universities Research Participant from Fresno State College, Fresno, Calif.
19. Chemical Technology Division.
20. Chemistry Division, Argonne National Laboratory, Argonne, Ill.
21. Physics Division.
22. Visiting scientist from the Federal Republic of Germany, Bonn.
23. Consultant, Department of Chemistry, University of Tennessee, Knoxville.
24. Oak Ridge Graduate Fellow from the University of Tennessee, Knoxville, under appointment with Oak Ridge Associated Universities.
25. Present address: Chemistry Department, Bronx Community College, Bronx, N.Y.
26. Plant and Equipment Division.

ISOTOPE CHEMISTRY

A. A. Palko, L. Landau, and J. S. Drury, "Chemical Fractionation of Carbon Isotopes," *Ind. Eng. Chem., Process Des. Develop.* **10**, 79 (1971).

G. Torsi,[27] G. Mamantov,[27] and G. M. Begun, "Raman Spectra of the $AlCl_3$-NaCl System," *Inorg. Nucl. Chem. Lett.* **6**, 553 (1970).

A. A. Palko, "Method for Fractionation of Carbon Isotopes," U.S. Pat. 3,535,079 (Oct. 20, 1970).

RADIATION CHEMISTRY

J. A. Ghormley and C. J. Hochanadel, "Production of H, OH, and H_2O_2 in the Flash Photolysis of Ice," *J. Phys. Chem.* **75**, 40 (1971).

J. A. Ghormley and C. J. Hochanadel, "Amorphous Ice: Density and Reflectivity," *Science* **171**, 62 (1971).

R. W. Matthews,[28] H. A. Mahlman, and T. J. Sworski, "Kinetics of the Oxidation of Cerium(III) by Peroxysulfuric Acids Induced by ^{60}Co Gamma Radiation," *J. Phys. Chem.* **74**, 2475 (1970).

R. W. Matthews,[28] H. A. Mahlman, and T. J. Sworski, "Kinetic Evidence That G_{OH} in the Radiolysis of Aqueous Sulfuric and Nitric Acid Solutions Is Proportional to Electron Fraction Water," *J. Phys. Chem.* **74**, 3835 (1970).

H. A. Mahlman, R. W. Matthews,[28] and T. J. Sworski, "Reduction of Cerium(IV) by Hydrogen Peroxide. Dependence of Reaction Rate on Hammett's Acidity Function," *J. Phys. Chem.* **75**, 250 (1971).

ORGANIC CHEMISTRY

C. J. Collins, B. M. Benjamin, V. F. Raaen, I. T. Glover,[29] and M. D. Eckart,[24,30] "Molekulare Umlagerungen XXVI. Ringöffnung durch Desaminierung von substituierten 2-*endo*-Bicyclo[2.2.1]heptylaminen," *Justus Liebigs Ann. Chem.* **739**, 7 (1970).

C. J. Collins and N. S. Bowman,[27] editors, *Isotope Effects in Chemical Reactions,* American Chemical Society Monograph, Van Nostrand Reinhold, New York, 1971.

PHYSICAL CHEMISTRY

G. Scatchard,[31] R. M. Rush, and J. S. Johnson, "Osmotic and Activity Coefficients for Binary Mixtures of Sodium Chloride, Sodium Sulfate, Magnesium Sulfate, and Magnesium Chloride in Water at 25°. III. Treatment with the Ions as Components,"[32] *J. Phys. Chem.* **74**, 3786 (1970).

R. J. Herdklotz,[24,33] "The Thermodynamic Properties of Aqueous Hydrochloric Acid–Sodium Chloride–Magnesium Chloride Mixtures as Calculated from Electromotive Force Measurements," Ph.D. thesis, University of Tennessee, Knoxville, July 1970.

L. Dresner, "Theory of the Porous-Frit Method of Measuring Self-Diffusion Constants,"[34] ORNL-4667 (March 1971).

---

27. Department of Chemistry, University of Tennessee, Knoxville.
28. Visiting scientist from the Australian Atomic Energy Commission Research Establishment, Lucas Heights, New South Wales.
29. Present address: Oak Ridge Associated Universities, Special Training Division.
30. Present address: Tennessee Eastman Corporation, Kingsport, Tenn.
31. Consultant; Professor of Physical Chemistry, Emeritus, Massachusetts Institute of Technology, Cambridge.
32. Research jointly sponsored by the Office of Saline Water, U.S. Department of the Interior, and by the U.S. Atomic Energy Commission under contract with Union Carbide Corporation and under Contract No. AT-(30-1)-905 with the Massachusetts Institute of Technology.
33. Present address: Chemistry Department, Bob Jones University, Greenville, S.C.
34. Research jointly sponsored by the ORNL-NSF Environmental Program and by the Office of Saline Water, U.S. Department of the Interior, under Union Carbide Corporation's contract with the U.S. Atomic Energy Commission.

R. J. Raridon and K. A. Kraus,[35] "Properties of Organic-Water Mixtures. Activity Coefficients of Sodium Chloride at Saturation in Aqueous Solutions of Some Oxy-Oxa Compounds at 25°C,"[36] *J. Chem. Eng. Data* **16**, 241 (1971).

J. J. Perona,[19,37] T. W. Pickel,[38] and K. A. Kraus,[35] "Hyperfiltration Studies XVIII. The Optimization of Two-Stage Plants for the Desalination of Brackish Waters,"[39] *Desalination* 8, 73 (1970).

R. J. Raridon and K. A. Kraus,[35] "Properties of Solutions," OSW Research and Development Report No. 685 (October 1970).

J. S. Johnson, Jr., and K. A. Kraus,[35] "Separations Processes," OSW Research and Development Report No. 508 (February 1970).

Water Research Program (J. A. Dahlheimer,[40,41] J. S. Johnson, W. R. Mixon,[40] and K. A. Kraus[35]), "Application of Hyperfiltration to Treatment of Municipal Sewage Effluents," Water Pollution Control Research Series, ORD-17030 EOHO1/70 (January 1970).

J. S. Johnson and K. A. Kraus,[35] "Method of Making a Dynamic Solute-Rejecting Membrane," U.S. Pat. 3,503,789 (Mar. 31, 1970).

A. E. Marcinkowsky,[42] J. S. Johnson, Jr., K. A. Kraus,[35] and J. R. Kuppers,[43] "Hyperfiltration Method of Removing Organic Solute from Aqueous Solutions," U.S. Pat. 3,537,988 (Nov. 3, 1970).

A. S. Dworkin and M. A. Bredig, "Pretransition Behavior of Solid Potassium and Thallium Sulfates from Heat Content and Thermal Expansion," *J. Phys. Chem.* 74, 3403 (1970).

A. S. Dworkin and M. A. Bredig, "Miscibility of Liquid Metals with Salts. IX. The Pseudobinary Alkali Metal–Metal Halide Systems: Cesium Iodide–Sodium, Cesium Iodide–Lithium, and Lithium Fluoride–Potassium," *J. Phys. Chem.* 74, 3828 (1970).

A. S. Dworkin and M. A. Bredig, "Enthalpy of Alkali Metal Fluoroborates from 298–1000°K. Enthalpies and Entropies of Fusion and Transition," *J. Chem. Eng. Data* **15**, 505 (1970).

A. S. Dworkin and M. A. Bredig, "Enthalpy of Lanthanide Chlorides, Bromides and Iodides from 298–1300°K. Enthalpies of Fusion and Transition," *High Temp. Sci.* **3**, 81 (1971).

C. W. Linsey,[44] "High Temperature Enthalpies of the Lead Halides: Enthalpies and Entropies of Fusion," Ph.D. Dissertation, North Texas State University, Denton, June 1970.

G. H. Cartledge, "Free Energies of Formation of Hydrous Oxides of Technetium in Its Lower Valencies," *J. Electrochem. Soc.* **118**, 231 (1971).

---

35. Director's Division.

36. Research sponsored by the Office of Saline Water, U.S. Department of the Interior, under Union Carbide Corporation's contract with the U.S. Atomic Energy Commission.

37. Present address: Department of Chemical Engineering, University of Tennessee, Knoxville.

38. General Engineering Division.

39. Research jointly sponsored by the Office of Saline Water, U.S. Department of the Interior, and by the U.S. Atomic Energy Commission under contract with Union Carbide Corporation.

40. Reactor Division.

41. Present address: WEDCO Corporation, Buchanan, N.Y.

42. Present address: Union Carbide Corporation, South Charleston, W.Va.

43. Oak Ridge Associated Universities Research Participant from the University of North Carolina, Charlotte.

44. Oak Ridge Graduate Fellow under appointment with Oak Ridge Associated Universities. Present address: Emporia College, Emporia, Kan.

R. E. Meyer, M. C. Banta,[45] P. M. Lantz, and F. A. Posey, "Chronopotentiometry and Voltammetry of the Ag-AgCl Electrode in Flowing Streams. I. Experimental,"[39] *J. Electroanal. Chem. Interfacial Electrochem.* **30**, 345 (1971).

F. A. Posey and R. E. Meyer, "Chronopotentiometry and Voltammetry of the Ag-AgCl Electrode in Flowing Streams. II. Theoretical,"[39] *J. Electroanal. Chem. Interfacial Electrochem.* **30**, 359 (1971).

CHEMICAL PHYSICS

Z. M. El Saffar[46] and G. M. Brown, "The Structure of Manganese Dichloride Tetrahydrate: A Neutron Diffraction Study," *Acta Crystallogr., Sect. B* **27**, 66 (1971).

L. H. Hall[47] and G. M. Brown, "The Crystal and Molecular Structure of N-Formylaminomethylferrocene, $[(C_5H_5)Fe(C_5H_4)]CH_2NHCHO$," *Acta Crystallogr., Sect. B* **27**, 81 (1971).

W. E. Thiessen and H. Hope,[48] "The Structure and Absolute Configuration of Solstitialin, $C_{15}H_{20}O_5$," *Acta Crystallogr., Sect. B* **26**, 554 (1970).

R. D. Ellison, C. K. Johnson, and H. A. Levy, "Glycolic Acid: Direct Neutron Diffraction Determination of Crystal Structure and Thermal Motion Analysis," *Acta Crystallogr., Sect. B* **27**, 333 (1971).

W. R. Busing, "An Interpretation of the Structures of Alkaline Earth Chlorides in Terms of Interionic Forces," *Trans. Amer. Crystallogr. Ass.* **6**, 57 (1970).

W. R. Busing, "Least-Squares Refinement of Lattice and Orientation Parameters for Use in Automatic Diffractometry," pp. 319–30 in *Crystallographic Computing,* edited by F. D. Ahmed, Munksgaard Publishing Co., 1970.

C. K. Johnson, "An Introduction to Thermal-Motion Analysis," pp. 207–19 in *Crystallographic Computing,* edited by F. D. Ahmed, Munksgaard Publishing Co., 1970.

C. K. Johnson, "The Effect of Thermal Motion on Interatomic Distances and Angles," pp. 220–26 in *Crystallographic Computing,* edited by F. D. Ahmed, Munksgaard Publishing Co., 1970.

C. K. Johnson, "Drawing Crystal Structures by Computer," pp. 227–30 in *Crystallographic Computing,* edited by F. D. Ahmed, Munksgaard Publishing Co., 1970.

C. K. Johnson, "ORTEP, a Fortran Thermal-Ellipsoid Plot Program for Crystal Structure Illustrations," ORNL-3794 (Second Revision, June 1970).

L. Blum,[49] "X-Ray Scattering from Liquids with Nearly Spherical Molecules," *J. Comput. Phys.* **7**, 222 (1971).

C. Folzer,[50] R. W. Hendricks,[51] and A. H. Narten, "Diffraction Pattern and Structure of Liquid Trimethylamine Decahydrate at 5°C," *J. Chem. Phys.* **54**, 799 (1971).

R. Livingston and H. Zeldes, "Paramagnetic Resonance Study of Liquids during Photolysis. VIII. An Emission Spectrum from Solutions of Tartaric Acid," *J. Chem. Phys.* **53**, 1406 (1970).

H. Zeldes and R. Livingston, "Paramagnetic Resonance Study of Liquids during Photolysis. IX. Oxalic Acid and Its Esters," *J. Phys. Chem.* **74**, 3336 (1970).

---

45. Summer faculty employee, 1969; present address: Department of Chemistry, Sam Houston State University, Huntsville, Tex.
46. Visiting scientist from Iraq, 1965–1966. Present address: Department of Physics, DePaul University, Chicago, Ill.
47. Oak Ridge Associated Universities Research Participant from Florida Atlantic University, Boca Raton, summer 1966. Present address: Department of Chemistry, Eastern Nazarene College, Wollaston, Mass.
48. Department of Chemistry, University of California, Davis.
49. Oak Ridge Associated Universities Research Participant from Department of Physics, University of Puerto Rico, Rio Piedras.
50. Visiting scientist from the University of Pittsburgh, Pittsburgh, Pa., 1970.
51. Metals and Ceramics Division.

R. Livingston, J. K. Dohrmann,[52] and H. Zeldes, "Paramagnetic Resonance Study of Liquids during Photolysis. X. Hyperfine Interactions from ^{13}C," *J. Chem. Phys.* **53**, 2448 (1970).

H. Zeldes and R. Livingston, "Paramagnetic Resonance Study of Liquids during Photolysis. XI. Citric Acid and Sodium Citrate in Aqueous Solution," *J. Amer. Chem. Soc.* **93**, 1082 (1971).

M. M. Abraham,[53] L. A. Boatner,[54] C. B. Finch,[51] R. W. Reynolds,[54] and H. Zeldes, "EPR Investigations of Divalent Americium and Trivalent Curium in Strontium Chloride," *Phys. Rev. B* **1**, 3555 (1970).

T. A. Carlson, C. W. Nestor, Jr.,[16] N. Wasserman,[55] and J. D. McDowell,[16] "Comprehensive Calculation of Ionization Potentials and Binding Energies for Multiply-Charged Ions," ORNL-4562 (July 1970).

L. D. Hulett[14] and T. A. Carlson, "Analysis of Compounds of Biological Interest by Electron Spectroscopy," *Clin. Chem.* **16**, 677 (1970).

B. P. Pullen,[24,56] T. A. Carlson, W. E. Moddeman,[57] G. K. Schweitzer,[27] W. E. Bull,[27] and F. A. Grimm,[27] "Photoelectron Spectra of Methane, Silane, Germane, Methyl Fluoride, Difluoromethane, and Trifluoromethane," *J. Chem. Phys.* **53**, 768 (1970).

W. E. Bull,[27] B. P. Pullen,[24,56] F. A. Grimm,[27] W. E. Moddeman,[57] G. K. Schweitzer,[27] and T. A. Carlson, "High-Resolution Photoelectron Spectroscopy of Carbon and Silicon Tetrafluorides," *Inorg. Chem.* **9**, 2474 (1970).

T. A. Carlson, C. C. Lu,[16] T. C. Tucker,[16] C. W. Nestor, Jr.,[16] and F. B. Malik,[58] "Eigenvalues, Radial Expectation Values, and Potentials for Free Atoms from $Z = 2$ to 126 as Calculated from Relativistic Hartree-Fock-Slater Atomic Wave Functions," ORNL-4614 (December 1970).

T. A. Carlson, C. W. Nestor, Jr.,[16] N. Wasserman,[55] and J. D. McDowell,[16] "Calculated Ionization Potentials for Multiply Charged Ions," *At. Data* 2, 63 (1970).

L. D. Hulett[14] and T. A. Carlson, "Measurements of Chemical Shifts in the Photoelectron Spectra of Arsenic and Bromine Compounds," *Appl. Spectrosc.* **25**, 33 (1971).

T. A. Carlson, "Spectroscopy, Photoelectron," pp. 400–402 in *McGraw-Hill Yearbook of Science and Technology, 1971.*

T. A. Carlson, "Angular Dependence of Vibrational Structure in the Photoelectron Spectra of N_2 and O_2," *Chem. Phys. Lett.* **9**, 23 (1971).

W. E. Moddeman,[57] "Auger Spectroscopy of Simple Gaseous Molecules," Ph.D. thesis, University of Tennessee, Knoxville, September 1970; ORNL-TM-3012 (September 1970).

S. Datz, H. O. Lutz,[59] L. B. Bridwell,[60] C. D. Moak,[21] H. D. Betz,[61,62] and L. D. Ellsworth,[61] "Electron Capture and Loss Cross Sections of Fast Bromine Ions in Gases," *Phys. Rev. A* 2, 430 (1970).

---

52. Visiting scientist from Institut für Physikalische Chemie der Freien Universität Berlin, Germany, 1969–1970.
53. Solid State Division.
54. Applied Technology Center, Inc., Dallas, Tex.
55. Oak Ridge Associated Universities Summer Student Trainee from Cornell University, Ithaca, N.Y., summer 1968.
56. Present address: Southeastern Louisiana State College, Hammond.
57. Graduate student from the University of Tennessee, Knoxville, supported by National Aeronautics and Space Administration research grant NGL 43-001-021, Supplement 3. Present address: Vanderbilt University, Nashville, Tenn.
58. Indiana University, Bloomington.
59. Present address: Kernforschungsanlage, Jülich, West Germany.
60. Present address: Physics Department, Murray State University, Murray, Ky.
61. Physics Department, Kansas State University, Manhattan.
62. Present address: Physics Department, Massachusetts Institute of Technology, Cambridge.

S. Datz, C. D. Moak,[21] B. R. Appleton,[53] M. T. Robinson,[53] and O. S. Oen,[53] "Energy Dependence of Channeled Ion Energy Loss Spectra," p. 374 in *Atomic Collision Phenomena in Solids,* edited by D. W. Palmer, M. W. Thompson, and P. D. Townsend, North-Holland Press, 1970.

J. Anderson,[63] S. Datz, P. Hvelplund,[63] and G. Sørensen,[63] "Channeling Effects in the Light Emission from Helium Ion Beams Excited by a Gold Single Crystal," *Phys. Lett. A* **33**, 121 (1970).

H. O. Lutz,[59] C. D. Moak,[21] and T. S. Noggle,[53] "Non-Equilibrium Charge States of 60 MeV I Ions Channeled in Au Single Crystals," *Phys. Lett. A* **33**, 309 (1970).

---

63. Institute of Physics, University of Aarhus, Denmark.

Papers Presented at Scientific and Technical Meetings

NUCLEAR CHEMISTRY

E. Eichler and S. Raman,*[1] "New Observations in the A = 49 Decay Chain; Levels in ^{49}Sc and ^{49}Ti," 1971 Spring Meeting, American Physical Society, Washington, D.C., Apr. 26–29; *Bull. Amer. Phys. Soc.* **16**, 494 (1971).

N. R. Johnson, "Spectroscopic Studies of Nuclear Structure," Southeast-Southwest Regional Meeting, American Chemical Society, New Orleans, La., Dec. 2–4, 1970; abstract NUCL-303 (invited).

N. C. Singhal,*[2] N. R. Johnson, E. Eichler, and J. H. Hamilton,[3] "The Decay of ^{104}Rh," 1971 Annual Meeting, American Physical Society, New York, Feb. 1–4; *Bull. Amer. Phys. Soc.* **16**, 14 (1971).

E. Collins,[3] J. H. Hamilton,*[3] P. E. Little,[3] A. V. Ramayya,[3] and N. R. Johnson, "γ-γ Directional Correlations of the 961-89 and 2089-89 keV Cascades in ^{156}Gd," International Conference on Angular Correlations in Nuclear Disintegrations, Delft, Netherlands, Aug. 17–21, 1970.

N. R. Johnson, A. F. Kluk,*[4] and J. H. Hamilton,[3] "Properties of the β- and γ-Vibrational Levels of ^{156}Gd Populated in the Decay of ^{156}Eu," 1971 Annual Meeting, American Physical Society, New York, Feb. 1–4; *Bull. Amer. Phys. Soc.* **16**, 130 (1971).

A. F. Kluk,*[4] N. R. Johnson, and J. H. Hamilton,[3] "Levels of ^{158}Gd Populated by the Decay of ^{158}Eu," 1971 Annual Meeting, American Physical Society, New York, Feb. 1–4; *Bull. Amer. Phys. Soc.* **16**, 130 (1971).

K. S. Toth*[5] and R. L. Hahn, "Search for New α-Emitters with N = 86 and N = 87," International Conference on the Properties of Nuclei Far from the Region of Beta-Stability, Leysin, Switzerland, Aug. 31–Sept. 4, 1970.

K. S. Toth*[5] and R. L. Hahn, "Search for New α-Emitters with N = 86 and N = 87," 160th National Meeting, American Chemical Society, Chicago, Ill., Sept. 14–18, 1970; abstract NUCL-62.

K. S. Toth*[5] and R. L. Hahn, "α Decay from High-Spin Isomers in ^{153}Ho and ^{154}Ho," 1970 Fall Meeting, American Physical Society, New Orleans, La., Nov. 23–25; *Bull. Amer. Phys. Soc.* **15**, 1358 (1970).

K. S. Toth,*[5] R. L. Hahn, and M. A. Ijaz,[6] "Search for the New Isotopes, ^{155}Tm and ^{156}Tm," 1971 Spring Meeting, American Physical Society, Washington, D.C., Apr. 26–29; *Bull. Amer. Phys. Soc.* **16**, 539 (1971).

G. D. O'Kelley,* J. S. Eldridge,[7] E. Schonfeld,[8] and P. R. Bell,[9] "Comparative Radionuclide Concentrations and Ages of Apollo 11 and Apollo 12 Samples from Nondestructive Gamma-Ray Spectrometry," Second Lunar Science Conference, Houston, Tex., Jan. 11–14, 1971.

E. Schonfeld*[8] and G. D. O'Kelley, "The Selenographic Orientation of Apollo 12 Rocks Determined by Nondestructive Gamma-Ray Spectroscopy," Second Lunar Science Conference, Houston, Tex., Jan. 11–14, 1971.

---

*Speaker.

1. Nuclear Data Project.
2. Graduate research assistant from Vanderbilt University, Nashville, Tenn.
3. Physics Department, Vanderbilt University, Nashville, Tenn.
4. Oak Ridge Graduate Fellow from Vanderbilt University, Nashville, Tenn., under appointment with Oak Ridge Associated Universities. Present address: U.S. Atomic Energy Commission, Washington, D.C.
5. Electronuclear Division.
6. Physics Department, Virginia Polytechnic Institute, Blacksburg.
7. Analytical Chemistry Division.
8. NASA Manned Spacecraft Center, Houston, Tex.
9. Formerly of the NASA Manned Spacecraft Center, Houston, Tex., now of the Director's Division.

J. S. Eldridge,*[7] K. J. Northcutt,[7] and G. D. O'Kelley, "Standards for Low-Level Gamma-Ray Spectrometry of Lunar and Geochemical Samples," Symposium on Standard Radioactive Materials and Their Uses, 161st National Meeting, American Chemical Society, Los Angeles, Calif., Mar. 28–Apr. 2, 1971; abstract NUCL-7.

CHEMISTRY AND PHYSICS OF TRANSURANIUM ELEMENTS

R. L. Hahn* and K. S. Toth,[5] "Emission of Charged Particles in Complex Nuclear Reactions on Heavy Targets," 160th National Meeting, American Chemical Society, Chicago, Ill., Sept. 14–18, 1970; abstract NUCL-17.

R. L. Hahn, "Recent Research with Heavy Ions and Heavy Elements at Oak Ridge," Heavy Ion Users' Meeting, Columbia University, New York, Feb. 5, 1971 (invited).

J. L. C. Ford, Jr.,*[10] P. H. Stelson,[10] R. L. Robinson,[10] F. K. McGowan,[10] W. T. Milner,[10] and C. E. Bemis, Jr., "Coulomb Excitation of ^{197}Au, ^{204}Hg, and ^{238}U," 1971 Spring Meeting, American Physical Society, Washington, D.C., Apr. 26–29; *Bull. Amer. Phys. Soc.* **16**, 515 (1971).

E. Eichler,* N. R. Johnson, C. E. Bemis, and R. O. Sayer,[11] "Coulomb Excitation of ^{242}Pu and ^{238}U with Heavy Ions," 1971 Spring Meeting, American Physical Society, Washington, D.C., Apr. 26–29; *Bull. Amer. Phys. Soc.* **16**, 494 (1971).

M. J. Zender,[12] C. E. Bemis, Jr., and M. R. Schmorak,*[1] "Rotational Parameters in the $A > 230$ Mass Region," 1970 Meeting, American Physical Society, Houston, Tex., Oct. 15–17; *Bull. Amer. Phys. Soc.* **15**, 1650 (1970).

M. R. Schmorak,[1] N. B. Gove,[13] C. E. Bemis, Jr.,* and M. J. Zender,[12] "Ground State Rotational Bands in Even-Even Actinide Nuclei," International Conference on Heavy Ion Physics, Dubna, U.S.S.R., Feb. 11–17, 1971 (invited).

Y. Y. Chu,[14] M. L. Perlman,[14] P. F. Dittner, and C. E. Bemis, Jr.,* "Electron Binding Energies and Fluorescent Yields in Curium (Z = 96)," International Conference on Heavy Ion Physics, Dubna, U.S.S.R., Feb. 11–17, 1971.

P. F. Dittner* and C. E. Bemis, Jr., "K X-Ray Energies and Intensities of Cm, Bk, Cf, Es, and Fm," 1971 Spring Meeting, American Physical Society, Washington, D.C., Apr. 26–29; *Bull. Amer. Phys. Soc.* **16**, 617 (1971).

Y. Y. Chu,[14] M. L. Perlman,[14] P. F. Dittner,* and C. E. Bemis, Jr., "Determination of Electron Binding Energies in Curium (Z = 96)," 1971 Spring Meeting, American Physical Society, Washington, D.C., Apr. 26–29; *Bull. Amer. Phys. Soc.* **16**, 618 (1971).

C. E. Bemis, Jr.,* P. F. Dittner, D. C. Hensley,[5] C. D. Goodman,[5] and R. J. Silva, "The Unequivocal Identification of Transfermium Elements by X-Ray Techniques," International Conference on Heavy Ion Physics, Dubna, U.S.S.R., Feb. 11–17, 1971 (invited).

R. J. Silva, "Recent Chemical Studies of the Transfermium Elements in the United States," Conference on Radiochemistry, Dubna, U.S.S.R., Sept. 28–Oct. 8, 1970.

O. L. Keller, Jr., "Investigations of Transuranium Elements as Sources of Radiation and Power," Journèes Techniques de Paris, 9ème Salon International de la Chimie, Apr. 19–24, 1971 (invited).

O. L. Keller, Jr., "Transactinide and Superheavy Elements," Southeast-Southwest Regional Meeting, American Chemical Society, New Orleans, La., Dec. 2–4, 1970 (invited).

L. J. Nugent, "Theory of the Tetrad Effect in the Lanthanide(III) and Actinide(III) Series," Southeast-Southwest Regional Meeting, American Chemical Society, New Orleans, La., Dec. 2–4, 1970.

---

10. Physics Division.
11. Physics Department, Furman University, Greenville, S.C.
12. Oak Ridge Associated Universities Research Participant from Fresno State College, Fresno, Calif.
13. Mathematics Division.
14. Department of Chemistry, Brookhaven National Laboratory, Upton, Long Island, N.Y.

J. H. Burns* and P. G. Laubereau,[15] "The Crystal and Molecular Structure of Uranium Triindenide Chloride," Winter Meeting, American Crystallographic Association, University of South Carolina, Columbia, Jan. 31–Feb. 4, 1971.

J. L. Atwood,*[16] J. H. Burns, and P. G. Laubereau,[15] "The Crystal and Molecular Structure of Tris(indenyl)samarium," Winter Meeting, American Crystallographic Association, University of South Carolina, Columbia, Jan. 31–Feb. 4, 1971.

J. R. Peterson,*[17] J. A. Fahey,[18,19] and R. D. Baybarz,[20] "The Preparation and Some Properties of Berkelium Metal," Fourth International Conference on Plutonium and Other Actinides, Santa Fe, N.M., Oct. 5–9, 1970.

J. R. Peterson,[17] "Chemistry of the Transplutonium Elements," Symposium on Advances in Nuclear Chemistry, Southeast-Southwest Regional Meeting, American Chemical Society, New Orleans, La., Dec. 2–4, 1970 (invited).

ISOTOPE CHEMISTRY

G. M. Begun,* G. Torsi,[21] and G. Mamantov,[21] "The Raman Spectra of Aluminum Trihalide–Sodium Halide System," Symposium on Molecular Structure and Spectroscopy, Ohio State University, Columbus, Sept. 12, 1970.

PHYSICAL CHEMISTRY

G. Scatchard,[22] J. S. Johnson, and R. M. Rush,* "Free Energies of Mixed Electrolyte Solutions," 160th National Meeting, American Chemical Society, Chicago, Ill., Sept. 14–18, 1970; abstract PHYS-42 (invited paper for H.S. Harned Memorial Symposium).

M. H. Lietzke* and R. J. Herdklotz,[18,23] "Activity Coefficient Behavior in Several Aqueous Four-Component Systems," 160th National Meeting, American Chemical Society, Chicago, Ill., Sept. 14–18, 1970; abstract PHYS-43 (invited paper for H. S. Harned Memorial Symposium).

M. H. Lietzke, "Activity Coefficient Behavior in Multicomponent Electrolyte Systems," Gordon Research Conference on Electrochemistry, Santa Barbara, Calif., Jan. 19, 1971.

K. A. Kraus,[24] H. O. Phillips, R. J. Raridon,* and S. B. Sachs,[25] "Some Properties of Electrolytes in Water-Organic Mixtures," 160th National Meeting, American Chemical Society, Chicago, Ill., Sept. 14–18, 1970; abstract PHYS-65 (invited paper for H. S. Harned Memorial Symposium).

J. S. Johnson, Jr., "Hyperfiltration," Gordon Research Conference on Separations and Purifications, New London, N.H., Sept. 4, 1970 (invited).

K. A. Kraus,[24] "Hyperfiltration and Related Methods," Symposium on Reverse Osmosis, Roswell, N.M., Nov. 5, 1970 (invited).

E. H. Taylor, "A Kinetic Argument against the Existence of Anomalous Water," 44th Annual Colloid Symposium, Lehigh University, Bethlehem, Pa., June 22–24, 1970.

---

15. Visiting scientist from the Federal Republic of Germany, Bonn.
16. Department of Chemistry, University of Alabama, University.
17. Consultant, Department of Chemistry, University of Tennessee, Knoxville.
18. Oak Ridge Graduate Fellow from the University of Tennessee, Knoxville, under appointment with Oak Ridge Associated Universities.
19. Present address: Chemistry Department, Bronx Community College, Bronx, N.Y.
20. Chemical Technology Division.
21. Department of Chemistry, University of Tennessee, Knoxville.
22. Consultant; Professor of Physical Chemistry, Emeritus, Massachusetts Institute of Technology, Cambridge.
23. Present address: Chemistry Department, Bob Jones University, Greenville, S.C.
24. Director's Division.
25. Visiting scientist from the Weizmann Institute of Science, Rehovoth, Israel.

CHEMICAL PHYSICS

G. M. Brown* and G. R. Freeman,[26] "Crystal Structure of $(C_6H_5C_6H_4)_3\dot{N}^+ClO_4^-$, Tri(*p*-biphenylyl)aminium Perchlorate," Winter Meeting, American Crystallographic Association, University of South Carolina, Columbia, Jan. 31–Feb. 4, 1971.

W. R. Busing* and E. C. Kostansek,[27] "Urea–Phosphoric Acid: Is It a Salt?" Winter Meeting, American Crystallographic Association, University of South Carolina, Columbia, Jan. 31–Feb. 4, 1971.

C. K. Johnson, "Thermal-Motion Skewness and ORTEP-II," Winter Meeting, American Crystallographic Association, University of South Carolina, Columbia, Jan. 31–Feb. 4, 1971.

A. H. Narten, "Water: X-Ray Scattering and Radial Distribution," Gordon Research Conference on Structural Aspects of Water and Aqueous Solutions, Tilton, N.H., June 14–19, 1970.

A. H. Narten, "Analysis and Interpretation of Diffraction Data from Liquids," Italian Crystallographic Society Congress, Cagliari, Italy, Sept. 27–Oct. 3, 1970.

F. Vaslow, "Salt-Induced Critical-Type Transitions in Aqueous Solution. Heats of Dilution of the Lithium and Sodium Halides," 160th National Meeting, American Chemical Society, Chicago, Ill., Sept. 14–18, 1970; abstract PHYS-192.

R. Livingston, "EPR of Transient Species Formed by Photolysis," Joint Conference of The Chemical Institute of Canada and the American Chemical Society, Toronto, Canada, May 24–29, 1970 (invited).

H. Zeldes, "Paramagnetic Resonance of Liquids during Photolysis," Second Southeastern Magnetic Resonance Conference, University of South Carolina, Columbia, Oct. 1–2, 1970 (invited).

L. D. Hulett*[7] and T. A. Carlson, "Applications of Electron Spectroscopy in Analytical Chemistry," Mid-America Spectroscopy Symposium, Chicago, Ill., June 2–5, 1970.

W. E. Moddeman,*[28] T. A. Carlson, M. O. Krause,[29] B. P. Pullen,[18,30] G. K. Schweitzer,[21] and W. E. Bull,[21] "Electronic States of the Singly and Doubly Positive Ions of Simple Molecules as Seen by Auger Spectroscopy," Mid-America Spectroscopy Symposium, Chicago, Ill., June 2–5, 1970.

T. A. Carlson, "Recent Work in Electron Spectroscopy at Oak Ridge," EUCHEM Research Conference on Electron Spectroscopy, Uppsala, Sweden, Sept. 7–9, 1970 (invited).

L. D. Hulett*[7] and T. A. Carlson, "Studies of Chemical Shifts in Inner Shell Binding Energies by Photoelectron Spectroscopy," 160th National Meeting, American Chemical Society, Chicago, Ill., Sept. 14–18, 1970.

W. E. Bull,*[21] W. E. Moddeman,[28] F. A. Grimm,[21] and T. A. Carlson, "Auger Spectra of CH_4, CH_3F, CH_2F_2, CHF_3, SiH_4, and SiF_4," Conference on Photoionization Phenomena and Photoelectron Spectroscopy, Oxford, England, Sept. 14–16, 1970.

M. O. Krause,[29] "Hard Photons – Soft X Rays; Use of $M\zeta$ Lines of Y to Rh in Photoelectron Spectrometry," Conference on Photoionization Phenomena and Photoelectron Spectroscopy, Oxford, England, Sept. 14–16, 1970.

---

26. Oak Ridge Graduate Fellow from North Texas State University, Denton, under appointment with Oak Ridge Associated Universities, 1968–69. Present address: University of Alabama Medical Center, Birmingham.

27. Oak Ridge Associated Universities Summer Student Trainee from Hiram College, Hiram, Ohio, summer 1969.

28. Graduate student from the University of Tennessee, Knoxville, supported by National Aeronautics and Space Administration research grant NGL 43-001-021, Supplement 3. Present address: Vanderbilt University, Nashville, Tenn.

29. Formerly of the Thermonuclear Division.

30. Present address: Southeastern Louisiana State College, Hammond.

T. A. Carlson,* M. O. Krause,[29] and W. E. Moddeman,[28] "Excitation Accompanying Photoionization in Atoms and Molecules and Its Relationship to Electron Correlation," Conference on Simple and Multiple Electronic Processes in the Region of X-Rays and Vacuum UV, Paris, France, Sept. 21–25, 1970.

M. O. Krause,*[29] T. A. Carlson, and W. E. Moddeman,[28] "Manifestation of Atomic Dynamics through the Auger Effect," Conference on Simple and Multiple Electronic Processes in the Region of X-Rays and Vacuum UV, Paris, France, Sept. 21–25, 1970.

M. O. Krause,[29] "Rearrangement of Inner Shell Ionized Atoms," Conference on Simple and Multiple Electronic Processes in the Region of X-Rays and Vacuum UV, Paris, France, Sept. 21–25, 1970 (invited).

M. O. Krause,[29] "Instruments and Methods in Electron Spectrometry," ASM Educational Symposium on Modern Microanalytical Techniques in Metallurgy, Oak Ridge, Tenn., Nov. 4, 1970 (invited).

R. Laubert,[31] B. R. Appleton,[32] S. Datz, C. D. Moak,[10] and I. A. Sellin,[10] "Inner Shell Excitation Cross Sections for Iodine and Silver in Collision," 1971 Annual Meeting, American Physical Society, New York, Feb. 1–4; *Bull. Amer. Phys. Soc.* **16**, 73 (1971).

S. Datz,* C. D. Moak,[10] and B. R. Appleton,[32] "Inner Subshell Competition for Vacancies in High-Energy Heavy-Ion Collisions," 1971 Spring Meeting, American Physical Society, Washington, D.C., Apr. 26–29; *Bull. Amer. Phys. Soc.* **16**, 563 (1971).

---

31. Physics Department, New York University, New York.
32. Solid State Division.

Lectures

NUCLEAR CHEMISTRY

G. D. O'Kelley, "A New Look at the Moon: Analysis of Samples from Apollo 11 and Apollo 12," American Chemical Society Local Section Speaker Tour: Jamestown, N.Y.; Erie, Pa.; Marietta, Youngstown, Mentor, Ashland, and Cleveland, Ohio; November 1970.

CHEMISTRY AND PHYSICS OF TRANSURANIUM ELEMENTS

C. E. Bemis, Jr., "The Unequivocal Identification of Transfermium Elements; Atomic and Nuclear Spectroscopy above $Z = 100$," Research Institute of Physics, Stockholm, Sweden, Feb. 8, 1971.

C. E. Bemis, Jr., "The Unequivocal Identification of Transfermium Elements via X-Ray Techniques," Instituut voor Kernphysisch Onderzoek, Amsterdam, Netherlands, Feb. 25, 1971.

R. L. Hahn, "RHETORIC – a Discourse on Research with Heavy-Element Targets at the ORIC," ORNL Physics Division Seminar, Sept. 25, 1970.

O. L. Keller, Jr., "Some Selected Topics in the Theory and Practice of Heavy and Superheavy Elements," University of Liege, Apr. 26, 1971; Technical University of Darmstadt, Apr. 27, 1971; Kernforschungszentrum, Karlsruhe, Apr. 28, 1971.

R. J. Silva, "Present Status of Superheavy Elements Experiments at Oak Ridge," Transplutonium Committee, AEC Headquarters, Germantown, Md., and Washington, D.C., Apr. 22, 1971.

R. J. Silva, "Present Status of Superheavy Elements," National Cross Sections Advisors Committee, Duke University, Durham, N.C., May 5, 1971.

J. R. Peterson,[1] "Recent Developments in the Chemistry of Berkelium," Seminar, Laboratoire Curie, Institut du Radium, Paris, France, July 2, 1970.

J. R. Peterson,[1] "Preparation and Properties of Berkelium Metal," Seminar, Centre d'Etudes Nucléaires, Fontenay-aux-Roses, France, July 3, 1970.

J. R. Peterson,[1] "Self-Radiation Effects on the Observed Properties of Curium by Utilizing Curium-248," Seminar, Centre d'Etudes Nucléaires, Fontenay-aux-Roses, France, July 3, 1970.

J. R. Peterson,[1] "A Study of the Chemistry of Curium-248," Seminar, University of Liege, Sart Tilman, Liege, Belgium, July 15, 1970.

J. R. Peterson,[1] "Microchemical Techniques Used in Transuranium-Element Research," Seminar, Appalachian State University, Boone, N.C., Dec. 11, 1970.

ORGANIC CHEMISTRY

C. J. Collins, "Isotopes and Organic Reaction Mechanisms," Fisk University, Nashville, Tenn., Nov. 4, 1970; Murray State University, Murray, Ky., Dec. 19, 1970; Virginia Polytechnic Institute, Blacksburg, Feb. 4, 1971; Brown University, Providence, R.I., Mar. 19, 1971.

---

1. Consultant, Department of Chemistry, University of Tennessee, Knoxville.

PHYSICAL CHEMISTRY

M. A. Bredig, "Molten Metal–Metal Halide Systems: Mobile Electrons in Fused Electrolytes," The Robert A. Welch Foundation Lectureship in Chemistry: Texas Christian University, Fort Worth, Dec. 7, 1970; Tarleton State College, Stephenville, Tex., Dec. 8, 1970; Southwest Texas State University, San Marcos, Dec. 9, 1970.

CHEMICAL PHYSICS

W. R. Busing, "Chemical Information from Neutron Diffraction Studies," Chemistry Department, University of Tennessee, Knoxville, Dec. 3, 1970.

R. Livingston, "Paramagnetic Resonance Studies of Free Radicals Formed in Liquids by Photolysis," Pensacola Section, American Chemical Society, Pensacola, Fla., Nov. 12, 1970.

T. A. Carlson, "Calculated X-Ray Energies for the Superheavy Elements," Research Institute for Physics, Stockholm, Sweden, Sept. 3, 1970.

T. A. Carlson, "High-Resolution Electron Spectroscopy in Chemical Analysis," Savannah River Laboratory, Aiken, S.C., Jan. 12, 1971.

T. A. Carlson, "Multiple Ionization and Excitation in Atoms and Molecules," University of Oklahoma, Oklahoma City, Mar. 11, 1971.

T. A. Carlson, "Research in ESCA at Oak Ridge," Brookhaven National Laboratory, Upton, Long Island, N.Y., Apr. 14, 1971.

M. O. Krause, "Elektronenspektrometrie des Photoeffekts," Colloquium DESY, Hamburg, Germany, Sept. 4, 1970.

M. O. Krause, "Einfache und mehrfache Photoionisationsprozesse," Colloquium, Gutenberg University, Mainz, Germany, Sept. 28, 1970.

M. O. Krause, "Electron Spectrometry of Solids," Seminar, ORNL Solid State Division, Apr. 22, 1971.

S. Datz, "Collision Processes in Chemical Dynamics," Lecture Series at University of Aarhus, Aarhus, Denmark, April–May 1970.

S. Datz, "Interatomic Potentials from High Energy Scattering in Solids," Max-Planck Institute for Gas Dynamics, Göttingen, West Germany, July 11, 1970; Ohio State University–Battelle Memorial Institute Joint Seminar, Oct. 9, 1970.

Supplementary Activities

STAFF

PROFESSIONAL AND EDUCATIONAL ACTIVITIES

Russell Baldock	Editorial Board, *International Journal of Mass Spectrometry and Ion Physics,* 1968–present.
R. H. Busey	Director, Calorimetry Conference, 1969–1971.
W. R. Busing	President, American Crystallographic Association, 1971.
C. J. Collins	Professor of Chemistry, part time, University of Tennessee, Knoxville, January 1964–present. NATO Award, Universities of Munich and Saarbrücken, May 14–July 9, 1971.
S. Datz	Program Committee, Division of Electron and Atomic Physics, American Physical Society, 1969–1970. Co-chairman, Conference on Dynamics of Molecular Collisions, Oak Ridge National Laboratory, Aug. 31–Sept. 4, 1970. Editorial Advisory Board, *Atomic Data,* 1969–present. Editorial Board, *Case Studies in Atomic Physics,* 1970–present. International Committee, International Conference on Atomic Collisions in Solids, 1970. Chairman, Gordon Research Conference on Particle-Solid Interactions, 1969–1970. Guest Professor, Institute of Physics, University of Aarhus, Aarhus, Denmark, April 13–July 12, 1970.
R. L. Ferguson	Fellowship from Deutsches Bundesministerium für Wissenschaftliche Forschung, Garching, Germany, July 1970–July 1971.
R. L. Hahn	Committee on Major Nuclear Facilities, Division of Nuclear Chemistry and Technology, American Chemical Society, 1970–1974. *Ad Hoc* Committee on the Outside Use of the Super-HILAC, American Physical Society, 1970.
C. K. Johnson	Member, National Research Council Committee on Chemical Crystallography. Consultant, Crystallographic Computing Committee, International Union for Crystallography.
O. L. Keller, Jr.	USAEC Transplutonium Program Committee, 1969–1972. Member, Nuclear Physics Survey Panel, National Academy of Sciences, 1969–1971.
K. A. Kraus	Editorial Board, *Journal of Chromatography,* 1958–present. Editorial Advisory Board, *Journal of Inorganic and Nuclear Chemistry,* 1958–present. Editorial Board, *Desalination,* 1966–present.
H. A. Levy	Discussion Leader, Welch Conference on Solid State Chemistry, Houston, Tex., November 1970. Consultant to Committee under Auspices of National Science Foundation to Study Feasibility of Reactivating the Materials Testing Reactor, 1971.
M. H. Lietzke	Professor of Chemistry, part time, University of Tennessee, Knoxville, January 1964–present.
Ralph Livingston	Professor of Chemistry, part time, University of Tennessee, Knoxville, January 1964–present. ORNL liaison officer for ORNL–University of Tennessee part-time teaching programs, 1968–present. Member, Graduate Council, University of Tennessee, Knoxville, January 1970–present. Co-Chairman, ESR Symposium, Division of Physical Chemistry, American Chemical Society, Athens, Ga., Dec. 7–9, 1970. Chairman, Third Southeastern Magnetic Resonance Conference, Oak Ridge, to be held Oct. 20–22, 1971. Editorial Board, *The Journal of Magnetic Resonance,* January 1971–present. Participant, Southern College University Union Planning Conference, Vanderbilt University, Nashville, Tenn., Aug. 25–27, 1970. Chairman-Elect, East Tennessee Section, American Chemical Society, 1971.
G. E. Moore	Instructor in Chemistry, National Science Foundation In-Service Institute for Secondary School Science Teachers, Knoxville College, Knoxville, Tenn., 1967–present.

G. D. O'Kelley	Professor of Chemistry, part time, University of Tennessee, Knoxville, January 1964–present. Subcommittee on Radiochemistry, National Academy of Sciences–National Research Council, 1962–present. Chairman, Division of Nuclear Chemistry and Technology, American Chemical Society, 1971.
J. R. Peterson[1]	North Atlantic Treaty Organization Postdoctoral Fellow in Sciences, University of Liège, Belgium, Aug. 18, 1969, to Aug. 21, 1970.
R. J. Raridon	State Sponsor of the Collegiate Division, Tennessee Academy of Science, 1965–present. President, Tennessee Academy of Science, 1971. Chairman, Committee on Collegiate Academies, Association of Academies of Science.
R. W. Stoughton	Editorial Advisory Board, *Journal of Inorganic and Nuclear Chemistry*, 1958–present.
E. H. Taylor	Board of Directors, Institute of Catalysis.
W. E. Thiessen	Member, Selection Committee for Contributed Papers to the XXIIIrd International Congress of Pure and Applied Chemistry.

FOREIGN MEETINGS AND ACTIVITIES

Meeting and/or Activity	Location	Staff Member(s)
Annual Meeting of Nuclear Scientists of Belgium, Apr. 15, 1970	University of Ghent Ghent, Belgium	J. R. Peterson[1]
Joint Conference, Chemical Institute of Canada and American Chemical Society, May 24–29, 1970	Toronto, Canada	R. Livingston
Summer Meeting, American Crystallographic Association, Aug. 15–21, 1970	Carleton University Ottawa, Canada	P. A. Agron W. R. Busing W. E. Thiessen
EUCHEM Research Conference on Electron Spectroscopy, Sept. 7–9, 1970	Uppsala, Sweden	T. A. Carlson M. O. Krause
Conference on Photoionization Phenomena and Photoelectron Spectroscopy, Sept. 14–16, 1970	Oxford, England	T. A. Carlson M. O. Krause
Conference on Simple and Multiple Electronic Processes in the Region of X-Rays and Vacuum UV, Sept. 21–25, 1970	Paris, France	T. A. Carlson M. O. Krause
Italian Crystallographic Society Congress, Sept. 27–Oct. 3, 1970	Cagliari, Italy	A. H. Narten
Conference on Molecular Motions in Liquid, Oct. 5–8, 1970	Herrenalb, Germany	A. H. Narten
Conference on Radiochemistry, Sept. 28–Oct. 8, 1970	Dubna, U.S.S.R.	R. J. Silva
International Conference on Heavy Ion Physics, Feb. 11–17, 1971	Dubna, U.S.S.R.	C. E. Bemis, Jr.
International Conference of Chemical Arts, Apr. 19–24, 1971	Paris, France	O. L. Keller, Jr.

COLLABORATIVE RESEARCH

Institution	Collaborator(s)	Subject	Staff Member(s)
Andrews University	M. C. Kelley J. R. Van Hise	Search for the 0^+ member of the two-phonon vibrational state in ^{110}Cd	N. R. Johnson
Australian Atomic Energy Commission Research Establishment	R. W. Matthews	Photooxidation and fluorescence of Ce(III)	T. J. Sworski
Brookhaven National Laboratory	M. L. Perlman	Electron binding energies in curium	C. E. Bemis, Jr. P. F. Dittner
Centenary College	R. F. Walker, Jr.	Properties of osmium alpha emitters	R. L. Hahn
Centre d'Etude de L'Energie Nucleaire, Mol, Belgium	P. Fettweis	Decay of ^{101}Tc	G. D. O'Kelley

1. Consultant, Department of Chemistry, University of Tennessee, Knoxville.

Institution	Collaborator(s)	Subject	Staff Member(s)
David Lipscomb College	J. W. Dawson	An investigation of radioactive ^{163}Tm	N. R. Johnson R. J. Silva
University of Delft, Netherlands	B. van Nooijen K. Rester	Properties of radioactive ^{84}Y and ^{86}Y	N. R. Johnson
University of Delhi, India	S. C. Pancholi	Investigations of the decay properties of ^{84}Y and ^{59}Fe	N. R. Johnson
Florida State University	R. K. Sheline	Levels in ^{161}Tb excited by the (^{3}He,*d*) reaction and by the decay of 3.7-min ^{161}Gd	N. R. Johnson G. D. O'Kelley
Furman University	R. O. Sayer	Coulomb excitation of heavy elements	E. Eichler N. R. Johnson
Indiana University	F. B. Malik	Use of atomic wave functions[2]	T. A. Carlson
Institute of Nuclear Research, Amsterdam, Netherlands	J. Konijn	Properties of radioactive ^{84}Y	N. R. Johnson
Lawrence Radiation Laboratory, Berkeley	D. K. Fujita B. B. Cunningham	Magnetic susceptibility studies of berkelium metal	J. R. Peterson[1]
Lawrence Radiation Laboratory, Livermore	R. G. Lanier	Search for the 0^{+} member of the two-phonon vibrational state in ^{110}Cd	N. R. Johnson
	R. G. Lanier R. A. Meyer	Levels in ^{161}Tb excited by the (^{3}He,*d*) reaction and by the decay of 3.7-min ^{161}Gd	N. R. Johnson G. D. O'Kelley
University of Liège, Belgium	M. Noé J. Fuger	Self-radiation effects on the physical and chemical properties of curium	J. R. Peterson[1]
Maryville College	P. J. Ogren	Pulse radiolysis and flash photolysis of oxygen	C. J. Hochanadel J. A. Ghormley J. W. Boyle
		Absorption spectrum of HO_2 radical in gas phase	C. J. Hochanadel J. A. Ghormley J. W. Boyle
Massachusetts Institute of Technology School of Chemical Engineering Practice, Oak Ridge Station	J. T. Day P. H. Wadia and various teams	Hyperfiltration with dynamically formed membranes	J. S. Johnson K. A. Kraus
Memphis State University	P. K. Sen Gupta	Studies of metallocenes	G. M. Brown
Middle East Technical University, Ankara, Turkey	N. K. Aras	Decay of ^{101}Tc	G. D. O'Kelley
University of Missouri	K. L. Cheng	Electron spectroscopy[2]	T. A. Carlson
University of Naples, Italy	G. Chilosi	Decay of ^{101}Tc	G. D. O'Kelley
NASA Manned Spacecraft Center	E. Schonfeld	Determination of primordial and cosmogenic radionuclide content of lunar material by gamma-ray spectrometry	G. D. O'Kelley
University of Puerto Rico	L. Blum	X-ray and neutron scattering from liquids	A. H. Narten
Purdue University	L. R. Morss	Thermodynamic systematics among the members of the lanthanide and actinide series	L. J. Nugent
	R. C. Hagenauer	Decay of neutron-deficient nuclides of mass 89 and 88	G. D. O'Kelley E. Eichler
University of Southern Mississippi	J. W. Pinson	Study of solid polymers from radiolysis of pentaborane-9 vapor	P. S. Rudolph R. Baldock

2. In collaboration with the Physics Division.

Institution	Collaborator(s)	Subject	Staff Member(s)
University of Tennessee	T. F. Williams A. Campion	Pulse radiolysis studies of electron-excess centers in succinonitrile and adiponitrile	J. A. Ghormley C. J. Hochanadel
	J. W. Larsen	Heats of formation of organic compounds in superacids	C. J. Collins V. F. Raaen
		NMR spectroscopy	C. J. Collins B. M. Benjamin
	G. Mamantov K. W. Fung	Crystal structure of trimercury chloro-aluminate	R. D. Ellison H. A. Levy
	W. E. Bull F. A. Grimm G. K. Schweitzer	Use of electron spectroscopy for chemical analysis[2]	T. A. Carlson
	F. K. Schmidt-Bleek	Chemical accelerator sources	S. Datz
Texas A and M University	R. A. Kuebbing	Highly retarded $E1$ transitions in ^{92}Nb and ^{94}Nb	E. Eichler
Tri-State College	J. R. Van Hise	Decay of ^{136}Pr and level structure of ^{136}Ce	B. H. Ketelle A. R. Brosi
Vanderbilt University	J. H. Hamilton A. V. Ramayya	Systematics of the $K^{\pi}=0^-$ and 1^- octupole bands in transitional nuclei	N. R. Johnson
		A study of the properties of some vibrational spherical nuclei	N. R. Johnson E. Eichler
		Studies of the vibrational behavior of deformed nuclei	N. R. Johnson
	G. D. Benson R. G. Albridge	Decay of ^{192}Au	G. D. O'Kelley
	G. D. Benson A. V. Ramayya R. G. Albridge	Decay of ^{194}Au to levels in ^{194}Pt	G. D. O'Kelley
Virginia Polytechnic Institute	M. A. Ijaz	Properties of rare-earth alpha emitters	R. L. Hahn
Washington University	D. G. Sarantites	Levels in ^{95}Tc	E. Eichler

ANNUAL INFORMATION MEETING AND ADVISORY COMMITTEE

The Annual Information Meeting of the Chemistry Division was held October 12 and 13, 1970, in the Central Auditorium, Building 4500N. Reports presented at the Meeting were:

Monday, October 12, 1970

E. H. Taylor	Introduction
L. J. Nugent	Electron-Transfer and $f \rightarrow d$ Absorption Bands of Some Lanthanide and Actinide Complexes and the Standard (III-IV) Oxidation Potentials for Each Member of the Lanthanide and Actinide Series
C. J. Collins	Memory Effects during Deaminations
W. E. Thiessen	Organic Crystal Structure Analysis without Heavy Atoms
C. J. Hochanadel	Effects of Water and Other Additives on Ozone Formation in the Pulse Radiolysis of Oxygen, Oxygen-Nitrogen, and Oxygen-Argon Mixtures
A. S. Dworkin	Thermochemistry and Crystal Structure of Alkali Metal Fluoroborates
J. S. Drury	Superheavy Elements

Tuesday, October 13, 1970

C. E. Bemis, Jr.	Nuclear Spectroscopy of the Transuranium Elements
E. Eichler	Coulomb Excitation of Heavy Nuclei
A. R. Brosi	Fast Coincidence Spectroscopy and the Decay of ^{136}Nd, ^{136}Pr, and ^{137}Nd

M. L. Mallory	Development of Heavy Ions on the Oak Ridge Isochronous Cyclotron (ORIC)
S. Datz	Atomic Potentials from Channeled-Ion-Energy-Loss Spectra

Members of the Advisory Committee were:

Dr. Gerhart Friedlander
Department of Chemistry
Brookhaven National Laboratory
Upton, Long Island, New York 11973

Prof. George S. Hammond
Department of Chemistry
California Institute of Technology
Pasadena, California 91109

Dr. Joseph J. Katz
Argonne National Laboratory
9700 South Cass Avenue
Argonne, Illinois 60493

Prof. Henry Taube
Department of Chemistry
Stanford University
Stanford, California 94305

VISITING SCIENTISTS

Name	Affiliation	ORNL Research Program	Sponsor
J. K. Dohrmann	Freie Universität Berlin, Institut für Physikalische Chemie	Microwave and Radio-Frequency Spectroscopy	Deutsche Forschungsgemeinschaft
W. H. Fletcher	University of Tennessee	Infrared Spectroscopy	Consultant
Leela Ganguly	Louisiana State University	Transuranium Research Laboratory	Louisiana State University
R. V. Gentry	Columbia Union College	Transuranium Research Laboratory	Columbia Union College
P. G. Laubereau	Anorganisch-Chemisches Laboratorium, Technische Hochschule München, Munich, Germany	Transuranium Research Laboratory	Bundesministerium für wissenschaftliche Forschung, Bonn, Federal Republic of Germany
P. G. Lenhert	Vanderbilt University	Crystallographic Computing	
P. J. Ogren	Maryville College	Radiation Chemistry	
J. R. Peterson	University of Tennessee	Transuranium Research Laboratory	Consultant
S. W. Peterson	Argonne National Laboratory	Neutron and X-Ray Diffraction	ANL
J. W. Pinson	University of Southern Mississippi	Mass Spectrometry	ORAU Faculty Research Participation Program
F. K. Schmidt-Bleek	University of Tennessee	Molecular Beam	Consultant
P. K. Sen Gupta	Memphis State University	Neutron and X-Ray Diffraction	ORAU Faculty Research Participation Program
R. M. Statnick		Molecular Beam	U.S. AEC Postdoctoral Fellowship Program
J. M. Williams	Argonne National Laboratory	Neutron and X-Ray Diffraction	ANL
F. Wuilleumier	Laboratoire de Chimie Physique de la Faculté des Sciences de Paris, Paris, France	Transuranium Research Laboratory	CNRS, France, and NATO
M. J. Zender	Fresno State College	Transuranium Research Laboratory	ORAU Faculty Research Participation Program

STUDENTS

GRADUATE

Name	Major Professor and/or Institution	Staff Advisor	Field of Research	Sponsor
Carol P. Anderson	W. E. Bull and F. A. Grimm, University of Tennessee	T. A. Carlson	Determination of molecular orbitals by photoelectron spectroscopy[2]	NSF Fellowship
Linda C. Cain	G. K. Schweitzer, University of Tennessee	T. A. Carlson	Study of bonding in second and third row transitional metal compounds[2]	NSF Fellowship
J. C. Carver	G. K. Schweitzer, University of Tennessee	T. A. Carlson	Study of bonding in metallic salts by photoelectron spectroscopy[2]	NSF Fellowship
L. L. Collins, Jr.	G. D. O'Kelley	G. D. O'Kelley N. R. Johnson E. Eichler	Nuclear spectroscopy	University of Tennessee
J. A. Fahey	J. R. Peterson, University of Tennessee	L. J. Nugent	Transuranium Research Laboratory	Oak Ridge Graduate Fellowship Program
L. Finkel	J. A. Marinsky, State University of New York at Buffalo	G. E. Boyd E. Eichler R. L. Ferguson	Independent fission yields of ^{101}Tc, ^{104}Tc, and ^{105}Tc from thermal-neutron induced fission of ^{235}U	Oak Ridge Graduate Fellowship Program
D. W. Gosbin	M. H. Lietzke, University of Tennessee	M. H. Lietzke	Application of a two structure model to aqueous electrolyte mixtures	
M. S. Green[3]	W. W. Wyatt, University of Tennessee	B. M. Benjamin	Stereochemistry of 1,2-glycols by nuclear magnetic resonance	ORAU Special Training Division
R. J. Herdklotz	M. H. Lietzke, University of Tennessee	M. H. Lietzke	Thermodynamic Properties of Aqueous HCl-NaCl-$MgCl_2$ Mixtures as Calculated from EMF Measurements (Ph.D. thesis, July 1970)	Oak Ridge Graduate Fellowship Program
F. D. Hwang	F. K. Schmidt-Bleek, University of Tennessee	S. Datz	Molecular Beam	University of Tennessee
A. E. Jonas	W. E. Bull and G. K. Schweitzer, University of Tennessee	T. A. Carlson	Photoelectron spectroscopy of gaseous molecules[2]	University of Tennessee NASA Research Grant
N. Kashihira	F. K. Schmidt-Bleek, University of Tennessee	S. Datz	Collision dynamics of alkali metal atoms and diatomic molecules	
A. F. Kluk	J. H. Hamilton, Vanderbilt University	N. R. Johnson	Vibrational behavior of deformed rare-earth nuclei	Oak Ridge Graduate Fellowship Program
C. W. Linsey	R. B. Escue, North Texas State University	R. H. Busey R. A. Gilbert	High-Temperature Enthalpies of the Lead Halides: Enthalpies and Entropies of Fusion (Ph.D. thesis, June 1970)	Oak Ridge Graduate Fellowship Program
G. E. McGuire	G. K. Schweitzer, University of Tennessee	T. A. Carlson	Study of complex metal salts by photoelectron spectroscopy[2]	NSF Fellowship
W. E. Moddeman	W. E. Bull and G. K. Schweitzer, University of Tennessee	T. A. Carlson	Auger Spectroscopy of Simple Gaseous Molecules (Ph.D. thesis, Sept. 1970)[2]	University of Tennessee, NASA Research Grant
Joyce Ann Monard	P. G. Huray, University of Tennessee	O. L. Keller, Jr. R. L. Becker[4] F. E. Obenshain[4]	Transuranium Research Laboratory	NSF Fellowship

3. M.Ed. candidate in the College of Education.
4. Physics Division.

Name	Major Professor and/or Institution	Staff Advisor	Field of Research	Sponsor
H. D. Harmon	J. R. Peterson,[1] University of Tennessee	C. F. Coleman[5]	Transuranium Research Laboratory	National Defense Education Act Title IV Fellow
G. L. Ostrom	F. K. Schmidt-Bleek, University of Tennessee	S. Datz	Sputtering studies	
P. R. Reed	F. K. Schmidt-Bleek, University of Tennessee	C. J. Hochanadel T. J. Sworski	Radiation chemistry of methane	AUA-ANL Pre-doctoral Fellowship
N. Singhal	J. H. Hamilton, Vanderbilt University	N. R. Johnson E. Eichler	Vibrational properties of even-even spherical nuclei	Vanderbilt University
J. N. Stevenson	J. R. Peterson,[1] University of Tennessee	O. L. Keller, Jr. L. J. Nugent	Transuranium Research Laboratory	Oak Ridge Graduate Fellowship Program

UNDERGRADUATE

Name	Institution	ORNL Research Program	Sponsor
D. J. Houser	DePauw University	Organic Chemistry	Great Lakes Colleges Association
J. S. Jones	DePauw University	Isotope Chemistry	Great Lakes Colleges Association
R. L. Lewis	Grinnell College	Radiation Chemistry	ORAU Summer Student Trainee Program
R. C. Thomas	Albion College	Neutron and X-Ray Diffraction	Great Lakes Colleges Association
M. T. Unger	Huntington College	Chemistry of Aqueous Systems	ORAU Summer Student Trainee Program
W. A. Wachter	La Salle College	Electrochemistry	ORAU Summer Student Trainee Program
J. R. Wiersig	Denison University	Organic Chemistry	Great Lakes Colleges Association

5. Chemical Technology Division.

ORNL-4706
UC-4 – Chemistry

INTERNAL DISTRIBUTION

1. Biology Library
2–4. Central Research Library
5. Laboratory Shift Supervisor
6. MIT Practice School
7. ORNL – Y-12 Technical Library Document Reference Section
8–43. Laboratory Records Department
44. Laboratory Records, ORNL R.C.
45. H. I. Adler
46. P. A. Agron
47. W. H. Baldwin
48. C. E. Bemis
49. D. S. Billington
50. F. F. Blankenship
51. E. G. Bohlmann
52. C. J. Borkowski
53–54. G. E. Boyd
55. M. A. Bredig
56. R. B. Briggs
57. H. R. Bronstein
58. A. R. Brosi
59. G. M. Brown
60. J. H. Burns
61. R. H. Busey
62. W. R. Busing
63. T. A. Carlson
64. G. H. Cartledge
65. C. J. Collins
66. D. R. Cuneo
67. F. L. Culler
68. M. D. Danford
69. S. Datz
70. J. S. Drury
71. A. S. Dworkin
72. E. Eichler
73. R. L. Ferguson
74. J. L. C. Ford
75. W. Fulkerson
76. J. L. Gabbard
77. J. A. Ghormley
78. J. H. Gibbons
79. R. A. Gilbert
80. J. H. Gillette
81. C. D. Goodman
82. W. R. Grimes
83. R. L. Hahn
84. J. Halperin
85. R. F. Hibbs
86. C. J. Hochanadel
87. H. P. Carter
88. C. K. Johnson
89–93. J. S. Johnson
94. N. R. Johnson
95. W. H. Jordan
96. O. L. Keller
97. H. W. Kohn
98. M. T. Kelley
99. B. H. Ketelle
100. K. A. Kraus
101. M. O. Krause
102. J. A. Lane
103. E. Lamb
104. H. A. Levy
105. M. H. Lietzke
106. T. A. Lincoln
107. J. L. Liverman
108. R. Livingston
109. R. S. Livingston
110. R. N. Lyon
111. H. G. MacPherson
112. Peter Mazur
113. J. R. McNally, Jr.
114–124. G. E. Moore
125. K. Z. Morgan
126. A. H. Narten
127. L. J. Nugent
128. G. D. O'Kelley
129. G. W. Parker
130–131. R. B. Parker
132. F. Plasil
133. J. J. Pinajian
134. F. A. Posey
135. A. S. Quist
136. Helen Raaen
137. R. J. Raridon
138. S. A. Reynolds
139. P. S. Rudolph
140. H. W. Schmitt
141. H. E. Seagren
142. E. D. Shipley
143. M. J. Skinner
144. H. G. Smith
145. A. H. Snell
146. P. H. Stelson

147. J. N. Stevenson
148. R. W. Stoughton
149. D. A. Sundberg
150. T. J. Sworski
151–204. E. H. Taylor
205. W. E. Thiessen
206. R. E. Thoma
207. K. S. Toth
208. D. B. Trauger
209. F. Vaslow
210. G. M. Watson
211. A. M. Weinberg
212. J. J. Katz (Advisory Committee)
213. Henry Taube (Advisory Committee)
214. George S. Hammond (Advisory Committee)

EXTERNAL DISTRIBUTION

215. H. Miller, Office of Isotope Development, AEC, Washington
216. R. H. Schuler, Radiation Research Laboratories, Mellon Institute, 4400 Fifth Ave., Pittsburgh 13, Pa.
217. Division of Research and Development, AEC, Washington
218. Boeing Airplane Company
219. Union Carbide Corporation, Chemicals Division (South Charleston)
220. North American Aviation, Inc.
221. Masaharu Kondo, Professor of Chemistry, Radiation Chemistry Laboratory, Tokyo Metropolitan University, 1-950, Fukasawa-cho, Setagaya-ku, Tokyo, Japan
222. M. Daniels, Department of Chemistry, University College of West Indies, Kingston 7, Jamaica
223. J. P. W. Houtman, Reactor Institute Delft, Technische Hogeschool, Delft, The Netherlands
224. Technion, Israel Institute of Technology, Department of Nuclear Science, Haifa, Israel
225. J. H. Green, Department of Nuclear and Radiation Chemistry, The University of New South Wales, P.O. Box 1, Kensington, N.S.W., Australia
226. Ingmar Bergstrom, Nobel Institute of Physics, Stockholm 50, Sweden
227. Riki Kobayashi, William Marsh Rice University, Houston, Texas
228. J. A. Swartout, 270 Park Avenue, New York 17, New York
229. W. W. Grigorieff, Assistant to the Executive Director, Oak Ridge Associated Universities
230. Enrico Cerrai, CISE, Milan, Italy
231. H. E. Podall, Office of Saline Water, U.S. Department of the Interior, Washington, D.C.
232. D. E. Troutner, Chemistry Department, University of Missouri, Columbia, Missouri
233. J. H. Hamilton, Physics Department, Vanderbilt University, Nashville, Tennessee
234. W. H. McCoy, Office of Saline Water, U.S. Department of the Interior, Washington, D.C.
235. W. A. Schwartz, Cincinnati Water Research Laboratory, 4676 Columbia Parkway, Cincinnati, Ohio
236. Sidney Langer, Gulf General Atomic, San Diego, California
237. J. R. Peterson, Department of Chemistry, University of Tennessee, Knoxville, Tennessee
238. Library, Wah Chang Albany Corporation, P.O. Box 460, Albany, Oregon
239. S. B. Sachs, Weizmann Institute of Science, Rehovoth, Israel
240. F. Schmidt-Bleek, Department of Chemistry, University of Tennessee, Knoxville, Tennessee
241. F. E. Walker, Chemistry Department, Lawrence Radiation Laboratory, Livermore, California
242. Robert Vandenbosch, Chemistry Department, University of Washington, Seattle, Washington
243. S. R. Mohanty, Department of Chemistry, Utkal University, Bhubaneswar 4, India
244. G. Czapski, Department of Physical Chemistry, The Hebrew University, Jerusalem, Israel
245. G. Scatchard, Professor of Physical Chemistry, Emeritus, Massachusetts Institute of Technology, Cambridge, Mass. 02139
246. Craig A. Brandon, Department of Mechanical Engineering, Clemson University, Clemson, S.C. 29631
247. Kenton J. Brown, Group Director, Pulping & Processing Research, Corporate Research Center, International Paper Co., P.O. Box 797, Tuxedo Park, N.Y. 10987
248. H. F. Gibbard, Jr., Department of Chemistry, Southern Illinois University, Carbondale, Illinois 62901
249. M. A. Ijaz, Physics Department, Virginia Polytechnic Institute, Blacksburg, Virginia
250. R. F. Walker, Jr., Physics Department, Centenary College, Shreveport, Louisiana 71104

251. Justin L. Bloom, U.S. Atomic Energy Commission, Washington, D.C. 20545
252. D. A. Bromley, Department of Physics, Yale University, New Haven, Conn.
253. M. L. Perlman, Department of Chemistry, Brookhaven National Laboratory, Upton, New York
254. R. A. Robinson, Department of Chemistry, University of Florida, Gainesville, Fla. 32601
255. Jerzy Jastrzebski, Institute for Nuclear Research, Swierk K. Otwocka, Poland
256. R. Bock, Physikalisches Institut, Max Planck Institut für Kernphysik, Heidelberg, West Germany
257. Director of the Institute for Nuclear Physics Research (I.K.O.), Ooster Ringdijk 18 a, Amsterdam, The Netherlands
258. Laboratory and University Division, AEC, ORO
259. Patent Office, AEC, ORO

260–459. Given distribution as shown in TID-4500 under Chemistry category (25 copies – NTIS)